

Antarctic Meteorology and Climatology

American Geophysical Union

ANTARCTIC
RESEARCH
SERIES

Physical Sciences

ANTARCTIC OCEANOLOGY

Joseph L. Reid, *Editor*

ANTARCTIC OCEANOLOGY II: THE AUSTRALIAN- NEW ZEALAND SECTOR

Dennis E. Hayes, *Editor*

ANTARCTIC SNOW AND ICE STUDIES

Malcolm Mellor, *Editor*

ANTARCTIC SNOW AND ICE STUDIES II

A. P. Crary, *Editor*

ANTARCTIC SOILS AND SOIL FORMING PROCESSES

J. C. F. Tedrow, *Editor*

DRY VALLEY DRILLING PROJECT

L. D. McGinnis, *Editor*

GEOLOGICAL INVESTIGATIONS IN NORTHERN VICTORIA LAND

Edmund Stump, *Editor*

GEOLOGY AND PALEONTOLOGY OF THE ANTARCTIC

Jarvis B. Hadley, *Editor*

GEOLOGY OF THE CENTRAL TRANSANTARCTIC MOUNTAINS

Mort D. Turner and John F. Spletstoesser,
Editors

GEOMAGNETISM AND AERONOMY

A. H. Waynick, *Editor*

METEOROLOGICAL STUDIES AT PLATEAU STATION, ANTARCTICA

Joost A. Businger, *Editor*

OCEANOLOGY OF THE ANTARCTIC CONTINENTAL SHELF

Stanley S. Jacobs, *Editor*

STUDIES IN ANTARCTIC METEOROLOGY

Morton J. Rubin, *Editor*

UPPER ATMOSPHERE RESEARCH IN ANTARCTICA

L. J. Lanzerotti and C. G. Park, *Editors*

THE ROSS ICE SHELF: GLACIOLOGY AND GEOPHYSICS

C. R. Bentley and D. E. Hayes, *Editors*

VOLCANOES OF THE ANTARCTIC PLATE AND SOUTHERN OCEANS

W. E. LeMasurier and J. T. Thomson, *Editors*

MINERAL RESOURCES POTENTIAL OF ANTARCTICA

John F. Spletstoesser and Gisela A. M. Dreschhoff,
Editors

MARINE GEOLOGICAL AND GEOPHYSICAL ATLAS OF THE CIRCUM-ANTARCTIC TO 30°S

Dennis E. Hayes, *Editor*

MOLLUSCAN SYSTEMATICS AND BIOSTRATIGRAPHY

Jeffery D. Stilwell and William J. Zinsmeister

THE ANTARCTIC PALEOENVIRONMENT: A PERSPECTIVE ON GLOBAL CHANGE

James P. Kennett and Detlef A. Warnke, *Editors*

PHYSICAL AND BIOCHEMICAL PROCESSES IN ANTARCTIC LAKES

William Green and E. Imre Friedmann, *Editors*

THE ANTARCTIC PALEOENVIRONMENT: A PERSPECTIVE ON GLOBAL CHANGE PART 2

James P. Kennett and Detlef A. Warnke, *Editors*

CONTRIBUTIONS TO ANTARCTIC RESEARCH I

David H. Elliot, *Editor*

CONTRIBUTIONS TO ANTARCTIC RESEARCH II

David H. Elliot, *Editor*

CONTRIBUTIONS TO ANTARCTIC RESEARCH III

David H. Elliot, *Editor*

American Geophysical Union

ANTARCTIC
RESEARCH
SERIES

Biological and Life Sciences

BIOLOGY OF THE ANTARCTIC SEAS

Milton O. Lee, *Editor*

BIOLOGY OF THE ANTARCTIC SEAS II

George A. Llano, *Editor*

BIOLOGY OF THE ANTARCTIC SEAS III

George A. Llano and Waldo L. Schmitt, *Editors*

BIOLOGY OF THE ANTARCTIC SEAS IV

George A. Llano and I. Eugene Wallen, *Editors*

BIOLOGY OF THE ANTARCTIC SEAS V

David L. Pawson, *Editor*

BIOLOGY OF THE ANTARCTIC SEAS VI

David L. Pawson, *Editor*

BIOLOGY OF THE ANTARCTIC SEAS VII

David L. Pawson, *Editor*

BIOLOGY OF THE ANTARCTIC SEAS VIII

David L. Pawson and Louis S. Kornicker, *Editors*

BIOLOGY OF THE ANTARCTIC SEAS IX

Louis S. Kornicker, *Editor*

BIOLOGY OF THE ANTARCTIC SEAS X

Louis S. Kornicker, *Editor*

BIOLOGY OF THE ANTARCTIC SEAS XI

Louis S. Kornicker, *Editor*

BIOLOGY OF THE ANTARCTIC SEAS XII

David L. Pawson, *Editor*

BIOLOGY OF THE ANTARCTIC SEAS XIII

Louis S. Kornicker, *Editor*

BIOLOGY OF THE ANTARCTIC SEAS XIV

Louis S. Kornicker, *Editor*

BIOLOGY OF THE ANTARCTIC SEAS XV

Louis S. Kornicker, *Editor*

BIOLOGY OF THE ANTARCTIC SEAS XVI

Louis S. Kornicker, *Editor*

BIOLOGY OF THE ANTARCTIC SEAS XVII

Louis S. Kornicker, *Editor*

BIOLOGY OF THE ANTARCTIC SEAS XVIII

Louis S. Kornicker, *Editor*

BIOLOGY OF THE ANTARCTIC SEAS XIX

Louis S. Kornicker, *Editor*

BIOLOGY OF THE ANTARCTIC SEAS XX

Louis S. Kornicker, *Editor*

BIOLOGY OF THE ANTARCTIC SEAS XXI

Louis S. Kornicker, *Editor*

BIOLOGY OF THE ANTARCTIC SEAS XXII

Stephen D. Cairns, *Editor*

ANTARCTIC TERRESTRIAL BIOLOGY

George A. Llano, *Editor*

TERRESTRIAL BIOLOGY II

Bruce Parker, *Editor*

TERRESTRIAL BIOLOGY III

Bruce Parker, *Editor*

ANTARCTIC ASCIDIACEA

Patricia Kott

ANTARCTIC BIRD STUDIES

Oliver L. Austin, Jr., *Editor*

ANTARCTIC PINNIPEDIA

William Henry Burt, *Editor*

ANTARCTIC CIRRIPEDIA

William A. Newman and Arnold Ross

BIRDS OF THE ANTARCTIC AND SUB-ANTARCTIC

George E. Watson

ENTOMOLOGY OF ANTARCTICA

J. Linsley Gressitt, *Editor*

HUMAN ADAPTABILITY TO ANTARCTIC CONDITIONS

E. K. Eric Gunderson, *Editor*

POLYCHAETA ERRANTIA OF ANTARCTICA

Olga Hartman

POLYCHAETA MYZOSTOMIDAE AND SEDENTIARIA OF ANTARCTICA

Olga Hartman

RECENT ANTARCTIC AND SUBANTARCTIC BRACHIOPODS

Merrill W. Foster


Volume 61

ANTARCTIC
RESEARCH
SERIES

Antarctic Meteorology and Climatology:

Studies Based on Automatic Weather Stations

David H. Bromwich
Charles R. Stearns
Editors

 American Geophysical Union
Washington, D.C.
1993

Volume 61

ANTARCTIC
RESEARCH
SERIES

Published under the aegis of the
Board of Associate Editors, Antarctic Research Series
David H. Elliot, Chairman
John B. Anderson, Robert Bindschadler,
Stephen D. Cairns, Rodney M. Feldmann, Stanley Jacobs,
John Prisco, Charles R. Stearns

Library of Congress Cataloging-in-Publication Data

Antarctic meteorology and climatology : studies based on automatic
weather stations / David H. Bromwich, Charles R. Stearns, editors.
p. cm. — (Antarctic research series ; v. 61)

Includes bibliographical references.

ISBN 0-87590-839-X

1. Antarctica—Climate. 2. Meteorology—Antarctica. 3. Automatic
weather stations. I. Bromwich, David H. II. Stearns, Charles R.
III. Series.

QC994.9.A58 1993

551.6998'9—dc20

94-3154
CIP

ISBN 0-87590-839-X

ISSN 0066-4634

Copyright 1993 by the American Geophysical Union
2000 Florida Avenue, N.W.
Washington, DC 20009

Figures, tables, and short excerpts may be reprinted in scientific books and journals if the source is properly cited.

Authorization to photocopy items for internal or personal use, or the internal or personal use of specific clients, is granted by the American Geophysical Union for libraries and other users registered with the Copyright Clearance Center (CCC) Transactional Reporting Service, provided that the base fee of \$1.00 per copy plus \$0.20 per page is paid directly to CCC, 222 Rosewood Dr., Danvers, MA 01923. 0066-4634/93/\$01.00+0.20.

This consent does not extend to other kinds of copying, such as copying for creating new collective works or for resale. The reproduction of multiple copies and the use of full articles or the use of extracts, including figures and tables, for commercial purposes requires permission from AGU.

Published by
American Geophysical Union
With the aid of grant DPP-89-15494 from the
National Science Foundation

Printed in the United States of America.

CONTENTS

The Antarctic Research Series: Statement of Objectives <i>Board of Associate Editors</i>	xi
Preface <i>David H. Bromwich and Charles R. Stearns</i>	xiii
Monthly Mean Climatic Data for Antarctic Automatic Weather Stations <i>Charles R. Stearns, Linda M. Keller, George A. Weidner, and Manuela Sievers</i>	1
Katabatic Winds in Adélie Coast <i>Gerd Wendler, Jean Claude André, Paul Pettré, Joan Gosink, and Thomas Parish</i>	23
Spatial and Temporal Characteristics of the Intense Katabatic Winds at Terra Nova Bay, Antarctica <i>David H. Bromwich, Thomas R. Parish, Andrea Pellegrini, Charles R. Stearns, and George A. Weidner</i>	47
Katabatic Winds Along the Transantarctic Mountains <i>Christopher J. Breckenridge, Uwe Radok, Charles R. Stearns, and David H. Bromwich</i>	69
Satellite and Automatic Weather Station Analyses of Katabatic Surges Across the Ross Ice Shelf <i>Jorge F. Carrasco and David H. Bromwich</i>	93
Sensible and Latent Heat Flux Estimates in Antarctica <i>Charles R. Stearns and George A. Weidner</i>	109
The Kernlose Winter in Adélie Coast <i>Gerd Wendler and Yuji Kodama</i>	139
Antarctic Climate Anomalies Surrounding the Minimum in the Southern Oscillation Index <i>Shawn R. Smith and Charles R. Stearns</i>	149
Variation in Aerosol Concentration Associated With a Polar Climatic Iteration <i>A. Hogan, D. Riley, B. B. Murphey, S. C. Barnard, and J. A. Samson</i>	175
Continuous Nanoclimate Data (1985–1988) From the Ross Desert (McMurdo Dry Valleys) Cryptoendolithic Microbial Ecosystem <i>Christopher P. McKay, James A. Nienow, Michael A. Meyer, and E. Imre Friedmann</i>	201

The Antarctic Research Series:

STATEMENT OF OBJECTIVES

The Antarctic Research Series provides for the presentation of detailed scientific research results from Antarctica, particularly the results of the United States Antarctic Research Program, including monographs and long manuscripts.

The series is designed to make the results of Antarctic fieldwork available. The Antarctic Research Series encourages the collection of papers on specific geographic areas within Antarctica. In addition, many volumes focus on particular disciplines, including marine biology, oceanology, meteorology, upper atmosphere physics, terrestrial biology, geology, glaciology, human adaptability, engineering, and environmental protection.

Topical volumes in the series normally are devoted to papers in one or two disciplines. Multidisciplinary volumes, initiated in 1990 to enable more rapid publication, are open to papers from any discipline. The series can accommodate long manuscripts and utilize special formats, such as maps.

Priorities for publication are set by the Board of Associate Editors. Preference is given to research manuscripts from projects funded by U.S. agencies. Because the series serves to emphasize the U.S. Antarctic Research Program, it also performs a function similar to expedition reports of many other countries with national Antarctic research programs.

The standards of scientific excellence expected for the series are maintained by the review criteria established for the AGU publications program. Each paper is critically reviewed by two or more expert referees. A member of the Board of Associate Editors may serve as editor of a volume, or another person may be appointed. The Board works with the individual editors of each volume and with the AGU staff to assure that the objectives of the series are met, that the best possible papers are presented, and that publication is timely.

Proposals for volumes or papers offered should be sent to the Board of Associate Editors, Antarctic Research Series, at 2000 Florida Avenue, N.W., Washington, D.C. 20009. Publication of the series is partially supported by a grant from the National Science Foundation.

Board of Associate Editors
Antarctic Research Series

PREFACE

This volume provides examples of the application of state-of-the-art technology to fundamental problems in Antarctic meteorology and climatology. The technology, particularly as related to instrumentation and satellite communication, has been developed and applied in response to definite scientific needs. In its original conception the volume contents were limited to the U.S. Antarctic automatic weather station (AWS) program at the University of Wisconsin-Madison and to the results flowing from analysis of the collected data. The focus subsequently shifted to include a broader collection of papers on atmospherically related topics. Thus this volume, in addition to illustrating the importance and usefulness of Antarctic automatic weather station data, can also serve as an introduction to a number of basic issues in Antarctic meteorology and climatology.

Automatic weather stations transmit messages that are picked up by the ARGOS data collection system on board the NOAA series of polar-orbiting meteorological satellites. The ARGOS system receives 256-bit data words transmitted at 60- to 200-second intervals at a frequency of 401.650 MHz from fixed and mobile platforms and makes possible the collection and distribution of year-round data from remote areas such as Antarctica for a wide variety of applications. The installed U.S. AWS units cover a large geographic area, extending from near Halley Station, at 20°W, westward to Dome C (Dome Charlie) at 123°E. The AWS units are serviced only when transportation and personnel are available during the austral summer season, usually between November and February. Units that are operating properly are normally not serviced. One advantage of the ARGOS system is that data from each AWS can be accessed by a telephone call to a computer data base, and plans can be made for repair of nonreporting units well before the start of the Antarctic field season.

An annual data book consisting of 3-hour observations and the monthly and annual means is published for the AWS units funded by the U.S. Antarctic Program. The data book is distributed to more than 250 individuals and organizations, including members of the Antarctic Treaty. The purposes of this publication from the Department of Atmospheric and Oceanic Sciences at the University of Wisconsin-Madison are to meet the requirements of the Antarctic Treaty regarding the sharing of data and to provide a survey of the data so that others may decide what data they would like to have on electronic media for scientific purposes. The

paper by Stearns et al. provides an overview of the AWS data and data collection systems. These data are at times superior to those collected by manned stations, particularly for temperature and pressure. Wind measurements continue to be problematic, especially for those areas with extreme wind conditions.

Four papers deal with aspects of the Antarctic katabatic winds. The initial katabatic wind study was started in Adélie Coast in 1980 down the slope from Dome C to near Dumont d'Urville, and was the first installation of AWS units for a specific experiment. The units did not operate properly at first, and several years were required for an adequate number of data to be collected. The paper by Wendler et al. summarizes the results from this decade-long program, which combined AWS analyses, field programs, airborne campaigns, and numerical modeling. This is the most successful of the experiments based on AWS. The AWS results from another experiment being conducted at Terra Nova Bay are reported by Bromwich et al. The Terra Nova Bay katabatic wind study is the most complete for converging airflow into and down a glacier valley because the AWS units are located at the top and bottom of Reeves Glacier and beyond and because there is additional support from five AWS installed by Progetto Antartide of Italy in the vicinity of Priestley Glacier. Breckenridge et al. report on the meteorological conditions accompanying prominent thermal infrared signatures of katabatic winds on winter satellite imagery of the Ross Ice Shelf near Byrd Glacier. Carrasco and Bromwich present case studies of the mesoscale and synoptic conditions accompanying the propagation of such satellite-observed katabatic wind signatures from Marie Byrd Land across the almost flat Ross Ice Shelf.

Other studies based primarily on AWS data include the paper on the coreless winter in Adélie Coast by Wendler and Kodama. Stearns and Weidner use AWS observations to infer sensible and latent heat fluxes in Antarctica and conclude that sublimation plays a much more important role in the surface mass balance of Antarctica than was previously thought. McKay et al. use AWS data to probe the conditions that allow microbes in the sandstones of the McMurdo Dry Valleys to survive during the long, harsh winter and prosper during the short summer.

Climatic studies that draw mostly on other data sources are presented by Hogan et al. and Smith and Stearns. Hogan et al. integrate a wide variety of material

PREFACE

to infer a decadal-scale variation of the atmospheric aerosol concentration at South Pole Station. Smith and Stearns present the evolution of the Antarctic surface pressure and temperature fields across all minima in the Southern Oscillation Index between 1957 and 1984.

The AWS units provide support to many groups and people not represented by the papers in this volume. The AWS data are received in real time at McMurdo Station, Antarctica, and are used to support air operations. The data are entered into the Global Telecommunications Systems (GTS) by the Naval Oceanography Center, Monterey, California, for worldwide distribu-

tion and are used in the preparation of synoptic analyses by the Navy meteorological offices at McMurdo Station and Christchurch, New Zealand. Other organizations known to be using the AWS data in near real time through the GTS are the European Center for Medium-Range Weather Forecasts, the Australian Bureau of Meteorology, and the New Zealand Meteorological Service.

The U.S. AWS program is supported by NSF grant DPP-9015586 to Charles R. Stearns.

David H. Bromwich and Charles R. Stearns

MONTHLY MEAN CLIMATIC DATA FOR ANTARCTIC AUTOMATIC WEATHER STATIONS

CHARLES R. STEARNS, LINDA M. KELLER, GEORGE A. WEIDNER, AND MANUELA SIEVERS

Department of Atmospheric and Oceanic Sciences, University of Wisconsin, Madison, Wisconsin 53706

Automatic weather station (AWS) units were installed at remote locations in Antarctica to supplement the few research stations making meteorological observations. Most AWS units were positioned in data sparse regions in support of field experiments. Monthly means and extremes for air pressure, air temperature, wind speed, and wind direction for the AWS sites are available in tabular form. Since data collection in such a hostile environment is difficult, possible errors and/or problems are discussed. Some analysis of the longer-term climatic record is included for specific AWS sites representing different climatic regimes. The data will show that research stations located in protected areas along the coast of Antarctica do not represent the meteorology of the interior of Antarctica. Comparisons made between the automatic weather stations and research stations show that the automatic weather stations do as well as the research stations in measuring air pressure and air temperature.

1. INTRODUCTION

Antarctica is a continent with few meteorological observations in the interior. For 1984, most research stations are along the coast as shown in Figure 1. As of 1992, Siple (75°55'S, 83°55'W), Russkaya (74°42'S, 136°51'W), and Leningradskaja (69°30'S, 159°23'E) have ceased collecting meteorological data. The sector of the Earth from South Pole along 85°W longitude to 30°S latitude, then along 30°S latitude to 175°W longitude, then along 175°W longitude to the south pole is one sixteenth of the Earth's surface and is the largest meteorological void with only South Pole Station collecting meteorological data.

Starting in February 1980 with four automatic weather station (AWS) units and continuing to 1989, about 30 AWS units have been installed by the United States Antarctic Program (USAP). Figures 2, 3, and 4 depict the locations of past and present AWS sites. Table 1 gives the latitude, longitude, elevation, and period of operation for each AWS unit. Monthly means of air temperature, air pressure, wind speed, and resultant wind speed and direction are available for those units which provided more than 25% of the possible data at 3-hour intervals during each month. An example of the data set is presented in Table 2. Values with an asterisk beside them indicate less than 50% of the month had data reported. Included in the data set are monthly maxima and minima for air pressure and temperature and the maximum wind speed and direction. Annual mean values are included when data are available for 12 months of the year.

2. AUTOMATIC WEATHER STATION SYSTEM

The AWS unit contains a small computer that controls the operating cycle. The wind speed, wind direction, and air temperature sensors are mounted at the top of the 3-m tower. Some AWS units measure relative humidity at the tower top and the vertical air temperature difference from the tower top down 2.5 m. Air pressure is measured at the enclosure near the midpoint of the tower. The height of the sensors is nominal and will vary with the changing snow level. The computer transmits a 256-bit data word in 1 s at 401.650 MHz every 200 s and updates the data every 10 min. The actual times vary from one AWS unit to another so that the transmissions do not overlap between units. The data word contains the present values of the four measurements and the four previous values of each which are 10 min apart. Relative humidity and vertical air temperature difference have two past values at 20-min intervals. Battery voltage, cycle, and a check sum are included in the transmission.

2.1. Calibration

The external and internal temperature are calibrated for 0°C using a 1000-ohm, 0.05% tolerance resistor in place of the platinum resistance thermometers. Because the other resistances in the temperature circuit are known only to 1%, the temperature calibration will vary from unit to unit. A correction factor is computed and programmed into the read-only memories for each unit. After the correction factors have been programmed into the AWS, a calibration box with 0.1% resistors is used

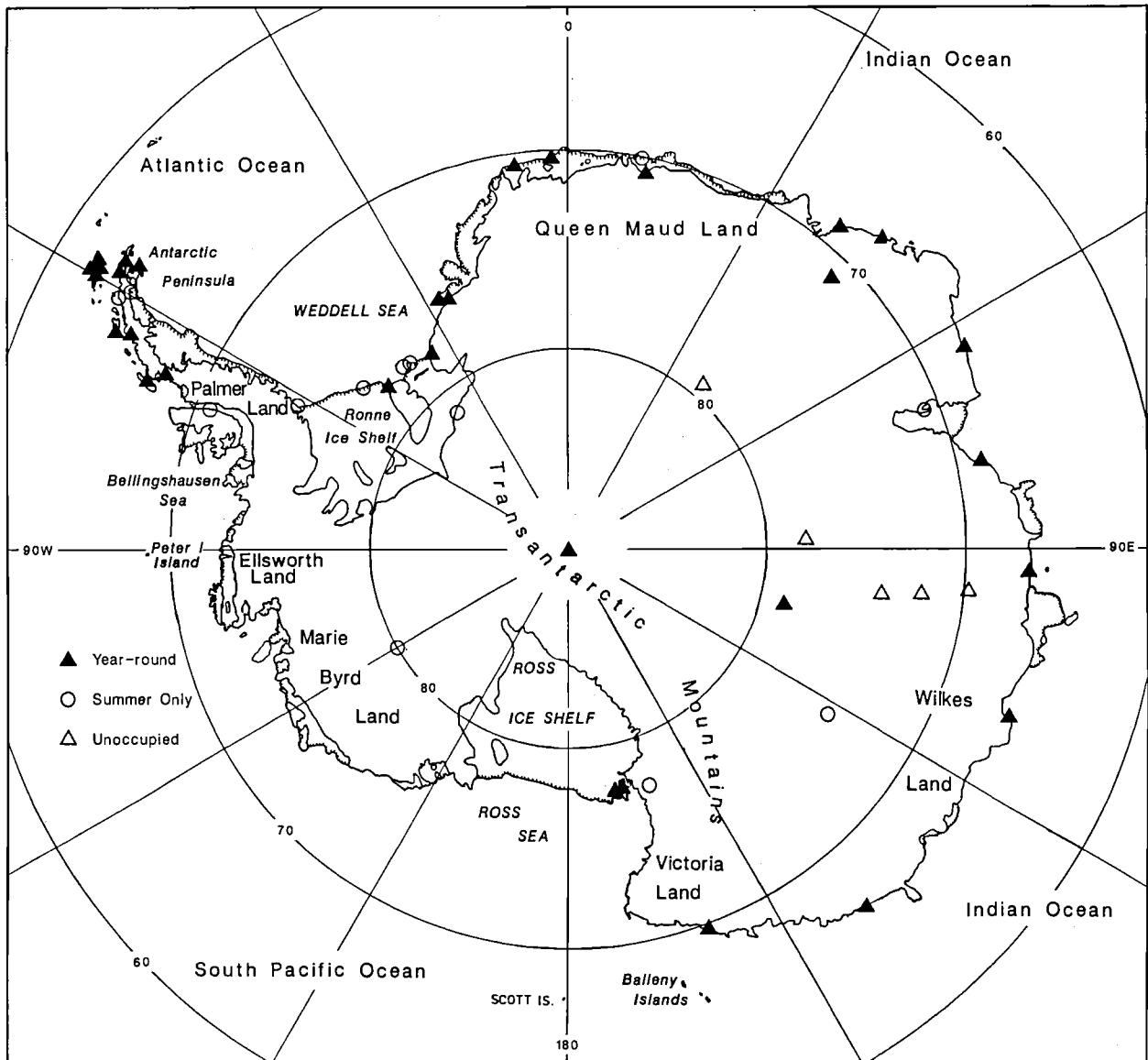


Fig. 1. Map of Antarctica showing the locations of research stations that made meteorological observations for 1984. Some stations may operate during the austral summer only on a regular basis, and others may operate intermittently during the summer.

in the field to check the resistance and thus the air temperature calibration of the AWS unit. The temperature resolution is 0.125°C .

The atmospheric pressure transducer is a Parascientific model 215 digiquartz pressure transducer. The transducer frequency changes from a nominal 40 kHz at zero mbar to about 36 kHz at 1000 mbar. The pressure resolution is about 0.05 mbar. Paulin aneroid barometers calibrated against a mercury barometer of 10-mm bore are used to check the pressure gauge calibration. Comparisons are made between AWS units, the aneroid barometer at McMurdo Station, and the mercury ba-

rometers at Scott Base, Antarctica. The calibrations should be within ± 0.2 mbar. The reference cell in the pressure transducer can outgas with time with a maximum observed 4-mbar shift to lower pressure for one pressure gauge after 5 years in the field. In 1987, Parascientific introduced a new model of the pressure gauge which has reduced the long-term drift by about an order of magnitude. Recalibration of each pressure transducer is desirable every 2–3 years.

The Belfort model 123 aerovane rotates a potentiometer wiper, and the fraction of full scale of the potentiometer is measured. The wind direction is checked by

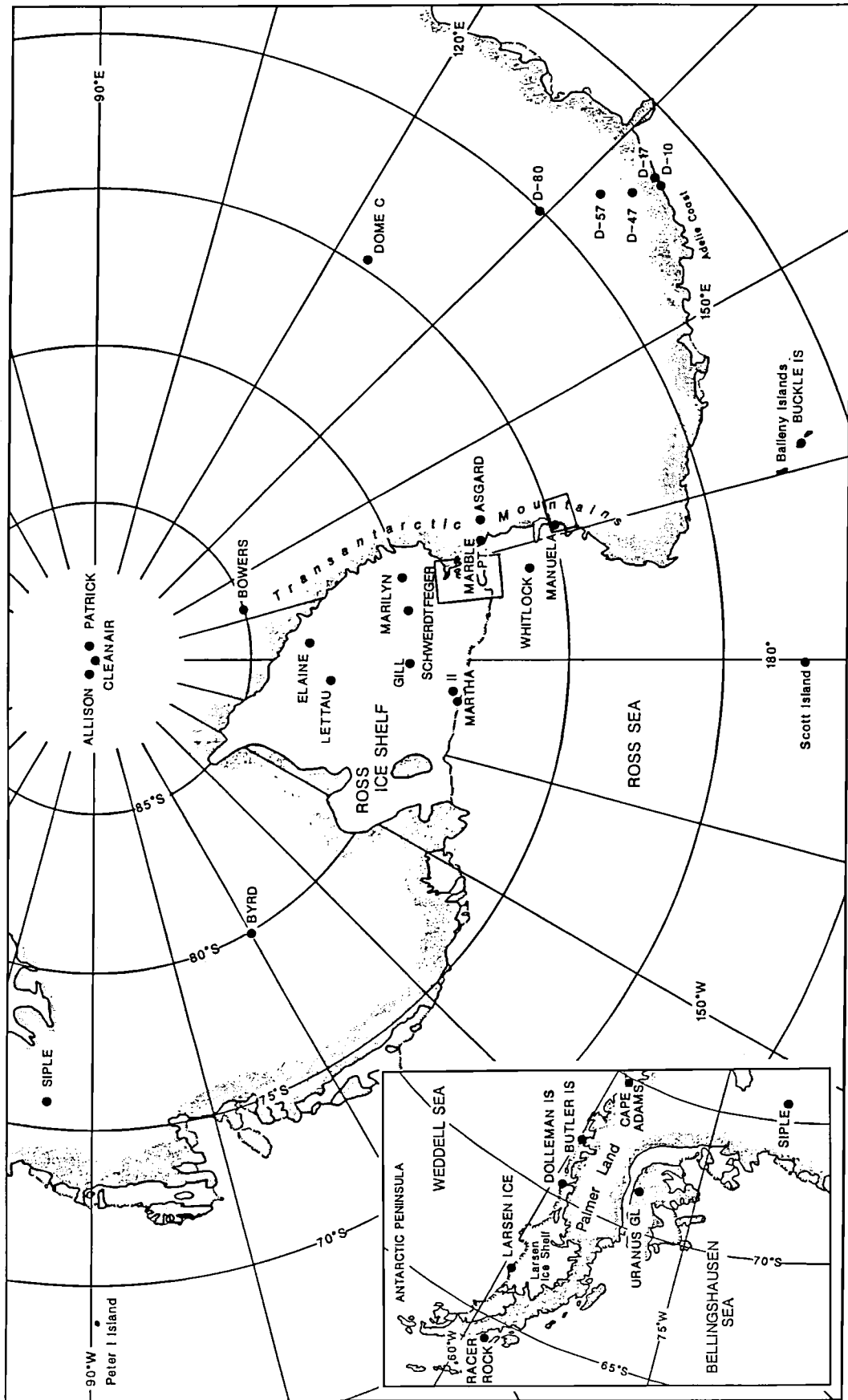


Fig. 2. Map of Antarctica showing the locations of widely spaced automatic weather station sites of the U.S. Antarctic Program installed from 1980 through 1989. Area in the box around Ross Island is shown in Figure 3. Area in the box around Manuela is shown in Figure 4.

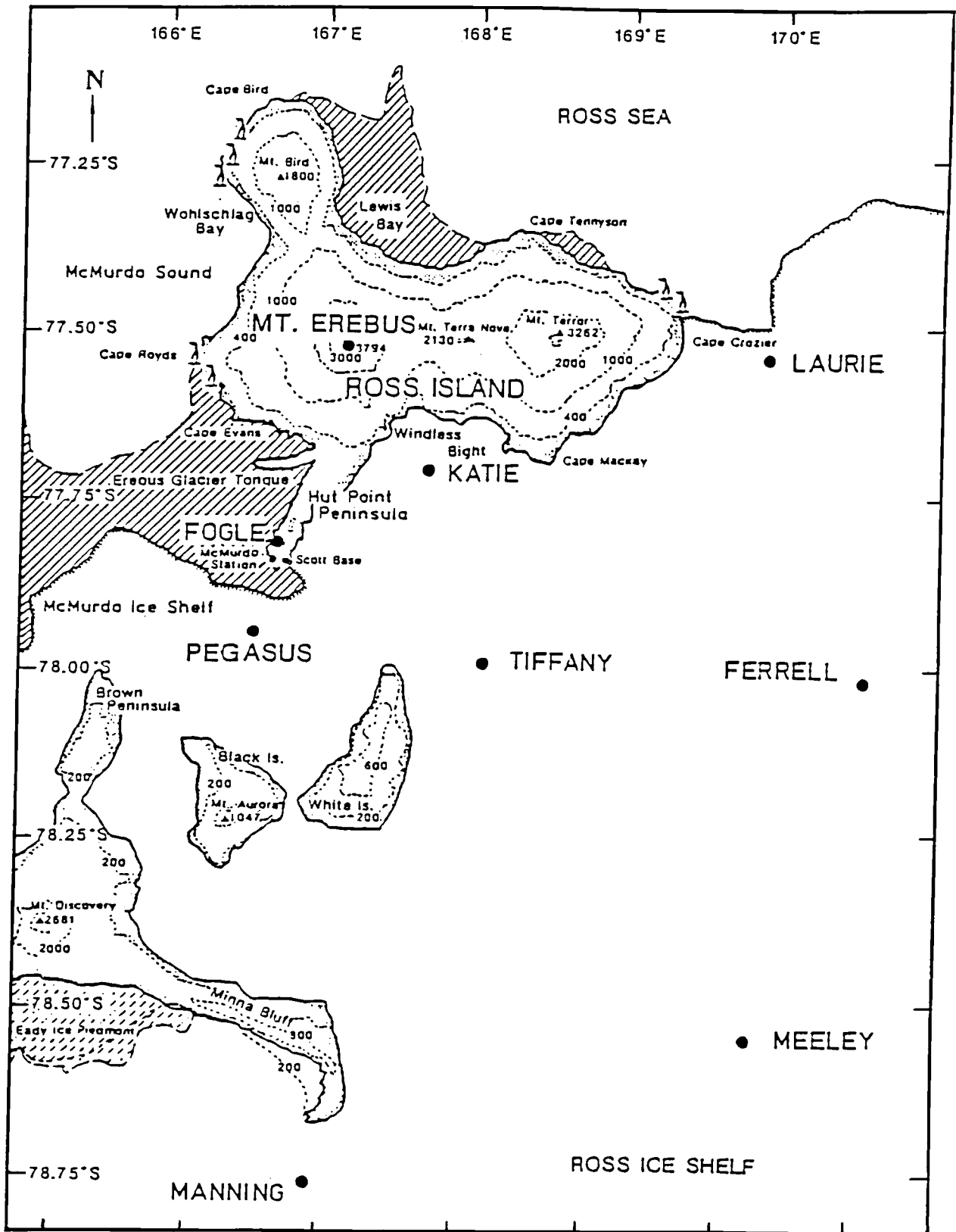


Fig. 3. Map of the vicinity of Ross Island, Antarctica, showing the locations of the automatic weather station units installed from 1980 through 1989.

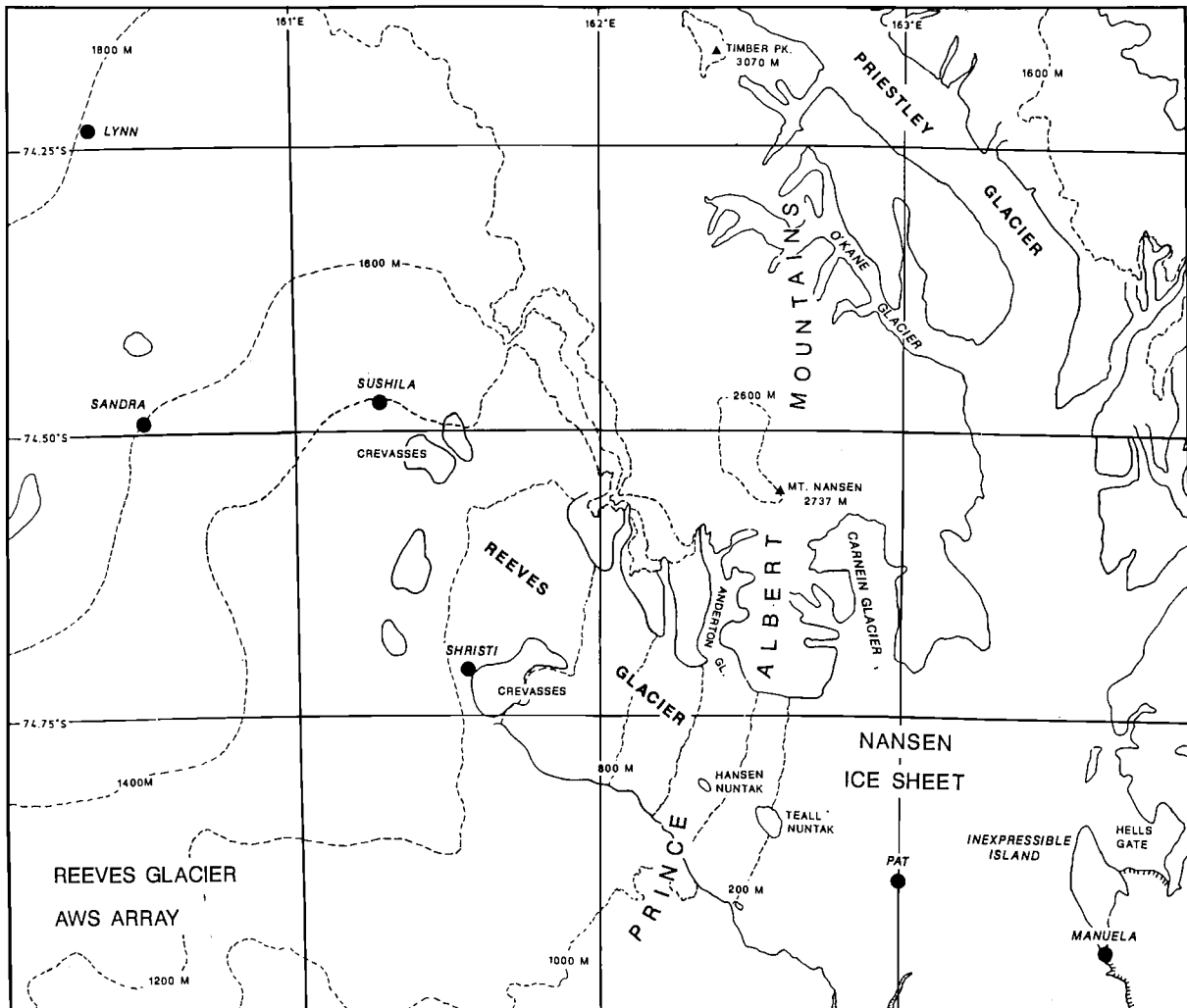


Fig. 4. Map of the vicinity of Reeves Glacier, Antarctica, showing the locations of the automatic weather station units installed from 1984 through 1989.

positioning the aerovane to the north, east, south, and west directions relative to the boom. North or zero on the potentiometer is toward the antenna on the boom and has a dead zone of less than 5° . In the field the boom is usually aligned along the north-south line as determined by the Sun's azimuth, location, and UT. In some cases the 180° or south end of the boom may point in a direction other than south. For example, at the Reeves Glacier array the south end of the boom is pointing upglacier, and a correction is added when the data are processed. At Byrd AWS site the dead zone of the potentiometer pointed north, and that was the most frequent wind direction. In January 1991 the boom was rotated 120° so that the potentiometer dead zone was at 240° .

Wind speed is determined from the aerovane tachom-

eter voltage output as 0.254 m s^{-1} per bit. The aerovane tachometer output is applied to a 1000-ohm resistor in series with a 71.5-ohm resistor. The input to the AWS unit is the voltage drop across the 71.5-ohm resistor. The maximum wind speed measurement is 64.8 m s^{-1} . The aerovane tachometer is spun at 1800 rpm to confirm that the output is $9.20 \pm 0.05 \text{ V dc}$ with a load of 1071.5 ohms resistance. The corresponding wind speed is 39.8 m s^{-1} .

The Vaisala HMP-31UT or HMP-35A humidity sensor output voltage varies linearly with relative humidity. The sensor is calibrated by placing it over saturated salt solutions with known relative humidities; sodium chloride (75%) and lithium chloride (12%) are used. In addition, an inert gas is forced past the sensor, giving a 0% relative humidity, and the sensor output can be

TABLE 1. AWS Locations From 1980 Through 1989

Site	Latitude, deg	Longitude, deg	Elevation, m	Date		Terrain
				Start	Stop*	
<i>Adélie Coast</i>						
D-10	66.70°S	139.80°E	240	Feb. 1980		snow
D-17	66.70°S	139.70°E	438	Jan. 1980	June 1980	snow
D-47	67.38°S	138.72°E	1560	Jan. 1983		snow
D-57	68.18°S	137.52°E	2105	Jan. 1981	Dec. 1988	snow
D-80	70.02°S	134.72°E	2500	Nov. 1984		snow
Dome C	74.50°S	123.00°E	3280	Feb. 1980		snow
<i>Summer Only Stations</i>						
Byrd Station	80.00°S	120.00°W	1530	Feb. 1980		snow
Siple Station	75.90°S	83.92°W	1054	Dec. 1987		snow
<i>Ross Island Region</i>						
Marble Point	77.43°S	163.75°E	120	Feb. 1980		rock
Manning	78.77°S	166.85°E	66	Dec. 1980	Jan. 1986	snow
Ferrell	78.02°S	170.80°E	45	Dec. 1980		snow
Asgard	77.60°S	160.10°E	1750	Feb. 1980	Dec. 1982	rock
Meeley	78.52°S	170.18°E	49	Dec. 1980	Jan. 1986	snow
Laurie	77.55°S	170.09°E	23	Dec. 1981	Jan. 1986	snow
Katie	77.70°S	167.70°E	40	Feb. 1983	Jan. 1986	snow
Fogle	77.82°S	166.75°E	202	Jan. 1984	Jan. 1985	rock
Tiffany	78.00°S	168.20°E	25	Jan. 1984	Jan. 1986	snow
Pegasus	77.97°S	166.49°E	10	Jan. 1989	Nov. 1989	hard ice
Mount Erebus	77.53°S	167.15°E	3700	Nov. 1989		rock
<i>Ocean Islands</i>						
Whitlock	76.24°S	168.70°E	275	Jan. 1982		rock
Buckle Island	66.87°S	163.24°E	520	Feb. 1987	Oct. 1988	snow
Scott Island	67.37°S	179.97°W	30	Dec. 1987		snow
<i>Ross Ice Shelf</i>						
Marilyn	79.98°S	165.03°E	75	Jan. 1984		snow
Schwerdtfeger	79.94°S	169.83°E	60	Jan. 1985		snow
Gill	80.00°S	179.00°W	55	Jan. 1985		snow
Bowers	85.20°S	163.40°E	2090	Jan. 1986	Jan. 1987	snow
Elaine	83.15°S	174.46°E	60	Jan. 1986	Jan. 1989	snow
Lettau	82.59°S	174.27°W	55	Jan. 1986		snow
Martha	78.31°S	172.50°W	42	Feb. 1984	May 1986	snow
Martha II	78.38°S	173.42°W	18	Feb. 1987		snow
<i>Reeves Glacier</i>						
Manuela	74.92°S	163.60°E	80	Feb. 1984		rock
Shristi	74.72°S	161.58°E	1200	Dec. 1987		snow
Sushila	74.41°S	161.28°E	1431	Jan. 1988		snow
Sandra	74.51°S	160.42°E	1525	Jan. 1988		snow
Lynn	74.23°S	160.29°E	1772	Jan. 1988		snow
Pat	74.90°S	163.10°E	30	Jan. 1989		hard ice
<i>Antarctic Peninsula</i>						
Larsen Ice Shelf	66.97°S	60.55°W	17	Oct. 1985		snow
Butler Island	72.20°S	60.34°W	91	March 1986		snow
Dolleman Island	70.58°S	60.92°W	396	Feb. 1986	June 1988	snow
Uranus Glacier	71.43°S	68.93°W	780	March 1986		snow
Cape Adams	75.01°S	62.53°W	25	Jan. 1989		snow
Racer Rock	64.16°S	61.54°W	17	Nov. 1989		rock
<i>South Pole Stations</i>						
Clean Air	90.00°S		2835	Jan. 1986		snow
Allison	89.88°S	60.00°W	2835	Jan. 1986	Jan. 1988	snow
Patrick	89.88°S	45.00°E	2835	Jan. 1986	Jan. 1988	snow

*If the site does not have a stop date, then the AWS unit is at the site in 1989.

zeroed. The gain setting is done directly using a saturated sodium chloride solution. The resolution of the humidity reading is about 1%, and the drift is 2–3% per year in the field. *Stearns and Weidner* [this volume] show the distribution of relative humidities with respect to air temperature for one AWS unit on the Ross Ice Shelf.

Two junction thermocouples are used to measure the air temperature difference between two levels on the tower. The output is about 78 μV for each degree difference between the junctions at 0°C, dropping to 60 μV at –80°C. The thermocouple output is amplified by a differential amplifier with a gain of about 425. Zero output is adjusted to 0.4 V, so that zero to 1 V corresponds to –6°C to +9°C temperature difference. The resolution is 0.05°C temperature difference. Calibrations of the individual systems are done by applying known voltages to the inputs of the amplifier.

2.2. Operation

The data are received by the SERVICE ARGOS data collection system (DCS) on board the polar-orbiting satellites of the National Oceanic and Atmospheric Administration (NOAA) series when the satellites are above the horizon at the AWS site. *Schwalb* [1978] describes the DCS for these satellites. In Antarctica the satellites are within view of the AWS units for 10–15 min for about 12 of the 14 orbits during a 24-hour period. Two satellites are usually in orbit, and the orbits are such that one satellite is usually in view every 50 min. Frequently, data are available every 10 min for a total of 144 data reports every 24 hours. The data are usually updated once during the satellite passage. The minimum number of 10-min values during 24 hours is about 100 and dependent on the phase of the orbits of the two satellites relative to each other. Some parts of Antarctica do not have as many satellite crossings as others. Data that are not received by the satellites occur in 50-min or longer gaps.

3. DATA COLLECTION SYSTEM

Magnetic tapes containing the AWS data are received at monthly intervals from SERVICE ARGOS and consist of all transmissions collected by the DCS on the satellites. The data tapes are processed by computer to eliminate duplicate transmissions, and a check sum is computed for comparison to the check sum transmitted in the data word. If the check sums are equal, then the data are accepted for conversion to meteorological units. The meteorological variables are checked to see if they are within the expected range for that particular site. The data are printed at this point and manually checked for errors.

3.1. Data Summaries

Data are selected at 3-hourly intervals to prepare a monthly summary for each AWS unit for survey purposes only. The summary includes the mean, maximum, and minimum values where appropriate, the resultant wind speed and direction, and frequency distributions of wind speed and direction. In order for the summary values to be calculated, more than 25% of the 3-hourly reports for the month must be present. Users should be aware that when the level of data present falls below 50%, the data can be clustered at the beginning or end of a month or spread throughout the month because of an AWS unit being removed, installed, or not performing properly (see the data problems section below for further description).

The monthly summaries that are printed do not have decimal values so that 1 month of data will fit on one page. Data prepared on magnetic media have one significant figure after the decimal point for air pressure, air temperature, and wind speed and, when measured, for relative humidity and the vertical air temperature difference if the bottom sensor is not buried in the snow. Data that were not received or that were not considered valid are indicated by a cross on the printed summaries and 444 in the data files.

The monthly summaries are distributed on paper or in data files on magnetic media (5 $\frac{1}{4}$ -inch or 3 $\frac{1}{2}$ -inch diskettes) to interested users. In addition, the monthly summaries along with other pertinent AWS unit information are published in an annual data book which is also available for distribution. The data books published for 1980–1989 are as follows: *Savage et al.* [1985a, b, c, d, e], *Sievers et al.* [1986, 1987, 1988], and *Keller et al.* [1989, 1990] and are supplied to most libraries containing material related to Antarctica. *Stearns* [1982, 1984, 1986, 1987, 1988, 1989], *Stearns and Savage* [1981], and *Stearns and Weidner* [1983, 1985] describe the activities during the austral summer in Antarctica. Similar material is available in the data books.

3.2. Data Problems

Missing or incorrect data can be the result of any number of events which occur while the AWS unit is unattended. Occasionally, the data are not collected by SERVICE ARGOS. The wind system (Bendix or Belfort aerovane) is the most vulnerable part of the AWS unit to adverse meteorological conditions. Extreme wind speeds, such as are found along the Adélie Coast, can literally tear the wind system apart. During the winter season, many of the AWS units show constant wind direction and zero wind speed. We have speculated that this is due to frost buildup on the aerovane coupling since the wind speed and direction begin to work again when the air temperatures rise, high wind speeds occur, and/or the Sun reappears. The aerovane may start operating when the wind speeds are higher

than $10\text{--}20\text{ m s}^{-1}$. Because this occurs at locations which have low air temperatures, there may be other explanations for this phenomenon.

The failure of other sensors on the tower is usually hardware related. Connections break because of corrosion, sensors drift over time, batteries run low, or any of the multitude of electronic parts in the AWS unit can fail. Complete AWS unit failure can result from any of the above problems. In addition, the transmitter frequency can drift beyond the range the satellite can receive, or the AWS unit can be buried in snow or even blown over. AWS units occasionally fail for no discernible reason; even after recovery and diagnostic testing in our laboratory, the failure can remain unexplained.

Subjective judgement is required to determine whether the data should be retained as valid or discarded. For example, during the summer an AWS unit may be in full Sun most of the day and also experience very light or calm winds. The air temperature may be questionably high. Periods of significant solar radiation can be detected by an increase in the battery voltage indicating that the batteries are being charged by the solar panel. When the air temperatures rise and fall over a large range in light winds, the air temperature at each time is compared to the internal AWS unit temperature at the air pressure gauge. If the internal temperature rises sharply at sunrise, then an attempt is made to determine when the air temperature is reflecting the true air temperature and when it is elevated a few degrees Celsius because of solar heating. Comparisons are made to nearby AWS sites, if possible. Occasional increases in wind speed and/or patchy cloudiness also give an indication of what the correct temperature might be. The decision to accept or reject the temperature data is then made. Since each set of AWS data is examined separately by at least two people, a consensus is reached on the validity of the questionable data. There should be a very good reason for removing data from the record. In spite of the efforts to eliminate erroneous data, some are surely missed. Users of the data are urged to keep this in mind when using the data. Be sure to check the wind speed when the air temperature is questionably high.

3.3. Data Tables

The AWS units have operated for up to 10 years in Antarctica. The data set contains monthly averages and extremes of the AWS data for those months when at least 25% of the possible 3-hourly observations were available. Table 2 presents an example of what is available in the full data set and how to obtain it. The order of the AWS units is the same as in Table 1. Table 1 also indicates (by the start and stop dates) the extent of the data for each station. Where no stop date is listed, data are available through December 1989. The header for the year that the AWS unit was installed contains the

site name, latitude, longitude, and elevation above sea level, followed by the year on the second line. The header for later years contains only the site name and the year. Occasionally, a site will have data missing for one or more years, and this will be noted after the header. The AWS data follow the header. If one month has less than 25% of the 3-hourly observations, then the month's name is listed without the data. The data are taken from the monthly summaries of the 3-hourly observations. The order of the data across Table 2 is as follows: short name of the month, mean air temperature, percent of missing data for the air temperature, maximum air temperature, minimum air temperature, mean wind speed, percent of missing data for wind speed and direction, resultant wind direction and speed, constancy of the wind determined as the ratio of the monthly mean vector wind speed to the scalar wind speed, direction and speed of the maximum wind speed, mean air pressure, percent of missing air pressure data, maximum air pressure, and minimum air pressure. The percent of missing data is based on the number of missing 3-hourly values divided by the number of possible values multiplied by 100%. The pressure data are the site or station pressure and are not corrected to sea level. The validity of the monthly data can be judged relative to the missing data. Information of this type is not usually available for mean values of meteorological data in Antarctica.

4. REGIONAL CLIMATES

The topography of the Antarctic continent is mainly responsible for the variety of regional climates that can be found. Several long-term AWS sites, chosen on the basis of height above sea level and/or location near specific geographical features, can be used to illustrate this variety. The names of the climate regimes based on elevation or location are merely descriptive of the area and should not be considered as definitive for each region.

Figure 5 illustrates the high plateau type of monthly mean air temperature climate based on site elevations greater than 2500 m. Dome Charlie (Dome C) is on one of the highest areas of the continent and illustrates the very light wind speeds and extremely cold temperatures which are associated with this climate regime. The elevation of Clean Air at the south pole is 445 m lower than the elevation of Dome C. Clean Air has slightly higher wind speeds, but the monthly mean air temperatures are remarkably similar to Dome C for most of the year. Both AWS sites illustrate the phenomenon known as the kernlose (coreless) winter defined by *Stearns and Wendler* [1988, p. 51] as "no systematic temperature changes taking place during the six winter months of April, May, June, July, August, and September." While the two sites agree very well, note that the records are not for the same times.

TABLE 2. Example of Monthly Mean Automatic Weather Station Data From 1980 to 1989

Mon	Mean % Of Air Month Temp Data °C Absent	Max Air Temp °C	Min Air Temp °C	Mean Wind Speed (m/s)	% Of Month Data Absent	Resultant Wind (dir vv)	Con	Max Wind Speed (dir vv)	Mean Air Press (mb)	% Of Month Data Absent	Max Air Press (mb)	Min Air Press (mb)			
<i>Marble Pt.</i>															
77.43°S				163.75°E				120 M							
1988															
Jan	-3.2	00	1.9	-8.4	2.8	00	124	0.7	.27	217	11	980.9	00	992.0	966.9
Feb	-10.0	07	-0.1	-19.0	4.0	07	170	3.2	.78	165	13	976.6	07	990.8	966.3
Mar	-18.3	01	-7.4	-29.4	4.3	01	178	3.6	.85	198	17	977.8	01	994.7	963.1
Apr	-19.1	06	-7.4	-29.6	4.1	06	201	2.7	.67	270	22	976.1	06	987.3	958.3
May	-20.5	00	-8.5	-31.8	4.1	00	189	3.0	.73	271	16	982.5	00	997.7	961.4
Jun	-20.7	06	-11.4	-32.0	5.2	06	181	4.3	.83	222	20	987.2	06	1002.3	967.3
Jul	-25.0	00	-10.8	-35.9	3.5	00	195	2.1	.58	129	22	969.2	00	985.2	944.5
Aug	-19.5	06	-4.1	-33.8	5.8	06	192	4.3	.75	137	28	968.5	06	997.5	942.9
Sep	-20.1	03	-7.1	-30.6	3.9	03	200	2.3	.59	127	20	976.3	03	1002.9	945.9
Oct	-12.9	01	-3.8	-30.0	4.2	01	182	2.7	.65	142	22	982.0	01	1002.4	952.8
Nov	-11.6	42	-2.4	-21.6	3.1	42	180	1.2	.38	163	11	972.4	42	992.6	961.8
Dec															
<i>Marble Pt.</i>															
1989															
Jan	-3.0	50*	1.8	-6.5	3.6	50*	133	2.8	.76	135	10	980.6	42	986.2	968.4
Feb	-9.2	00	-1.3	-15.3	5.8	00	147	5.5	.95	189	21	977.7	00	993.8	961.8
Mar	-14.6	00	-6.1	-22.8	3.7	00	160	3.2	.86	146	12	977.3	00	998.5	961.8
Apr	-18.1	04	-2.3	-37.4	4.0	04	161	3.1	.78	151	23	980.9	04	1001.5	944.9
May	-23.4	02	-9.5	-34.8	2.5	02	175	1.8	.71	163	11	965.3	02	981.5	949.3
Jun	-28.4	00	-17.3	-37.3	2.7	00	163	1.9	.72	147	17	974.1	00	993.3	957.4
Jul	-23.9	03	-13.4	-37.0	3.4	03	167	2.5	.74	232	14	972.9	03	992.3	953.2
Aug	-26.4	01	-0.8	-38.8	3.0	01	169	2.1	.71	189	19	977.6	01	1003.5	958.8
Sep	-22.7	00	-4.0	-37.5	3.4	00	174	2.4	.70	154	17	976.9	00	999.6	951.2
Oct	-16.1	03	-7.8	-27.5	3.2	03	182	1.7	.54	151	15	968.3	03	987.2	943.0
Nov	-8.3	01	1.0	-17.0	3.6	01	149	2.2	.62	129	17	969.2	01	983.0	947.4
Dec	-1.9	01	4.8	-8.4	3.0	01	095	0.8	.26	337	11	981.7	01	995.3	961.7
MEAN	-16.3				3.5		158	2.4	.70			975.2			

The column header at the top of each page contains Mon for month, mean air temperature, percent of missing data for the air temperature, maximum air temperature, minimum air temperature, mean wind speed, percent of missing data for wind speed and direction, resultant wind direction and speed, constancy of the wind determined as the ratio of the monthly mean vector wind speed to the scalar wind speed, direction and speed of the maximum wind speed, site mean air pressure, percent of missing pressure data, maximum air pressure, and minimum air pressure. The header for the first year that the AWS unit delivered data contains the site name, latitude, longitude, and elevation above sea level, followed by the year on the second line. The header for later years contains only the site name and the year. Occasionally a site will have data missing for one or more years and this will be noted after the header. The AWS data for the year follows the header. Table 2 is available in its entirety on the disk (in ASCII format) enclosed inside the back cover of this book or as paper copy from C. R. Stearns, 1225 West Dayton Street, Madison, Wisconsin 53706 (telephone 608-262-0780; email chucks@ssec.wisc.edu).

Figure 6 shows AWS sites at an intermediate elevation (1000–1500 m) in West Antarctica. Byrd AWS site is 490 m higher than Siple AWS site and has slightly colder temperatures. The largest difference occurs in July, August, and September when Byrd’s air temperature continues to drop while Siple warms slightly. This may be due to the inland location of Byrd versus the location of Siple, which is closer to the coast. On the basis of the map of the streamlines of katabatic winds

from *Parish and Bromwich* [1987], Siple lies in an area much like Dome C, which is reflected in the nearly constant low wind speeds throughout the year. Byrd is positioned in a more diffluent region with somewhat higher winds speeds, except in the summer months.

The coastal climate (Figure 7) can be the most varied depending on the slope of the terrain. For example, D-10 is on a steeply sloped area of the coast and experiences strong downslope winds while Marble Point

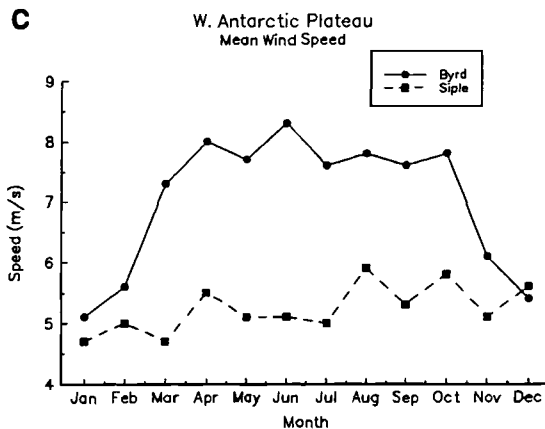
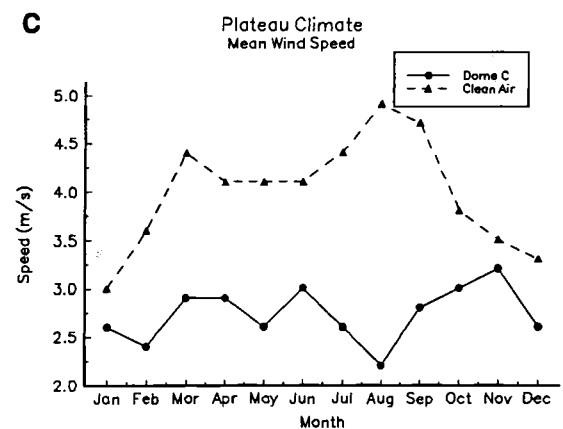
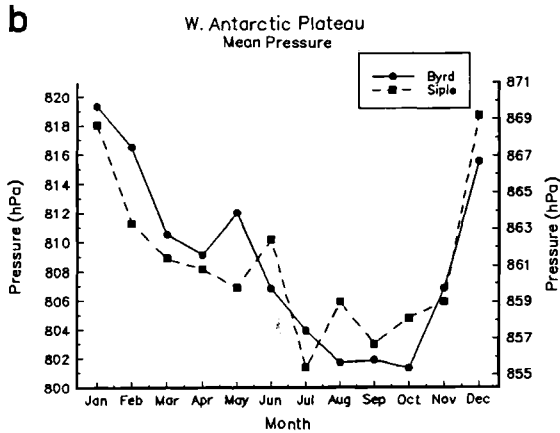
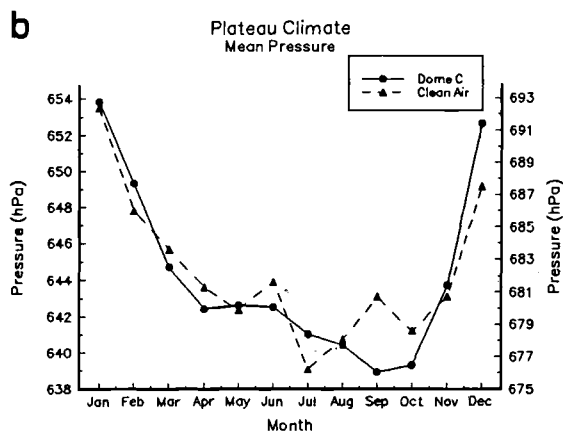
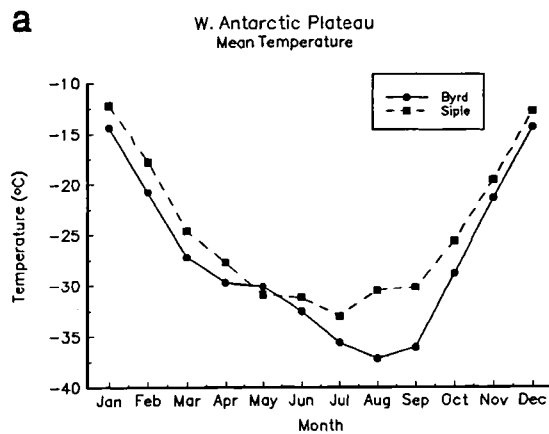
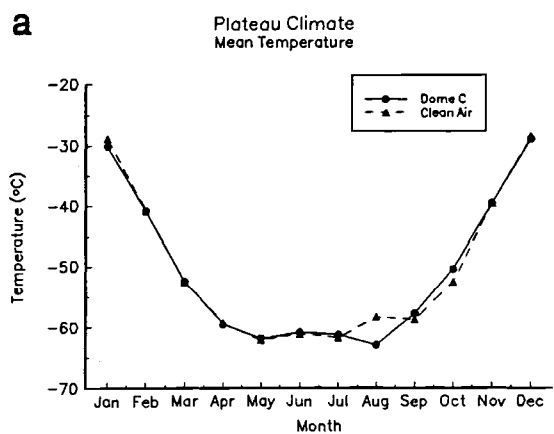


Fig. 5. Annual graph of the monthly mean (a) air temperature, (b) air pressure, and (c) wind speed for high-elevation AWS sites Dome C (1980–1989) and Clean Air (1986–1989). In Figure 5b the air pressure axis for Dome C is on the left; the air pressure axis for Clean Air is on the right.

Fig. 6. Annual graph of the monthly mean (a) air temperature, (b) air pressure, and (c) wind speed for intermediate-elevation AWS sites Byrd (1980–1988) and Siple (1982–1989). In Figure 6b the air pressure axis for Byrd is on the left; the air pressure axis for Siple is on the right.

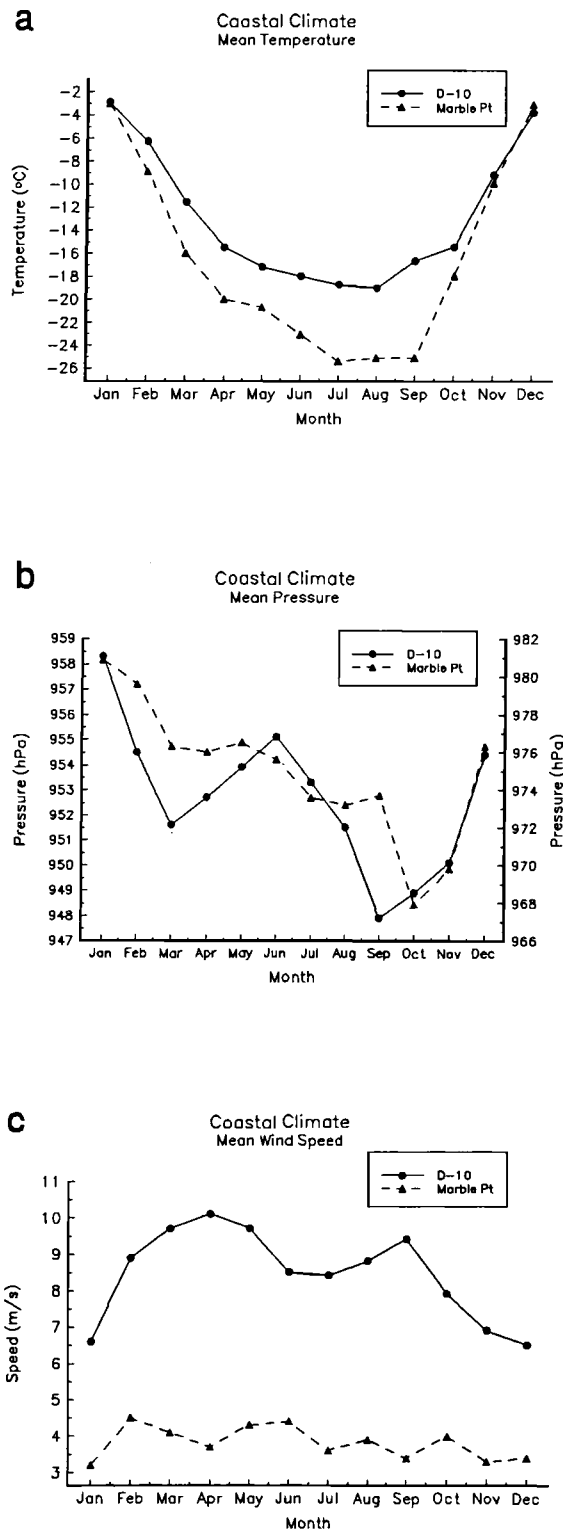


Fig. 7. Annual graph of the monthly mean (a) air temperature, (b) air pressure, and (c) wind speed for coastal AWS sites D-10 (1980–1989) and Marble Point (1980–1989). In Figure 7b the air pressure axis for D-10 is on the left; the air pressure axis for Marble Point is on the right.

is in a relatively flat region on the coast of McMurdo Sound near the Transantarctic Mountains, and the monthly resultant wind direction is parallel to the mountains. This difference is most apparent in the wind speeds. Marble Point has light mean wind speeds throughout the year while D-10 experiences fairly strong winds except in the summer. D-10 is also in a confluent region for katabatic wind flow as shown by *Parish and Bromwich* [1987]. Even though Marble Point is 120 m lower in elevation than D-10, their summer air temperatures are very similar. D-10 is much warmer in the winter, which is a reflection of the adiabatic warming associated with the katabatic flow. Note that the air pressure patterns (D-10 axis on the left, Marble Point on the right) are similar although Marble Point does not show as great a variability between months as D-10. In addition, Marble Point lags D-10 by a month in the major reversals of monthly mean air pressure.

Some of the best examples of katabatic flow are found in the glacial regions of the Transantarctic Mountains. The region around Terra Nova Bay, at the base of the Reeves Glacier, has been extensively studied [see *Bromwich, 1989a, b; Parish, 1992*]. One of the AWS units is located on Inexpressible Island (Manuela), which is at the base of this glacier. Figure 4 shows the AWS sites down the Reeves Glacier from Lynn site at 1772 m to Pat site at 30 m. Figure 8 shows the monthly mean air temperature, air pressure, and wind speed for Manuela site on Inexpressible Island. The temperature illustrates the coreless winter found at several of the AWS sites. The most interesting feature of Manuela site is the high mean wind speeds found in all except the summer months. This illustrates the intensity and constancy of the katabatic flow during the colder seasons. During the months of February through October the constancy of the wind is greater than 0.90.

The only long-term island AWS site (Whitlock, Figure 2) is on Franklin Island in the Ross Sea (Figure 9). This AWS site shows the highest wind speeds in February and March, tapering to slightly lower levels for April through November, and falling to minimum levels during December and January. The pressure pattern indicates the highest monthly mean air pressures in January and the lowest in October. While the month of the lowest monthly mean air pressure may vary from September to November, most AWS sites follow this same pattern of pressure. The monthly mean air temperature at Whitlock site shows a slightly different pattern from the coreless winter. The monthly mean air temperature for May is only slightly colder than that for April. This AWS site is not the only one to exhibit this temperature pattern, and so the concept of all of Antarctica's having coreless winters must be amended.

The last region to be examined is the Ross Ice Shelf (Figure 2). The array of AWS sites on the Ross Ice Shelf allows both latitudinal and longitudinal cross sections of the region to depict variations in both east-west and

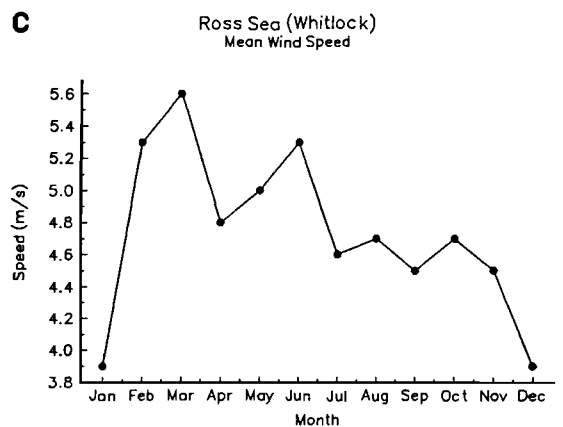
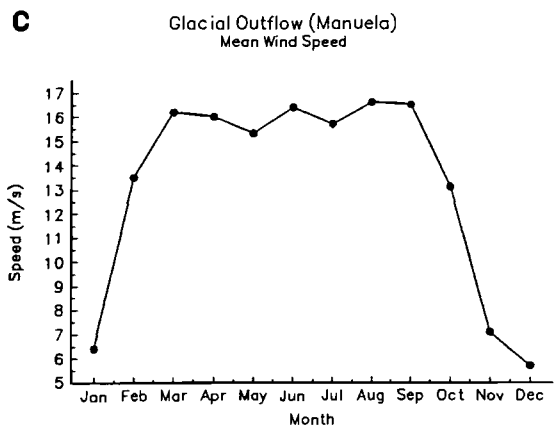
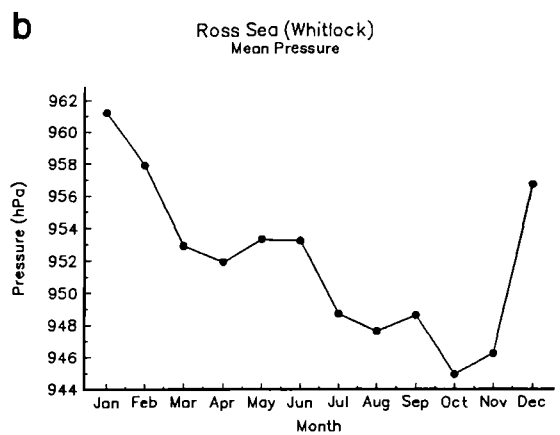
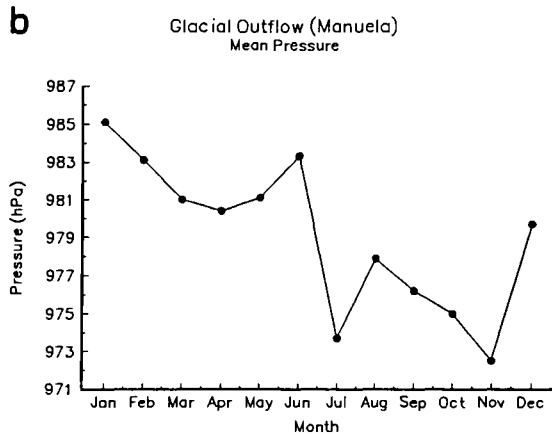
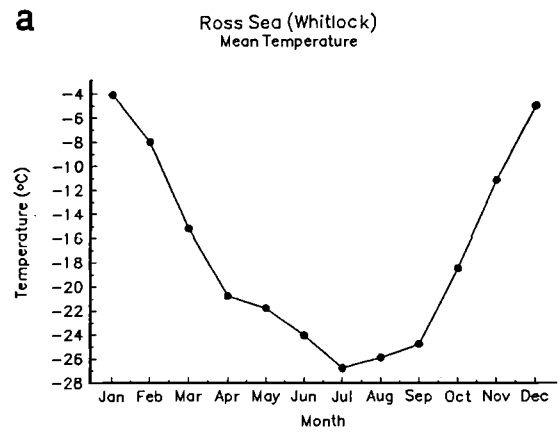
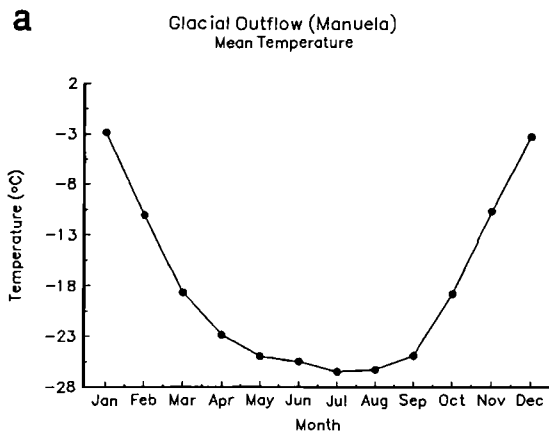


Fig. 8. Annual graph of the monthly mean (a) air temperature, (b) air pressure, and (c) wind speed for Manuela site (1984–1989).

Fig. 9. Annual graph of the monthly mean (a) air temperature, (b) air pressure, and (c) wind speed for Whitlock site (1982–1989).

north-south directions. The latitudinal cross section is along approximately 80°S (Figure 10). The monthly mean air temperatures are quite similar in the summer but diverge as the colder seasons progress. Marilyn, which is closest to the Transantarctic Mountains, has the warmest air temperatures from March through September, most probably because of the warming due to the katabatic flow down the glaciers onto the Ross Ice Shelf [see *Bromwich, 1989b*]. This AWS site also has the highest monthly mean wind speeds from March through October. Schwerdtfeger is to the east of Marilyn and shows slightly colder monthly mean air temperatures and lower monthly mean wind speeds. Gill is the farthest east of the three AWS sites and has the coldest monthly mean air temperatures, lowest monthly mean wind speeds, and generally lowest site monthly mean air pressures of the three AWS units. In summary, as the eastward distance from the Transantarctic Mountains increases, the air temperatures become colder and the wind speeds lighter.

In the longitudinal direction, along approximately 180°, a slightly different pattern emerges (Figure 11). The monthly mean air temperatures for Gill, Lettau, and Martha II are very similar, except for July, August, and September when Gill is colder. This shows an interesting phenomenon, because Gill is the middle AWS site in this cross section. Lettau is farther south into the interior of the Ross Ice Shelf, and Martha II is farther north at the edge of the Ross Ice Shelf. The monthly mean air pressures show that Lettau has the highest site air pressures while Martha II generally has the lowest and Gill is in between. However, Gill usually has the lowest monthly mean wind speeds while Martha II has the highest monthly mean wind speeds except in January and September through November. This indicates that the coldest spot on the Ross Ice Shelf is not deep in the interior, but in the middle of the shelf nearer to the Ross Sea. It may well be that this particular location is far enough inland that it is not influenced by synoptic activity along the coast and far enough away from the confluence zones on the east and west sides of the Ross Ice Shelf so that the influence of the higher wind speeds and adiabatically warmed air due to katabatic flow down the surrounding slopes is diminished or deflected before reaching this area.

5. COMPARISON OF AWS SITES AND RESEARCH STATION OBSERVATIONS

A comparison between research station data where the observations are collected and processed by the station personnel and the AWS sites for monthly mean values of air temperature and air pressure can be made using the Byrd, Scott Base, Amundsen-Scott (South Pole) and Dumont d'Urville research stations. The air temperature and pressure record for the stations of Byrd, South Pole, Dumont d'Urville, McMurdo, and

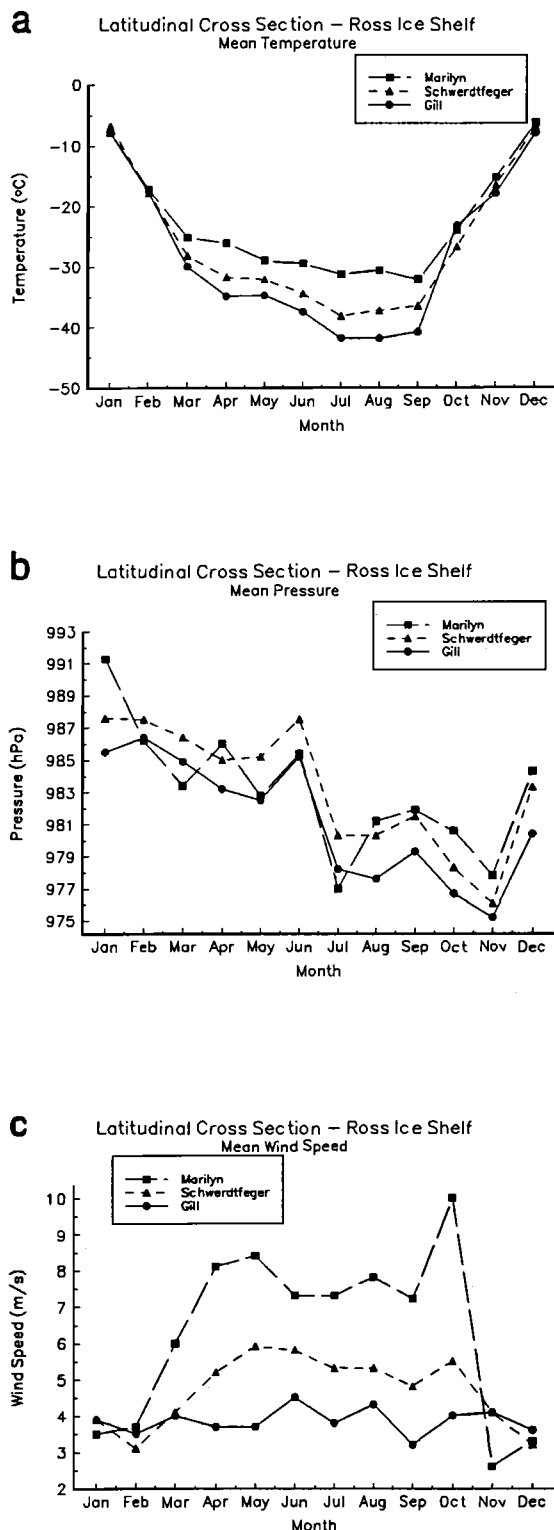


Fig. 10. Annual graph of the monthly mean (a) air temperature, (b) air pressure, and (c) wind speed for a latitudinal cross section along approximately 80°S. The AWS sites in this cross section are Marilyn (1984–1989), Schwerdtfeger (1985–1989), and Gill (1985–1989).

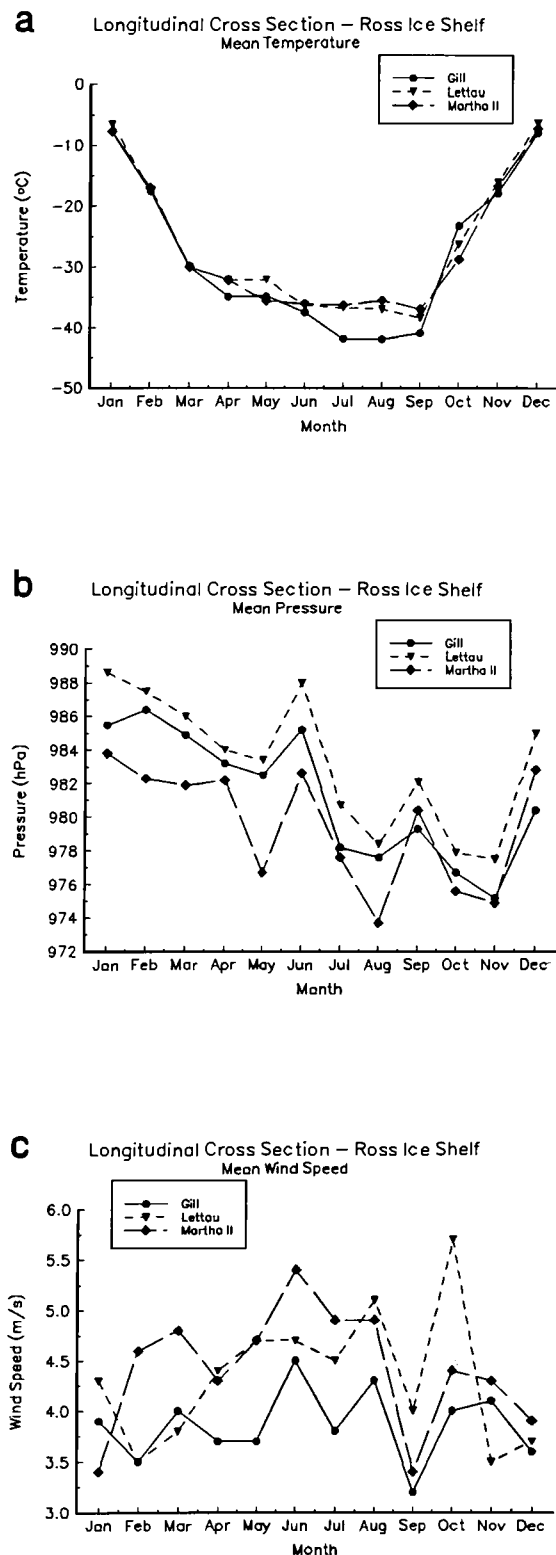


Fig. 11. Annual graph of the monthly mean (a) air temperature, (b) air pressure, and (c) wind speed for AWS sites Lettau, Gill, and Martha II, which are at approximately the same longitude of 180° on the Ross Ice Shelf.

Scott Base are from *Smith [1991]* and *Jones and Limbert [1987]*. This comparison will provide a test of both methods of making meteorological observations.

Figure 12 shows graphs of the annual cycle of the monthly mean air temperature for Byrd station and Byrd AWS site, for South Pole station and Clean Air AWS site, for Dumont d'Urville station and D-10 AWS site, and for McMurdo station, Scott Base, and Marble Point AWS site. Figure 12a is for the Byrd AWS site and the Byrd station record. The Byrd AWS site is about 2 km from Byrd station, and the period of record does not overlap. The monthly mean air temperature record for Byrd station could be continued using the AWS data. Clean Air AWS site is about 400 m from the South Pole meteorology office. South Pole (Amundsen-Scott station) and Clean Air AWS in Figure 12b show good agreement during the months of September through March despite the small overlap between the two records. The monthly mean air temperature record at South Pole station could be checked against the AWS data in the future. Figure 12c shows the annual cycle of the monthly mean air temperature for D-10 and Dumont d'Urville. Dumont d'Urville is a rocky island a few kilometers off the Adélie Coast of Antarctica. D-10 is on snow, 193 m higher in elevation, and 10.3 km from Dumont d'Urville. Figure 12d shows the annual cycle of the monthly record for McMurdo, Scott Base, and Marble Point AWS. The Marble Point AWS site is 93.5 km from McMurdo and 95.7 km from Scott Base. The elevation of the Marble Point AWS site is 96 m above McMurdo and 104 m above Scott Base. The Marble Point AWS site is rocky and is not snow covered during the summer. The agreement with McMurdo station is good during the period November through February even though the overlap of the records is small. Scott Base is on the south end of Ross Island on a point of land facing the Ross Ice Shelf to the south and, as expected, the air temperature climate is colder than the other two sites. The Marble Point site monthly mean air temperature data could be used as a surrogate for McMurdo.

A similar set of four graphs in Figure 13 compare the annual cycles of the monthly mean air pressure records for the same locations as in Figure 12. Compared to air temperature, the air pressure records are much more variable but generally have the same shape during the year. The Byrd AWS site is approximately 2 km from the station, and the AWS site elevation relative to the elevation of the Byrd station barometer is not known. Figure 13a shows the annual cycle of the monthly mean air pressure for Byrd station and Byrd AWS site. Although the two records do not overlap, the agreement between the monthly mean pressures is very good. The shape of the monthly mean pressure during the year is similar except for the months of May and September. In Figure 13b, Clean Air AWS site and South Pole monthly mean air pressure records overlap for 4 years,

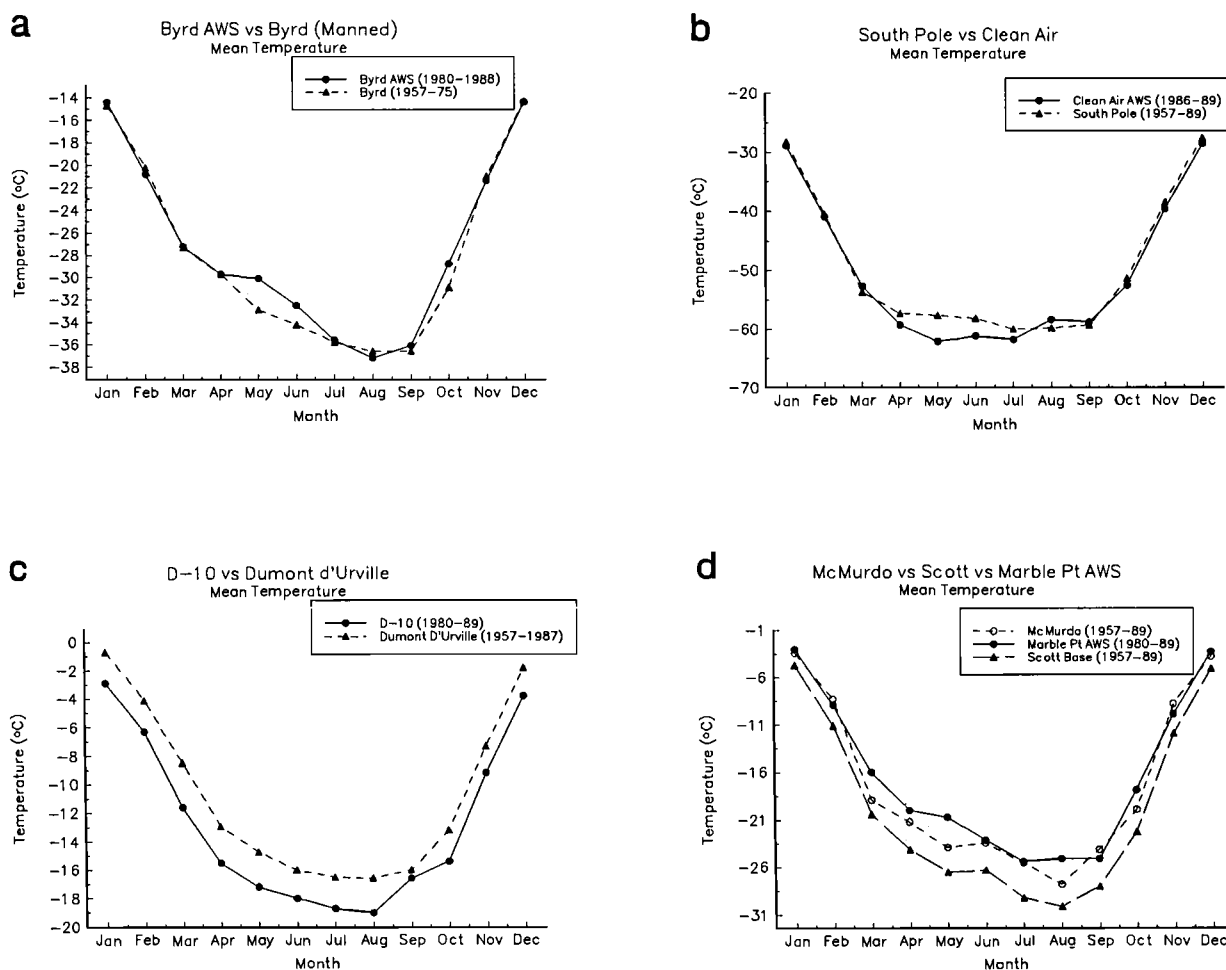


Fig. 12. Annual graph of the monthly mean air temperature from a nearby AWS site and a research station for (a) Byrd, (b) South Pole (Amundsen-Scott), (c) Dumont d'Urville, and (d) McMurdo and Scott Base. The data periods are not the same, and the sites may not be collocated.

and again there is a significant air pressure difference between the two records for the month of September. Figure 13c shows the monthly mean pressures for D-10 AWS site and Dumont d'Urville station. The pressure at Dumont d'Urville is between 20 and 25 mbar higher than the pressure at D-10 site. The difference in height between the two locations is 193 m. The pressure difference is larger in the cold months than in the warm months as is expected since the air temperature is lower. Figure 13d shows the annual cycle of the monthly mean air pressures for McMurdo, Scott Base, and Marble Point AWS site. The elevations above sea level are as follows: McMurdo, 24 m; Scott Base, 16 m; and Marble Point AWS, 120 m. The 10-year record from the Marble Point AWS site does not differ significantly from the Scott Base and McMurdo record, although the Marble Point AWS site is about 95 km from the comparison sites. Scott Base monthly mean pressure data are missing from the records of Smith [1991] for January

1985 through 1986. The comparison between McMurdo and Scott Base is poor considering that the locations are only 2.2 km apart.

Monthly mean air temperatures and pressures for McMurdo and the AWS sites of Marble Point, Ferrell, and Katie can be compared to the monthly mean data for Scott Base. The data for Scott Base and McMurdo were published by Jones and Limbert [1987] with some corrections and additions to the Jones and Limbert data made by Smith [1991]. The distance between Scott Base and the other sites is as follows: McMurdo, 2.2 km; Marble Point, 95.7 km; Ferrell, 85.9 km; and Katie, 28.6 km. Ferrell AWS site is on the Ross Ice Shelf south of Cape Crozier, and Katie AWS site is in Windless Bight on the Ross Ice Shelf (Figure 3). The surface at Ferrell and Katie sites is snow throughout the year, while at Marble Point and McMurdo the surface is usually bare ground during the austral summer.

Figure 14 is a point by point monthly mean air

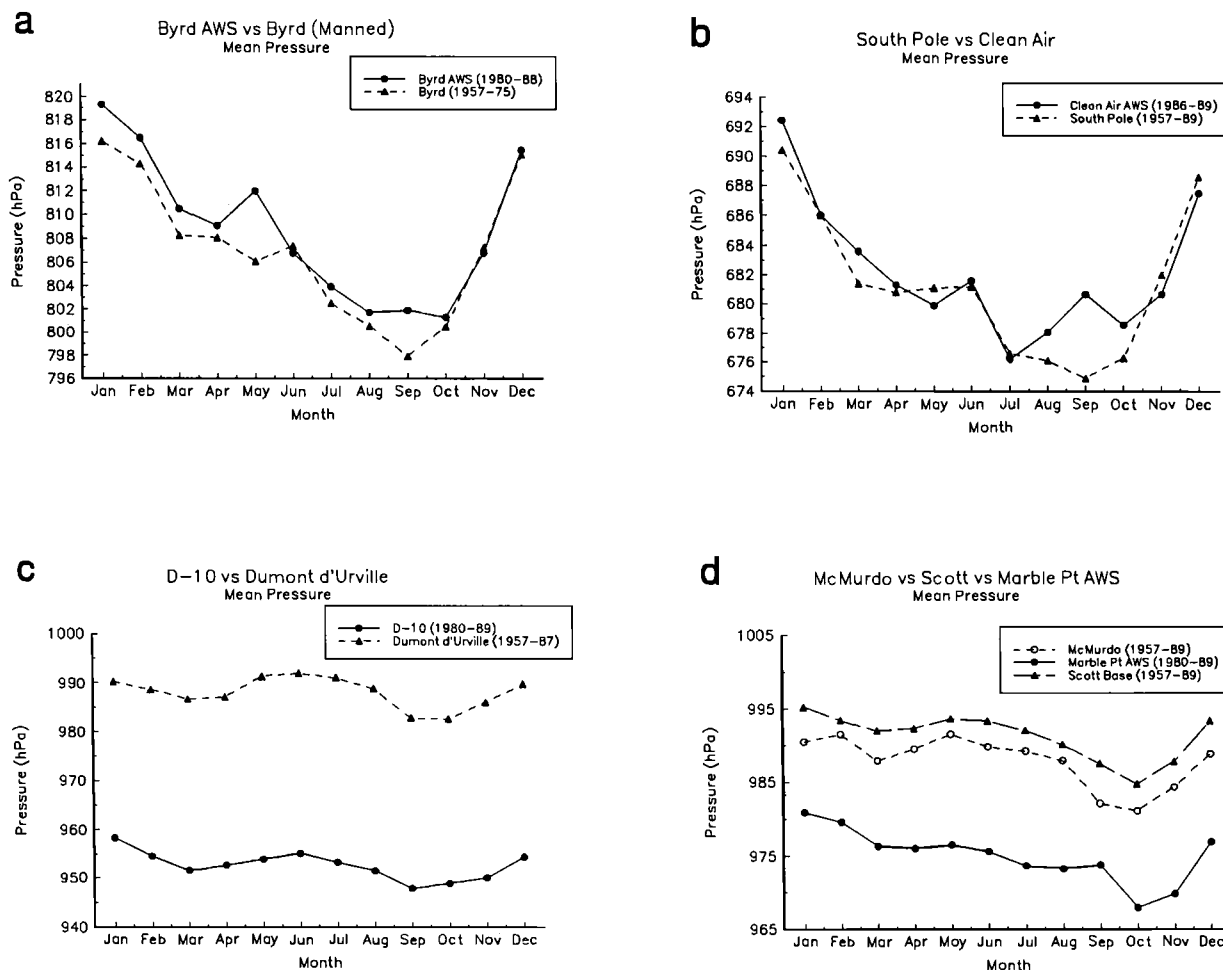


Fig. 13. Annual graph of the monthly mean site air pressure from a nearby AWS site and a research station for (a) Byrd, (b) South Pole (Amundsen-Scott), (c) Dumont d'Urville, and (d) McMurdo and Scott Base. The data periods are not the same, and the sites may not be collocated.

temperature comparison between Scott Base as the horizontal axis and each of the other four sites of McMurdo, Marble Point AWS, Ferrell AWS, and Katie AWS on the vertical axis. Table 3 gives the results of a linear least squares fit between Scott Base and each of the other four sites. McMurdo has the lowest correlation coefficient with Scott Base and the longest record. Scott Base is on the edge of the Ross Ice Shelf, and McMurdo is screened from the Ross Ice Shelf by Hut Point Peninsula. The most noticeable difference in Figure 14a is that McMurdo does not have the low monthly mean air temperature experienced by Scott Base and the scatter of the points is large. The maximum monthly mean air temperatures are about the same. Figure 14b shows the monthly mean air temperature for Marble Point AWS site versus Scott Base. The maximum monthly mean air temperatures are about the same while the minimum monthly mean air temperatures are higher for Marble Point. In Table 3 the correlation

coefficient between Marble Point site and Scott Base is higher than the correlation coefficient between McMurdo and Scott Base. Figure 14c is the comparison between the monthly mean air temperatures for Ferrell AWS site and Scott Base. The two points in Figure 14c that look out of place represent two months for Ferrell site with about 50% of the possible data. Katie site (Figure 14d) has the highest correlation coefficient with Scott Base although the number of data points is the smallest of the four locations in Figure 14. The agreement between the two locations is very good and should be expected. Ferrell and Katie sites are colder than Scott Base.

Figure 15 is a comparison of the monthly mean air pressure between Scott Base on the horizontal axis and McMurdo Station, Marble Point, Ferrell, and Katie. Table 3 gives the results of the linear least squares fit between Scott Base and the four other sites. The correlation coefficient between McMurdo and Scott

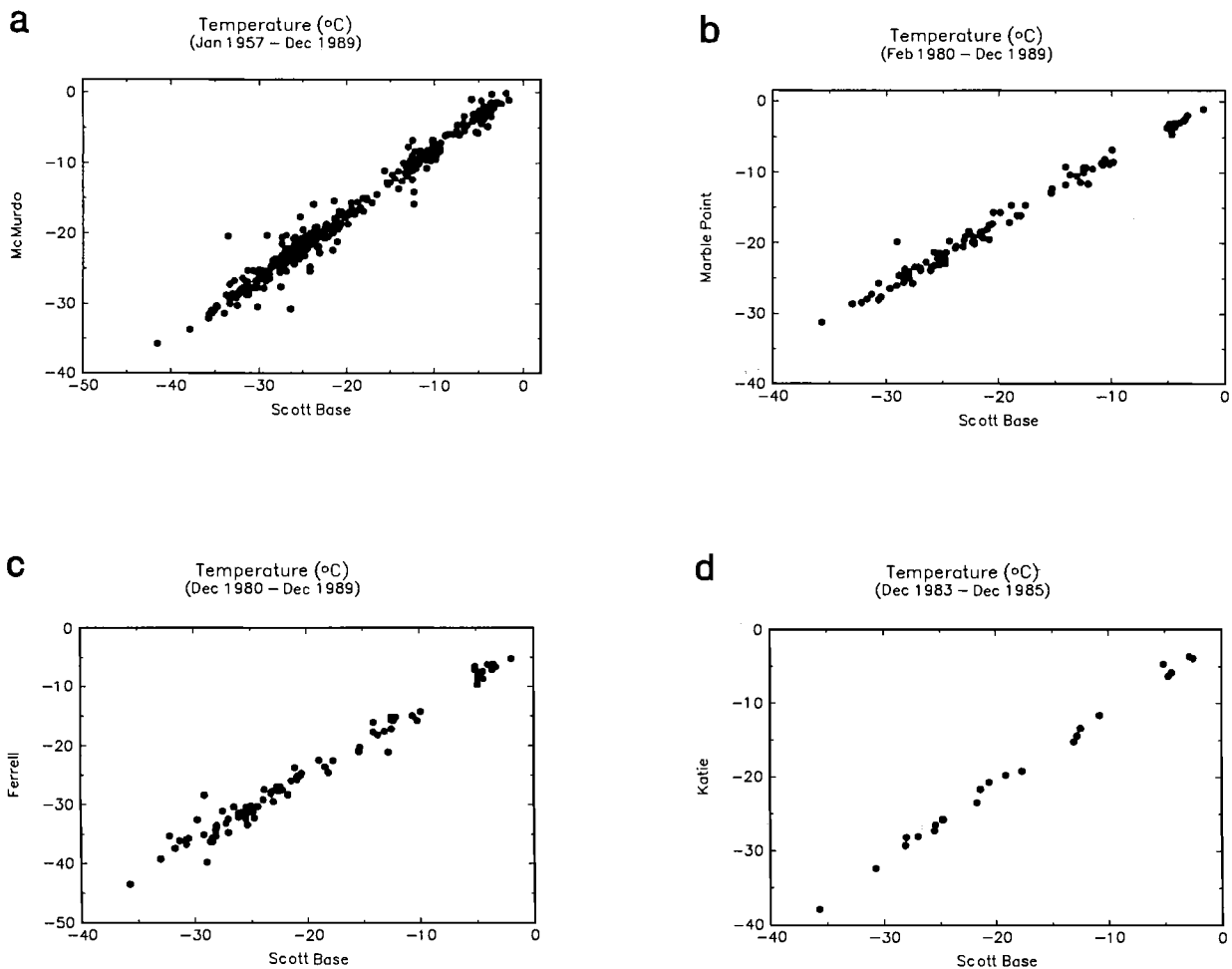


Fig. 14. Graph of the monthly mean air temperature for Scott Base versus (a) McMurdo, (b) Marble Point, (c) Ferrell, and (d) Katie.

Base is the lowest of the four sites, and the graph in Figure 15a between the monthly mean air pressures for Scott Base and McMurdo shows two possible trend lines and considerable spread in the data points. The locations are only 2.2 km apart. The question that arises is which air pressure data are the most nearly correct? Figure 15b is the comparison between Scott Base and Marble Point AWS site. The scatter of the points in Figure 15b is less than in Figure 15a, and there are fewer points. Figure 15c is the comparison between Scott Base and Ferrell AWS site. There are two outlying points. One is for August 1989 when only 65% of the data were collected from Ferrell site, and the other is for January 1981 when only 52% of the Ferrell site data were collected because the first 2 weeks of data were lost in the transfer of data from Stanford University to the University of Wisconsin. The three graphs in Figure 15 for Marble Point, Ferrell, and Katie against Scott base for roughly the same time period indicate good agreement with Scott Base and give no reason for

questioning the Scott Base monthly mean air pressure data.

Since Scott Base and the AWS sites of Marble Point, Ferrell, and Katie agree better than Scott Base and McMurdo, in spite of the short distance between Scott Base and McMurdo, the monthly mean air pressure difference for Scott Base minus McMurdo as a function of time starting on January 1980 and ending on December 1989 is plotted in Figure 16. The differences in the monthly mean air pressure for Scott Base minus McMurdo are large enough to seriously question the value of the McMurdo monthly mean air pressure data. The spread of the data in Figure 16 is smaller starting in 1987, but it is still 2.5 mbar wide. The spread of the Ferrell AWS monthly mean pressure data is also about 2.5 mbar wide neglecting the months with significant missing data. The Ferrell AWS site is 86 km from Scott Base. The McMurdo meteorology office does not have a mercury barometer for checking the setting of the

TABLE 3. The Results of a Linear Least Squares Fit Between Pairs of Sites for Air Temperature and Air Pressure Data

	r	b	t	$S1$	$S2$	n	N
<i>Air Temperature</i>							
McMurdo–Scott Base	0.988	0.913	124.056	8.673	9.387	373	396
Marble Point–Scott Base	0.993	0.902	82.482	7.868	8.663	102	119
Ferrell–Scott Base	0.989	1.106	60.892	10.050	8.986	87	109
Katie–Scott Base	0.998	1.009	69.238	9.724	9.611	23	25
D-10–Dumont d’Urville	0.990	0.970	58.185	5.961	6.085	72	84
Clean Air–South Pole	0.991	0.947	47.045	11.745	12.286	42	48
<i>Air Pressure</i>							
McMurdo–Scott Base	0.883	0.923	34.773	6.090	5.827	344	396
Marble Point–Scott Base	0.968	1.000	36.429	6.030	5.838	90	119
Ferrell–Scott Base	0.986	1.000	50.111	5.491	5.411	76	109
Katie–Scott Base	0.998	0.962	48.825	5.792	6.009	13	25
D-10–Dumont d’Urville	0.976	0.994	36.376	5.858	5.748	69	84
Clean Air–South Pole	0.921	0.917	15.164	5.818	5.847	43	48

The results are correlation coefficient (r), slope (b), Student t test (t), standard deviation for the first site ($S1$), standard deviation for the second site ($S2$), number of observations used (n), and the possible observations over the time period (N).

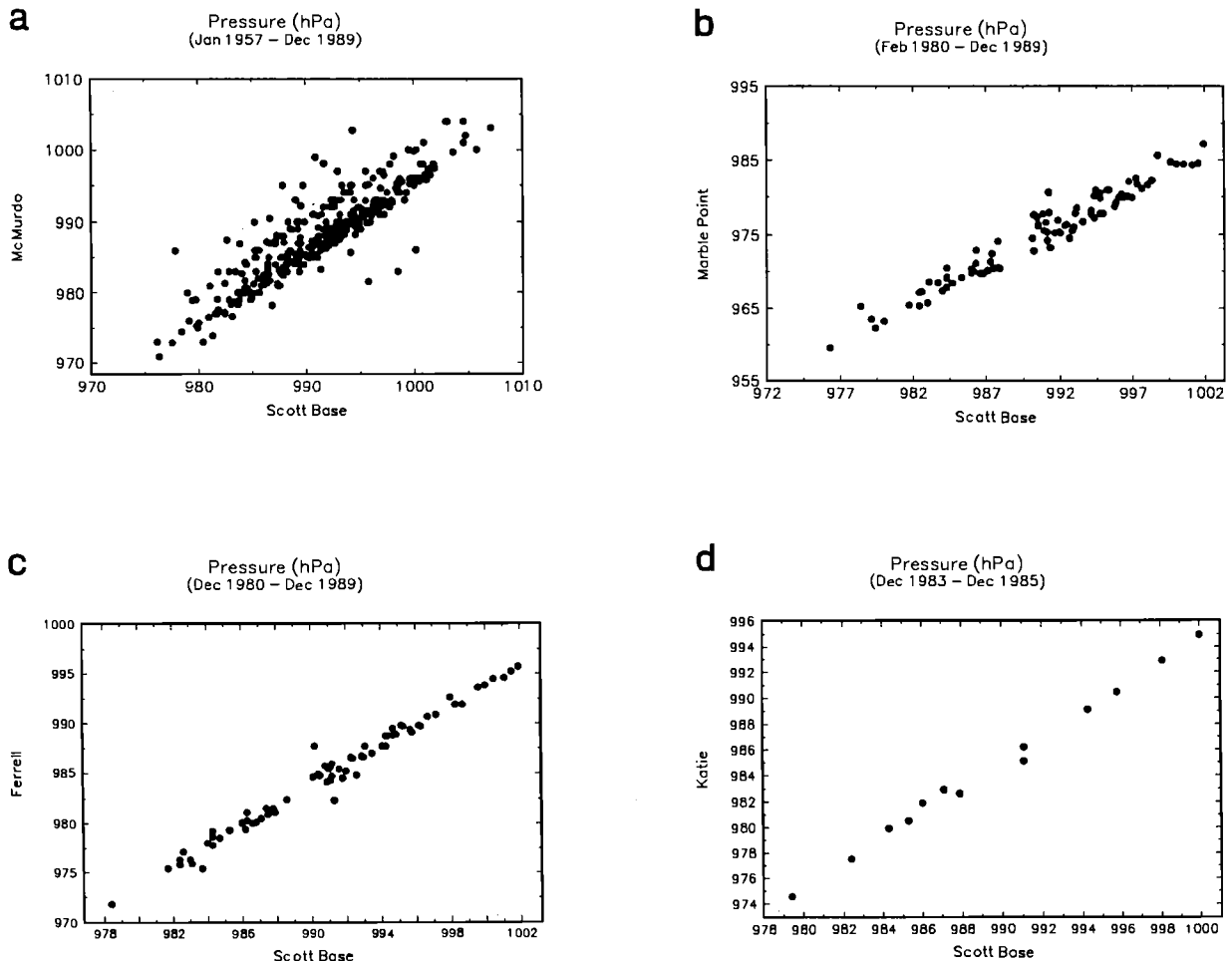


Fig. 15. Graph of the monthly mean air pressure for Scott Base versus (a) McMurdo, (b) Marble Point, (c) Ferrell, and (d) Katie.

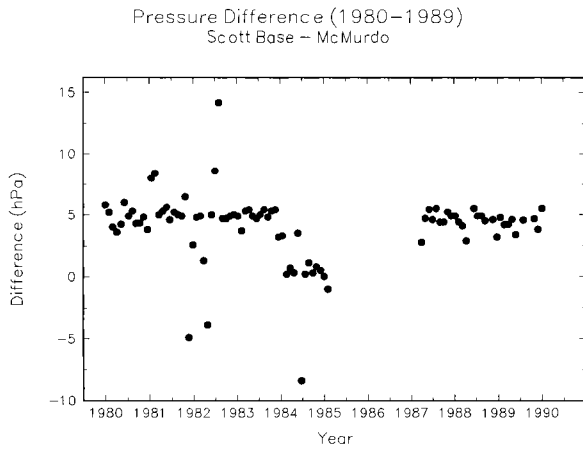


Fig. 16. Graph of the monthly mean station pressure difference for Scott Base pressure minus McMurdo from January 1980 to January 1990.

aneroid barometer. Scott Base has two Kew type mercury barometers.

In Figures 17a and 17b the graphs compare the monthly mean temperature and pressure for Clean Air to the South Pole data and show good agreement for the air temperature. The clear outlying point for the air pressure comparison is an error in the South Pole pressure data. Hogan *et al.* [this volume] made comparisons between the AWS sites around South Pole and the South Pole station data at 3-hourly intervals and for monthly means of air pressure, air temperature, and wind speed. In Figure 9 of Hogan *et al.* [this volume] are shown monthly mean values of wind speed, air temperature, and the monthly minimum air temperature for AWS sites Clean Air, Patrick, and Allison versus South Pole station data. The largest differences are in wind speed especially for AWS Patrick and Allison sites, which are about 13 km away from the South Pole.

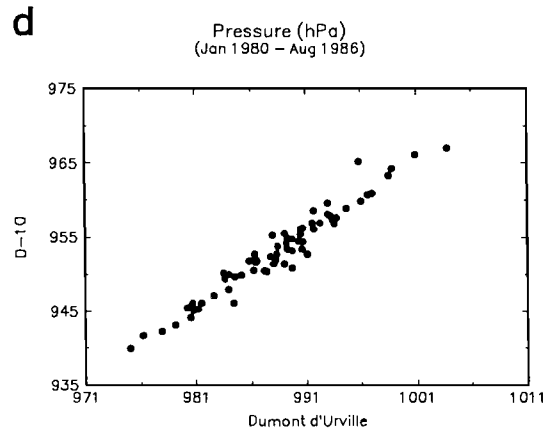
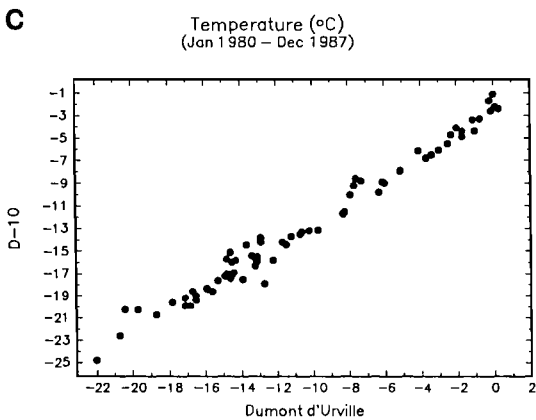
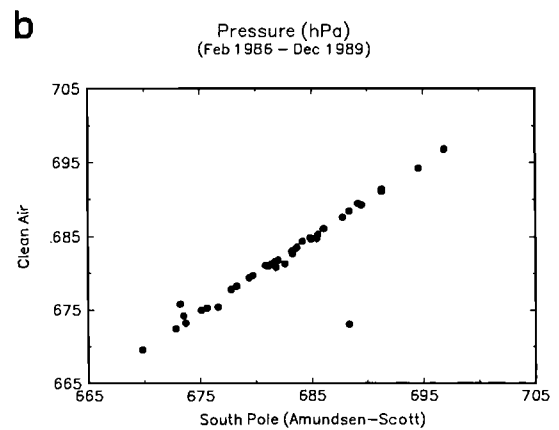
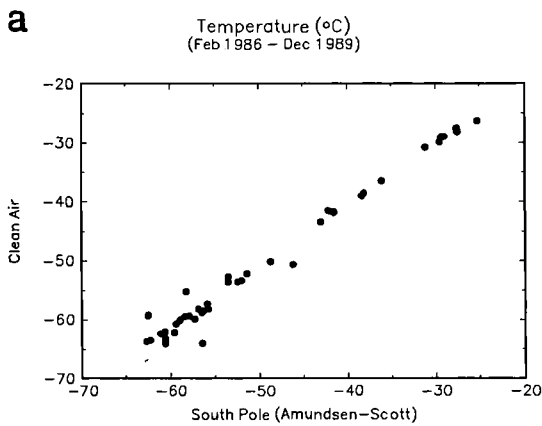


Fig. 17. Graph of the South Pole versus AWS Clean Air site monthly mean (a) air temperature and (b) air pressure, and of Dumont d'Urville versus AWS D-10 site monthly mean (c) air temperature and (d) air pressure.

The air temperature and wind speed at Clean Air site shows the best agreement with the South Pole data. Figure 10 of Hogan *et al.* [this volume] shows values of air temperature and wind speed at 3-hourly intervals for South Pole official measurements and AWS Patrick from August 15 to August 26, 1986. AWS Patrick site is approximately 13 km northeast of Amundsen-Scott station, and differences between the two sets of observations should be expected. The bulk of the data points overlap.

Figures 17c and 17d are a comparison between D-10 and Dumont d'Urville for monthly mean air temperature and air pressure. The agreement between the two sites is reasonable considering the differences in the locations. The results of the least squares fit for the data in Figure 17 are given in Table 3.

Some of the AWS sites have sufficient data so that one should be able to detect long-term trends in the climate as defined by the monthly mean air temperature, wind speed, and air pressure. There are small trends in the data for Ferrell, Byrd, and Whitlock, but none that we believe are indicative of changes in the climate. Dome C, D-10, and Marble Point AWS sites showed no noticeable trends.

The best coverage of a region by AWS units that could have a similar climate is on the Ross Ice Shelf. The elevations of the AWS units are within a few meters of each other, and the surface is uniform snow without significant changes in elevation. Figures 10 and 11 show significant differences in the climate based on monthly mean air temperature and wind speed on the Ross Ice Shelf. Stearns and Weidner [this volume] show significant differences in the monthly mean sensible heat flux to the air on the Ross Ice Shelf. Along the line of AWS sites from Marilyn site to Gill site, the magnitude of the sensible heat flux decreases from a large negative (toward the surface) value at Marilyn site to a small negative value at Gill site, with Schwerdtfeger site having an intermediate value. A similar trend in the sensible heat flux is observed at Elaine and Lettau sites. The monthly mean air temperatures on the Ross Ice Shelf are lowest at Gill site in the middle of the Ross Ice Shelf and higher south, west, and north of Gill site, and there are east to west changes in the sensible heat fluxes to the surface. On the basis of the above results the Ross Ice Shelf does not have a uniform climate in any direction.

6. CONCLUSIONS

The measurements of air pressure and, in particular, air temperature by the AWS units appear to be good enough that the data can be used for climate purposes. The maintenance of the AWS sites and the deployment of the AWS units into the meteorological void of Antarctica should continue. The comparison between Scott Base and the nearby AWS sites and McMurdo indicates

that the AWS units may be more reliable than some research stations.

The AWS units can miss data for a number of reasons. The AWS unit does not have the advantage of a research station in that the equipment can be readily checked when the unit is not operating properly. The data collection system operated by SERVICE ARGOS may miss 1 day or more. The wind speed and direction is subject to the whims of the elements, and the wind systems may not operate properly for extensive time periods, especially during the colder months, resulting in missing data. When using the AWS data for climate purposes, one should check that the AWS site has a significant amount of data before using the data. The percent of missing data is included in the complete data set for that purpose.

The many interesting variations in patterns of pressure and temperature (e.g., the lack of a coreless winter conditions at some locations) during the year require further analysis which we are pursuing. The connection between Antarctic climate and other hemispheric and global meteorological phenomena is only beginning to be explored. It is hoped that the data provided here will stimulate further research into the many types of phenomena on this continent and the teleconnections with the rest of the global atmosphere.

Acknowledgments. This research was funded by the National Science Foundation's Division of Polar Programs grants 8818171 and 9015586.

REFERENCES

- Bromwich, D. H., An extraordinary katabatic wind regime at Terra Nova Bay, Antarctica, *Mon. Weather Rev.*, *117*, 688-695, 1989a.
- Bromwich, D. H., Satellite analyses of Antarctic katabatic wind behavior, *Bull. Am. Meteorol. Soc.*, *70*, 738-749, 1989b.
- Hogan, A., D. Riley, B. B. Murphey, S. C. Barnard, and J. A. Samson, Variation in aerosol concentration associated with a polar climatic iteration, this volume.
- Jones, P. D., and D. W. S. Limbert, A data bank of Antarctic surface temperature and pressure data, *Rep. DOE/ER/60397-H2, Dist. Category UC-11*, 52 pp., U.S. Dep. of Commer., Springfield, Va., 1987.
- Keller, L. M., G. A. Weidner, C. R. Stearns, and M. F. Sievers, Antarctic automatic weather station data for the calendar year 1988, report, 329 pp., Dep. of Meteorol., Univ. of Wis., Madison, 1989.
- Keller, L. M., G. A. Weidner, and C. R. Stearns, Antarctic automatic weather station data for the calendar year 1989, report, 354 pp., Dep. of Meteorol., Univ. of Wis., Madison, 1990.
- Parish, T. R., On the interaction between Antarctic katabatic winds and tropospheric motions in the high southern latitudes, *Aust. Meteorol. Mag.*, *40*, 149-167, 1992.
- Parish, T. R., and D. H. Bromwich, The surface wind field over the Antarctic ice sheets, *Nature*, *328*, 51-54, 1987.
- Savage, M. L., C. R. Stearns, and D. Fleming, Antarctic automatic weather station data for the calendar year 1980,

- report, 72 pp., Dep. of Meteorol., Univ. of Wis., Madison, 1985*a*.
- Savage, M. L., C. R. Stearns, and D. Fleming, Antarctic automatic weather station data for the calendar year 1981, report, 149 pp., Dep. of Meteorol., Univ. of Wis., Madison, 1985*b*.
- Savage, M. L., C. R. Stearns, and D. Fleming, Antarctic automatic weather station data for the calendar year 1982, report, 185 pp., Dep. of Meteorol., Univ. of Wis., Madison, 1985*c*.
- Savage, M. L., C. R. Stearns, G. A. Weidner, and D. Fleming, Antarctic automatic weather station data for the calendar year 1983, report, 192 pp., Dep. of Meteorol., Univ. of Wis., Madison, 1985*d*.
- Savage, M. L., C. R. Stearns, G. A. Weidner, and D. Fleming, Antarctic automatic weather station data for the calendar year 1984, report, 243 pp., Dep. of Meteorol., Univ. of Wis., Madison, 1985*e*.
- Schwalb, A., The TIROS-N/NOAA A-G satellite series, *NOAA Tech. Memo. NESS 95*, 95 pp., U.S. Dep. of Commer., Washington, D. C., 1978.
- Sievers, M., G. A. Weidner, and C. R. Stearns, Antarctic automatic weather station data for the calendar year 1985, report, 254 pp., Dep. of Meteorol., Univ. of Wis., Madison, 1986.
- Sievers, M., G. A. Weidner, and C. R. Stearns, Antarctic automatic weather station data for the calendar year 1986, report, 268 pp., Dep. of Meteorol., Univ. of Wis., Madison, 1987.
- Sievers, M., G. A. Weidner, and C. R. Stearns, Antarctic automatic weather station data for the calendar year 1987, report, 299 pp., Dep. of Meteorol., Univ. of Wis., Madison, 1988.
- Smith, S., Antarctic climate anomalies associated with the minimum of the Southern Oscillation index, M.S. thesis, Dep. of Meteorol., Univ. of Wis., Madison, 1991.
- Stearns, C. R., Antarctic automatic weather stations, austral summer 1981–1982, *Antarct. J. U.S.*, 17(5), 217–219, 1982.
- Stearns, C. R., Antarctic automatic weather stations, austral summer 1983–1984, *Antarct. J. U.S.*, 19(5), 189–191, 1984.
- Stearns, C. R., Antarctic automatic weather stations, austral summer 1985–1986, *Antarct. J. U.S.*, 21(5), 189–191, 1986.
- Stearns, C. R., Antarctic automatic weather stations, austral summer 1986–1987, *Antarct. J. U.S.*, 22(5), 270–272, 1987.
- Stearns, C. R., Antarctic automatic weather stations, austral summer 1987–1988, *Antarct. J. U.S.*, 23(5), 183–186, 1988.
- Stearns, C. R., Antarctic automatic weather stations, austral summer 1988–1989, *Antarct. J. U.S.*, 24(5), 242–243, 1989.
- Stearns, C. R., and M. Savage, Automatic weather stations, 1980–1981, *Antarct. J. U.S.*, 16(5), 190–192, 1981.
- Stearns, C. R., and G. A. Weidner, Antarctic automatic weather stations, austral summer 1982–1983, *Antarct. J. U.S.*, 18(5), 245–246, 1983.
- Stearns, C. R., and G. A. Weidner, Antarctic automatic weather stations, austral summer 1984–1985, *Antarct. J. U.S.*, 20(5), 233–234, 1985.
- Stearns, C. R., and G. A. Weidner, Sensible and latent heat flux estimates in Antarctica, this volume.
- Stearns, C. R., and G. Wendler, Research results from Antarctic automatic weather stations, *Rev. Geophys.*, 26, 45–61, 1988.

(Received September 15, 1991;
accepted April 16, 1993.)

KATABATIC WINDS IN ADÉLIE COAST

GERD WENDLER,¹ JEAN CLAUDE ANDRÉ,² PAUL PETTRÉ,² JOAN GOSINK,³ AND THOMAS PARISH⁴

A decade ago, a joint U.S.-French experiment commenced in Adélie Coast, eastern Antarctica. The experiment is called IAGO, for Interactions-Atmosphere-Glace-Océan. One of the main purposes of this investigation is to obtain a better understanding of the katabatic wind, which is very well developed in this area. This paper summarizes some of the findings so far. It discusses the climatology of the area, detailed vertical measurements through the boundary layer, radiative and energy budget fluxes, blowing snow and its effects on the gravity flow, the hydraulic jump (Loewe phenomenon), and modeling efforts.

1. INTRODUCTION

Most of the data discussed in this paper were collected by automatic weather stations (AWS). These stations were originally designed by A. Peterson's group at Stanford University, but since 1981 C. Stearns' group from the University of Wisconsin at Madison has taken care of them [Stearns, 1982; Weidner, 1987]. The first stations were established in Adélie Coast in 1980, so that now up to 10 years of data are available. The stations measure wind speed and direction, temperature, and atmospheric pressure, besides some nonmeteorological parameters. Lately, we have added humidity sensors and dual wind sensors for extremely windy areas. However, this paper is based on data from the original stations.

Data are transmitted by the Argos system from polar-orbiting satellites which have a period of about 104 min. There are normally two satellites available. For transmission the stations can store, at 10-min intervals, up to four data sets besides the instantaneous values. Hence under ideal circumstances a steady data flow at 10-min intervals can be obtained.

The stations are in remote locations and are normally serviced once a year. Hence a visual inspection is not possible. It is believed that the wind sensors can occasionally become frozen; this can be deduced from data analysis. It does not present a serious problem for Adélie Coast since, with the exception of Dome Charlie (Dome C), wind speeds are strong. Further, some radiation errors will occur during times of bright sunshine and low wind speed; the temperature sensors are

shielded but not ventilated. The height of measurements above the surface is not constant, since snow accumulates throughout the year. No corrections are made for the height, which normally varies between 1.5 m and 3.0 m. This especially affects the wind speed.

There is a long-term manned meteorological station in the area, at Dumont d'Urville, the main French Antarctic base. Data have been collected here for more than 30 years, and we sometimes refer to this data base [Périad and Pettré, 1991].

The meteorological program which has been carried out during the last decade is U.S.-French, and more recently there has been in cooperation with the Australians who have stations to the west of us [Radok and Wendler, 1991]. Figure 1 shows the locations of our stations, and Tables 1a and 1b have specifics on observation time and geographic setting. Note that the length of the observation periods varies greatly and does not necessarily overlap.

It should be pointed out that in this paper, results from field investigations and AWS in Adélie Coast are discussed. There are many more AWS from the United States and other nations. Stearns and Wendler [1988] summarized the results from U.S. stations.

2. RESULTS

2.1. Climatology

Temperature. Antarctica is a dome of ice, with a high plateau in its interior of 4000 m elevation (the highest mountain in Antarctica is the Vinson Massif at 5140 m), and sloping toward its perimeter at sea level. The radiation budget is negative on an annual basis because of the high reflectivity of snow [Hoinkes, 1961; Rusin, 1961; Dalrymple et al., 1966; Kuhn et al., 1977; Ishikawa et al., 1982; Carroll, 1982]. Therefore the air layer near the surface is cooled for most of the year. Hence strong inversion conditions develop which are persistent and can be seen over nearly the entire conti-

¹Geophysical Institute, University of Alaska, Fairbanks, Alaska 99775.

²Centre National de Recherches Météorologiques, Toulouse, France.

³School of Mining, Golden, Colorado 80401.

⁴Department of Atmospheric Science, University of Wyoming, Laramie, Wyoming 82071.

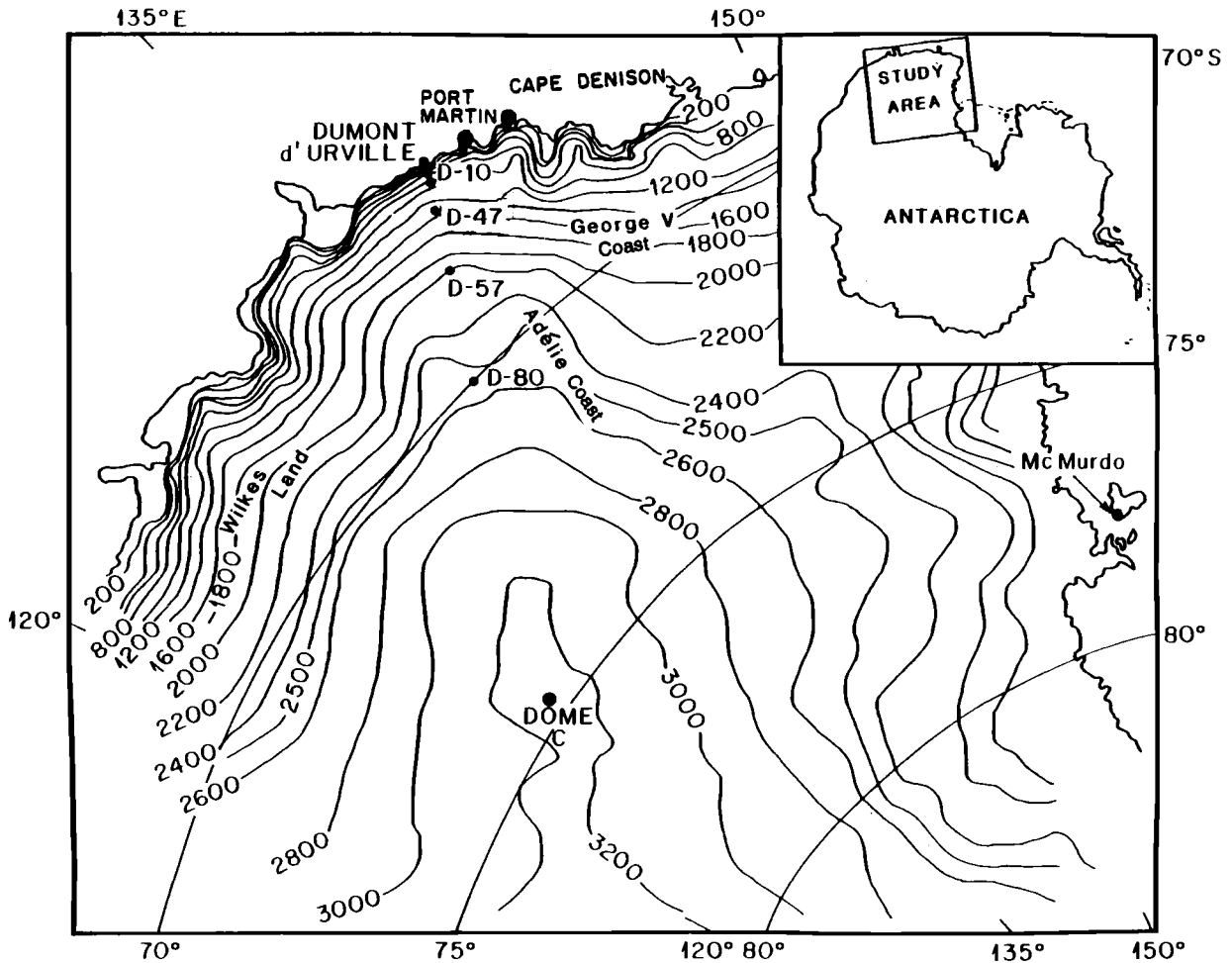


Fig. 1. Location map of AWS station in Adélie Coast. Altitude lines are in meters.

ment for much of the year. Therefore the surface layer of air has a lower temperature than the free air at a point downslope at the same altitude, which starts a gravitational air movement down the slopes [Defant, 1951; Ball, 1956]. This gravity flow dominates the surface wind regime of Antarctica [Schwerdtfeger, 1984]. No where else on Earth does one single meteorological element have such an overwhelming influence on the climate of an entire continent.

In confluence zones on or near the coast, where topographic funneling occurs, very strong winds are observed. Adélie Coast has such places. At the historic stations of Port Martin and Cape Denison, mean annual wind speeds of close to 20 m s^{-1} were observed [Loewe, 1972]. These are the strongest winds observed anywhere on Earth close to sea level [Parish and Wendler, 1991; Wendler, 1990a, b]. These katabatic winds occur not only in the coastal areas but also influence most of the inland stations, which are normally located on sloped terrain. The slope angle might be small and not

visible to the naked eye, as for example at D80; nevertheless gravitational flow has a dominant influence on the wind direction. The only AWS in Adélie Coast which is not influenced by katabatic flow is at the top of Dome C, a flat-topped dome with an elevation of 3280 m, a site originally chosen for a drilling experiment.

In Table 2 the monthly mean minimum and maximum temperatures are presented. The temperatures are not given for D17, as the record is very short (7 months). Dome C is very cold; an absolute minimum of -84.6°C was recorded, and the average winter temperature hovers around -60°C . It can also be seen that the winter is kernlose; that is, no systematic changes in temperature are observed during the winter months. This phenomenon is discussed separately [Wendler and Kodama, this volume] and hence is not further mentioned here. Even in summer, Dome C is cold, with the warmest monthly temperature around -30°C . The highest temperature ever measured was well below the freezing point. Dome C, of course, lies in the dry snow zone [Giovinetto,

TABLE 1a. Location of AWS in Adélie Coast

Station	Location	Altitude, m	Distance From Coast, km	Slope	Azimuth of Maximum Upslope, deg	Date Installed
D10	66°42'S 139°48'E	240	5	2×10^{-2}	210	Jan. 1980
D47	67°23'S 138°43'E	1560	110	5.5×10^{-3}	210	Jan. 1982
D57	68°11'S 137°32'E	2103	210	6.5×10^{-3}	210	Jan. 1981
D80	70°01'S 134°43'E	2450	440	1.8×10^{-3}	210	Jan. 1983
Dome C	74°30'S 123°00'E	3280	1080			Jan. 1980

1961], where melting never occurs. In the coastal areas, really cold temperatures are never observed (Figure 2). At D10, a station 5 km from the edge of the continent, temperatures below -40°C have never been measured. For Dumont d'Urville, some 10 km away from D10, a record of more than 30 years exists, and again the temperature has never dropped below -40°C . In summer, which consists mainly of December and January, the temperatures are close to the freezing point and frequently go through the freezing cycle over the course of the day. These relatively mild temperatures induced the French to nickname the area the "Riviera of Antarctica." However, these mild temperatures are found for larger coastal areas, for example, for the Australian station Mawson. A precondition for the absence of very cold temperatures is a strong katabatic wind, which weakens the surface inversion because of forced mixing.

In Figure 3 the potential temperature differences (monthly mean) between D10 and Dome C are given. It can be seen that with the exception of midsummer (December, January), large temperature differences were observed. In midwinter, temperature differences of 15°C above the adiabatic lapse rate are occurring, showing a strong meridional temperature gradient at this time of year.

In Figure 4 the diurnal variation in temperature is given for Dome C and D10 for March, June, and December. In midwinter (June), no systematic temperature variation is observed for either of the stations, as they are south of the Antarctic circle and the Sun is below the horizon. In autumn (March), there is a great deal of temperature variation with the maximum in the early afternoon. The variation is much larger for Dome C (about 10°C) than for the coastal station D10 (about 2°C). The reason for this is not easy to find because it is the result of the coupled processes of heat exchange at the surface and conditions in the boundary layer. An explanation was first offered by Simpson [1919], the foremost meteorologist of Scott's expedition. The larger heat conductivity of snow and ice in the coastal areas

suppresses extremes in temperature, while the drier and lower-density snow of inland areas has a poor heat conductivity and capacity, thereby enhancing extremes. An additional reason for this is believed to be found in the much stronger forced mixing at D10 owing to the higher wind speeds. These stronger winds do not allow the diurnal buildup of the boundary layer to the same extent.

In midsummer (December) the diurnal variation is again more pronounced at Dome C than in the coastal areas. Near the coast the oceans, which are ice free at this time of year, have a moderating effect. Further, there is a great deal of forced turbulent mixing, and the heat characteristics of the underlying surface are different. A large diurnal temperature range, as observed for Dome C at times when the Sun is above the horizon all day, has previously been noted in Antarctica by Simpson [1919], Hisdal [1960], and Wendler and Kodama [1984].

Pressure. In Figure 5 the annual course of the atmospheric pressure is given for D10 and Dome C. A well-pronounced semiannual variation can be seen. Minima are observed in autumn and spring, with the spring minimum being larger, while the maxima are observed in summer and winter. They are caused by two out-of-phase oscillations [van Loon, 1967], one with equinoctial pressure maxima in latitudes 30° – 55°S , reaching its largest amplitude between 40° and 50°S , and one with a equinoctial pressure minima having its largest amplitude at 65° – 70°S . In Figure 6 the mean temperature of D10 and Dome C is plotted against the pressure difference between these two stations for monthly values. It can be seen that with decreasing temperature the pressure difference increases, a result to be expected; the relationship is fairly good.

The interdiurnal pressure variation gives an indication of the cyclonic activity [Schwerdtfeger, 1970]. For example, at Dome C, values of 3.48, 4.09, and 5.47 mbar were observed for December, March, and June 1982, respectively. One can see that the highest values are found in winter, the lowest in the summer. This is in

TABLE 1b. Time of Observations of

Station	1980	1981	1982	1983
	JFMAMJJASOND	JFMAMJJASOND	JFMAMJJASOND	JFMAMJJASOND
D10	XXXXXXXXXXXX	XXXX X	XXXXXXXXXXXX	XXXXXXXXXXXX
D47			XX	XXXXXXXXXXXX
D57		XXXXXXXXXXXX	XXXXXXXXXXXX	XXXXXXXXXXXX
D80				XXXXXXXXXX
Dome C	XXXXXXXXXXXX	XXXXXXXXXXXX	XXXXXXXXXXXX	

Spaces indicate months during which the stations did not operate.

agreement with *Wexler* [1958], who showed that the increased horizontal latitudinal temperature gradient in the Antarctic atmosphere in winter increases cyclonic activity, even though the circumpolar trough is farthest away from the continent in winter.

Wind. In Figure 7 the annual course of the wind speed is presented. The wind speeds at Dome C are very light. A comparison with other inland stations shows that Dome C experiences the lowest wind speeds of any inland station in Antarctica. A mean value of about 3 m s⁻¹ was observed with no pronounced annual cycle. This is unique, as a freely exposed station at a height of 3280 m on any other continent would have higher wind speeds than lower-lying stations.

In winter (June), there is no diurnal variation in wind speed at Dome C. The Sun is, of course, below the horizon, and no systematic variation in surface heating can occur. This was also shown by the absence of any variation in temperature (Figure 4). However, in summer (December), higher wind speeds are observed in the afternoon (Figure 8). Assuming no gravitational flow for Dome C, the stronger inversions at night hinder the transfer of momentum to the surface, whereas in the afternoon the inversions are weaker. *Wendler and Nicpon* [1975] showed these effects for the Subarctic (interior of Alaska) quantitatively.

This diurnal course contrasts the one observed for the slope stations, where a maximum in summer wind speeds is observed in the very early morning hours, shortly after the inversion strength has reached its maximum. The minimum wind speeds are observed in the afternoon, normally 2–3 hours after the maximum in temperature (Figure 8). In winter, no systematic diurnal variation is observed, as for Dome C.

When going down the slope, we find a steady increase in wind speed when approaching the coast. A latitudinal cross section is presented in Figure 9. The maximum wind speed is, however, not observed at the coast but some distance inland. These observations confirm *Parish's* [1984] modeling results.

With the exception of Dome C, all slope stations show a strong constancy in wind direction, which is defined as the ratio of the mean wind vector to the scalar mean wind speed (see Table 3). A value of 1.0 means that the

wind blows constantly from one direction, whereas a value of 0.0 means that winds from opposite directions with equal strengths are equally frequent. There is no place where 0.0 is found, as the general circulation has preferred directions. The strong directional constancy for the slope stations indicates that the downslope gravitational flow is a major determining factor and that cyclonic disturbances have only a modifying effect for these stations. Only at Dome C, where gravitational flow cannot take place, is a large variation in wind direction observed.

In Figure 10 the temperature difference between the cold interior of Antarctica (Dome C) and the coastal area (D10) is plotted against the wind speed at D10. If the winds would be solely of gravitational nature, increasing wind speeds would be expected with increasing temperature differences. A fairly well established linear relationship can be seen, which is significant at the 99.9% confidence level.

In Figure 11 the temperature is plotted against the wind speed. For Dome C, no relationship is observed, but a well-established dependency is found for all slope stations; D80 is shown as an example in Figure 11. Colder months have stronger winds, a result to be expected. Cold temperatures normally are associated with strong inversions and hence strong gravitational flow.

2.2. Radiative Fluxes and Surface Energy Balance

During Austral summer 1985/1986 a large field program was carried out in Adélie Coast. Three stations were simultaneously occupied, located some 5 km, 100 km, and 200 km from the edge of the continent. Two were occupied by French personnel and one by a U.S. team. Included in these measurements were detailed radiative and surface heat balance observations at the U.S. site, D47. A description of the climate during this time is given by *Ishikawa et al.* [1990].

The high surface reflectivity has a dominant influence on the radiative fluxes and the surface energy budget. With the exception of areas very close to the coast the albedo stays very high year-round, and most of the

AWS in Adélie Coast

1984	1985	1986	1987	1988
JFMAMJJASOND	JFMAMJJASOND	JFMAMJJASOND	JFMAMJJASOND	JFMAMJJA
XXXXXXXXXXXX	XXXXXXXXXXXX	XXXXXXXXXX XX	XXXXXXXXXXXX	XXXXXXXXXX
XXXXXXXXXXXX	XXXXXX XX	XXXXXXXXXXXX	XXXXXXXXXXXX	XXXXXXXXXX
XXXXXXXXXXXX	XXXX XX	XXXXXXXXXXXX	XXXXXXXXXXXX	XXXXXXXXXX
XX	XXXX X	XXXXXXXXXXXX	XXXXXXXXXXXX	XXXXXXXXXX
XXXXXXXXXXXX	XXXXXXXXXXXX	XXXXXXXXXXXX	XXXXXXXXXXXX	XXXXXXXXXX

energy is reflected back to space. At D47, in the dry snow zone some 100 km from the edge of the continent, melting of snow never occurs [Giovinetto, 1961]. We found the reflectivity for the summer to be 82.6%, a high but not unreasonable value. The high surface albedo results in a counterintuitive process: with increasing global radiation the net radiation is decreasing (see Figure 12). Loewe [1956] making measurements in 1951/1952 at Port Martin, Adélie Coast, was the first to point this out. Both the shortwave and the long-wave radiation budget depend on cloudiness, the shortwave budget increasing, the long-wave radiation budget decreasing

with decreasing cloudiness. In Figure 13 the relationship between the long-wave and the shortwave radiation budget is given. A very nice negative correlation coefficient ($r = -0.963$) was calculated. One can see from the slope of this figure (note that the axes have identical scales) that with increasing positive shortwave radiation budget, the long-wave radiation decreases by a larger amount. Hence with increasing cloudiness the net radiation becomes more positive, for which Ambach [1974] coined the phrase “radiation paradox.” He observed this in Greenland, also an area with a high surface reflectivity. We were able to model this effect using the radiative data from Adélie Coast as input [Wendler, 1986]. These calculations showed that a surface reflectivity in excess of 60% is a precondition for this phenomenon.

TABLE 2. Temperatures in Degrees Centigrade (Mean, Maximum, and Minimum) for the AWS Stations in Adélie Coast

Station	T	T_{max}	T_{min}
<i>D10</i>			
II-IV	-11.1	8.2	-29.1
V-VII	-17.8	-0.1	-35.2
VIII-X	-17.1	-2.0	-35.4
XI-I	-4.8	14.0	-21.9
Annual	-13.5	14.0	-35.4
<i>D47</i>			
II-IV	-22.9	-4.6	-40.0
V-VII	-31.0	-10.7	-44.2
VIII-X	-28.9	-2.0	-41.1
XI-I	-16.2	5.7	-26.1
Annual	-24.8	-2.0	-44.2
<i>D57</i>			
II-IV	-28.6	-7.7	-49.7
V-VII	-36.8	-13.6	-55.4
VIII-X	-30.4	-12.0	-61.1
XI-I	-20.1	-3.2	-41.2
Annual	-29.0	-3.2	-61.1
<i>D80</i>			
II-IV	-39.7	-11.2	-60.0
V-VII	-42.3	-13.5	-69.7
VIII-X	-45.3	-18.0	-71.2
XI-I	-27.7	-5.5	-50.5
Annual	-36.2	-5.5	-71.2
<i>Dome C</i>			
II-IV	-48.3	-13.1	-79.7
V-VI	-57.9	-13.5	-82.2
VIII-X	-54.2	-17.6	-84.6
XI-I	-29.8	-15.0	-67.4
Annual	-47.5	-13.1	-84.6

While the individual radiation fluxes are large, the all-wave radiation balance, or net radiation, is small in summer as the positive shortwave radiation budget is nearly canceled by a negative long-wave radiation budget. In Table 4 the mean and extreme daily values are given for a 33-day period in summer for a station some 100 km from the edge of the continent. Figure 14 shows

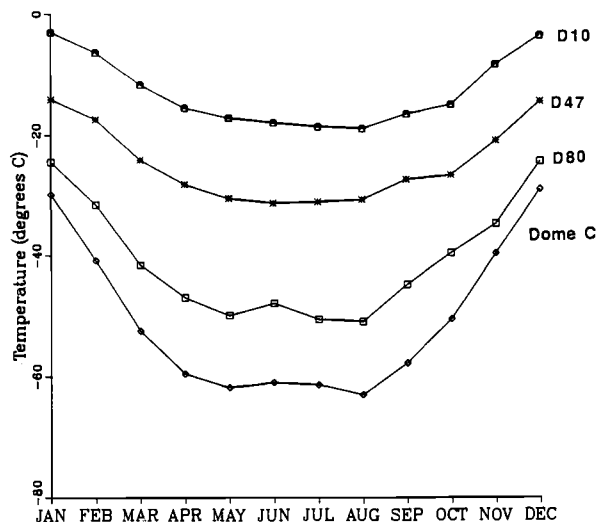


Fig. 2. The annual course of temperature for AWS stations in Adélie Coast, eastern Antarctica.

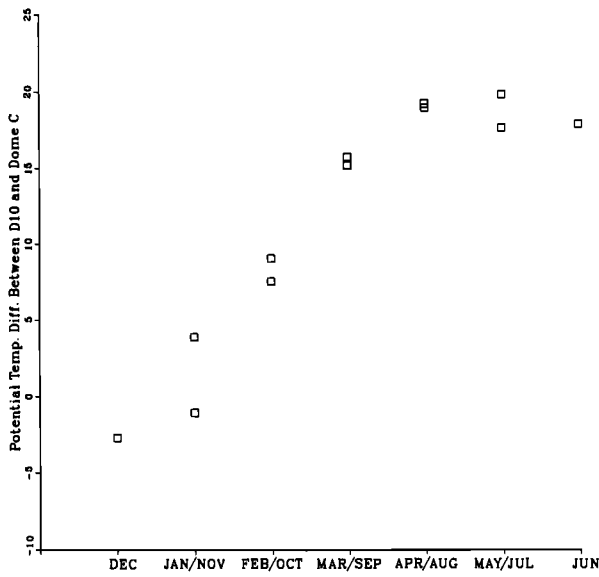


Fig. 3. Difference in potential temperature between the interior (Dome C) and the coastal region (D10). Note that the temperature difference is for most of the year above the adiabatic rate with a minimum in difference during summer.

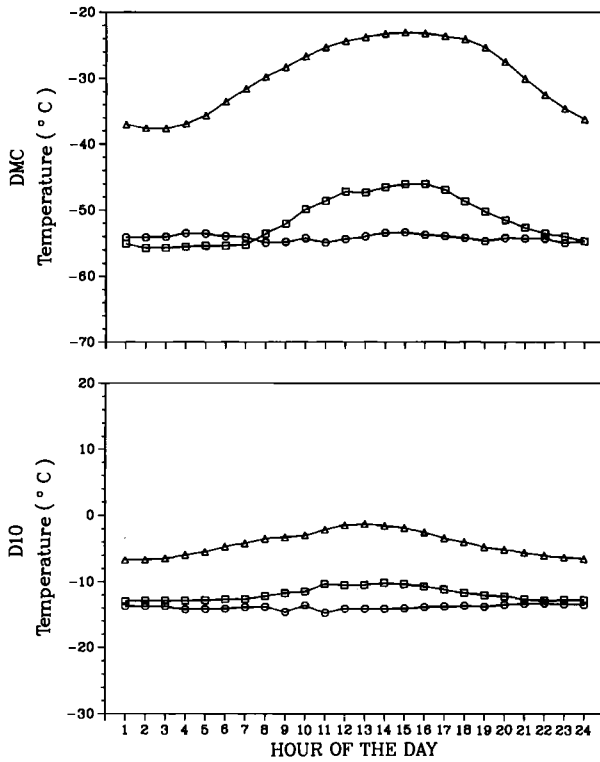


Fig. 4. Mean diurnal variation of temperature for March, June, and December for coastal and inland station in Antarctica (triangle, December; square, March; circle, June). Time axis is in local time.

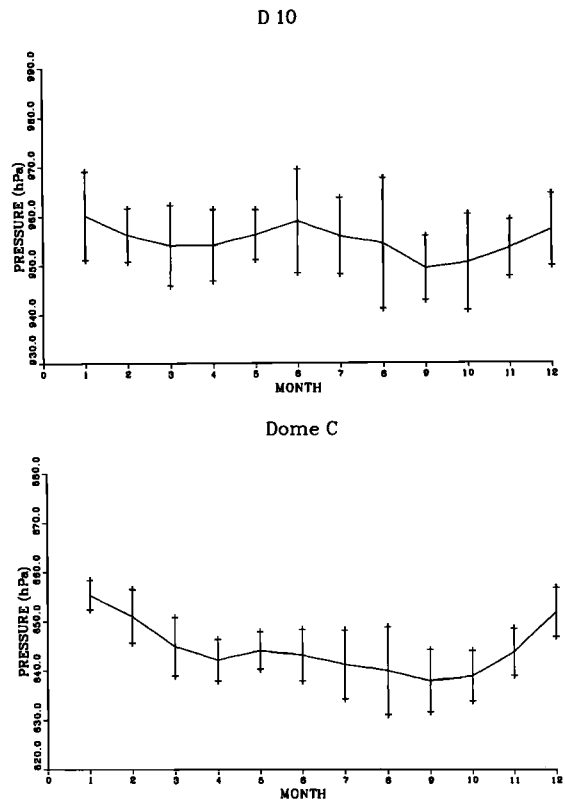


Fig. 5. Mean annual course of atmospheric pressure for D10 and Dome C. The bars denote one standard deviation.

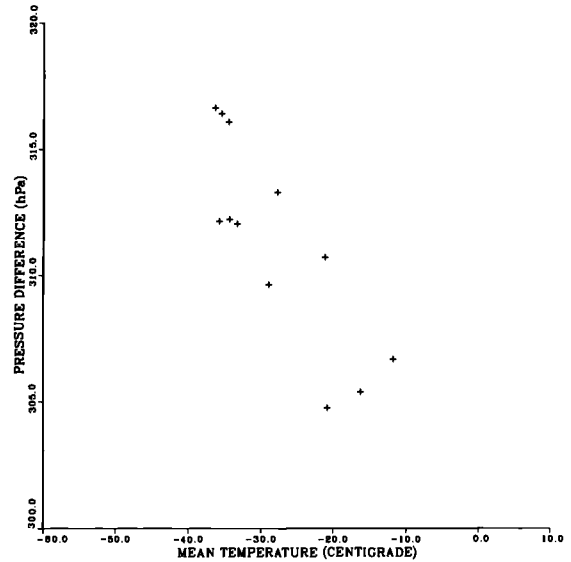


Fig. 6. Pressure difference between D10 and Dome C plotted against the mean temperature of these two stations.

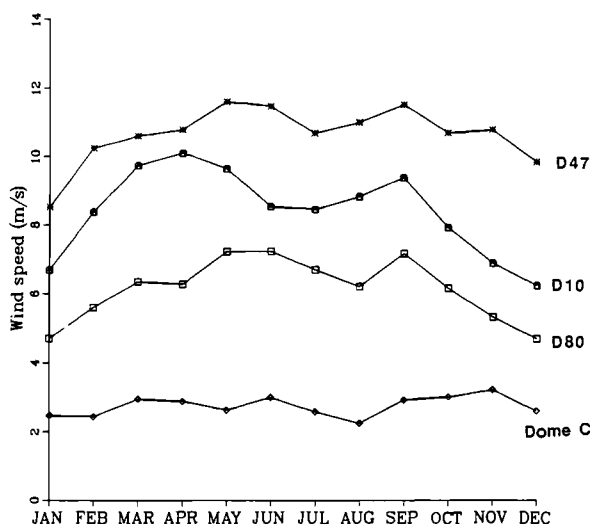


Fig. 7. The annual course of the wind speed for AWS stations in Adélie Coast, eastern Antarctica.

the mean diurnal variation of the net radiation for the same period. A nice sinusoidal curve can be observed, with negative values for about 12 hours and positive values around noon. The negative values occur with the Sun above the horizon; the solar elevation is, however, insufficient to supply larger amounts of energy to the surface [Wendler *et al.*, 1988a].

Values of Ångström's turbidity coefficient β of about 0.04 were found, and typical values of Linke's turbidity factor T were about 2. These values are in general agreement with findings of other authors [e.g., Forgan *et al.*, 1988]. Our data showed further that the decrease in intensity with increasing optical air mass was less pronounced for longer wavelengths than for shorter ones, a result to be expected. In general, it can be stated

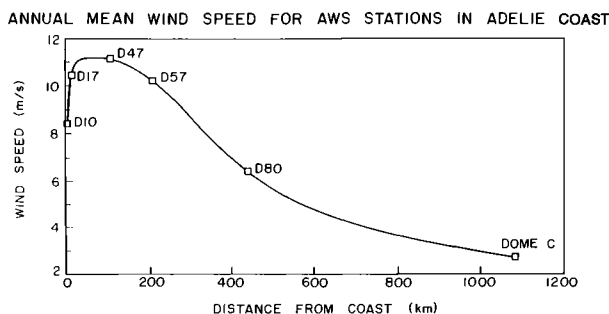


Fig. 9. Wind speed as a function of the distance from coast. Note that the wind speed increases velocity when going down from Dome C toward the coast but reaches its maximum a certain distance before the edge of the continent.

that the air is much cleaner than in the Arctic [Wendler and Ishikawa, 1988].

Turbidity measurements have been carried out for over three decades by different authors. Even though these measurements are somewhat difficult to compare because of their different locations and altitudes, no obvious change in turbidity could be detected (Table 5).

Because of the low turbidity, and even more so because of the relatively low amount of cloudiness, the incoming global radiation (G) is large [Wendler, 1986], as can be seen from Figure 15, in which the daily mean values of the global radiation are presented. The encompassing curve represents the extraterrestrial radiation (ET^*) which was reduced to the horizontal surface and corrected for the Earth-Sun distance. Calculating the ratio of G/ET^* , which is also called the clearness index (K_T), a mean value of 0.81 was found. This means that 81% of the radiation on top of the atmosphere penetrates throughout the atmosphere and is measured at the surface either as direct or diffuse radiation. A mean value of 0.89 was found for 0/10 cloudiness, a very high

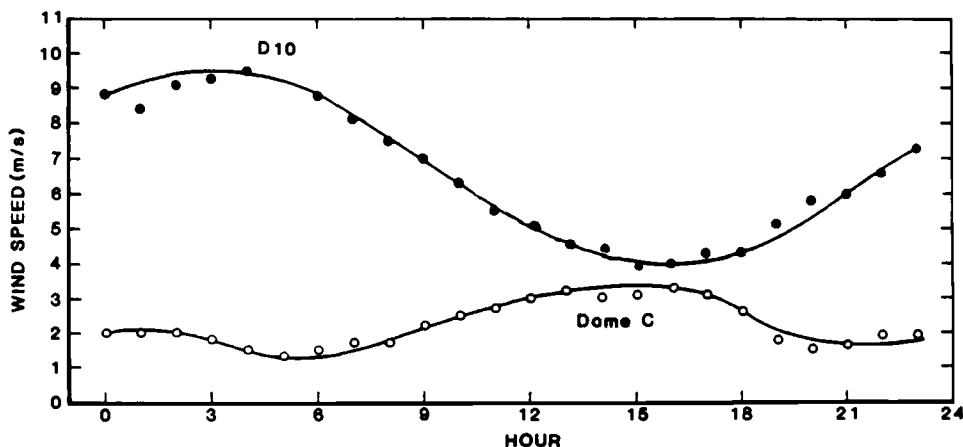


Fig. 8. Diurnal variation in wind speed, summer, Dome C and D10.

TABLE 3. Wind Direction Constancy for the AWS Stations in Adélie Coast

Month	D10*	D47†	D57‡	D80§	Dome C
Jan.	0.91	0.92	0.92	0.82	0.62
Feb.	0.93	0.95	0.93	0.84	0.54
March	0.94	0.93	0.93	0.90	0.59
April	0.94	0.89	0.93	0.94	0.67
May	0.93	0.92	0.96	0.97	0.58
June	0.81	0.95	0.87	0.88	0.67
July	0.93	0.92	0.84	0.87	0.55
Aug.	0.92	0.90	0.95	0.90	0.63
Sept.	0.92	0.89	0.80	0.90	0.51
Oct.	0.92	0.90	0.91	0.80	0.61
Nov.	0.84	0.92	0.89	0.83	0.68
Dec.	0.87	0.90	0.94	0.81	0.72
Annual	0.90	0.92	0.91	0.87	0.61

*Latitude, 66°42'S; longitude, 139°48'E; altitude, 240 m.

†Latitude, 67°23'S; longitude, 138°43'E; altitude, 1560 m.

‡Latitude, 68°11'S; longitude, 137°32'E; altitude, 2100 m.

§Latitude, 70°01'S; longitude, 134°43'E; altitude, 2500 m.

||Latitude, 74°30'S; longitude, 123°00'E; altitude, 3280 m.

value indeed, even for totally clear skies. This shows that the atmosphere in Antarctica is not only very clean but also contains very little water vapor. The lowest K_f value was observed for 10/10 cloudiness (mean 0.57), indicating that clouds are normally "thin," a result *Loewe* [1956] observed already for the same general area more than three decades ago. This is due to the fact that the atmosphere is cold and hence unable to hold large amounts of water vapor.

For the same time period the mean diurnal variation in temperature, relative humidity, and wind speed at 2 m above the surface are given in Figure 16. Even though the Sun was above the horizon between 22 and 24 hr d^{-1} , there was a strong diurnal variation in temperature. The minimum of nearly $-22^{\circ}C$ occurred at 0300 local standard time (LST), while the maximum occurs at 1400 LST with a temperature of $-13^{\circ}C$. The curve is sinusoidal and smooth, an effect of averaging over the 33-day period.

The relative humidity shows the reciprocal diurnal variation. Maxima are found at night (86%), while a minimum occurs at the time when the temperature reaches its maximum (65%). This, of course, does not mean that there is less water vapor in the air during the day, as the saturation water vapor pressure is strongly dependent on the temperature.

The wind speed has its maximum in the early morning hours (0500 LST) while the minimum is observed between 1800 and 1900 LST. The range of the diurnal variation is 3 m s^{-1} . There is a 4-hour shift from the extremes in temperature, which appears to be the time lag required for the gravity-driven wind to react to changes in the inversion strength.

Profile measurements allowed us to calculate the eddy fluxes. In Figure 17 the diurnal variation of the sensible and latent heat flux are presented. It can be seen that the

surface warms the air for the average summer day (negative flux), while at night the flux is in the opposite direction. The average latent heat flux is mostly negative, with larger values during the day and slightly positive values around midnight.

The heat flux into or out of the snow was obtained from the temperature in the snow. The tautochrones for a clear day are given in Figure 18. A strong warming during the day can be observed. The lag time from the maximum solar height is larger than for the air temperature. These temperature profiles make it possible to calculate the heat flux in the snow surface at hourly intervals. During the daytime a flux into the snow

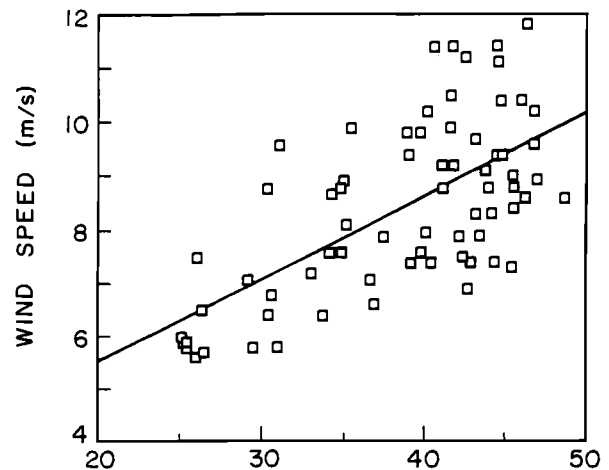


Fig. 10. The wind speed near the coast (D10) is plotted against the temperature difference (degrees Centigrade) between this coastal station and Dome C. The points represent monthly mean values. A regression line was put through the points.

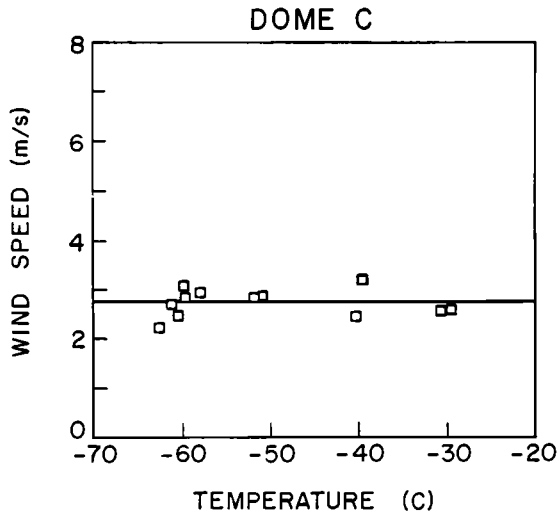
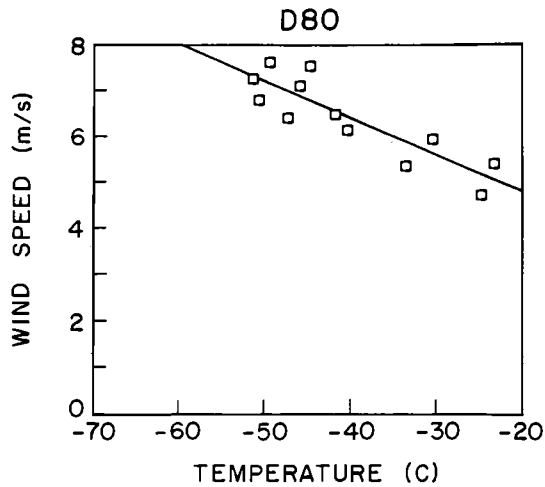


Fig. 11. Monthly mean values of temperature plotted against the wind speed of the same stations. For Dome C, no relationship was found, while for the station over sloped terrain the wind speed increases with decreasing temperature.

TABLE 4. Radiative Fluxes at D47, Adélie Coast, for the Time Period November 20 to December 22, 1985

	Mean	Maximum*	Minimum*
Shortwave incoming	407.9	474.3	256.7
Shortwave reflected	337.9	385.2	228.7
Shortwave balance	70.0	96.6	25.0
Albedo	0.83	0.90	0.78
Long-wave incoming	163.8	237.5	123.2
Long-wave outgoing	232.0	260.7	217.6
Long-wave balance	-68.2	-2.5	-97.0
All-wave balance	1.8	22.5	-12.4

Values are in watts per square meter.

*The extremes are the highest and lowest daily values.

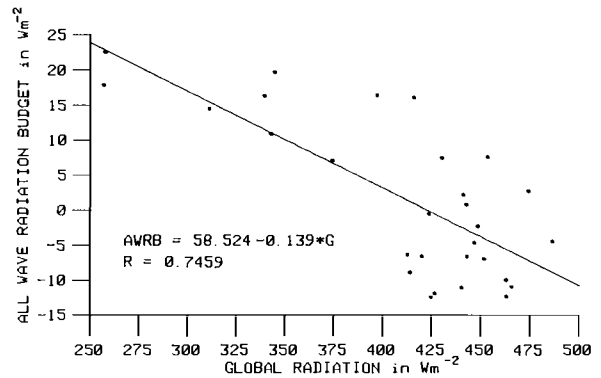


Fig. 12. Relation between global radiation (G) and all-wave radiation budget (AWRB).

surface is generally observed, while at night the flux has the opposite direction (positive flux).

On the average, the snow heat flux is negative, indicating that the snow was warmed after the cold winter. The snow heat flux is small, about 2 orders of magnitude less than the global radiation, and also smaller than the sensible heat flux, since conduction is a much less efficient way to transport energy than convection. Additionally, snow is a fairly good insulator.

Now the heat balance can be calculated as a whole, its components being presented for the mean of the entire period in Figure 19. The net shortwave radiation supplies most of the energy toward the surface. The second positive flux is the sensible heat, which means the air above the surface is cooled, on the average. Most of the energy received is lost as long-wave radiation. Further, and to a smaller degree, energy is used for sublimation of snow and to heat the snow cover.

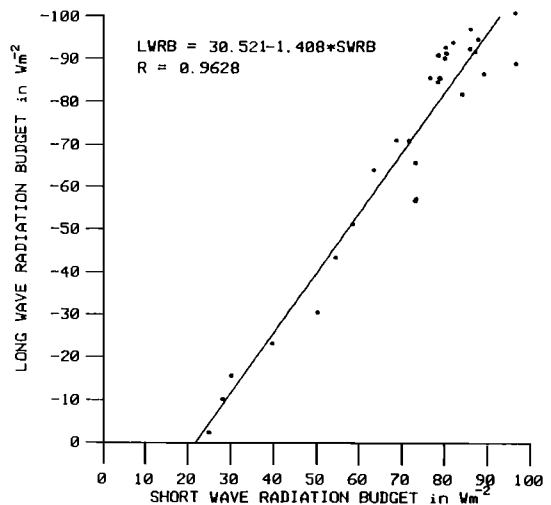


Fig. 13. Relation between the shortwave radiation budget (SWRB) and the long-wave radiation budget (LWRB) (note: y axis is inverted).

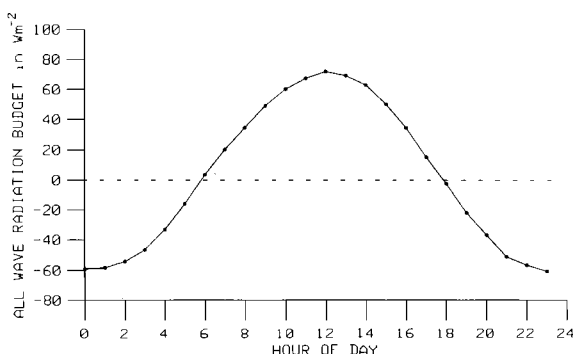


Fig. 14. Mean diurnal variation of the all-wave radiation budget for November 20 to December 22, 1985.

The imbalance of the fluxes is 3%, which might give an estimate of the accuracy of the estimations; a more detailed discussion of this is given by *Wendler et al.* [1988a].

2.3. Boundary Layer Measurements

In austral summer 1982/1983 and again in 1985/1986, measurements through the boundary layer were carried out in Adélie Coast. In the 1982/1983 profile, measurements were carried out (not simultaneously) at D47, D57, and D80, that is, from about 100 km to about 440 km inland. *Sorbjan et al.* [1986] reported on the results. In 1985/1986, three stations were occupied: D10 and D57 by French teams and D47 by a U.S. team. Part of the results were reported by *Kodama et al.* [1989] and *André et al.* [1993]. The second experiment was much larger. For the inland stations, balloons and kites were used as carriers; in the coastal area, drones were used in addition to balloons and kites.

In Figure 20 the mean profiles of potential temperature, wind speed, and wind direction are plotted at 3-hour intervals for D47. The data are from November/December 1985. The number of profiles used in obtaining the mean profiles varies. There were a total of 52

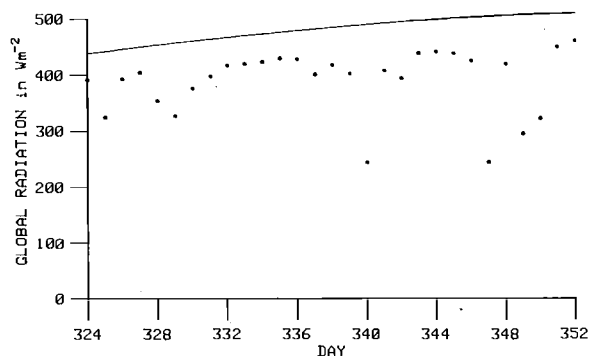


Fig. 15. Daily mean values of global radiation for D47, eastern Antarctica. The encompassing curve is the extraterrestrial radiation on the horizontal for this latitude, corrected for Earth-Sun distance.

successful profile measurements. For any specific time, however, the number of observations was not constant; for example, for the morning observation (0900 LST), which was a "standard" observation carried out simultaneously at the three slope stations, profile measurements were made most frequently. For more details, see *Kodama et al.* [1989]. These differences in numbers of observations might cause variations in the meteorological parameters, which should otherwise be small for the upper part of the profile for 3-hour intervals.

In the potential temperature profiles, two distinctive layers are seen: the lowest atmosphere influenced by the cooling and heating at the ground surface and the constant lapse rate layer aloft, which is insensitive to the variation of the thermal condition at the surface. The average of the vertical potential temperature gradient is 6.7°K per 1000 m. In Table 6 the depths of the thermal boundary layer are shown. They are defined here as the heights to which significant cooling or heating extends, as judged from the evolution of the profiles of the potential temperature deficit or surplus. At 1800 LST the potential temperature gradient in the lowest layer is almost the same as that in the free atmosphere. At 2100

TABLE 5. Direct Beam Solar Radiation Measurements for the Optical Air Mass 2 for Selected Polar Stations

	Latitude	Longitude	Altitude, m	Radiation, $W m^{-2}$	Reference
<i>Arctic Stations</i>					
Devon Ice Cap	75°30'N	83°10'W	1320	912	<i>Holmgren</i> [1971]
McCall Glacier	69°18'N	143°48'W	1740	906	<i>Shaw and Wendler</i> [1972]
Carrefour Greenland	69°49'N	47°26'W	1850	905	<i>Ambach and Markl</i> [1981]
<i>Antarctic Stations</i>					
Maudheim Station	71°03'S	10°56'W	37	954	<i>Liljequist</i> [1956]
Little America V	78°11'S	162°10'W	44	960	<i>Hoinkes</i> [1961]
Adélie Coast	67°23'S	138°43'E	1560	997	<i>Wendler et al.</i> [1988b]
Mizuho Station	70°42'S	44°20'E	2230	1034	<i>Yamanouchi</i> [1983]
Plateau Station	79°15'S	40°30'E	3265	1065	<i>Kuhn</i> [1971]

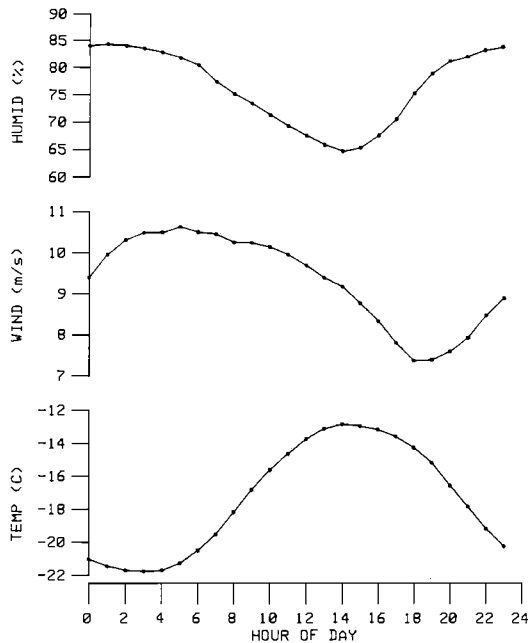


Fig. 16. Mean diurnal variation in hourly intervals of temperature, relative humidity, and wind speed on November 20 to December 22, 1985.

LST the cooling is developed at the lowest layer of the atmosphere and reaches a height of 200 m. At 0300 LST it is further developed, and the height of the inversion layer reaches 400 m. In the morning, at 0900 LST, the

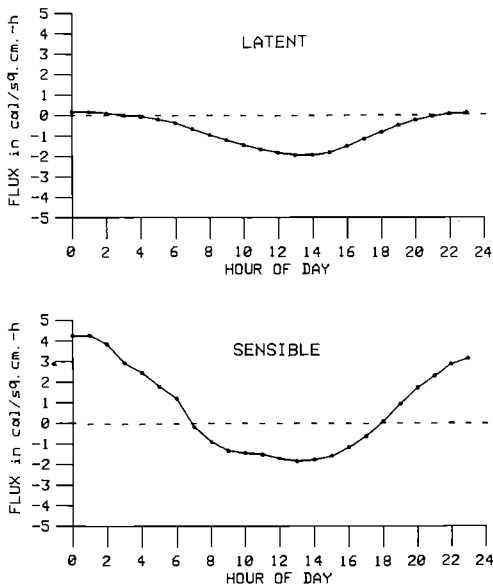


Fig. 17. Mean diurnal variation of the sensible and latent heat flux, November 20 to December 22, 1985. The diurnal curve of the latent heat flux was smoothed with a 3-point running mean.

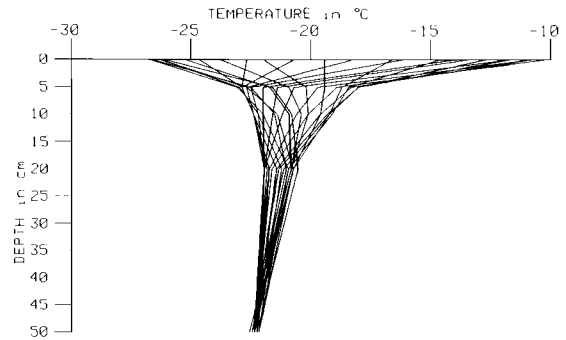


Fig. 18. Tautochrones of the snow temperature in hourly intervals for a totally clear summer day (November 29, 1985).

cooling is reduced from the ground surface, while the thermal boundary layer is increased to 500 m. At 1200 LST the constant potential temperature zone is seen, indicating that a mixing layer exists. At 1500 LST the lowest layer of the atmosphere has a slightly smaller lapse rate than that of the free atmosphere.

The general picture emerging from the wind profiles (Figure 20) is a pronounced low-level jet in all profiles. The wind increases from the surface to about 120–200 m in height, depending on the time of the day, having the local maximum wind speed at that height. Then it decreases to a height of 800–900 m, where the local minimum of the wind speed is seen. Further up, the wind speed increases with height.

The variations of the mean profiles of wind direction do not show a distinguished diurnal pattern; however, the change in wind direction is very small in both the boundary layer and the free atmosphere.

Figure 21 shows the average temperature profile obtained at D57 and Dumont d'Urville (Figure 1) at the hour 0900 LST during the experiment. The temperature profile at D57 shows an inversion layer from the surface (average surface pressure of 750 mbar) to the 720-mbar level, a constant temperature layer from the 720-mbar level to the 690-mbar level, and a constant lapse layer above the 690-mbar level. The temperature difference between D57 and Dumont d'Urville above the 690-mbar level is about 5°C. Since the distance between D57 and Dumont d'Urville is 200 km, the horizontal temperature gradient is 2.5°C per 100 km, which is equivalent to the horizontal temperature gradient calculated from the geostrophic wind shear observed at D47.

Figures 22a and 22b show the daytime and nighttime wind hodographs, respectively. One remarkable feature of the hodograph is the pronounced "spiraling" in the nighttime hodograph, especially at 0300 LST, when the cooling in the boundary layer is large. The spiraling is smaller for the daytime hodographs. Further, the change in the wind vector in the upper level can be approximated by a linear regression line, if the wind at that level is assumed to be in geostrophic shear and is

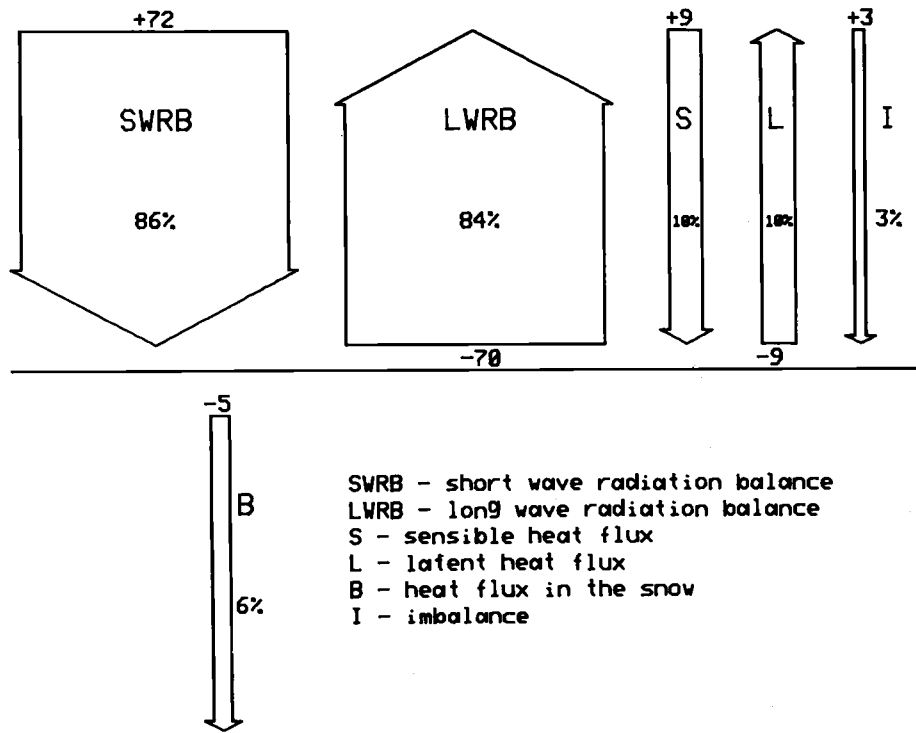


Fig. 19. Mean fluxes of the components of the heat balance for the period November 20 to December 22, 1985. The values are expressed in watts per square meter and in percent. For the calculation of the imbalance, the sum of all the outgoing fluxes was assumed to be 100%.

related to the mesoscale horizontal temperature gradient. The averaged geostrophic shear can be calculated using all the profile data ($N = 52$). This gives an average value of 8.2 m s^{-1} per 1000 m, pointing 58° from the fall line to the right. This corresponds to a horizontal temperature gradient of 2.5°C per 100 km to the north. The reason for this observed strong horizontal temperature gradient could be sought in the difference in thermal properties between the coastal areas and the open ocean.

Figure 22c shows the actual wind speed profiles and the calculated geostrophic wind profiles for 0300 LST and 1500 LST. The solid triangle (H) indicates the actual wind speed, and the solid line is the extrapolated regression line taken from the geostrophic wind profiles above 1000 m. At 0300 LST the actual wind speed (H) in the boundary layer is far larger than the calculated geostrophic wind (solid line), indicating the strong cooling at the surface. For the profiles at 1500 LST the actual wind speed profile is not substantially different from the calculated geostrophic wind, indicating weak cooling or heating at the sloping surface, which is also seen from the potential temperature profiles (Figure 20).

The extrapolation of the regression line described here to the ground surface gives the surface geostrophic wind $V_{gs} = [u_g(0), v_g(0)]$. It is due to the mesoscale

horizontal temperature gradient in the free atmosphere, and it is also the approximate surface geostrophic wind in the absence of katabatic wind. The average of the surface geostrophic wind obtained using all the profiles ($N = 52$) is 6.2 m s^{-1} in magnitude and points 316° from the north, almost normal to the fall line. If the katabatic and Coriolis forces are balanced, the wind direction should be normal to the fall line (210°) or 300° , assuming no temperature gradient exists along an altitude line. The observed average geostrophic wind,

$$6.0 \text{ m s}^{-1} = 6.2 \cos(316^\circ - 300^\circ) \text{ m s}^{-1}$$

would then correspond to the inversion intensity, $\Delta\theta = fV_g\theta/g\alpha$, of 3.3°K , assuming $f = 1.4 \times 10^{-4} \text{ s}^{-1}$, $\theta = 253^\circ\text{K}$, $g = 9.8 \text{ m s}^{-2}$, and $\alpha = 6.5 \times 10^{-3}$. This inversion intensity is typical for nighttime in summer. The difference of these two is found in that the surface geostrophic wind described here is semipermanent and the katabatic wind changes diurnally, strong during the night because of the strong cooling over the slope and weak during the day because of the heating at the ground.

We can now explain the reasons for the high wind directional constancy and the low-level jet. During nighttime the high constancy and low-level jet are

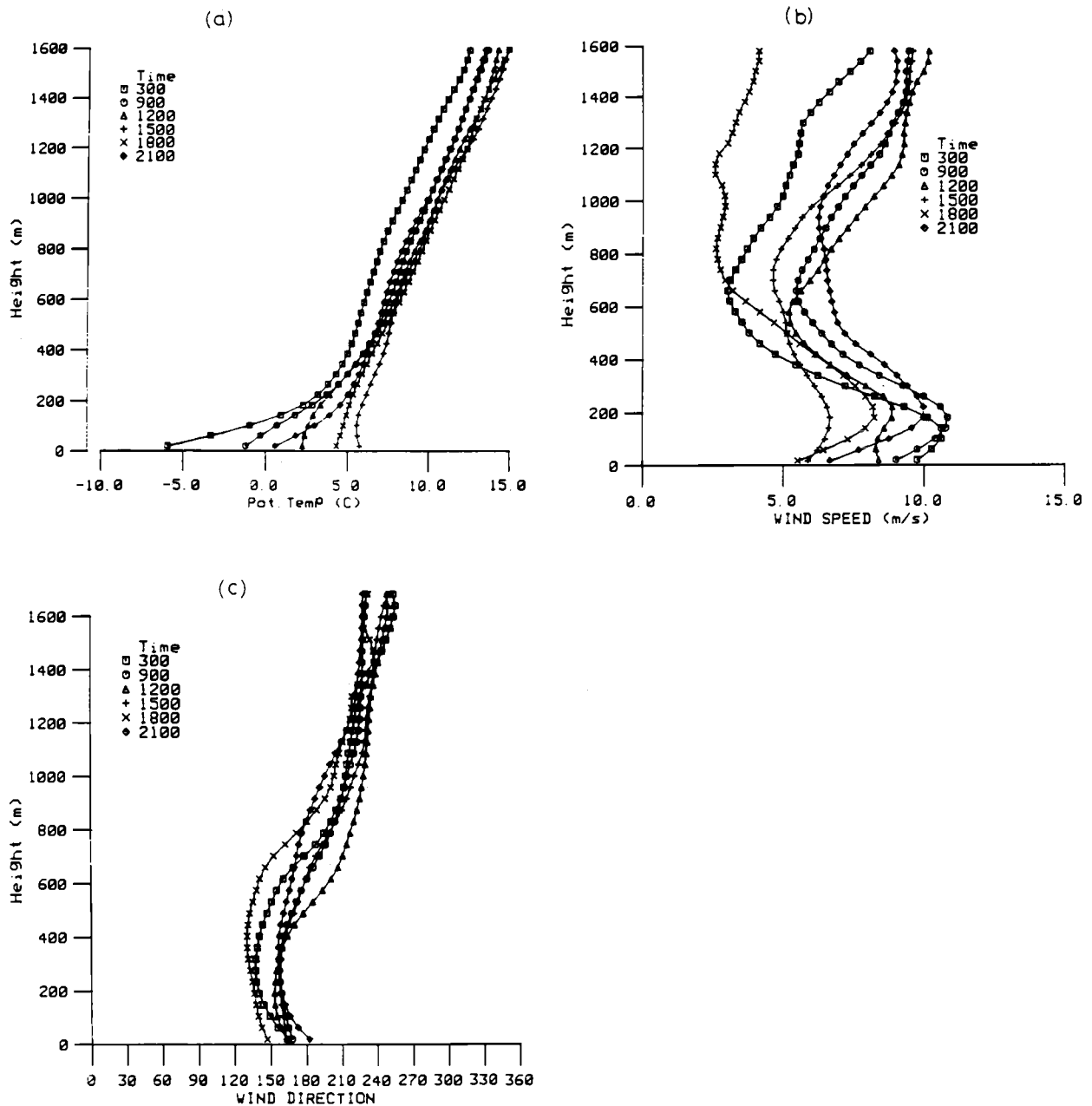


Fig. 20. Profile of (a) temperature, (b) wind speed, and (c) wind direction through the boundary layer, summer, Adélie Coast.

supported by the presence of an inversion layer over the sloping terrain, which generates katabatic wind. During daytime the surface geostrophic wind due to the mesoscale horizontal temperature gradient remains and acts just like the katabatic wind at night.

2.4. Blowing Snow

Strong winds over a snow surface transport snow. At moderate wind speeds this transport takes place close to

the surface and is called drifting snow. At higher wind speeds, normally values around 10 m s^{-1} , the snow is elevated to greater heights, and one speaks of blowing snow. A manifestation of this transport of snow is to be found in sastrugi, a kind of snow dune, which cover large parts of Antarctica. They are normally directed along the resultant wind vector. *Mather and Miller* [1967] used the direction of these sastrugi to deduce the mean wind field over Antarctica. Their results are in good agreement

TABLE 6. The Depth of the Thermal Boundary Layer (h_θ), the Height (h_u), and the Wind Speed ($W(h_u)$) of the Low-Level Wind Maximum

Hour	Number of Observations	h_θ , m	h_u , m	$W(h_u)$, m s^{-1}
0300	4	400	120	10.6
0900	20	500	150	10.8
1200	4	500	200	8.6
1500	6	600	200	6.6
1800	5	500	200	8.0
2100	13	200	150	10.0

with modeling studies which were carried out more than a decade later [Parish, 1982; Parish and Bromwich, 1987]. Such sastrugi are very pronounced in Adélie Coast and can reach heights exceeding 1 m.

Blowing snow can transport large amounts of snow, and this distribution can have great importance for glaciological studies [Radok, 1970]. It has been described as a low-level avalanche moving slowly to the edge of the Antarctic continent and then out to the ocean. Therefore it is of importance for the mass balance of Antarctica [Loewe, 1970]; however, the magnitude of this mass flux is poorly known [Polar Research Board, 1984].

All devices which catch snow particles directly have a certain collection efficiency, which can be fairly low and is often not known very well. Hence some 20 years ago the concept of detecting snow particles photoelectrically was first applied. Such instrumentation was first tested in Antarctica by the Australian Antarctic Division [Landon-Smith and Woodberry, 1965]. Hollung *et al.* [1966] developed the instrument further. Their work indicated the possibility of detecting individual snow particles by their shadows on photosensitive semiconductors. Not only the number of particles but also information on size and speed could be obtained. The instrument was further refined in the following years, mainly to avoid obstruction of the wind flow and to increase the signal to noise ratio. Finally, Schmidt

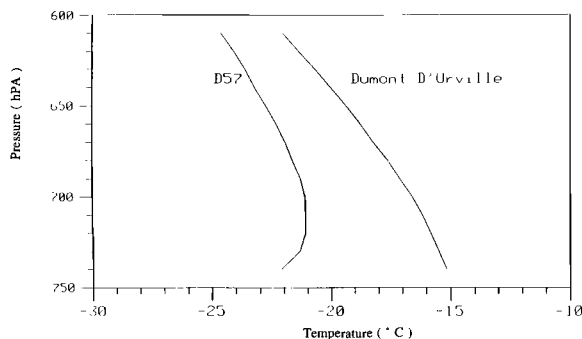


Fig. 21. The averaged temperature profile at 0900 LST at D57 and Dumont d'Urville.

[1977] wrote a detailed paper on the snow particle counter including design criteria. Following his basic design, but making a few improvements, two instruments were built and tested at the south pole [Wendler, 1990a, b].

One of the advantages of the instrument is the fact that linear relationships were found between both the number and size of particles and the output voltage. After successful calibration in the laboratory and testing at Pole Station, measurements were carried out in Adélie Coast [Wendler, 1988a, b, 1990a, b].

This device has two advantages over traditional snow traps: (1) little or no disturbance of the wind field and (2) high time resolution, about 2 orders of magnitude better than the traditional ones, which makes it much easier to relate wind speed variation to blowing snow flux.

Our measurements gave typical snow particle sizes in the 80- to 300- μm range, while the frequency was from

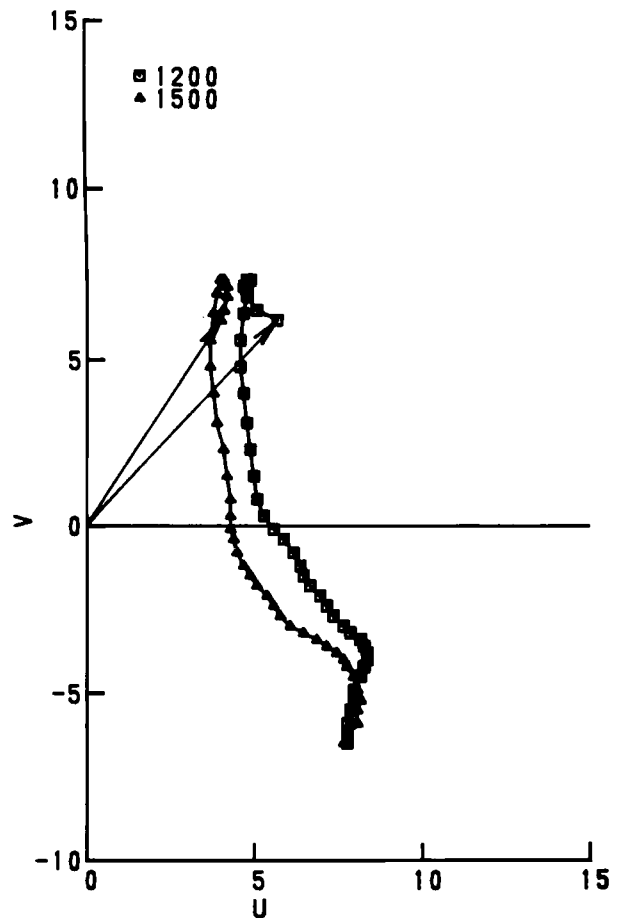


Fig. 22a. Wind hodograms through the boundary layer, summer, Adélie Coast: 1200 and 1500. U and V are in meters per second.

several hundred to a few thousand particles per square centimeter and second.

In Figure 23 the frequency (number of particles) and the mean size of the particles is plotted for one specific event of 2 minutes duration. Points were taken at 4-s intervals. It can be seen that stronger winds stir up not only more particles but also larger ones. While the blowing snow has been studied for a long time, the effects of the blowing snow on the katabatic wind have been much less investigated [Gosink, 1989]. There are at least two effects of the wind speed:

1. Snow suspended in the air increases the density of the air and thus increases the katabatic force.
2. Air moving down the Antarctic slope is adiabatically warmed, which results in unsaturated air. When blowing snow is present, the surface area of the snow is substantially increased, and the air will stay closer to saturation pressure all the time. This sublimation of snow particles cools the air.

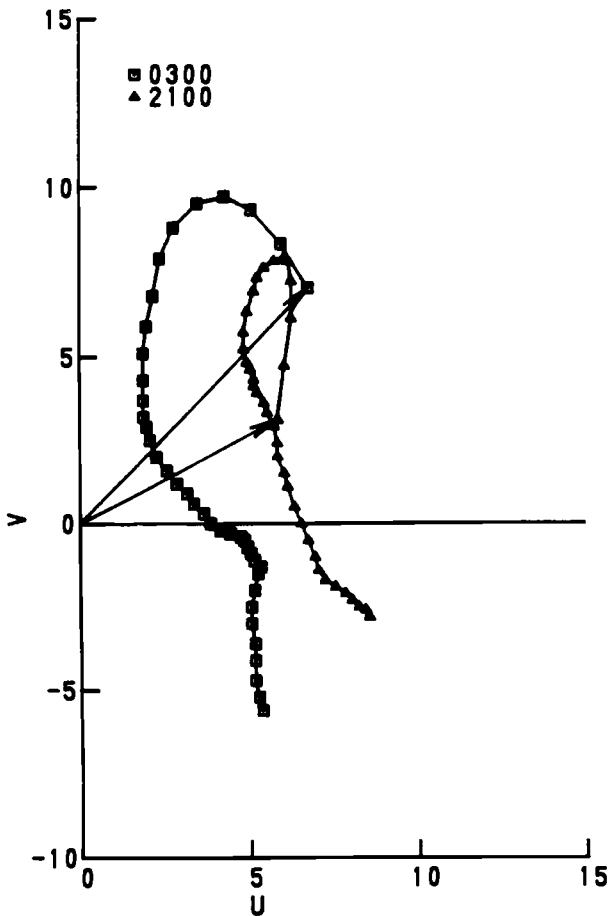


Fig. 22b. Wind hodograms through the boundary layer, summer, Adélie Coast: 0300 and 2100. *U* and *V* are in meters per second.

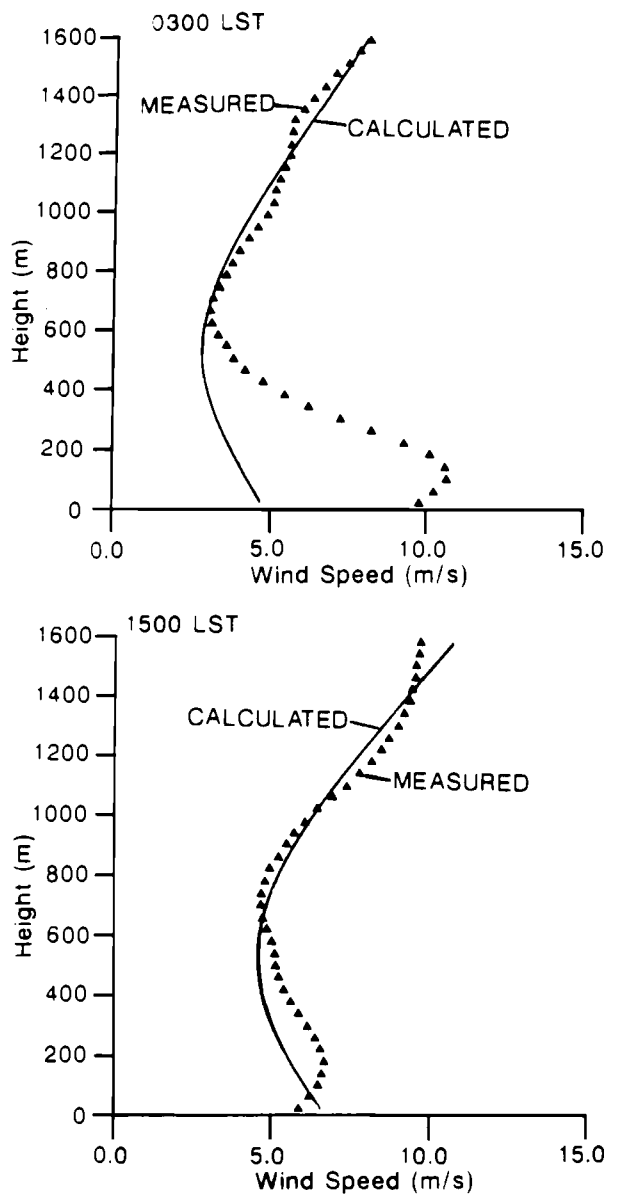


Fig. 22c. The actual wind profiles and the calculated geostrophic wind profiles for 0300 and 1500 LST, summer, D47, Adélie Coast.

A third, but probably less important effect of blowing snow is the change of the roughness parameter, which increases with blowing snow [König, 1985; Wendler, 1990a, b].

Kodama *et al.* [1985] investigated the two prior effects in greater detail. They expressed the increase in flux density due to the blowing snow as an additional cooling and therefore an increase in the katabatic force. For example, a snow load of 10 g m^{-3} means an increase of density equivalent to a cooling of 2°C [Loewe, 1974], which is equivalent to the average inver-

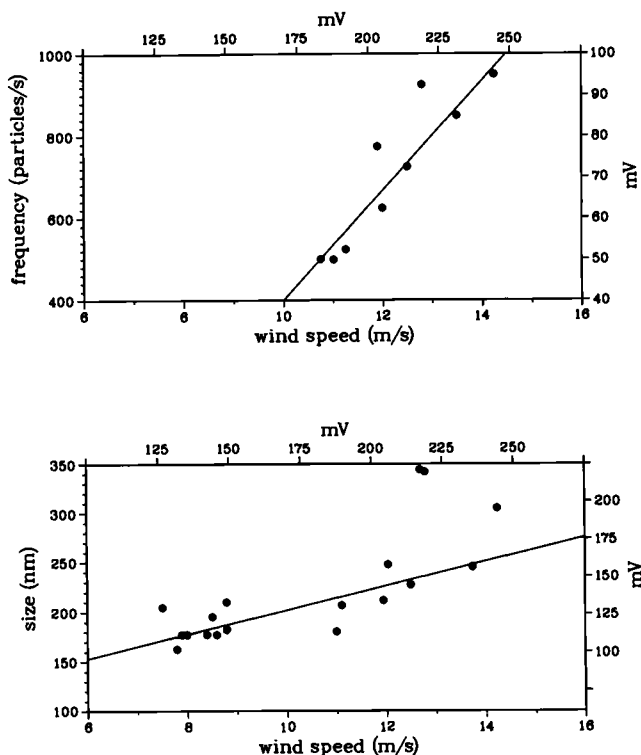


Fig. 23. Number of particles per second (frequency) and mean size of the particles against wind speed for one specific event (December 1, 1985) and one specific height (30 cm) at D47, eastern Antarctica.

sion strength in summer months in Antarctica [Phillpot and Zillman, 1970]. The cooling becomes important for the blowing snow density of a few grams per cubic meter. This density and higher ones were frequently observed for the wind speeds above 18 m s^{-1} at 10-m level at Byrd Station in Antarctica [Budd *et al.*, 1966].

The increased density in the katabatic flow layer due to the entrainment of blowing snow particles leads to stronger wind speeds as the result of increased katabatic force. Temperature and atmospheric pressure are, however, not directly affected by the entrained snow particles. This is one of the main reasons why the study of blowing snow is difficult. The katabatic force, KF , in case of blowing snow can be expressed in the following form:

$$KF = KF_a + KF_{bs}$$

where $KF_a = g\alpha(\Theta_f - \Theta_s)/\Theta$ and $KF_{bs} = g\alpha\rho_{bs}/\rho$. KF_a is the katabatic force in the case without blowing snow, and KF_{bs} is an additional force due to blowing snow; g and α are gravitational acceleration and slope of terrain, respectively; and ρ and Θ are density and potential temperature, respectively. The subscripts s , bs , and a indicate surface, blowing snow, and atmosphere. KF_{bs} cannot be calculated from the tempera-

ture and pressure because these two parameters are not directly changed by blowing snow.

According to the slab model of katabatic wind [Ball, 1956], wind speed is proportional to the cube root of katabatic force, i.e.,

$$V^3 = (KF)Q/k$$

where $Q = uh$ expresses net downslope transport of the medium, and where u , h , and k are downslope components of wind speed, depth of katabatic flow, and friction coefficient, respectively. For this derivation Ball assumed (1) negligible synoptic pressure gradient and (2) quadratic shear stress. Since the effect of snow particles entrained into the flow does not affect the value of temperature and pressure, KF_a in case of blowing snow becomes

$$KF_a = kV^3/Q - KF_{bs}$$

The transport rate of snow by wind, $\rho_{bs}Q$, can also be expressed to be about proportional to the cube of wind speed [Kobayashi, 1972; Dyunin, 1967]. Since KF_{bs} is proportional to ρ_{bs} , KF_{bs} is proportional to V^3/Q . Thus from the equation above it follows that

$$KF_a = (K - c)V^3/Q$$

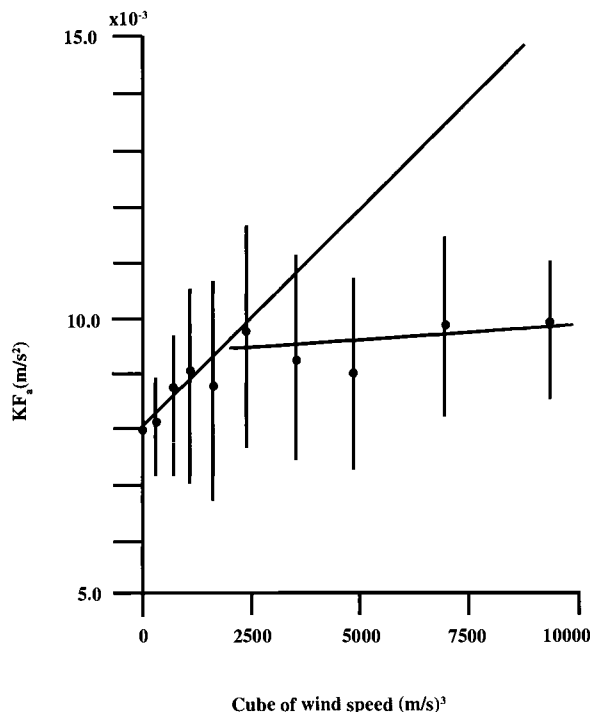


Fig. 24. Katabatic force and wind speed. Circles show averages for wind speed intervals of 2 m s^{-1} ; lines give 2 times the standard deviation. Two linear regression lines were drawn using lower six points and upper five points.

where c is a constant. The slope of the relationship of KF_a and V^3 is expected to be smaller for the case of blowing snow.

In Figure 24, KF_a is plotted against the cube of wind speed for D47. The solid circles indicate averages for wind speed intervals of 2 m s^{-1} . The length of the line attached to each circle gives twice the standard deviation. The numerical values above the abscissa give the number of observations for the interval. Two linear regression lines are drawn using the lower six points and the upper five points. It is obvious from Figure 24 that the slope for weaker wind speeds is steeper than that for stronger wind speeds. This may indicate the effect of blowing snow, as the stronger wind speeds, which reflect the effect of blowing snow, are increased with the relatively small increase in KF which does not take account of the effect of blowing snow. The wind speed at the terminal point of two regression lines (12.4 m s^{-1}) agrees quite well with the wind speed at which blowing snow density can be more than 1 g m^{-3} according to *Budd et al.* [1966] and our own observations in Adélie Coast.

In order to test whether the increase in wind velocity which occurs at wind speeds stronger than 12.4 m s^{-1} could be due to the increased density of the air with the entrained blowing snow, we compare the measured intensification of the wind with the theoretical intensification from entrained blowing snow. KF_{bs} is defined by the above given equation and appears in Figure 24 as the

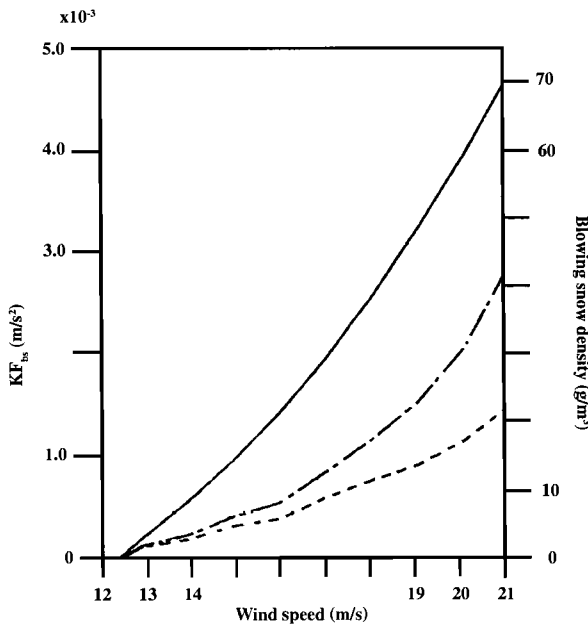


Fig. 25. KF_{bs} and wind speed. The right-hand ordinate is density of suspended snow required to explain the increase of wind speed. The dashed-dotted is the blowing snow density at 3 m for corresponding wind speed [*Budd et al.*, 1966]. The dashed line is the total effect of blowing snow including sublimation from the suspended snow particles.

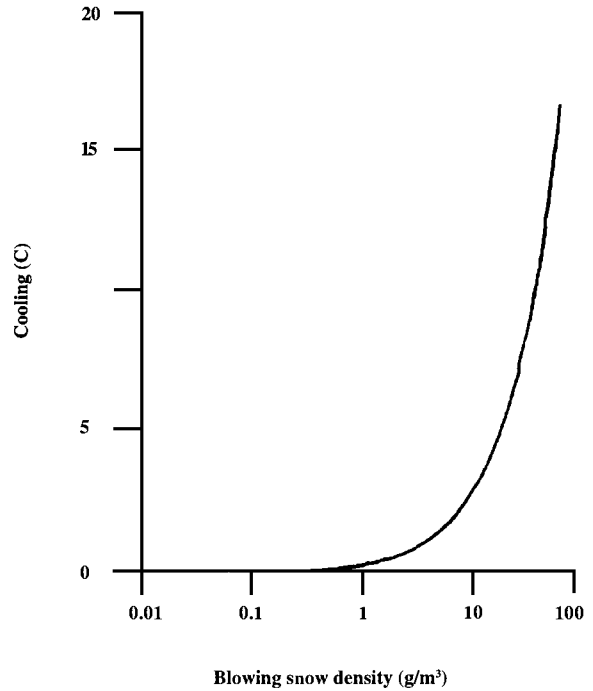


Fig. 26. Equivalent cooling by density increase due to blowing snow and blowing snow density. Curve is calculated for surface temperature of -20°C and inversion strength of 10°C .

difference between the two regression lines. It is plotted against wind speed (solid line) in Figure 25. The ordinate on the right of the figure is the amount of suspended snow required to explain the total increase of wind speed. This ordinate may be determined from Figure 26. For a wind speed of 18 m s^{-1} , for example, 39 g m^{-3} of suspended snow would be required. However, according to *Budd et al.* [1966], the amount of suspended snow is about one third of this value. A realistic amount of suspended snow as a function of wind speed is also given in Figure 25 (dashed line). Hence there must be an additional accelerative force.

A candidate to fill the gap is the additional cooling due to sublimation from blowing snow particles. Sublimation from blowing snow particles occurs because of the difference in vapor pressure at the surface of snow particles and the ambient air. It is difficult to achieve an accurate estimate of sublimation without knowledge of moisture in the katabatic flow. However, a rough estimation was done by assuming the following conditions: (1) The air is kept saturated with respect to ice. (2) Flow is downslope and stationary. (3) Sublimation occurs because of temperature increase by compression warming during descent. (4) Time for travel of air parcel is fixed to a time scale of gravity flow [after *Gosink*, 1983], so that the distance of descent depends on the wind speed. (5) The average sublimation of the whole layer is proportional to the depth of the blowing snow layer with

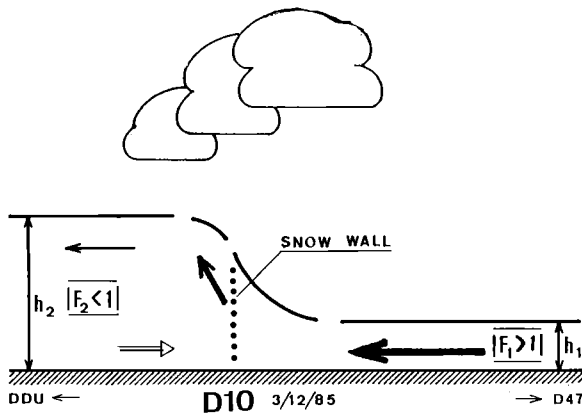


Fig. 27. Sketch of the Loewe phenomenon which occurred on December 3, 1985, at D10 near Dumont d'Urville, Adélie Coast, Antarctica. F represents the Froude number (see text).

densities of more than 1 g m^{-3} . Estimated cooling under these conditions is converted to the equivalent blowing snow density and added to Figure 25. This effect adds another 20–30% to the katabatic force. Hence suspended snow and sublimation of the snow particles can explain about two thirds of KF_{bs} .

2.5. Hydraulic Jump

The hydraulic jump, also called Loewe phenomenon from the first observer's name, generally occurs after the katabatic wind has persisted during several hours or even several days.

The jump itself can be seen as a frontal region where very strong variations of wind speed, temperature, and pressure take place. This front can be either stationary or slowly move downslope or upslope. It separates two regions: on the upstream side the wind is very strong with gales and blowing snow reducing the visibility, while on the downstream side one observes calm conditions [André, 1987].

Figure 27 shows the jump which occurred on December 3, 1985, as described by Pettré and André [1991]. The position of the jump is clearly marked at surface by a snow wall due to local strong turbulence and aloft by a line of cumulus due to ascending air moving with the jump. On December 3 a wind reversal was recorded after the snow wall had just passed the station at D10.

Figure 28 shows the surface measurements as the jump slowly moves upslope. The southerly surface wind suddenly drops from 20 m s^{-1} to -5 m s^{-1} as pressure simultaneously increases from 958.5 hPa to 964.2 hPa. Some minutes later, potential temperature increases from 264.6°K to 267.0°K, probably because

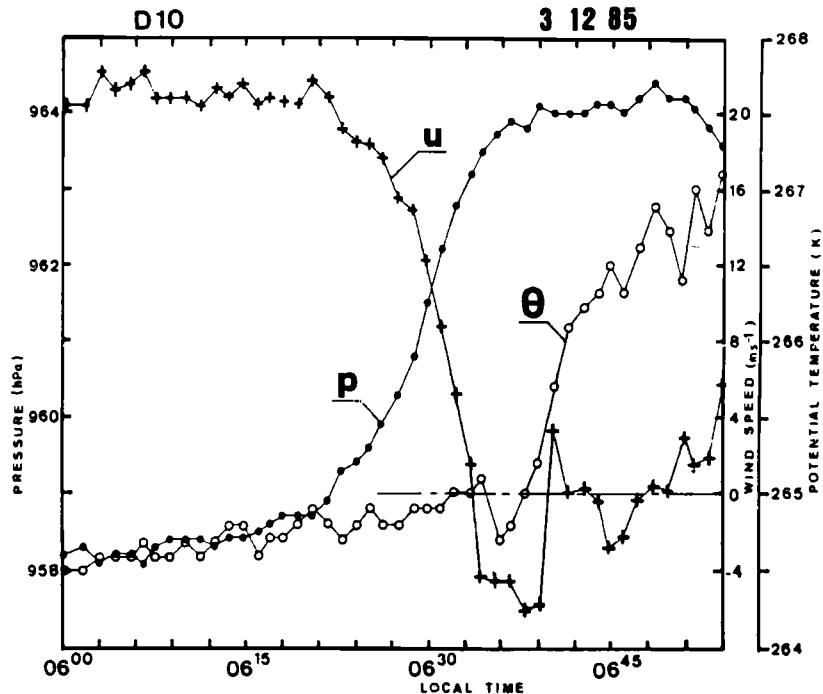


Fig. 28. Surface measurements of pressure (solid circles), potential temperature (open circles), and downslope wind speed (crosses) as function of local time during the phenomenon.

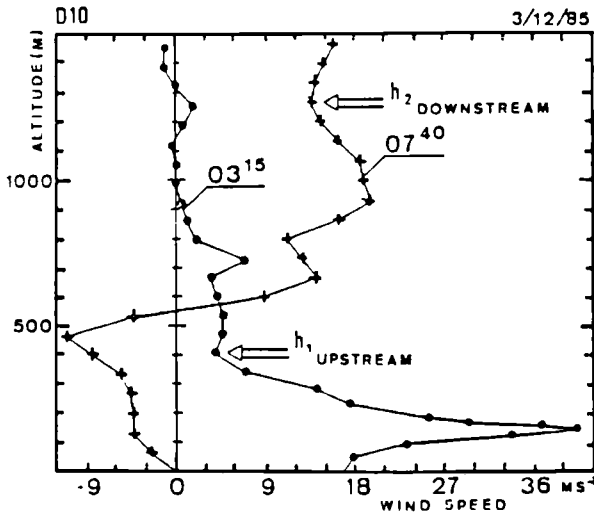


Fig. 29. Vertical profiles of downslope wind at D10 before/after upstream (0315 LT) and after/downstream (0740 LT) the December 3 jump.

of turbulent mixing with upper warmer air associated to the jump. Figure 29 shows the vertical profiles of the downslope component of the wind, before and after the jump, also interpreted as upstream and downstream conditions.

The usual method for evaluating the pressure change through the jump is based on analogy with hydraulic jumps in channels [Ball, 1956]. Following Ball, we consider a two-layer flow: the upper layer density is ρ' , and one supposes that the pressure P_H is constant over an horizontal surface at height H . Denoting by h the depth of the lower layer of density ρ , one can derive the surface pressure P using the hydrostatic approximation

$$P = P_H + \rho' g H + (\rho - \rho') g h.$$

The pressure jump through the hydraulic jump is then estimated as

$$\Delta P / \rho = (\Delta \rho / \rho) g \Delta h$$

with $\Delta \rho = \rho - \rho'$ or, using the Boussinesq approximation, as

$$\Delta P / \rho = (-\Delta \theta / \theta) g \Delta h$$

with $\Delta \theta = \theta - \theta'$.

A pressure jump $\Delta P = 0.9$ hPa is predicted from this last equation using observed data on December 3. It is very small in comparison with the observed value of 5.7 hPa, even taking into account the large errors made in estimating the parameters due to very difficult experimental conditions in Antarctica. Following Ball's method the change in depth of the katabatic layer is given by

$$h_2 / h_1 = \frac{1}{2} [(1 + 8F_1^2)^{1/2} - 1]$$

where $F_1 = U_1 / (g'h_1)^{1/2}$ is the upstream Froude number of the katabatic layer. Combining these last two equations, the change in depth becomes

$$\Delta P = \frac{\rho u_1^2}{2} \left\{ \frac{(1 + 8F_1^2)^{1/2} - 3}{F_1^2} \right\}$$

It is found from this equation that the maximum pressure change is always reached for $F_1^2 = 2 + 3(2)^{1/2}$. Consequently, the maximum pressure increase only depends on the kinetic energy of the katabatic layer upstream of the jump. On December 3, estimating an upstream wind velocity of 22.5 m s^{-1} , the maximum pressure change is 2.1 hPa, almost 3 times smaller than the observed value of 5.7 hPa.

It is then clear that, even taking into account various difficulties associated with data uncertainties, Ball's method is not able to predict large pressure changes as they are frequently observed in Antarctica (see also Lied [1964], who has observed a pressure change of 20 hPa through a hydraulic jump).

We propose below a new approach to estimating the pressure jump. Figure 30 shows the vertical structure of the downslope flow over 100 km from D47 to Dumont d'Urville, 8 hours before the jump occurrence at D10 (10 km upstream of Dumont d'Urville). The downstream sounding shows an unstable layer ($\chi \theta / \partial z < 0$) overlaying the katabatic layer, with a depth of about 570 m. It can then be safely assumed that turbulent mixing, due to the wind shear resulting from the downslope wind acceleration under katabatic effect, occurs just above the katabatic layer.

These experimental observations lead to schematically depicting the vertical cross section of the katabatic flow before the occurrence of the jump as in Figure 30. Let us consider two streamlines located very near each other at the top of the katabatic layer in the upstream part of the flow. Going downslope, these streamlines separate [Smith, 1985]: the lower one remains at the top of the katabatic layer, but the upper one caps an unstable layer as shown in Figure 31. These streamlines pass through layers where the Richardson number is large. Consequently, the turbulent effects can be safely neglected, making it possible to apply Bernoulli's theorem along two streamlines.

It is also assumed that the density variations are only due to temperature variations. Using the Boussinesq approximation, one derives the Boussinesq form of Bernoulli's theorem as

$$H = \frac{1}{2} \rho_0 q^2(z) + \Delta p - \rho_0 g \frac{\Delta T}{\bar{T}} z = \text{const}$$

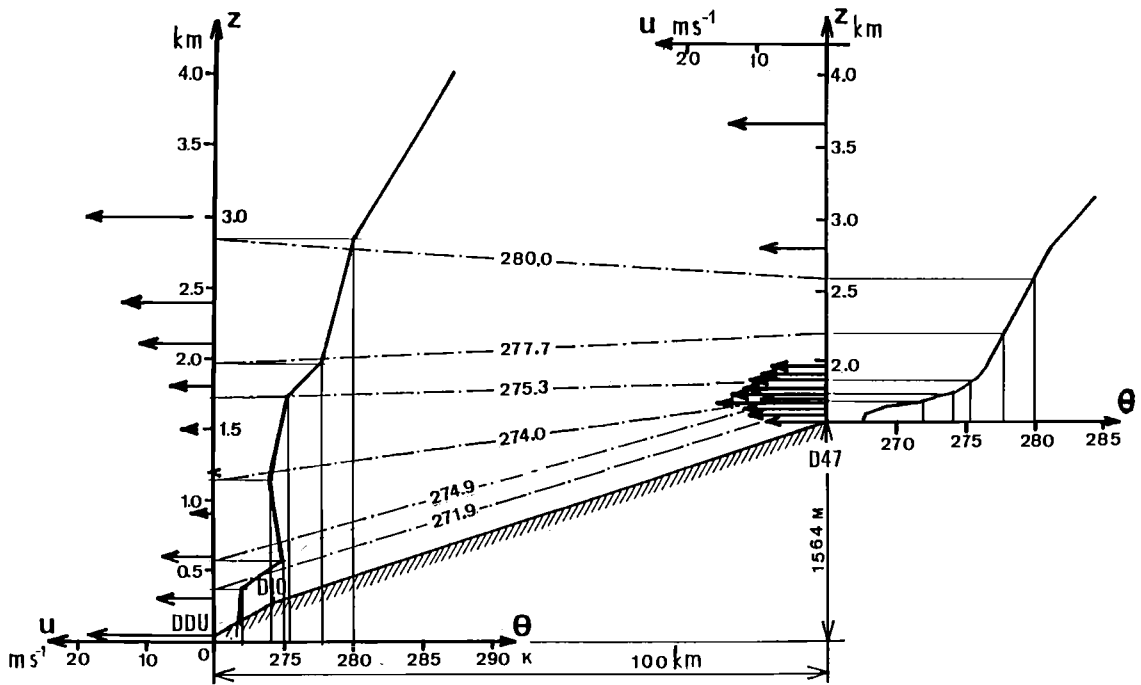


Fig. 30. Vertical cross section of the katabatic flow from D47 to Dumont d'Urville, 8 hours before the occurrence of the jump at D10.

where Δp and ΔT are the deviation of pressure and temperature, respectively, from a reference state with mean pressure \bar{p} and mean temperature \bar{T} .

Given the definition of the lower and upper streamlines as the lower and upper boundaries of the adiabatic layer with $\partial\theta/\partial z = 0$ between r_1 and r_2 , one easily shows that $\Delta T(z_1) = \Delta T(z_2) = \Delta T^*$. As disturbances above the upper streamline either vanish or are very small, it can be assumed that $\Delta p(z_2) = 0$. The pressure deviation along the lower streamline then reduces to

$$\Delta p(z_1) = -\frac{1}{2}\rho_0[q^2(z_1) - q^2(z_2)] - \rho_0 g \frac{\Delta T^*}{\bar{T}}(z_2 - z_1)$$

It is well known that Antarctic katabatic winds blow very severely. Our experimental data confirm that along the lower branch of the streamline, the wind velocity $q(z_1)$ is large because it scales with the katabatic wind speed, while, on the contrary, along the upper branch the velocity $q(z_2)$ scales with geostrophic wind and is much smaller.

As the wind drops through the hydraulic jump, unperturbed flow conditions are restored, and the pressure deviation can be neglected at point r'_1 downstream of the jump. As both r_1 and r'_1 lie at the same level z_1 , the reference pressure is the same at these two locations, so that

$$p_{r_1'} - p_{r_1} = -\Delta p(z_1) = \frac{1}{2}\rho_0[q^2(z_1) - q^2(z_2)] + \rho_0 g \frac{\Delta T^*}{\bar{T}}(z_2 - z_1)$$

The pressure jump is then given by the last equation, which for the conditions of December 3 is 5.7 hPa, while the strength of the inversion is 3°K, leading to a value of the velocity in the upper part of the katabatic layer of 29

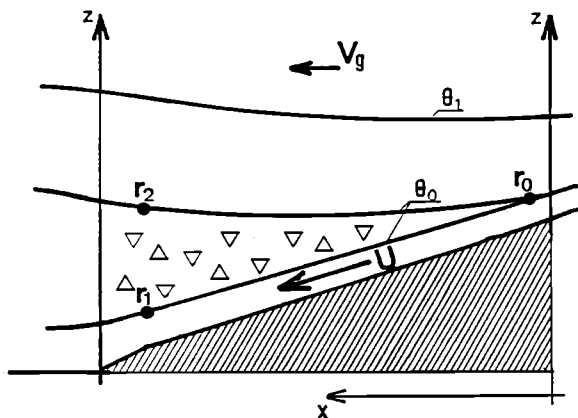


Fig. 31. Idealized flow cross section before the occurrence of the jump. Triangles indicate the unstable layer.

m s^{-1} , in good agreement with the experimental evidence (see Figure 29).

In summary, the careful study of the surface pressure change through a hydraulic jump has shown the following two features: (1) Bernoulli's theorem can be applied along the two streamlines at the top and at the base of the unstable layer as there the eddy stress can be neglected. (2) During strong wind periods the surface pressure is reduced, and the large surface pressure jump observed at the end of these periods is interpreted as a return to unperturbed conditions.

There is consequently an analogy between the vertical structure of strong katabatic flow and the severe downslope winds, with a transitional neutral or unstable layer developing, along the slope, over the surface layer with strong winds.

2.6. Modeling the Adélie Coast

Katabatic Winds

Numerical simulations have been conducted to explain the strong katabatic winds found in Adélie Coast. The model used is a three-dimensional, hydrostatic, primitive equation system adapted from *Anthes and Warner* [1978]. The model is written in terrain-following sigma coordinates; prognostic equations include the horizontal equations of motion, temperature, and continuity. Details of the equation system can be found in the work of *Parish and Waight* [1987].

A numerical simulation was carried out for Adélie Coast [*Parish and Wendler*, 1991]. This study incorporates a bulk treatment of the planetary boundary layer in which the entire planetary boundary layer is represented by a single layer. No explicit representation of the turbulent fluxes of heat and momentum is attempted within the boundary layer; rather, fluxes are related to surface conditions and the temperature and wind within the bulk layer. The boundary layer height is held constant at approximately 125 m corresponding to the height above ground level of the first sigma level in the model. The bulk approach is most suited for well-mixed boundary layers, which have been observed for Adélie Coast [*Kodama et al.*, 1985]. Such assumptions have also been used in previous studies of Antarctic winds [*Ball*, 1957, 1960]. The momentum flux in the lowest layer follows that of *Ball* [1960]. The frictional drag coefficient was set at 5.5×10^{-6} on the basis of comparisons with a two-dimensional version of the model incorporating a high-resolution boundary layer parameterization [*Pickett*, 1989]. The cooling rate within the lowest layer includes both radiational and sensible heat fluxes. A constant surface cooling rate of approximately 120 W m^{-2} was imposed. This value was obtained from results of the two-dimensional model as described by *Parish and Waight* [1987]; model-produced well-developed katabatic winds over the steep coastal slopes suggested strong downward directed tur-

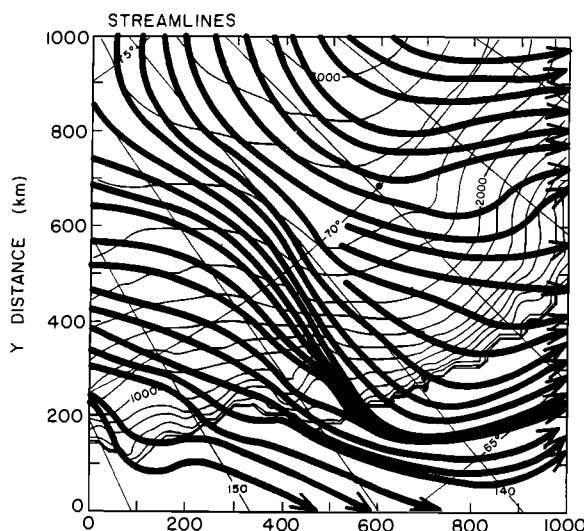


Fig. 32. Twelve-hour model results of streamlines for Adélie Coast katabatic wind simulation.

bulent heat fluxes of the order of 100 W m^{-2} and upward radiative heat fluxes near 20 W m^{-2} .

The model simulation for the Adélie Coast region encompasses a 51×51 model domain with a grid spacing of 20 km. Height values of the Adélie Coast terrain were obtained from a digitized version of the detailed map of *Drewry* [1983]. The simulation emphasizes the terrain-driven slope flows; effects of synoptic forcing are not included. The model is initialized about a state of rest in which the geostrophic wind components in the free atmosphere are set to zero. The model equations were integrated for a period of 12 hours, by which time near-steady conditions prevail.

Figure 32 illustrates the streamline pattern of the modeled drainage flow in the lowest sigma layer after the 12-hour integration period. Note that a marked confluence of the katabatic wind streamlines extends some 300 km from the interior of Adélie Coast to near Commonwealth Bay. The position and orientation of this modeled confluence zone agrees well with that shown by *Parish and Bromwich* [1987]. As discussed by *Parish* [1984], the confluence of negatively buoyant air in the interior of the continent provides a large supply of cold air available downslope. Persistent katabatic flow requires replenishment of negatively buoyant air; as noted by *Lettau and Schwerdtfeger* [1967], even moderate katabatic winds rapidly exhaust upwind reservoirs of radiatively cooled air. This confluence zone enables the katabatic winds along the axis of confluence and downwind to the coast to become significantly enhanced. This suggests that it is impossible to infer katabatic wind characteristics solely on the basis of local terrain slopes. It is essential that the katabatic

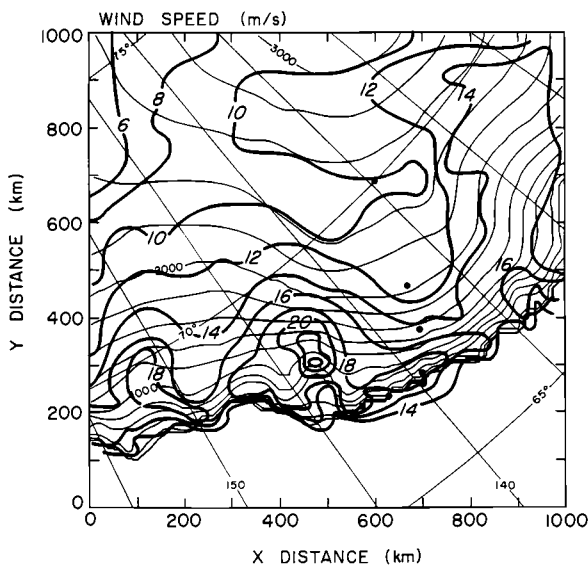


Fig. 33. Wind speed in meters per second after 12-hour model run for Adélie Coast katabatic wind simulation.

regime be viewed in a larger context; the pattern of upwind drainage currents is critical.

From Figure 32 the mean wind direction can be obtained. We did this for the locations of the AWS and found for D80, D57, D47, and D10 the following wind directions, respectively: 145°, 150°, 155°, and 155°. This is with the exception of D80 in agreement with the ground observation. The wind direction was taken for the nonsummer month, which is the time for which the model is valid. Less than 10° difference between model and observations was observed, which is in the same order with which the direction can be obtained from the map or the monthly observed changes of the ground observations [Wendler and Kodama, 1984]. However, for D80, the highest station, the observed wind direction was 170°, 25° more downslope than the model predicted. For the two coastal stations of Port Martin and Cape Denison, slightly more cross-slope winds were observed, as the model showed; however, as there is relatively a great deal of curvature in the flow lines, the determination of the direction from the map is not very accurate.

Results of the katabatic wind speeds in the lowest level of the model after the 12-hour integration are shown in Figure 33. The coupling between the katabatic wind speeds and the confluence zone is evident upon comparison of Figures 32 and 33. The strongest winds in excess of 24 m s⁻¹ are found along the axis of confluence in the vicinity of Commonwealth Bay and extending southeastward into the interior of the continent. Note that the strongest winds are not at the coast, but at some distance inland, a fact well confirmed by observations (Figure 9).

TABLE 7. Comparison of Modeled Wind Speed With Those Observed From the AWS

Station	Wind Speed (Modeled), m s ⁻¹	Wind Speed (Observed), m s ⁻¹
D80	10.0	6.8
D57	11.5	10.0
D47	14.5	12.8
D10	18.0	9.9
Port Martin	17.5	21.0
Cape Denison	18.5	23.0

When comparing the modeled speeds with those observed from the AWS, the agreement is good to fair. Again, as with the wind directions, the nonsummer month were used (see Table 7).

The model overestimates the winds in the interior (D80) but does a good job when going toward the coast. At the coast itself, it overestimates the speeds in the Dumont d'Urville area but underestimates the wind speed in the Port Martin/Cape Denison area.

In general, it can be stated that the model simulated well the overall diverse conditions of Adélie Coast, doing somewhat better in determining the directions than the speeds.

Acknowledgments. Many people helped in over a decade in making the measurements in Antarctica. There are too many to list by name; however, we are very thankful to all of them. U.S. Antarctic Research Program and Expeditions Polaires Françaises gave logistic support and NSF DPP, TAAF, and INSU gave financial support which is gratefully acknowledged.

REFERENCES

- Ambach, W., The influence of cloudiness on the net radiation balance of a snow surface with high albedo, *J. Glaciol.*, 13(67), 73–84, 1974.
- Ambach, W., and G. Markl, Messungen der atmosphärischen Trübung am Grönländischen Inlande während der Internationalen Glaziologischen Grönlandexpedition 1959 and 1967, *Polarforschung*, 51, 129–137, 1981.
- André, J. C., Des chercheurs dans le vent: Vous avez dit blizzard?, *Recherche*, 18(192), 1254–1256, 1987.
- André, J. C., P. Pettré, G. Wendler, and M. Zephoris, Vertical structure and downslope evolution of antarctic katabatic flows, in *Waves and Turbulence in Stably Stratified Flows*, edited by S. D. Mobbs and J. C. King, pp. 91–104, Clarendon, Oxford, 1993.
- Anthes, R. A., and T. T. Warner, The development of hydrodynamical models suitable for air pollution and other mesometeorological studies, *Mon. Weather Rev.*, 106, 1045–1078, 1978.
- Ball, F. K., The theory of strong katabatic winds, *Aust. J. Phys.*, 9(3), 373–386, 1956.
- Ball, F. K., The katabatic winds of Adélie Land and King George V. Land, *Tellus*, 9, 201–208, 1957.
- Ball, F. K., Winds on the icy slopes of Antarctica, in *Antarctic Meteorology*, pp. 9–16, Pergamon, New York, 1960.
- Budd, W. F., W. R. J. Dingle, and U. Radok, The Byrd snow drift project: Outline and basic results, in *Studies in Antarc-*

- tic Meteorology, Antarct. Res. Ser.*, vol. 9, edited by M. J. Rubin, pp. 71–134, AGU, Washington, D. C., 1966.
- Carroll, J. J., Long-term means and short-term variability of the surface energy balance at the south pole, *J. Geophys. Res.*, 87(6), 4277–4286, 1982.
- Dalrymple, P., H. Lettau, and S. Wollaston, South pole micrometeorology program: Data analysis, in *Studies in Antarctic Meteorology, Antarct. Res. Ser.*, vol. 9, edited by M. J. Rubin, pp. 13–57, AGU, Washington, D. C., 1966.
- Defant, F., Local winds, in *Compendium of Meteorology*, pp. 655–672, American Meteorological Society, Boston, Mass., 1951.
- Drewry, D. J., The surface of the Antarctic ice sheet, in *Antarctica: Glaciological and Geophysical Folio*, edited by D. J. Drewry, atlas sheet 2, Scott Polar Research Institute, Cambridge, England, 1983.
- Dyunin, A. K., Fundamentals of the mechanics of snow storms, in *Physics of Snow and Ice*, vol. 1(2), edited by H. Oura, pp. 1063–1076, Institute of Low Temperature Science, Sapporo, Japan, 1967.
- Forgan, B. W., I. Allison, A. Butterworth, and M. Gould, Aerosol optical depth measurements at Davis Base, Antarctica, in *Baseline Atmospheric Program (Australia), 1986*, edited by B. W. Forgan and P. J. Fraser, pp. 16–21, Department of Administrative Services/Bureau of Meteorology, Melbourne, Australia, 1988.
- Giovinetto, M., Mass accumulation in West Antarctica, *Eos Trans. AGU*, 42(3), 386–389, 1961.
- Gosink, J. P., Analysis of katabatic wind data between Dome Charlie and Dumont d'Urville, *Pure Appl. Geophys.*, 120, 506–526, 1983.
- Gosink, J. P., The extension of density current model of katabatic winds to include the effects of blowing snow and sublimation, *Boundary Layer Meteorol.*, 49, 367–394, 1989.
- Hisdal, V., Norwegian-British-Swedish Antarctic Expedition 1949–1952, scientific results: Temperature, *Norsk Polarinst. Oslo*, 1(2), 125, 1960.
- Hoinkes, H., Studies of solar radiation and net radiation in the Antarctic, *Arch. Meteorol. Geophys. Bioklimatol.*, Ser. B, 10, 175–181, 1961.
- Hollung, O., W. E. Rogers, and J. A. Businger, Development of a system to measure the density of drifting snow, joint technical report, 54 pp., Electr. Eng., Dep. Atmos. Sci., Univ. of Wash., Seattle, 1966.
- Holmgren, B., Climate and energy exchange on a subpolar ice cap in summer, in *Arctic Institute of North America, Devon Island Expedition 1961–1963*, pp. 107–112, Meddelanden fran Uppsala Universitets Meteorologiska Institution, Uppsala, Sweden, 1971.
- Ishikawa, N., S. Kobayashi, T. Ohtake, and S. Kawaguchi, Some radiation properties at Mizuho Station, East Antarctica in 1980, *Memo. Spec. Issue 24*, pp. 19–31, Natl. Inst. of Polar Res., Tokyo, 1982.
- Ishikawa, N., Y. Kodama, and G. Wendler, Meteorological features in Adélie Land during the austral summer season, *Pure Appl. Geophys.*, 132, 439–455, 1990.
- Kobayashi, D., Studies of snow transport in low-level drifting snow, *Contrib. Inst. Low Temp. Sci.*, Ser. A, 24, 1–58, 1972.
- Kodama, Y., G. Wendler, and J. Gosink, The effect of blowing snow on katabatic winds in Antarctica, *Ann. Glaciol.*, 6, 59–62, 1985.
- Kodama, Y., G. Wendler, and N. Ishikawa, On the diurnal variation of the boundary layer in summer in Adélie Land, eastern Antarctica, *J. Appl. Meteorol.*, 28(1), 16–24, 1989.
- König, G., Roughness length of an Antarctic ice shelf, *Polarforschung*, 55(1), 27–32, 1985.
- Kuhn, M., Messung und Analyse der spektralen Transparenz der Ostantarktischen Atmosphäre, dissertation, Univ. of Innsbruck, Innsbruck, Austria, 1971.
- Kuhn, M., L. S. Kundla, and L. A. Stroschein, The radiation budget at Plateau Station, Antarctica 1966–1967, in *Meteorological Studies at Plateau Station, Antarctica, Antarct. Res. Ser.*, vol. 25, edited by J. A. Businger, pp. 41–73, AGU, Washington, D. C., 1977.
- Landon-Smith, I. H., and B. Woodberry, The photo-electric metering of windblown snow, *Interim Rep. Ser. A(IV), Glaciol. Publ. 79*, 18 pp., Antarct. Div., Dep. of External Affairs, Melbourne, Australia, 1965.
- Lettau, H. H., and W. Schwerdtfeger, Dynamics of the surface wind regime over the interior of Antarctica, *Antarct. J. U.S.*, 2(5), 155–158, 1967.
- Lied, N. T., Stationary hydraulic jumps in a katabatic flow near Davis, *Aust. Meteorol. Mag.*, 47, 40–51, 1964.
- Liljequist, G. H., Energy exchange of an Antarctic snow-field, in *Norwegian-British-Swedish Antarctic Expedition 1949–1952, Scientific Research II: Short Wave Radiation*, Norsk Polarinstitut, Oslo, 1956.
- Loewe, F., *Études de Glaciologie en Terre Adélie 1951–1952, Expédition Polaires Françaises-Paris*, p. 148, Hermann, 1956.
- Loewe, F., The transport of snow on ice sheet by the wind, in *Studies of Drifting Snow*, vol. 13, 69 pp., Meteorology Department, University of Melbourne, Melbourne, Australia, 1970.
- Loewe, F., The land of storms, *Weather*, 1972, 110–121, 1972.
- Loewe, F., Considerations concerning the winds of Adélie Land, *Z. Gletscherkd. Glazialgeol.*, 10, 189–197, 1974.
- Mather, K. B., and G. S. Miller, The problem of katabatic wind on the coast of Terre Adélie, *Polar Rec.*, 13, 425–432, 1967.
- Parish, T. R., Surface airflow over East Antarctica, *Mon. Weather Rev.*, 110, 84–90, 1982.
- Parish, T., A numerical study of strong katabatic winds over Antarctica, *Mon. Weather Rev.*, 112, 545–554, 1984.
- Parish, T. R., and D. H. Bromwich, The surface windfield over the Antarctic ice sheets, *Nature*, 328, 51–54, 1987.
- Parish, T. R., and K. T. Waight, The forcing of Antarctic katabatic winds, *Mon. Weather Rev.*, 115, 2214–2226, 1987.
- Parish, T., and G. Wendler, The katabatic wind regime at Adélie Land, *Int. J. Climatol.*, 11, 97–107, 1991.
- Périard, C., and P. Pettré, Climatology of Dumont d'Urville, Adélie Land, Antarctica, *Rep. 2*, 19 pp., Centre Natl. De Rech. Meteorol., Toulouse, France, 1991.
- Pettré, P., and J. C. André, On the surface pressure change through Loewe's phenomena and katabatic flow jumps: Study of two cases in Adélie Land, Antarctica, *J. Atmos. Sci.*, 48, 557–571, 1991.
- Phillip, H. R., and J. W. Zillman, The surface temperature inversion over the Antarctic Continent, *J. Geophys. Res.*, 75, 4161–4169, 1970.
- Pickett, J. L., A mixed-layer model of katabatic winds, M.S. thesis, Dep. of Atmos. Sci., Univ. of Wyo., Laramie, 1989.
- Polar Research Board, *The Polar Regions and Climatic Change*, National Academy of Sciences, Washington, D. C., 1984.
- Radok, U., Boundary processes of drifting snow, in *Studies of Drifting Snow*, vol. 13, 20 pp., Meteorology Department, University of Melbourne, Melbourne, Australia, 1970.
- Radok, U., and G. Wendler, Plateau Weather, a synoptic study of IAGO and ANARE AWS observations in East Antarctica, in *Proceedings of the Symposium on Global Change in Polar Regions*, vol. 1, edited by G. Weller, C. Wilson, and B. Severin, pp. 192–198, Fairbanks, Alas., 1991.
- Rusin, N. P., *Meteorological and Radiational Regime of Antarctica, Leningrad* (in Russian), 355 pp., 1961. (English translation Israel Program for Scientific Translations, Jerusalem, 1964.)
- Schmidt, R. A., A system that measures blowing snow, *Forest*

- Serv. Res. Pap. RM-194*, 80 pp., U.S. Dep. of Agric., Washington, D. C., 1977.
- Schwerdtfeger, W., *World Survey of Climatology*, vol. 14, *The Climate of Antarctica*, pp. 253–355, Elsevier, New York, 1970.
- Schwerdtfeger, W., *Weather and Climate of the Antarctic*, 261 pp., Elsevier Science, New York, 1984.
- Shaw, G., and G. Wendler, Atmospheric turbidity measurements at McCall Glacier in northeast Alaska, in *Conference on Atmospheric Radiation, August 1972, Fort Collins, Colorado*, pp. 181–187, Boston, Mass., 1972.
- Simpson, G. C., *British Antarctic Expedition 1910–1913, Meteorology*, vol. 1, *Discussion*, 326 pp., Tacker, Spink, Calcutta, India, 1919.
- Smith, R. B., On severe downslope winds, *J. Atmos. Sci.*, **42**, 2598–2603, 1985.
- Sorbjan, Z., Y. Kodama, and G. Wendler, Observational study of the atmospheric boundary layer over Antarctica, *J. Clim. Appl. Meteorol.*, **25**(5), 641–651, 1986.
- Stearns, C., Automatic weather station technical manual, Dep. of Meteorol., Univ. of Wis., Madison, 1982.
- Stearns, C., and G. Wendler, Research results from Antarctic automatic weather stations, *Rev. Geophys.*, **26**, 45–61, 1988.
- van Loon, H., The half-yearly oscillation in middle and high southern latitudes and the coreless winter, *J. Atmos. Sci.*, **24**, 472–486, 1967.
- Weidner, G., Automatic weather station technical manual, Dep. of Meteorol., Univ. of Wis., Madison, 1987.
- Wendler, G., The “radiation paradox” on the slopes of the Antarctic Continent, *Polarforschung*, **56**, 33–41, 1986.
- Wendler, G., Blowing snow in eastern Antarctica, *Antarct. J.*, **22**, 1987 review, 264–265, 1988a.
- Wendler, G., Measuring blowing snow in Adelie Land, eastern Antarctica, paper presented at Second Conference on Polar Meteorology and Oceanography, Am. Meteorol. Soc., Madison, Wis., 1988b.
- Wendler, G., Strong gravity flow observed along the slope of eastern Antarctica, *Meteorol. Atmos. Phys.*, **43**, 127–135, 1990a.
- Wendler, G., On the blowing snow in Adelie Land, eastern Antarctica, in *Glacier Fluctuations and Climatic Change*, edited by J. Oelemans, pp. 261–279, Kluwer Academic, Hingham, Mass., 1990b.
- Wendler, G., and N. Ishikawa, Measurements of atmospheric turbidity at D47, Adélie Land, Antarctica, *Polarforschung*, **58**(1), 41–46, 1988.
- Wendler, G., and Y. Kodama, On the climate of Dome C, Antarctica, in relation to its geographical setting, *J. Climatol.*, **4**, 495–508, 1984.
- Wendler, G., and Y. Kodama, The kernlose winter in Adélie Land, this volume.
- Wendler, G., and P. Nicpon, Low-level temperature inversions in Fairbanks, central Alaska, *Mon. Weather Rev.*, **103**, 34–44, 1975.
- Wendler, G., N. Ishikawa, and Y. Kodama, On the heat balance of the icy slope of Adelie Land, eastern Antarctica, *J. Appl. Meteorol. Oceanogr.*, **27**, 52–65, 1988a.
- Wendler, G., N. Ishikawa, and Y. Kodama, On the heat balance of the icy slope of Adélie Land, eastern Antarctica, *J. Appl. Meteorol.*, **27**, 52–65, 1988b.
- Wexler, H., The “kernlos” winter in Antarctica, *Geophysika*, **6**, 577–595, 1958.
- Yamanouchi, T., Variations of incident solar flux and snow albedo on the solar zenith angle and cloud cover at Mizuho Station, Antarctica, *J. Meteorol. Soc. Jpn.*, **61**, 879–893, 1983.

(Received October 15, 1991;
accepted October 5, 1992.)

SPATIAL AND TEMPORAL CHARACTERISTICS OF THE INTENSE KATABATIC WINDS AT TERRA NOVA BAY, ANTARCTICA

DAVID H. BROMWICH,¹ THOMAS R. PARISH,² ANDREA PELLEGRINI,³ CHARLES R. STEARNS,⁴ AND GEORGE A. WEIDNER⁴

Two years of automatic weather station observations describing the linkage between the inland confluence zone and the intense coastal katabatic wind regime at Terra Nova Bay, Antarctica, are analyzed. A highly stable wind regime is described by the data with the air over the plateau converging into the head of Reeves Glacier, descending dry adiabatically to the Nansen Ice Sheet, and apparently accelerating horizontally down the local pressure gradient to Inexpressible Island, which is situated along the western shore of Terra Nova Bay. This low-level jet of cold air is laterally confined and is only slightly responsive to synoptic forcing. The internal dynamics of the airstream is the dominant factor determining its behavior. Lateral fluctuations in the katabatic wind are primarily controlled by buoyancy variations.

1. INTRODUCTION

The surface wind field over the sloping ice fields of Antarctica has a small vertical extent of a few hundred meters, and a continent-wide horizontal scale of thousands of kilometers. From a broad perspective [Mather and Miller, 1967], surface air blows radially away from the highest points of the terrain toward the coast. Because of continuity considerations this low-level divergence requires inflow aloft and sinking motion over the continent. This tropospheric convergence generates cyclonic vorticity via conservation of angular momentum and plays a key role in centering the circumpolar vortex over the crest of the East Antarctic ice sheet [James, 1989; Parish and Bromwich, 1991a]. This asymmetry of the circumpolar vortex with respect to the rotation axis of the Earth is thought to excite a wave number one response which contributes to the development of the primary region for blocking in the southern hemisphere near New Zealand [James, 1988; Watterson and James, 1992]. Thus the Antarctic katabatic wind regime has a far greater tropospheric impact than would be expected from the shallow nature of the flow.

With the development of accurate topographic maps of the Antarctic ice masses by the glaciological commu-

nity [e.g., Drewry, 1983], it became possible to diagnose the time-averaged streamline pattern of surface airflow over Antarctica [Parish, 1982] from the simple equation system of Ball [1960]. This expresses a steady state force balance between the pressure gradient due to the presence of cold near-surface air over sloping terrain, the Coriolis force, and friction. From estimates of the terrain slopes and of the temperature stratification of the lower atmosphere, Parish and Bromwich [1987] diagnosed the airflow pattern over Antarctica (Figure 1) from the Ball model. In contrast to earlier depictions, the airflow was found to exhibit very marked spatial variations; as air flows away from the summit of the ice sheet, it converges into a limited number of narrow zones just inland from the steep coastal ice slopes. In these so-called "confluence zones," radiatively cooled air from a large interior section of the ice sheet is concentrated. These features provide an enhanced supply of negatively buoyant air to downwind coastal slopes allowing the katabatic winds to be intensified and more persistent. This situation has been advanced as the primary explanation for the intense katabatic wind regimes found at Cape Denison/Port Martin in Adélie Coast [Parish, 1981] and Terra Nova Bay [Bromwich and Kurtz, 1984].

For the last few years a comprehensive program has been underway near Terra Nova Bay to understand the critical linkage between the inland confluence zone and the intensified katabatic winds near the coast. Study strategies have included aircraft measurements of the planetary boundary layer characteristics [Parish and Bromwich, 1989a], airborne mapping of the streamline pattern over the plateau [Bromwich et al., 1990a],

¹Byrd Polar Research Center, The Ohio State University, Columbus, Ohio 43210.

²Department of Atmospheric Science, University of Wyoming, Laramie, Wyoming 82071.

³ENEA, Antarctic Project, Rome, Italy.

⁴Department of Atmospheric and Oceanic Sciences, University of Wisconsin, Madison, Wisconsin 53706.

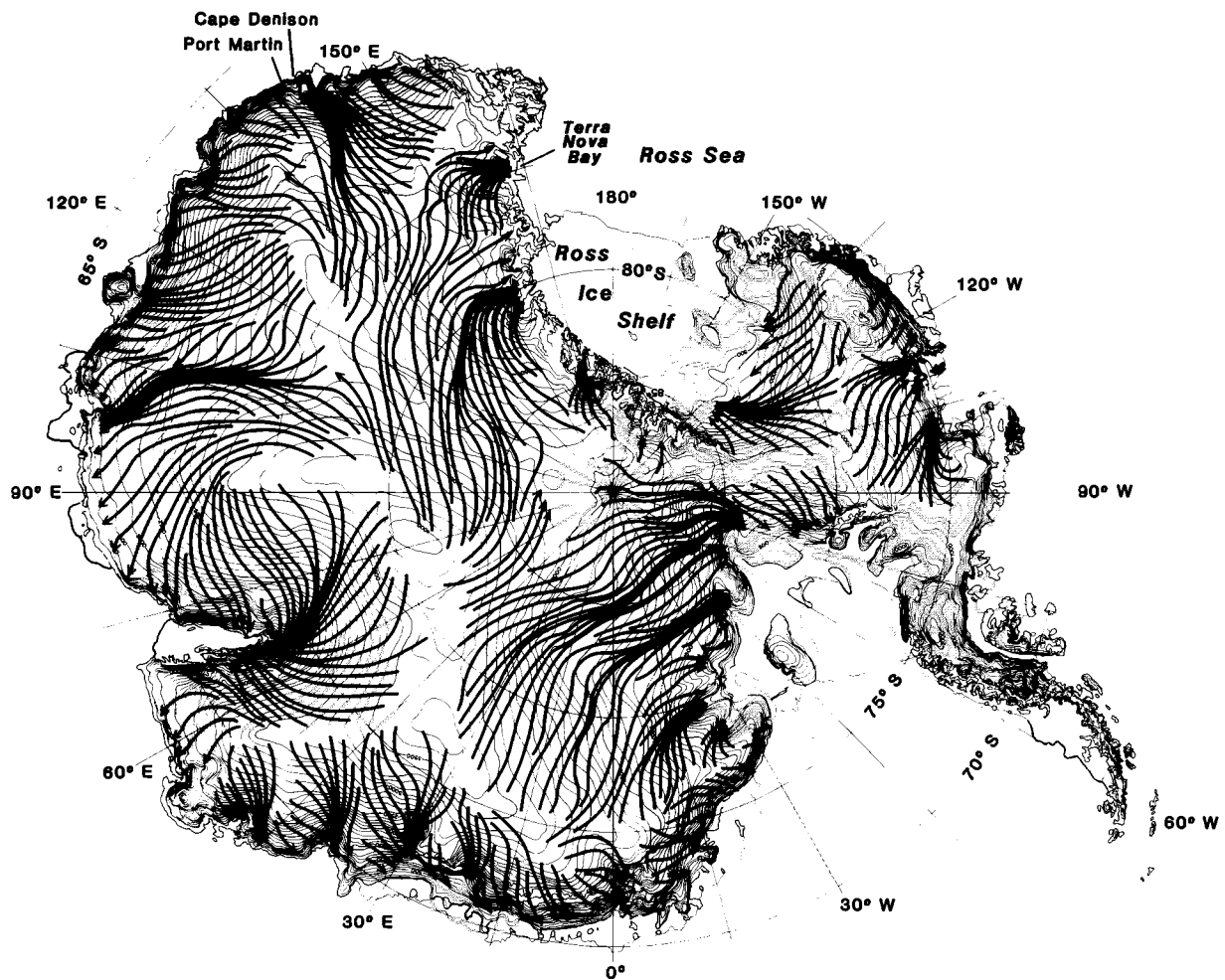


Fig. 1. Time-averaged streamlines (heavy lines) of winter airflow over Antarctica from *Parish and Bromwich* [1987]. Light lines are elevation contours in 100-m increments.

numerical modeling [*Parish and Bromwich*, 1989b; *Bromwich et al.*, 1990a], and investigations of satellite-observed wind signatures at thermal-infrared wavelengths [*Bromwich*, 1989a; *Bromwich and Geer*, 1991; *Bromwich and Ganobcik*, 1992]. In early 1988 an array of four automatic weather stations (AWS; 09, 21, 23, and 27) on the plateau was added to the coastal unit at Inexpressible Island (05) which was first deployed in 1984 (Figure 2). The results from 4 years of intermittent data collection at the latter site are described by *Bromwich* [1989b]. These five U.S. platforms were complemented by four AWS (50, 51, 52, and 53) deployed a year earlier by the Italian Antarctic Program. In 1989 another U.S. AWS (site 31) was located on the Nansen Ice Sheet halfway between the foot of Reeves Glacier and Inexpressible Island. Stations 06 and 13 have been operating since the early 1980s. The knowledge ob-

tained by analyzing nearly 2 years of data (1988 and 1989) from the full AWS array (see Table 1) is reported here and is integrated with the findings from the diverse analyses referenced above. The period starts in February 1988, the first full month for which all stations were deployed. A brief summary of the results for February 1988 to January 1989 was presented by *Bromwich et al.* [1990b], and some related analyses were conducted by *Parish and Bromwich* [1991b]. In the next section, data limitations from AWS deployments in such a windy area are discussed. Section 3 outlines the time-averaged characteristics of the interior and coastal winds and temperatures. Section 4 presents an analysis of the time-varying behavior of the fields on daily, synoptic, seasonal, and interannual time scales, and the final section provides an overview and offers some ideas for closing the remaining gaps in knowledge.

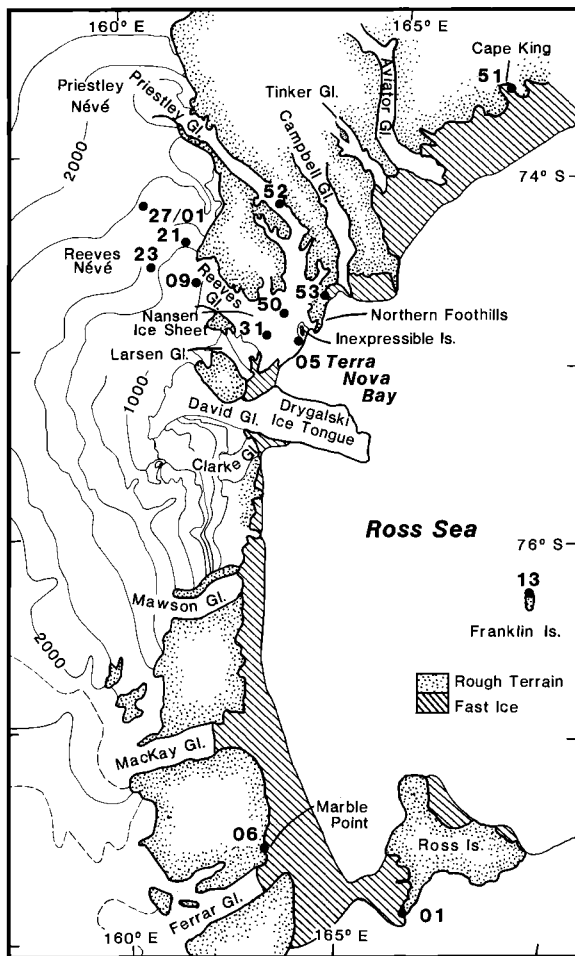


Fig. 2. Map of Terra Nova Bay area identifying points of interest and showing AWS sites (dots with attached numbers). McMurdo Station is located very close to AWS 01.

2. DATA ASPECTS

Before proceeding to discussion of the analysis results, it is necessary to consider the inherent shortcomings in the available data. Automatic weather stations are devices to remotely measure near-surface continuous values of at least temperature, pressure, wind speed, and wind direction, and these data are transmitted to the National Oceanic and Atmospheric Administration (NOAA) polar-orbiting meteorological satellites [Stearns and Wendler, 1988]. The platforms are deployed in remote areas during summer and usually are not visited until the next summer field season. They must therefore perform flawlessly in these remote and inhospitable environments for periods of a year or more in order for a complete data set to be collected. Naturally, this ideal performance is not attained for all sites in all years. Figure 3 summarizes the data availability for all stations in the array. We use the fairly stringent

requirement that 80% or more of the possible observations need to be available for a station to avoid being classified as having missing data for any month. During 1988 the polar plateau above Reeves Glacier was monitored by two AWS (09 and 27) during the first part of the year and by three AWS in the second half (09, 21, and 23). The Italian stations 50–53 only worked satisfactorily during the warmer months with the data gap lasting from April to September; this was due to a temperature dependent problem with the transmitter (P. Grigorini, personal communication, 1993). During 1989 the polar plateau was monitored by roughly three stations throughout the year. All Italian stations except 51 continuously transmitted. For both years the coastal behavior of the katabatic airstream from Reeves Glacier was well monitored but was enhanced in 1989 by the operation of AWS 31 at the center of the Nansen Ice Sheet.

In addition to data not being available because of transmission problems, malfunctions of particular sensors can severely limit the monitoring of particular parameters. Table 2 summarizes the identified problems. The most serious breakdown was associated with the anemometer at station 09. Anomalously low speeds abruptly started to be recorded on October 14, 1988, and persisted to the end of the year; however, the regional speed variations were preserved. As the anemometer was not serviced during that summer, the problem persisted until mid-September 1989 when a further but more severe degradation in the wind speed readings was noted. Comparisons between the wind speed records at AWS 09 and those at surrounding sites both before and after the abrupt change indicated that the recorded speeds after October 13, 1988, could be multiplied by a constant factor of 2.12. This factor was only used until the end of January 1989, and the corrected wind speeds thereafter were ignored because of doubts about the stability of the correction factor. The cause of this anemometer problem has subsequently been identified as being caused by the brushes on the commutator; these wear away, and the resulting dust buildup reduces the amplitude of the output voltage.

To illustrate the validity of the correction procedure for the wind speed readings at station 09 between mid-October 1988 and January 1989, the 5-day average wind speeds at stations 09 and 05 are compared in Figure 4 between January 1988 and January 1989. As will be seen below, AWS 09 is directly upwind of AWS 05, and their katabatic wind speed fluctuations are closely related. The corrected AWS 09 winds for the lighter wind period of November 1988 to January 1989 are similar to those reliably measured in January 1988 in that the average speed is slightly smaller than that for AWS 05. On a small number of occasions during both periods the AWS 09 speed is higher than that at AWS 05. In addition, their speed variations are closely correlated. It is concluded that overall the correction procedure produces realistic

TABLE 1. AWS Site Characteristics

Station*	Site Name	Site Location	Latitude and Longitude	Elevation, m	Height of Anemometer Above Surface, m	Local Slope	Shortest Distance to the Ocean
(89)05	Manuela	Inexpressible Island	74°55'S 163°36'E	80	1.5	N/A	along coast
(89)06	Marble Point	Marble Point	77°26'S 163°45'E	120	3	N/A	along coast
(89)09	Shristi	head of Reeves Glacier	74°42'S 161°34'E	1200	3	2.4×10^{-2} to 119°	67 km
(89)13	Whitlock	Franklin Island	76°14'S 168°42'E	275	3	N/A	offshore island
(89)21	Sushila	Reeves Névé	74°18'S 161°18'E	1441	3	1.3×10^{-2} to 180°	90 km
(89)23	Sandra	Reeves Névé	74°29'S 160°29'E	1525	3	1.1×10^{-2} to 122°	106 km
(89)27/01	Lynn	Reeves Névé	74°14'S 160°22'E	1772	3	7.8×10^{-3} to 135°	120 km
(89)31	Pat	Nansen Ice Sheet	74°53'S 163°00'E	30	3	N/A	18 km
(73)50	Sofia	Nansen Ice Sheet	74°48'S 163°19'E	87.1	10	N/A	16 km
(73)51	Alessandra	Cape King	73°35'S 166°38'E	183	10	N/A	along coast
(73)52	Zoraida	Priestley Glacier	74°15'S 163°09'E	650	10	1.9×10^{-2} to 137°	50 km
(73)53	Eneide	Tethys Bay	74°41'S 164°06'E	88	10	N/A	along coast

* Parentheses are around that part of the station number that is not used in this paper.

wind speed variations at AWS 09. It should be emphasized that the corrected wind speeds for AWS 09 are used only in estimating the role of site 09 in the time-averaged spatial structure of the wind field.

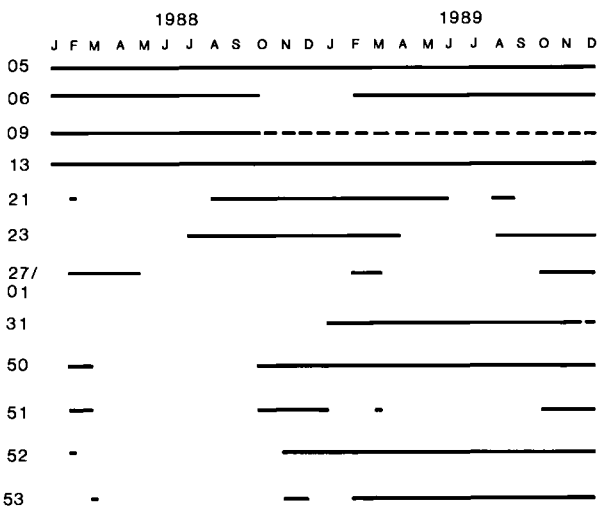


Fig. 3. Automatic weather station monthly data during 1988 and 1989 based upon 80% or more of possible observations (horizontal lines). Dashed line for AWS 09 after mid-October 1988 indicates that the wind speed record is uncertain.

Some anemometer problems were noted for station 05 and perhaps station 31 in 1989. Physically unrealistic dead calms, persisting for days at a time, signal the interruption of the electronic recording of wind speed. The contact with the anemometer slip rings can be restored by vigorous vibration, with the wind speed record then resuming. Inspection of all available platform transmissions (typically at 10-min intervals) can usually identify such events. The wind speeds were not used when this occurred. For station 31 such events were suspected but could not be conclusively demonstrated by comparison with station 05 observations. No wind speed observations from this site were omitted.

3. SPATIAL CHARACTERISTICS

To examine the typical spatial characteristics of the surface wind field near Terra Nova Bay from the AWS records, it is necessary to reduce all the records to a common period and to account for the missing data described in Figure 3 and the instrument malfunctions in Table 2. The following strategy was used from February 1988 to January 1989. Stations 05 and 09 operated continuously during this period, and their observations were used as reference time series for the coastal (AWS 50, 51, 52, and 53) and interior (AWS 21, 23, and 27) stations, respectively, with significant amounts of miss-

TABLE 2. Instrumental Malfunctions for the Various Automatic Weather Station Sites Between February 1988 and December 1989

Station	1988		1989	
	Problem	Action Taken	Problem	Action Taken
05			Intermittent extended calms March to Sept. due to anemometer malfunction.	Speeds put to missing when appropriate, judged from all transmissions.
09	Anomalously low speeds started abruptly on Oct. 14.	Measured speeds after Oct. 13 multiplied by a fixed correction factor of 2.12, based on before and after comparisons with fully functional surrounding stations.	Problem continues all year. Another major deterioration in mid-Sept.	Reported wind speeds ignored for entire year.
	Intermittent directional sticking after Feb., but particularly for Oct. to mid-Nov.	No correction made.	Direction sticks at times starting in May. Does not change from mid-Sept. to end of Nov.	Ignored because of high directional constancy at site.
13			Some extended calm periods in Aug. and Sept., probably due to rime buildup on anemometer.	No corrections made.
27/01			5-hPa pressure jumps throughout the year.	Instantaneous values are questionable, but averages are probably satisfactory and were not corrected.
31	N/A		Possible anemometer problem like station 05 starting in Feb. Inspection of transmissions during extended light winter periods suggest that these may be real. AWS tower fell over on Dec. 4. No wind observations after this date.	No corrections made.
52	No pressure observations until mid-Jan.			
53	Intermittent spurious anemometer readings.	Edited out.		

ing data. The correction strategy for missing wind speeds at a station depended on the ratio of speed at that station to the value at the reference station when both were operating without significant amounts of missing data. Monthly ratios were averaged for the summer (November–January) and winter (February–October) wind periods (see the next section) and then were combined by weighted averaging according to seasonal duration. The reference station's annual mean speed was multiplied by the combined ratio to yield an estimate of the annual mean speed at the station with significant amounts of missing data. Where necessary, speeds were adjusted to a height of 3 m above the surface (see Table 1) by assuming a logarithmic wind speed profile and a roughness length of 0.1 mm [Budd et

al., 1966]. The resultant wind direction and directional constancy values for summer and winter were taken directly from each station's available data because these parameters do not exhibit much intraseasonal variability. These values were then combined by weighted averaging according to seasonal duration to yield annual estimates. The vector-averaged speed is equal to the product of the mean speed and the directional constancy. For potential temperature the correction procedure followed that for wind speed but was based on the difference between simultaneous readings at the station and the reference location.

The correction procedure for wind speeds at interior stations differed during calendar year 1989 because the speed observations at the 1988 reference station 09 were

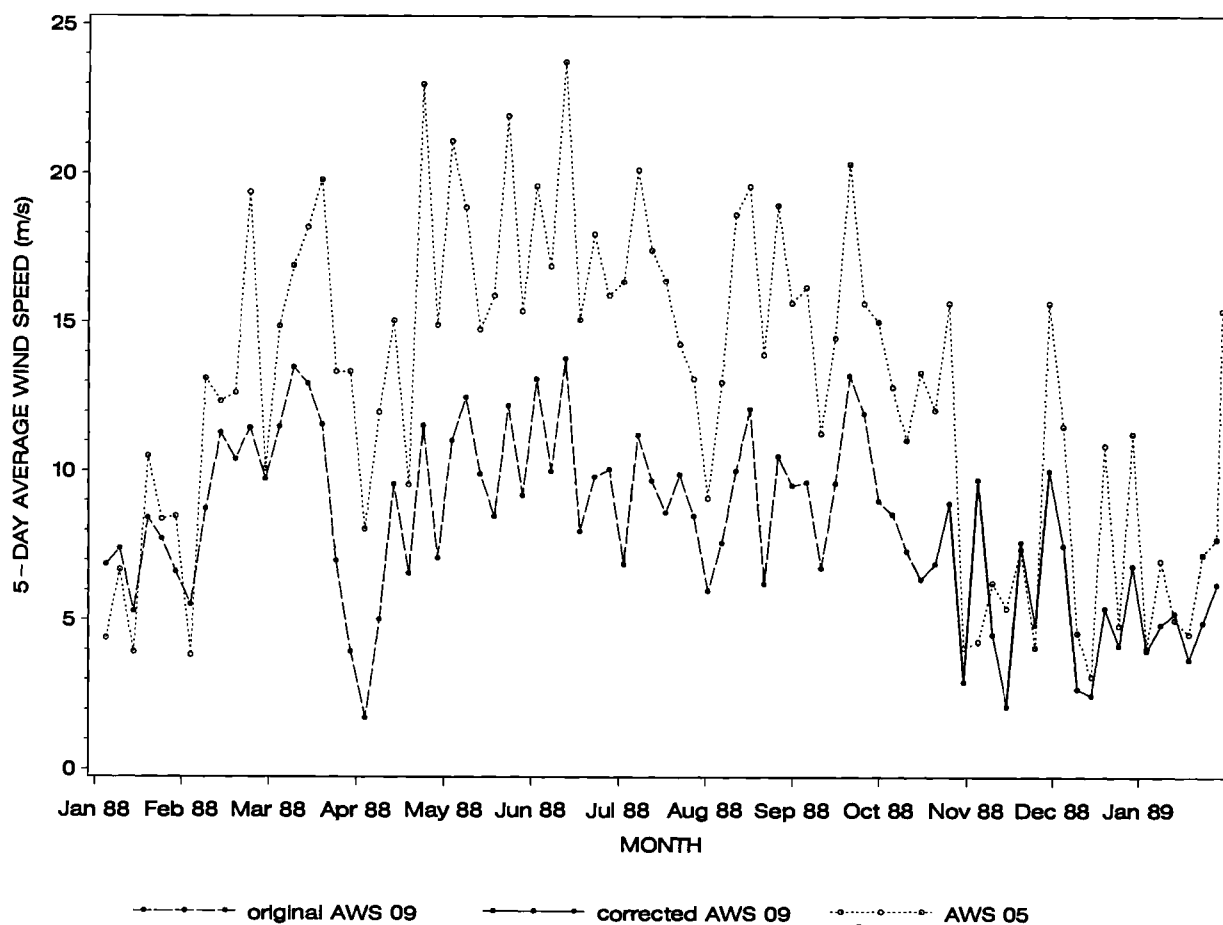


Fig. 4. Comparison of 5-day average wind speeds from AWS 05 and 09 to illustrate validity of correction procedure implemented for AWS 09 speeds after October 13, 1988.

unreliable, as described previously. For station 09 the resultant direction and directional constancy found for February 1988 to January 1989 were used for calendar year 1989. An estimate of annual wind speed was obtained from the product of the speed ratio between station 09 and station 05 for the earlier annual period and the 1989 mean speed at station 05. This was inferred to be a very adequate procedure because in 1988 the daily mean speed variations at the two sites were highly correlated (see the next section and Figure 4).

Station 23 was used as the reference AWS for wind speeds at the interior stations during calendar year 1989. Figure 3 shows that this site had significant amounts of missing data only during May–July, the best performance on the plateau. Use of the wind speed record from this site requires a speed estimate for each of May, June, and July. As station 52 operated throughout the year, the values were estimated from the winter speed ratios (23/52) before and after the data gap at AWS 23 and the speeds at AWS 52 during May–July. Resultant wind directions and directional constancies for the

missing 3 months at station 23 were estimated from the winter data at AWS 23 before and after.

Figure 5 summarizes the wind and temperature fields resulting from the above manipulations; the vector-averaged wind, the directional constancy, the mean 3-m speed, and the mean potential temperature for 1988 (February 1988 to January 1989) and 1989 (January to December 1989) are plotted for all sites. A very stable wind regime is present over the polar plateau with annual directional constancies of 0.89 and greater. The airflow clearly converges into the head of Reeves Glacier with slightly more persistent winds being found in this area. This airflow pattern over the interior closely fits with that derived from the airborne sastrugi surveys [Bromwich *et al.*, 1990a]. The mean speeds exceed 8 m s^{-1} with slightly stronger winds near the head of Reeves Glacier. The airflow accelerates as it descends Reeves Glacier [cf. Parish and Bromwich, 1989a] and arrives at station 31 with an average speed of 10.5 m s^{-1} . Somewhat remarkably, the airflow appears to accelerate as it crosses the flat Nansen Ice Sheet to reach the Inexpressible Island AWS

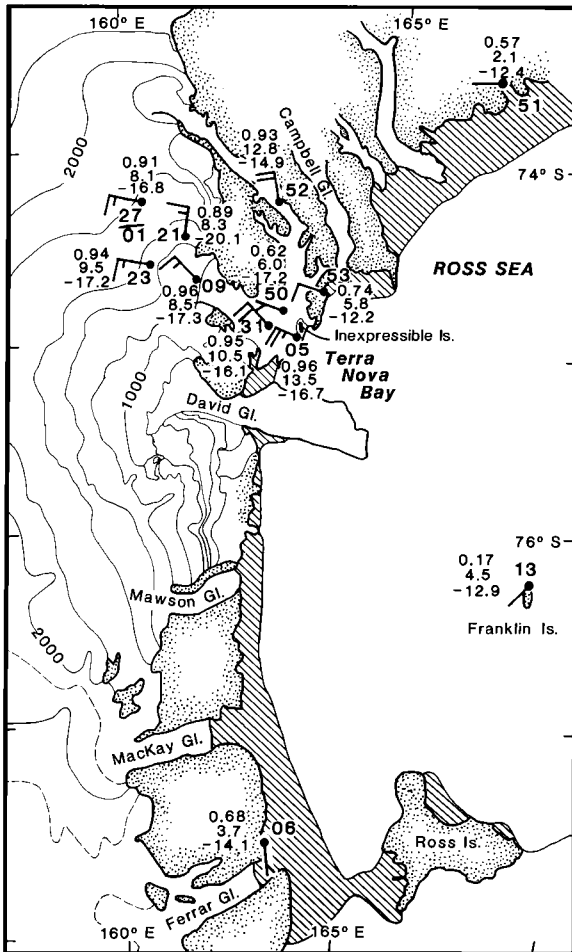


Fig. 5. Annual average wind and temperature fields near Terra Nova Bay from the AWS observations for 1988 and 1989. For each AWS site the following data are listed vertically from top to bottom: the directional constancy, the mean 3-m wind speed in meters per second, and the average potential temperature in degrees Celsius. The vector-averaged 3-m winds are plotted for each AWS in conventional notation.

where the mean speed is 13.5 m s^{-1} (discussed further below). Similarly high and nearly unidirectional airflow regimes are found at AWS 31 and 05.

The Italian stations to the north illustrate the highly confined nature of the katabatic airstream from Reeves Glacier. Station 50 was located along the northern edge of the katabatic wind generated ablation zone shown on Landsat band 7 imagery of the Nansen Ice Sheet [Bromwich and Kurtz, 1984]. The wind record indicates that it is intermittently embedded within the katabatic airstream. The wind speed versus wind direction plot of the 1989 observations from this site (Figure 6) shows that most of the strong winds ($>15 \text{ m s}^{-1}$) come from the direction of Reeves Glacier (250° – 280°). Fairly frequent flow from the north (350° – 10°) occurs with speeds up to 15 m s^{-1} , and this is katabatic airflow from Priestley Glacier (discussed

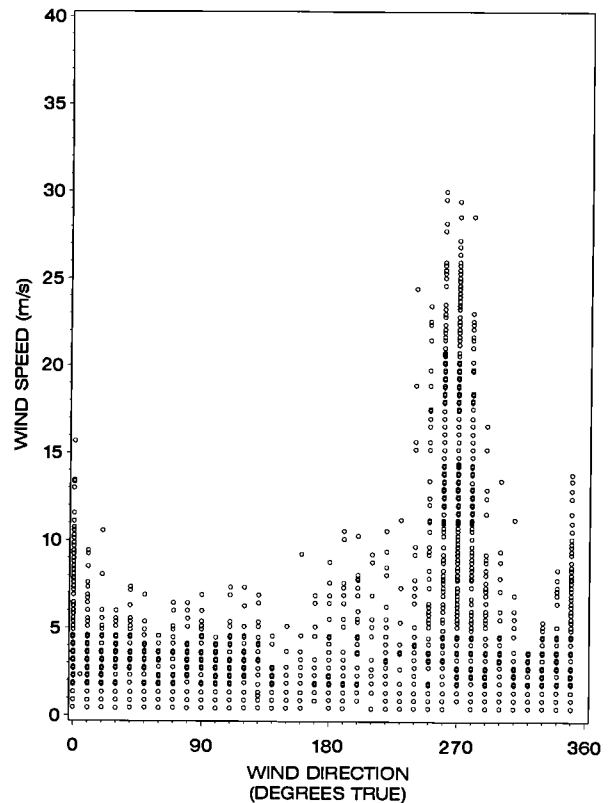


Fig. 6. Wind speed versus wind direction plot for AWS 50 during 1989.

more below). The combination of strong winds from primarily one direction and lighter winds from many directions yields a directional constancy of 0.62, a mean speed of 6.0 m s^{-1} , and a resultant wind direction that points from the direction of Reeves Glacier.

Station 52 reveals a katabatic wind regime down Priestley Glacier that is nearly as intense as that at Inexpressible Island. Both the mean speed and the directional constancy at this site are slightly smaller than at AWS 05. The resultant wind direction is parallel to the steep sides of the glacier valley immediately upwind from the site. The wind speed versus wind direction plot for AWS 52 (Figure 7) shows that the wind speeds stronger than 20 m s^{-1} are confined to the directional range from 320° to 10° via north, consistent with katabatic flow parallel to the valley walls just upwind. Winds from other directions are infrequent and light. A secondary directional clustering is centered around 140° , which corresponds to weak upslope flow parallel to the valley walls at lower elevations. These events are concentrated in the warmer months (November–February) when the katabatic winds are weaker (see next section) and occur in conjunction with relatively warm and moist conditions, i.e., are associated with synoptic invasions of warm moist air from the southeast.

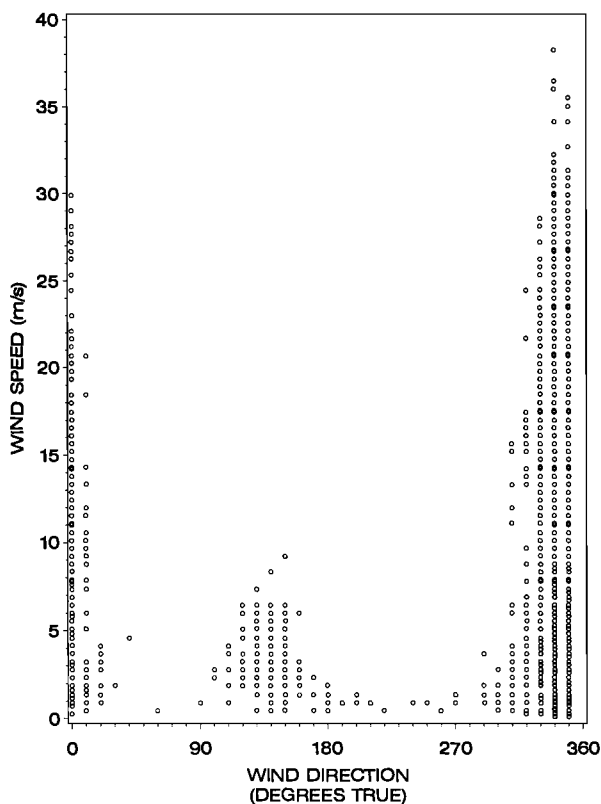


Fig. 7. Same as Figure 6 but for station 52.

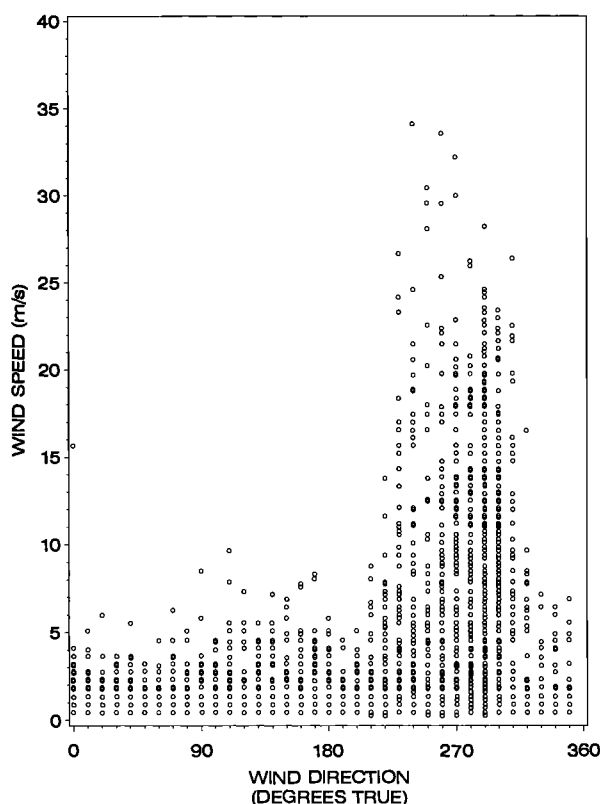


Fig. 8. Same as Figure 6 but for station 53.

Station 53 is located on the eastern side of the Northern Foothills, and the resultant wind direction shows frequent airflow down the locally high terrain. The speed versus direction plot for this site (Figure 8) reveals that speeds stronger than 15 m s^{-1} are almost confined to the sector of 230° – 310° , i.e., spanning the directions that could include direct katabatic airflow from Reeves and Priestley glaciers. *Bromwich and Parish* [1989] and *Bromwich* [1989a] present examples where the katabatic airflow from these glaciers is clearly reaching site 53 despite the large topographic obstacles between the glaciers and the site. Presumably, the stability and momentum conditions (low Froude number) of the katabatic airstreams are such as to allow them to surmount the obstructing obstacles.

The potential temperature field shows that the airflow on the plateau which converges toward the head of Reeves Glacier is nearly dry adiabatic apart from air blowing southward past AWS 21 which is significantly colder and may originate in the high continental interior. The katabatic air that arrives at station 31 is over 1°C warmer than the air at the head of Reeves Glacier (station 09), perhaps reflecting the stronger winds and reduced stratification at the former site [cf. *Parish and Bromwich*, 1989a]. The 0.6°C lower potential temperature at AWS 05 in comparison to AWS 31 may be a

consequence of colder air from very near the surface of the Nansen Ice Sheet blowing over the southern part of Inexpressible Island. This potential temperature contrast persisted on a monthly mean basis throughout the year. The lower potential temperature at site 50 than at either site 31 or site 05 reflects its intermittent exposure to the katabatic airstream from Reeves Glacier, thus allowing radiative cooling to produce lower air temperatures during periods of light wind conditions. Comparison between the potential temperatures at sites to the north and south shows that the intense katabatic airstream blowing into Terra Nova Bay is indeed a source of cold boundary layer air for the southwestern Ross Sea, as inferred by *Bromwich* [1989b]. Using the average of the potential temperatures at AWS 06 and 51 as an estimate of the regional near-surface environment temperature, we see that the katabatic airstream from Reeves Glacier is 3.4°C colder on an annual basis ($-16.7 - (-14.1 - 12.4)/2$).

The potential temperature of the Priestley Glacier katabatic wind at station 52 is about 2°C warmer than that of the katabatic airstream blowing down Reeves Glacier, indicating that on average the former is positively buoyant in relation to the latter. As a further demonstration of this, the northerlies at station 50 which were previously identified as being caused by katabatic

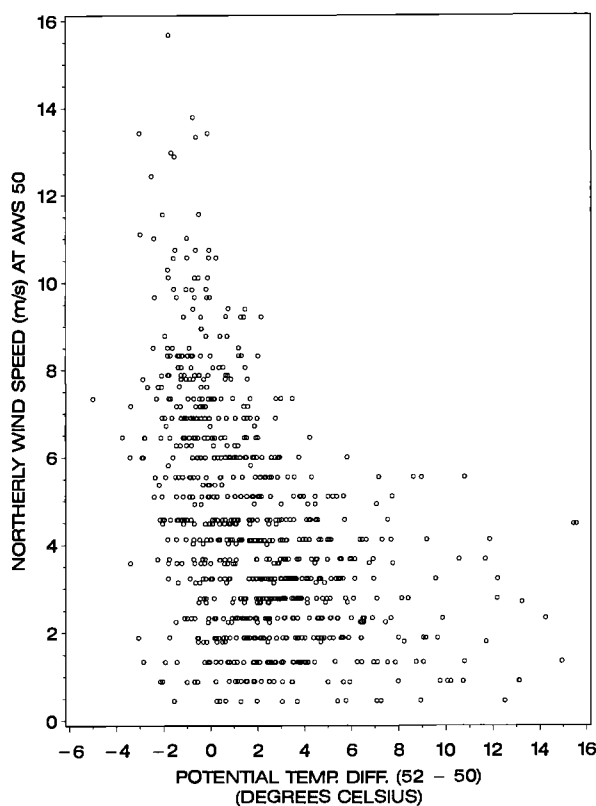


Fig. 9. Speed of northerly winds at station 50 versus potential temperature difference between station 52 and station 50 during 1989.

airflow from Priestley Glacier were examined in relation to the potential temperature difference between station 52 and station 50. Moderately strong northerlies (approximately greater than 8 m s^{-1}) only appeared when this difference approached zero (see Figure 9), i.e., indicating that katabatic air from Priestley Glacier had reached site 50. The moderate northerlies were also associated with a small potential temperature difference between site 52 and site 31, indicating that this katabatic airstream only appeared at the surface of the northern fringes of the Nansen Ice Sheet when the two katabatic airstreams were of similar buoyancy.

Argentini et al. [1992] report cases during the austral summer when an acoustic sounder near AWS 50 monitored the drainage flow from Reeves Glacier overriding the flow from Priestley Glacier. At this time the potential temperature of the Priestley Glacier wind (AWS 52) was lower than that from Reeves Glacier (AWS 09). This is primarily caused by the more pronounced summer warming at AWS 09 than at AWS 52. The marked seasonal variation of the thermal contrast between the Reeves and Priestley Glacier katabatic airstreams, probably caused by conditions in the continental interior, deserves further investigation.

The potential temperature at station 53 is much

warmer than that at any of the sites close by, and in particular than those at stations 05 and 52, representing the katabatic airflows from Reeves and Priestley glaciers, respectively. To further examine the origins of the air at AWS 53, the speed of the winds blowing from the direction of Reeves Glacier (WSW) was compared with the potential temperature difference between AWS 53 and AWS 50. In Figure 10a, winds stronger than 15 m s^{-1} are associated with comparatively small potential temperature differences, indicating that this air plausibly came from the Nansen Ice Sheet. In Figure 10b the speed of the winds at AWS 53 from the direction of the Priestley Glacier (WNW) is compared to the potential temperature difference between AWS 53 and AWS 52. Little association between the variables can be seen, suggesting that most of the WNW winds at AWS 53 are not surface level katabatics from Priestley Glacier.

A possible explanation is that these WNW winds at AWS 53 originate in the upper part of the katabatic layer blowing down Priestley Glacier. Such air should usually be somewhat potentially warmer than the near-surface air monitored by AWS 52, consistent with the typical potential temperature differences in Figure 10b. If the WNW wind speed at AWS 53 depends primarily on the wind speed in the upper part of the katabatic layer in Priestley Glacier, it should be largely independent of the surface level potential temperature difference between AWS 53 and AWS 52, as in Figure 10b, but somewhat dependent on surface wind speed at AWS 52, as in Figure 10c. The higher-level katabatic air from Priestley Glacier will encounter smaller topographic obstacles on its path to Tethys Bay ($74^{\circ}41'S$, $164^{\circ}06'E$) than surface level air. The near-surface katabatic wind may separate from the higher-level air at the sharp southward bend in the Priestley Glacier valley and sometimes continue all the way down the valley to be recorded as a northerly (katabatic) wind by AWS 50.

The sea level pressure field for February 1988 to December 1989 was also derived. This variable is subject to the same data gaps as summarized by Figure 3. The same correction procedure was followed as for potential temperature with station 05 serving as the reference location. The gaps at station 06 were filled by reference to AWS 13. Observations from stations with elevations greater than 300 m were omitted because of the large uncertainties introduced by the reduction to sea level during winter. Figure 11 presents the sea level pressure field. In Figure 11a a marked trough axis lies right along the center of the Nansen Ice Sheet and Reeves Glacier. This means that the apparent acceleration of the katabatic airflow from station 31 to station 05 noted previously in the discussion of Figure 5 takes place down the local pressure gradient. A broader-scale view of the pressure field is provided by Figure 11b. To fill missing gaps in the data given by *Keller et al.* [1989, 1990], procedures similar to those described by *Bromwich* [1991] were used for stations on the Ross Ice Shelf. The

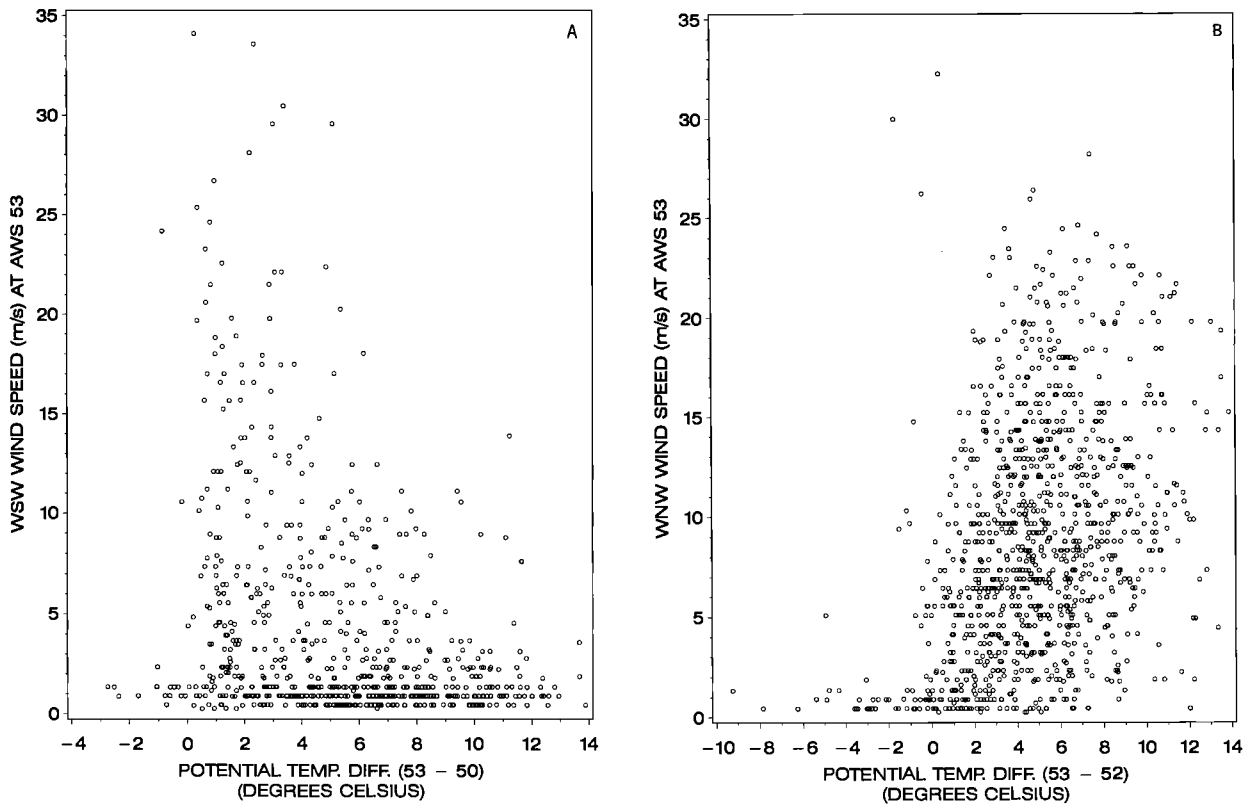


Fig. 10. Speed of winds at AWS 53 from (a) the WSW versus potential temperature difference between AWS 53 and AWS 50, (b) the WNW versus potential temperature difference between AWS 53 and AWS 52, and (c) the WNW versus the wind speed at AWS 52, during 1989.

resulting pattern is very similar to that found by *Bromwich* [1991] for 1985 with the characteristic fall of pressure from the Transantarctic Mountains to the northeast being present, as is troughing southward across Ross Island. Farther north this Ross Island trough merges with the trough that projects up Reeves Glacier.

As a finale to this section, it is possible to check the plausibility of some of the extensive correction procedures used to fill the data gaps of wind and temperature. From Figure 3 it can be noted that stations 50, 52, and 53 had significant amounts of missing data from April to September/October in 1988, whereas the observations were nearly complete in 1989. The differences between the averages at these sites for the 2 years can be compared to the differences at station 05 which operated continuously throughout the period. Note, however, that data from AWS 05 were used to fill data gaps in wind speed, potential temperature, and sea level pressure at AWS 50, 52, and 53 for April to September/October 1988, so part of the interannual changes are implicitly determined by AWS 05 observations. The changes in annual mean potential temperature between 1988 and 1989 (1989 minus 1988) at stations 50, 52, and

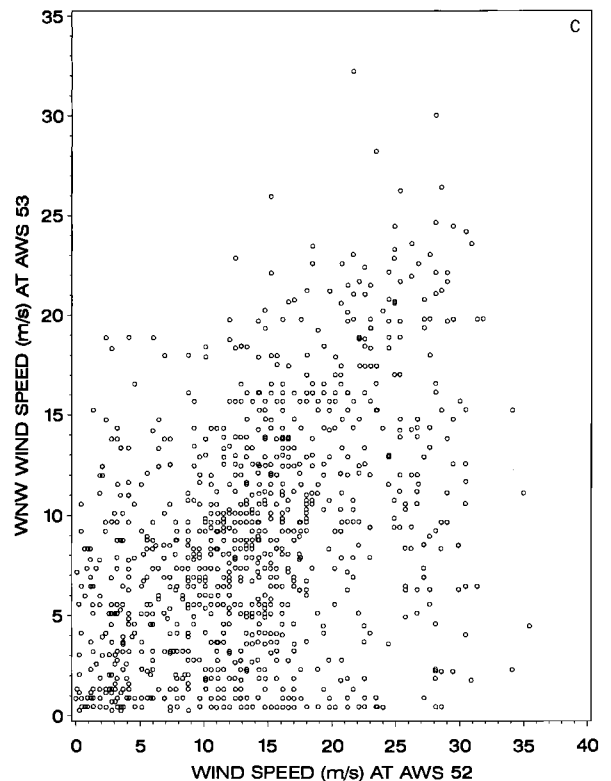


Fig. 10. (continued)

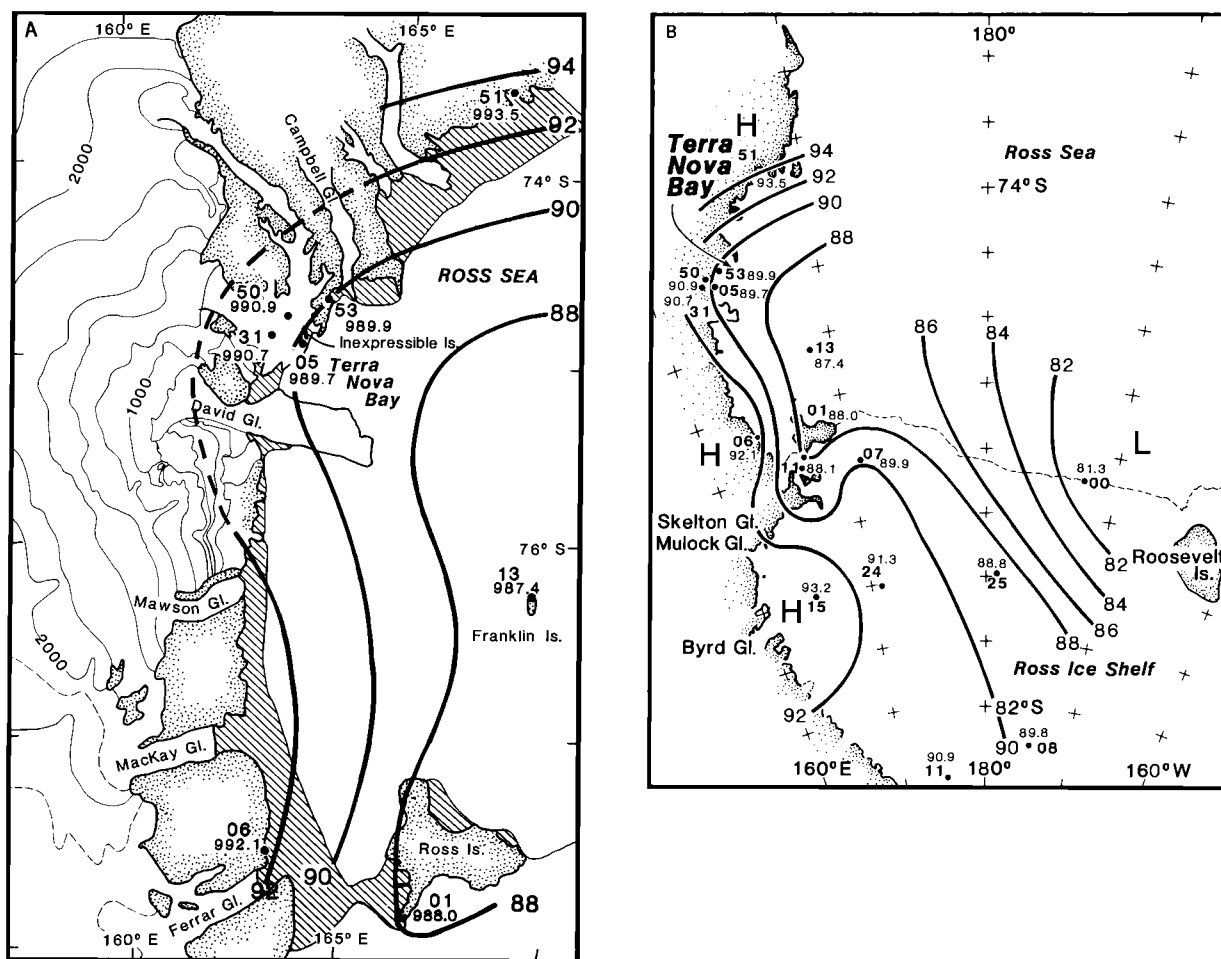


Fig. 11. Annual average sea level pressure field (a) near Terra Nova Bay and (b) in the Ross Sea/Ross Ice Shelf area for 1988 and 1989. $88 \equiv 988$ hPa. In Figure 11b, 900 has been subtracted from the pressure values plotted for each AWS. Also, two AWS 11 pressure values are plotted in Figure 11b; the southern station operated in 1988, and the northern one in 1989.

53 were -1.2°C , -1.5°C , and -1.0°C , respectively, compared to -0.7°C at station 05 and -0.9°C at station 09. For wind speed the respective changes were $+0.2$, $+0.7$, and -0.8 m s^{-1} compared to $+0.05$ m s^{-1} at station 05. For directional constancy the changes were -0.02 , $+0.03$, and $+0.03$ compared to 0.0 at station 05. For resultant direction the changes were (positive for clockwise rotation from 1988 to 1989) $+4^{\circ}$, -5° , and -12° versus 0° change for station 05. For sea level pressure only the changes at stations 50 and 53 are relevant because the high elevation of station 52 introduces substantial uncertainties into the reduction of its pressure to sea level. The changes from one year to the next at stations 50 and 53 were -2.2 and -3.7 hPa compared to -2.9 hPa at station 05. From these comparisons it can be seen that the temperature and wind corrections for stations 50 and 52, and the pressure corrections for AWS 50, in 1988 were probably realistic.

Although the temperature and pressure corrections for station 53 appear reliable, the situation for the wind regime is less clear. Considering the atypical wind regime at site 53 with a significant contribution from higher-level katabatic flows from Priestley Glacier, the wind differences could reflect real interannual variability, but an artifactual result cannot be ruled out. It is concluded that the adopted procedures properly corrected, at least qualitatively, for the missing observations.

4. TEMPORAL VARIATIONS

4.1. Diurnal Changes

In the summer half year a small part of the incident solar radiation is absorbed by the generally highly reflective snow surface and leads to a pronounced daily cycle in the stratification of the near-surface air layer. The temperature variation is much larger over exposed

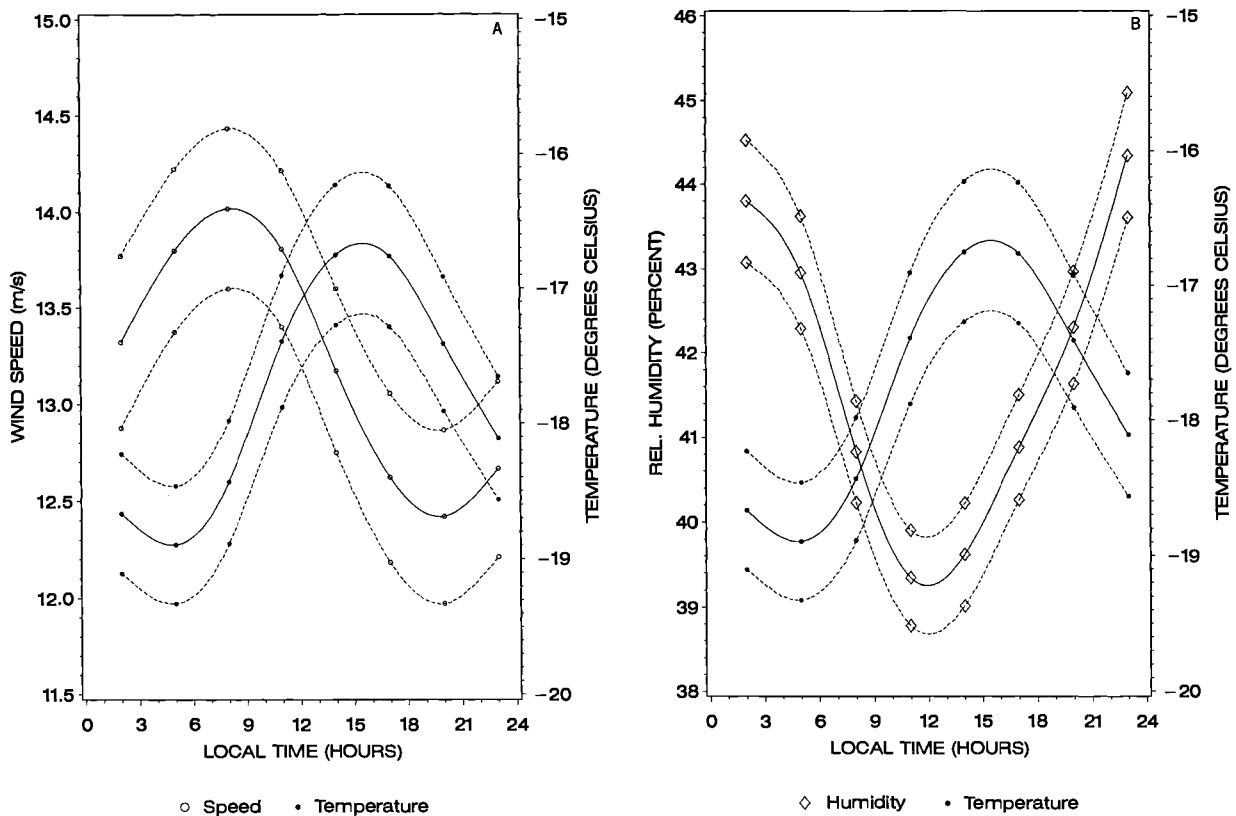


Fig. 12. Diurnal variations of (a) wind speed and air temperature and (b) temperature and relative humidity at the Inexpressible Island AWS during December 1988. Dashed lines denote plus/minus one standard error of the mean.

rock surfaces [Mastrantonio *et al.*, 1990]. Fairly uniform changes are experienced in the snow-covered areas in the vicinity of Terra Nova Bay. At Inexpressible Island, for example (Figure 12a shows December 1988), the summer diurnal temperature range is 3° – 5°C with maxima around 1700 and minima near 0400 hours local solar time (UTC + 11 hours). The wind speed exhibits a less well defined cycle of 2 – 4 m s^{-1} with maxima near 0600 and minima around 2000 hours. That is, the strongest winds lag the lowest temperatures by about 2 hours, and vice versa. There is no clear daily variation of wind direction. The relative humidity (Figure 12b shows December 1988) undergoes a weak diurnal change, becoming moistest between 2300 and 0200 hours and driest between 1100 and 1400 hours; for certain summer months the range can be as large as 17%.

Similar cycles are present over the plateau above Terra Nova Bay. At station 23 the temperature cycle has the same phase as at the coast but nearly double the range (5° – 8°C). The corresponding wind speed variation is weaker (1 – 3 m s^{-1}). The wind direction is more downslope at the time of highest speeds (0500) and more cross-slope at the time of lowest speeds (1600); the range increases on average to 30° near the summer

solstice. Kodama *et al.* [1989] found a similar diurnal wind pattern in the interior of Adélie Coast. The daily relative humidity changes at station 09 are very similar to those at the coast.

4.2. Seasonal Cycle

Composite depictions of the annual course of state parameters for the entire AWS array have been prepared for both calendar year 1988 and calendar year 1989. The trends were computed by first determining daily averages (vector averages for wind) and then passing the time series through a nine-point low-pass filter to remove some of the high-frequency variance. The weights of the smoothing function are proportional to binomial coefficients, and therefore the smoothing function has a shape of a normal curve [see Panofsky and Brier, 1968]. Figure 13 shows the evolution of potential temperature, wind speed, and pressure during the course of 1988 for the AWS units 05 (Inexpressible Island) and 09 (head of Reeves Glacier). Potential temperatures undergo a dramatic decrease during the early austral autumn period from mid-February to mid-March. The rapid change is in all likelihood a result of

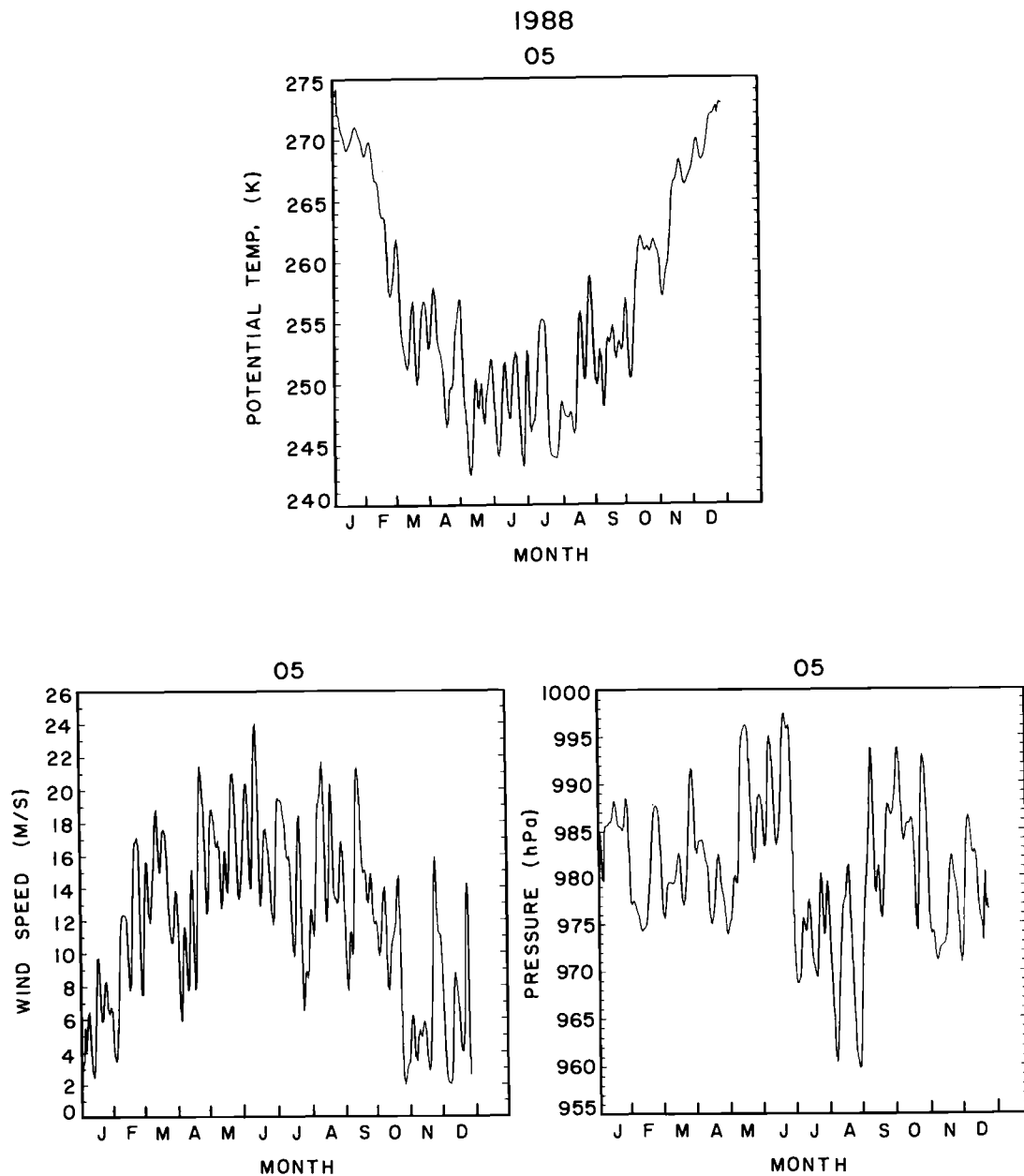


Fig. 13a. Annual course of potential temperature, wind speed, and pressure at station 05 (Inexpressible Island) during 1988.

the rapidly changing solar geometry and resulting decrease in solar insolation. This sudden onset of winter has been alluded to by Bromwich [1989b].

Accompanying the abrupt temperature decrease is a pronounced increase in the intensity of the katabatic wind. In a period of approximately 1 month, resultant wind speeds increase in excess of 100%. By the end of April, winter conditions are fully established with daily resultant wind speeds of approximately 15 m s^{-1} at station 05 and mean potential temperatures near 250 K.

Note that the potential temperature trends at station 09 are nearly identical to those found at station 05, indicating similar synoptic influences and/or local radiative conditions. As noted in the aircraft studies of katabatic winds near Terra Nova Bay by Parish and Bromwich [1989a], and seen in AWS averages presented in the previous section, values of potential temperature are very close at the head and beyond the foot of Reeves Glacier. This feature has also been noted in modeling studies [Parish and Waight, 1987] and is characteristic

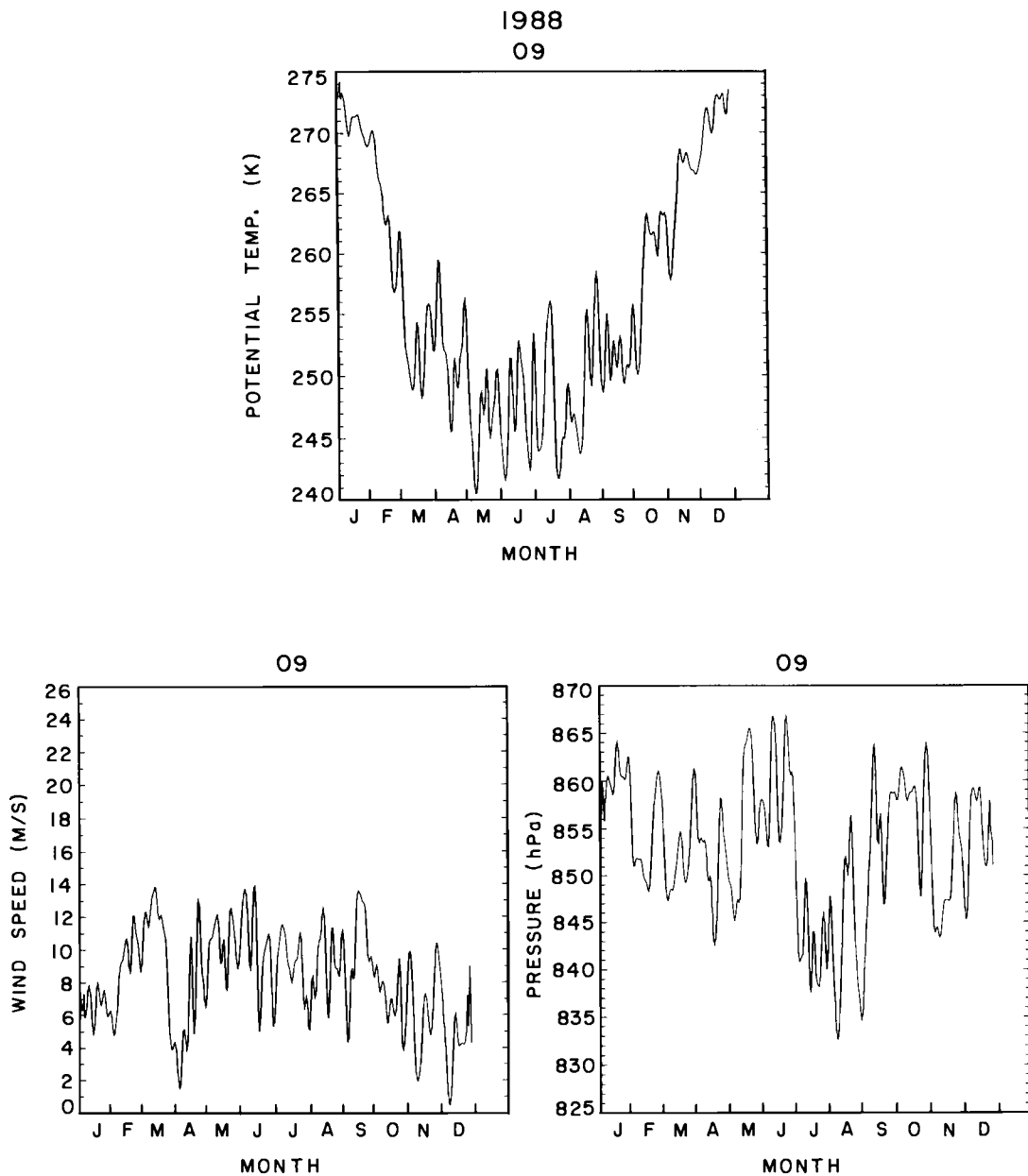


Fig. 13*b*. Annual course of potential temperature, wind speed, and pressure at station 09 (head of Reeves Glacier) during 1988.

of katabatic-prone areas. As in the time-averaged situation, the wind speeds seen at station 09 are consistently some $3\text{--}5\text{ m s}^{-1}$ less than corresponding wind speeds at station 05, implying that the katabatic flow accelerates down Reeves Glacier and across the Nansen Ice Sheet. Only minor enhancements to the fall changes are observed during the following 5 months. The temperature trend observed during the winter months suggests a “kernlose” or coreless winter; little if any temperature decrease can be detected. Both temperature and wind

speed trends suggest a similar although possibly weaker return to summertime conditions during the austral springtime months of October and November. Short-term variations, presumably due to the effects of transient synoptic systems, are present in both potential temperature and wind speed throughout the entire year.

The annual cycle of surface pressure during 1988 shows short-term fluctuations similar to those of wind speed and temperature. A notable longer-term feature is the marked drop in pressure commencing near the end

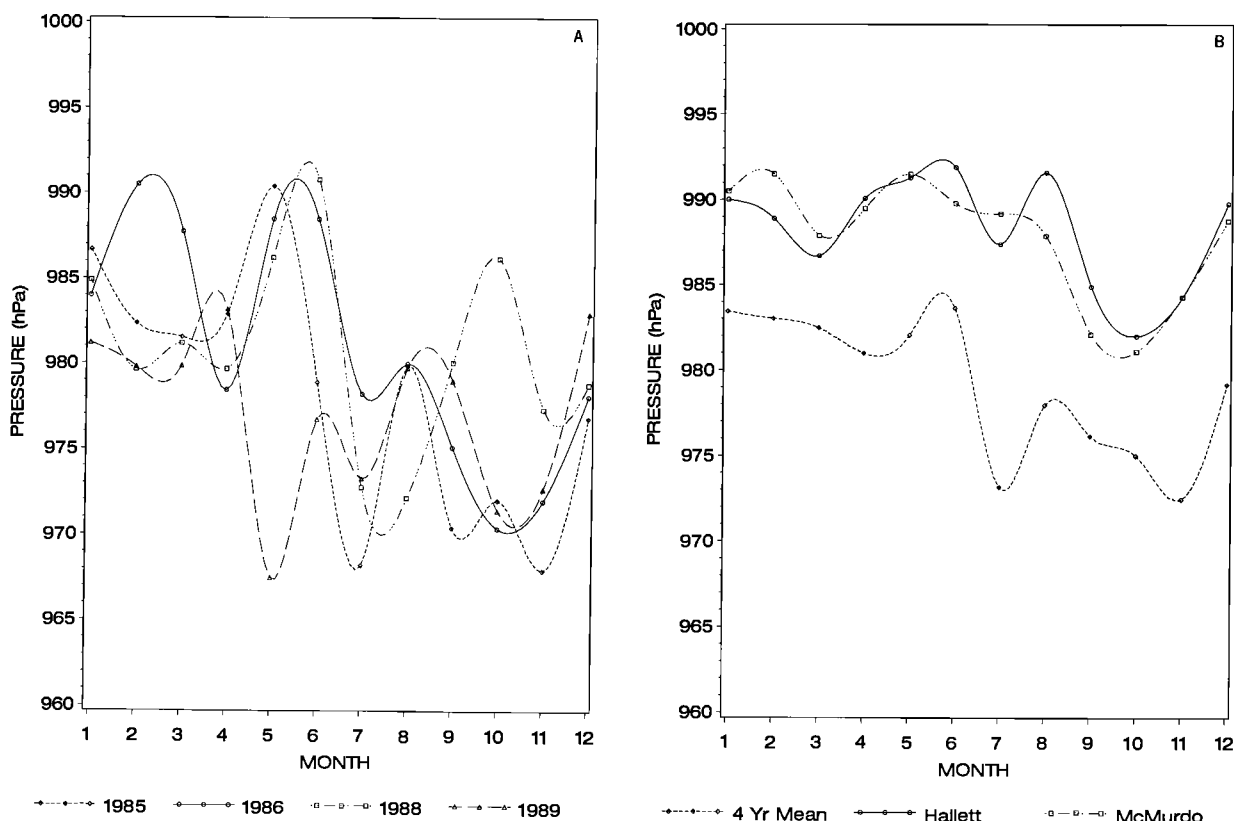


Fig. 14. Seasonal station pressure variations at Inexpressible Island for (a) 1985, 1986, 1988, and 1989 and (b) the 4-year mean in relation to the climatological values for McMurdo and Hallett stations.

of June and continuing until the end of August; this feature is characteristic of all AWS records in the Terra Nova Bay area during 1988. No corresponding change can be seen in either temperature or wind speed. To put this variation into a longer-term perspective, Figure 14 has been prepared. Figure 14a shows the monthly mean station pressures at Inexpressible Island for all years with “complete” records: 1985, 1986, 1988, and 1989. The sharp pressure fall from June to July occurred in three of the four years, with pressure values similar to or higher than those in July being recorded in August. Typically, another pressure minimum develops in September–November. Figure 14b compares the 4-year average at Inexpressible Island with the climatological station pressures at McMurdo and Hallett stations [Schwerdtfeger, 1970] which are located respectively to the south and north of Terra Nova Bay along the Victoria Land coast. The Inexpressible Island mean shows the sharp drop from June to July and a broad minimum from July to November. The Hallett record contains a reflection of the sharp June to July drop, but there is no evidence in the curve from McMurdo. Both climatological records contain a notable minimum in September–October. The well-defined pressure minimum during July–August 1988 was probably due to

interannual variations in the time that the circumpolar trough moves poleward and intensifies during the spring phase (September–October) of the semiannual pressure variation [van Loon, 1967; Stretten, 1980].

Pressure maxima (Figure 14b) occur during summer and May–June. For the first (well marked) maximum there is a north to south variation in the timing: December at Hallett, January at Terra Nova Bay, and February at McMurdo Station. The second (weak) seasonal pressure maximum comes about 3 weeks earlier at McMurdo than at the other two sites. Between around March and April there is a weak minimum associated with the fall phase of the semiannual pressure variation. The annual pressure variation in this area exhibits several characteristics in common with that over the Antarctic plateau [Schwerdtfeger, 1984, pp. 221–223].

4.3. Interdiurnal Variability

To depict interrelationships between the various AWS sites, records were subjected to spectrum and cross-spectrum analysis. All time series were detrended to remove spurious low-frequency noise and then tapered to reduce spectral leakage from neighboring frequencies [Stull, 1989]. The results of spectrum analysis presented here employ the original, 3-hour data. Vari-

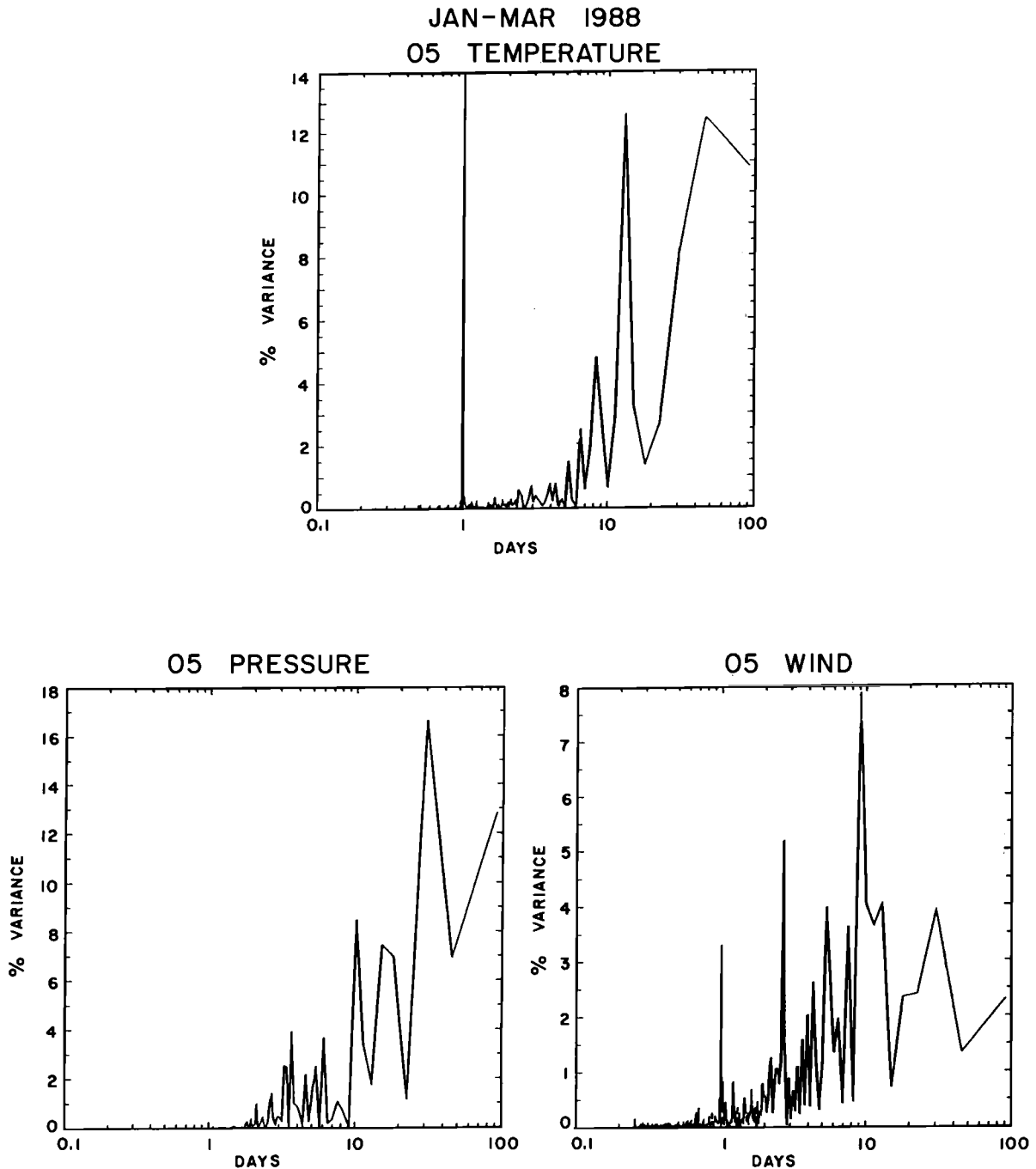


Fig. 15. Power spectra of temperature, pressure, and wind speed at station 05 during January–March 1988.

ous low-pass filters were used in preliminary tests; the final results to be presented here are not sensitive to filtering over frequencies of meteorological interest, mainly the 1-day period and beyond. The Nyquist frequency corresponds to a time interval of 6 hours; focusing on events having time scales of at least 1 day

assures that the 3-hour sampling period is adequate. Spectrum analysis will focus on the AWS data for 1988, the year with the most complete record.

Power spectra of the surface temperature, pressure, and wind at station 05 (Inexpressible Island) for the 1988 “summer” period January–March are shown in Figure 15.

As outlined above, the diurnal cycle is pronounced in both temperature and wind during the summer months. In addition, there is a suggestion of synoptic variability; secondary peaks in the percent variance explained are present in all analyses over the 2- to 10-day time scale. Power spectra for station 05 for the winter months May–July 1988 (Figure 16) suggest appreciable variance in wind speed over time scales of 2–4 days and again for the 6- to 10-day period. Again, this variance is presumably associated with transient synoptic activity and is consistent with the observed variance in pressure seen over time scales of 2–10 days. There appears to be a correlation between wind speed and pressure at station 05. During the months January–March and May–July, correlation coefficients of -0.259 and -0.261 , respectively, were calculated. These coefficients are significantly above what would be expected by chance for a 3-month period (1% probability originating from uncorrelated populations would give a correlation coefficient of 0.10 [see *Panofsky and Brier*, 1968]). Such values are somewhat smaller than those reported by *Loewe* [1974] for the historic site of Port Martin (record from 1950 to 1951) situated along the coast of East Antarctica but still suggest that the strongest winds at Inexpressible Island are associated with low-pressure events. Wintertime power spectra for surrounding AWS stations are qualitatively very similar to that shown in Figure 16. In all cases, wind speed is negatively correlated with pressure, with magnitudes of the correlation coefficients ranging from -0.23 to -0.30 .

In conducting cross-spectrum analysis, a low-pass filter was applied to the spectra weights of the particular time series. Cross-spectrum analysis shows that the individual state parameters measured by the AWS units are highly coherent with each other. As an example, wind speeds for January–March 1988 at sites on Inexpressible Island (05) and at the head of Reeves Glacier (09) show a correlation coefficient of 0.68 (compare with Figure 4). As shown in Figure 17, a high degree of coherence is seen over the diurnal and synoptic time scales. Similarly, high coherence in wind speed (values in excess of 0.65) can be seen over nearly all frequencies at surrounding AWS stations near Reeves Glacier and situated on the sloping Antarctic ice fields. Pressure differences between the head of the Reeves Glacier and Inexpressible Island and the wind speed at Inexpressible Island were also shown to be significantly correlated (correlation coefficient of 0.61). This indicates that the katabatic winds are enhanced by acceleration down the local horizontal pressure gradient and represents a modulation of the time-averaged situation sketched in Figure 11. Figure 18 shows the cross spectra. Note that a high degree of coherence is present over time scales longer than about 1 day; no phase lag is seen between the katabatic wind at Inexpressible Island and the pressure difference along Reeves Glacier. Similar results have been obtained using 2-month records (September–October) for the same two AWS sites as well as

the September–October record at stations 05 and 23, situated further into the hinterland upslope from Reeves Glacier.

These results confirm earlier studies that the association between large-scale synoptic pressure patterns out over the Ross Sea is not a good indicator of katabatic wind events at Terra Nova Bay [*Bromwich*, 1989b] and that the local horizontal pressure gradients over the ice sheet can be dramatically different than those seen several hundred kilometers offshore [cf. *Bromwich and Parish*, 1989], in terms of both magnitude and direction. It can be concluded that there appears to be some large-scale modulation of the Inexpressible Island katabatic wind regime, but that such an effect is probably secondary to the locally forced drainage circulation along and above Reeves Glacier.

4.4. Interannual Changes

The records available for evaluation of the longer-term trends in the environment of the katabatic winds issuing from Reeves Glacier are limited because of the early AWS measurement difficulties at Inexpressible Island [cf. *Bromwich*, 1989b], primarily relating to the extreme stress exerted by the high-momentum airstream on the AWS. Table 3a summarizes the longest wind record available from the Inexpressible Island AWS, that for the months of February to April. It appears that there is a substantial downward trend in the intensity of the fall wind speeds at Inexpressible Island starting in about 1985. This corresponds to a less sharply defined start to the “winterlike” wind conditions [*Bromwich*, 1989b] in 1988 and 1989, as can be seen from the March and April averages. There is no corresponding trend in the mean air temperatures or sea level pressures.

The available annual record of temperatures and sea level pressures at Inexpressible Island is summarized in Table 3b. The two variables over this short period of record vary in phase, increasing and then decreasing back to close to the 1985 values by 1989. The 4-year means are -18.1°C and 989.8 hPa. The former is only 0.1°C colder than the annual average given by *Bromwich* [1989b], and the latter is 1.7 hPa higher than that quoted by *Bromwich* [1991] for 1985.

5. CONCLUSIONS AND REMARKS

The results from monitoring the intense katabatic wind regime at Terra Nova Bay for 2 years with a comprehensive AWS array have been presented. The coastal katabatic winds at Inexpressible Island are not as intense as previously thought; these winds are 6 and 3 m s^{-1} less on the annual average than those at the extraordinary katabatic sites at Cape Denison and Port Martin in Adélie Coast, respectively. However, this

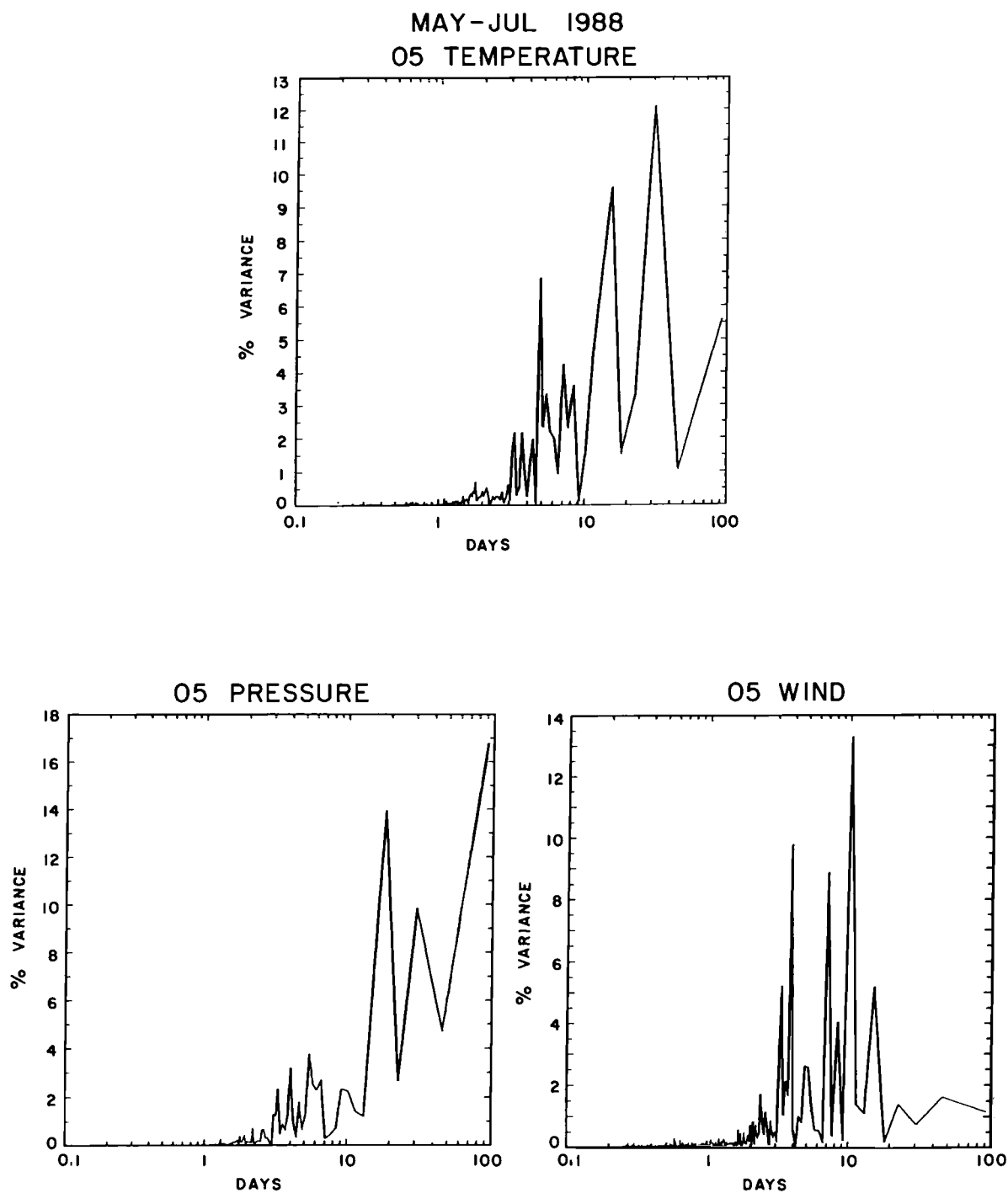


Fig. 16. Same as Figure 15 but for May-July 1988.

comparison is complicated by the substantial downward trend in fall wind speeds in recent years at Inexpressible Island (also applies to the annual means?) and by the fact that the results for Cape Denison and Port Martin are for 1912-1913 and 1950-1951, respectively. The

complications introduced by interannual variability can be circumvented by simultaneously monitoring the katabatic winds at all three sites, a task now being attempted with commencement of AWS measurements at the Adélie Coast sites in 1990 [Wendler and André,

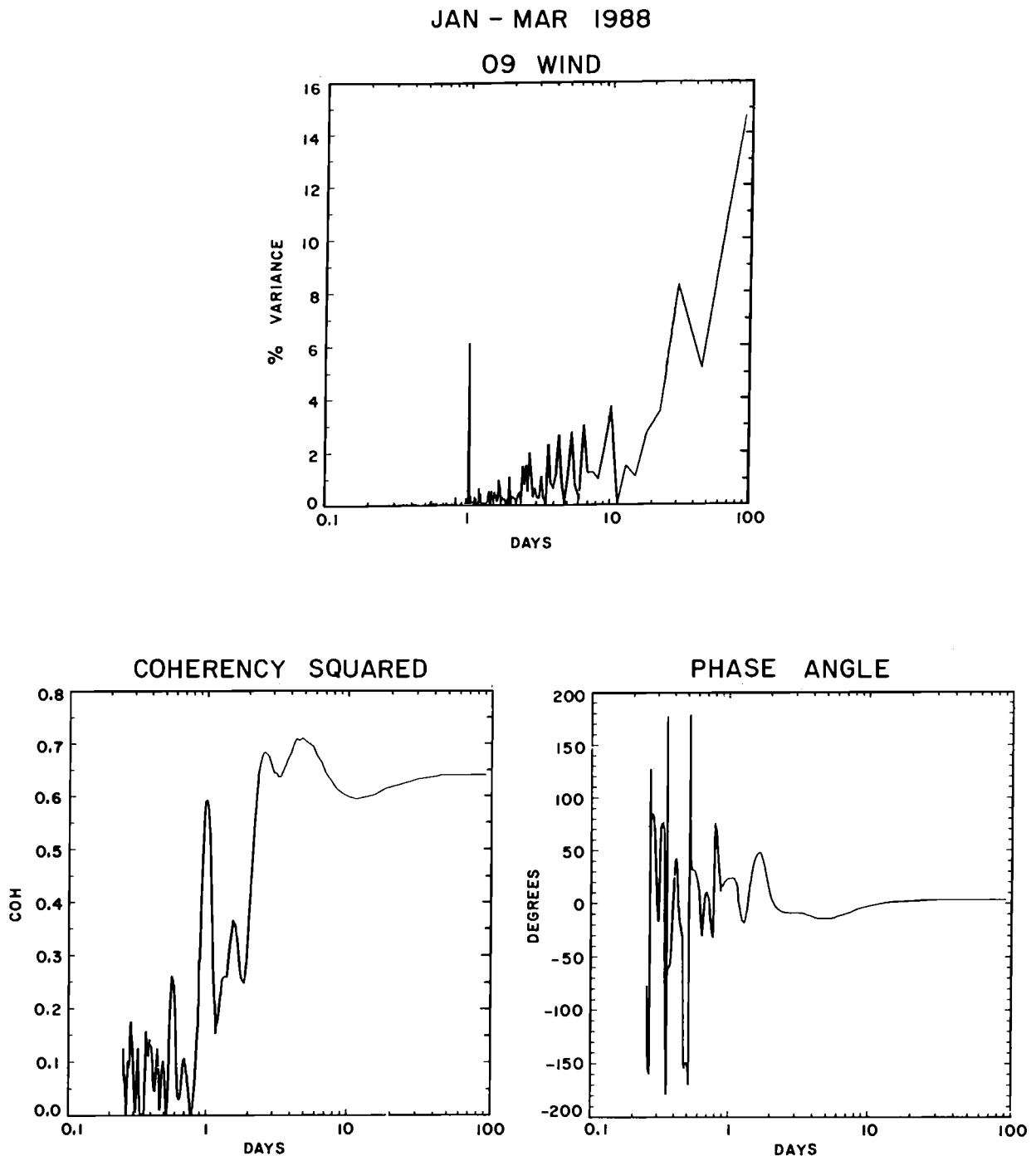


Fig. 17. Cross spectrum of wind for stations 05 and 09 for January-March 1988. (Top) Power spectra of station 09 wind and (bottom) coherency and phase spectra are shown.

1990]. The different physical settings of the sites should also be kept in mind when making the above comparison. Both Cape Denison and Port Martin sit right at the base of fairly uniform ice slopes, whereas Inexpressible Island is located 34 km horizontally downwind from the

exit to the Reeves Glacier through which the airflow is channeled. The picture is further complicated by the apparent acceleration of the airflow across the Nansen Ice Sheet.

The intense katabatic winds at Inexpressible Island

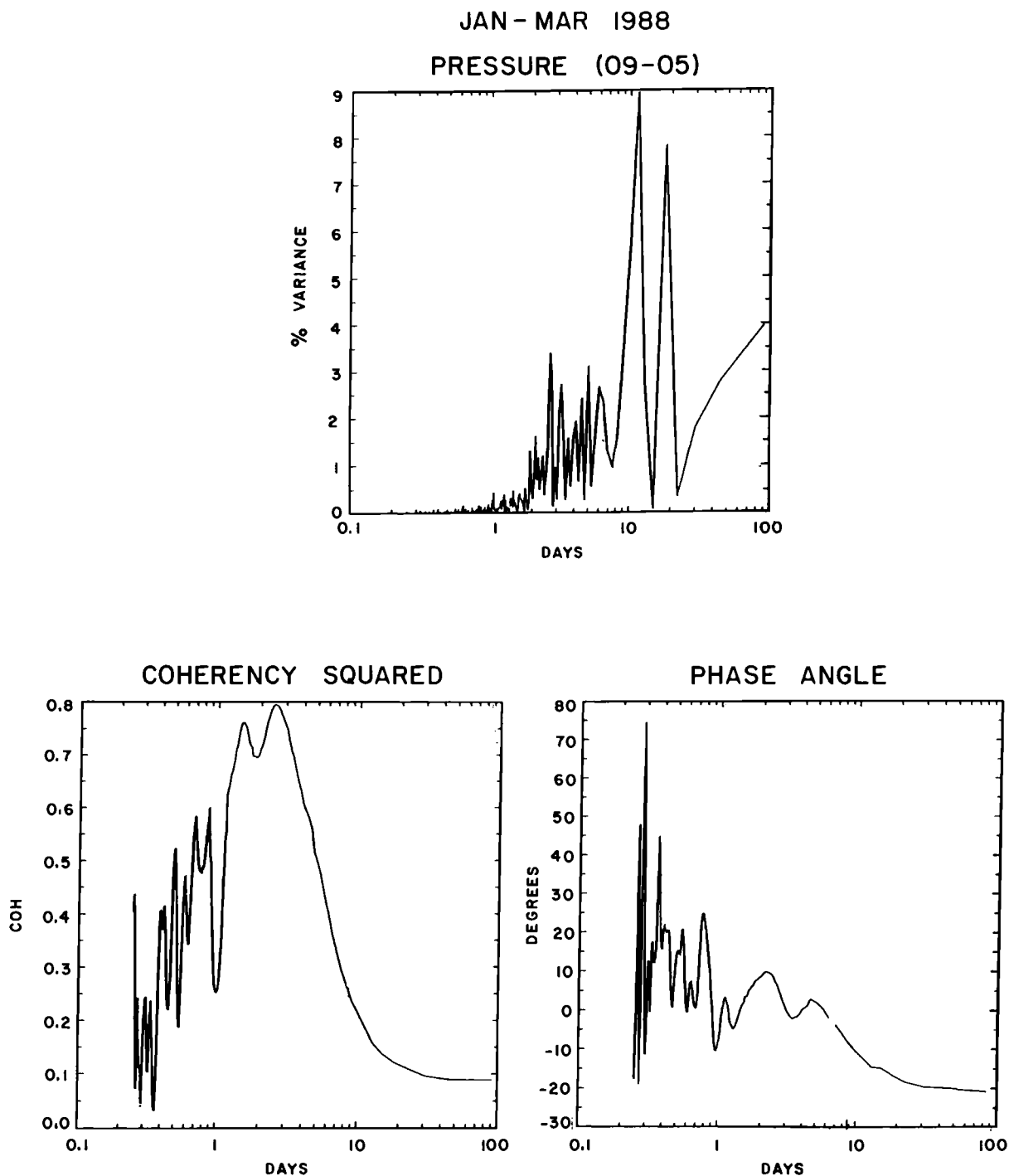


Fig. 18. Cross spectrum of pressure differences between station 05 and station 09 and wind speed at station 05 for January-March 1988. (Top) Power spectra of pressure differences and (bottom) coherency and phase spectra are shown.

result from two effects. The annual average speed increases by 2 m s^{-1} as a result of descent of 1000 m from AWS 09 to AWS 31. The speed increases further by 3 m s^{-1} across the Nansen Ice Sheet from AWS 31 to

AWS 05. This acceleration takes place down the local pressure gradient and is increased in association with short-term strengthening of the pressure gradient. It is possible that part of the wind speed enhancement at

TABLE 3a. Interannual Variations in Environmental Conditions at the Inexpressible Island AWS: Fall Wind Speeds (in Meters per second at 3-m Height)

Year	Wind Speed, m s ⁻¹				February–April Average		
	Jan.	Feb.	March	April	Wind Speed, m s ⁻¹	Air Temperature, °C	Station Pressure, hPa
1984	...	14.1	18.3	17.0	16.5	-17.4	977.5
1985	...	16.9	18.7	17.5	17.7	-17.7	981.9
1986	-15.8	985.5
1987	...	15.3*	17.8	17.0	16.7	-18.8	982.8
1988	6.9	12.2	15.7	13.4	13.8	-18.0	980.2
1989	6.6	11.5	11.4	16.9	13.5	-17.6	980.9

* Denotes one half month of data.

AWS 05 is due to the impact of horizontal airflow around Inexpressible Island [Bromwich, 1985]. Further investigations are needed to define the governing dynamics, which possibly involves complicated three-dimensional air motions [Argentini *et al.*, 1992].

The katabatic winds at Terra Nova Bay are sustained by radiatively cooled air which converges in the continental interior, but with the convergence being most marked near the head of Reeves Glacier [Parish and Bromwich, 1989a; Bromwich *et al.*, 1990a]. This is manifested by fairly uniform fluctuations in the state variables throughout the confluence zone–katabatic wind region. External influences on the airstream, such as synoptic forcing, seem to be of secondary importance to its internal dynamical controls. Variations in the behavior of the katabatic wind in its marginal areas can, to first order, be explained by buoyancy variations.

The intense katabatic winds issuing from Reeves Glacier form a spatially confined jet of cold air which Bromwich [1991] and Carrasco [1992] have shown is subject to frequent low-level baroclinic instability some distance offshore on the cyclonic shear side. The strong spatial gradients in this area's environmental properties can be adequately appreciated by resorting to remote-sensing observations from satellites and aircraft [Bromwich, 1989a; Bromwich *et al.*, 1990a] in conjunction with those from AWS. Such a complexity is expected to be the norm in the Antarctic because topographically forced alterations to stable airflow behavior readily generate such situations.

TABLE 3b. Annual Mean Air Temperatures and Sea Level Pressures

Year	Temperature, °C	Sea Level Pressure, hPa
1984
1985	-18.4	988.1
1986	-17.4	991.4
1987
1988	-17.8	991.4
1989	-18.7	988.2

With the increasing realization that Antarctic katabatic winds play a central role in the climate of high southern latitudes and with confluence zones being a key part of this circulation regime [Parish and Bromwich, 1987, 1991a], all these areas should be monitored because at each location their time-averaged observations represent a spatial integration of the climatic variations over a large section of the ice sheet. In addition, continuing efforts are needed to understand the governing dynamics of the confluence zone–coastal katabatic wind linkage. For this project analyses have been significantly impeded by the observations being largely confined to the near-surface layers; for example, direct measurements of stability variations and vertical wind shear [cf. Mastrantonio *et al.*, 1990; Argentini *et al.*, 1992] have not been generally possible. A comprehensive field program is being considered to characterize the full three-dimensional time dependent structure of this complex airstream, using surface-based remote-sensing and aircraft campaigns. Emphasis will be concentrated on the near-coastal areas where the most dramatic changes (e.g., the apparent horizontal acceleration across Nansen Ice Sheet) are taking place.

Acknowledgments. This research was funded in part by National Science Foundation grants DPP-8916134 to D. H. Bromwich, DPP-8916998 to T. R. Parish, and DPP-8818171 and 9015586 to C. R. Stearns. Byrd Polar Research Center contribution 846.

REFERENCES

- Argentini, S., G. Mastrantonio, G. Fiocco, and R. Ocone, Complexity of the wind field as observed by a sodar system and by automatic weather stations on the Nansen Ice Sheet, Antarctica, during summer 1988–89: Two case studies, *Tellus, Ser. B*, 44, 422–429, 1992.
- Ball, F. K., Winds on the ice slopes of Antarctica, in *Antarctic Meteorology, Proceedings of the Symposium, Melbourne, 1959*, pp. 9–16, Pergamon, New York, 1960.
- Bromwich, D. H., Katabatic wind interaction with Inexpressible Island, Terra Nova Bay, *Antarct. J. U.S.*, 20(5), 196–198, 1985.
- Bromwich, D. H., Satellite analyses of Antarctic katabatic

- wind behavior, *Bull. Am. Meteorol. Soc.*, 70, 738–749, 1989a.
- Bromwich, D. H., An extraordinary katabatic wind regime at Terra Nova Bay, Antarctica, *Mon. Weather Rev.*, 117, 688–695, 1989b.
- Bromwich, D. H., Mesoscale cyclogenesis over the southwestern Ross Sea linked to strong katabatic winds, *Mon. Weather Rev.*, 119, 1736–1752, 1991.
- Bromwich, D. H., and S. H. Ganobcik, Katabatic wind dynamics at Terra Nova Bay, Antarctica from the satellite image perspective, in *Third Conference on Polar Meteorology and Oceanography*, pp. J125–J128, American Meteorological Society, Boston, Mass., 1992.
- Bromwich, D. H., and J. K. Geer, Satellite analyses of katabatic winds near Terra Nova Bay, *Antarct. J. U.S.*, 26(5), 268–271, 1991.
- Bromwich, D. H., and D. D. Kurtz, Katabatic wind forcing of the Terra Nova Bay polynya, *J. Geophys. Res.*, 89, 3561–3572, 1984.
- Bromwich, D. H., and T. R. Parish, A strong katabatic wind event at Terra Nova Bay, *Antarct. J. U.S.*, 24(5), 223–225, 1989.
- Bromwich, D. H., T. R. Parish, and C. A. Zorman, The confluence zone of the intense katabatic winds at Terra Nova Bay, Antarctica, as derived from airborne sastrugi surveys and mesoscale numerical modeling, *J. Geophys. Res.*, 95, 5495–5509, 1990a.
- Bromwich, D. H., T. R. Parish, and A. Pellegrini, The katabatic wind regime near Terra Nova Bay, Antarctica, *Antarct. J. U.S.*, 25(5), 267–269, 1990b.
- Budd, W. F., W. R. J. Dingle, and U. Radok, The Byrd snowdrift project: Outline and basic results, in *Studies in Antarctic Meteorology, Antarct. Res. Ser.*, vol. 9, edited by M. J. Rubin, pp. 71–134, AGU, Washington, D. C., 1966.
- Carrasco, J. F., A mesoscale cyclogenesis study along the Pacific coast of Antarctica, M.S. thesis, 179 pp., Atmos. Sci. Program, Ohio State Univ., Columbus, 1992.
- Drewry, D. J., The surface of the Antarctic ice sheet, in Antarctica: Glaciological and geophysical folio, edited by D. J. Drewry, sheet 2, Scott Polar Res. Inst., Cambridge, England, 1983.
- James, I. N., On the forcing of planetary-scale Rossby waves by Antarctica, *Q. J. R. Meteorol. Soc.*, 114, 619–637, 1988.
- James, I. N., Antarctic drainage flow: Implications for hemispheric flow on the southern hemisphere, *Antarct. Sci.*, 1, 279–290, 1989.
- Keller, L. M., G. A. Weidner, C. R. Stearns, and M. F. Sievers, Antarctic automatic weather station data for the calendar year 1988, report, 329 pp., Dep. of Meteorol., Univ. of Wis., Madison, 1989.
- Keller, L. M., G. A. Weidner, and C. R. Stearns, Antarctic automatic weather station data for the calendar year 1989, report, 354 pp., Dep. of Meteorol., Univ. of Wis., Madison, 1990.
- Kodama, Y., G. Wendler, and N. Ishikawa, The diurnal variation of the boundary layer in summer in Adélie Land, eastern Antarctica, *J. Appl. Meteorol.*, 28, 16–24, 1989.
- Loewe, F., Considerations concerning the winds of Adélie Land, *Z. Gletscherkd. Glazialgeol.*, 10, 189–197, 1974.
- Mastrantonio, G., R. Ocone, S. Argentini, and G. Fiocco, Aspects of the Antarctic boundary layer observed by a triaxial Doppler sodar, in *Second Workshop Italian Research on Antarctic Atmosphere, Conference Proceedings*, vol. 27, edited by M. Colacino, G. Giovanelli, and L. Stefanutti, pp. 73–83, Italian Physics Society, Bologna, 1990.
- Mather, K. B., and G. S. Miller, Notes on the topographic factors affecting the surface wind in Antarctica, with special reference to katabatic winds, and bibliography, *Rep. UAG-189*, Geophys. Inst., Univ. of Alaska, Fairbanks, 1967.
- Panofsky, H. A., and G. W. Brier, *Some Applications of Statistics to Meteorology*, 224 pp., Pennsylvania State University, University Park, 1968.
- Parish, T. R., The katabatic winds of Cape Denison and Port Martin, *Polar Rec.*, 21, 525–532, 1981.
- Parish, T. R., Surface airflow over East Antarctica, *Mon. Weather Rev.*, 110, 84–90, 1982.
- Parish, T. R., and D. H. Bromwich, The surface windfield over the Antarctic ice sheets, *Nature*, 328, 51–54, 1987.
- Parish, T. R., and D. H. Bromwich, Instrumented aircraft observations of the katabatic wind regime near Terra Nova Bay, *Mon. Weather Rev.*, 117, 1570–1585, 1989a.
- Parish, T. R., and D. H. Bromwich, Observational and modeling studies of the katabatic winds at Terra Nova Bay, *Antarct. J. U.S.*, 24(5), 221–223, 1989b.
- Parish, T. R., and D. H. Bromwich, Continental-scale simulation of the Antarctic katabatic wind regime, *J. Clim.*, 4, 135–146, 1991a.
- Parish, T. R., and D. H. Bromwich, Automatic weather station observations of strong katabatic winds near Terra Nova Bay, Antarctica, *Antarct. J. U.S.*, 26(5), 265–267, 1991b.
- Parish, T. R., and K. T. Waight, The forcing of Antarctic katabatic winds, *Mon. Weather Rev.*, 115, 2214–2226, 1987.
- Schwerdtfeger, W., The climate of the Antarctic, in *World Survey of Climatology*, vol. 14, *Climate of the Polar Regions*, edited by S. Orvig, pp. 253–355, Elsevier, New York, 1970.
- Schwerdtfeger, W., *Weather and Climate of the Antarctic*, 261 pp., Elsevier, New York, 1984.
- Stearns, C. R., and G. Wendler, Research results from Antarctic automatic weather stations, *Rev. Geophys.*, 26, 45–61, 1988.
- Streten, N. A., Some synoptic indices of the southern hemisphere mean sea level circulation 1972–1977, *Mon. Weather Rev.*, 108, 18–36, 1980.
- Stull, R. B., *An Introduction to Boundary Layer Meteorology*, 666 pp., Kluwer Academic, Hingham, Mass., 1989.
- van Loon, H., The half-yearly oscillations in middle and high southern latitudes and the coreless winter, *J. Atmos. Sci.*, 24, 472–486, 1967.
- Watterson, I. G., and I. N. James, Baroclinic waves propagating from a high-latitude source, *Q. J. R. Meteorol. Soc.*, 118, 23–50, 1992.
- Wendler, G., and J. C. André, Winds in the coastal area of Adélie Land, *Antarct. J. U.S.*, 25(5), 265–267, 1990.

(Received December 15, 1991;
accepted April 29, 1993.)

KATABATIC WINDS ALONG THE TRANSANTARCTIC MOUNTAINS

CHRISTOPHER J. BRECKENRIDGE,¹ UWE RADOK,² CHARLES R. STEARNS,¹ AND DAVID H. BROMWICH³

Thermal infrared satellite imagery of the Ross Ice Shelf area of Antarctica often indicates dark streaks emanating from the major glaciers of the Transantarctic Mountains. Past authors have shown that these streaks indicate katabatic wind activity. In the present study, satellite imagery, automatic weather station (AWS) data, and synoptic analyses are used to characterize such activity for the 1982 austral winter. Over 50% of all available thermal infrared satellite images (those both with and without cloud cover) containing the Ross Island area and Skelton, Mulock, and Byrd glaciers show katabatic winds at one or more of these glaciers. However, it is likely that katabatic winds are present in nearly all the sufficiently cloud-free imagery. The overall frequency of katabatic activity may also be higher depending on its occurrence during cloudy conditions. Comparison of a case of intense katabatic winds in June 1982 with a case during July 1982 devoid of such winds indicates a dramatic difference in the supply of radiationally cooled near-surface air over the polar plateau. During the intense katabatic event, surface temperatures recorded by an AWS on the East Antarctic plateau are up to 45°C colder than surface temperatures at AWS sites on the Ross Ice Shelf, with potential temperatures up to 15 K lower. By contrast, during the case without katabatic winds, surface temperatures on the plateau are up to 15°C warmer (potential temperatures up to 45 K higher) than those on the Ross Ice Shelf. Thus the katabatic winds are likely of the "fall" type (i.e., requiring a supply of cold air at high elevations). A synoptic scale low-pressure area over the eastern Ross Sea/Ross Ice Shelf also appears conducive for intense katabatic activity.

1. INTRODUCTION

The East Antarctic ice sheet has an average elevation of over 2 km. The interior surface slopes are small: from the maximum interior elevation of 4270 m to the top of Beardmore Glacier at 2000 m, the average slope is 2.1 m km⁻¹. From the top of the Beardmore Glacier there is a 2-km fall over a horizontal distance of only 200 km, yielding a slope of 10 m km⁻¹. Along the Transantarctic Mountains and the continental coasts these abrupt surface slopes allow for the development of katabatic winds.

Using NOAA 2 (National Oceanic and Atmospheric Administration) infrared imagery from the very high resolution radiometer (VHRR), *Swithinbank* [1973] noticed dark gray streaks emanating from the major glaciers of the Transantarctic Mountains, principally Byrd, Mulock, and Skelton (see Figure 1 for locations). These dark gray streaks were seen to extend from the glacial base out 150 km onto the Ross Ice Shelf, beginning about 60 km up the valley from the foot of each glacier. (An example of this phenomenon is presented later in Figure 3.) *Swithinbank* [1973] proposed that the dark

streaks represented katabatic winds draining down the major glacial valleys from the polar plateau and warming adiabatically 25°C to 30°C. *D'Aguzzo* [1986] used NOAA advanced very high resolution radiometer (AVHRR) thermal infrared satellite images to document a case of katabatic winds down the glaciers of the Transantarctic Mountains, showing the katabatic airstreams to be up to 15 K warmer than the surrounding environment. *Godin* [1977] studied a case of katabatic winds through the Transantarctic Mountains which occurred in October 1973 by using Defense Meteorological Satellite Program (DMSP) thermal infrared satellite imagery. He conjectured that the katabatic winds appeared darker on the infrared imagery as a result of blowing snow. *Bromwich* [1989] has provided an overview of satellite-observed katabatic winds in the western Ross Sea area. *Bromwich et al.* [1992] examined satellite-observed katabatic winds originating from southern Marie Byrd Land in West Antarctica, which sometimes continue across the Ross Ice Shelf for distances of up to 1000 km.

A katabatic wind may be defined as "any wind blowing down an incline" [*Huschke*, 1959, p. 325]. *Schwerdtfeger* [1984] has classified katabatic flow into two types. In the "foehn" type the wind at the bottom of the slope is warmer than the displaced air. The "bora" (a fall wind) has the katabatic wind at the bottom of the slope being colder than the displaced air.

¹Department of Atmospheric and Oceanic Sciences, University of Wisconsin, Madison, Wisconsin 53706.

²Cooperative Institute for Research in Environmental Sciences, University of Colorado, Boulder, Colorado 80309.

³Byrd Polar Research Center, The Ohio State University, Columbus, Ohio 43210.

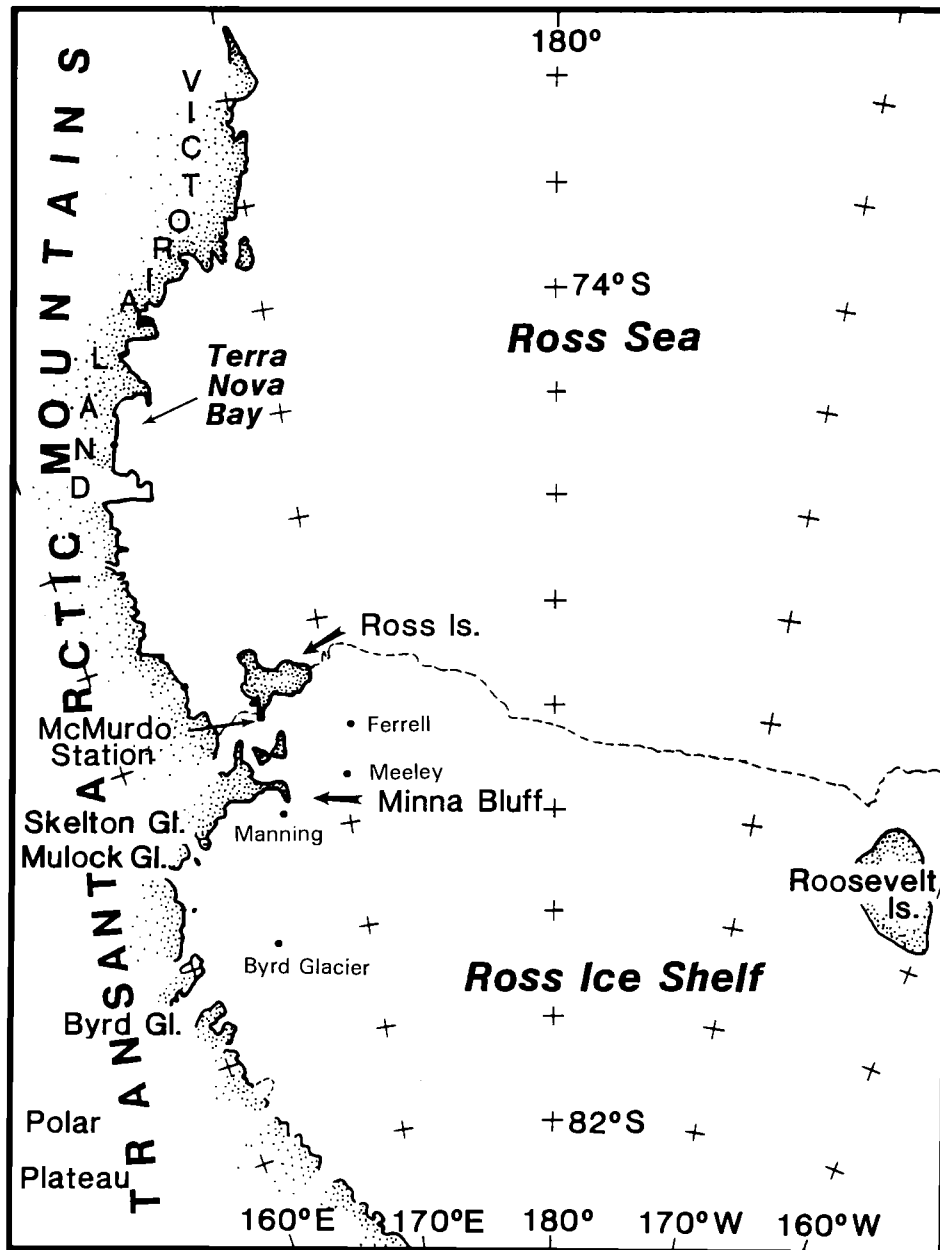


Fig. 1. Location map for western Ross Sea/Ross Ice Shelf area of Antarctica. Dots on the Ross Ice Shelf indicate AWS locations.

The foehn (föhn), quoting from the *Glossary of Meteorology* [Huschke, 1959, p. 226], is defined as “a warm, dry wind on the lee side of a mountain range, the warmth and dryness of the air being due to adiabatic compression upon descending the mountain slopes . . . It is associated with cyclonic scale motions, being produced only when the circulation is sufficiently strong and deep to force air completely across a major mountain range in a short period of time.” In contrast, the fall (or bora) wind is defined as [Huschke, 1959, p.

218] “a strong, cold, downslope wind. A fall wind differs from a foehn in that the air is initially cold enough so that it remains relatively cold despite adiabatic warming upon descent . . . a fall wind prerequisites an accumulation of cold air at high elevations.” The difficulty in determining the type of katabatic winds through the Transantarctic Mountains lies in their paradoxical qualities of resulting from drainage of the large pool of radiationally cooled air over the plateau of East Antarctica and yet appearing dark (i.e., warm with respect to

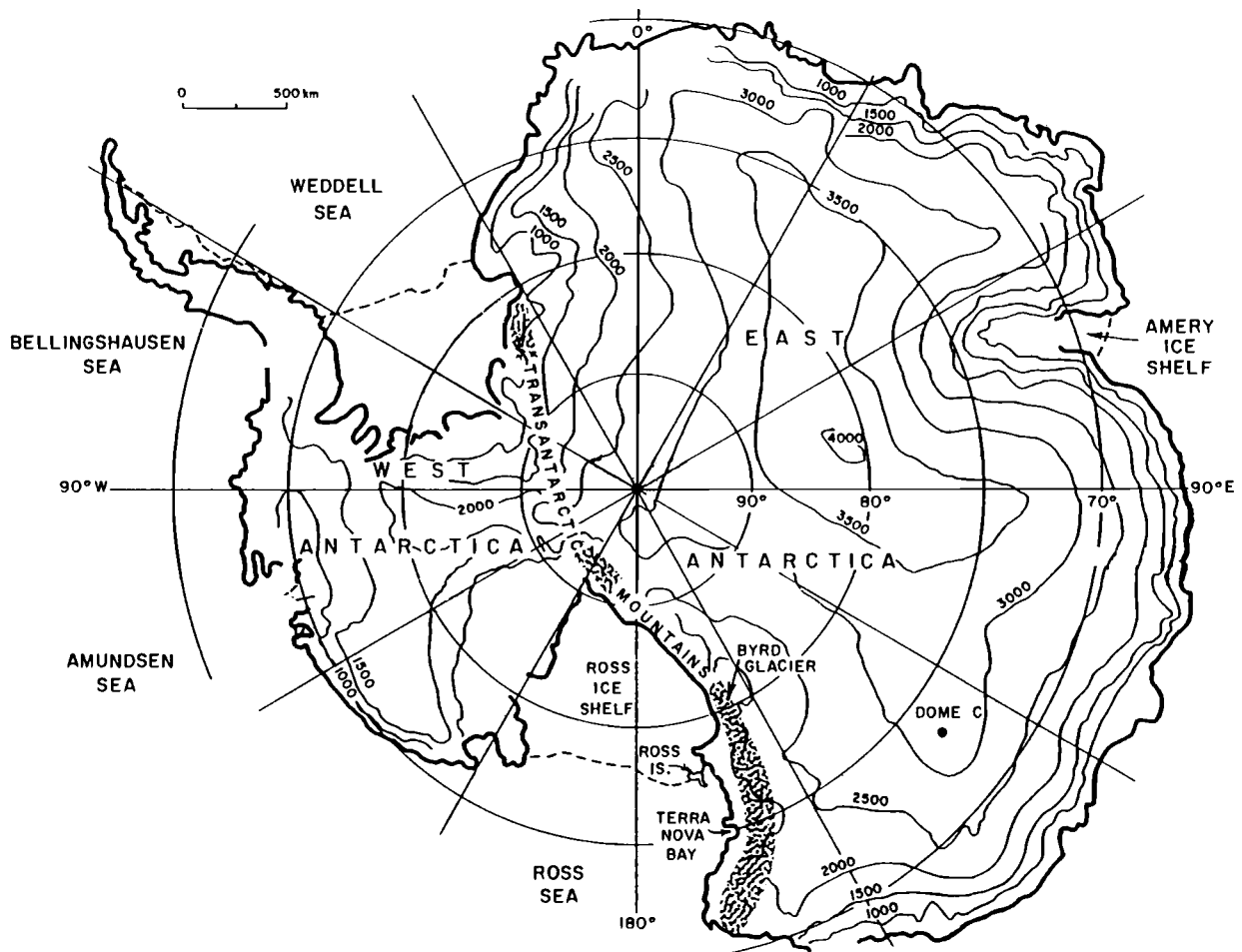


Fig. 2. Location map for the entire Antarctic continent, with terrain heights from 1000 to 4000 m, contoured every 500 m. Location of the Dome C AWS is indicated by the dot in East Antarctica.

their surroundings) on thermal infrared satellite imagery. The current amount of observational data does not yet allow for a conclusive answer to this question. However, *Bromwich* [1989] inferred that these katabatic winds are mainly of the fall type and explained their warm thermal infrared signatures as being due to surface warming resulting from the breakup of the strong low-level inversion common to the region; the air column as a whole is colder and more negatively buoyant than the surrounding air. Support for this explanation is found in the work of *Parish and Bromwich* [1989], where instrumented aircraft flights through katabatic airstreams near Terra Nova Bay on successive days in November 1987 showed these airstreams to be colder than the surrounding environment, even though these airstreams appeared warm on the infrared imagery.

2. DATA SOURCES

This study uses satellite imagery in the 10.5- to 11.5- μm band, surface and upper air synoptic charts,

and surface automatic weather station (AWS) data both to explore the synoptic setting for extended katabatic wind outbreaks along the Transantarctic Mountains and to obtain statistical information regarding katabatic wind occurrence and duration. The climatic state of the ice shelf, based on mean values of AWS data, will be compared to the katabatic wind state.

The AWS sites used in this study are Manning (8905), Ferrell (8907), and Meeley (8915) on the Ross Ice Shelf near Ross Island (Figure 1) and Dome Charlie (Dome C) (8904) on the East Antarctic plateau (Figure 2). Mean data from the Byrd Glacier (or Marilyn, 8921; see Figure 1) AWS are also discussed. Details of Antarctic AWS operation are given by *Stearns et al.* [this volume].

Hemispheric surface and upper air synoptic analyses consisting of surface pressure and 1000- to 500-hPa thickness analyses, 500-hPa geopotential height analyses, and 250-hPa geopotential height analyses will be used in the case studies of the katabatic and nonkatabatic wind events. These are produced every 12 hours at 0000 UTC

TABLE 1. Multiannual Monthly Mean AWS Data From Ferrell Site (78.0°S, 170.8°E, 44-m Elevation), From December 1980 to August 1983

Month	Mean Temperature, °C	Maximum Temperature, °C	Minimum Temperature, °C	Mean Wind Speed, m s ⁻¹	Resultant Wind Direction, deg true	CON, %	Maximum Wind Speed and Direction, m s ⁻¹ /deg true	Mean Sea Level Pressure, hPa	Maximum Sea Level Pressure, hPa	Minimum Sea Level Pressure, hPa
Jan.	-7.5	4.9	-21.6	3.6	206	61	15.0/194	993.6	1010.1	978.4
Feb.	-15.8	0.5	-35.2	4.8	195	71	18.7/207	995.4	1015.2	979.5
March	-25.1	-8.4	-42.1	6.0	204	78	26.7/211	990.3	1011.4	969.5
April	-30.9	-8.8	-55.9	6.5	210	81	28.2/225	990.1	1020.3	961.1
May	-30.5	-12.9	-50.1	7.3	205	90	26.3/218	991.7	1015.5	963.5
June	-33.7	-12.9	-53.4	6.2	209	81	26.5/214	988.7	1030.3	952.2
July	-36.5	-16.6	-55.4	5.2	216	77	21.7/219	992.2	1028.9	962.6
Aug.	-34.0	-15.9	-56.9	6.9	209	81	26.5/211	988.9	1032.2	956.0
Sept.	-36.9	-15.5	-53.1	5.6	207	80	21.7/210	988.9	1029.6	959.2
Oct.	-27.3	-11.2	-48.1	5.3	215	79	24.1/221	986.5	1008.2	962.6
Nov.	-16.8	-0.8	-31.6	6.0	211	87	21.3/224	986.7	1004.2	962.9
Dec.	-7.3	4.6	-16.1	4.7	207	72	16.6/217	992.2	1012.9	969.7
Average	-25.2	-7.8	-43.3	5.8	208	79	22.8/215	990.7	1018.2	964.8
Maximum	-7.3	4.9	-16.1	7.3	216	90	28.2/224	995.4	1032.2	978.4
Minimum	-36.9	-16.6	-56.9	3.6	195	61	15.0/194	986.5	1004.2	952.2

Ferrell AWS was out of service August–November 1983. The 44-m elevation is the elevation at the end of the averaging period. Routine resurveying of AWS elevations is responsible for the different value reported by *Stearns et al.* [this volume].

and 1200 UTC and are based on the U.S. Navy analyses constructed at McMurdo Station. For the surface pressure and 1000- to 500-hPa thickness analyses, contours are not drawn over the interior, as these would be of dubious validity given the high surface elevations of both the East and the West Antarctic ice sheets.

Up until the year 1972, orbiting satellites were flying too high to adequately resolve many interesting surface features. With the advent of the NOAA 2 satellite launched on October 15, 1972, this problem was rectified by the use of scanning radiometers such as the VHRR. Scanning radiometers provide both stored picture coverage and direct transmission of cloud or ice cover images to local receiving stations worldwide. The VHRR allowed for the combination of large areal coverage and high resolution where each image covers 2200 by 2200 km at a resolution of 4 km.

The satellite images used in this study were taken by the NOAA 7 polar-orbiting satellite launched on June 23, 1981. (The hard copies of these images were recorded at McMurdo Station.) With an orbital period of 101.9 min, this satellite utilized an AVHRR which differs from the VHRR (for the purposes of this study) in that it carries an additional infrared channel. The infrared band of the utilized images is from 10.5 to 11.5 μm .

3. BACKGROUND CONDITIONS

3.1. Climatic State

The climate of the Ross Island region near McMurdo can be described by mean values from the Meeley, Manning, Ferrell, and Byrd Glacier AWS sites. The re-

sults serve as a background to the study of katabatic wind outbreaks from Byrd, Mulock, and Skelton glaciers. Tables 1–3 are climatic summaries for Ferrell, Meeley, and Manning sites for an approximately 3-year period (late 1980 to late 1983). Table 4 gives similar data for Byrd Glacier but only for a period of about 7 months (because of station operation problems). This latter incomplete data set is used to get an idea of what may typically occur near the base of one of the glaciers. Pressure values used in the climate summaries are reduced to sea level via the use of the hypsometric equation. “CON” refers to wind constancy (vector mean wind speed divided by mean scalar wind speed). The means in these tables were computed by taking the simple average of the station’s 3-hourly data for the indicated periods.

It is clear by looking at Tables 1–4 that for the months of June through August Manning had warmer average temperatures than either Meeley or Ferrell. For example, in the month of July, Manning’s average temperature is -33.8°C . This is 2.4°C warmer than Meeley’s climatic mean of -36.2°C and 2.7°C warmer than the mean at Ferrell. For the period of June through August, Manning averages 2.5°C warmer than Ferrell and 2.2°C warmer than Meeley.

Although the data from Byrd Glacier AWS are quite limited, some interesting observations can be made from them. Table 4 indicates that this station was warmer in the winter of 1984 than the ice shelf stations in the mean. For example, the mean temperature for July 1984 at Byrd Glacier was -31.4°C , at least 2°C warmer than the other ice shelf AWS sites. Thus the station located directly at the base of a glacier is the

TABLE 2. Multiannual Monthly Mean AWS Data From Meeley Site (78.5°S, 170.2°E, 52-m Elevation), December 1980 to November 1983

Month	Mean Temperature, °C	Maximum Temperature, °C	Minimum Temperature, °C	Mean Wind Speed, m s ⁻¹	Resultant Wind Direction, deg true	CON, %	Maximum Wind Speed and Direction, m s ⁻¹ /deg true	Mean Sea Level Pressure, hPa	Maximum Sea Level Pressure, hPa	Minimum Sea Level Pressure, hPa
Jan.	-7.5	2.7	-18.4	4.0	219	70	13.6/217	993.7	1010.5	978.4
Feb.	-16.0	-3.0	-35.7	4.8	207	75	17.5/219	995.5	1015.2	980.5
March	-25.2	-9.1	-42.6	6.1	209	85	24.8/232	990.6	1009.0	970.3
April	-31.5	-8.0	-55.4	6.4	208	84	28.2/225	990.0	1020.3	961.1
May	-30.2	-12.9	-49.0	7.1	206	86	26.3/218	991.7	1015.7	960.8
June	-32.5	-12.6	-53.7	7.4	213	88	25.3/194	988.5	1030.2	952.2
July	-36.2	-16.6	-55.4	4.2	218	87	24.2/215	991.8	1028.5	960.6
Aug.	-34.5	-13.2	-55.5	6.6	210	89	23.9/218	988.9	1032.4	956.4
Sept.	-36.1	-15.4	-54.5	5.4	213	87	24.6/200	989.0	1022.6	953.0
Oct.	-26.1	-10.2	-47.5	6.3	214	90	22.2/217	982.7	1007.3	951.1
Nov.	-16.4	-2.0	-31.7	5.7	212	88	21.7/207	983.6	1003.9	960.9
Dec.	-7.0	2.7	-14.9	4.8	212	79	15.1/211	991.7	1012.5	968.4
Average	-24.9	-8.2	-42.9	5.7	212	84	22.3/215	990.1	1017.3	962.8
Maximum	-7.0	2.7	-14.9	7.4	219	90	28.2/225	995.5	1032.4	980.5
Minimum	-36.2	-16.6	-55.5	4.0	205	70	13.6/217	982.7	1003.9	951.1

Wind data for April–May 1981 and for May–July 1982 are from Ferrell AWS because of aerovane freeze-up at Meeley. Meeley AWS was out of service June–July 1983; data from Ferrell AWS were used (0.8 hPa was subtracted from sea level pressures to account for elevation difference between the two sites). Elevation is as stated in Table 1.

warmest of all. This is consistent with the high frequency of katabatic wind activity observed along the Transantarctic Mountains, as will be discussed.

At Byrd Glacier the resultant winds are consistently from the southwest and west-southwest. This direction corresponds to that of the fall line of the glacier; in general, the winds tend to be directed straight down the

face of the glacier and out onto the ice shelf. Compare this to the resultant surface wind direction over the Ross Ice Shelf at Meeley site which is from the south-southwest (Table 2). The limited climatic data from Byrd Glacier AWS are consistent with frequent katabatic wind activity down Byrd Glacier.

Table 5 compares mean winter (June, July, August;

TABLE 3. Multiannual Monthly Mean AWS Data From Manning Site (78.8°S, 166.9°E, 74-m Elevation), December 1980 to November 1983

Month	Mean Temperature, °C	Maximum Temperature, °C	Minimum Temperature, °C	Mean Wind Speed, m s ⁻¹	Resultant Wind Direction, deg true	CON, %	Maximum Wind Speed and Direction, m s ⁻¹ /deg true	Mean Sea Level Pressure, hPa	Maximum Sea Level Pressure, hPa	Minimum Sea Level Pressure, hPa
Jan.	-7.0	6.0	-19.0	3.5	275	69	11.6/248	996.0	1009.3	976.7
Feb.	-15.6	-1.4	-36.7	3.6	268	75	15.5/229	995.8	1015.2	980.3
March	-24.3	-6.6	-44.6	4.5	268	72	21.3/252	991.4	1012.9	969.3
April	-29.1	-5.5	-54.7	5.9	250	85	22.2/236	991.0	1020.9	962.0
May	-28.7	-9.1	-51.1	5.1	250	75	20.8/256	993.2	1019.1	961.7
June	-31.3	-11.1	-56.6	5.1	251	70	23.2/239	989.5	1031.8	953.5
July	-33.8	-14.9	-56.5	4.0	266	70	20.9/240	992.5	1029.5	963.8
Aug.	-31.6	-11.9	-55.1	6.4	249	83	23.7/218	990.4	1033.8	959.0
Sept.	-34.7	-12.6	-52.5	4.3	271	71	18.7/236	989.6	1024.8	956.3
Oct.	-25.7	-8.8	-51.1	6.5	249	86	19.3/242	983.6	1009.5	953.1
Nov.	-14.6	-3.6	-34.0	5.2	253	79	17.4/249	984.4	1004.4	961.0
Dec.	-6.1	5.2	-20.7	4.2	261	74	18.4/262	991.5	1011.4	969.8
Average	-23.5	-6.9	-44.4	4.9	257	76	19.4/242	990.7	1018.6	963.9
Maximum	-6.1	6.0	-19.0	6.5	275	85	23.7/218	996.0	1033.8	980.3
Minimum	-34.7	-12.6	-56.6	3.5	249	69	11.6/248	983.6	1004.5	953.1

Mean wind data missing March–November 1981 because of aerovane malfunction at low wind speeds. Elevation is as stated in Table 1.

TABLE 4. Monthly Mean AWS Data From Byrd Glacier Site (Marilyn, 80.0°S, 165.0°E, 75 m Elevation), February 1984 to July 1984

Month	Mean Temperature, °C	Maximum Temperature, °C	Minimum Temperature, °C	Mean Wind Speed, m s ⁻¹	Resultant Wind Direction, deg true	CON, %	Maximum Wind Speed and Direction, m s ⁻¹ /deg true	Mean Sea Level Pressure, hPa	Maximum Sea Level Pressure, hPa	Minimum Sea Level Pressure, hPa
Feb.	-17.0	-0.9	-39.1	4.0	244	65	14.5/258	997.7	1009.9	987.1
March	-21.9	-7.6	-37.7	8.1	246	84	24.4/257	986.4	997.8	964.0
April	-24.4	-4.9	-38.2	7.7	241	88	18.3/237	988.2	998.8	954.7
May	-26.4	-8.8	-42.9	8.8	240	83	29.5/208	994.8	1017.9	961.5
June	-29.1	-9.6	-46.6	7.2	223	72	23.1/192	989.8	1011.3	958.3
July	-31.4	-10.7	-48.7	6.2	230	75	26.4/198	983.3	999.7	962.1

Because of the lack of year-round coverage, overall statistics are not included. Byrd Glacier AWS was operating from 0300 UTC on January 16, 1984, through 1800 UTC on August 6, 1984.

June and July only for Byrd Glacier site) values from Tables 1–4 with mean winter values from these same AWS sites for longer time periods (potentially through 1989, but of differing lengths for each AWS [see *Stearns et al.*, this volume]). Differences in the means between the two sets of time periods are minor for Manning, Meeley, and Ferrell sites. The larger differences for Byrd Glacier site are not surprising, as its shorter time period only encompassed data from a single year. All of the conclusions and comparisons of this paper based upon the shorter time periods are also valid when the means from the longer time periods are considered.

3.2. Katabatic Wind Activity Statistics

Swithinbank [1973] first documented the occurrence of katabatic wind activity along the Transantarctic Mountains but made no attempt to determine how common this activity was. *Bromwich* [1989] found, as a result of surveying thermal infrared imagery for April through October for both 1984 and 1985, that 98% of the images where Byrd, Mulock, and/or Skelton glaciers were visible displayed katabatic winds. For the present study the frequency of this phenomenon is provided by examining the satellite images for the months of June–

TABLE 5. Winter (June, July, August) Means of AWS Data for Ferrell, Meeley, Manning, and Byrd Glacier (Marilyn) Sites Over Two Time Periods

Time Period	Mean Temperature, °C	Mean Wind Speed, m s ⁻¹	Resultant Wind Direction, deg true	Constancy, %	Mean Sea Level Press,* hPa
<i>Ferrell</i>					
1981–1983	-34.7	6.1	211	80	989.9
1981–1989	-34.0	6.2	212	82	990.0
<i>Meeley</i>					
1981–1983	-34.4	6.1	214	88	989.7
1981–1983, 1985†	-35.0	6.1	214	88	989.1
<i>Manning</i>					
1981–1983	-32.2	5.2	255	74	990.8
1981–1985	-32.7	4.3	258	73	991.1
<i>Byrd Glacier‡</i>					
1984	-30.3	6.7	227	74	986.6
1984, 1987–1989	-30.2	7.1	241	80	990.4

The first is that found in Tables 1 through 4. The second is based on all available data from each site through 1989, based on data presented by *Stearns et al.* [this volume].

*For comparison purposes, elevations used to compute both mean sea level pressures for each station are those valid at the end of 1983 (1984 for the Byrd Glacier site).

†No wind data are available from 1985; therefore wind-related means from the two periods are identical.

‡Mean data cover June and July only.

[Redacted]

[Redacted]

[Redacted]

[Redacted]

[Redacted]

[Redacted]

[Redacted]

[Redacted]

[Redacted]

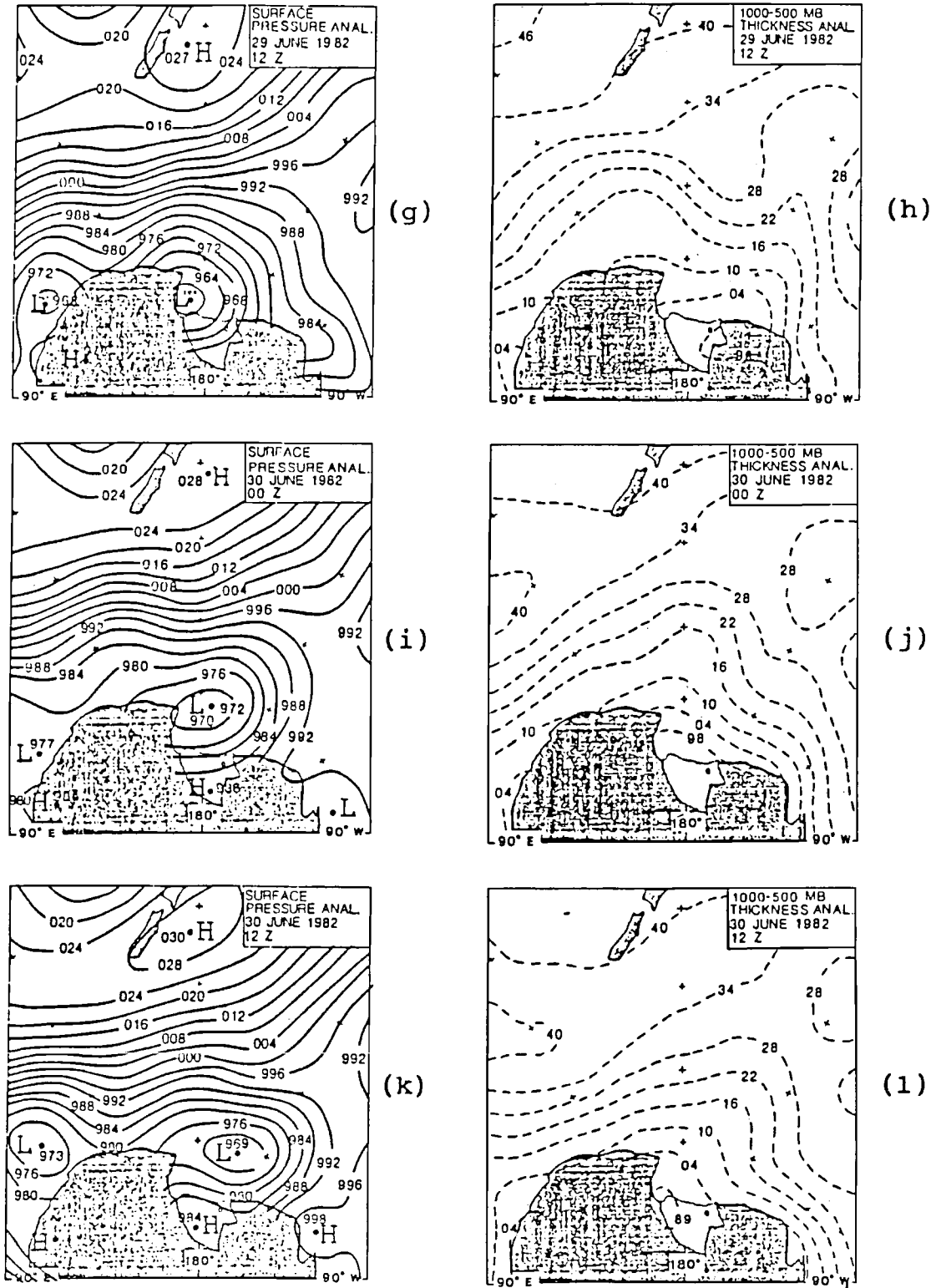


Fig. 4. (continued)

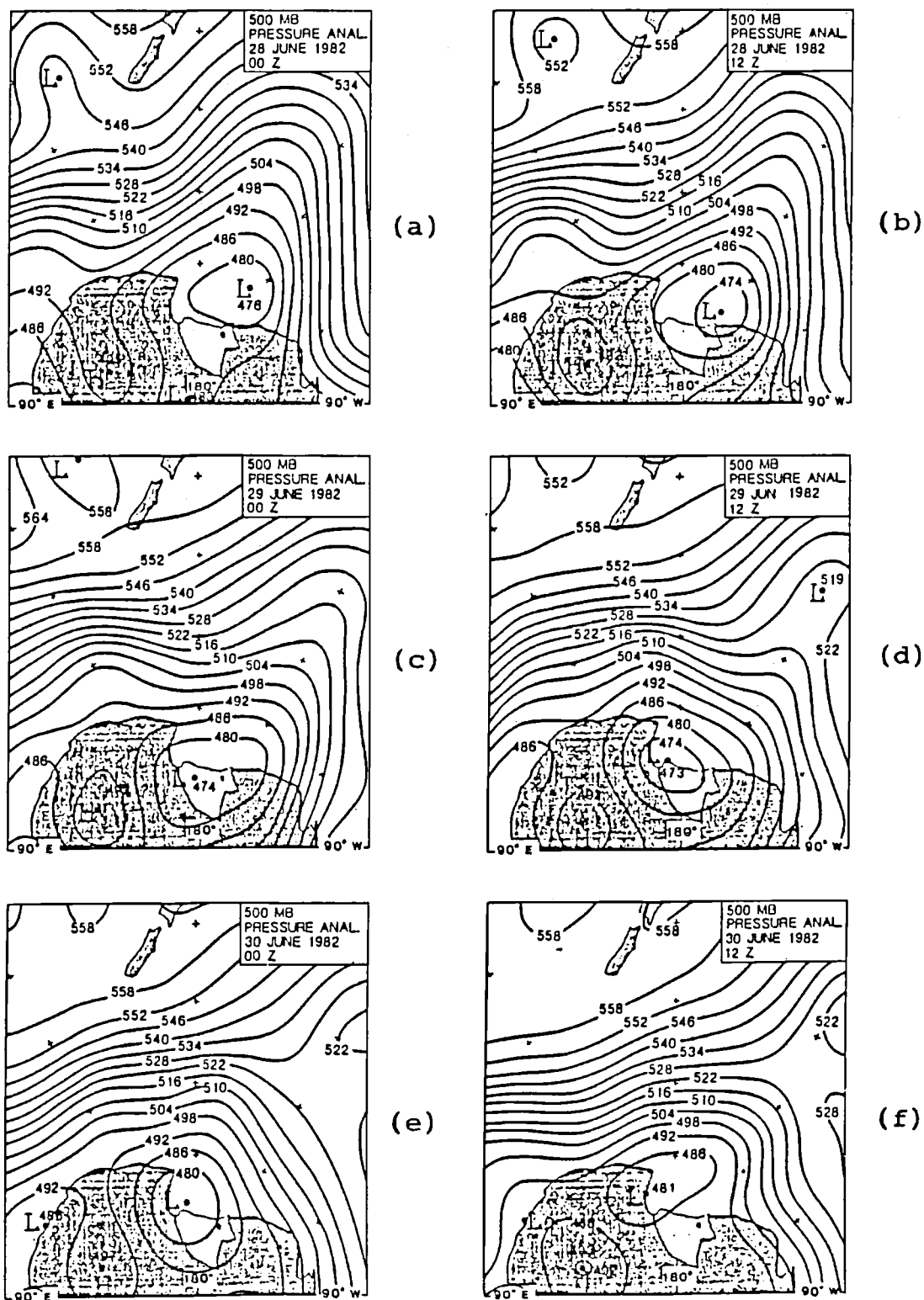


Fig. 5. The 500-hPa geopotential height analyses (6-gpdam contour interval) for the following 1982 times: (a) 0000 UTC on June 28, (b) 1200 UTC on June 28, (c) 0000 UTC on June 29, (d) 1200 UTC on June 29, (e) 0000 UTC on June 30, and (f) 1200 UTC on June 30.

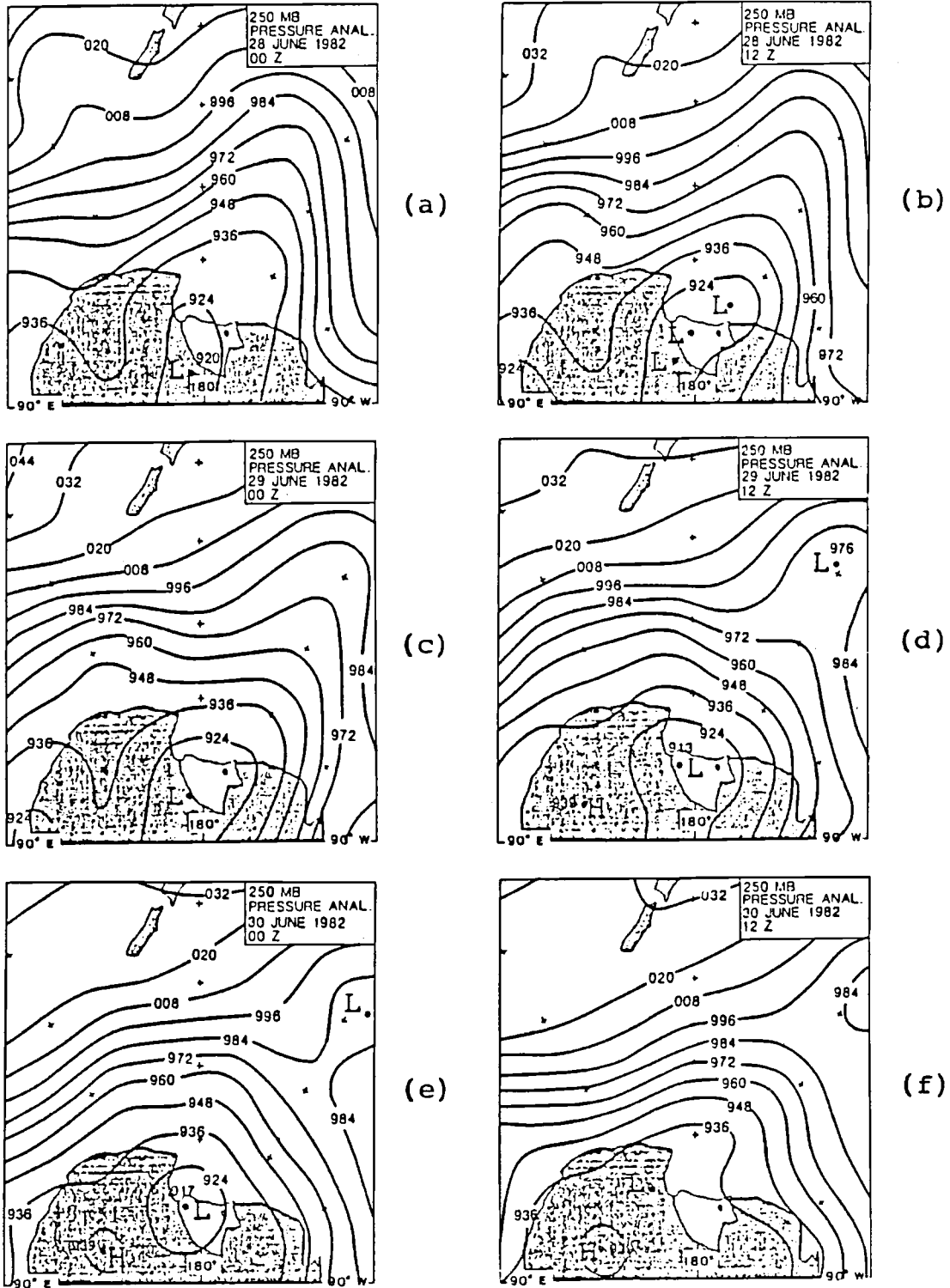


Fig. 6. The 250-hPa geopotential height analyses (12-gpdam contour interval). The times for this sequence of maps are the same as those in Figure 5.

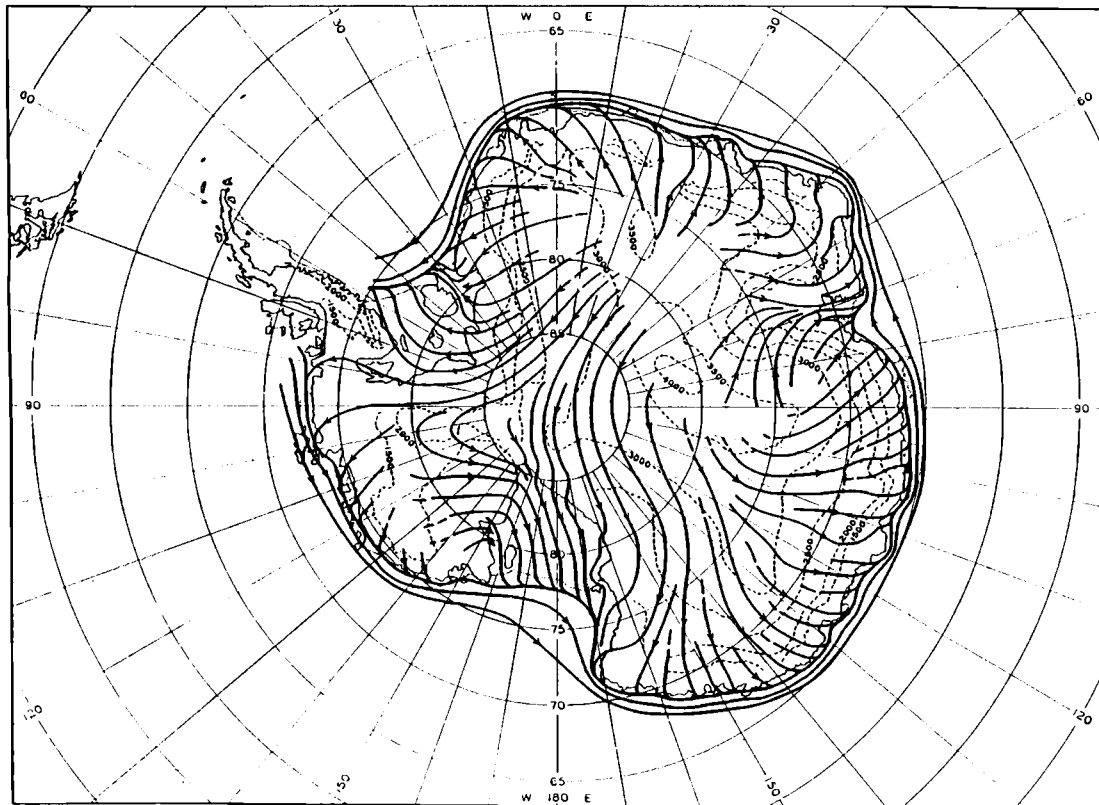


Fig. 7. Streamlines of average surface wind flow over Antarctica, inferred from traverse and station records [after Mather and Miller, 1967].

high of 988 hPa is situated with its center south of Byrd Glacier. AWS pressure readings for 0003 UTC confirm this: Manning registers 988.8 hPa, Ferrell 985.4 hPa, and Meeley 986.0 hPa. The dominant feature for this case is the large cyclone positioned to the north of Marie Byrd Land near 140°W, 75°S, with a 960-hPa analyzed central pressure. Satellite imagery showed the cyclonic cloud shield ahead of the warm front extending over the eastern Ross Ice Shelf, with the trailing cold front nearly coinciding with the north-south-oriented thickness lines (Figure 4b).

According to the satellite photos for June 26 and 27, this storm moved in from the northwest and at 0000 UTC on June 28 is no longer deepening but is an occluded system losing its definition; at this stage it is difficult to accurately locate its surface center from the satellite imagery. Several small eddies were seen in the satellite imagery behind the cold front over the Ross Sea. The trailing cold front is now of the inactive type, consisting of broken bands of cumuliform and stratiform clouds. This implies a weaker baroclinic zone with weak cold air advection and vertical shear. All of this is consistent with the storm becoming occluded. At 0327 UTC on June 28, McMurdo Sound and Ross Island are obscured by stratiform clouds found west of the warm

frontal cloud shield; the glaciers south of Byrd Glacier are not as obscured, and subsequently katabatic wind activity is observed.

At 0327 UTC on June 28, Dome C records a temperature of -70.7°C while Manning's temperature is -27.7°C and Meeley's is -31.6°C . At this time the potential temperature at Dome C is 16.8 K colder than that at Manning. The orientation of the cloud bands and the dark streaks extending out from the glacial bases suggests moderate south-southwesterly flow in association with the cyclone to the east. This is confirmed by the AWS data. The winds at 0327 UTC on June 28 are 9.2 m s^{-1} from 217° at Manning, 11.3 m s^{-1} from 194° at Ferrell, and 12.0 m s^{-1} from 210° at Meeley. Surface flow thus approximates the mean flow (Figure 7) with a component directed across the mountains and toward the east. At Beardmore Glacier (see Figure 3 for location) winds appear in the satellite imagery (via the dark signatures) to be nearly south to north across the mountains; subsequently, extensive katabatic wind activity is observed there.

At 0000 UTC on June 28 the 500-hPa closed low (Figure 5a) is located at 160°W , 73°S , near the center of the cloud spiral in the satellite imagery. The surface and 500-hPa low centers are nearly vertically stacked, im-

peding development and intensification. Figures 5a and 6a show the positions of the 500-hPa and 250-hPa troughs. Their axes extend northward from the Ross Ice Shelf out over the South Pacific at nearly 160°W. The axes' positions change very slowly over the next 24 hours; by 0000 UTC on June 29 the axes lie at nearly 150°W (Figures 5c and 6c).

The 0831 UTC June 28 satellite image shows the dark streaks abruptly turning to the left as they advance onto the ice shelf. Strong southerly winds are observed at this time on the ice shelf: Meeley records winds from 198° at 13.9 m s⁻¹, and Ferrell records winds from 214° at 8.5 m s⁻¹.

By 1200 UTC on June 28 the cyclone has a central pressure of 961 hPa (Figure 4c). The storm has moved slightly westward. Satellite imagery shows that the clouds around the system have gradually dissipated, leaving the western Ross Ice Shelf partially cloud-free. Pressures have fallen over the past 12 hours by 11 hPa at Manning and 10 hPa at Meeley. The cold front as seen on satellite imagery still coincides with the north-south-oriented thickness lines (Figure 4d). The surface winds at the AWS sites have been decreasing over the past 12 hours. At 500 hPa (Figure 5b), geostrophic winds are directed nearly parallel to the western Transantarctic Mountains.

The time 1200 UTC on June 28 is of maximum interest, being very near the time that the katabatic wind activity is at its peak intensity. The 1515 UTC June 28 image (Figure 3) clearly displays the dark, thick streaks representing adiabatically warmed air flowing down from the major Transantarctic Mountain glaciers onto the Ross Ice Shelf. Flow off Byrd, Skelton, and Mulock glaciers is extremely strong; as the warming air hits the base of the glacier and starts flowing out onto the ice shelf, it is deflected slightly to the left by the Coriolis force.

The AWS data support the existence of katabatic wind activity at 1200 UTC on June 28. The observed surface winds at 1155 UTC on June 28 have a directional component across the mountains and toward the east. Meeley reports 6.7 m s⁻¹ from 200°, Ferrell 4.2 m s⁻¹ at 239°, and Manning 2.2 m s⁻¹ from 222°. Note that the winds at the AWS sites have weakened by the time of most intense katabatic activity as revealed by the satellite imagery. This is due to the eastward direction of the main body of the katabatic airstreams as they leave Byrd, Mulock, and Skelton glaciers (Figure 3), passing to the south of the AWS sites.

An important factor contributing to the intensity of the katabatic wind outbreak appears to have been the temperature difference between Dome C and the ice shelf stations. From 0000 UTC on June 28 to 1200 UTC on June 28 the 498 geopotential dekameter (gpdam) cold pool has apparently translated west, and now this colder air likely lies over the eastern plateau (Figures 4b and 4d). At 0900 UTC on June 26 the temperature at Dome

C was as high as -50°C; by 0000 UTC on June 28 it had dropped to -71°C with a potential temperature of 229.5 K. Dome C temperatures remained near -70°C from 0000 UTC through 1200 UTC on June 28, with the potential temperatures near 229 K, indicating a buildup of very cold air on the plateau. (The lowest temperature for the month, -76.4°C, had occurred at 1438 UTC on June 7.) The ice shelf station temperatures for 1200 UTC on June 28 range in the negative low to mid thirties. At 1155 UTC on June 28, Manning measured -30.4°C, Ferrell -34.4°C, and Meeley -31.4°C. Thus a 40°C temperature difference existed between Dome C and the ice shelf.

Station potential temperatures also seem to favor severe katabatic wind activity. At 1155 UTC on July 28, Dome C records 231.2 K while Manning reads 245.0 K and Ferrell reads 240.8 K. From 0000 UTC to 1200 UTC on July 28, Dome C's potential temperature was lower than Manning's by an average of 15.7 K. This potential temperature gradient indicates that the air flowing from the plateau down to the ice shelf did not come from as far away as Dome C but from a lower elevation nearer the Transantarctic Mountains. However, the Dome C temperatures indicate a large supply of cold air over the interior of the ice sheet.

The 1656 UTC June 28 satellite image continues to show katabatic streaks extending outward onto the shelf and not sharply turned, but spreading out in all directions. At this time there is a weaker pressure gradient between Manning and Meeley than 12 hours previously; the pressure difference is only 0.4 hPa at 1656 UTC, as opposed to 2.8 hPa at 0831 UTC. Meeley reports a calm, and Ferrell has 2.5 m s⁻¹ from 170°. Thus the AWS winds have weakened still further, as the katabatic streaks continue to largely bypass these locations.

4.1.2. *June 29, 1982.* The 0000 UTC June 29 surface analysis (Figure 4e) shows that the dominant cyclone has moved west-southwestward. It lies over the northwestern Ross Ice Shelf with a central pressure of 963 hPa. By 0300 UTC on June 29 the entire Ross Ice Shelf with the exception of the northwest tip is obscured by clouds. Satellite photos show that the storm has slowly progressed westward. The 0315 UTC June 29 satellite image depicts moderate katabatic wind activity still occurring from Byrd through Skelton glaciers. The pressure gradient over the ice shelf stations remains weak with a pressure difference between Manning and Meeley of 0.7 hPa. AWS units indicate that the lowest pressures reached were at 2351 UTC on June 28 when Meeley recorded 971.5 hPa, Ferrell 970.3 hPa, and Manning 970.8 hPa. From this period on all station sea level pressures rose steadily.

Temperature data at Dome C for the period 1200 UTC on June 28 through 0315 UTC on June 29 continue to show a cold pool on the plateau (temperatures of -69°C to -70°C). Thus plenty of cold, dense air was still available to drain down the glaciers.

By 1200 UTC on June 29 the cyclone has strengthened slightly and moved to the northwest, now lying over the western Ross Sea just off the eastern coast of Victoria Land (Figure 4g). Despite the presence of some obscuring cloud cover, katabatic wind activity is still observable at Byrd and Mulock glaciers. Low pressures are still observed at the AWS sites; at 1135 UTC on June 29, Manning records 975.2 hPa, Ferrell 973.8 hPa, and Meeley 973.6 hPa. The pressure gradient has strengthened: the pressure difference between Meeley and Manning is 1.8 hPa with the gradient directed from Manning to Meeley (toward the Ross Sea). Surface winds have intensified and are directed from the west through the southwest; winds at Manning are 5.6 m s^{-1} from 293° , those at Ferrell are from 240° at 4.4 m s^{-1} , and winds of 9.9 m s^{-1} from 228° are seen at Meeley.

The 500-hPa and 250-hPa height analyses for 1200 UTC on June 29 indicate little change (Figures 5d and 6d); the long-wave trough axes have remained quite stationary at 150°W for the past 12 hours. The 1200 UTC June 29 thickness analysis indicates little change over the past 12 hours (Figure 4h); correspondingly, temperatures at Dome C have remained constant over the period. At 1155 UTC on June 29 a large temperature difference between Dome C and the ice shelf stations is still observed: while Dome C reads -69.6°C , Manning reports -28.0°C , and Ferrell reports -36.4°C .

4.1.3. *June 30, 1982.* As of 0000 UTC on June 30 the entire ice shelf including the McMurdo Sound region and most of the Transantarctic Mountains is obscured by mid- to low-level stratiform clouds. The 0303 UTC June 30 satellite image indicates ridge line cirrus curving from the Ross Sea inland over the eastern ice shelf and out over central Marie Byrd Land. Figures 5e–5f depict a shortwave ridge building into that area with its axis near 140°W . In addition, a 500-hPa low can be seen over the western Ross Sea corresponding to the position of the analyzed surface low center in Figure 4i. Surface pressures at the AWS stations remain low but are slowly rising. At 2339 UTC on June 29, Manning reports 975.8 hPa, Ferrell 975.1 hPa, and Meeley 974.9 hPa. Whether or not the cold air on the plateau was draining down the glaciers at this time is impossible to determine by direct examination of the satellite photos. However, it is quite possible that cold air drainage is occurring at the surface beneath the cloud layers, even though it is not consistently observable on the satellite imagery via the presence of dark streaks. Indeed, from 1200 UTC on June 29 through 1200 UTC on June 30, katabatic wind activity remains visible in some satellite imagery, with dark streaks on several of the Transantarctic glaciers including Byrd, Mulock, and Beardmore.

By 2339 UTC on June 29 the temperatures at Dome C have risen nearly 13°C over the past 24 hours; the station now records -55.9°C , Manning reads -25.1°C , Ferrell reads -24.5°C , and Meeley reads -24.5°C . The

temperature difference is decreasing which should aid in diminishing the intensity of the katabatic wind activity.

The 0000 and 1200 UTC June 30 surface analyses (Figures 4i and 4k) show the main cyclone moving east-northeastward and into the South Pacific Ocean. Thus this storm has made a loop of the Ross Sea area, moving in from the northeast, then northward along the Transantarctic Mountains, and then to the northeast out of the area.

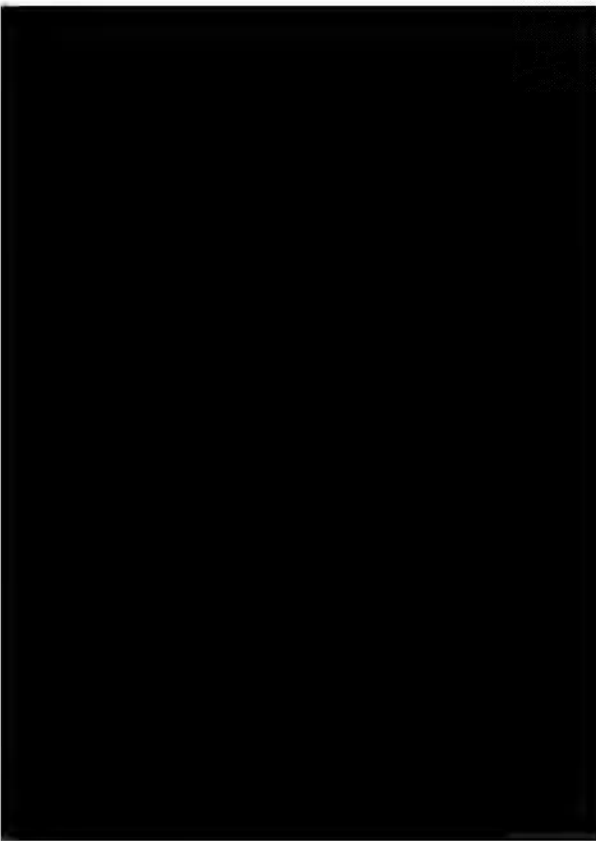
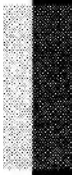
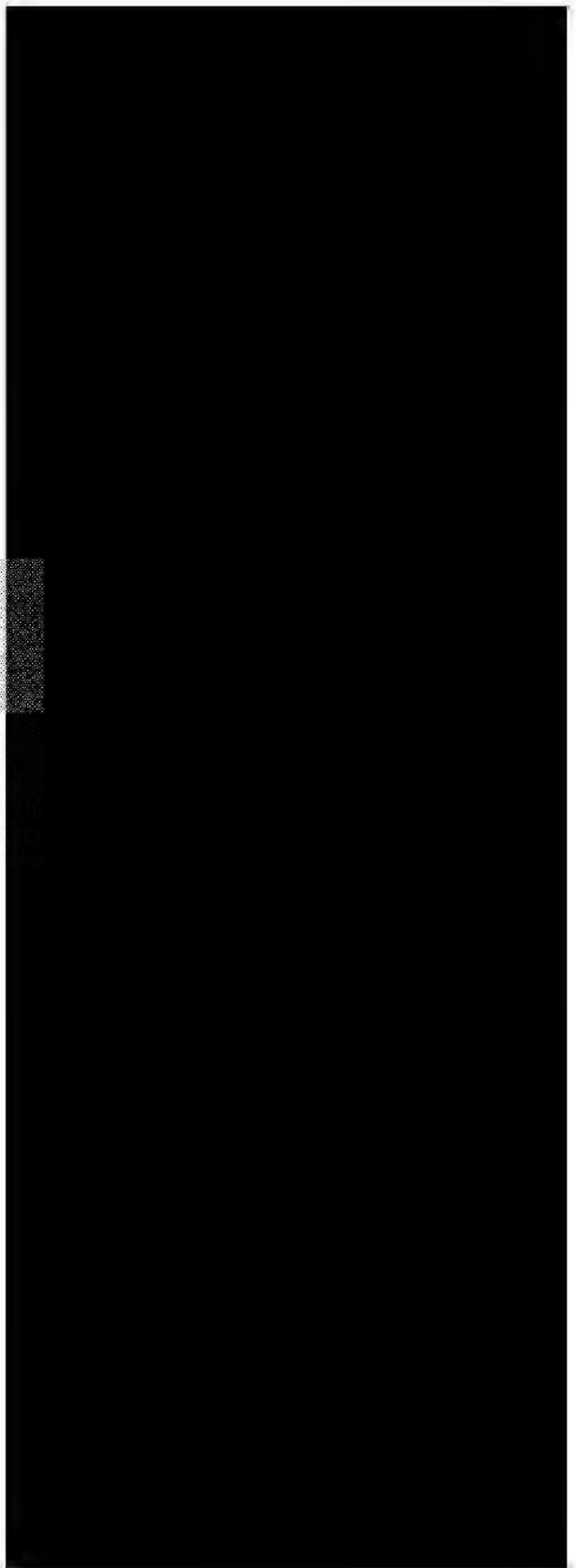
The 0948 UTC June 30 satellite photo shows the presence of the low-pressure system analyzed on the 1200 UTC June 30 surface chart (Figure 4k), with its center at 160°W , 70°S . Pressures at Manning are currently 4–5 hPa greater than those at Meeley and Ferrell; corresponding to this intense pressure gradient, the surface winds have strengthened from the directions south through southwest. At 0948 UTC on June 30, Manning records winds from 245° at 12.6 m s^{-1} , and Meeley reports winds of 16.2 m s^{-1} from 217° . These directions are similar to those at 1200 UTC on June 28 when the katabatic wind activity was at its peak intensity, though the speeds are roughly twice as strong as they were at that time.

4.1.4. *Case summary.* The following aspects highlight this case study. Two important factors to consider are the temperature and potential temperature differences between the plateau, here represented by Dome C, and the ice shelf. A $30^\circ\text{--}40^\circ\text{C}$ temperature and a 10–18 K potential temperature difference between Dome C and Manning (the ice shelf) may be needed for the occurrence of extensive katabatic wind activity. This indicates the presence of a pool of very cold air on the plateau which warms adiabatically as it flows out and onto the ice shelf. This cold pool is created by intense radiational cooling in conjunction with the high pressure over the plateau, which brings clear skies and weak winds.

The position of the surface low appears to be important; the low should be over the eastern Ross Sea or western Marie Byrd Land such that the resulting surface winds are directed parallel to the northeast, with the pressure gradient directed from Manning to Meeley. Strong katabatic winds may also be associated with upper air height contours oriented such that the geostrophic wind has a directional component across the Transantarctic Mountains from west to east. It is this combination of above mentioned temperature factors with these special wind and pressure fields that appears to lead to intense katabatic wind outbreaks.

4.2. A Case Without Katabatic Winds

In comparison to the intense katabatic wind outbreak, we will examine the opposite situation: an extended episode of negligible katabatic wind activity along the glaciers of the Transantarctic Mountains. Figure 8 is a satellite photo representative of the conditions which



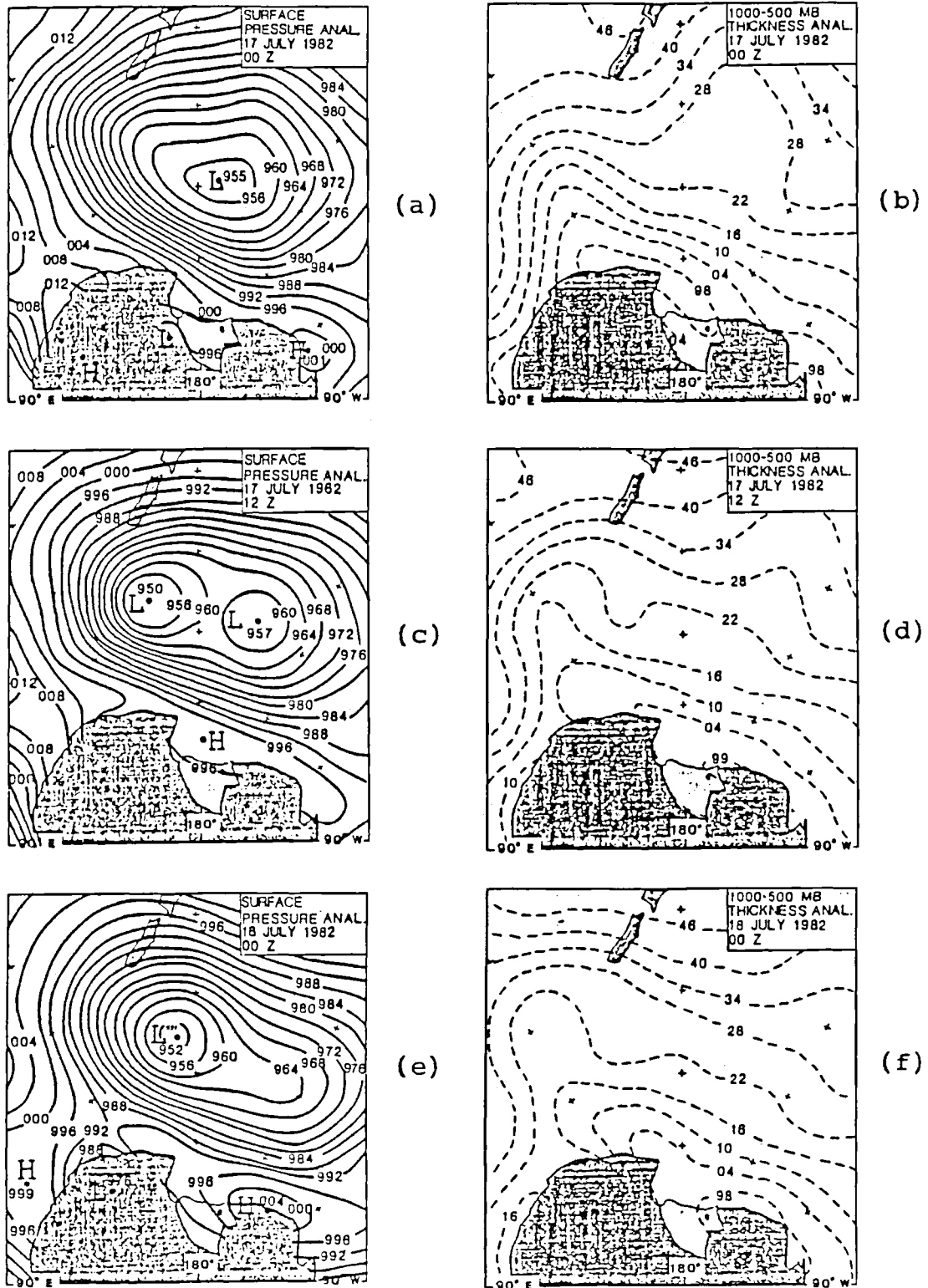


Fig. 9. (Left) Surface pressure analyses (4-hPa contour interval) and (right) the 1000- to 500-hPa thickness analyses for the corresponding time (6-gpdm contour interval; 98 = 498, 04 = 504, etc.) for the following 1982 times: (a)-(b) 0000 UTC on July 17, (c)-(d) 1200 UTC on July 17, (e)-(f) 0000 UTC on July 18, (g)-(h) 1200 UTC on July 18, (i)-(j) 1200 UTC on July 19.

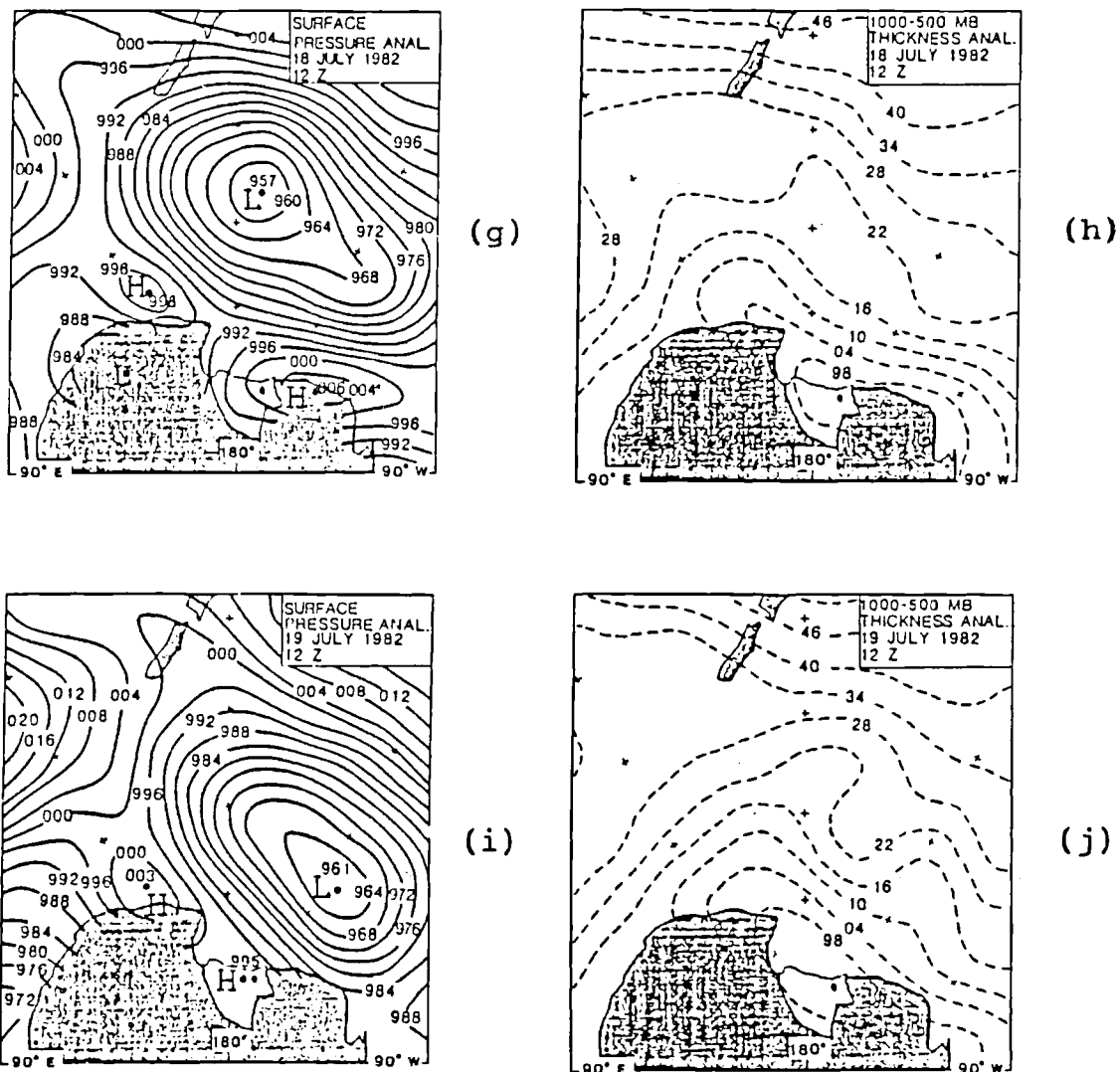


Fig. 9. (continued)

temperature difference between Dome C and the ice shelf show that the 498-gpdam cold pool has decreased and translated eastward to northwestern Marie Byrd Land. Over the past 12 hours, Dome C temperatures have risen; at 1128 UTC on July 17, AWS 8904 registers -41.7°C , a warming of 12.0°C over the 12-hour period. Temperatures at Meeley and Ferrell have remained nearly constant; at 1128 UTC on July 17 Meeley reads -43.5°C , and Ferrell -44.1°C . The ice shelf temperatures are now lower than those on the plateau. The potential temperature at 1128 UTC on July 17 at Dome C is 260.3 K versus 229.7 K at Meeley, 229.0 K at Ferrell, and 237.3 K at Manning.

Both upper air charts (Figures 10b and 11b) suggest southerly flow across the mountains with an west-to-east component. Upper air winds are likely very weak

over the ice shelf given the small geopotential height gradients.

4.2.2. July 18, 1982. By 0000 UTC on July 18, 1982, the high over Marie Byrd Land and the Ross Ice Shelf has continued to strengthen (Figure 9e). At 0108 UTC on July 18, Ferrell records 1010.3 hPa and Manning registers 1011.2 hPa, indicating increases of 4–5 hPa over the previous 12 hours.

The image for 0000 UTC on July 18 represents the peak of inactivity. Roosevelt Island, Ross Island, Minna Bluff, Black Island, and White Island all show up clearly outlined on this image as darker than the surrounding ice, and there are no dark streaks. The major reason for the lack of katabatic wind activity is that the air over the plateau is very warm compared to that on the ice shelf. At 0108 UTC on July 18, Dome C's potential tempera-

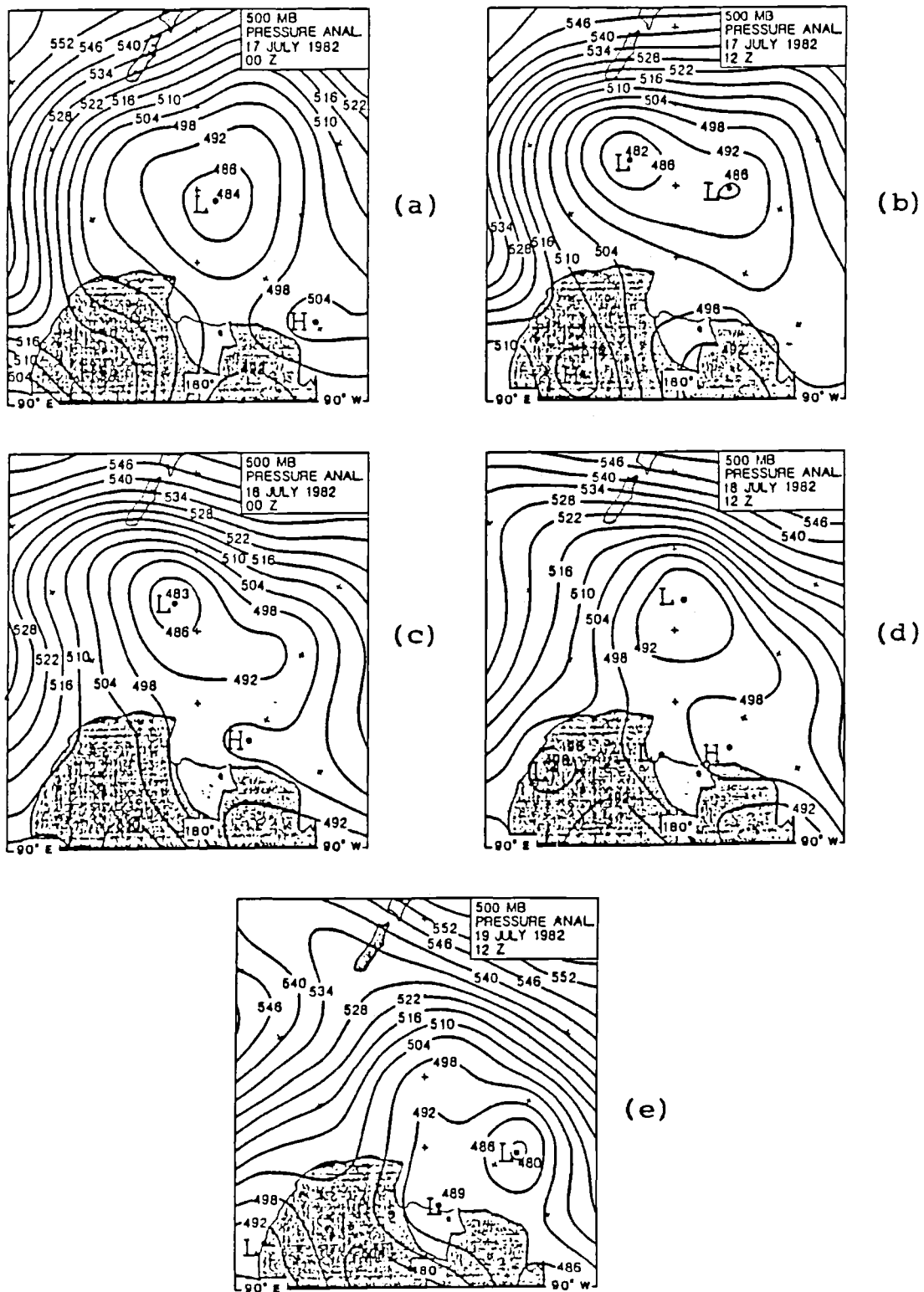


Fig. 10. The 500-hPa geopotential height analyses (6-gpdam contour interval) for the following 1982 times: (a) 0000 UTC on July 17, (b) 1200 UTC on July 17, (c) 0000 UTC on July 18, (d) 1200 UTC on July 18, (e) 1200 UTC on July 19.

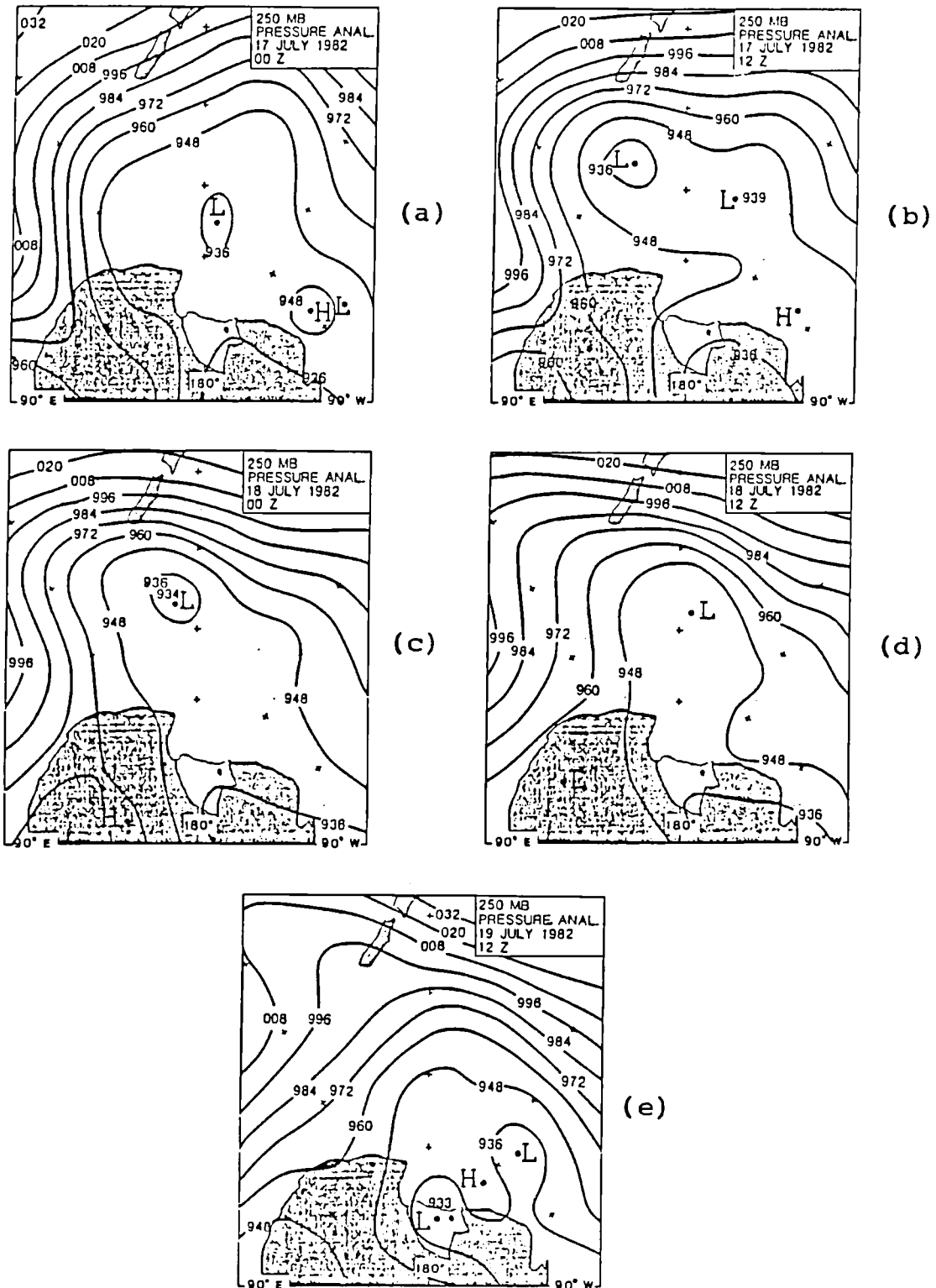


Fig. 11. The 250-hPa geopotential height analyses (12-gpdam contour interval). The times for this sequence of maps are the same as those in Figure 10.

ture was 266.5 K while Manning recorded 224.5 K, Meeley 220.7 K, and Ferrell 220.2 K; this is the largest contrast since the beginning of this case.

The thickness analysis of Figure 9*f* shows the 498-gpdam cold pool over Marie Byrd Land; the values increase westward until 516-gpdam thicknesses are observed off the East Antarctic coast near Dome C and northeastern Wilkes Land. The highest Dome C temperature for this case, -35.0°C , occurred at 2000 UTC on July 17. At 0108 UTC on July 18, Dome C registered -37.5°C . Values at Meeley, Ferrell and Manning for that time were -52.2°C , -52.7°C , and -48.5°C , respectively. During this period of minimal katabatic wind activity, ice shelf station temperatures were up to 15.2°C colder than those at Dome C. By contrast, the 0700 UTC June 28 (during the case described in section 4.1) Dome C temperature was 42.7°C colder than that at Ferrell, and at 1200 UTC on June 28 (the period of peak katabatic wind activity), Dome C was 39.6°C colder than the ice shelf. The corresponding potential temperatures on the high plateau were up to 14 K lower than those on the ice shelf. The case analyzed here thus highlights the very (relatively) warm air over the plateau.

The warm air over the plateau was advected in from the Indian Ocean by a large ridge with its axis near 130°E (Figures 10*b* and 11*b*). The McMurdo analyses indicated that a 70-knot (35 m s^{-1}) jet at 250 hPa was located off the coast between 110°E and 140°E (not shown); the 1600 UTC July 17 satellite image indicates extensive ridge line cirrus extending over the eastern plateau reaching inland to Dome C. Additionally, such cirrus clouds hindered the radiational cooling necessary for production of cold air over the plateau.

Surface winds over the ice shelf at 0108 UTC on July 18 are light south-southwesterlies. Meeley registers calm winds, and Ferrell registers winds from 211° at 2.4 m s^{-1} . Winds at Manning fluctuate from northwest to southwest; at 0108 UTC on July 18 they are from 224° at 1.5 m s^{-1} . The 0431 UTC July 18 satellite image indicates scattered cloudiness over the plateau. The entire ice shelf is of a uniform white; no katabatic wind activity is visible. The 0934 UTC July 18 satellite image is also a picture of tranquility; the ice shelf is of a uniform white, and the plateau a uniform light gray indicating its higher temperature. No katabatic wind activity is visible at any of the glaciers.

Figure 9*g* is the surface analysis for 1200 UTC on July 18. The South Pacific low has progressed eastward and weakened by 6 hPa. It is now located near 175°W , 56°S . The high over Marie Byrd Land has strengthened a little over the past 12 hours; its position has remained roughly the same. This high has dominated the weather over the Ross Ice Shelf for the past 24 hours. At 0935 UTC on July 18, Manning records 1013.0 hPa, Ferrell 1011.0 hPa, and Meeley 1011.4 hPa.

South to southwesterly winds have occurred at Fer-

rell since 1200 UTC on July 17. At 0935 UTC on July 18, Ferrell reports 2.8 m s^{-1} from 221° . Manning's winds for the past 24 hours have been light westerlies. Speeds have been very low for most of this case study because of the high-pressure cell and corresponding weak pressure gradient; values have ranged from 2 to 4 m s^{-1} . Figures 10*d* and 11*d* indicate nearly calm conditions at 1200 UTC on July 18 for the upper levels as well.

Figure 9*h* shows the 498-gpdam cold pool covering the ice shelf and most of Marie Byrd Land at 1200 UTC on July 18. Moving west across the Transantarctic Mountains, thicknesses increase until the warm pool near Dome C is reached. At 1145 UTC on July 18, Dome C registers -39.4°C , Meeley has cooled to -53.0°C , and Ferrell has cooled to -54.1°C .

4.2.3. *July 19, 1982.* The final analyses are for 1200 UTC on July 19; the 0000 UTC July 19 maps were unavailable. Widespread high pressure extends over the entire ice shelf and presumably much of the central plateau from South Pole to Dome C (Figure 9*i*). For the past 24 hours, pressures have slowly fallen by roughly 6 hPa to 1104 UTC July 19 readings of near 1005 hPa at Meeley, Ferrell, and Manning.

The weak pressure gradient over the ice shelf corresponds with the very weak surface winds for the past day; at 1100 UTC on July 19, Manning was calm, and Ferrell registered only 2.4 m s^{-1} . These low winds have been south to southwesterly at Ferrell and Meeley and southwest to northwesterly at Manning. These are climatologically common directions for these stations (Figure 7), especially during low wind speed situations.

Figure 9*j* shows that the plateau thicknesses have likely decreased over the past 24 hours. Correspondingly, the temperature at Dome C has decreased since 2000 UTC on July 17. By 0526 UTC on July 19 the plateau and ice shelf station temperature values were equal: Dome C reads -52.6°C , and Meeley -52.2°C . By 1244 UTC on July 19, Dome C has cooled to -63.5°C , and the ice shelf station temperatures have remained nearly constant with Meeley at -54.7°C and Ferrell at -53.5°C . Thus the temperature gradient has now reversed to become more conducive to katabatic wind activity, with the plateau colder than the ice shelf. The potential temperature differences between plateau and ice shelf still remain positive although much smaller than during the first half of July 18: Dome C's potential temperature is 238.5 K, while Manning records 231.3 K and Meeley records 218.6 K.

The 0900 UTC July 19 satellite image shows signs of renewed katabatic wind activity; from the base of Byrd Glacier a light gray streak extends 65 km straight out onto the ice shelf. By 1600 UTC on July 19 this streak is darker and extends out about 120 km. There are, however, no signs of katabatic wind activity at any of the other glaciers.

4.2.4. *Case summary.* This case provides an excellent contrast to that of section 4.1. For several days

TABLE 7a. AWS Data During Katabatic Wind Events With Departure From Monthly Mean Data

Variable	Example 1: 00 UTC, June 17, to 05 UTC June 19, 1982	Example 2: 00 UTC, June 28, to 12 UTC, June 30, 1982*	Example 3: 01 UTC, July 1, to 16 UTC, July 2, 1982	Example 4: 05 UTC, July 25, to 20 UTC, July 26, 1982	Example 5: 04 UTC July 29, to 17 UTC, July 31, 1982
	<i>Manning</i>				
Pressure, hPa	981.5	977.5	985.5	978.1	986.9
anomaly	-8.0	-12.0	-7.0	-14.4	-5.6
Temperature, °C	-42.5	-27.9	-33.9	-29.7	-29.1
anomaly	-11.2	+3.4	-0.1	+4.1	+4.7
Wind speed, m s ⁻¹	3.6	5.3	5.5	...†	...†
anomaly	-1.5	+0.2	+1.5	...†	...†
Wind direction, deg true	225	248	268	...†	...†
anomaly	-26	-3	+2	...†	...†
	<i>Meeley</i>				
Pressure, hPa	980.1	975.6	983.6	977.1	985.0
anomaly	-8.4	-12.9	-8.2	-14.7	-6.8
Temperature, °C	-39.6	-30.1	-34.3	-32.8	-32.2
anomaly	-7.1	+2.4	+1.9	+3.4	+4.0
Wind speed, m s ⁻¹	8.0	9.0	8.6	...†	6.7
anomaly	+0.6	+1.6	+4.4	...†	+2.5
Wind direction, deg true	197	216	225	...†	207
anomaly	-16	+3	+7	...†	-11
	<i>Ferrell</i>				
Pressure, hPa	981.5	976.1	984.4	977.2	985.2
anomaly	-7.2	-12.6	-7.8	-15.0	-7.0
Temperature, °C	-38.1	-32.1	-36.5	-34.6	-33.5
anomaly	-4.4	+1.6	0.0	+1.9	+3.0
Wind speed, m s ⁻¹	5.7	7.3	6.0	5.1	6.5
anomaly	-0.5	+1.1	+0.8	-0.1	1.3
Wind direction, deg true	184	214	232	232	216
anomaly	-25	+5	+16	+16	0
	<i>Frequency of Temperature Differences, %</i>				
Manning > Meeley	21	56	68	83	85
Manning > Ferrell	28	72	63	87	91
Meeley > Ferrell	36	69	79	74	70

For monthly mean data, see Tables 1–3.

*See section 4.1.

†Missing wind data were due to AWS malfunction.

there was no katabatic wind activity along the glaciers of the Transantarctic Mountains. Instead of a strong low-pressure area east of the mountains supporting surface flow down the glaciers, the region was dominated by high pressure over the ice shelf and eastern plateau. Wind speeds were very low over the entire period, corresponding to a lack of a supporting pressure gradient over the area. The principal reason for the lack of intense katabatic wind activity was the reversal of the temperature and potential temperature gradients from the plateau to the ice shelf. These factors all contributed to the absence of katabatic winds.

Although the majority of this period contained no observable katabatic wind activity, Manning was consistently warmer than the other two stations. In some instances, Manning's temperature was over 16°C higher than those at Meeley and Ferrell. But the wind direction at Manning was opposite to that expected for adiabati-

cally warmed air because of katabatic winds. Throughout this period, when Manning registered a calm, its temperatures were much higher than those of the other two ice shelf AWS sites. With light winds the temperatures approximated those of the other stations. This strongly suggests an instrumental defect at Manning.

4.3. Katabatic and Nonkatabatic Wind Events as Climatic Anomalies

Finally, the average pressures, temperatures, and winds during several katabatic wind events and during the nonkatabatic wind period described in section 4.2 are compared in Table 7 with the climatic values for their months of occurrence (June and July). The relative frequencies with which the temperatures at one AWS exceeded that at the other two during these events are also given in that table. Table 7 demonstrates both the

TABLE 7b. AWS Data During the Nonkatabatic Wind Event (Section 4.2) With Departure From Monthly Mean Data

Variable	00 UTC, July 17, to 12 UTC, July 19, 1982
<i>Manning</i>	
Pressure, hPa	1009.2
anomaly	+16.7
Temperature, °C	-45.0
anomaly	-11.2
Wind speed, m s ⁻¹	1.2
anomaly	-2.8
Wind direction, deg true	272
anomaly	+6
<i>Meeley</i>	
Pressure, hPa	1008.5
anomaly	+16.7
Temperature, °C	-50.7
anomaly	-14.5
Wind speed, m s ⁻¹	...*
anomaly	...*
Wind direction, deg true	...*
anomaly	...*
<i>Ferrell</i>	
Pressure, hPa	1008.1
anomaly	+15.9
Temperature, °C	-48.2
anomaly	-11.7
Wind speed, m s ⁻¹	2.7
anomaly	-2.5
Wind direction, deg true	204
anomaly	-12
<i>Frequency of Temperature Differences, %</i>	
Manning > Meeley	96
Manning > Ferrell	92
Meeley > Ferrell	58

For monthly mean data, see Tables 1-3.

*Missing wind data were due to AWS malfunction.

climatic diversity of katabatic wind scenarios and some of their common elements. They are reviewed and summarized in the concluding section.

The beginning points and endpoints for these examples were chosen arbitrarily as many satellite images do not contain the McMurdo Sound area. Each day from 1800 UTC to 2400 UTC the satellite is focused on the other half of the continent; thus the region of McMurdo Sound is not visible. Other images are blacked out in the region of interest because of satellite-tracking errors. Image discontinuity thus makes it very difficult or impossible to tell exactly when a katabatic wind outbreak begins or ends, even though on more than one half of all "valid" images, katabatic wind activity is occurring with widely varying intensity; the dark streaks above and beneath the glaciers vary from light to dark gray.

The examples in Table 7a are arranged in order of occurrence and represent katabatic winds of above

average intensity. Example 2 is the strong katabatic wind case discussed in section 4.1. Example 5 will be called the "Terra Nova Bay" storm because, for a large portion of the episode, the bay appears black, indicating open water caused by strong winds blowing offshore and pushing the ice out to sea. One of the most interesting aspects of this episode is seen on the image for 1536 UTC on July 30 (not shown). Minna Bluff and Black and White islands to the north are visible as a darker gray compared to the white of the ice shelf. The air, visible as dark streaks, flows down off of Byrd, Skelton, and Mulock glaciers and combines into an expanding stream of relatively warm air moving toward Manning site and then past it toward the northwest. This warming air appears to miss both Meeley and Ferrell sites (Ferrell is furthest removed from the warm airstream). This effect shows up clearly in the station temperatures for this time. At 1536 UTC, Manning reads -24.9°C, Meeley registers -29.6°C, and Ferrell records -36.9°C. There is a 12.0°C difference between Manning site, which is directly in the relatively warm airflow, and Ferrell, which is not.

Example 1 was chosen to illustrate the point that even though katabatic wind activity may be occurring, the temperature patterns can be completely reversed. On this occasion the flow from Byrd Glacier was quite active, while those from Mulock and Skelton glaciers were not. From the temperature observations in Table 7 one might not have deduced the presence of katabatic wind activity. To detect it, it was very important to have access to satellite imagery.

Finally, during the nonkatabatic wind period (Table 7b) the temperature at Manning was higher on average than temperatures at the other two AWS sites, and very much higher during calms at Manning which should have strengthened the surface inversion and lowered the temperature there. As discussed in section 4.2, an instrumental malfunction of the Manning AWS is suspected to have occurred in this case.

5. CONCLUSIONS

Katabatic winds occur extensively along the Transantarctic Mountains, from Skelton Glacier to Beardmore Glacier. NOAA 7 infrared satellite images in the 10.5- to 11.5- μm band show the presence of dark streaks extending out from the glacial bases to distances of more than 320 km onto the Ross Ice Shelf. These streaks vary in darkness depending on the intensity of the katabatic wind outbreak; the warmer the surface air, the darker the streak.

For the winter months of June through August, katabatic wind activity was commonly observed; the intensities of the outbreaks varied greatly. Over 50% of the satellite images (both with and without clouds) in which the region was in the potential field of view (not blacked out because of satellite-tracking errors) displayed katabatic

batic wind activity occurring at Byrd, Mulock, and/or Skelton glaciers. This represents a lower bound, as these winds may also be present in those images where the McMurdo Sound region was obscured by cloud cover. Katabatic wind activity was also common at the Beardmore Glacier during these episodes.

Case studies reported here cover two widely contrasting synoptic situations: one in which katabatic wind activity was at a peak, the other where it was at a minimum. These cases involved very different temperature, potential temperature, and pressure patterns in addition to strongly differing surface and upper air wind fields. Particularly striking was the contrast in relative temperatures (and potential temperatures) between the East Antarctic plateau (as represented by Dome C) and the Ross Ice Shelf (as represented by the Meeley, Manning, and Ferrell). During the strong katabatic wind activity described in section 4.1, the surface air over the high plateau was up to 45°C colder than the air over the ice shelf, and potential temperatures were up to 15 K lower. In sharp contrast, during the case of minimal katabatic winds described in section 4.2, the temperature at Dome C was up to 15°C warmer than temperatures on the Ross Ice Shelf, with the Dome C potential temperature up to 45 K higher. This highlights the dramatic lack of cold air over the East Antarctic plateau and thus the absence of drainage winds through the Transantarctic Mountains, for this case. This indicates that the katabatic winds described in section 4.1 are of the “fall” type, as discussed in section 1, as an accumulation of presumably radiationally cooled air (as indicated by Dome C potential temperatures) was required over the East Antarctic plateau for these winds to occur. This cold air converges into the heads of these glaciers (especially Byrd) and results in the strong and persistent katabatic winds observed in this region. Support for this scenario is also found in the work of *Parish and Bromwich* [1987], who found a pronounced convergence of modeled wintertime cold-air drainage from the East Antarctic plateau into the head of Byrd Glacier.

In the other examples cited in Table 7, differences of 0–10 K between the potential temperatures at Dome C and the potential temperatures at the AWS sites on the Ross Ice Shelf were common. However, in those other examples, katabatic wind activity was observed on the satellite images even though the potential temperature at Dome C was 0–10 K above that at the ice shelf stations. There are a couple of reasons for this. Dome C is too far from the ice shelf to represent the air involved in the katabatic wind currents, and the atmospheric forcing alone can be strong enough in some cases to drive even moderately cold air down the glaciers.

Other conditions favoring katabatic wind outbreaks include the presence of a low-pressure system located over either the Ross Ice Shelf, the southern Ross Sea, or northwest Marie Byrd Land. This is clearly illustrated in Table 7a by the substantially lower than normal sea

level pressures at the AWS sites during each katabatic wind example. The 1000-hPa isobars should either parallel the mountains or cut across them such that the surface flow has a westerly component. An upper level geostrophic flow directed across the Transantarctic Mountains with a component toward the northeast may also aid in these outbreaks.

Satellite images directly show the existence of katabatic winds, but even AWS data alone may show that a katabatic wind event is occurring. It is important to note that the following trends and features do not always imply the presence of katabatic winds. As can be seen in Figure 3, the katabatic airstreams have fairly well defined edges. Thus the fixed AWS sites may reflect widely different conditions during katabatic wind events depending on their locations with respect to the main body of the katabatic winds.

During katabatic winds, low pressure is commonly observed at the AWS sites, with a pressure gradient directed toward the Ferrell site from the Manning site. Average station pressures tend to be generally 7–15 hPa below the climatic norms for the given month. The strength of the pressure gradient between the stations does not appear to be an important factor. Winds are generally mild to moderate at between 4 and 10 m s⁻¹. Winds at Manning are usually west-southwesterly, while at Meeley and Ferrell, persistent southerlies and south-southwesterlies are observed.

The temperature pattern is the most interesting feature. It is quite probable that katabatic winds are occurring if together with the other key factors Manning records the highest temperature of the three stations. Meeley should be the next warmest station, with Ferrell being the coldest. The average temperature difference between Manning and Ferrell is commonly 2°–3°C and can be as high as 6°C for the duration of the outbreak. This results from the fact that the topography of Minna Bluff forces the air past Manning and toward the northeast where it is further from and has less of an effect on Meeley and Ferrell sites.

The AWS winds most commonly came from south through southwest, with southwest the most common direction. It was postulated that this was an effect of the katabatic winds which occur with great frequency and varying intensities. We have shown in section 4.3 that, indeed, katabatic winds are commonly of moderate, above average speed and usually come from south-southwest or southwest. In addition, katabatic winds are often warmer by several degrees Celsius than the monthly means for all three stations.

An AWS located on the ice sheet above Byrd Glacier would help in obtaining a greater understanding of the katabatic wind phenomenon. Some clues have already been provided by the data from the temporary station at the base of Byrd Glacier (Table 4) which show down-glacier winds to be of common occurrence; also,

monthly mean temperatures at the site were 2°C to 5°C higher than those at the other AWS sites.

Acknowledgments. A preliminary version of this work constituted the 1985 M.S. thesis of C.J.B. Michael Savage of the Madison Academic Computing Center provided both suggestions and computer-programming assistance. Mannie Sievers assisted in the preparation of the maps and charts used in this paper. Thanks also to Lyle H. Horn, John A. Young, and George A. Weidner for their suggestions. This research was funded by U.S. National Science Foundation Division of Polar Programs grants DPP-8306265 to Charles Stearns and DPP-8916134 to David Bromwich. Byrd Polar Research Center contribution 856.

REFERENCES

- Bromwich, D. H., Satellite analyses of Antarctic katabatic wind behavior, *Bull. Am. Meteorol. Soc.*, 70, 738–749, 1989.
- Bromwich, D. H., J. F. Carrasco, and C. R. Stearns, Satellite observations of katabatic-wind propagation for great distances across the Ross Ice Shelf, *Mon. Weather Rev.*, 120, 1940–1949, 1992.
- D'Aguanno, J., Use of AVHRR data for studying katabatic winds in Antarctica, *Int. J. Remote Sens.*, 7, 703–713, 1986.
- Godin, R. H., An investigation of synoptic and associated mesoscale patterns leading to significant weather days at McMurdo Station, Antarctica, M.S. thesis, 114 pp., Nav. Postgrad. Sch., Monterey, Calif., June 1977.
- Huschke, R. E., *Glossary of Meteorology*, 638 pp., American Meteorological Society, Boston, Mass., 1959.
- Mather, K. B., and G. S. Miller, Notes on topographic factors affecting the surface wind in Antarctica, with special reference to katabatic winds; and bibliography, *Tech. Rep. UAG-R-189*, 125 pp., Univ. of Alaska, Fairbanks, 1967.
- Parish, T. R., and D. H. Bromwich, The surface windfield over the Antarctic ice sheets, *Nature*, 328, 51–54, 1987.
- Parish, T. R., and D. H. Bromwich, Instrumented aircraft observations of the katabatic wind regime near Terra Nova Bay, *Mon. Weather Rev.*, 117, 1570–1585, 1989.
- Schwerdtfeger, W., *Weather and Climate of the Antarctic*, p. 41, Elsevier Science, New York, 1984.
- Stearns, C. R., L. M. Keller, G. A. Weidner, and M. Sievers, Monthly mean climatic data for Antarctic automatic weather stations, this volume.
- Swithinbank, C., Higher resolution satellite pictures, *Polar Rec.*, 16, 739–751, 1973.

(Received September 15, 1991;
accepted May 14, 1993.)

SATELLITE AND AUTOMATIC WEATHER STATION ANALYSES OF KATABATIC SURGES ACROSS THE ROSS ICE SHELF

JORGE F. CARRASCO¹ AND DAVID H. BROMWICH

Byrd Polar Research Center and Atmospheric Sciences Program, The Ohio State University, Columbus, Ohio 43210

Thermal infrared satellite images from three winter months in 1988 were studied to evaluate the occurrence of dark (warm) signatures coming from southern Marie Byrd Land and extending across the Ross Ice Shelf in a direction generally parallel to the Transantarctic Mountains. The presence of these features around Siple Coast was found to be a very frequent event and is inferred to be caused by the persistent katabatic drainage from Marie Byrd Land. At times the signatures extended all the way across the ice shelf to the Ross Sea, a horizontal distance of about 1000 km. This took place even though the downslope buoyancy force is near zero over the ice shelf. Periods of maximum decrease of pressure over the northeastern Ross Ice Shelf and/or around the Russkaya Station area were associated with the occurrence of this phenomenon. Synoptic analyses indicated that the pressure decreases were caused by the passage of synoptic storms over the southern Amundsen Sea. This led to an increase of the pressure gradient over Marie Byrd Land and the Ross Ice Shelf, which primarily supported the horizontal propagation of katabatic winds from West Antarctica for great distances across the Ross Ice Shelf. Three detailed case studies are presented to illustrate the typical characteristics of these events.

INTRODUCTION

Dark (that is, warm) signatures of Antarctic downslope winds during winter are commonly observed on thermal infrared satellite images [Bromwich, 1989a, b]. One of these warm features is often seen around Siple Coast and at times can project to the north across the Ross Ice Shelf (Figure 1). The pattern of time-averaged, near-surface wintertime streamlines of airflow over West Antarctica [Parish and Bromwich, 1986; Bromwich, 1986] suggests the existence of intensified katabatic winds around Siple Coast as a result of inland confluence of drainage winds (Figure 2). The warm signature revealed by the satellite images can be associated with the katabatic winds which blow down onto the ice shelf. The north or northwestward movement of the warm signature that generally parallels the Transantarctic Mountains is supported by the regional pressure field. The extension of these features can cross the entire Ross Ice Shelf and reach its northern edge, causing an enlargement of the polynya (area of open water/thin ice surrounded by sea ice) along the ice shelf edge, mainly on its northwest side.

Dark signatures are often found coming from the glacier valleys through the Transantarctic Mountains, indicating that they are associated with katabatic winds which converge into the heads of these valleys and then

descend to the Ross Ice Shelf [Swithinbank, 1973; Breckenridge, 1985; D'Aguanno, 1986; Bromwich, 1989a]. Therefore the warm surface signature observed at the southeast corner of the Ross Ice Shelf can be related to the cold airflow coming down from West Antarctica through Siple Coast. As described by Bromwich [1989a, b], such airflows produce vigorous vertical mixing and transport of drift snow within stable boundary layers, and cause a temperature increase of the air close to the surface and within the katabatic jet. The result is a horizontal contrast in snow surface emissions between the area affected by katabatic airflow (warm) and the surrounding regions (cold); higher up in the boundary layer the katabatic jet is significantly colder than the surrounding air masses. This situation explains the apparent paradox of warm satellite signatures actually reflecting the presence of negatively buoyant air (compare also Parish and Bromwich [1989]). Thus the dark signatures captured by infrared satellite imagery qualitatively reflect the intensity of the katabatic winds. Although the network of automatic weather stations (AWS) does not cover some katabatically dominated areas of key importance to this study, when warm features have been present over AWS sites, the wind direction recorded by those stations has been parallel to the dark signature, and the wind speed stronger. Also, the surface temperatures recorded in these cases have been warmer than at surrounding locations [Bromwich, 1989a].

Bromwich [1989b], using thermal infrared satellite

¹On leave from Direccion Meteorologica de Chile, Santiago, Chile.

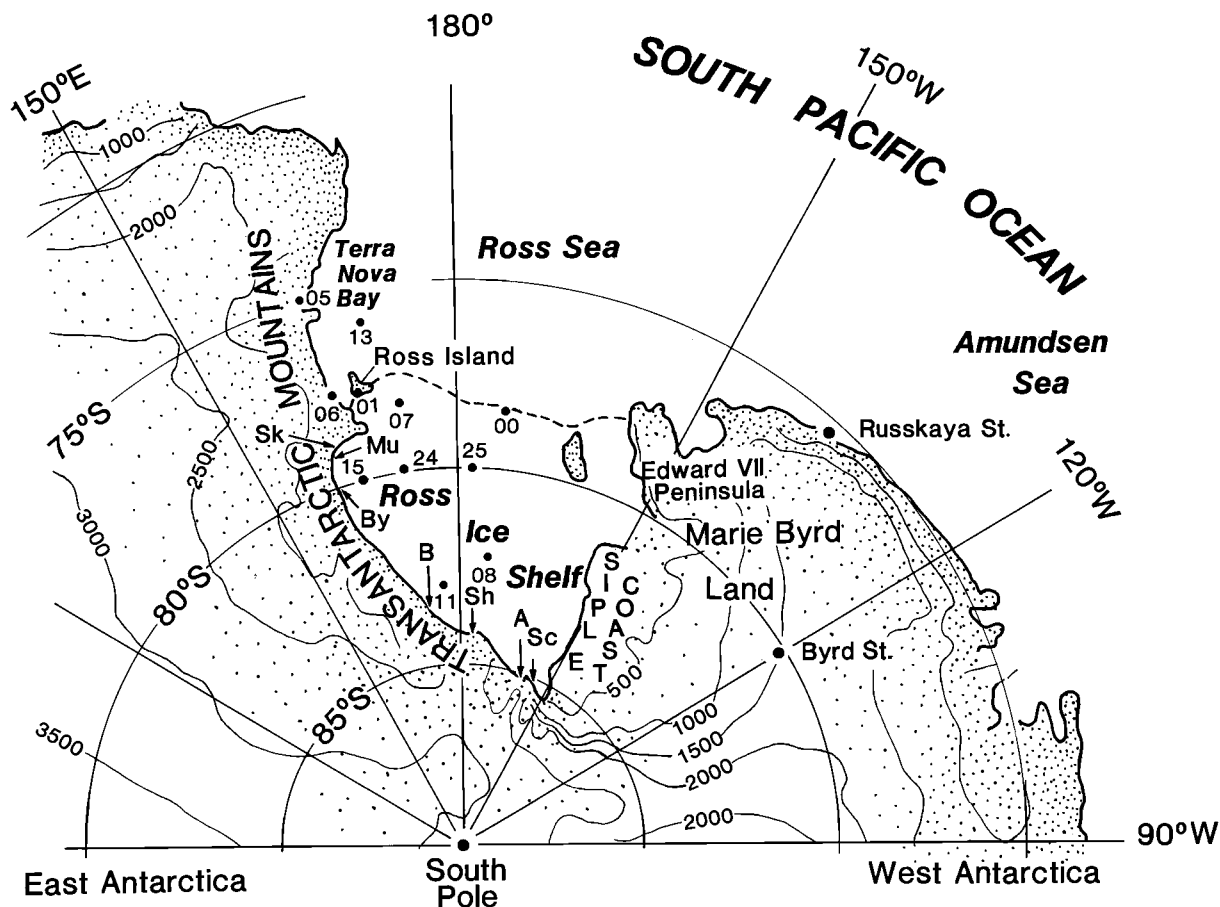


Fig. 1. Location map of the Ross Ice Shelf, Marie Byrd Land, Ross Sea, and Amundsen Sea. Solid circles with attached numbers represent AWS sites. B, Beardmore Glacier; Sh, Shackleton Glacier; A, Amundsen Glacier; Sc, Scott Glacier; By, Byrd Glacier; Sk, Skelton Glacier; and Mu, Mulock Glacier.

images, evaluated the frequency and utility of katabatic wind signatures within and beyond the Siple Coast confluence zone from mid-May to mid-June in 1988. His results indicate that warm signatures coming from Siple Coast area and propagating horizontally toward the north across the entire Ross Ice Shelf are a frequent phenomenon. This takes place even though there is little downslope forcing on katabatic air over the ice shelf, and requires assistance from the large-scale pressure field. This paper is a study of this phenomenon from June to August 1988, including part of the period studied by Bromwich. For this interval, all available satellite images that covered almost the entire 3 months were examined. Automatic weather station data were studied to evaluate the mesoscale environment on the Ross Ice Shelf. Also, surface and 500-hPa synoptic analyses prepared by the Australian Bureau of Meteorology were reviewed to examine the broad scale circulation associated with extension of the warm signatures. Emphasis is placed on case studies which illustrate recurring char-

acteristics of the events rather than on a detailed discussion of the composited results, which is presented elsewhere for a longer period [Bromwich *et al.*, 1992].

The paper is organized as follows. The next section contains the results obtained by examining the infrared satellite images and is followed by a summary of the AWS analyses. A brief description of the typical synoptic scale environment precedes an in-depth presentation of the three case studies. The final section gives an overview and discusses the governing dynamics.

INFRARED SATELLITE IMAGERY ANALYSIS

In order to evaluate the frequency of the warm signatures at the foot of the slope to Marie Byrd Land and their projection toward the north, all available satellite images for June, July, and August 1988 were examined. The routine collection of high-resolution picture transmission (HRPT) data from the TIROS-N/NOAA satellites, which includes the advanced very

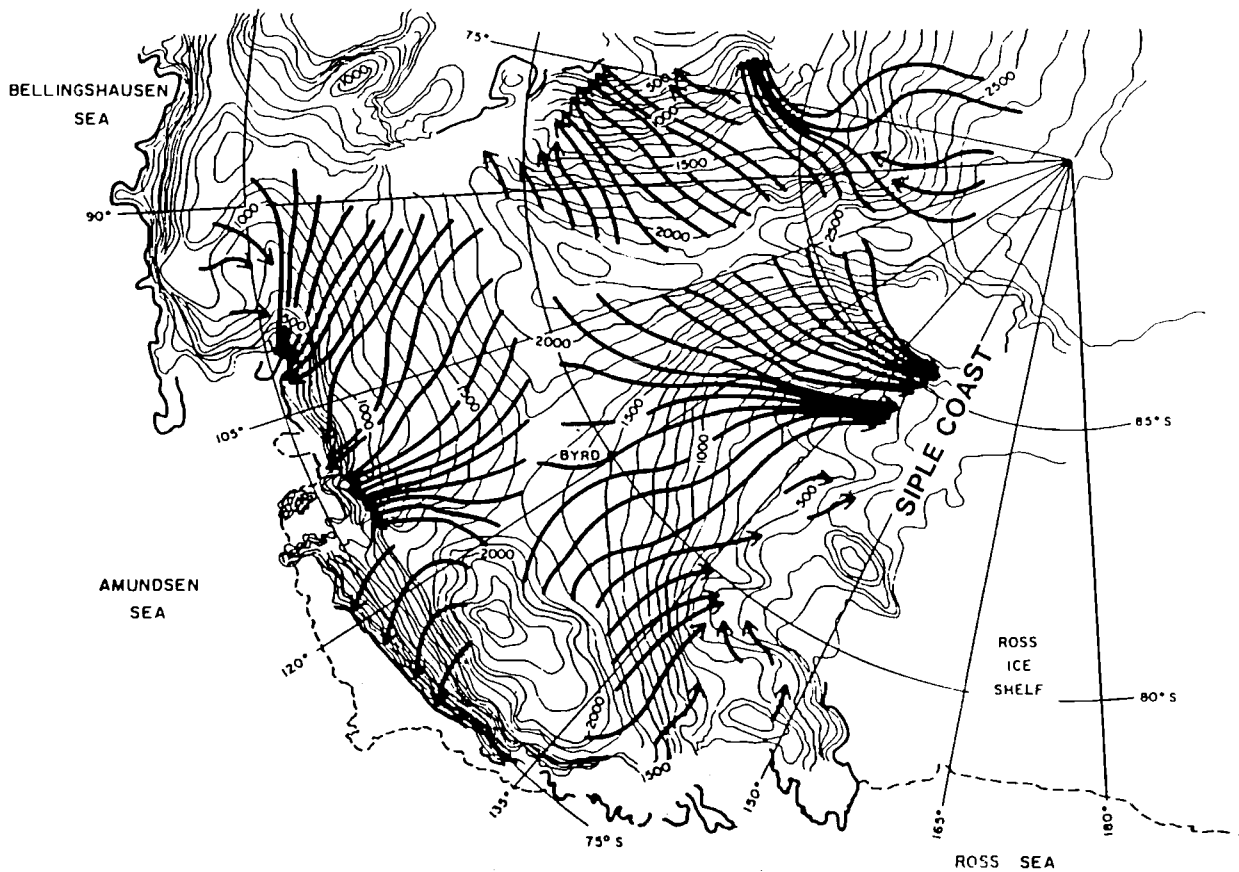


Fig. 2. Time-averaged near-surface wintertime streamlines (heavy arrows) of cold air drainage over West Antarctica [from Parish and Bromwich, 1986]. Light lines are elevation contours in 100-m increments.

high resolution radiometer data (AVHRR) [Kidwell, 1986; Schwab, 1982], has been carried out at McMurdo Station on Ross Island since October 1987 [Antarctic Journal of U.S., 1988; Van Woert et al., 1992]. This provides satellite observations for evaluation of different phenomena that occur over the Ross Ice Shelf, southern Ross Sea, and surrounding areas. These data were obtained from the Antarctic Research Center at Scripps Institution of Oceanography and processed on a SUN 4/110 workstation using the TeraScan software package supplied by SeaSpace. The images were sampled at a spatial resolution of 2.2 km for thermal infrared channel 4 (10.5–11.3 μm). The evaluation criterion used was that all dark signatures that extended to the north of AWS 08 and 11 (Figure 1) were counted as a northward projection of the warm signature. If the above did not occur, then the warm signature was counted as present just on the southeast corner of the ice shelf (to the southeast of AWS 08 and 11). The following results (Table 1) were obtained:

1. Warm surface signatures propagating from the sloping ice fields of West Antarctica, crossing Siple Coast, but staying on the flat southeast corner of the

Ross Ice Shelf were frequently noted. When these signatures could be detected, they were present on 89% of such days.

2. The north or northwestward projection of the warm signature across the entire Ross Ice Shelf (called signature days) was clearly found on 12% of the total days examined and on 18% of the days on which the surface was observable (termed analyzable days). Bromwich [1989b] obtained similar results.

The satellite images indicate that katabatic winds descending through the Shackleton, Amundsen, and Scott glaciers, which dissect the Transantarctic Mountains around the southeast corner of the Ross Ice Shelf, were more prominent in conjunction with the northward extension of the dark signatures from Siple Coast than when these features were absent. This suggests that when katabatic winds from southern Marie Byrd Land propagate across the shelf, katabatic winds coming through the above glaciers are intensified.

Sixteen satellite images showed a northward projection of warm surface air, corresponding to 11 signature days (four in June, five in July, and two in August).

TABLE 1. Summary of the Results of Three Months (June–August, 1988) of Katabatic Airflow Coming From Southern Marie Byrd Land Onto the Ross Ice Shelf (156 AVHRR Images Examined)

	Percentage
Total days ($n = 92$) which were overcast or without data*	33%
Total days with surface wind signature at foot of Marie Byrd Land slope	60%
Analyzable days ($n = 62$) with surface wind signature at foot of Marie Byrd Land slope	89%
Total days with surface wind signature all the way across the Ross Ice Shelf (called "signature" days, $n = 11$)	12%
Analyzable days which are signature days	18%
Signature days with synoptic storms over southern Ross and/or Amundsen seas	81%
Signature days with reduced pressure over the eastern Ross Ice Shelf	81%

Analyzable days are those for which, in the opinion of the analyst, the ice surface conditions can be determined on at least one image. Thin, nonobscuring cloud cover may be present on analyzable days.

*The remaining days are called analyzable.

AWS ANALYSES

Automatic weather stations have been giving information on the air temperature, air pressure, wind speed, and wind direction since 1980, when they started to be routinely deployed on the Antarctic continent by the U.S. Antarctic Program (USAP) [Stearns and Wendler, 1988]. The AWS data [Keller *et al.*, 1989] from selected stations were used to analyze the behavior of the above parameters during the 3 months under consideration. AWS 08, 11, and 25 are the stations on the Ross Ice Shelf closest to Siple Coast. To examine the temperature behavior around the southeast side of the shelf, and for comparison with the satellite observations, the daily mean temperature (measured at 1.5 m above the surface [Stearns and Wendler, 1988]) for each day was evaluated. At AWS 08, 11, and 25, these temperatures were respectively warmer than the corresponding monthly averages for eight, nine, and six of the 11 signature days. The mean temperature for signature days was significantly warmer (at better than the 95% confidence level) than the 3-month average for the composite of AWS 08, 11, and 25 and for AWS 11. Changes at AWS 08 and 25 were not significant. Warmer temperatures were also recorded for other days, but because the area under consideration was cloudy or the satellite information was not available, they could not be associated with the presence of a dark signature over the ice shelf. Therefore it is possible that katabatic airflows from Marie Byrd Land propagate far across the Ross Ice Shelf more frequently than 12% of the time obtained by examining all satellite images, but probably do exceed the 18% frequency obtained from just analyzable days.

In order to analyze the association between the pressure variation over the northeastern Ross Ice Shelf and the presence of warm signatures across the shelf, pressure data recorded by AWS 00 and at Russkaya Station were examined. The latter were read directly from the Australian surface charts. The difference between daily mean pressure for each day and the respective monthly average was calculated. For nine of the 11 signature days the pressure recorded at both stations was lower than the respective monthly average. In addition, at both sites the mean pressure for signature days was significantly smaller (in a statistical sense) than the mean pressure for the 3 months. By integrating the above results, it was found that for eight of the 11 signature days the temperatures recorded by AWS 08, 11, and/or 25 were above average and the pressures recorded by AWS 00 and/or Russkaya Station were below average.

To analyze the wind behavior around the southeast part of the ice shelf, wind speed and direction observations at AWS 08, the station closest to Siple Coast, were examined. Eighty percent of the time the daily mean wind speed for signature days was higher than the respective monthly average. Also, the average wind speed for signature days was significantly stronger (by 2.3 m s^{-1}) than the average for the entire 3 months. The vector-averaged speed showed a statistically significant difference of 2.9 m s^{-1} in favor of signature days, but little difference was found in vector-averaged direction. However, the directional constancy for signature days was 0.90, compared with 0.76 for the 3 months. Seventy percent of the signature days were characterized by above-average wind speeds and temperatures at AWS 08 and below-average pressures over the northeastern Ross Ice Shelf.

Little difference was found in the wind behavior at AWS 11 apart from the vector-averaged direction for signature days pointing more toward Beardmore Glacier. This suggests that this site is strongly affected by katabatic airflow from Beardmore Glacier during katabatic surge events from West Antarctica.

SYNOPTIC ANALYSES

The above analyses for signature days were complemented by an examination of the hemispheric surface and 500-hPa charts produced by the Australian Bureau of Meteorology. A synoptic storm passing over the southern Amundsen Sea, usually associated with a dissipating front over Marie Byrd Land that acquired the characteristics of a warm front, was analyzed on most of the days for which dark signatures were observed across the ice shelf. These fronts were confirmed, and corrected when necessary, using the satellite information. The common pattern revealed by the synoptic analyses for these days was a definite cyclonic circulation over Marie Byrd Land and the Ross Ice

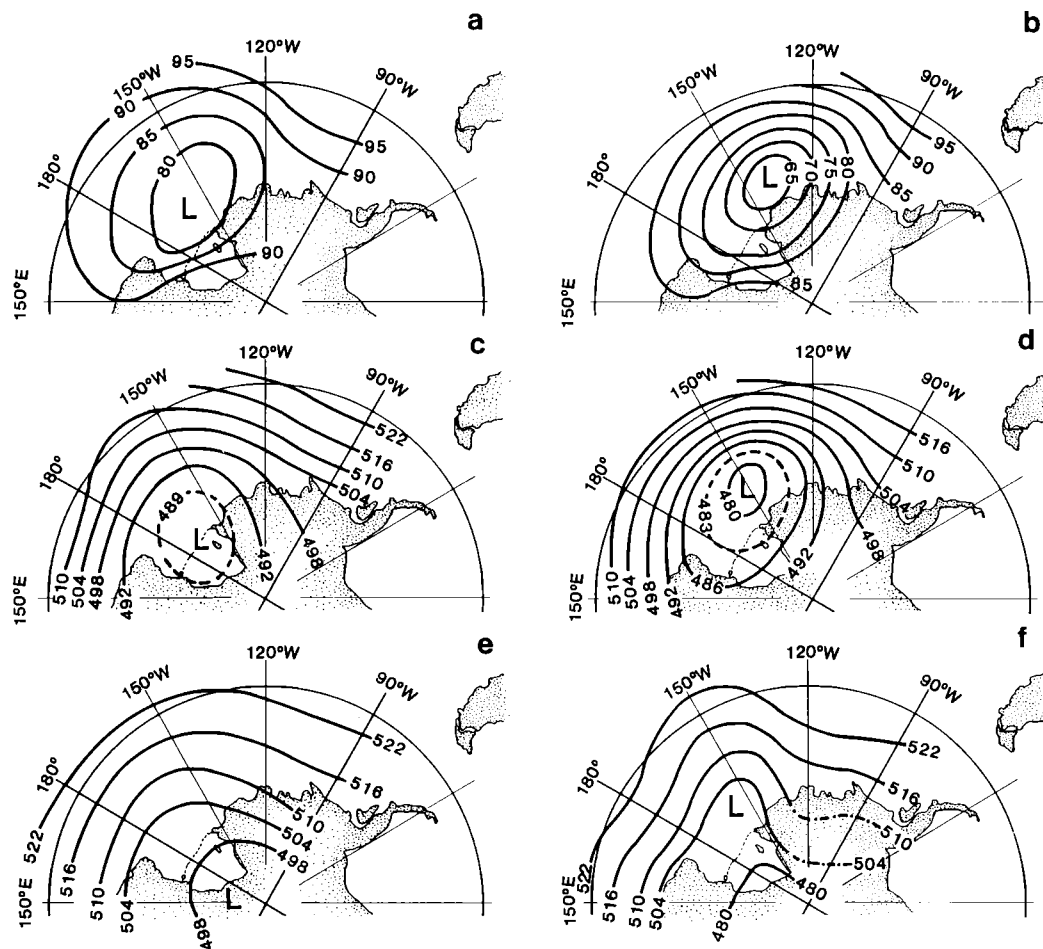


Fig. 3. (a) The mean sea level pressure field ($80 \equiv 980$ hPa) for the 3 months derived from the daily analyses (0000 UTC) produced by the Australian Bureau of Meteorology. (b) Same as Figure 3a but for the days that the warm satellite signatures were observed to project far to the northwest across the Ross Ice Shelf (signature days). (c) Same as Figure 3a but for the mean 500-hPa geopotential height field in dekameters. (d) Same as Figure 3b but for the 500-hPa geopotential height. (e) Same as Figure 3a but for the mean 1000- to 500-hPa thickness in dekameters. (f) Same as Figure 3b but for the 1000- to 500-hPa thickness.

Shelf with the vortex centered over the Amundsen Sea or Ross Sea.

The average sea level pressure field for signature days was compared with the average sea level pressure for the 3 months. The average pressure at each point of a grid, formed by the intersection of the longitude and latitude lines at 10° intervals, was calculated from pressure values given by the Australian surface analyses. Also, AWS data were used to describe the pressure field in the Ross Ice Shelf sector; the pressure behavior on the northern side of Marie Byrd Land was analyzed with the aid of Russkaya Station data obtained directly from the Australian charts. Figure 3a is the average sea level pressure for the 3 months under consideration. It shows the typical quasi-stationary low-pressure area slightly to

the northeast of the Ross Ice Shelf [cf. Schwerdtfeger, 1970]. Figure 3b is the average that includes only those days with a northward projection of dark signatures across the Ross Ice Shelf. Comparing the two figures, it can be noted that the presence of dark features was associated with an intensification and northeastward movement of the quasi-stationary synoptic low, i.e., with the passage of synoptic vortices which on average were deeper than the 3-month average. Statistically significant changes were found in the southern Amundsen Sea. The pressure field in Figure 3b also shows a more well defined cyclonic circulation over Marie Byrd Land and the Ross Ice Shelf; the isobars are almost parallel to the Transantarctic Mountains and coincide with the orientation of the warm satellite signatures.

TABLE 2. Sea Level Mean Pressure Differences Between Some Locations for Monthly Average Field and Signature Days

Locations	Monthly Average Field	Signature Days
Difference between AWS 08 and Russkaya Station	7.4	12.6
Difference between AWS 00 and Russkaya Station	-2.8	6.0
Difference between AWS 08 and 70°S/140°W	11.3	16.1

All signature day entries are significantly different from the corresponding monthly average field entries at better than the 95% confidence level using a two-tail *t* test.

Table 2 compares the mean pressures between several points to demonstrate that for signature days the pressure gradient over Marie Byrd Land was stronger by a statistically significant amount than for the 3-month average.

The 500-hPa analyses revealed that the general pattern was the presence of a midtropospheric vortex centered over the Amundsen Sea or Ross Sea, giving Marie Byrd Land and the Ross Ice Shelf a well-defined cyclonic circulation. The average 500-hPa geopotential height fields for signature days and for the 3 months were calculated from the values given by the Australian synoptic analyses. Figure 3c presents the results for the entire period under consideration. It shows the typical weak midtropospheric vortex over the Ross Ice Shelf and southern Ross Sea [cf. *Schwerdtfeger*, 1970]. Figure 3d, which is the average for signature days, clearly shows a deeper midtropospheric vortex centered slightly to the northwest of Russkaya Station. Once again, the position of the vortex gives a more definite (midtropospheric) cyclonic circulation over Marie Byrd Land and the Ross Ice Shelf.

The 1000- to 500-hPa average thickness fields, for the 3 months (Figure 3e) and for the days with northward projection of dark signatures (Figure 3f), were derived from the surface and 500-hPa average fields. Comparing the two figures, the latter shows a well-defined lower tropospheric cold trough over the Ross Sea with lower geopotential thicknesses, while over Marie Byrd Land a warm thickness ridge is analyzed. This reveals the presence, or advection, of cold air over the Ross Sea and warm air over Marie Byrd Land.

To summarize, the average fields for the 3 months show patterns similar to those described by *Schwerdtfeger* [1970, 1984], emphasizing that Marie Byrd Land and the Ross Ice Shelf are almost always affected by the quasi-stationary synoptic cyclone located over the southern Ross Sea. The synoptic analyses showed a more definite cyclonic circulation over Marie Byrd Land and the Ross Ice Shelf for those days when dark

signatures were clearly observed with a northward projection. In addition, the analyses revealed that this phenomenon is associated with the passage of synoptic storms close to Russkaya Station. The displacement of the time-averaged synoptic vortices to the southern Amundsen Sea results in statistically significant changes in relation to the 3-month averages and emphasizes that the increased pressure gradient over Marie Byrd Land plays an important role in the northwest extension of dark signatures from southern Marie Byrd Land across the Ross Ice Shelf.

CASE STUDIES

Three cases are included in this section as examples of katabatic airflow coming from southern Marie Byrd Land and extending across the Ross Ice Shelf. The first two cases, June 5 and July 11–12, clearly show the most common mesoscale and synoptic scale patterns associated with the occurrence of this phenomenon. The third case reveals the importance of a favorable pressure field distribution over the ice shelf for the northwestward extension of the katabatic airflow coming through Siple Coast.

Case 1: June 5, 1988

The temperature readings given by AWS 08 and AWS 11 show that the area around these stations was affected by warm surface air between June 2 and June 7. Also, the pressures recorded by AWS 00 and Russkaya Station were lower than the respective monthly averages (Figure 4). The satellite images during these days revealed the presence of dark signatures around Siple Coast every day, but only on June 3 and June 5 did they show a clear northward projection across the Ross Ice Shelf. One of the most spectacular examples found in this study occurred on June 5. Three consecutive images showed dark signatures which crossed the entire ice shelf parallel to the Transantarctic Mountains, a horizontal distance of around 1000 km.

The mesoscale analysis at 0300 UTC on June 5, 1988 (Figure 5), revealed warmer surface temperatures around AWS 08 and 25. The temperature field showed the presence of cool air over the northeast side of the ice shelf and adjacent to AWS 24. The daily average temperature at AWS 08 (Figure 4) showed a gradual increase from -35.6°C on June 1 to -19.2°C on June 5. Over the same period the daily average wind speed at this site increased from 4 m s^{-1} to 13.6 m s^{-1} (8.2 m s^{-1} greater than the monthly average), with the strongest winds occurring between 1500 UTC on June 4 and 0900 UTC on June 5. Also, during the first 6 days in June, AWS 25 showed warmer daily temperatures than the June average; however, the warmest temperature (-27°C) was recorded between 2100 UTC on June 4 and 0000 UTC on June 5, which is 8.3°C warmer than the

monthly average. The satellite image at 0338 UTC on June 5 (Figure 6a) showed a distinctive dark signature coming from the Siple Coast area and extending toward the northwest, passing over AWS 08 and 25 but skirting AWS 11. Compare this with the AWS temperature field analysis in Figure 5. At this time the warm surface air had already reached the northern edge of the ice shelf. The prior satellite image at 0339 UTC on June 4 did not clearly reveal this dark feature. The warmest temperatures recorded by AWS 08 and 25 coincide, in time and space, with the dark signature shown by the satellite image at 0338 UTC on June 5, suggesting that the northwestward propagation of the katabatic winds could have occurred late on June 4. No significant warming was observed at AWS 11, although the temperature anomalies (Figure 4) indicate a warming from June 2 to June 3 and from June 5 to June 6, while a cooling is suggested on June 4. This coincides with the dark signature observed on satellite images on June 3 and 5 but not on June 4.

At 0600 UTC on June 5, the AWS analysis showed almost the same mesoscale arrangement as at 0300 UTC (Figure 5), only the cool air located over the southwest side of the shelf was not as well defined because of the temperature rises at AWS 11 and 24. Also, the dark

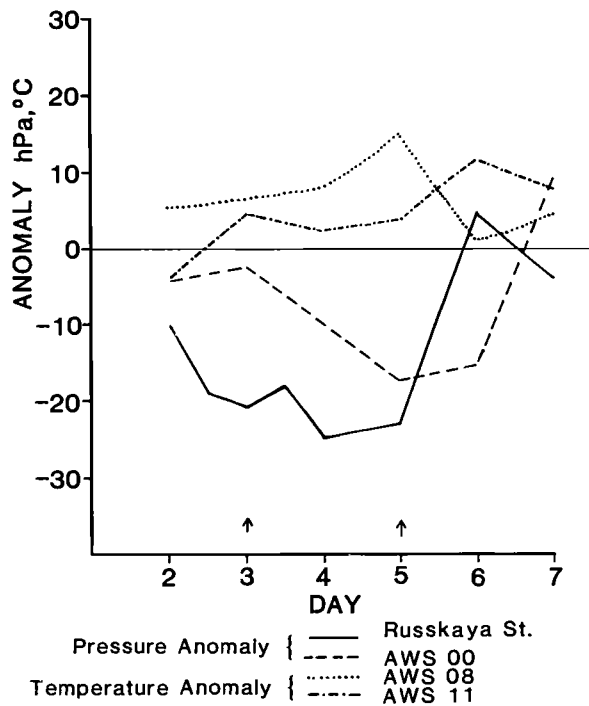


Fig. 4. Pressure and temperature anomalies between June 2 and June 7, 1988. Solid and dashed lines correspond to the pressure anomalies (daily mean minus monthly average) at Russkaya Station and AWS 00, respectively. Dotted line and dotted-dashed line represent temperature anomalies at AWS 08 and AWS 11, respectively. Arrows indicate the days for which dark signatures were observed across the Ross Ice Shelf.

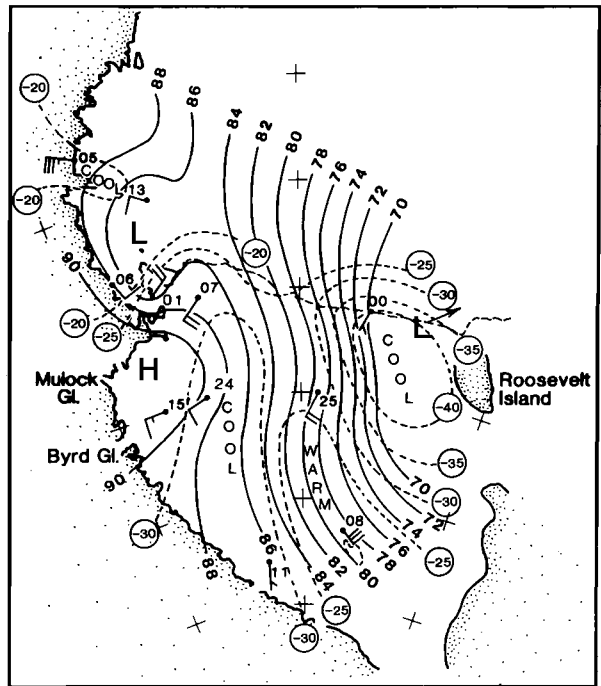
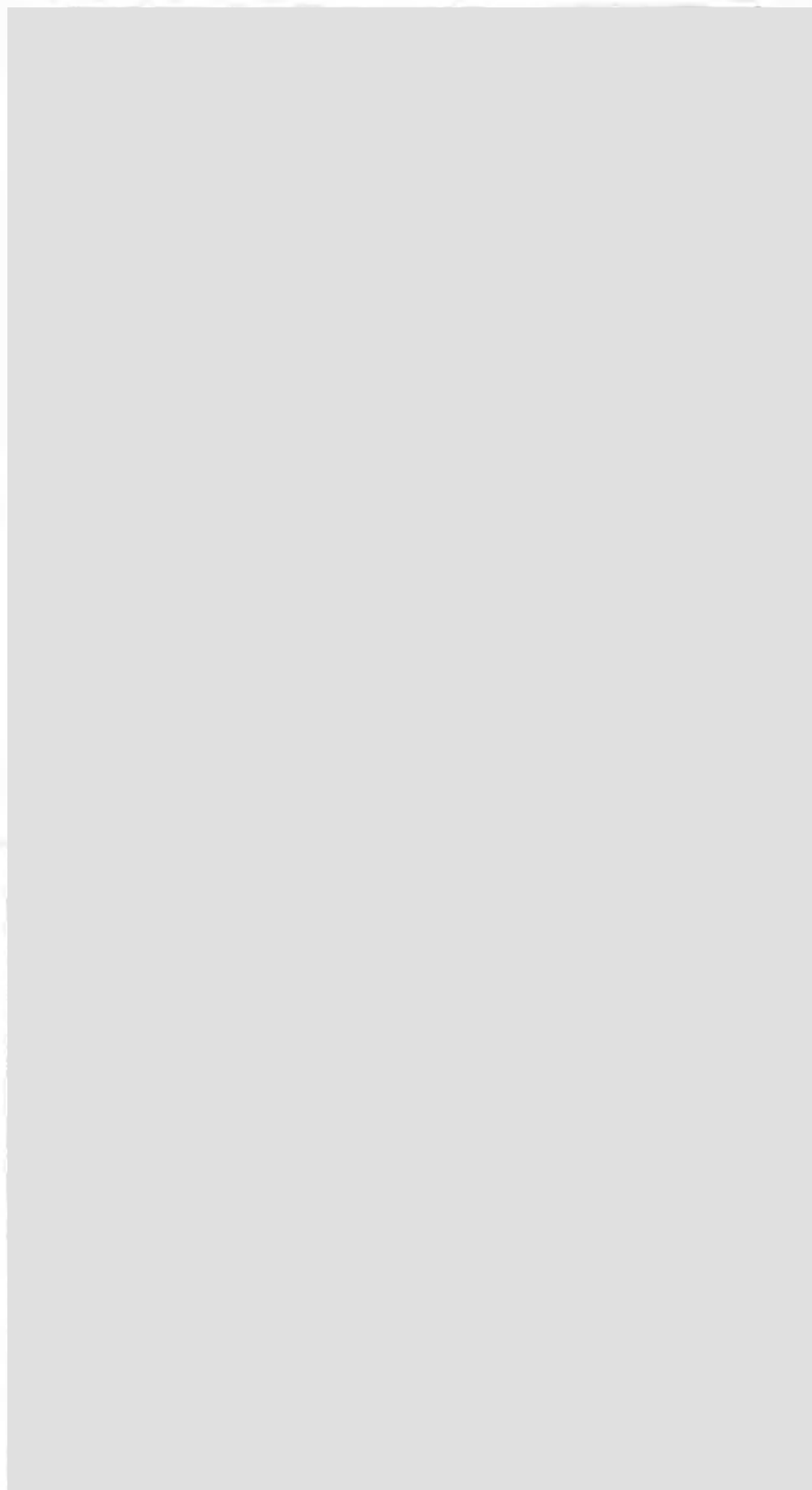


Fig. 5. Regional sea level pressure analysis at 0300 UTC on June 5, 1988. Solid lines are isobars (hPa), and dashed lines are isotherms (degrees Celsius).

signature on the image at 0652 UTC had almost the same orientation. By 0900 UTC the cool air located over the northeastern side of the shelf had moved slightly toward the southwest, as shown by the temperature decrease at AWS 25. Automatic weather stations along the Transantarctic Mountains showed an increase of temperature which continued thereafter. At 1200 UTC the AWS mesoscale analysis (Figure 7) indicated that the temperature had increased 13°C at AWS 11, 10°C at AWS 24, and 4°C at AWS 07 during the last 9 hours. The last station continued recording a temperature increase until 1800 UTC, when it was 9°C warmer than the monthly average. The image at 1053 UTC (not reproduced) showed almost the same signature projection, but displaced slightly toward the west and still parallel to the Transantarctic Mountains. The three images showed a polynya along the northwest edge of the Ross Ice Shelf as a result of the warm surface air being advected off the ice shelf. Figure 6b, which corresponds to the satellite image at 0652 UTC, shows the polynya located in the path of the dark signature.

The synoptic analysis at 1200 UTC on June 4, 1988, showed a front and its vortex over the Amundsen Sea. At 0000 and 1200 UTC June 5 (Figure 8) the charts revealed the movement of the system toward Marie Byrd Land and its gradual weakening, which was confirmed by satellite imagery. Its weak vortex was analyzed as being centered to the northeast of Russkaya Station. The 500-hPa analysis at 1200 UTC on June 5



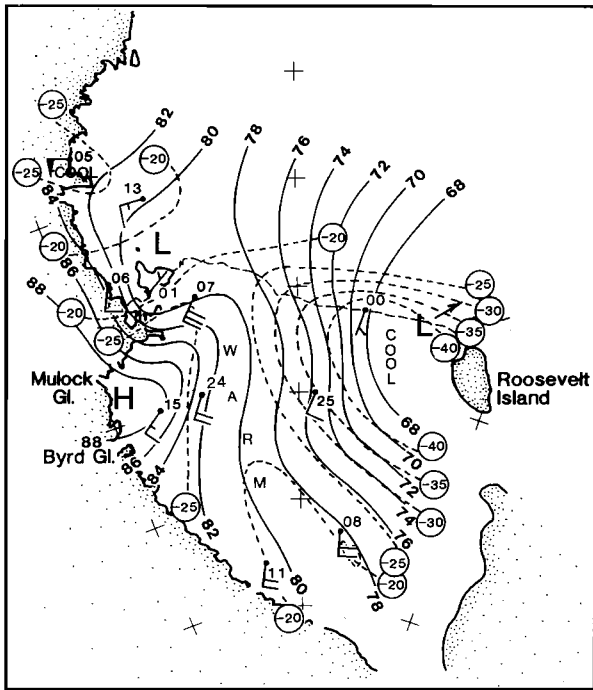


Fig. 7. Same as Figure 5 but for 1200 UTC on June 5, 1988.

(Figure 9) showed a midtropospheric vortex over the Ross Sea which was associated with the warm front and its synoptic low. It can be seen that both surface and 500-hPa analyses suggest cyclonic circulation over Marie Byrd Land and the Ross Ice Shelf.

Case 2: July 11–12, 1988

According to AWS deployed on the south side of the ice shelf, this area was affected by warm surface tem-

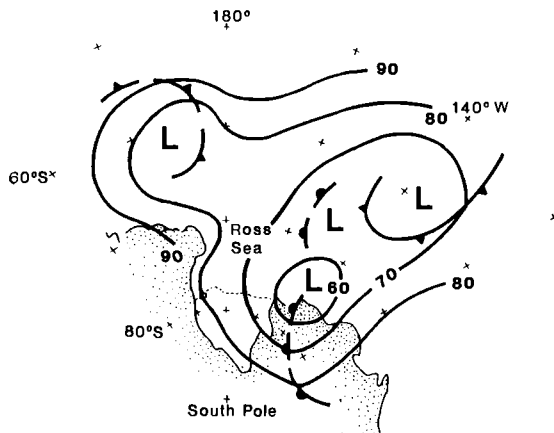


Fig. 8. Modified Australian surface analysis at 1200 UTC on June 5, 1988. The lines are isobars which are labeled by the two least significant digits (990 hPa = 90).

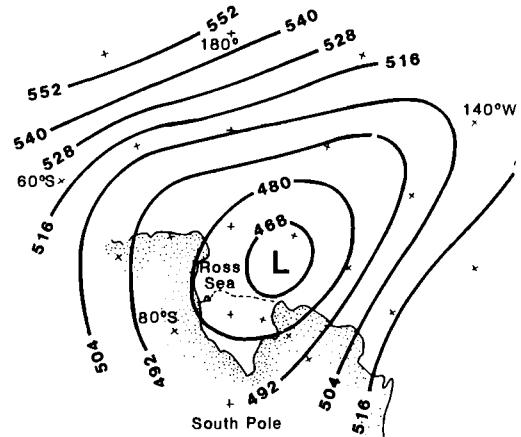


Fig. 9. The Australian 500-hPa synoptic analysis at 1200 UTC on June 5, 1988. The contours are labeled in geopotential dekameters.

peratures between July 3 and July 14. During this period, synoptic analyses showed the passage of synoptic storms close to Russkaya Station. During the first 8 days the presence of a warm signature could not be confirmed by the satellite images because they were not available or because the Ross Ice Shelf was completely overcast. Warmer temperatures recorded between July 10 and July 14 by AWS 08 and 11 (Figure 10) were supported by satellite images on July 11 and July 12.

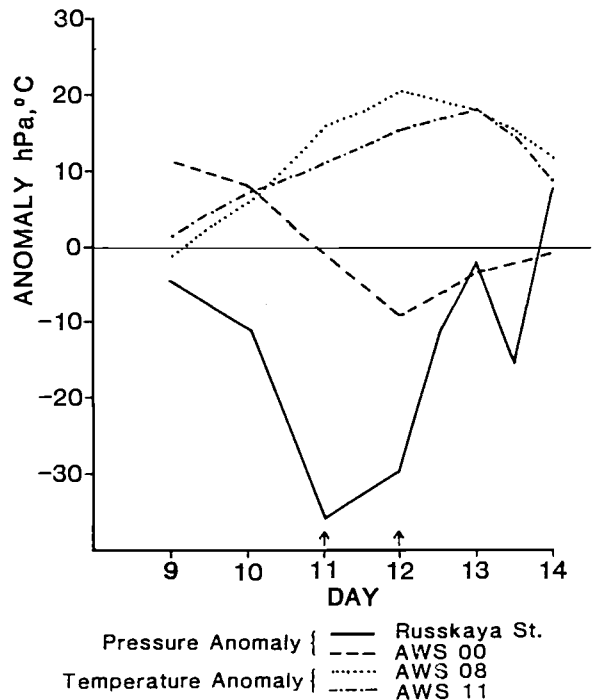


Fig. 10. Same as Figure 4, but for the period between July 9 and July 14, 1988.

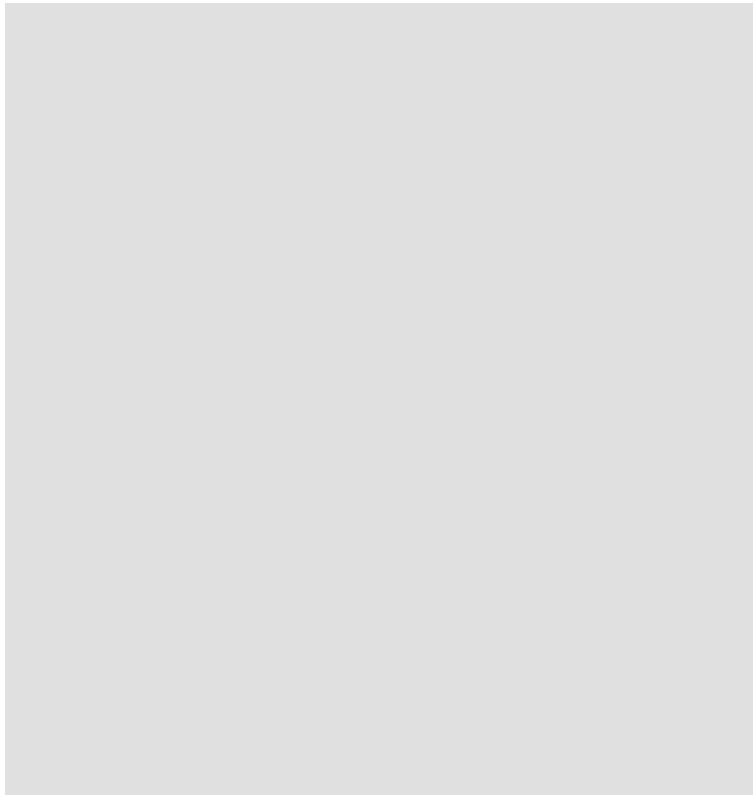


Fig. 11. NOAA 9 AVHRR thermal infrared image at 0702 UTC on July 11, 1988.

They showed warm signatures with a northward projection across the ice shelf. The previous satellite image, at 1721 UTC on July 10 (not reproduced), showed the dark signature restricted to the bottom of the Ross Ice Shelf. A significant increase of the daily average temperatures from -30.1°C to -20.4°C occurred between July 10 and July 11 at AWS 08 (Figure 10), as well as at AWS 25 (from -37.1°C to -27.4°C), which may reveal the time when the northwestward propagation of the katabatic winds took place. Maximum anomalies occurred at these two stations and at AWS 00 on July 12, indicating the persistence of the katabatic winds on this day. Significant increases in the temperature at AWS 11, 15, and 24 on July 10 may also suggest an intensification of the katabatic drainage from East Antarctica, adding mass to the katabatic winds coming from West Antarctica. The temperatures recorded at AWS sites and the satellite images indicate that the northwestward propagation of the katabatic airflow took place sometime between July 10 and July 11.

The satellite image at 0702 UTC on July 11, 1988 (Figure 11), showed a dark signature over the Siple Coast area which extended toward the northwest across the Ross Ice Shelf. AWS analysis at 0600 UTC (Figure 12) revealed the presence of warm surface air around

Fig. 12. Same as Figure 5 but for 0600 UTC on July 11, 1988.

Fig. 13. NOAA 9 AVHRR thermal infrared image at 0659 UTC on July 12, 1988.

AWS 08 and 11 which seemed to project toward AWS 24. Also, cooler air was present around AWS 07 and 00. At 0900 and 1200 UTC the mesoscale analysis indicated that the warm air could have extended toward the north between AWS 07 and AWS 00. The satellite image at 1205 UTC (not reproduced) showed a polynya between these stations, and the dark signature situated in accord with the AWS temperature data.

The satellite image at 0659 UTC on the next day (Figure 13) still showed the dark signature across the ice shelf. The AWS analysis at 0600 UTC (Figure 14) revealed that the eastern half of the shelf continued to be affected by warm air. The temperatures recorded at AWS 08 and 11 were -10°C and -14°C ; these were 26°C and 18°C warmer than the respective monthly averages. Cool air only remained around AWS 07. In general, the satellite images showed a dark signature over the area where warmer surface temperatures were recorded. The polynya was clearly observed along the northeastern edge of the ice shelf, indicative of the position of the warm surface air on this day (Figure 13).

The front analyzed by the Australian Bureau of Meteorology at 0000 and 1200 UTC on July 11 over Marie Byrd Land was confirmed by the satellite images, which also indicated that it slowly moved toward the

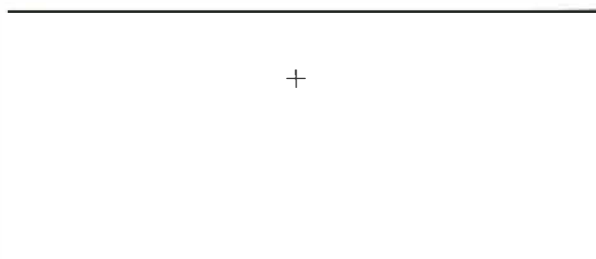


Fig. 14. Same as Figure 5 but for 0600 UTC on July 12, 1988.

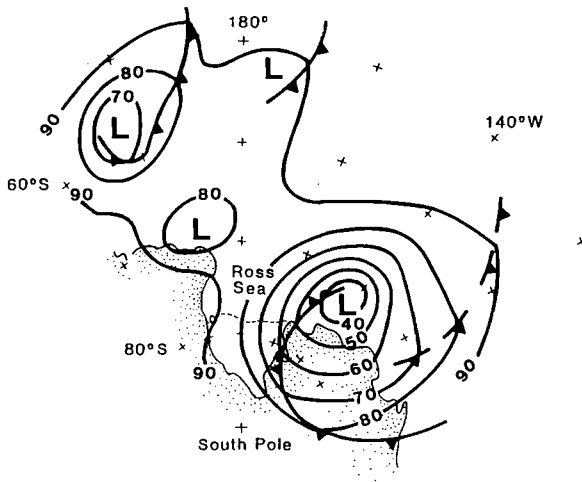


Fig. 15. Same as Figure 8 but for 1200 UTC on July 11, 1988.

west, passing over the Ross Ice Shelf thereafter. The surface synoptic analyses revealed that the synoptic vortex associated with the front was over the Amundsen Sea on July 10 and near Russkaya Station at 1200 UTC on July 11, 1988 (Figure 15). At this time the pressure recorded by this station was 36 hPa lower than its monthly average (Figure 10), which was associated with the passage of the synoptic storm; the cyclone then moved slowly toward the west over the Ross Sea. According to the satellite image at 0659 UTC on July 12 (Figure 13), the warm front was over Siple Coast. Figure 16, which is a modified surface synoptic analysis at 1200 UTC on July 12, shows the synoptic environment on this day. The 500-hPa analyses revealed an almost stationary vortex to the north of Russkaya Station for the 2 days. Figure 17 shows the position of the vortex at 0000 UTC on July 12, according to the Australian

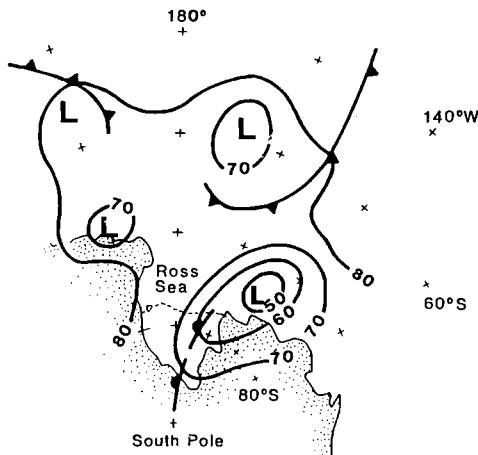


Fig. 16. Same as Figure 8 but for 1200 UTC on July 12, 1988.

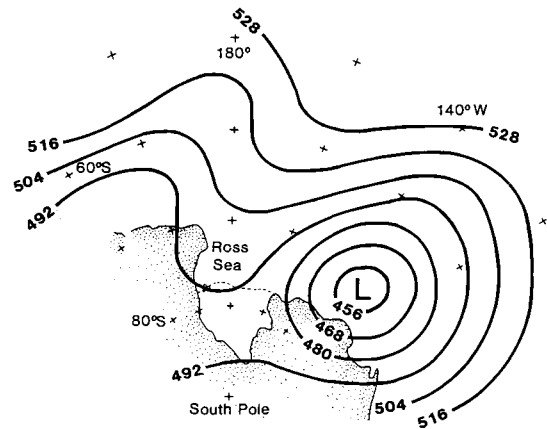


Fig. 17. Same as Figure 9 but for 0000 UTC on July 12, 1988.

Bureau of Meteorology analysis. Once again, cyclonic circulation over Marie Byrd Land and the Ross Ice Shelf is suggested by both surface and 500-hPa analyses.

Case 3: August 24, 1988

The satellite image at 1048 UTC on August 24, 1988 (Figure 18), showed a well-defined dark signature along the Transantarctic Mountains and over the southwest side of Marie Byrd Land; another signature was present over Edward VII Peninsula. Sparse low cloud seems to be present with these features. No above-average temperatures were recorded by the AWS sites; however, the mesoscale analysis at this time suggested that the warm surface air was over the area depicted by the satellite image. According to the AWS mesoscale analyses at 0600 and 1200 UTC on August 24 (Figures 19a and 19b), the presence of cool air, covering most of the Ross Ice Shelf, was revealed by AWS 00, 07, 08, 24, and 25, which recorded colder temperatures than their respective monthly averages. Only AWS 11 recorded a temperature similar to its monthly average. Although the pressure recorded by Russkaya Station was higher than its monthly average (Figure 20), the analysis indicated that it decreased and reached a minimum on August 24. The same behavior, but with a minimum value on August 25, was exhibited by the pressure readings from AWS 00. The regional pressure analysis resolved a mesoscale cyclone to the north of AWS 11 (Figures 19a and 19b). Satellite imagery at 0917 UTC on August 23 (not reproduced) showed a mesoscale cyclone over the Ross Ice Shelf, slightly to the southeast of AWS 24. Katabatic signatures coming from Skelton, Mulock, and Byrd glaciers are also shown by the satellite image; however, no dark signature was observed along the Transantarctic Mountains at this time. The mesoscale analyses suggested that the mesoscale vortex developed between 0600 and 0900 UTC on August 23, to the southeast of the location given by

Fig. 18. NOAA 9 AVHRR thermal infrared image at 1048 UTC on August 24, 1988.

image at 0917 UTC. The elements that could be involved in the formation of this vortex are as follows:

1. A strong, persistent westerly wind (around 16 m s^{-1}) recorded at AWS 24 for the preceding 24 hours indicates the presence of katabatic winds coming from East Antarctica. Such a katabatic airflow can induce the development of boundary layer baroclinicity [Bromwich, 1989c].

2. A surface trough over the Ross Ice Shelf along the Transantarctic Mountains was resolved by the mesoscale analyses starting at 2100 UTC on August 22.

At the same time a ridge extending from West Antarctica was analyzed over the southeastern side of the shelf. Boundary layer baroclinicity and a trough, which appear to be sufficient conditions for formation of mesoscale cyclones, were present at the time when the mesoscale cyclone formed. The AWS analyses suggest that the ridge located over the eastern side of the shelf could have inhibited northward extension of warm surface air coming from southern Marie Byrd Land. This ridge started to weaken at around 2100 UTC on August 23, with the isobars over southern parts of the shelf becoming more parallel to the Transantarctic Mountains. This configuration, which remained until 0600 UTC on August 24 (Figure 19a), allowed the warm surface air coming through Siple Coast to move toward

the northwest; the increase of the temperature at AWS 11 and the dark signature observed on the satellite image at 1048 UTC on August 24 confirm this. The apparent cyclonic circulation of this feature suggests that the mesoscale vortex remained around the center of the Ross Ice Shelf and could support the northwestward propagation of the katabatic winds coming from Siple Coast. After 0900 UTC on August 24 the ridge developed again over the eastern side of the shelf and moved rapidly over to the western side, weakening the mesoscale cyclone. The 3-hourly regional analyses suggest that this vortex moved northward crossing AWS 24 and 25 at around 1800 and 2100 UTC on August 24.

The surface analyses from the Australian Bureau of Meteorology showed that the region of the Ross Sea and Ross Ice Shelf was affected almost continuously by a cyclonic circulation between August 18 and August 27. According to the synoptic analyses and satellite information, the decrease of the pressure recorded by Russkaya Station and AWS 00 was associated with the passage of a synoptic storm through the southern Ross and Amundsen seas. The surface synoptic analysis at 0000 UTC on August 24 (Figure 21) showed an occluded front across Marie Byrd Land and its synoptic vortex located near Russkaya Station. At 1200 UTC the Australian analysis showed the front displaced to the east

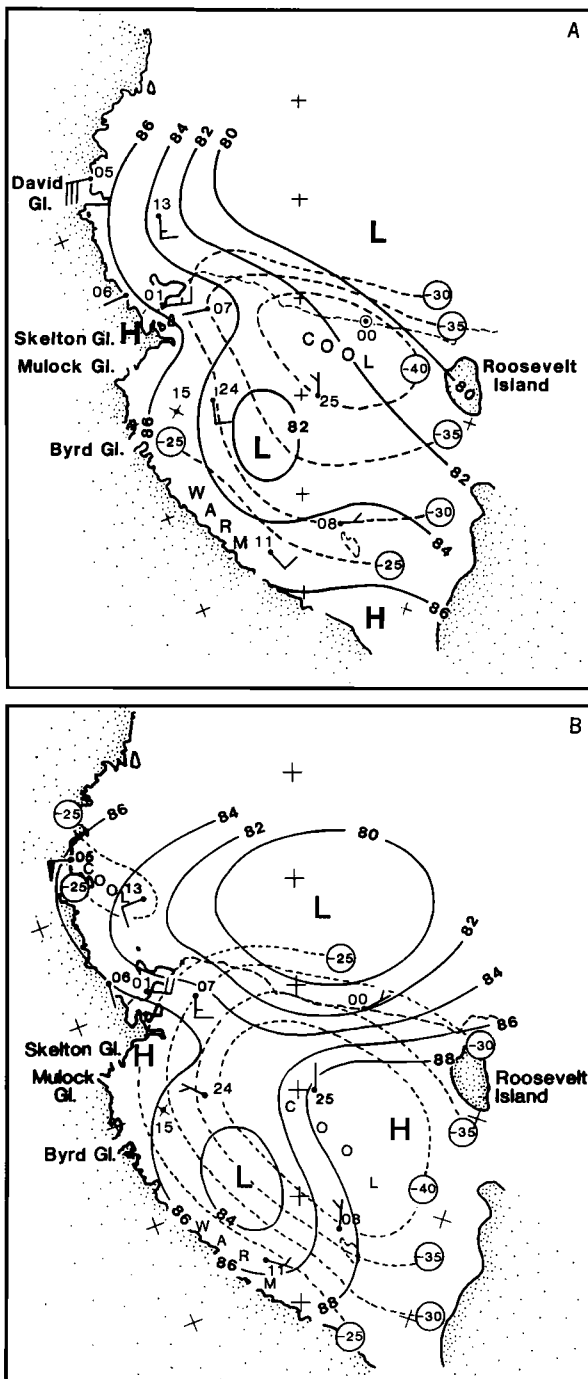


Fig. 19. Same as Figure 5 but for (a) 0600 UTC and (b) 1200 UTC on August 24, 1988.

over the Bellingshausen Sea; however, the satellite image at 1048 UTC on August 24 (Figure 18) indicated that the front, at least its southern part associated with the weak vortex near Russkaya Station, was still over Marie Byrd Land. Also at 1200 UTC on August 24 the Australian synoptic chart showed a subsynoptic cyclone

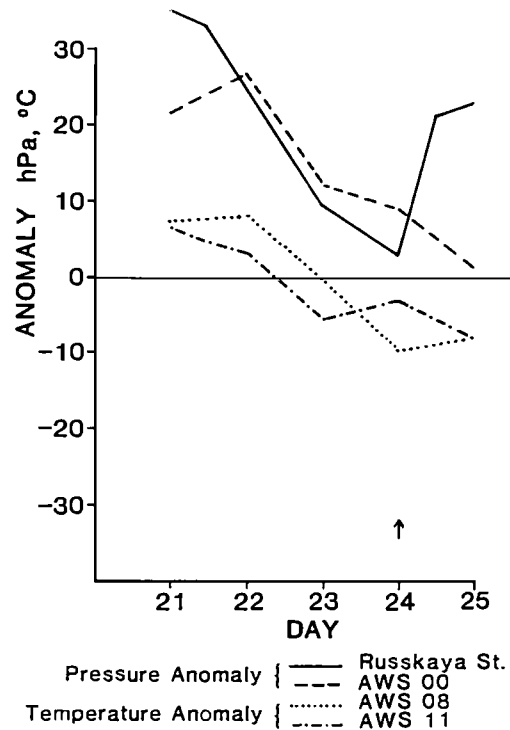


Fig. 20. Same as Figure 4 but for the period between August 21 and August 25, 1988.

over the southern Ross Sea, slightly to the northwest of AWS 00, which coincided with the AWS regional analysis. A cyclonic cloud feature shown by the satellite image (Figure 18) over the Ross Sea can be associated with this system. According to the synoptic analyses this subsynoptic vortex seem to be the remnant of a synoptic cyclone that moved into the region earlier on August 22. Subsequent analyses indicate that this subsynoptic vortex moved slightly toward the northeast, being analyzed for the last time at 1200 UTC on August 26. However, because of the lack of surface data over the Ross Sea, and the sporadic satellite information and synoptic analyses, the above could not be confirmed. The 500-hPa geopotential height analyses indicate a cyclonic circulation over the Ross Sea and Ross Ice Shelf. The 500-hPa chart at 0000 UTC on August 24 (Figure 22) showed a weak midtropospheric vortex over the Ross Sea, to the west of Russkaya Station. Over the next 12 hours it was displaced slightly to the west.

To summarize, in spite of the AWS not recording warm temperatures over the ice shelf, the satellite images clearly revealed their presence along the Transantarctic Mountains. Also, the warm surface air generated by katabatic winds coming from West Antarctica seemed to extend toward the northwest only when the pressure field distribution was favorable, i.e., when the isobars were almost parallel to the mountains [cf. Bro-

mwich, 1989b]. This took place early on August 24, when the subsynoptic ridge that affected the east side of the Ross Ice Shelf started to weaken. On the other hand, the broad scale cyclonic circulation given by surface and 500-hPa synoptic analyses was present throughout.

DISCUSSION

Katabatic winds play an important role in the development of mesoscale phenomena around and within the Antarctic continent. Thus, for example, over the Ross Ice Shelf and adjacent to Terra Nova Bay, katabatic winds coming from East Antarctica generate boundary layer baroclinicity, which, in conjunction with a weak trough, establishes conditions for mesoscale cyclogenesis [*Bromwich, 1989c, 1991*]. Also, polynyas are associated with persistent katabatic winds that blow onto the Ross Sea [*Kurtz and Bromwich, 1983, 1985; Bromwich and Kurtz, 1984*]. Therefore the temporal and climatological behavior of meteorological parameters can be strongly influenced by katabatic winds. Dark signatures that are observed on satellite images qualitatively reflect the intensity of katabatic airflow, while the warmer temperatures recorded by AWS located within the dark plumes reveal the passage and the effect of katabatic winds propagating onto the Ross Ice Shelf.

Throughout the 3 months studied, warm satellite signatures on the southeast side of the ice shelf were a common phenomenon which indicates the persistence of the katabatic winds coming from southern Marie Byrd Land. Unfortunately, the lack of AWS data close to Siple Coast is an impediment to precise evaluation of this situation. However, data from AWS 08, 11, and 25 seem to indicate that this phenomenon can occur quite frequently. Periods of warmer temperatures recorded at these sites were associated with below-average pressure (or periods of pressure decrease) around AWS 00 and/or

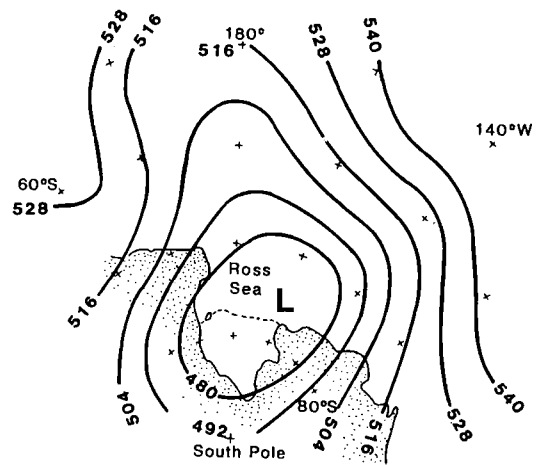


Fig. 22. Same as Figure 9 but for 0000 UTC on August 24, 1988.

Russkaya Station. The dark signatures observed across the Ross Ice Shelf were confirmed as warm surface air by the AWS analyses, and they occurred in conjunction with periods of lower pressure. This high correlation indicates that the north or northwestward projection of the warm satellite signatures, generally parallel to the Transantarctic Mountains, has broad-scale synoptic support. The synoptic analyses provided by the Australian Bureau of Meteorology revealed that the periods of pressure decrease associated with warmer signatures across the ice shelf were caused by the passage of synoptic storms over the southern Ross and Amundsen seas (Table 1). These storms increase the pressure gradient over Marie Byrd Land and the Ross Ice Shelf and support the northwestward propagation of katabatic airflow across the Ross Ice Shelf. Katabatic winds propagating into previously quiescent areas initiate low-level vertical mixing and produce an increase of temperature in the air layer immediately above the ice surface. This mechanism causes the warm satellite signature.

Derivation of the time-averaged winter streamline pattern of surface airflow over Antarctica [*Parish and Bromwich, 1986, 1987*] is based on the assumption that synoptic-scale cyclones do not have an important influence on the average behavior of the winds in the interior of the continent. Therefore, on average, the winds coming from West Antarctica are a consequence mainly of the orography and the surface temperature inversion, i.e., are pure katabatic winds [*Ball, 1960*]. However, the present research indicates that at times synoptic influence becomes important in the interior of the continent when storms, usually associated with warm fronts, pass close to Russkaya Station. When this occurs, the synoptic pressure gradient force over Marie Byrd Land acts nearly at right angles to the force generated by the

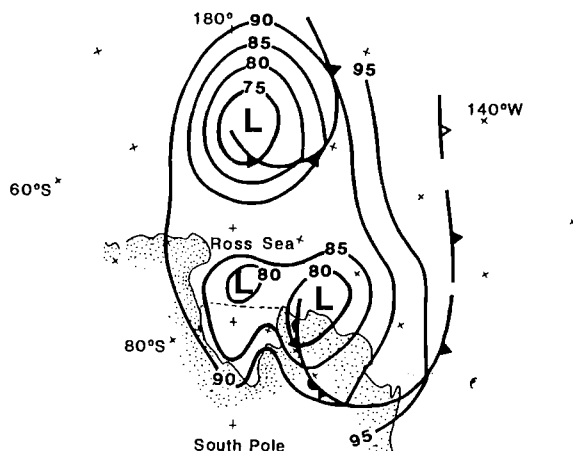


Fig. 21. Same as Figure 8 but for 0000 UTC on August 24, 1988.

presence of cold air over sloping terrain (katabatic force). Increases in katabatic wind speed over Marie Byrd Land due to enhanced convergence of drainage airflow are possible [Ball, 1960] but require further study for verification. Through analysis of signature days it was noted that the isobars over the Ross Ice Shelf were oriented in the same direction as the dark signatures. This suggests that the northward projection of the features requires geostrophic support. That is, the large-scale pressure field organizes and supports horizontal propagation of katabatic airflows from Marie Byrd Land for great distances across the Ross Ice Shelf. This appears to be the primary impact of the synoptic pressure field. Analysis of data from AWS 08 for signature days indicates that 80% of the time, the wind speed was faster and the temperature higher than the monthly average. This result is consistent with the frequent presence of katabatic winds over AWS 08.

All the satellite images showing dark signatures across the ice shelf indicated that the katabatic airflow coming from southern Marie Byrd Land in conjunction with katabatic winds coming from East Antarctica via the various glacial valleys enlarged the polynya along the northern edge of the ice shelf. The typical synoptic pattern associated with dark signatures across the ice shelf and subsequent enlargement of the polynya, which is described in this paper, is similar to that described by Zwally *et al.* [1985].

Unfortunately, data from AWS 03 (Byrd Station) were not available because this site failed in March 1988 [Keller *et al.*, 1989]. Therefore accurate analyses of the atmospheric conditions over Marie Byrd Land could not be conducted. AWS 03 is an important location for this type of study, and its contribution to future research will be significant.

Acknowledgments. This research was sponsored by National Science Foundation grants DPP-8716339 and DPP-8816792 to D.H.B. The satellite imagery was recorded by U.S. Navy personnel at McMurdo Station and obtained from Robert Whritner of the Antarctic Research Center at Scripps Institution of Oceanography (NSF grant DPP-8815818). Collection and distribution of U.S. Antarctic AWS data are supported by NSF grant DPP-8818171 to Charles R. Stearns. John Nagy drafted the figures. Contribution 817 of Byrd Polar Research Center.

REFERENCES

- Antarctic Journal of U.S.*, McMurdo Station gets satellite-image processing system, 23(2), 8–9, 1988.
- Ball, F. K., Winds on the ice slopes of Antarctica, in *Antarctic Meteorology*, pp. 9–16, Pergamon, New York, 1960.
- Breckenridge, C. J., Foehn events along the Transantarctic Mountains, M.S. thesis, 118 pp., Univ. of Wis., Madison, 1985.
- Bromwich, D. H., Surface winds in West Antarctica, *Antarct. J. U.S.*, 21(5), 235–237, 1986.
- Bromwich, D. H., Satellite analyses of Antarctic katabatic wind behavior, *Bull. Am. Meteorol. Soc.*, 70, 738–749, 1989a.
- Bromwich, D. H., Satellite observations of katabatic winds blowing from Marie Byrd Land onto the Ross Ice Shelf, *Antarct. J. U.S.*, 24(5), 218–221, 1989b.
- Bromwich, D. H., Subsynoptic-scale cyclone developments in the Ross Sea sector of the Antarctic, in *Polar and Arctic Lows*, edited by P. F. Twitchell, E. A. Rasmussen, and K. L. Davidson, pp. 331–345, A. Deepak, Hampton, Va., 1989c.
- Bromwich, D. H., Mesoscale cyclogenesis over the southwestern Ross Sea linked to strong katabatic winds, *Mon. Weather Rev.*, 119, 1736–1752, 1991.
- Bromwich, D. H., and D. D. Kurtz, Katabatic wind forcing of the Terra Nova Bay polynya, *J. Geophys. Res.*, 89, 3561–3572, 1984.
- Bromwich, D. H., J. F. Carrasco, and C. R. Stearns, Satellite observations of katabatic wind propagation for great distances across the Ross Ice Shelf, *Mon. Weather Rev.*, 120, 1940–1949, 1992.
- D'Aguanno, J., Use of AVHRR data for studying katabatic winds in Antarctica, *Int. J. Remote Sens.*, 7(5), 703–713, 1986.
- Keller, L. M., G. A. Weidner, C. R. Stearns, and M. F. Sievers, Antarctic automatic weather station data for the calendar year 1988, 329 pp., Dep. of Meteorol., Univ. of Wis., Madison, 1989.
- Kidwell, K. B., NOAA polar orbiter data (TIROS-N, NOAA-6, NOAA-7, NOAA-8, NOAA-9, and NOAA-10) users guide, Natl. Oceanic and Atmos. Admin./Natl. Environ. Satell., Data and Inf. Serv., Washington, D. C., 1986.
- Kurtz, D. D., and D. H. Bromwich, Satellite observed behavior of the Terra Nova Bay polynya, *J. Geophys. Res.*, 88(C14), 9717–9722, 1983.
- Kurtz, D. D., and D. H. Bromwich, A recurring, atmospherically forced polynya in Terra Nova Bay, in *Oceanology of the Antarctic Continental Shelf*, *Antarct. Res. Ser.*, vol. 43, edited by S. S. Jacobs, pp. 177–201, AGU, Washington, D. C., 1985.
- Parish, T. R., and D. H. Bromwich, The inversion wind pattern over West Antarctica, *Mon. Weather Rev.*, 114, 849–860, 1986.
- Parish, T. R., and D. H. Bromwich, The surface windfield over the Antarctic ice sheets, *Nature*, 328, 51–54, 1987.
- Parish, T. R., and D. H. Bromwich, Instrumented aircraft observations of the katabatic wind regime near Terra Nova Bay, *Mon. Weather Rev.*, 117, 1570–1585, 1989.
- Schwalb, A., Modified version of the TIROS-N/NOAA A-G satellite series (NOAA E-J)—Advanced TIROS-N (ATN), *NOAA Tech. Memo. NESS*, 116, 1982.
- Schwerdtfeger, W., The climate of the Antarctic, in *Climates of the Polar Regions*, World Surv. of Climatol., vol. 14, edited by S. Orvig, pp. 253–355, Elsevier, New York, 1970.
- Schwerdtfeger, W., *Weather and Climate of the Antarctic*, vol. 15, *Developments in Atmospheric Science*, 261 pp., Elsevier Science, New York, 1984.
- Stearns, C. R., and G. A. Wendler, Research results from Antarctic automatic weather stations, *Rev. Geophys.*, 26(1), 45–61, 1988.
- Swithinbank, C., Higher resolution satellite pictures, *Polar Rec.*, 16, 739–741, 1973.
- Van Woert, M. L., R. H. Whritner, D. E. Waliser, D. H. Bromwich, and J. C. Comiso, ARC: A source of multi-sensor satellite data for polar science, *Eos Trans. AGU*, 73(6), 65 and 75–76, 1992.
- Zwally, H. J., J. C. Comiso, and A. L. Gordon, Antarctic offshore leads and polynyas and oceanographic effects, in *Oceanology of the Antarctic Continental Shelf*, *Antarct. Res. Ser.*, vol. 43, edited by S. S. Jacobs, pp. 203–226, AGU, Washington, D. C., 1985.

(Received October 15, 1991;
accepted October 14, 1992.)

SENSIBLE AND LATENT HEAT FLUX ESTIMATES IN ANTARCTICA

CHARLES R. STEARNS AND GEORGE A. WEIDNER

Department of Atmospheric and Oceanic Sciences, University of Wisconsin-Madison, Madison, Wisconsin 53706

The United States Antarctic Program started installing reliable automatic weather stations on the Antarctic continent in 1980. The initial units were equipped to measure wind speed, wind direction, air pressure, and air temperature. During the 1983–1984 field season in Antarctica, three units were installed that measured a vertical air temperature difference between the nominal heights of 0.5 m and 3.0 m and relative humidity at a nominal height of 3 m. The measurements of the vertical air temperature difference and the relative humidity are the minimum required to estimate the sensible and latent heat fluxes to the air and also do not exceed the available energy requirements for the weather stations. The attempt to obtain estimates of the sensible and latent heat fluxes was in response to the need for this information to better understand the weather and climate of Antarctica. The results are at best an estimate because the surface roughness of the snow is not known, the height of the sensors is not known after installation because of snow accumulation, and the sensors, especially the relative humidity sensor at low temperatures, can be in error. The units are unattended and may not be visited for several years. The monthly mean values of the sensible heat fluxes on the Ross Ice Shelf are negatively large near the Transantarctic Mountains during the winter months and less negative to the east of the Transantarctic Mountains. During the summer months the monthly mean sensible heat fluxes are positive on the Ross Ice Shelf. At one site on the blue ice at the base of the Reeves Glacier, the estimated annual sublimation of ice equivalent was 0.23 m, and the estimate of the actual ablation of the ice was 0.26 m. The estimates of the net annual sublimation and deposition on the Ross Ice Shelf amount to 20–80% of the annual accumulation. The conclusion is that the assumption that annual sublimation and deposition are zero is not valid under Antarctic conditions.

1. INTRODUCTION

The surface area of Antarctica is about 14×10^6 km² with an average elevation above sea level greater than 2000 m. Antarctica is largely snow-covered ice representing about 75% of the Earth's known fresh water. The annual mean air temperatures in Antarctica range from -10°C along the coast to -50°C on the high plateau. The establishment of stations for making meteorological observations in Antarctica is strongly influenced by the ice conditions and the logistics of supplying a station. Figure 1 is a map of Antarctica showing the locations of stations conducting meteorological observations throughout the year and during the summer season. Aside from the west side of the Antarctic Peninsula, the stations are poorly distributed around the continent, being mainly in protected areas along the coast with a large gap between 75°W and 180° . There are only three interior stations representing an area equal to the continental United States and Canada south of 60°N .

The Workshop on Antarctic Meteorology [Warburton, 1975], and later the Scientific Committee for Antarctic Research (SCAR) [Allison, 1983], recommended that automatic weather station (AWS) units be used for determining the fluxes of heat, moisture, and momen-

tum from the Antarctic snow surface, temperature, wind, and snow drift in katabatic flow and homogeneous climate areas. As a result of these recommendations that automatic weather stations be used in remote areas of Antarctica, the National Science Foundation's Division of Polar Programs initiated the development of an AWS that would utilize a satellite-based data collection system on board polar orbiting satellites of the National Oceanic and Atmospheric Administration (NOAA) series. The AWS units were developed by the Radio Science Laboratory, Stanford University, California, under the direction of A. Peterson.

The low energy consumption of the AWS units allows them to be located in remote areas of Antarctica. The units are powered by six to 12 40 A h gel cell batteries charged by 10-W solar panels and have sufficient energy to operate the AWS unit for more than 1 year. The United States Antarctic Program (USAP) automatic weather station initially measured wind speed, wind direction, and air temperature at a nominal height of 3 m and air pressure at the electronics enclosure. In 1980 the deployment of the units started at Adélie Coast, the Ross Ice Shelf, and along the east side of the Antarctic Peninsula with additional deployments being made each year thereafter. Figure 2 shows the locations of AWS

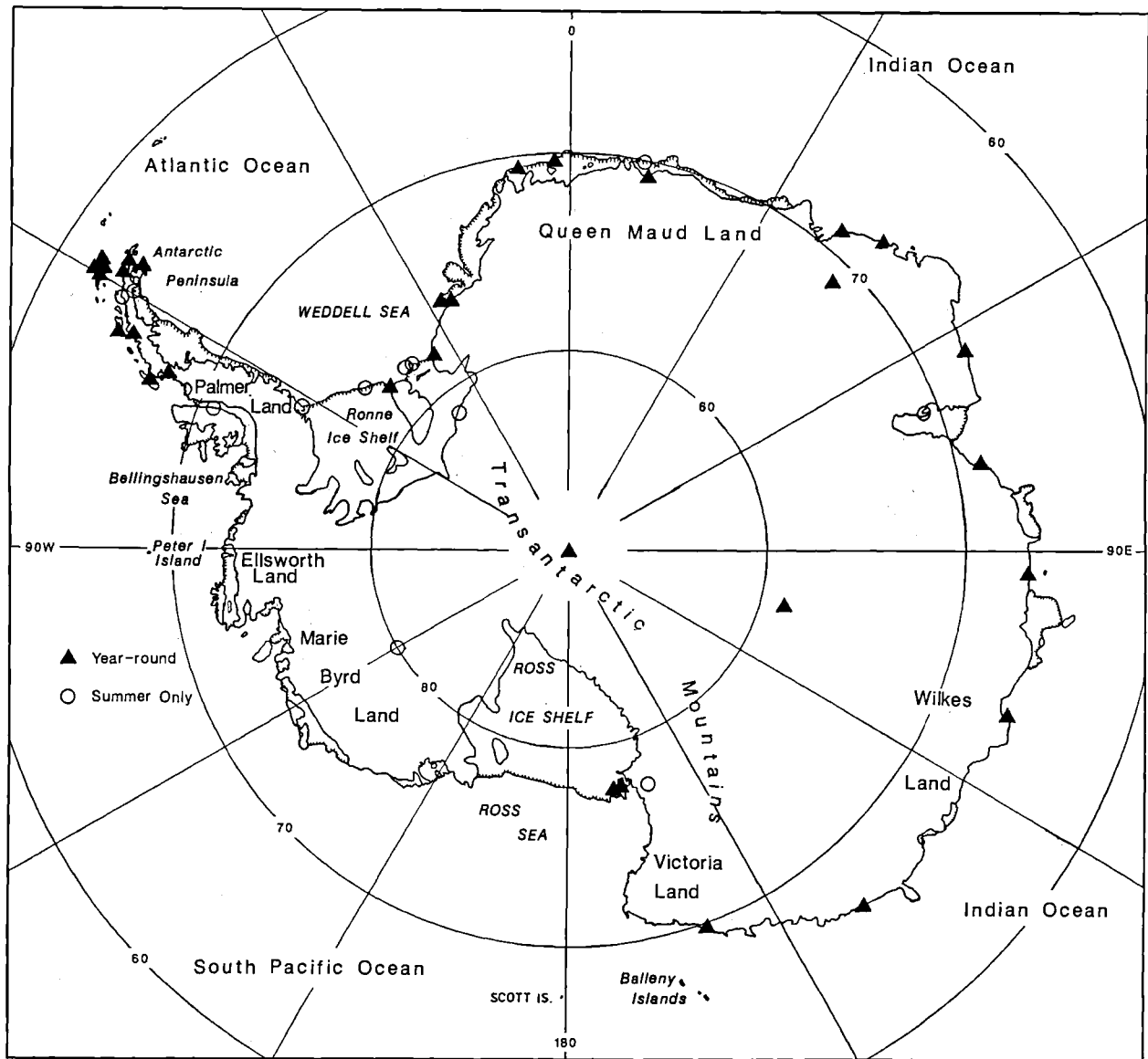


Fig. 1. Map of Antarctica showing the research stations open throughout the year (solid triangles) and those open for the summer only (open circles) for 1990. The largest gap along the coast of Antarctica is between 75°W and 180°W . Meteorological observations are not available on a regular basis in the above sector from the south pole to 30°S .

units for 1992, and Table 1 gives the site names, locations, and site start and stop dates for all the AWS units deployed in Antarctica by the USAP. In 1984 the measurements of the vertical air temperature difference between the nominal height of 3.0 and the nominal height of 0.5 m and the relative humidity at 3.0 m were added to some AWS units in the Ross Island area to see if the measurements could be made reliably. Figure 3 is a layout of the AWS unit used in Antarctica.

Antarctica is considered a sink for atmospheric energy. One mechanism would be a flux of sensible and

latent heat to the surface and the eventual loss by long-wave radiation to space. There is a temperature increase with respect to height in the near-surface atmosphere over most of Antarctica, and it is generally assumed that this condition exists throughout the year. The assumed temperature increase with respect to height at the surface would lead to a sensible heat flux toward the surface. The positive temperature gradient in the air close to the surface does not necessarily mean that the vapor pressure gradient for ice is also positive. As the air temperature near the Earth's surface is very

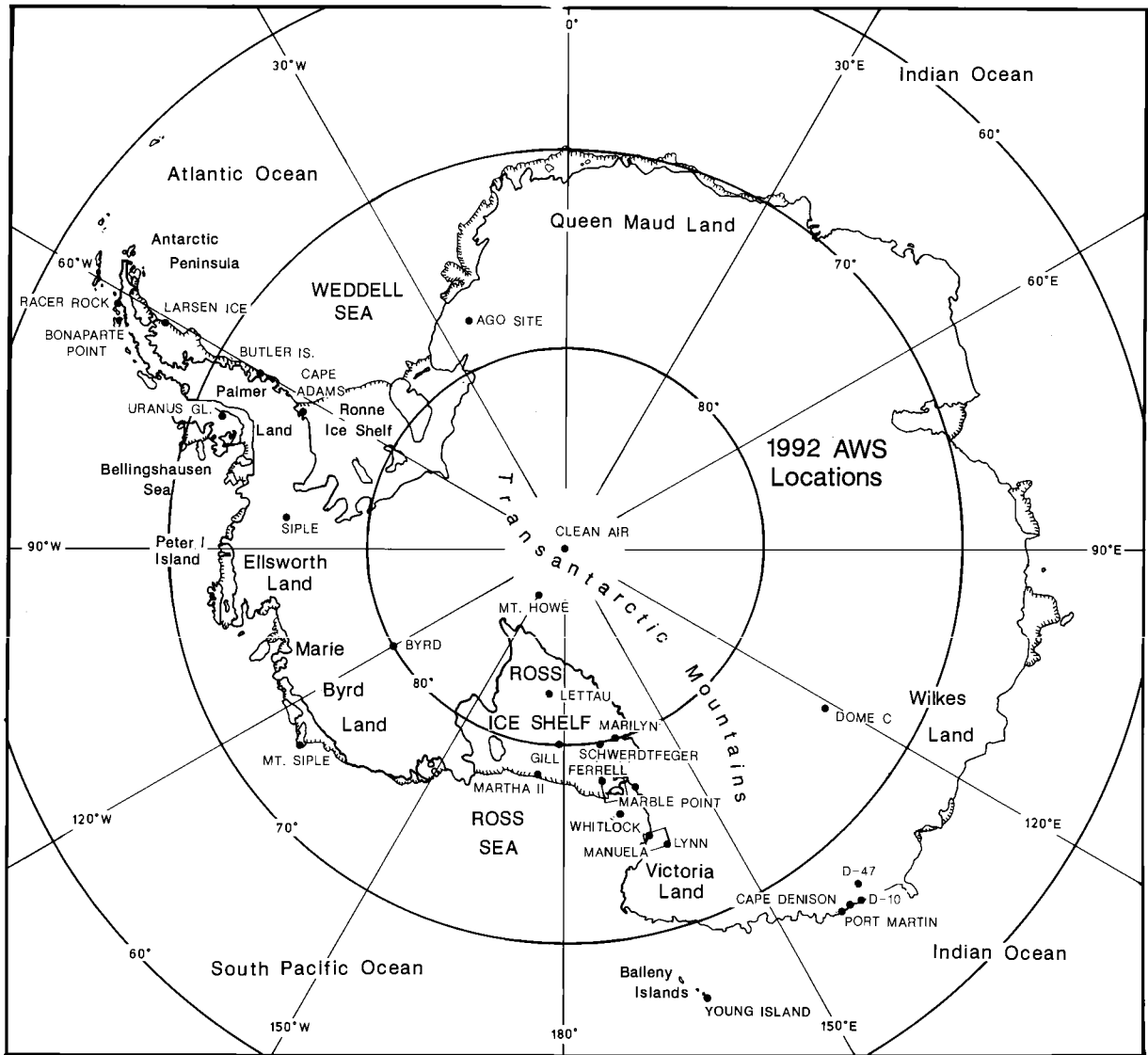


Fig. 2. Map of Antarctica showing the locations of the automatic weather stations of the United States Antarctic Program for 1992.

low, the ice vapor pressure is also very low, and differences with respect to height near the Earth's surface should also be very small but not necessarily positive with respect to height.

The net yearly flux of water vapor to or from the Antarctic snow surface has an effect on the estimation of precipitation based on snow accumulation measurements. At a point the snow surface can accumulate mass by precipitation, condensation, deposition, and wind transport. The snow may be removed from a point by evaporation, sublimation, and wind transport. Evaporation and condensation assume that the phase change of water is between the vapor and the liquid phase, and sublimation and deposition assume that the phase

change of water is between the solid and the vapor phase of water. Since most of the surface air temperatures of Antarctica are usually well below 0°C, the liquid phase of water is seldom present and will be disregarded. Measurements are needed to determine the direction and the magnitude of the latent heat flux on the Antarctic continent as the process represents either an annual surface addition or a removal of water mass.

The meteorological measurements at the manned stations usually do not support estimates of sublimation or wind deposition mass losses. Even if the stations did do an excellent job of making the necessary measurements, the stations are frequently in protected areas of Antarctica, and there are only three stations that could

TABLE 1. AWS Locations From 1980 to 1992

Site	Latitude, deg	Longitude, deg	Altitude, m	Date		World Meteorological Organization Number
				Start	Stop	
<i>Adélie Coast</i>						
D-10	66.70°S	139.80°E	240	Feb. 1980		89832
D-17	66.70°S	139.70°E	438	Jan. 1980	June 1980	
D-47	67.38°S	138.72°E	1560	Jan. 1983		89834
D-57	68.18°S	137.52°E	2105	Jan. 1981	Dec. 1988	
D-80	70.02°S	134.72°E	2500	Nov. 1984		89836
Dome Charlie	74.50°S	123.00°E	3280	Feb. 1980		89828
Port Martin	66.82°S	141.39°E	39	Jan. 1990		
Cape Denison	67.02°S	142.68°E	31	Jan. 1990		
<i>Stations</i>						
Byrd Station	80.00°S	120.00°W	1530	Feb. 1980		89324
Siple Station	75.90°S	83.92°W	1054	Jan. 1982		89284
Mount Siple	73.20°S	127.05°W	30	Feb. 1992		
<i>Ross Island Region</i>						
Marble Point	77.43°S	163.75°E	120	Feb. 1980		89866
Manning	78.77°S	166.85°E	66	Dec. 1980	Jan. 1986	
Ferrell	78.02°S	170.80°E	45	Dec. 1980		89872
Asgard	77.60°S	160.10°E	1750	Feb. 1980	Dec. 1982	
Meeley	78.52°S	170.18°E	49	Dec. 1980	Jan. 1986	
Jimmy	77.87°S	166.81°E	202	Dec. 1981		
Laurie	77.55°S	170.09°E	23	Dec. 1981	Jan. 1986	
Nancy	77.91°S	168.17°E	25	Jan. 1983	Nov. 1983	
Katie	77.70°S	167.70°E	40	Feb. 1983	Jan. 1986	
Fogle	77.82°S	166.75°E	202	Jan. 1984	Jan. 1985	
Tiffany	78.00°S	168.20°E	25	Jan. 1984	Jan. 1986	
Pegasus	77.97°S	166.49°E	10	Jan. 1989	Nov. 1989	
Pegasus North	77.95°S	166.51°E	10	Jan. 1990		89667
Pegasus South	78.03°S	166.60°E	10	Jan. 1991		
Minna Bluff	78.50°S	166.51°E	900	Jan. 1991		
Linda	78.50°S	168.35°E	50	Jan. 1991		
Mount Erebus	77.53°S	167.15°E	3700	Nov. 1989	Dec. 1990	89867
Willie Field	74.23°S	160.29°E	40	Jan. 1992		
<i>Ocean Islands</i>						
Whitlock	76.24°S	168.70°E	275	Jan. 1982		89865
Buckle Island	66.87°S	163.24°E	520	Feb. 1987	Oct. 1988	
Scott Island	67.37°S	179.97°W	30	Dec. 1987	Feb. 1991	89371
Young Island	66.28°S	162.33°E	30	Dec. 1990		89660
<i>Ross Ice Shelf</i>						
Marilyn	79.98°S	165.03°E	75	Jan. 1984		89869
Schwerdtfeger	79.94°S	169.83°E	60	Jan. 1985		89868
Gill	80.03°S	178.63°W	55	Jan. 1985		89863
Bowers	85.20°S	163.40°E	2090	Jan. 1986	Jan. 1987	
Elaine	83.15°S	174.46°E	60	Jan. 1986	Jan. 1989	
Lettau	82.59°S	174.27°W	55	Jan. 1986		89377
Martha I	78.31°S	172.50°W	42	Feb. 1984	May 1986	
Martha II	78.38°S	173.42°W	18	Feb. 1987	Feb. 1992	89374
<i>Reeves Glacier</i>						
Manuela	74.92°S	163.60°E	80	Feb. 1984		89864
Shristi	74.72°S	161.58°E	1200	Dec. 1987		89862
Sushila	74.41°S	161.31°E	1441	Jan. 1988		
Sandra	74.48°S	160.48°E	1525	Jan. 1988		89861
Lynn	74.21°S	160.39°E	1772	Jan. 1988		89860
Pat	74.90°S	163.10°E	30	Jan. 1989	Jan. 1991	

TABLE 1. (continued)

Site	Latitude, deg	Longitude, deg	Altitude, m	Date		World Meteorological Organization Number
				Start	Stop	
<i>Antarctic Peninsula</i>						
Larsen Ice Shelf	66.97°S	60.55°W	17	Oct. 1985		89262
Butler Island	72.20°S	60.34°W	91	March 1986		89266
Dolleman Island	70.58°S	60.92°W	396	Feb. 1986	June 1988	
Uranus Glacier	71.43°S	68.93°W	780	March 1986		89264
Cape Adams	75.01°S	62.53°W	25	Jan. 1989		89268
Racer Rock	64.16°S	61.54°W	17	Nov. 1989		89261
Halley Bay	75.50°S	26.65°W	52	March 1990	Nov. 1990	
BAS-AGO	77.52°S	23.74°W	1545	Jan. 1991		89024
Bonaparte Point	64.78°S	63.06°W	8	Jan. 1992		
<i>South Pole Station</i>						
Clean Air	90.00°S		2835	Jan. 1986		89208
Allison	89.88°S	60.00°W	2835	Jan. 1986	Jan. 1988	
Patrick	89.88°S	45.00°E	2835	Jan. 1986	Jan. 1988	
Mount Howe	87.32°S	149.55°W	2400	Jan. 1992		

If the site does not have a stop date, then the AWS unit is at the site in 1992. The ARGOS identification and World Meteorological Organization number are for 1992.

represent the Antarctic interior. Three stations are unlikely to give good estimates of the surface mass balance changes for Antarctica that could be extrapolated over the entire continent.

The purpose of this paper is to describe the method used to estimate the sensible and latent heat fluxes using

the USAP automatic weather stations and to present the results. Estimating the sensible and latent heat fluxes from the AWS units would allow measurements in remote areas of Antarctica using an array of stations over periods of several years for survey purposes. Previous sensible and latent heat flux measurements are single-point measurements with a duration usually less than 1 year.

Sublimation is the conversion of water from the solid phase to the vapor phase and is represented by a positive latent heat flux from the surface. Deposition is the opposite of sublimation and is represented by a negative latent heat flux.

Dalrymple et al. [1966] reported results of a micrometeorological program at South Pole during 1958 that included monthly mean estimates of the latent heat flux as a residual of the measurements of the net radiation, the submedium heat flux, and the sensible heat flux to the air. The latent heat flux values did not indicate a positive latent heat flux large enough to level the snow significantly [Gow, 1965]. Unfortunately, values were not available during the months of January and December. The results are given in Table 2.

Loewe [1962] states that deposition on the Antarctic plateau contributes as much moisture to the surface as sublimation removes during a year. *Schwerdtfeger* [1984] reported that the assumption that deposition and sublimation during the year are approximately equal has been generally accepted for the Antarctic plateau but may not hold for places 1000–2000 km from the pole. He concluded that on the ice shelves, sublimation may remove more than deposition supplies in the course of a year. *Schwerdtfeger* pointed out that the field measurements had not been made to support any conclusions about the sum of deposition and sublimation during the course of a year.

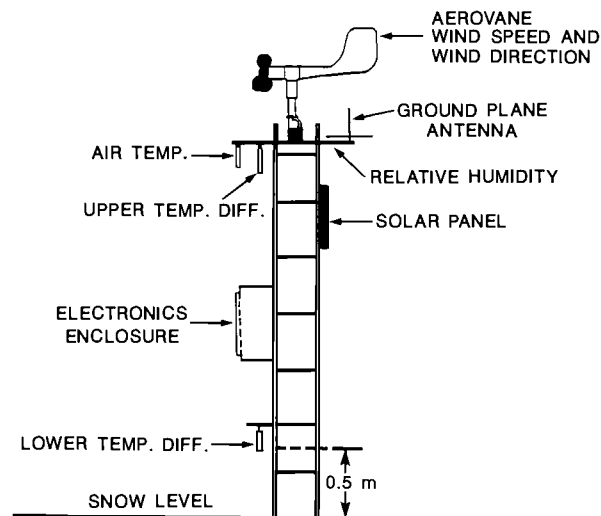


Fig. 3. Layout of the United States Antarctic Program automatic weather station used in Antarctica since 1980. The aerovane measures the wind speed and direction and sets above the boom. The air temperature, upper sensor for the vertical air temperature difference, and the relative humidity are measured on the under side of the boom. The air pressure is measured at the electronics enclosure. The lower sensor for the vertical temperature difference is mounted approximately 0.5 m above the snow at the time of installation.

In December 1960, Gow [1965] dug 3-m snow pits at South Pole and was surprised to "observe a relatively uniform and systematic stratigraphy in the pit wall since with the relatively low rate of accumulation (20 cm snow per year) and occurrence of some high sastrugi in the immediate vicinity of the pit, rather irregular layering might have been expected. Particularly rough surface relief with sastrugi up to 40 cm. high is observed at the end of winter at the south pole. However, a very considerable reduction of this surface relief was observed to take place during the summer and by mid-January even the largest sastrugi had been substantially leveled." Gow pointed out that sublimation and deflation could level the snow surface during the austral summer. Weller [1969] measured the heat balance components of the faces of snow blocks at Plateau Station and concluded that there was a considerable loss of mass from the sloping snow surfaces during the austral summer. Gow's and Weller's conclusion that there is a movement of mass in the snow surface layer indicates that during the austral summer there must be considerable sublimation taking place on the polar plateau.

Sublimation and deposition were measured at Mizuho Station and reported by Fujii and Kusunoki [1982] for 1977. The results were $0.2 \text{ g cm}^{-2} \text{ month}^{-1}$ deposition for May through July 1977. The average latent heat flux is -2.1 W m^{-2} , and the water equivalent depth of deposition is 2 mm month^{-1} . The average sublimation from November 24, 1977, to January 11, 1978, was $62 \text{ mg cm}^{-2} \text{ d}^{-1}$ for 48 days. The latent heat flux equivalent is an average of 20.3 W m^{-2} for the 48-day period, and the water equivalent depth is $-19 \text{ mm month}^{-1}$.

Wendler *et al.* [1988] measured the sensible, latent, and submedium heat fluxes from November 20 to De-

TABLE 3. Sensible (Q_0), Latent (E_0), and Submedium (S_0) Heat Fluxes Reported by Wendler *et al.* [1988] November 20 to December 22, 1985, for D-47 at 67.38°S , 138.72°E , 1560 m

Item	Mean	Minimum	Maximum
Q_0	-8.6	-57.1	15.1
E_0	8.7	-14.3	17.0
S_0	4.8	-1.2	11.4

Mean is the mean daily value, maximum is the mean daily maximum, and minimum is the mean daily minimum for the period. The sign of the heat fluxes is opposite that of Wendler *et al.* [1988]. The water equivalent depth for the period based on the average latent heat flux of 8 mm .

ember 22, 1985, at D-47. The results are given in Table 3 as the mean, mean maximum for the day, and mean minimum for the day for the above period. The water equivalent depth of the mean latent heat flux for the 31-day period is -8 mm .

Faure and Buchanan [1991] measured the ablation rates for the ice fields in the region of the Allan Hills, Antarctica, using wooden sticks implanted in the ice and measuring the lowering of the ice relative to the dowels. Ablation rates were determined at the end of the field season and 2 years later. The ablation amounts apparently were in centimeters of ice and were converted to millimeters of water equivalent. The results for Elephant Moraine ($76^\circ17'\text{S}$, $157^\circ20'\text{E}$) are 38 mm yr^{-1} , for Reckling Moraine ($76^\circ15'\text{S}$, $158^\circ40'\text{E}$) are 44 mm yr^{-1} , and for Allan Hills ($76^\circ47'\text{S}$, $159^\circ25'\text{E}$) are 49 mm yr^{-1} .

Simmonds and Budd [1991] used a 21-wave general circulation model (GCM) for July to estimate the sensitivity of the southern hemisphere circulation to leads in the Antarctic pack ice. One of the outputs from the GCM was the latent heat flux immediately south of the sea ice on the edge of the Antarctic continent. The result was 20.3 W m^{-2} or $1.99 \text{ mm month}^{-1}$ water equivalent removed by sublimation.

2. USAP AUTOMATIC WEATHER STATIONS

The standard automatic weather station used by the United States Antarctic Program in Antarctica to estimate the sensible and latent heat fluxes measures air temperature, air pressure, wind speed and direction, relative humidity, and the vertical air temperature difference. The data are updated at nominal 10-min intervals and transmitted to the NOAA series of polar-orbiting satellites at 200-s intervals.

The layout of the AWS unit is shown in Figure 3. The reference for height measurement is the top of the boom which is installed about 3 m above the snow surface. The wind speed is measured 0.43 m above the boom, air temperature and the top temperature difference sensor are 0.15 m below the boom, relative humidity is measured at 0.05 m under the boom, and the lower temper-

TABLE 2. Heat Budget Data From South Pole During 1958 Reported by Dalrymple *et al.* [1966]

Month	R_0		Q_0		S_0		E_0	
	S.P.	Patr.	S.P.	Patr.	S.P.	Patr.	S.P.	Patr.
Feb.	-19.2		-8.6	22.5	-1.4		-9.1	3.5
March	-31.2		-17.8	-2.2	-3.4		-10.1	0.3
April	-28.8		-17.8	-3.3	-3.4		-7.8	0.2
May	-25.9		-30.7	-7.7	-1.9		+6.7	0.0
June	-25.9		-21.6	-4.9	-1.0		-3.4	0.1
July	-28.3		-27.4	-8.2	-1.4		+0.5	0.1
Aug.	-24.0		-18.2	-18.0	-1.4		-4.3	0.1
Sept.	-22.1		-17.8	-13.4	-0.5		-3.8	0.0
Oct.	-14.9		-15.4	6.4	+2.4		-1.9	0.6
Nov.	+6.7		-4.3	51.5	+4.8		+6.2	6.4
Dec.				77.2	+4.8			23.4

The original units were langley per day and were converted to watts per square meter. R_0 is net radiation; Q_0 , sensible heat flux; S_0 , submedium heat flux; and E_0 , latent heat flux. The estimates of the sensible heat flux and the latent heat flux from Patrick AWS unit for 1986 from Table 4 are included for comparison. S.P. indicates South Pole results, and Patr. indicates Patrick AWS results.

TABLE 4. Meteorological Variable, Sensor, and Resolution for the Polar, Automatic Weather Stations

Variable	Sensor	Resolution
Air pressure	Parascientific model 215	0.05 mbar
Air temperature	Platinum resistance thermometer	0.125°C
Wind speed	Belfort aerovane model 123	0.25 m s ⁻¹
Wind direction	Belfort aerovane model 123	2°
Relative humidity	Vaisala HMP-31UT	1%
Temperature difference	two thermocouple junctions	0.05°C

The pressure sensor drifts less than 0.2 mbar yr⁻¹.

ature difference sensor is 2.5 m below the boom. A particular installation may result in significantly different heights for the boom above the surface and the height of the lower vertical temperature difference sensor. The temperature heights are given to the level where the temperature probe resides inside the shield. Table 4 gives the sensor's description and resolution.

The data are received at monthly intervals from Service ARGOS and are processed to scientific units. Each transmission contains five values 10 min apart of air temperature, air pressure, wind speed, and wind direction and three values 20 min apart for relative humidity and the vertical air temperature difference. Between 100 and 144 measurements are available every 24 hours. Data are selected at 3-hourly intervals ± 1 hour for general use and are used here for the estimations of the sensible and latent heat fluxes.

The purpose of the vertical air temperature and relative humidity measurements was to estimate the vertical fluxes of latent and sensible heat. Usual methods of measuring the vertical fluxes of sensible and latent heat require considerable amounts of power, constant attention, and elaborate data-logging systems. The measurements of the vertical air temperature difference and the relative humidity are the minimum measurements necessary to estimate the sensible and latent heat fluxes to the air and could be made without significantly increasing the energy requirements of the AWS units. The measurement of solar and net radiation was not considered because the potential for frequent accumulation of an unknown amount of frost on the instruments would make the measurements uncertain.

3. METHOD USED TO ESTIMATE THE SENSIBLE AND LATENT HEAT FLUX

The surface heat budget equation is

$$R_0 = SW \downarrow (1 - a) + LW \downarrow - LW \uparrow = S_0 + Q_0 + E_0 \quad (1)$$

where

- R_0 net radiation;
- $SW \downarrow$ global solar radiation down;
- a surface albedo;

- $LW \downarrow$ long-wave radiation down;
- $LW \uparrow$ long-wave radiation up;
- S_0 submedium heat flux;
- Q_0 sensible heat flux to the air;
- E_0 latent heat flux to the air.

The latent heat flux can be converted to the water equivalent depth as follows:

$$wed = -E_0 t L^{-1} \rho_v^{-1} \quad (2)$$

where

- wed water equivalent depth removed during the time t (m);
- t time for the average of E_0 (s);
- E_0 average latent heat flux ($W m^{-2}$);
- L latent heat of sublimation ($2.833 \times 10^6 J kg^{-1}$);
- ρ_v density of water ($1000 kg m^{-3}$).

The wind speed and potential air temperature profile theory used is based entirely on the work of *Lettau* [1979]. The wind speed and temperature profile and the profile structure dependence on the surface friction and sensible heat flux must be solved together because of the interdependence of the relationships. The relationships used are the wind profile, potential air temperature profile, *Monin and Obukhov* [1954] nondimensional height, and corrections for the departures of the wind and temperature profiles from a logarithmic variation with respect to height.

3.1. Profile Theory

The equation used to represent the horizontal wind speed profile is

$$u(z) = u^* k^{-1} [\ln (zz_0^{-1}) - \psi(z)] \quad (3)$$

where

- $u(z)$ horizontal wind speed at height z above the surface;
- u^* friction velocity;
- k von Karman constant, equal to 0.36;
- $z = z' - d$, equal to the height above the surface $z \leq h$;
- h height of the surface or constant flux layer;

- z' height above the surface at the time of installation;
 d displacement height of the surface;
 z_0 surface roughness and a characteristic of the surface structure;
 $\psi(z)$ the wind profile departure from logarithmic.

The equation for the air temperature as a function of height is

$$\theta(z) - \theta(z_0) = -\theta^* k^{-1} [\ln(z z_0^{-1}) - \Psi(z)] \quad (4)$$

where

- $\theta(z)$ potential air temperature at the height z ;
 $\theta(z_0)$ potential air temperature at the surface;
 $\Psi(z)$ the temperature profile departure from logarithmic;

$$\theta^* = Q_0 (\rho C_p u^*)^{-1} \quad (5)$$

where Q_0 is the sensible heat flux to the air, ρ is the air density, and C_p is the specific heat of the air at constant pressure. The *Monin and Obukhov* [1954] nondimensional height ζ is defined as

$$\zeta = -gkzQ_0(\rho C_p T_0 u^{*3})^{-1} \quad (6)$$

where T_0 is the Kelvin surface temperature and g is the acceleration of gravity. For $\zeta < 0$ or $Q_0 > 0$, $\psi(z)$ for the wind profile is

$$\psi(z) = \ln(1-x)^2 + \ln(1+x^2) + x - 2 \tan^{-1} x - 0.5086 \quad (7)$$

where

$$x = (1 - 15\zeta)^{1/4},$$

and $\Psi(z)$ for the temperature profile is

$$\Psi(z) = \ln(1+X+X^2)^{3/2} - 3^{1/2} \tan^{-1} [(1+2X)3^{-1/2}] + 0.1659 \quad (8)$$

where

$$X = (1 - 22.5\zeta)^{1/3}.$$

For $\zeta > 0$ or $Q_0 < 0$, $\psi(z)$ for the wind profile is

$$\psi(z) = \ln(1+y)^2 + \ln(1+y^2) - 2 \tan^{-1} y - 4y^3(3^{-1}) + 0.8247 \quad (9)$$

where

$$y = (1 + 5\zeta)^{1/4},$$

and $\Psi(z)$ for the temperature profile is

$$\Psi(z) = \ln(1+Y)^2 - 2Y - 2Y^3(3^{-1}) + 1.2804 \quad (10)$$

where

$$Y = (1 + 5\zeta)^{1/2}.$$

3.2. Sensible Heat Flux

Initially, (3) is solved for u^* assuming that $\psi(z) = 0$:

$$u^* = u(z)k/[\ln(z z_0^{-1}) - \psi(z)] \quad (11)$$

using the anemometer height, wind speed, and surface roughness.

An initial estimate of Q_0 is made assuming $\Psi(z_2)$ and $\Psi(z_1)$ equal zero and using (4) as

$$Q_0 = -\rho C_p u^* k [T(z_2) - T(z_1)] / [\ln(z_2 z_1^{-1}) - \Psi(z_2) + \Psi(z_1)]. \quad (12)$$

The term $\theta(z_2) - \theta(z_1)$ is replaced with the actual temperature difference between the two heights z_2 and z_1 .

The above steps give values of u^* and Q_0 that can be used in (6) to determine the values of $\psi(z)$ and $\Psi(z)$ and then in a return to (11) and (12) to make another estimate of Q_0 until the difference between two successive values of Q_0 is less than 0.01 W m^{-2} . There is only one value of Q_0 for one value each of wind speed and vertical air temperature difference. Five to ten trials are usually required to select the value of the sensible heat flux. After the sensible heat flux is determined, the surface temperature is estimated using (4) and the air temperature measured at the level of the upper temperature difference sensor. If the surface temperature is greater than 0°C , then the sensible heat flux estimate is rejected on the assumption that the surface temperature of the snow would not be above the melting temperature.

The wind speed has a resolution of 0.25 m s^{-1} , and the temperature difference has a resolution of 0.1°C . The adiabatic temperature difference from 3 to 0.5 m is -0.025°C , which is less than the temperature difference resolution, so the departures from adiabatic were neglected.

3.3. Latent Heat Flux

The relative humidity and the air temperature are used to calculate the pressure of the water vapor in the air using the air temperature to get the saturation vapor pressure of the air with respect to a pure flat water surface. Then, using the air pressure, the specific humidity is calculated. The surface specific humidity is needed to determine the latent heat flux. The surface temperature is estimated from (4), and the surface temperature is used to get the saturation vapor pressure of ice at the surface which is converted to specific humidity.

The equation for the latent heat flux estimate is

$$E_0 = -\rho u^{*2} L [q(z) - q(z_0)] u(z)^{-1} \quad (13)$$

where

- ρ air density (kg m^{-3});
- E_0 latent heat flux (W m^{-2});
- u^* friction velocity (m s^{-1});
- $q(z)$ specific humidity at the height z ;
- $q(z_0)$ specific humidity at the surface;
- $L = 2.833 \times 10^6 \text{ J kg}^{-1}$, equal to the latent heat of sublimation for ice.

The assumptions are that the eddy diffusivities for momentum and moisture are equal and that at zero wind speed the latent heat flux is zero. Equation (2) will give the water equivalent depth removed because of the change of water from the solid to the vapor phase and is a negative change in depth if $E_0 > 0$.

Figure 4 gives the wind speed versus the vertical temperature difference between 3.0 and 0.5 m for constant values of the sensible heat flux. Negative temperature differences correspond to positive heat fluxes, and the estimation of the sensible heat flux is largely dependent on the measurement of the vertical air temperature difference. The same is true for the negative heat fluxes if the vertical temperature difference is less than $+1^\circ\text{C}$ but is more dependent on the wind speed as the air temperature difference becomes more positive. The method for determining the sensible heat flux does not always converge to a solution if the wind speed is below 3 m s^{-1} and the vertical air temperature difference is greater than 0°C . The sensible and latent heat fluxes are set equal to zero and counted. Approximately 10% of the observations are in this category.

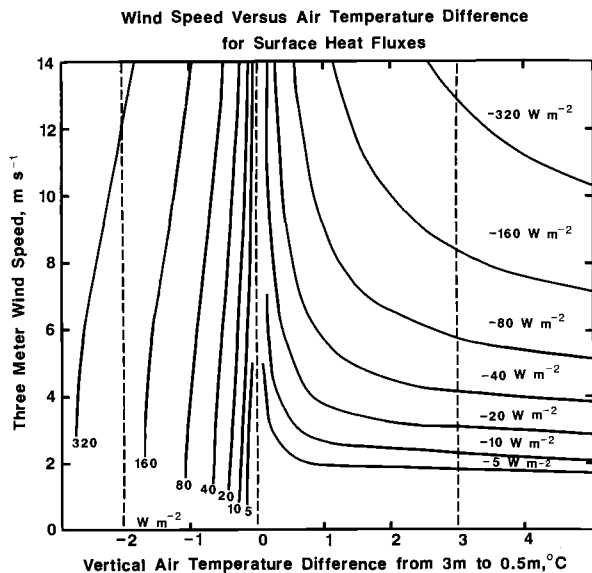


Fig. 4. Wind speed at 3.4 m versus the vertical temperature difference between 3.0 and 0.5 m for constant values of the sensible heat flux based on the theory of Lettau [1979].

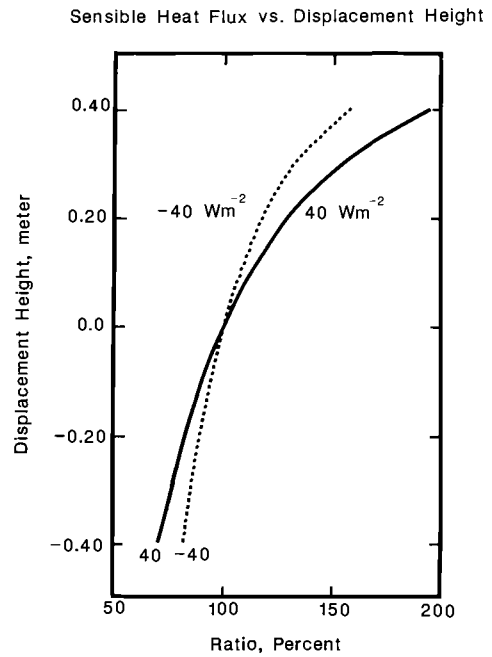


Fig. 5. The error in the sensible heat flux due to the changes in the displacement height. The surface roughness is 0.5 mm , the wind speed is 6 m s^{-1} , and the sensible heat flux to the air is $\pm 40 \text{ W m}^{-2}$.

3.4. Errors

The AWS unit will be isolated for several years, and this isolation may result in errors in the estimates of the sensible and latent heat fluxes due to changes in height and structure of the snow surface. Snow will have a net accumulation at the sites, and this accumulation will decrease the height of the sensors relative to the surface. Changes in the surface structure [Gow, 1965] may change the surface roughness by an unknown amount.

The sensors will introduce errors due to a lack of resolution, lack of response at low temperatures, and times when the sensor or the AWS system does not operate properly. The lack of sufficient resolution is apparent in the vertical air temperature difference. The range of the response of the relative humidity sensor appears to decrease as the air temperature decreases. The wind system frequently does not operate during the austral winter on the Ross Ice Shelf perhaps because of the accumulation of frost on the wind system.

3.4.1. *Displacement height.* The snow accumulation on the Ross Ice Shelf is between 100 and 300 mm yr^{-1} and will decrease the sensor height above the snow [Schwerdtfeger, 1984, p. 201]. Figure 5 shows the error in the sensible heat flux due to a change in the displacement height from -0.4 m to 0.4 m . A positive displacement height means that the level of the snow is increasing and the sensor height above the surface is decreasing. The method used to determine an error due

to a change in the displacement height is to solve for the vertical potential air temperature difference between 3.0 and 0.5 m given the sensible heat flux and the wind speed at 3.43 m with a surface roughness of 0.5 mm and a displacement height of 0.0 m using (3)–(11). The wind speed and vertical air temperature difference at displacement heights from -0.4 m to 0.4 m are used to calculate the sensible heat for comparison to the true value at 0.0 m displacement height. The calculations are performed for sensible heat fluxes ranging from -160 W m^{-2} to 160 W m^{-2} . The ratios of the computed to the correct sensible heat flux in Figure 5 are for ± 40 W m^{-2} . The results are similar for the other sensible heat fluxes. For displacement height changes from $+0.40$ m to -0.40 m, the range of percent error increases for increases in the positive sensible heat flux and decreases as the negative sensible heat flux decreases. Obviously, mounting the sensors higher initially causes a smaller error in the sensible heat flux estimate, but the vertical air temperature difference is smaller, thus introducing a larger uncertainty in the vertical air temperature difference since the resolution remains at 0.1°C .

Changes in the displacement height are assumed to be zero in solving for the sensible and latent heat fluxes, so the uncertainty in each of the fluxes is approximately $\pm 50\%$.

3.4.2. Surface roughness. The reported roughness of snow surfaces ranges from 0.1 mm to 15 mm as reported by Inoue [1989]. The surface roughness at South Pole in May 1958 was estimated to be less than 0.1 mm [Dalrymple *et al.*, 1966].

On the basis of a wind speed of 6 m s^{-1} at 3.43 m, sensible heat fluxes from -160 W m^{-2} to 160 W m^{-2} , a displacement height of 0 m, and a surface roughness of 0.5 mm, the friction velocity and the vertical potential air temperature difference from 3.0 to 0.5 m are calculated using the wind speed, vertical potential air temperature difference, and (3)–(12). Then the sensible heat flux and friction velocity are calculated for surface roughnesses from 0.1 to 1.0 mm in steps of 0.1 mm using the wind speed and the vertical potential air temperature difference. The change in the sensible heat flux was less than 1% . The conclusion is that surface roughness changes will not significantly change the estimates of the sensible heat flux, so the surface roughness was assumed to be 0.5 mm.

3.4.3. Relative humidity. The sensor used for the measurement of relative humidity is identified in Table 4. The vapor pressure of the atmosphere is difficult to measure at very low temperatures. The sensor relative humidity response is with respect to liquid water according to the manufacturer. Figure 6 shows the measured relative humidity versus the air temperature for an AWS unit installed for several years on the Ross Ice Shelf. The sensor did not indicate ice saturation very often and, at temperatures of -40°C and below, did not detect large changes in relative humidity. Upon retriev-

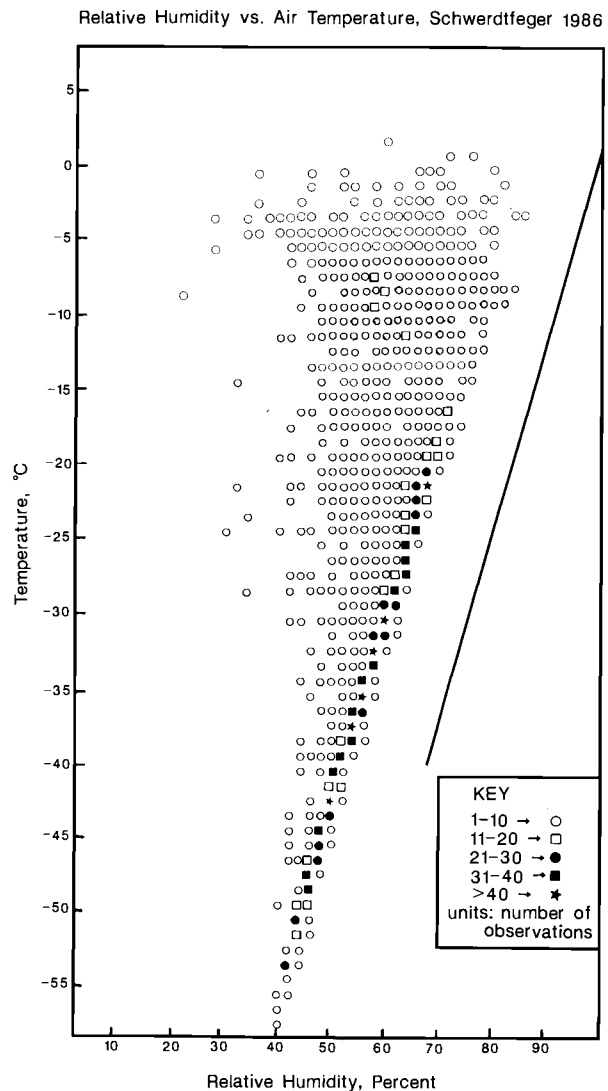


Fig. 6. Relative humidity versus air temperature from Schwerdtfeger site during 1986 for the HMP-31UT humidity sensor used on the AWS units in Antarctica. The relative humidity response of the sensor is with respect to liquid water. The sensor does not reach the saturation relative humidity with respect to ice shown by the slanting solid line. There were 2873 data points.

ing the humidity sensor after several years on the Ross Ice Shelf, the calibration was within 2% of the original calibration. The record shown in Figure 6 is very similar to the record of all the moisture sensors installed on the Ross Ice Shelf.

The relative humidity is converted to specific humidity using the air pressure and air temperature measured at that time by the AWS unit.

3.4.4. Air temperature. The air temperature will have a radiation error if the wind speed is less than 1 m s^{-1} and the Sun is shining. Therefore all wind speeds

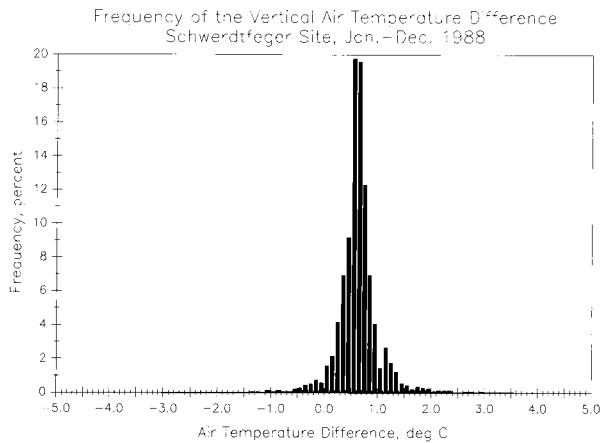


Fig. 7. Frequency of the vertical air temperature difference between 3.0 and 0.5 m at Schwerdtfeger during 1988 in increments of 0.2°C .

less than 1 m s^{-1} are not used to estimate the sensible and latent heat fluxes.

3.4.5. Vertical air temperature difference. The vertical temperature differences are also subject to a radiation error in the presence of sunlight and are not used when the wind speed is less than 1 m s^{-1} . Vertical air temperature differences outside the range of -2.0° to 3.0°C are not used because of the occasional large magnitude of the sensible heat flux estimates. Figure 7 shows the frequency distribution of the vertical temperature difference for Schwerdtfeger site during 1988. More than 99% of the values are within the range of -2.0° to 3.0°C . The vertical temperature difference is recorded to the nearest $\pm 0.1^{\circ}\text{C}$, introducing a range of sensible heat flux values for each 0.1°C interval. Figure 8 gives the error in the sensible heat flux as a function of the wind speed for four values of the sensible heat flux using the theory given in (3)–(11). As the wind speed increases, the uncertainty in the sensible heat flux increases at a rate of approximately 1 W m^{-2} per 0.1°C for each 1 m s^{-1} increase in the wind speed. The uncertainty could be reduced by increasing the resolution of the vertical air temperature difference.

3.4.6. Wind speed. The wind speed is the least reliable measurement on the AWS unit. During the winter the wind speed will read zero, and the wind direction will be constant for extended time periods. Sometimes the wind direction will be constant, but the wind speed will not be zero. If either the wind speed is zero or the direction is constant for extended time periods, the data are not used. As the AWS units are unattended during the winter, the reasons for the failures are not known. Most probably, frost builds up on the wind system. Occasionally, the wind system will start operating again with a wind speed above 10 m s^{-1} . The units usually start operating when the Sun gets above the horizon.

3.5. Latent and Sensible Heat Flux Estimates

The sensible and latent heat fluxes are calculated for each valid observation of the wind speed, wind direction, air temperature, air pressure, relative humidity, and vertical air temperature difference at 3-hourly intervals. The vertical air temperature difference must be in the interval of -2.0°C and 3.0°C to be used for estimating the heat fluxes. The surface roughness is assumed to be 0.5 mm , and the displacement height is assumed to be 0.0 m . Table 5 presents an example of what is available in the full data set (monthly averages for air temperature, air pressure, wind speed, surface stress, estimated surface temperature, vertical air temperature difference, sensible heat flux, latent heat flux, specific humidity of the air, specific humidity at the surface, and the number of observations for the month) and how to obtain it. The maximum number of observations in a month is 8 times the number of days in the month. An AWS unit installed in January of any year will likely have a short record, and the record will be removed if there are less than 80 observations in the month because the record is biased toward the end of the month. During the austral winter, data from the AWS unit may not be reliable particularly if the wind direction is not changing normally or the

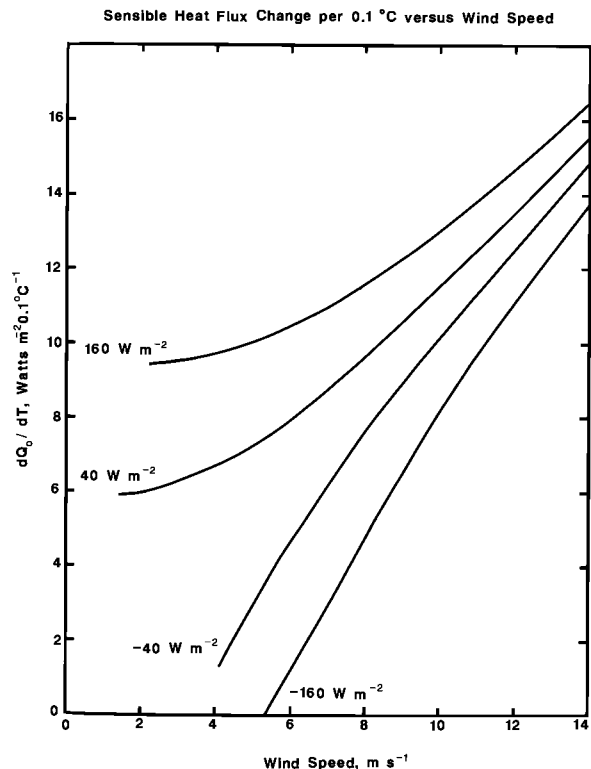


Fig. 8. The change in the sensible heat flux with respect to the vertical air temperature interval of 0.1°C , the resolution of the vertical temperature difference.

TABLE 5. Monthly Mean Data Related to the Sensible and Latent Heat Fluxes Determined From Automatic Weather Stations in Antarctica From 1984 Through 1990

Month	T_3	PP , mbar	VV , $m\ s^{-1}$	Tau	T_0	δT	Q_0 , $W\ m^{-2}$	E_0 , $W\ m^{-2}$	q_3	q_0	OBS
1984 8908 Laurie											
1	-8.98	998.30	4.60	6.53	-7.49	-0.17	18.70	21.27	1.44	2.09	73
2	-13.45	991.55	6.52	11.61	-12.76	-0.12	9.66	9.80	1.11	1.40	206
3	-20.28	981.37	5.58	9.46	-19.62	0.16	19.25	8.02	0.62	0.78	188
4	-22.05	981.57	7.39	15.20	-21.67	0.05	19.47	6.52	0.59	0.66	193
5	-25.43	989.74	6.53	12.94	-25.50	0.43	7.36	2.26	0.45	0.47	197
1984 8911 Tiffany											
2	-13.98	991.92	3.99	5.37	-13.94	0.41	-0.18	6.98	0.89	1.30	178
3	-19.41	981.32	3.68	4.04	-19.84	0.72	-6.85	1.90	0.61	0.76	166
4	-21.45	982.25	3.95	4.28	-22.80	1.29	-19.22	-1.95	0.55	0.56	125
5	-26.35	990.48	4.42	7.15	-26.43	0.73	-16.44	-3.03	0.36	0.41	88
1984 8921 Marilyn											
1	-8.97	996.36	2.98	2.02	-9.76	0.41	-5.82	6.79	1.32	1.73	87
2	-17.16	988.26	4.39	5.06	-18.79	0.73	-20.21	0.44	0.76	0.86	210
3	-21.58	976.85	8.23	17.78	-24.37	0.84	-53.45	-5.48	0.57	0.48	238
4	-24.25	978.70	8.09	16.55	-27.70	1.02	-66.49	-5.12	0.42	0.33	222
5	-26.07	984.73	8.78	21.00	-28.84	1.01	-45.18	-3.11	0.40	0.34	226
6	-28.77	979.82	7.82	16.37	-32.21	1.20	-61.62	-4.42	0.34	0.26	205
7	-31.86	975.22	6.23	10.93	-33.47	0.90	-30.19	-2.08	0.25	0.22	162
1985 8911 Laurie											
2	-16.76	990.68	5.47	8.37	-17.41	0.28	-8.73	5.08	0.80	0.99	210
3	-21.54	988.33	7.94	19.25	-22.98	0.54	-29.11	-3.02	0.57	0.55	215
5	-27.68	990.60	10.03	30.42	-29.27	0.50	-40.73	-3.09	0.35	0.32	210
11	-15.72	975.63	4.95	7.52	-16.14	0.26	-7.45	7.43	0.70	1.04	174
12	-7.92	982.91	6.94	13.82	-8.30	0.12	-11.40	17.59	1.36	1.97	209
1985 8924 Schwerdtfeger											
2	-19.78	985.81	3.43	2.91	-20.37	0.49	-5.77	3.70	0.59	0.79	191
3	-25.26	984.29	5.54	8.44	-27.22	0.74	-27.40	0.02	0.37	0.38	231
5	-33.73	987.26	6.44	11.10	-36.48	0.95	-42.08	-0.80	0.18	0.17	214
7	-46.15	972.59	4.84	7.75	-47.70	1.04	-24.98	-0.10	0.04	0.04	194
8	-38.88	982.79	4.60	6.01	-40.56	1.11	-23.17	-0.29	0.10	0.10	225
9	-33.98	972.67	5.85	9.58	-36.03	0.84	-31.61	-0.50	0.17	0.17	196
10	-27.26	974.28	5.57	8.25	-28.43	0.43	-18.50	1.71	0.30	0.36	215
11	-17.11	969.67	3.81	3.87	-17.15	0.15	-1.64	6.53	0.65	0.97	184
12	-7.84	977.96	4.89	6.14	-9.05	0.45	-15.68	10.55	1.38	1.84	205
1985 8925 Gill											
2	-18.33	984.66	4.18	4.53	-18.66	0.14	-2.75	4.71	0.72	0.91	191
3	-26.22	981.01	5.50	8.61	-26.93	0.21	-10.07	1.60	0.35	0.40	207
7	-49.96	971.90	3.95	5.50	-50.77	0.45	-9.30	0.37	0.02	0.03	183
8	-42.07	980.36	4.60	6.01	-43.18	0.41	-13.70	0.49	0.05	0.07	220
9	-40.31	970.60	4.38	5.69	-40.45	0.24	-1.41	0.94	0.08	0.11	204
10	-29.24	971.76	5.16	7.62	-29.20	0.14	-0.34	2.93	0.25	0.35	211
11	-17.16	969.15	4.70	6.34	-16.32	-0.08	7.48	9.48	0.70	1.04	210
12	-9.17	976.62	4.07	4.41	-8.90	0.02	1.17	12.98	1.29	1.88	204

T_3 is the mean air temperature at 3 m, PP is the mean pressure, VV is the mean wind speed, tau is the surface stress in 100 Pa, T_0 is the mean estimated surface temperature, δT is the mean vertical temperature difference, Q_0 is the mean sensible heat flux, E_0 is the mean latent heat flux, q_3 is the mean mixing ratio at 3 m, q_0 is the mean mixing ratio at the surface based on the estimated surface temperature, and OBS is the number of solutions for the latent and sensible heat flux for the month. Table 5 is available in its entirety on the disk (ASCII format) enclosed inside the back cover of this book or as paper copy from C. R. Stearns, 1225 West Dayton Street, Madison, Wisconsin 53706 (telephone 608-262-0780; email chuck@ssec.wisc.edu).

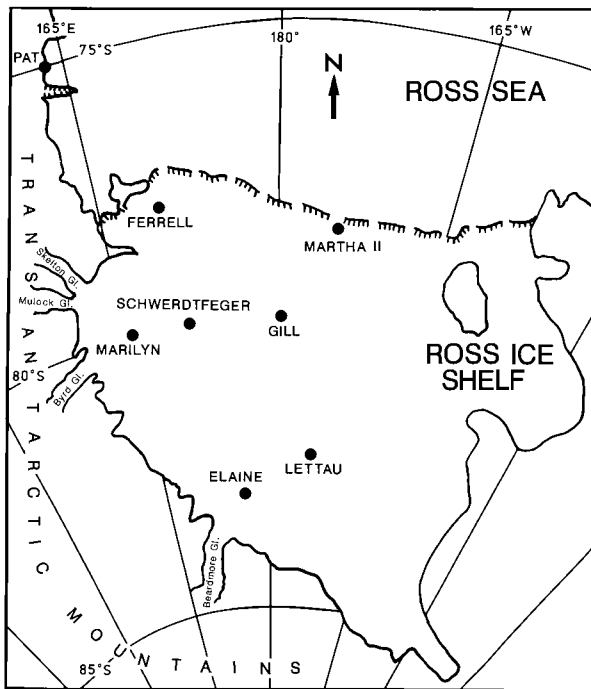


Fig. 9. Locations of the AWS units on the Ross Ice Shelf and on the Reeves Glacier that are discussed here. Ferrell site was not equipped to estimate the sensible and latent heat fluxes.

wind speed is zero, but the record will be retained because conditions are not changing rapidly as they are in January. The mean values will not be exactly those given by *Stearns et al.* [this volume] because the samples may be slightly different.

3.6. Verification of the Latent Heat Flux Estimates

Because of the many sources of error in the sensible and latent heat fluxes, the results presented here are called estimates. The one site that could provide some confirmation of the method is Pat site (Figure 9) at the bottom of the Reeves Glacier near Terra Nova Bay, Antarctica. Pat site was located on blue ice with abundant evidence of sublimation because the rocks in the nearby glacial moraine are sitting on top of the ice. The AWS unit was installed in December 1988 and was anchored by four 10×10 cm by 1 m wooden posts placed in holes drilled into the ice. The unit fell over in December 1989 because the anchors ablated out of the ice. The unit fell over in December 1989 because the anchors ablated out of the ice. The unit was reerected by members of the Italian Progetto Antartide in January 1990. We do not have a record of the level at which the unit was installed relative to the ice. In December 1990, Pat site was visited, and the AWS unit was tipped at an angle of about 60° relative to the vertical because

of the ablation of the anchors. The unit was removed because we needed a better anchoring method and were not able to do it at that time. Photographs were taken of the site before the unit was disturbed. The displacement of the base above the ice was 0.26 m on the assumption that the base was level with the ice surface when the members of Italian team installed the unit in January 1990. The sublimation from February 1990 to mid December 1990 was -0.21 m water equivalent depth or about -0.23 m of ice. The estimated ice ablation of -0.26 m compares well to the sublimation of -0.23 m of ice estimated from the latent heat flux. The possible melting of the ice at Pat site was not considered because the indicated air temperature was seldom above freezing.

4. VERTICAL AIR TEMPERATURE DIFFERENCES ON THE ROSS ICE SHELF

Figure 9 is a map of the Ross Ice Shelf showing the locations of the AWS units that are discussed here. The first records of the climate on the Ross Ice Shelf started in 1980 when AWS units were initially installed. Ferrell site, shown in Figure 9, has operated since 1980 (Table 1), and the record is presented by *Stearns et al.* [this volume], including a description and tables of the climate for all AWS units in Antarctica. Some of the features on the Ross Ice Shelf are that the winds are from the south and stronger and the air temperatures are warmer near the Transantarctic Mountains than in the middle of the Ross Ice Shelf. Measurements of the vertical air temperature differences on the Ross Ice Shelf were started in 1984. Previous information was strictly speculation and was without any validity. The data to be presented are from the AWS units at Marilyn, Schwerdtfeger, Gill, Elaine, and Lettau sites (Figure 9) as they provide an interesting data set because of the influence of the katabatic flow down the glaciers of the Transantarctic Mountains onto the Ross Ice Shelf. Some features of the katabatic flow are described by *Radok et al.* [this volume].

The vertical air temperature differences for the AWS units at Martha II, Marilyn, Schwerdtfeger, Gill, Elaine, and Lettau sites are sorted into intervals of 0.1°C , the resolution of the vertical air temperature difference. The frequency of occurrence at each interval and the mean wind speed at that interval are presented in Figures 10–15 for the common record available from January through August 1988. At Martha II site (Figure 10) the higher wind speeds are associated with extremes and rarely occurring vertical air temperature differences. The bulk of the vertical air temperature differences ranges from -2.0°C to 3.0°C with a maximum frequency at 0.2°C air temperature difference. The results for Marilyn site are shown in Figure 11. The highest frequencies are at 0.7° , 0.8° , and 1.0°C , and the mean wind

ANTARCTIC METEOROLOGY AND CLIMATOLOGY

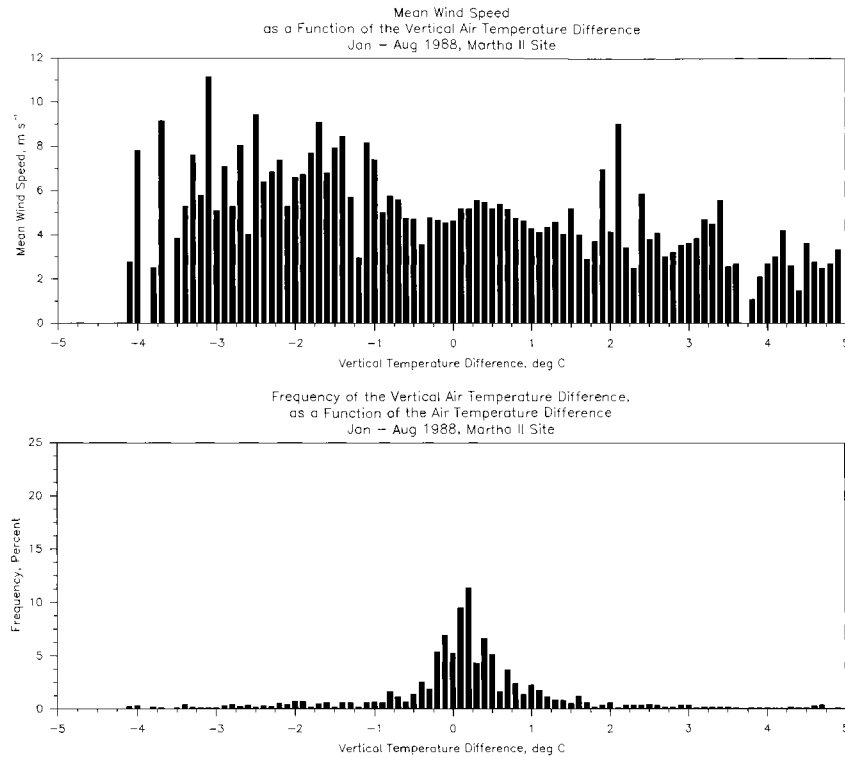


Fig. 10. Mean wind speed and frequency of occurrence as a function of the air temperature difference from 3.0 to 0.5 m for Martha II site for January through August 1988. The vertical air temperature difference interval is 0.2°C .

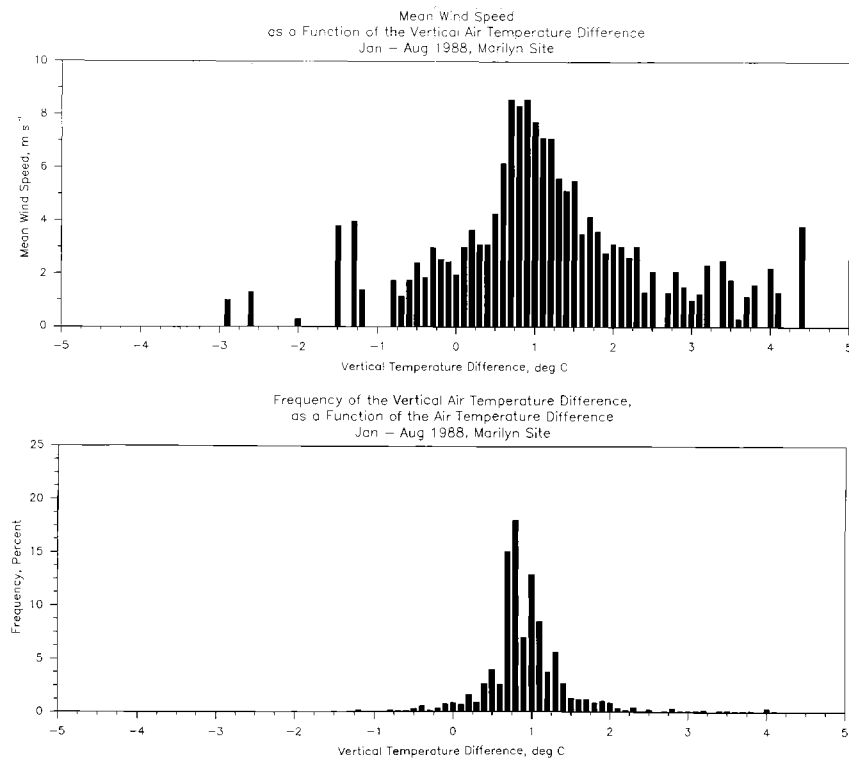


Fig. 11. Mean wind speed and frequency of occurrence as a function of the air temperature difference from 3.0 to 0.5 m for Marilyn site for January through August 1988. The vertical air temperature difference interval is 0.2°C .

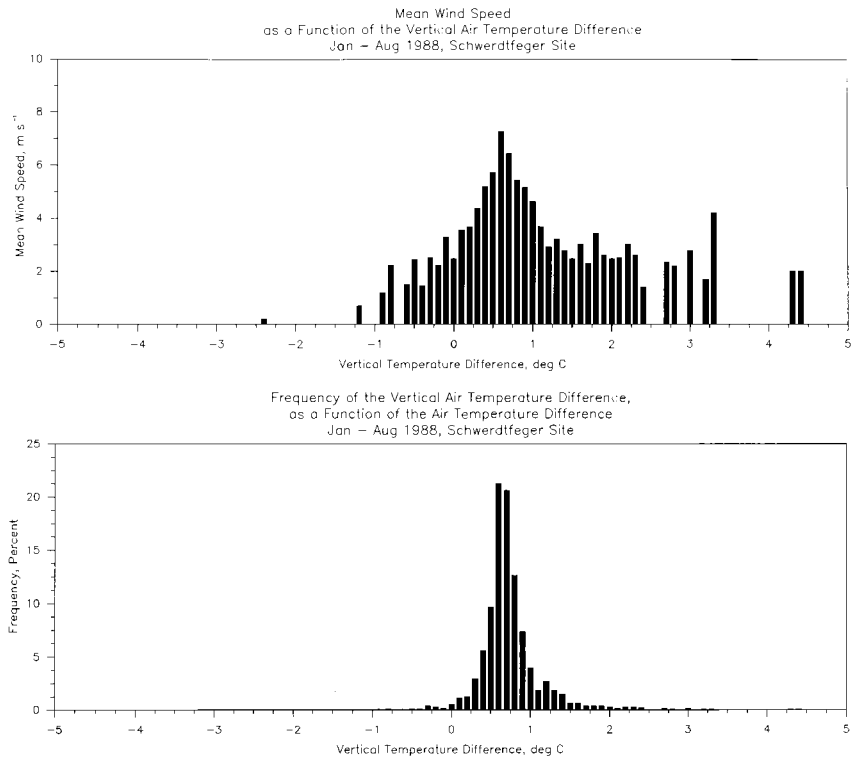


Fig. 12. Mean wind speed and frequency of occurrence as a function of the air temperature difference from 3.0 to 0.5 m for Schwerdtfeger site for January through August 1988. The vertical air temperature difference interval is 0.2°C.

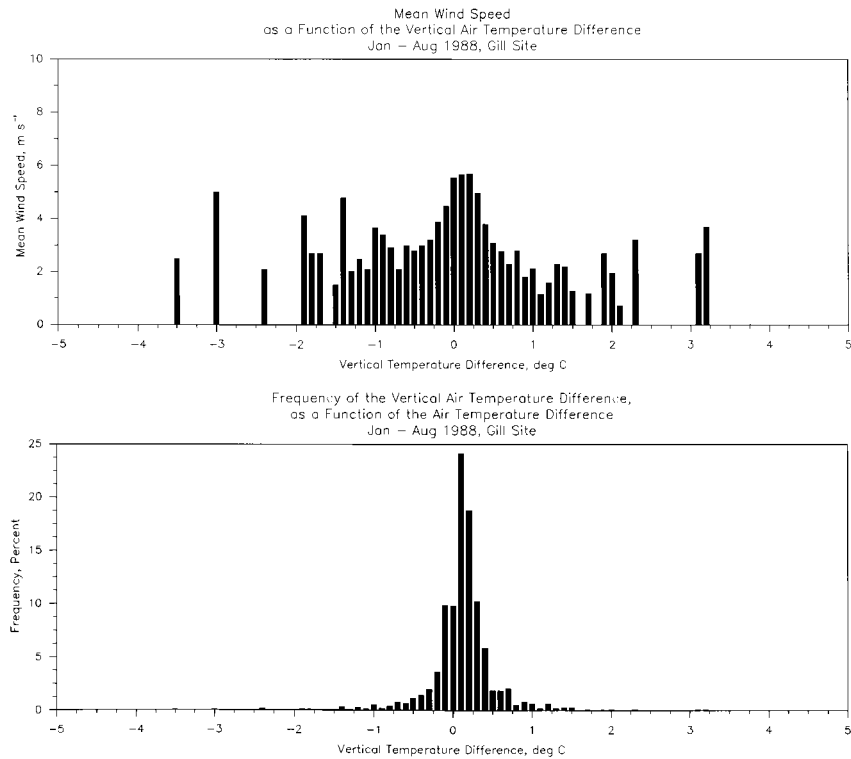


Fig. 13. Mean wind speed and frequency of occurrence as a function of the air temperature difference from 3.0 to 0.5 m for Gill site for January through August 1988. The vertical air temperature difference interval is 0.2°C.

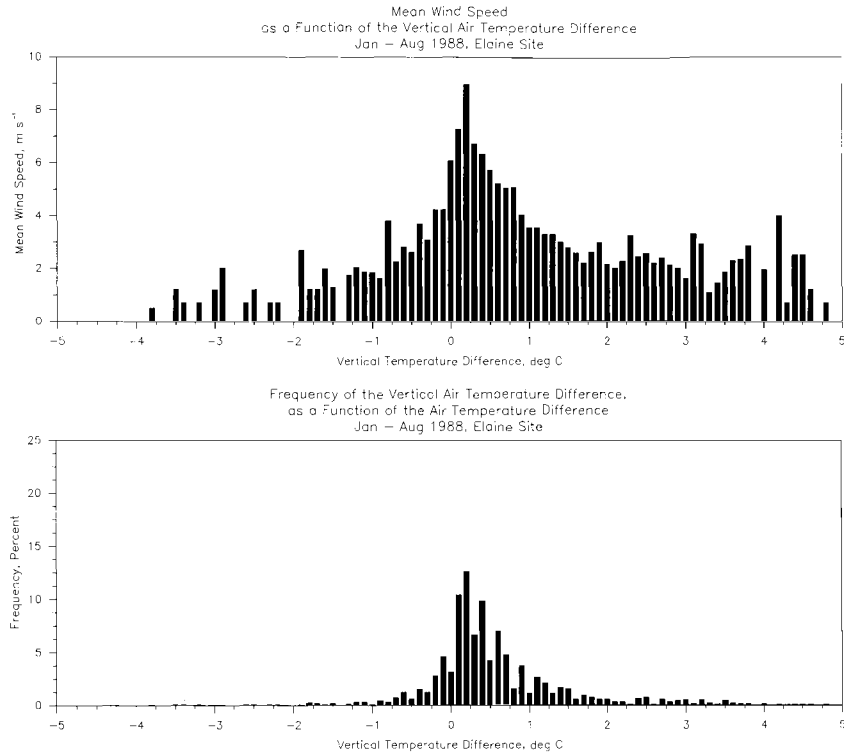


Fig. 14. Mean wind speed and frequency of occurrence as a function of the air temperature difference from 3.0 to 0.5 m for Elaine site for January through August 1988. The vertical air temperature difference interval is 0.2°C.

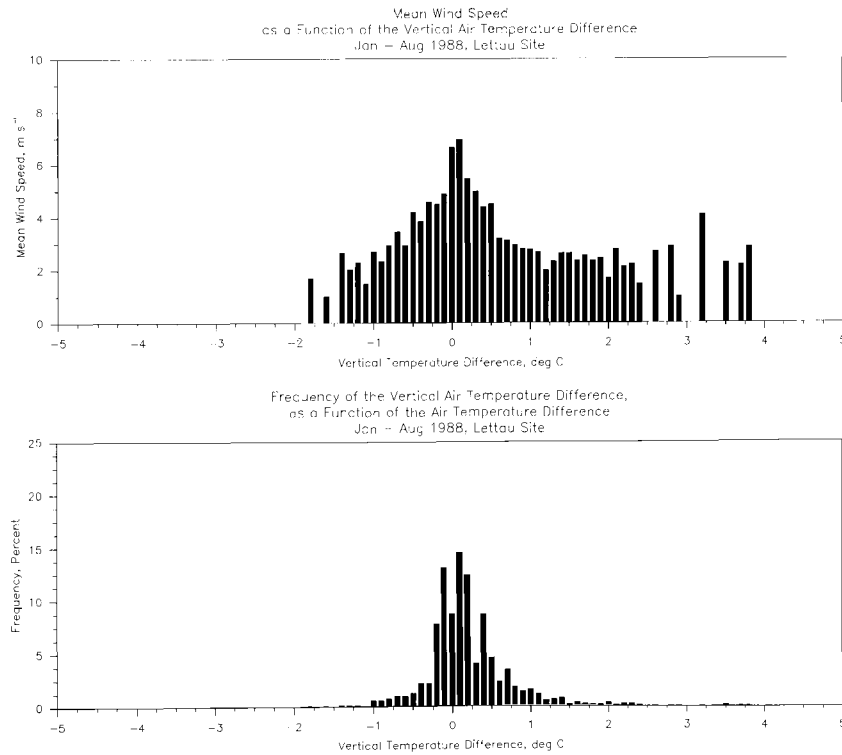


Fig. 15. Mean wind speed and frequency of occurrence as a function of the air temperature difference from 3.0 to 0.5 m for Lettau site for January through August 1988. The vertical air temperature difference interval is 0.2°C.

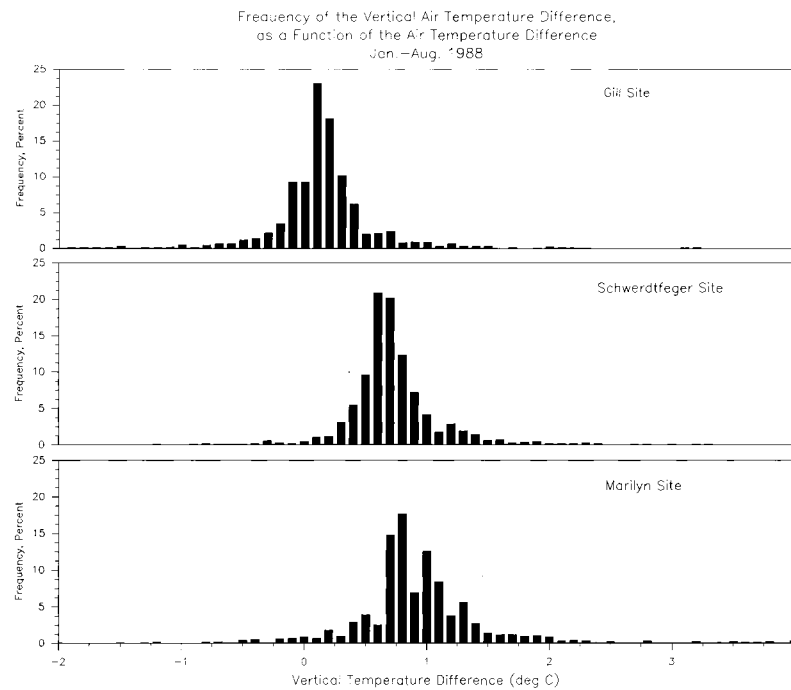


Fig. 16. Comparison of the frequency of the vertical air temperature difference from 3.0 to 0.5 m for Gill, Schwerdtfeger, and Marilyn sites.

speeds are at a maximum in the same region. Schwerdtfeger site (Figure 12) is farther east from the Transantarctic Mountains and Byrd Glacier than Marilyn site. The most frequent air temperature difference intervals are 0.6° and 0.7°C, corresponding to the maximum mean wind speed. Farther east at Gill site (Figure 13) the most frequent vertical air temperature difference is 0.1°C along with the highest mean wind speed. Figure 16 compares the frequency of the vertical air temperature differences for the sites of Marilyn, Schwerdtfeger, and Gill. The systematic shift in the distribution with distance eastward from the Transantarctic Mountains is apparent. An examination of Figures 11, 12, and 13, relative to the distance eastward from the Transantarctic Mountains, shows that the wind speeds decrease eastward and the peak frequency of the vertical air temperature difference shifts toward 0.0°C. A similar pattern is shown in Figures 14 and 15 for Elaine and Lettau sites.

Marilyn site seems to be strongly influenced by the Foehn type katabatic flow down the Byrd Glacier. The 3-hourly observations at Marilyn site for 1987 were sorted for the frequency of the wind direction, mean wind speed, vertical air temperature difference, and the sensible heat flux. The valid record included January through August 1988. Figure 17 shows four graphs relating the wind direction to frequency, wind speed, vertical temperature difference, and sensible heat flux. The direction toward Byrd Glacier from Marilyn site is

242°. From Figure 17a the most frequent wind direction is in the sector from 240° to 250° which contains the direction of Byrd Glacier from Marilyn site. Figure 17b shows that the highest mean sector wind speed is from 240° to 250°, and the next highest mean sector wind speed is from 170° to 180°. Figure 17c shows that the vertical air temperature difference is around 1°C in the westerly directions, and the mean sector sensible heat flux shown in Figure 17d is largest in the direction of Byrd Glacier.

Table 6 gives mean data for each month of the sensible and latent heat fluxes on the Ross Ice Shelf and includes the mean vertical air temperature difference. The monthly mean vertical air temperature differences for Marilyn site are usually higher than Schwerdtfeger site, which are usually higher than Gill site. Elaine site usually has monthly mean vertical air temperature differences higher than Lettau site.

5. SENSIBLE HEAT FLUXES ON THE ROSS ICE SHELF

Table 5 presents the monthly mean sensible heat flux for the AWS units equipped with the vertical air temperature difference and relative humidity. The results from some of the AWS units are discussed below.

Figures 18–22 show the mean monthly sensible heat flux record for Marilyn, Schwerdtfeger, Gill, Elaine, and Lettau sites. Marilyn site (Figure 18) is interesting

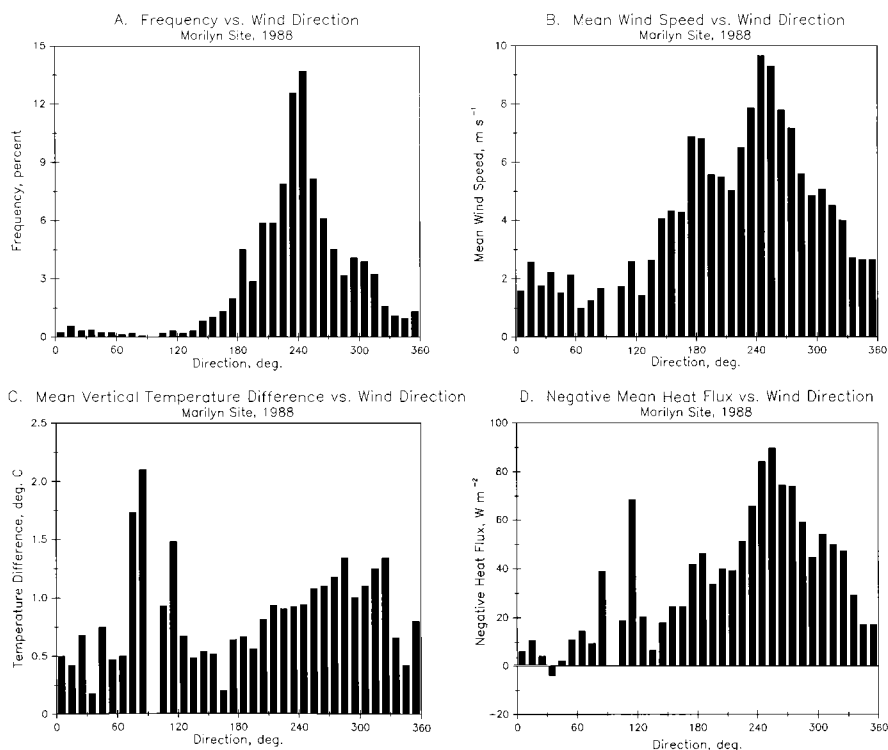


Fig. 17. Frequency of the (a) wind direction, (b) sector mean wind speed, (c) sector mean vertical air temperature difference from 3.0 to 0.5 m, and (d) sector mean sensible heat flux versus 10° wind direction sectors for Marilyn site from January through August 1988.

because of the large negative values of the sensible heat compared to the other sites. Unfortunately, Marilyn site had problems with the antenna, wind system, and the AWS electronics, so an analysis of a full annual record is not available at present. The large negative sensible heat fluxes are associated with high wind speed and large vertical air temperature as shown in Figure 11. The occurrence of the combination of high wind speeds and large vertical air temperature differences is apparently associated with katabatic flow down the Byrd Glacier onto the Ross Ice Shelf.

Figure 19 presents the monthly mean sensible heat flux for Schwerdtfeger site from 1985, when the site was established, through 1990. In 1987 the aerovane failed, the lower air temperature difference sensor was buried, and the record stopped after August. The unit was repaired in January 1988 and the tower raised. The record for 1988, 1989, and 1990 shows a systematic decrease in the magnitude of the annual mean sensible heat flux from -26.40 W m^{-2} to -24.97 W m^{-2} to -20.57 W m^{-2} , respectively, when a positive increase in the displacement height, due to snow accumulation at the site, would be expected to increase the magnitude of the sensible heat flux estimates because the vertical temperature difference would be greater nearer the surface.

The results for Gill site are shown in Figure 20. Data from the unit stopped being received reliably in August 1989. Gill site shows positive monthly mean sensible heat fluxes during the austral summer in contrast to the negative sensible heat fluxes at Schwerdtfeger and Marilyn sites. Figure 23 compares Gill, Schwerdtfeger, and Marilyn sites for 1988 showing clearly that the monthly mean sensible heat fluxes are less negative as the eastward distance from the Transantarctic Mountains increases.

Reception from Elaine site stopped in October 1988. In contrast to Marilyn and Schwerdtfeger sites there are positive monthly mean sensible heat fluxes during the months of November, December, and January. At Lettau site (Figure 22) the monthly mean sensible heat flux is positive during the months of November, December, January, and February and for 3 years in October. Also, the monthly mean sensible heat flux increases eastward from the Transantarctic Mountains as is shown in Figure 24 for Lettau, Elaine, Schwerdtfeger, and Gill sites for 1986.

Patrick site (Table 1) near South Pole provides a special case because comparison can be made with sensible heat flux measurements at the south pole in 1958 [Dalrymple *et al.*, 1966]. The frequency of the Patrick site vertical air temperature difference is given in Table 6.

TABLE 6. Frequency of the Vertical Air Temperature Differences in Percent for Each Month for Patrick Site Near South Pole in 1986

$\delta T, ^\circ\text{C}$	1	2	3	4	5	6	7	8	9	10	11	12	TOT	$VV, \text{m s}^{-1}$
-2.0		0.5									4.6	<u>7.8</u>	1.1	3.7
-1.9	6.3									0.8	2.1	3.5	0.7	3.6
-1.8		2.2	0.4							2.3	5.1	3.0	1.1	3.2
-1.7	9.4	1.8								1.3	4.6	4.8	1.2	2.6
-1.6	3.1									1.3	1.3	2.2	0.5	3.0
-1.5	9.4	3.5	0.4							0.4	3.0	6.1	1.3	3.0
-1.4	3.1	3.1	1.3							1.3	3.8	4.4	1.3	2.6
-1.3	6.3	1.3	0.4								2.1	0.4	0.5	2.7
-1.2	9.4	1.8	0.4							0.8	4.2	3.0	1.0	3.0
-1.1	<u>15.6</u>	4.0	0.9							1.7	2.5	2.2	1.2	3.0
-1.0	3.1	1.8								0.4	3.8	0.4	0.6	3.6
-0.9	<u>15.6</u>	4.5								1.7	<u>8.0</u>	0.9	1.5	3.7
-0.8	3.1	4.9								3.4	5.9	2.2	1.5	3.8
-0.7	3.1	4.0	0.8	0.4							2.1	0.4	0.7	3.8
-0.6	3.1	11.6	1.3	0.4						1.3	3.0	1.7	1.7	3.4
-0.5	3.1	<u>20.1</u>	2.6							2.1	1.7	0.4	2.4	4.0
-0.4		10.7	1.7	0.4			0.4			2.5	0.8	0.4	1.5	4.4
-0.3		16.5	5.6	3.3		0.8				0.8	1.3		2.5	4.5
-0.2		4.0	8.6	6.3	0.8	5.5	0.8			6.8	2.1	0.4	3.2	4.7
-0.1		0.9	5.6	2.5	2.0	2.1	2.8	0.4	0.5	1.7	1.7	0.9	1.9	4.6
0.0		0.9	<u>13.9</u>	8.8	1.6	6.3	5.3	1.6		5.5	2.1	0.4	4.2	4.7
0.1			11.6	<u>9.6</u>	3.6	4.2	9.3	5.3		<u>10.6</u>	1.3	0.4	5.1	<u>5.3</u>
0.2			3.9	4.2	1.6	0.8	7.7	2.0		2.5	0.8		2.2	5.2
0.3			6.9	7.5	9.3	4.6	9.3	6.5	2.5	5.1	0.4		4.8	5.0
0.4			6.5	8.3	11.3	6.7	9.7	12.2	4.6	5.9	0.4		6.0	5.0
0.5			1.7	4.6	7.3	4.6	4.1	4.5	4.0	1.7			3.0	4.1
0.6			5.2	7.9	16.5	9.2	<u>12.2</u>	12.2	7.6	3.8			<u>6.8</u>	3.9
0.7			3.5	7.9	<u>16.9</u>	7.6	8.5	<u>13.0</u>	13.6	2.5	0.4		6.7	3.4
0.8			1.7	1.3	6.9	1.7	2.0	6.1	5.6	0.8			2.3	3.3
0.9			3.0	4.6	7.7	5.5	4.0	8.1	10.1	5.9			4.4	3.6
1.0			3.0	1.7	4.0	<u>9.7</u>	6.1	6.5	<u>14.7</u>	1.3	0.4		4.1	2.8
1.1			1.3	2.1	1.2	1.3	1.2	2.8	2.5				1.1	2.1
1.2			1.3	2.9	2.8	6.7	3.2	5.3	10.6	2.1	0.4		3.1	1.8
1.3			1.7	2.1	2.0	6.7	2.4	2.0	6.6	1.7			2.2	2.2
1.4			0.4	0.8	1.2	2.5	1.2	1.2	1.5	0.4			0.8	1.6
1.5			0.9	2.1	1.6	3.4	1.2	1.6	4.6	0.4			1.4	2.2
1.6				0.8	0.4	4.2	2.8	1.2	2.5	1.3	0.4		1.2	1.9
1.7			0.4	0.4	0.4	0.4		0.4		0.4			0.2	2.0
1.8			0.4	1.3	0.4	2.1	0.4	0.8	2.0	0.8			0.7	1.9
1.9			0.9	1.7		1.3	1.6	2.8	1.0	0.4			0.9	1.3
2.0			0.4	1.3		0.4	0.8		0.5	0.4			0.3	1.9
2.1			0.4	0.4				0.8	0.5	0.8			0.3	1.0
2.2				0.8	0.4	0.4		1.2	1.0	1.3			0.5	1.7
2.3			0.4				0.4	0.8	0.5	0.8			0.3	1.4
2.4						0.8	0.4		1.0	1.3			0.3	1.8
2.5							0.4	0.4	0.5				0.1	1.7
2.6				0.8					0.5				0.1	0.9
2.7				0.8						1.3			0.2	0.9
2.8				0.4			0.4			1.3			0.2	1.6
2.9			0.4	0.4									0.1	1.0
TOTAL	94	98	99	99	100	100	99	100	99	91	70	46	91	
OBS	32	224	232	240	248	238	247	247	198	237	237	230	2610	

T is the vertical air temperature difference. TOT is the percent of the vertical air temperature difference for the year, and VV is the mean wind speed for the year at that temperature difference. At the end of the table, "total" the percent of the observations in the column above, and OBS is the number of observations.

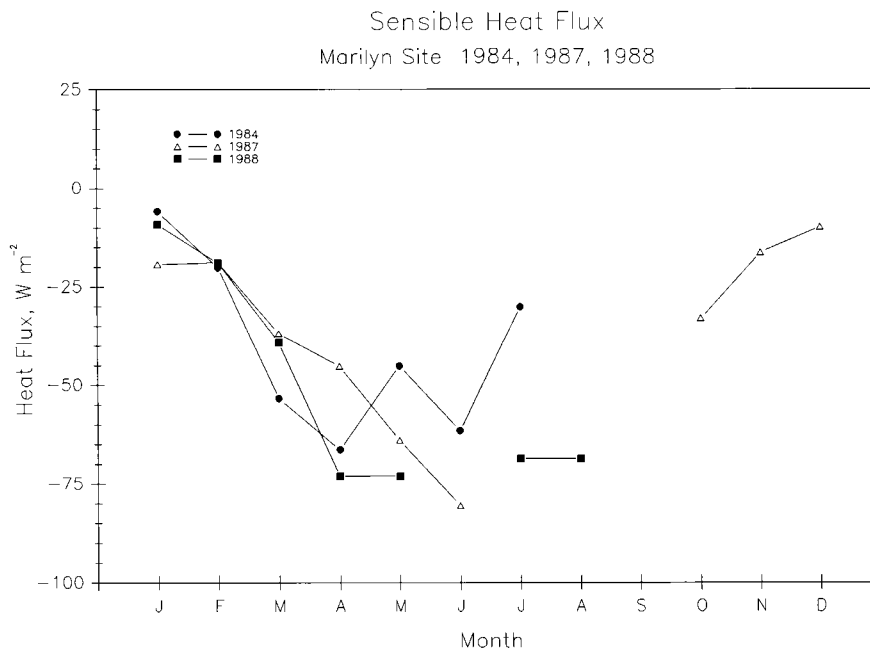


Fig. 18. Monthly mean sensible heat flux versus month of the year for Marilyn site for 1984, 1987, and 1988.

The record shows extensive periods with negative vertical air temperature differences and a positive monthly mean sensible heat flux in November and December 1986, while *Dalrymple et al.* [1966] report negative values for the same

months. Table 2 gives a side by side comparison between the two data sets. *J. S. Obremski et al.* (unpublished manuscript, 1988) observed negative vertical temperature differences at the south pole during January 1985. Of the

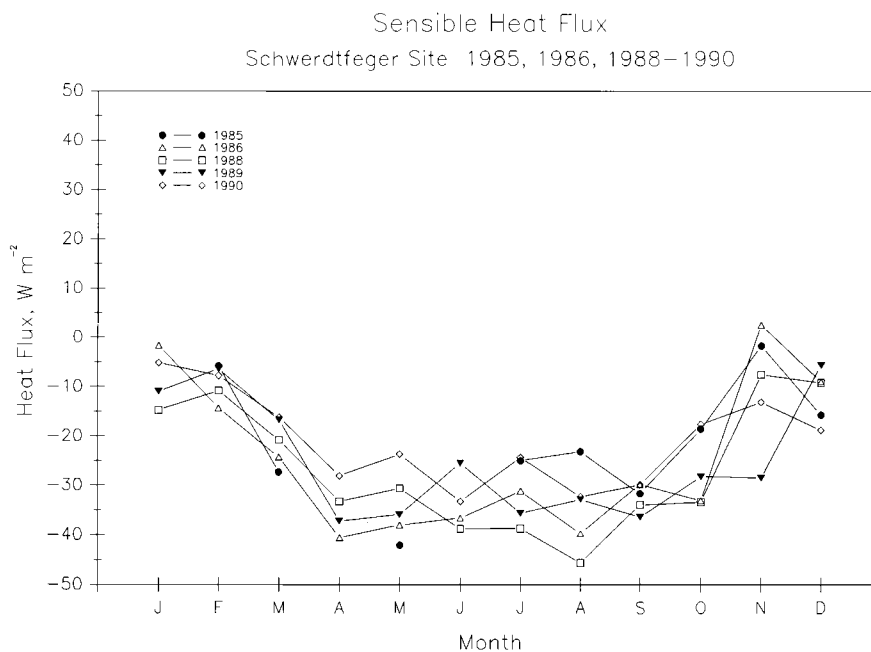


Fig. 19. Monthly mean sensible heat flux versus month of the year for Schwerdtfeger site for 1985 through 1990 except for 1987.

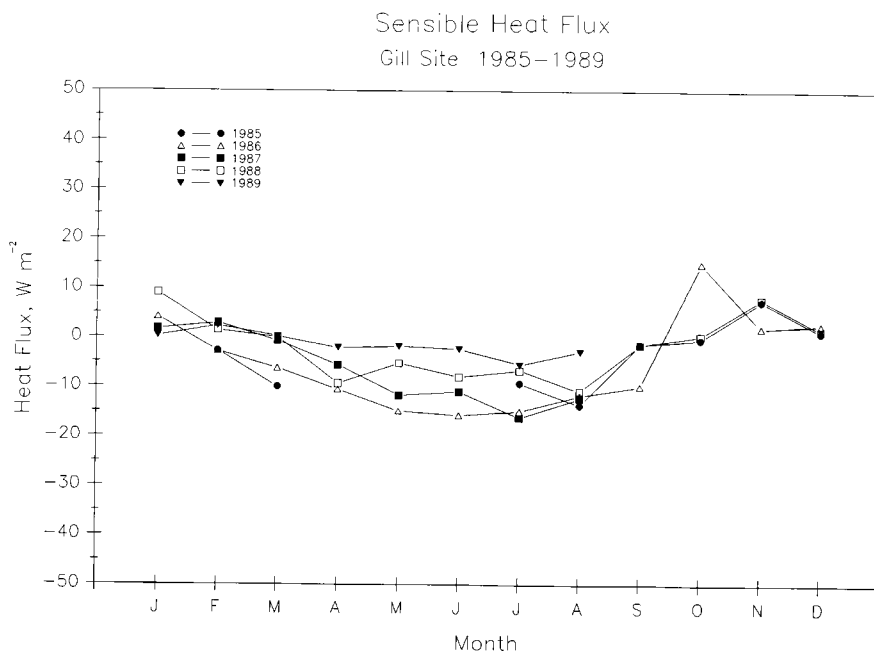


Fig. 20. Monthly mean sensible heat flux versus month of the year for Gill site 1985 through August 1989.

39 temperature profiles measured at the south pole, 29 were neutral or had negative temperature differences with height.

Schwerdtfeger site is used as an example of the

frequency of the sensible heat flux values in 1988 because the record was nearly complete. Figure 25 shows the frequency in percent versus the sensible heat flux.

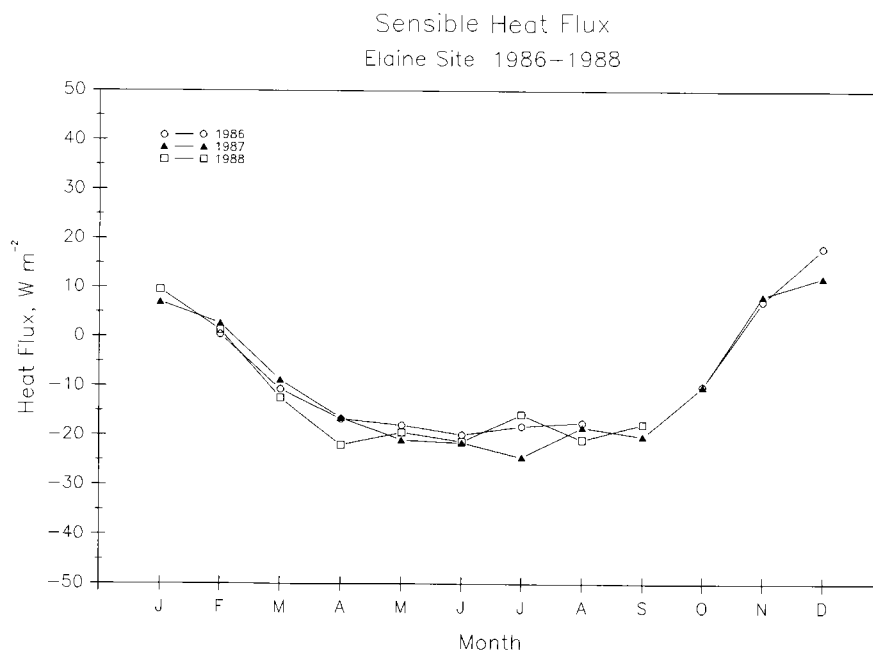


Fig. 21. Monthly mean sensible heat flux versus month of the year for Elaine site for February 1986 through September 1988.

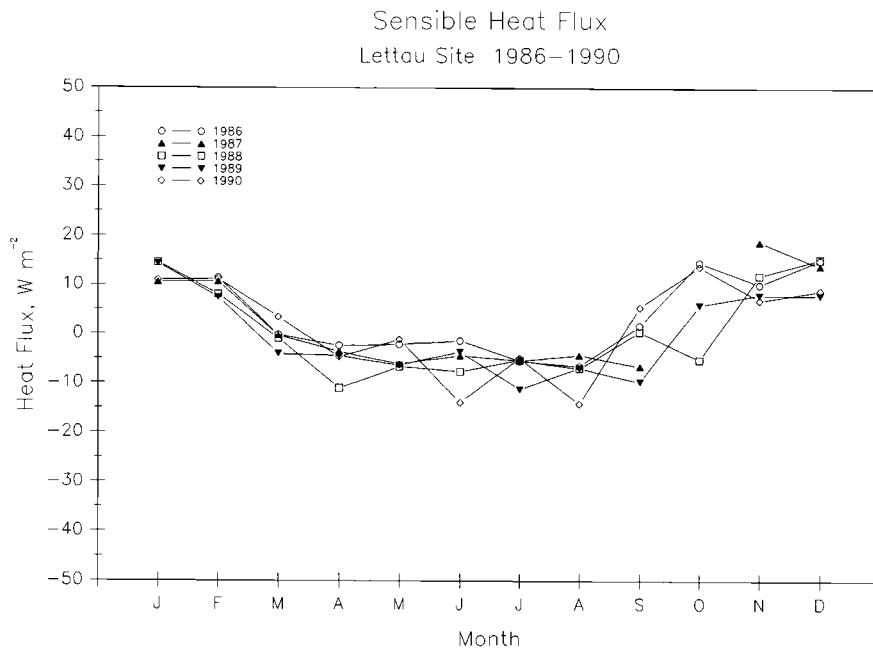


Fig. 22. Monthly mean sensible heat flux versus month of the year for Lettau site for February 1986 through December 1990.

6. LATENT HEAT FLUXES ON THE ROSS ICE SHELF AND SOUTH POLE

Latent heat flux is more interesting than the sensible heat flux because water mass is being added or sub-

tracted to the surface, and this will influence the assumption that the annual sum of the sublimation and deposition is close to zero. Table 5 presents the data for all AWS units in Antarctica equipped to measure the latent heat flux from the surface. Table 5 includes the

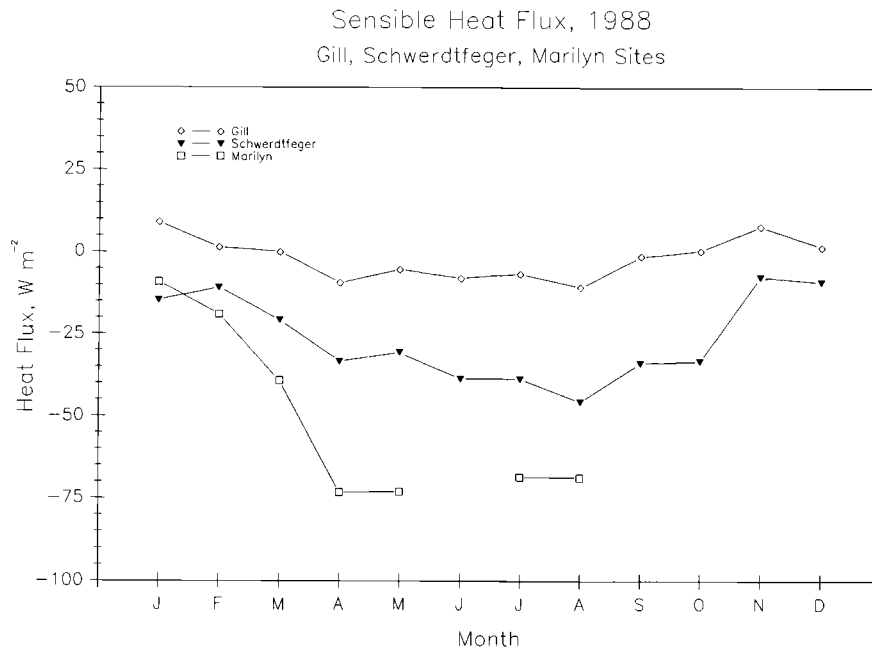


Fig. 23. Monthly mean sensible heat flux for Gill, Schwerdtfeger, and Marilyn sites versus month of the year for 1988.

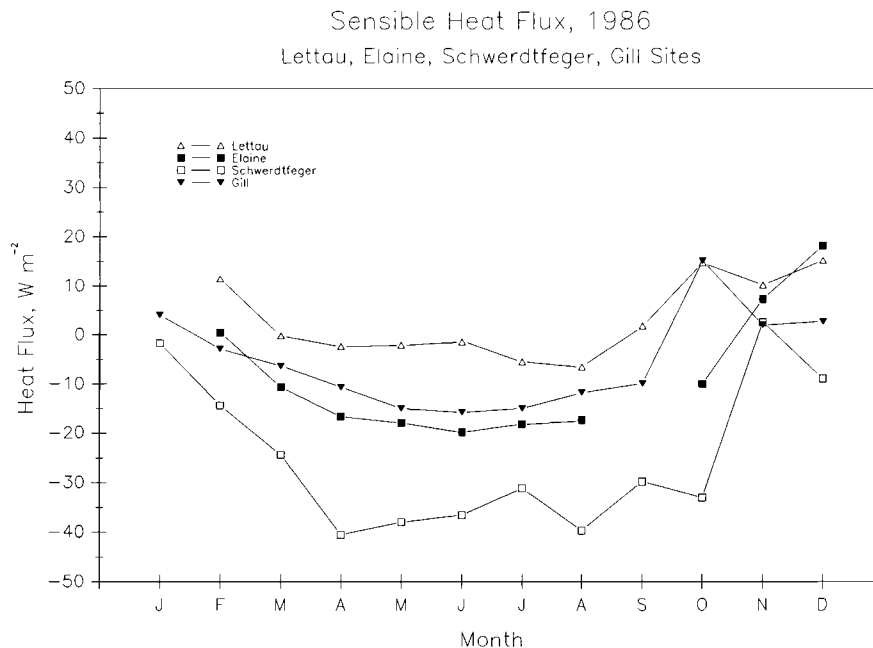


Fig. 24. Monthly mean sensible heat flux for Lettau, Elaine, Schwerdtfeger, and Gill sites versus month of the year for 1986.

mean surface temperature and the specific humidity at 3 m and the surface.

Table 2 gives Patrick site latent heat flux for the months of February through December 1986. Without January data the average monthly sublimation for the

year was 3.12 W m^{-2} , and the water equivalent depth removed during the 11 months was 32 mm. In summer, every monthly mean latent heat flux was positive. The winter months have negative monthly mean latent heat fluxes. These measurements support Gow's hypothesis

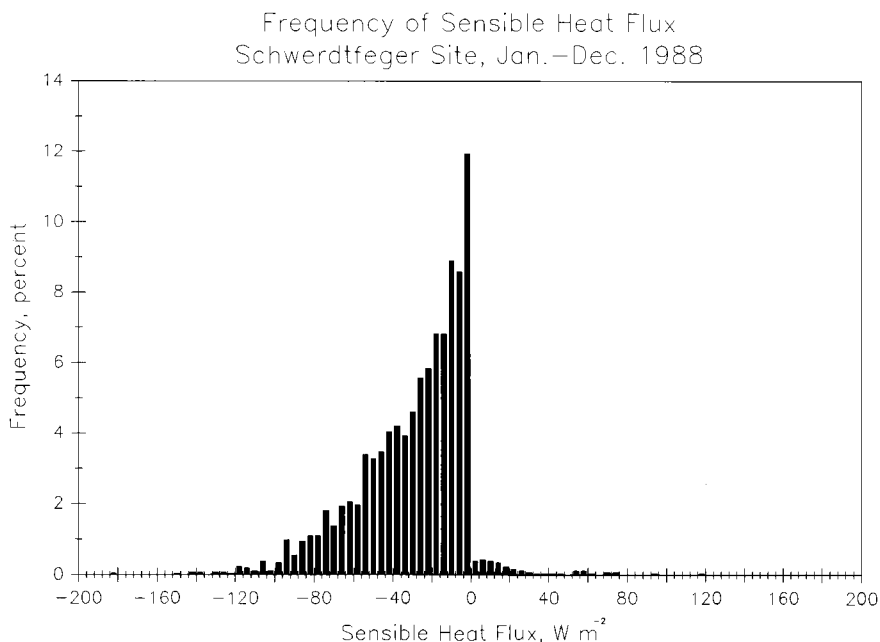


Fig. 25. Frequency of the sensible heat flux at 3-hourly intervals versus the sensible heat flux intervals of 4 W m^{-2} for Schwerdtfeger site for 1988.

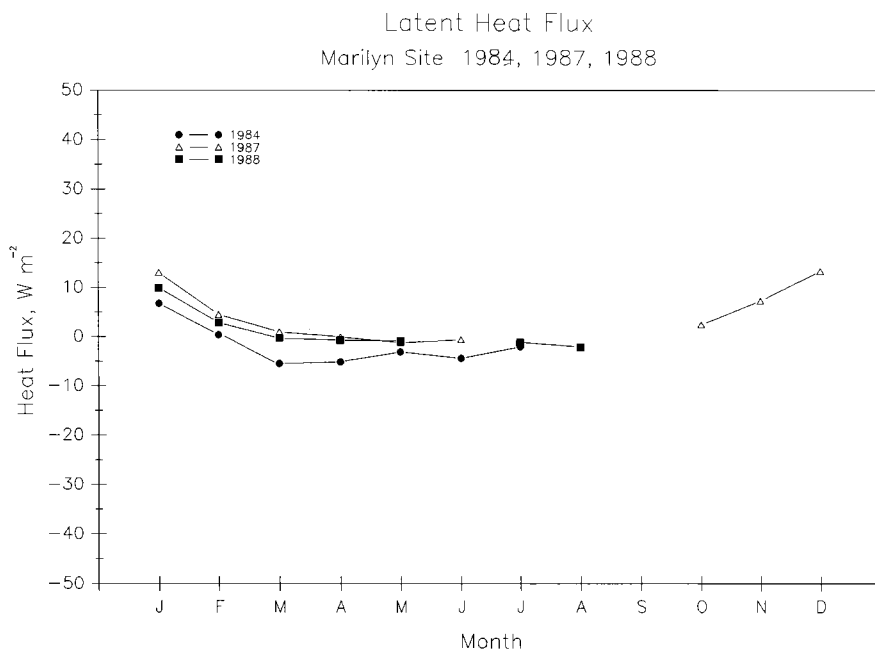


Fig. 26. Monthly mean latent heat flux versus month of the year for Marilyn site for 1984, 1987, and 1988.

that sublimation is one of the methods leveling the snow surface during the austral summer at South Pole [Gow, 1965; Weller, 1969]. Table 2 contains the heat budget data reported by Dalrymple *et al.* [1966] converted from

langley's per day to watts per square meter including the latent heat fluxes, estimated as the balance of the heat budget equation, and the estimated latent heat flux at Patrick site.

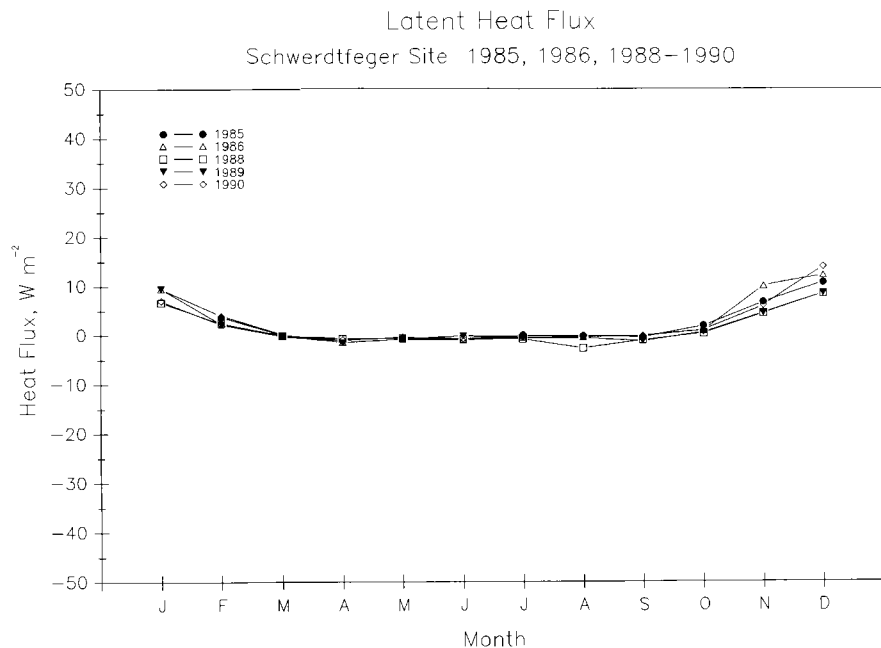


Fig. 27. Monthly mean latent heat flux versus month of the year for Schwerdtfeger site for 1985 through 1990 except for 1987.

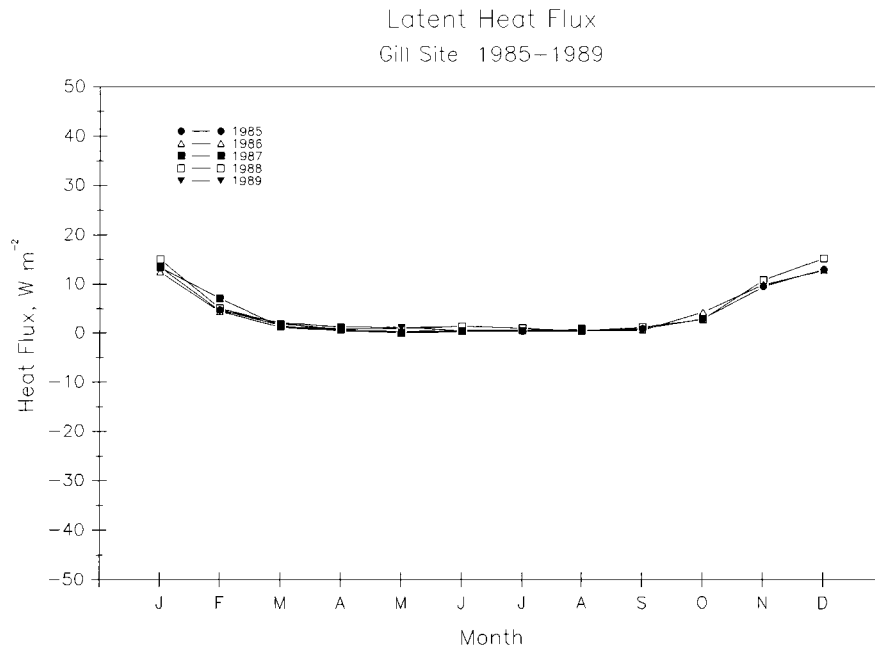


Fig. 28. Monthly mean latent heat flux versus month of the year for Gill site for 1985 through 1989.

Figures 26-30 show the monthly mean latent heat flux for each of the five individual AWS units on the Ross Ice Shelf. The year to year variation for each of the five AWS units is smaller than the year to year variation in the monthly mean sensible heat flux. Figure 31 shows

the monthly mean latent heat flux for Gill, Schwerdtfeger, and Marilyn sites for 1988. The three AWS units agree with each other very well in contrast to the monthly mean sensible heat flux which shows large variations in time and a trend with respect to distance from the

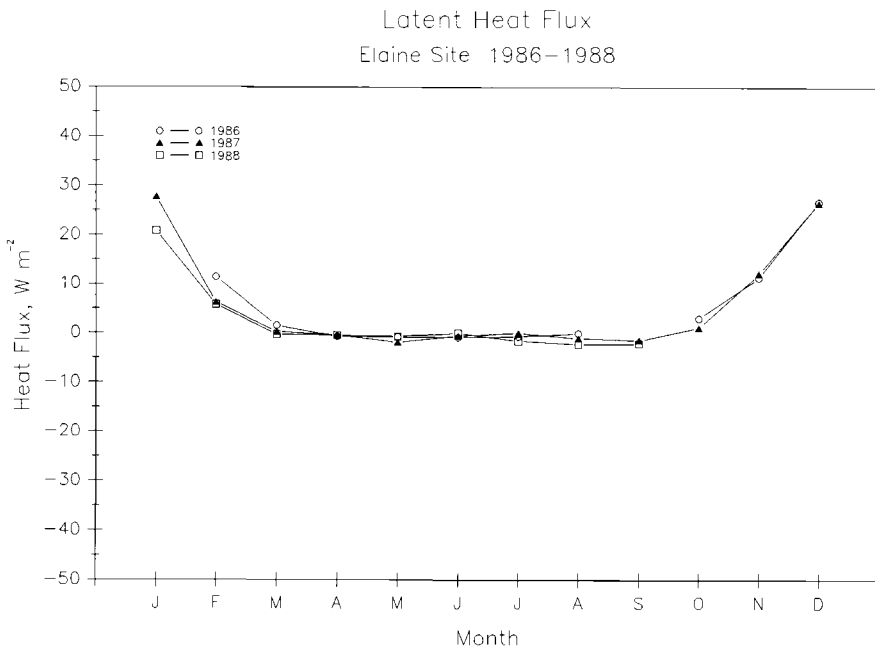


Fig. 29. Monthly mean latent heat flux versus month of the year for Elaine site for 1986 through 1988.

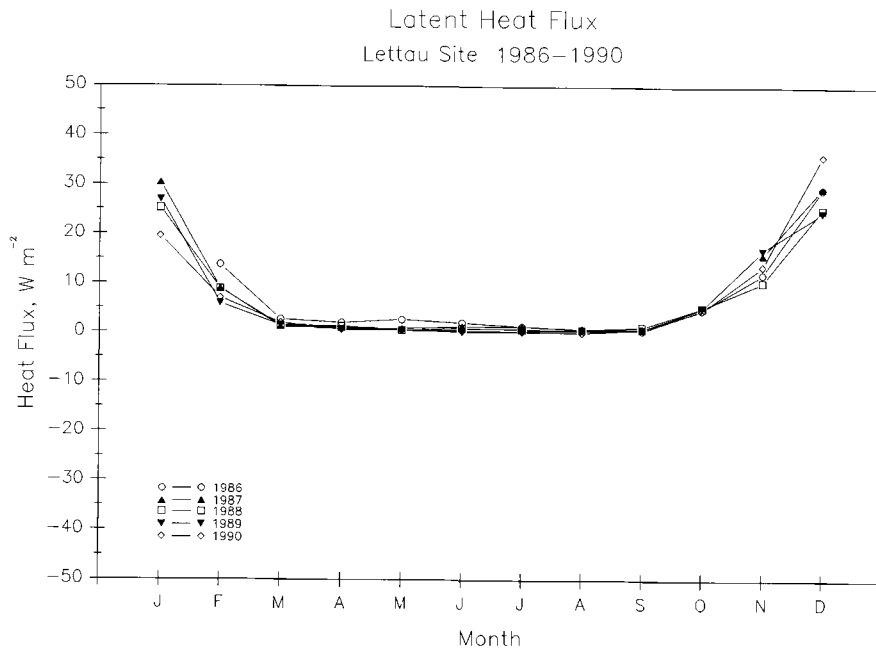


Fig. 30. Monthly mean latent heat flux versus month of the year for Lettau site for 1986 through 1990.

Transantarctic Mountains. Gill site has slightly higher values. Figure 32 shows the monthly mean latent heat flux for Lettau, Elaine, Schwerdtfeger, and Gill sites for 1986. Elaine and Lettau have higher monthly mean latent heat

fluxes in February and December in comparison to Schwerdtfeger and Gill sites. The differences in sensible heat flux related to the distance from the Transantarctic Mountains are not apparent in the latent heat flux.

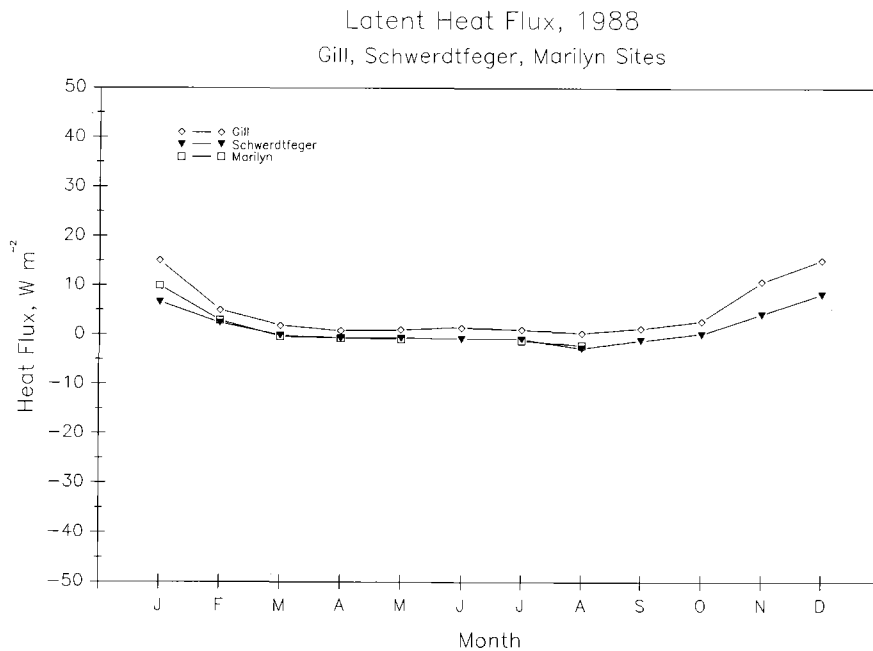


Fig. 31. Monthly mean latent heat flux versus month of the year for Gill, Schwerdtfeger, and Marilyn sites for 1988.

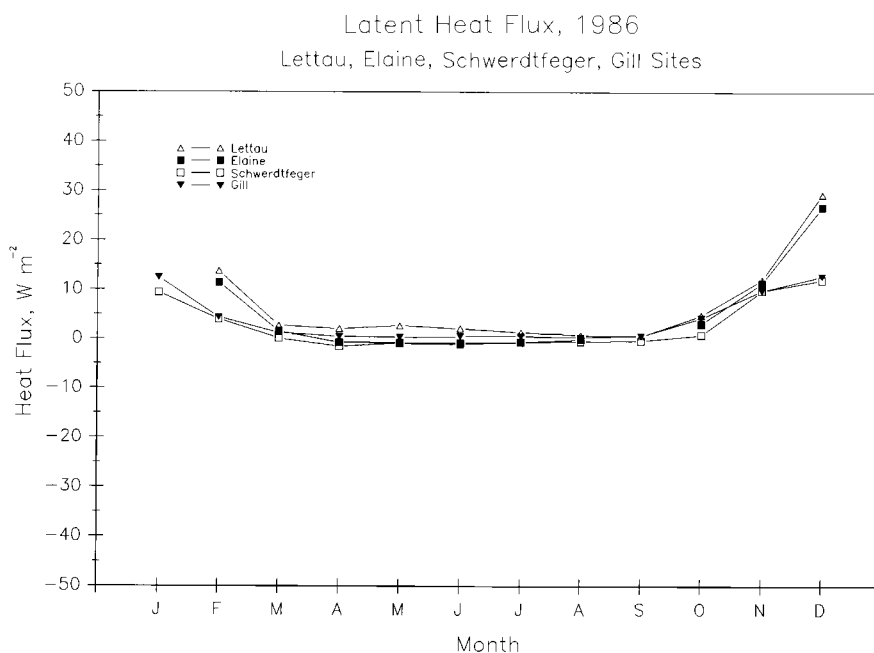


Fig. 32. Monthly mean latent heat flux versus month of the year for Lettau, Elaine, Schwerdtfeger, and Gill sites for 1986.

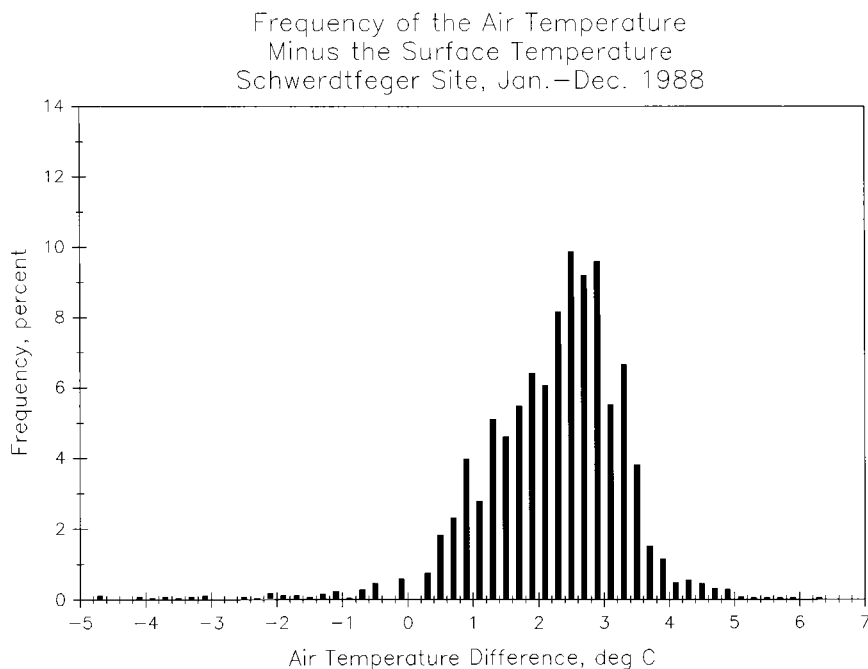


Fig. 33. Frequency of the difference in air temperature at 3.0 m and the surface temperature in 0.2°C intervals versus the temperature difference for Schwerdtfeger site during 1988.

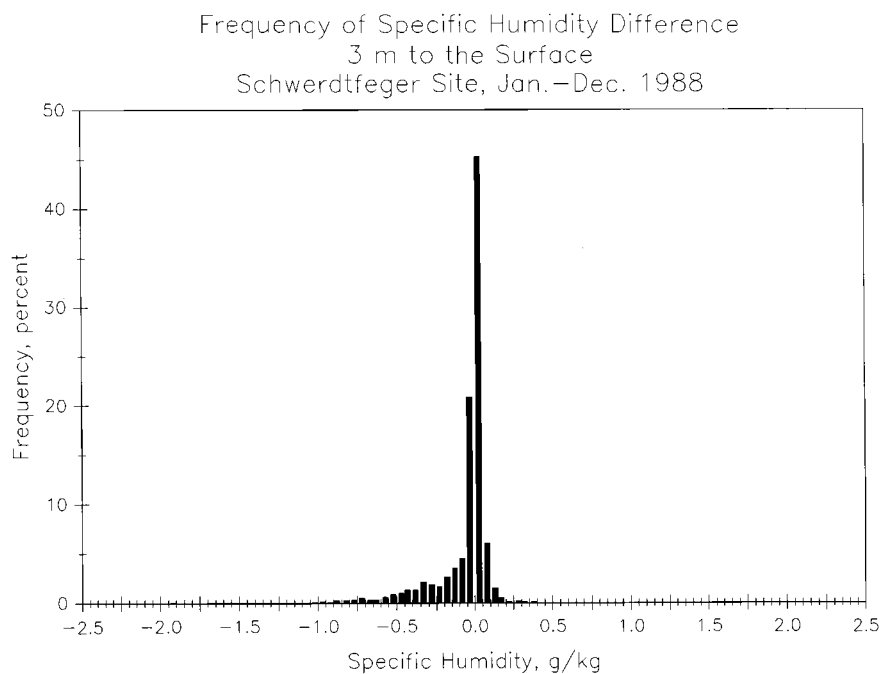


Fig. 34. Frequency of the specific humidity difference between 3.0 m and the surface in 0.05 g kg^{-1} intervals versus the specific humidity for 1988.

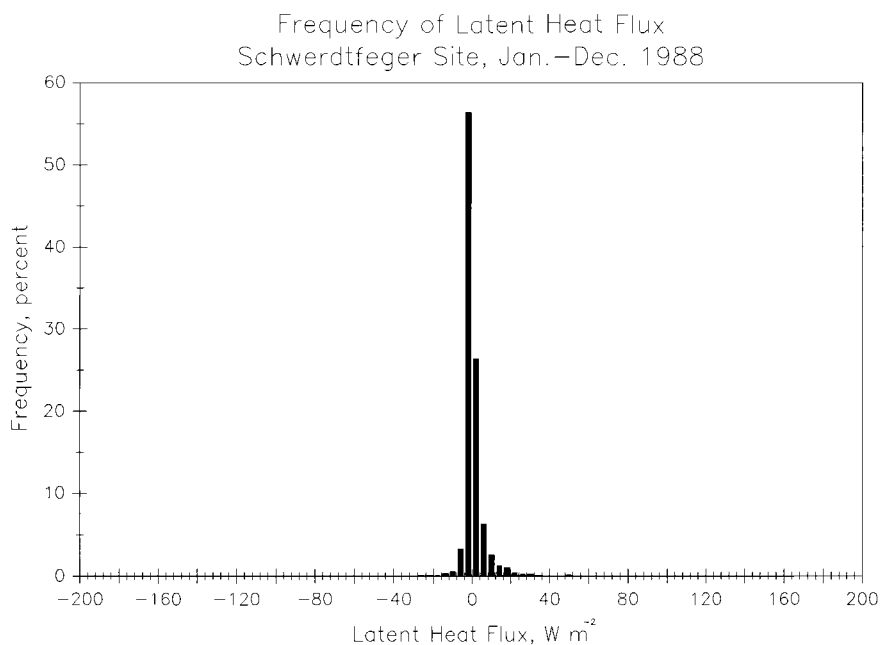


Fig. 35. Frequency of the latent heat flux in 4 W m^{-2} intervals versus the latent heat flux for Schwerdtfeger site for 1988.

TABLE 7. Depth Changes Due to Sublimation and the Accumulation Based on the Data of *Schwerdtfeger* [1984]

AWS Site	1986	1987	1988	1989	1990	Accumulation
Patrick	-32 (11)					
Lettau	-95	-86	-76	-78	-80	100
Elaine	-73	-64				140
Schwerdtfeger	-29	-45	-13	-18	-24	120
Gill	-44		-48	-53		110
Marilyn		-36 (9)	-6 (8)			140
Martha II		-39 (10)				180
Pat				-227 (11)	-208 (11)	
Pegasus				-19 (9)		
Pegasus North					-70 (11)	

Data are in millimeters per year. The numbers in parentheses is the number of months in the year used to calculate the depth change. Some years overlap slightly so that a complete year would be available. The overlap can be seen in Table 4.

Schwerdtfeger site is used to show the frequency of the air temperature minus the surface temperature estimated by the determination of the sensible heat flux (Figure 33). The surface temperature is used to calculate the surface vapor pressure assuming ice saturation. The relative humidity and the surface vapor pressure are used for the specific humidity difference from 3 m to the surface and are used to estimate the latent heat flux. Figure 34 shows the frequency of the specific humidity difference. The frequency distribution of the latent heat fluxes are given in Figure 35 using the same scale for latent heat flux as Figure 25 for the sensible heat flux.

7. CONCLUSIONS

The method used to obtain estimates of the sensible and latent heat flux over the snow surfaces has several features that indicate that the estimates should be reliable. The results from Pat site show there is strong agreement between the latent heat flux converted to the water equivalent depth and the estimated ablation of the ice in the vicinity of the AWS unit. The estimates of the latent heat flux at South Pole indicating a substantial removal of moisture support *Gow's* [1965] leveling of the snow. The dissimilarities between the south pole results of *Dalrymple et al.* [1966] and the Patrick AWS unit given in Table 2 may be due to the difference between the two methods. The latent heat fluxes reported by *Dalrymple et al.* were based on the remainder of the heat budget where net radiation, submedium heat flux, and sensible heat flux were measured. There is the agreement of the latent heat fluxes between the results reported by *Fujii and Kusunoki* [1982] of -2.1 W m^{-2} from May through July and the AWS units on the Ross Ice Shelf and at South Pole. The results of *Fujii and Kusunoki* during December of a latent heat flux of 20.3 W m^{-2} also agree well with the December results for the AWS units on the Ross Ice Shelf. The results of *Wendler et al.* [1988] give negative average sensible heat flux and positive average latent heat flux from Novem-

ber 20 to December 22 and are similar to December mean values on the Ross Ice Shelf.

Schwerdtfeger [1984] presents the results of snow accumulation measurements on the Ross Ice Shelf. Table 7 gives the estimated accumulation at each of the AWS sites on the Ross Ice Shelf. Also given are the depth changes due to sublimation, where possible, in millimeters for the year. Lettau site is of interest because the accumulation is the lowest but the removal by sublimation is about 80 mm yr^{-1} making the precipitation estimate 180 mm for the year. Gill site has 110 mm of accumulation and 48 mm lost for the year because of sublimation. Similar comparisons can be made for the other AWS sites. On the Ross Ice Shelf the addition of the sublimation to the accumulation will alter the precipitation total for each AWS site and the precipitation pattern. The assumption of *Loewe* [1962] that sublimation and deposition cancel each other is not true at the locations where the AWS units have made the necessary measurements. Another indication that moisture is added to the air on the Ross Ice Shelf is that in January, when sublimation is positive, the monthly mean specific humidity at Lettau site is lower than Gill site. The air flow is from Lettau site toward Gill site.

Improvements will be made in the AWS units particularly in increasing the resolution of the measurement of the vertical temperature difference. Sufficient experience has been gained about the frequency distribution of the vertical temperature differences to indicate that the resolution could be reduced about 0.5. The relative humidity sensor is very questionable. AWS units are planned for installation around the south pole again, and comparison could be made to measurements at the Clean Air Facility. The sensible and latent heat flux estimates from the AWS units are only to be considered as estimates for survey purposes until further comparisons can be made to other and more reliable measuring systems.

Acknowledgment. The above research was supported by National Science Foundation Division of Polar Programs grant 9015586.

REFERENCES

- Allison, I. (Ed.), Proposals for the implementation of a programme of Antarctic research contributing to the world climate research programme, report, 65 pp., Scott Polar Res. Inst., Cambridge, England, 1983.
- Dalrymple, P. C., H. H. Lettau, and S. H. Wollaston, South pole micrometeorological program: Data analysis, in *Studies in Antarctic Meteorology, Antarct. Res. Ser.*, vol. 9, edited by M. J. Rubin, pp. 13–57, AGU, Washington, D. C., 1966.
- Faure, G., and D. Buchanan, Ablation rates of the ice fields in the vicinity of the Allan Hills, Victoria Land, Antarctica, in *Contributions to Antarctic Research II, Antarct. Res. Ser.*, vol. 53, edited by D. H. Elliot, pp. 19–31, AGU, Washington, D. C., 1991.
- Fujii, Y., and K. Kusunoki, The role of sublimation and condensation in the formation of ice sheet surface at Mizuho Station, Antarctica, *J. Geophys. Res.*, 87, 4293–4300, 1982.
- Gow, A. J., On the accumulation and seasonal stratification of snow at the south pole, *J. Glaciol.*, 5(40), 467–477, 1965.
- Inoue, J., Surface drag over the snow surface of the Antarctic plateau, 2, Seasonal change of the surface drag in the katabatic wind region, *J. Geophys. Res.*, 94, 2219–2224, 1989.
- Lettau, H. H., Wind and temperature profile prediction for diabatic surface layers including strong inversion cases, *Boundary Layer Meteorol.*, 17, 443–464, 1979.
- Loewe, F., On the mass economy of the interior of the Antarctic ice cap, *J. Geophys. Res.*, 67, 5171–5177, 1962.
- Monin, A. S., and A. M. Obukhov, Basic laws of turbulent mixing in the atmosphere near the ground, *Tr. Akad. Nauk SSSR, Geofiz. Inst.*, 24, 163–187, 1954.
- Radok, U., C. Breckenridge, and C. Stearns: Foehn events along the Transantarctic Mountains, this volume.
- Schwerdtfeger, W., *Weather and Climate of the Antarctic*, 261 pp., Elsevier Science, New York, 1984.
- Simmonds, I., and W. F. Budd, Sensitivity of the southern hemisphere circulation to leads in the Antarctic pack ice, *Q. J. R. Meteorol. Soc.*, 117, 1003–1024, 1991.
- Stearns, C. R., L. Keller, and G. Weidner, Monthly mean climatic data for Antarctic automatic weather stations, this volume.
- Warburton, J. A. (Ed.), Report of Polar Meteorology Workshop, Reno, Nevada, *Ser. P, Tech. Rep. 18*, 117 pp., Desert Res. Inst., Reno, Nev., 1975.
- Weller, G., The heat and mass balance of snow dunes on the central Antarctic plateau, *J. Glaciol.*, 8(53), 277, 1969.
- Wendler, G., N. Ishikawa, and Y. Kodama, On the heat balance of the icy slope of Adélie Land, eastern Antarctica, *J. Appl. Meteorol.*, 27, 52–65, 1988.

(Received July 2, 1992;
accepted December 31, 1992.)

THE KERNLOSE WINTER IN ADÉLIE COAST

GERD WENDLER

Geophysical Institute, University of Alaska, Fairbanks, Alaska 99775

YUJI KODAMA

Institute of Low Temperature Sciences, University of Hokkaido, Sapporo, Japan

Five automatic weather stations (AWS) provided for the first time year-round data in a region in Antarctica stretching from near the ocean to the high plateau at 3280 m altitude. All of these stations displayed the typical pattern of a kernlose winter, which means there is no systematic temperature change for the six winter months. Some of the more interesting results for the six winter months are as follows: (1) No relationship between temperature and wind speed could be established for any slope stations. Only for the station on Dome Charlie (Dome C), located on a flat ice dome, did increasing wind speeds bring milder temperatures. (2) The wind direction showed a stronger downslope component during cold spells for all slope stations. (3) The atmospheric pressure difference between stations was larger during cold spells than during warm spells. (4) The absolute temperature variation in winter increased when going inland away from the ocean. (5) The interdiurnal pressure variation, which can be taken as an index of cyclonic activity, was not related to temperature. (6) During cold spells, low atmospheric pressure was observed, while for warm spells the atmospheric pressure was above normal. While the first four points can be easily understood, the latter two are surprising and more difficult to explain. Some explanations are offered.

INTRODUCTION

The annual course of air temperature in polar regions can have a well-developed minimum, as first demonstrated by *von Middendorf* [1899]. *Hann* [1911], when quoting *von Middendorf*, spoke of a “kern” or “core.” However, a kern in the winter temperature was not found everywhere in the Arctic. In the European part of the Arctic the winter temperature did not follow the same trend. Here the winter temperature was flat or “kernlose,” reversals of the temperature can happen during any time of the winter, and frequently a midwinter month is warmer than the two neighboring months. *Pollog* [1924] studied these widespread uniform winter temperatures in great detail.

Simpson, the well-known meteorologist participating in Scott's tragic Antarctic expedition, made year-round measurements in the Ross Sea area. He was the first to demonstrate that for high southern latitudes, no “kern” existed in the winter temperature. To quote him directly [*Simpson*, 1919, p. 90],

From April to August in the south . . . no insolation is received. The temperature in the south during these months is nearly stationary, the drop being only 4°F . . .

For the high plateau of Antarctica the annual course of the temperature was not known for many decades to come, even though the summer plateau temperatures

were known before Scott's last expedition [*Shackleton*, 1909]. Paul Siple was the first scientist to stay year-round at the south pole in 1956, and according to *Schwerdtfeger* [1984, p. 28] his observations were as follows:

When Paul Siple came to the south pole on 30 November 1956, the first scientist to stay for a full year at that far-out place, he did not hesitate to dig, in 4 days of hard work, a 5.5 meter-deep pit. The purpose was to measure the temperature which at that depth comes close to the mean annual value. Knowing about the summer temperature on the plateau from Amundsen's and Scott's reports, and assuming the temperature of the coldest month should be as much below the annual mean as the summer values are above it (“like it is in most other places”), he concluded the average temperature of the coldest month might drop below -84°C (-120°F), a possibility he considered “half in apprehension and half in excitement” (*Siple* 1959). Ten months later, he was surprised as well as relieved to find that the winter of the Antarctic Plateau is different. In 1957, the coldest month was September with a mean temperature of -62.2°C and the lowest minimum of -74°C .

His observations indicated that he was not aware of Simpson's work, or more likely that he believed it did not apply to the interior stations of Antarctica, a very reasonable assumption.

Since then, a large number of data have been gathered in Antarctica, and a number of substantial papers have

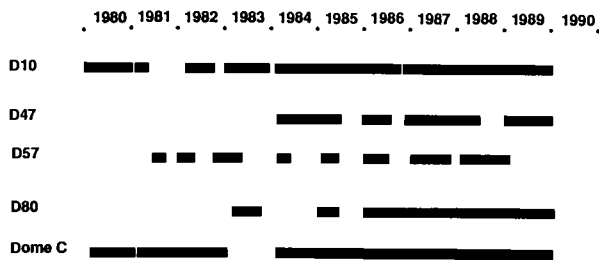


Fig. 1. Periods for which data are available from automatic weather stations in eastern Antarctica.

been written on this subject [Wexler, 1958; Van Loon, 1967; Loewe, 1969; Thompson, 1969; Schwerdtfeger, 1970; Kuhn *et al.*, 1975].

INSTRUMENTATION AND OBSERVATIONAL SITES

Previously, meteorological measurements at manned stations were the only ones available on a year-round basis in Antarctica. These stations are generally far apart from each other, and their locations were often chosen for territorial or logistic reasons rather than for their potential scientific value. These stations have shown that kernlose winters are a widespread phenomenon in Antarctica, holding true for both coastal and interior stations.

During the austral summer of 1979–1980, as part of a joint U.S.–French experiment [Wendler and Poggi, 1981], automatic weather stations (AWS) were installed in Adélie Coast. These stations were designed by Stanford University (Peterson's group) and have been maintained and improved by the University of Wisconsin, Madison (C. R. Stearns' group). In contrast to earlier stations [Sumner, 1965, 1966], these stations do not record on site, but send their data back via satellite. The interrogation is carried out by polar-orbiting satellites, which pass over the stations at intervals of about 104 min. Normally, two satellites are used. Data are transmitted via the Argos System to Toulouse, France, where they are recorded on magnetic tape. The data tapes are sent to the University of Wisconsin, Madison, where they are translated into meteorological units [Stearns, 1984] and sent to us for further analysis.

There are five long-term stations, stretching from near the ocean in the vicinity of Dumont d'Urville (D10) to 1080 km inland for the highest station, located on an ice dome, Dome Charlie (Dome C), at 3280 m altitude. The other stations are located at intermediate points: D47 at 1560 m, D57 at 2103 m, and D80 at 2450 m altitude. The times of their operation can be taken from Figure 1. Dome C and the coastal station D10 have the best track record, while breakdowns occurred more frequently at the intermediate stations. Nevertheless, for all stations there are several years of data available. Their exact

locations can be taken from Figure 2 or Table 1, respectively. The station at Dome C is powered by a radioisotope thermoelectric generator (RTG) and can run year-round without being serviced. All other stations are powered by a battery array in connection with photovoltaic cells. These photovoltaic cells are mounted in a vertical position and face to the north (see Figure 3); they charge the battery bank during the summer half year. These stations are normally serviced once annually.

The following meteorological data are measured at a level about 3 m above the snow surface: (1) air temperature, (2) atmospheric pressure, (3) wind speed, and (4) wind direction.

Also, some "housekeeping" data, such as internal temperature and the voltage of the power supply, are recorded but are of no special interest under normal running conditions. If some "dubious" data occur, the housekeeping data become of interest, since they might, for example, indicate an insufficient supply voltage.

The air temperature is measured with a platinum resistance thermometer (Weed Instrument Co.), the atmospheric pressure with a digiquartz pressure transducer system (Paroscientific Inc.), and wind speed and direction with a Bendix aerovane. The automatic weather stations are described by Renard and Salinas [1977], Stearns and Savage [1981], Scarbro [1982], Renard *et al.* [1983], and Weidner [1987].

The stations also have a storage capability of four previous values of the meteorological parameters, sampled at 10-min intervals. Therefore under the best conditions, with two satellites in orbit, a steady data flow at 10-min intervals can be obtained. A photograph of the station at D10 is given in Figure 3. These and other AWS made substantial progress of Antarctic meteorology possible during the last decade [Stearns and Wendler, 1988].

RESULTS

In Figure 4 the annual course of temperature is presented. It shows that the temperature drops with increasing altitude. The higher stations are furthermore the ones which are situated further to the south, that is, closer to the pole. While Dome C measured an absolute minimum of -84.6°C , the temperatures in the coastal area are relatively mild. The temperature at D10 never dropped below -40°C . This is in good agreement with temperatures measured at Dumont d'Urville, which is located on an island some 10 km to the north, for which long-term observations are available. Here the absolute minimum ever recorded is -36.5°C .

In Figure 5 the winter temperatures (absolute maximum, mean, and absolute minimum) are given for one station (D10) in greater detail. The winter consists of 6 months, April through September. It can be seen that no systematic trend exists for this time period. Warm spells

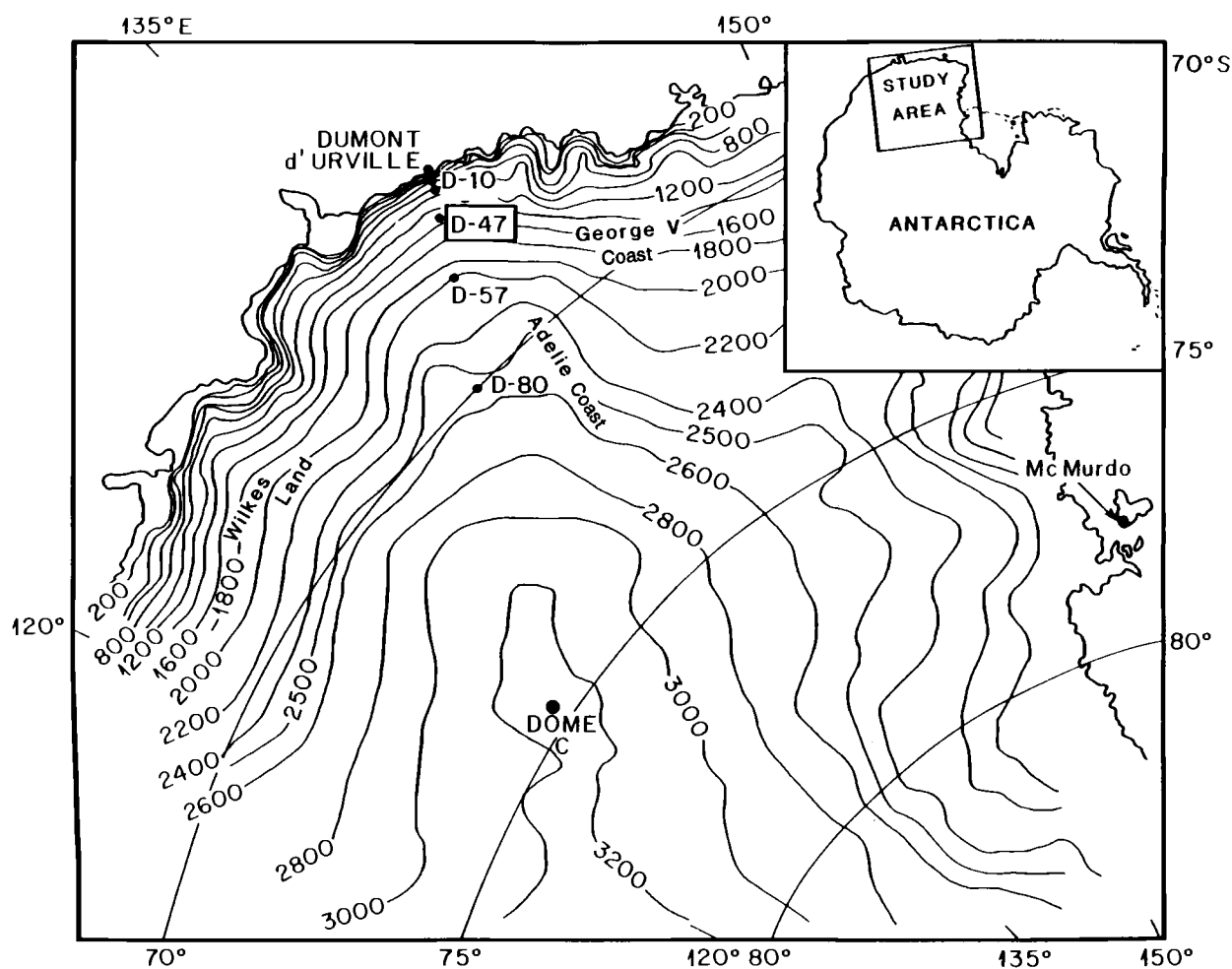


Fig. 2. Location map of the automatic weather stations in Antarctica.

TABLE 1. The Geographic Setting of the Automatic Weather Stations (AWS) in Adélie Coast, Antarctica

Station	Location	Height, m	Distance From the Coast, km	Slope	Azimuth of Upslope, deg
D10	66°42'S 139°48'E	240	5	2×10^{-3}	210
D47	67°23'S 138°43'E	1560	110	5.5×10^{-3}	210
D57	68°11'S 137°32'E	2103	210	6.5×10^{-3}	210
D80	70°01'S 134°43'E	2450	440	1.8×10^{-3}	210
Dome C	74°30'S 123°00'E	3280	1080		

The distance from the coast is measured along the line between Dumont d'Urville and Dome C.

[Redacted]

[Redacted]

[Redacted]

[Redacted]

[Redacted]

[Redacted]

[Redacted]

[Redacted]

[Redacted]

[Redacted]

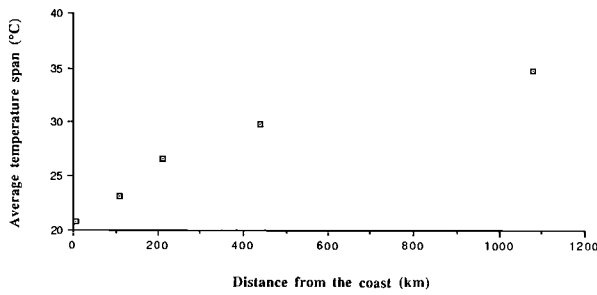


Fig. 6. Span of temperature in winter (absolute maximum minus absolute minimum) as function of distance from the coastline.

D80 and $-0.94^{\circ}/100$ m for D10 to Dome C. However, in winter, stable conditions prevail, with temperature gradients of $-1.41^{\circ}/100$ m and $-1.42^{\circ}/100$ m for the same two stretches, respectively.

In Figure 7 the monthly frequency distributions of mean daily temperature are given for D10. The figure shows that the temperature variation is much larger in winter when compared with the summer. During the

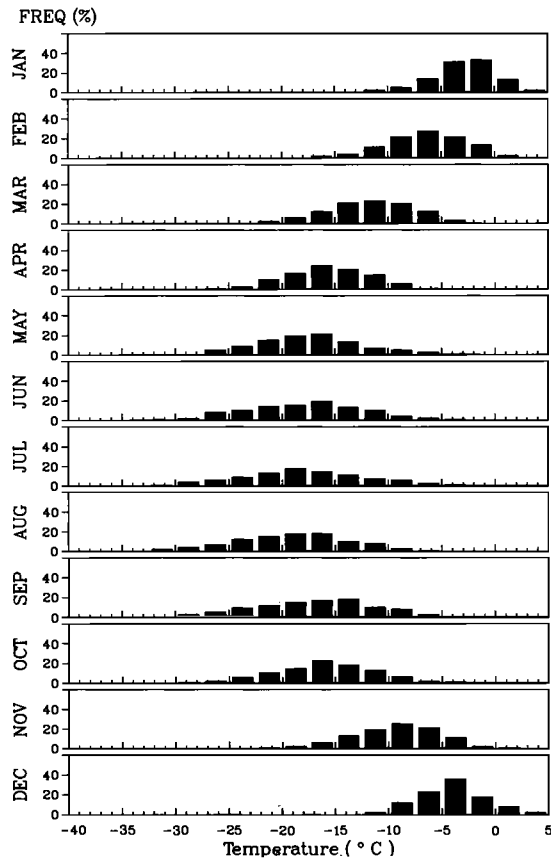


Fig. 7. Frequency distributions of the temperature in 2.5°C intervals at automatic weather station D10 on a monthly basis.

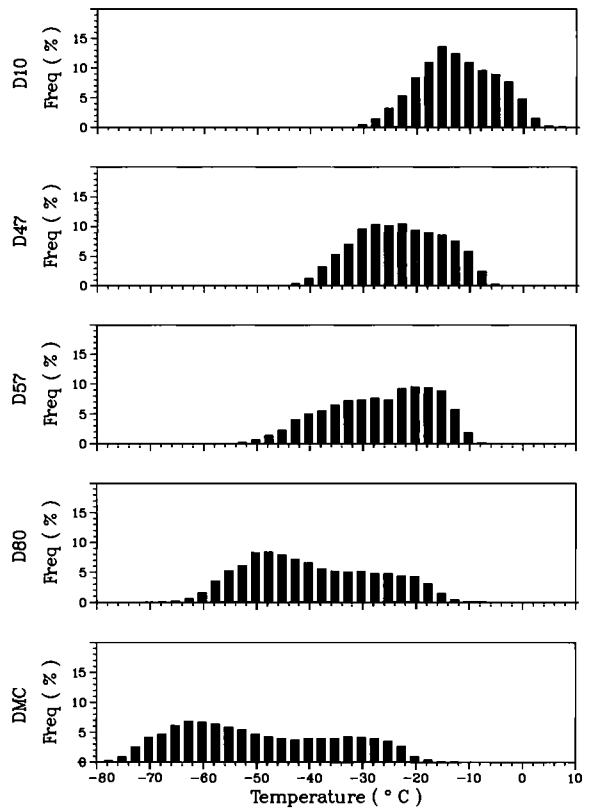


Fig. 8. Frequency distribution of temperature at the automatic weather stations in Adélie Coast on an annual basis.

two summer months of December and January, 80% of the data fall in a temperature range of 5°C , with the most frequent values just below freezing. In winter the temperature range between -10°C and -20°C is the most frequent, but there is no specific small temperature interval that is dominant. The most frequent temperature interval changes even from one winter month to the next.

Figure 8 shows the frequency distribution of mean daily temperature on an annual basis. It can be seen that for D80 and Dome C the distribution is positively skewed, the most frequent value (mode) being lower than the mean. This was already indicated in Figures 4 and 7, as the summer is short, about 2 months, while the winter is very long, 6 months. For D57, winter observations were frequently missing, and therefore the annual temperature frequency distribution for this station is not very meaningful. For the two stations close to the coast, the distribution is fairly symmetric, as winter temperatures are not very low. The figure shows further that the distribution becomes broader when going inland, which was already indicated in Figure 6.

Harmonic analyses of the curve of the mean monthly temperatures can be used to determine the presence and strength of kernlose winters. After *Meinardus* [1938] the

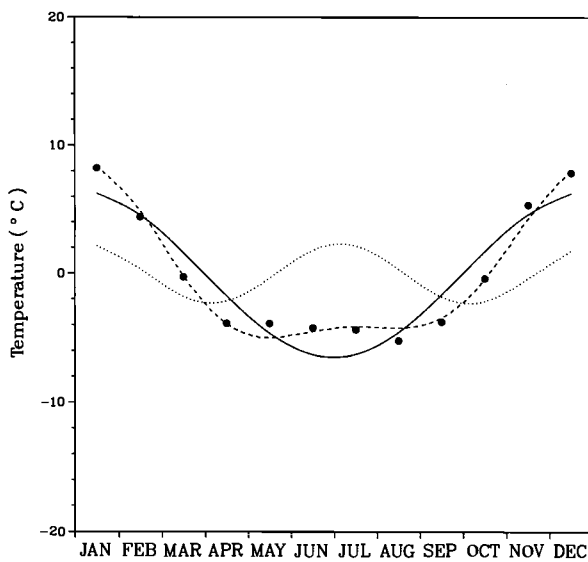


Fig. 9. The first and the second harmonics of the temperature curves for the automatic weather station D10 in Adélie Coast. Further, the combined curve and the actual measurements are given. Note the relatively large amplitude of the second harmonic, which is typical of corelessness.

corelessness can be expressed by the ratio of the amplitude of the first and second harmonics. Normally, the annual temperature curve is fairly well presented by the first two amplitudes. *Schwerdtfeger* [1984] showed for long-term inner Antarctic stations that above 99% of the variance could be explained in this manner. A typical coreless winter will have a second harmonic with a relatively big amplitude when compared to the fundamental oscillation. In Figure 9 the annual mean temperature curve as well as the first and second harmonics are shown for D10. We found a value of a_1/a_2 of 2.7, which is low and typical for a coreless winter. It is also in good agreement with the literature [e.g., *Kuhn et al.*, 1975].

In Figure 10, values of the atmospheric pressure are plotted against temperature. The graph shows that there is a dependency between pressure and temperature; high pressure is associated with high temperatures, and vice versa. Correlation factors between 0.22 and 0.25 were found, which are significant at the 99% confidence level. This is at first glance a very astonishing result. It has been suggested that warm spells are associated with increased advection [*Wexler*, 1958], the latter being normally connected with increased cyclonic activity, which in turn is normally associated with low pressure. A modified version of this idea is that warming does not have to occur by direct advection of warm air at the surface, even though the latter one is the most effective. However, warm air aloft also increases the long-wave incoming radiation, hence warming the surface. This is especially effective if there is an increase in cloudiness, which would tend to further increase the long-wave

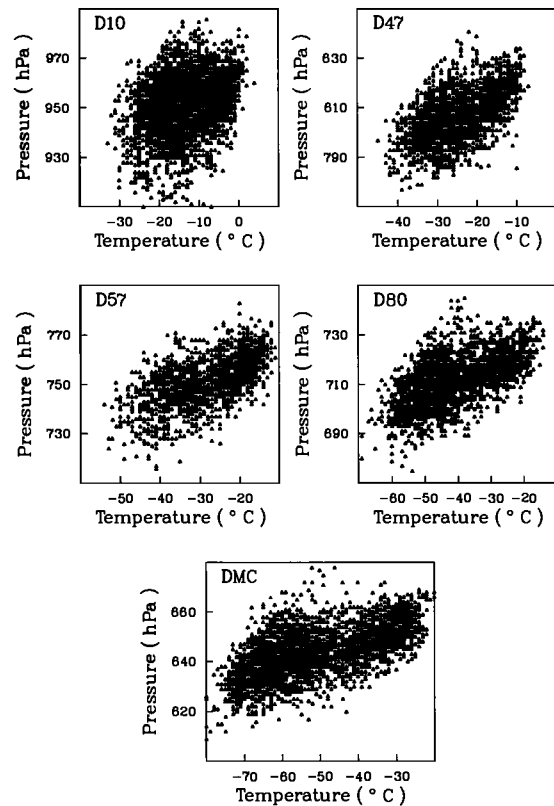


Fig. 10. Atmospheric pressure (hectopascals) measurements plotted versus temperature (degrees Celsius) for five automatic weather stations in Adélie Coast, Antarctica, in winter (April through September).

back radiation of the atmosphere [*van Loon*, 1967]. Again, cloudiness is more frequently associated with cyclonic systems and low atmospheric pressure, and not with anticyclonic situations, which normally display a low amount of cloudiness.

However, more recent findings [*Bromwich*, 1988] can explain that the pressures are generally high in conjunction with above-average temperature, as it was shown that poleward moist air advection occurred in conjunction with warm ridges from the north.

In Figure 11 the deviations of temperature, atmospheric pressure, and wind speed are given for D10. Zero is the mean value, +1 is one positive standard deviation, etc. No trends can be seen for any of the parameters throughout the winter. There appears to be a correlation between temperature and pressure, which could be seen more clearly in Figure 9. We defined temperature deviations larger than one standard deviation as warm or cold spells, respectively, and summarized the data in Table 2. This table shows that during warm spells $[(T - \bar{T}) > \sigma_t]$ the atmospheric pressure is higher than the averages for all five stations and lower for colder spells $[(T - \bar{T}) < \sigma_t]$. The table shows

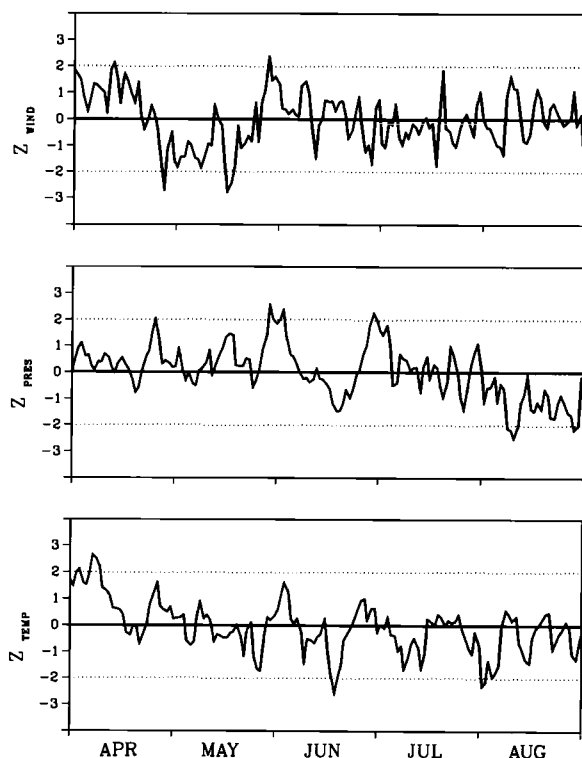


Fig. 11. The course of temperature, atmospheric pressure, and wind speed of the automatic weather station D10 in winter. $Z_x = (X - \bar{X})/\sigma_x$, where Z is the normalized variable; X is T , P , and u (temperature, pressure, and wind speed); \bar{X} is the mean; σ is the standard deviation. Zero denotes the average, +1 denotes one positive standard deviation, -1 denotes one negative standard deviation, etc.

further that the resultant wind direction for warm spells is more cross-slope than normal and more downslope than normal for cold spells except for Dome C. Most of the time, wind speeds are lower for both warm and cold spells when compared to the average conditions. Fur-

thermore, the analysis of the automatic weather stations' data shows the following results:

1. The differences in pressure between the stations are smaller for warm spells and larger for cold spells, a result to be expected.

2. The pressure is falling 66% of the time when warm spells are observed and rising about 70% of the time cold spells are observed.

3. The interdiurnal variation in atmospheric pressure, which can be usually taken as a sign of the cyclonic activity [Schwerdtfeger, 1970], was not related to the temperature and pressure.

4. Only for one station (Dome C) did increasing wind speeds bring warmer temperatures.

The last point can be explained as follows. Normally, the temperature is related to the inversion strength, meaning that the coldest days have normally the strongest inversion. The inversion strength is the main driving force of the katabatic wind over sloped terrain; hence from this point of view, cold spells should be related to the strongest winds. On the other hand, strong winds weaken the intensity of the inversion due to forced mixing, as shown by Thompson [1969]. This fact should work in the opposite direction. Therefore it is not astonishing that no relationship between temperature and wind speed could be found for the slope station. However, for Dome C, where gravity flow does not exist, higher wind speeds are related to higher temperatures (Figure 12), which is in agreement with Thompson [1969].

The fact that high atmospheric pressure is connected with above-normal temperatures is not easy to explain. High atmospheric pressure in Adélie Coast is generally an indicator that the anticyclone over the Antarctic plateau is stronger than normal. This extends and intensifies the pressure ridge between the two semipermanent cyclones which are situated at about 100°E and 170°W just off the coast of the Antarctic continent [Schwerdtfeger, 1970]. This in turn increases the advective

TABLE 2. Differences in the Atmospheric Pressure, Resultant Wind Speed, and Direction From Their Averages for Cases of the Winter Temperatures Which Deviate More Than One Standard Deviation From the Average for Five Stations in Adélie Land, Antarctica

	$T - \bar{T}$	$P - \bar{P}$, hPa	$WS - \bar{WS}$, m s^{-1}	$WD - \bar{WD}$, deg
D10	$\sigma_t=4.02 > \sigma_t$	6.9	-0.4	-10.9
	$\sigma_t=4.02 < -\sigma_t$	-7.4	-2.0	7.4
D47	$\sigma_t=4.57 > \sigma_t$	9.9	-0.7	-0.7
	$\sigma_t=4.57 < -\sigma_t$	-7.2	-0.3	8.7
D57	$\sigma_t=6.61 > \sigma_t$	11.1	-2.6	-31.4
	$\sigma_t=6.61 < -\sigma_t$	-8.8	0.7	14.8
D80	$\sigma_t=7.13 > \sigma_t$	12.4	-0.6	-12.5
	$\sigma_t=7.13 < -\sigma_t$	-9.3	-0.5	4.2
Dome C	$\sigma_t=7.91 > \sigma_t$	7.8	1.9	146.3
	$\sigma_t=7.91 < -\sigma_t$	-9.6	-1.2	-8.4

The overbar denotes the average.

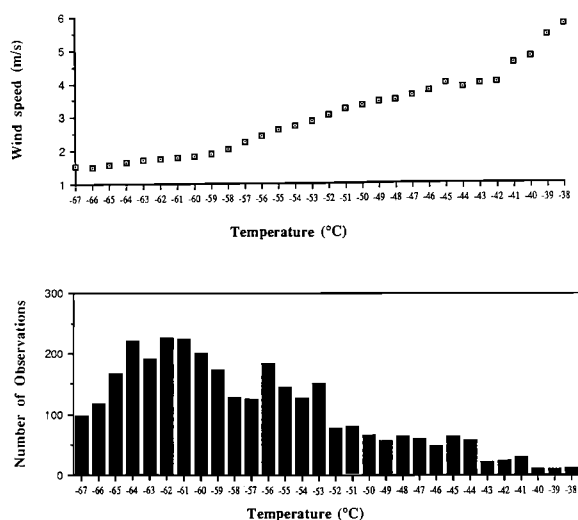


Fig. 12. Temperature plotted against wind speed for Dome C in winter. Note that with increasing wind speed the temperature rises.

tion of warm air into Adélie Coast as well as further inland on the continent. Kodama [1985] showed that this was correct for two specific synoptic events of winter 1983. Such intensified advection of warm air can explain warm spells in Adélie Coast, even though the distance between D10 and Dome C is rather large at 1080 km, and all stations show it simultaneously. Further, Kuhn *et al.* [1975, p. 265] found similar results for Plateau Station. They state, "It is interesting to note that most minima of T (temperature) in winter are accompanied, or shortly preceded, by minima in p (pressure)."

As Plateau Station is too far away from our stations in Adélie Coast to be influenced by the same cyclonic system, other factors also have to play a role. There are two additional arguments that can be made:

1. In a cyclone the air movement is upward, while in an anticyclone it is downward. Hence for a high-pressure situation the relatively warm air aloft can be brought more easily to the surface.

2. The surface temperature of Antarctica is controlled by the radiation budget [Wendler *et al.*, 1988]; in winter, in the absence of solar radiation, it is solely controlled by the long-wave or infrared radiation budget. The back radiation of the relatively warm air aloft causes the surface temperature not to cool further than observed, cooling in this way the air aloft, and warming the surface. Relatively warm air is advected aloft and drains as a thin surface layer (katabatic wind) around the periphery of Antarctica [Mather and Miller, 1967; Parish, 1984]. This drainage of cold air in the boundary layer is fairly steady, while the advection of warm air aloft is steered by cyclonic disturbances and is therefore

less steady. Hence low surface air pressure means that the advection of warm air has been disrupted for a while; the air aloft has been cooled by long-wave radiation and is not anymore to the same extent able to "warm" the surface by long-wave back radiation.

Acknowledgments. The study was supported by NSF grant DPP-90-17969. Our thanks to many people who made it possible to obtain these data, more specifically to Stanford University (A. Peterson's group) and the University of Wisconsin (C. Stearns' group). Many people of U.S. Antarctic Research Program and the Expéditions Polaires Françaises were helpful in carrying out this work, for which we are indebted. Finally, our thanks go to G. Weller and D. Bromwich, whose valuable comments on the manuscript improved this paper.

REFERENCES

- Bromwich, D., Snowfall in high southern latitudes, *Rev. Geophys.*, 26, 149–168, 1988.
- Hann, J., *Handbuch der Klimatologie*, vol. III, 635 pp., J. Engelhorn, Stuttgart, Germany, 1911.
- Kodama, Y., Katabatic wind in Adélie Land, Antarctica, Ph.D. thesis, 191 pp., Univ. of Alaska, Fairbanks, 1985.
- Kuhn, M. H., A. J. Riordan, and I. A. Wagner, The climate of Plateau Station, in *Climate of the Arctic*, edited by G. Weller and S. A. Bowling, pp. 255–267, Geophysical Institute, University of Alaska, Fairbanks, 1975.
- Loewe, F., On the coreless winter of the polar regions, *Gerlands Beitr. Geophys.*, 78(6), 453–476, 1969.
- Mather, K. B., and G. S. Miller, Notes on topographic factors affecting the surface winds in Antarctica, with special reference to katabatic winds; and bibliography, *Tech. Rep. UAG-R-189*, 125 pp., Univ. of Alaska, Fairbanks, 1967.
- Meinardus, W., Klimakunde der Antarktis, in *Handbuch der Klimatologie*, edited by W. Koeppen and R. Geiger, 135 pp., Bornträger, Berlin, 1938.
- Parish, T., A numerical study of strong katabatic winds over Antarctica, *Mon. Weather Rev.*, 112, 545–554, 1984.
- Periard, C., and P. Pettré, Climatologie of Dumont d'Urville, Adélie Land, Antarctica, *Notes Centre 2*, 19 pp., Centre National de Recherches Météorologiques, Toulouse, France, 1991.
- Pollog, C. H., Untersuchung von jährlichen Temperaturkurven zur Charakterisierung des Polarklimas, *Mitt. Geogr. Ges. München*, 17(2), 165–253, 1924.
- Renard, R. J., and M. G. Salinas, The history, operation and performance of an experimental automatic weather station in Antarctica, *Rep. NPS-63Rd7710*, 57 pp., Nav. Postgrad. School, Monterey, Calif., 1977.
- Renard, R. J., W. J. Thompson, and S. P. Hervey, Analysis of pressure, temperature and wind data from remote-site automatic weather stations near McMurdo, Antarctica, paper presented at First Int. Conf. on Southern Hemisphere Meteorol., Am. Meteorol. Soc., Sao Jose dos Campos, Brazil, July 21–Aug. 6, 1983.
- Scarbro, K. M., Analysis of Antarctic remote-site automatic weather station data for period January 1979–February 1980, Master's thesis, 78 pp., Dep. of Meteorol., Nav. Postgrad. School, Monterey, Calif., 1982.
- Schwerdtfeger, W., The climate of the Antarctic, in *World Survey of Climatology*, vol. 14, *Climates of the Polar Regions*, pp. 253–355, Elsevier, New York, 1970.
- Schwerdtfeger, W., *Weather and Climate of the Antarctic*, vol. 15, *Developments in Atmospheric Science*, 261 pp., Elsevier Science, New York, 1984.

- Shackleton, E. H., *The Heart of the Antarctic*, 2 vols., William Heinemann, London, 1909.
- Simpson, G. C., *British Antarctic Expedition 1910–1913, Meteorology*, vol. 1, *Discussion*, 326 pp., Tacker, Spink and Co., Calcutta, India, 1919.
- Siple, P., *90° South: The Story of the American South Pole Conquest*, 384 pp., Putnam's, New York, 1959.
- Stearns, C., Antarctic automatic weather stations, austral summer 1983–1984, *Antarct. J. U.S.*, 19(5), 189–191, 1984.
- Stearns, C., and M. Savage, Automatic weather stations, 1980–1981, *Antarct. J. U.S.*, 16(5), 190–192, 1981.
- Stearns, C., and G. Wendler, Research results from Antarctic automatic weather stations, *Rev. Geophys.*, 26, 45–61, 1988.
- Streten, N., A review of the climate of Mawson—A representative strong wind site in East Antarctica, *Antarct. Sci.*, 2(1), 79–89, 1990.
- Sumner, C. J., A long period recorder of Antarctic katabatic winds, *Q. J. R. Meteorol. Soc.*, 91, 364–375, 1965.
- Sumner, C. J., A sunshine sensing device for long period recording, *Q. J. R. Meteorol. Soc.*, 92, 567–574, 1966.
- Thompson, D. C., The coreless winter at Scott Base, Antarctica, *Q. J. R. Meteorol. Soc.*, 95, 404–407, 1969.
- van Loon, H., The half yearly oscillations in middle and high southern latitudes and the coreless winter, *J. Atmos. Sci.*, 24, 472–486, 1967.
- von Middendorf, T. H., *Reise in den äussersten Norden und Osten Sibiriens*, pp. 1848–1875, Imperial Academy of Science, St. Petersburg, Russia, 1899.
- Weidner, G., *Automatic Weather Station Technical Manual*, Department of Meteorology, University of Wisconsin, Madison, 1987.
- Wendler, G., and Y. Kodama, On the climate of Dome C, Antarctica, in relation to its geographical setting, *J. Climatol.*, 4, 495–508, 1984.
- Wendler, G., and Y. Kodama, Some results on the climate of Adélie Land, eastern Antarctica, *Z. Gletscherk. Glazialgeol.*, 21, 319–327, 1985.
- Wendler, G., and A. Poggi, Measurement of the katabatic wind in Antarctica, *Antarct. J. U.S.*, 15(5), 193–195, 1981.
- Wendler, G., N. Ishikawa, and Y. Kodama, On the heat balance of the icy slope of Adélie Land, eastern Antarctica, *J. Appl. Meteorol.*, 27(1), 52–65, 1988.
- Wexler, H., The “kernlose” winter in Antarctica, *Geophysika*, 6, 577–595, 1958.

(Received October 15, 1991;
accepted September 16, 1992.)

ANTARCTIC CLIMATE ANOMALIES SURROUNDING THE MINIMUM IN THE SOUTHERN OSCILLATION INDEX

SHAWN R. SMITH¹ AND CHARLES R. STEARNS

Department of Meteorology, University of Wisconsin-Madison, Madison, Wisconsin 53706

Composites of Antarctic monthly surface pressure and temperature anomalies and the Southern Oscillation Index (SOI) were used to analyze the relationships between the climate of Antarctica and the El Niño/Southern Oscillation (ENSO). Annual composites created for the year before and the year after the minimum in the SOI utilized data surrounding six SOI minima occurring between 1957 and 1984. Comparisons were made between these ENSO warm phase composites and similar annual composites for non-warm phase years. We further compared the six individual ENSO warm phases to the warm phase annual composites to determine the reliability of the composites. Three-month composites for the 24 months surrounding the SOI minimum look at the evolution of the Antarctic anomalies in a warm phase. We found a distinct change in the sign of the annual pressure and temperature anomalies between the year before and the year after the minimum in the SOI. Furthermore, the 3-month temperature composites showed smoother transitions from one 3-month period to the next than did the 3-month pressure composites. Using a simple thickness argument, we derive a hypothetical 500-mbar pattern for the Antarctic coastline from 120°W to 60°E by modifying the normal thickness pattern with the composite pressure and temperature anomalies surrounding the SOI minimum. We further hypothesize, using other authors' works, a connection between the derived 500-mbar pattern, a 500-mbar block common to New Zealand, and the Australian branch of the SO.

1. INTRODUCTION

The El Niño/Southern Oscillation (ENSO) is a major interannual climate fluctuation that affects the globe. *Philander and Rasmusson* [1985] described ENSO as a coupled system linking an oceanic branch, the El Niño, and an atmospheric branch, the Southern Oscillation (SO). They outlined the SO as a negative correlation between the sea level pressure (SLP) fluctuations in the southeast Pacific high and the north Australian-Indonesian low. The oceanic branch of the ENSO system was defined by large sea surface temperature (SST) anomalies covering the tropical Pacific Ocean from the west coast of Peru to the dateline between 30°N and 30°S latitudes. The term El Niño specifically defines the ENSO phase where the SST anomalies are positive. During a warm phase, described in detail by *Philander and Rasmusson* [1985] and *Rasmusson and Carpenter* [1982], the SO has lower SLP in the southeast Pacific high and higher SLP in the north Australian-Indonesian low. Upon occasion, during the years between warm events, the opposite atmospheric and oceanic conditions occur, and a cold phase of ENSO, the La Niña, exists [*van Loon and Shea*, 1985].

Since the ENSO system was defined, researchers have been searching for the mechanisms that drive this coupled ocean-atmosphere system. In the process, many authors have shown that ENSO is dynamically linked to weather patterns around the globe. *Philander and Rasmusson* [1985] gave an overview of some of these dynamic links, called teleconnections. *Mo and White* [1985] analyzed southern hemisphere teleconnections and hinted at a possible link between the SO and the southern polar latitudes. *Mo and White* found high teleconnectivity values in the summer SLP field over Antarctica, and even though they discounted their results because they felt the SLP data over Antarctica were suspect, their work revealed that an Antarctic-ENSO link may exist.

Since *Mo and White* [1985], other authors have pointed out possible relationships between ENSO and the higher southern latitudes. *Van Loon and Shea* [1985, 1987] found reversals in the signs of the seasonal SLP anomalies between the year before (yr_{-1}) and the year of (yr_0) an ENSO warm event. *Van Loon and Shea* [1987] concluded that the area of Australasia and the subtropical South Pacific Ocean likely play a major role in forcing the SO. *Carleton* [1988] found similar pressure reversals in the SLP fields for yr_{-1} and yr_0 in the Weddell Sea area near Antarctica. *Carleton* also revealed an associated change in the sea ice concentration from yr_{-1} to yr_0 . *Bromwich et al.* [1991] briefly re-

¹Now at the Byrd Polar Research Center, Ohio State University, Columbus, Ohio 43210.

viewed other papers that discuss possible ENSO relationships to the snow accumulation rates on the Ross Ice Shelf and the horizontal extent of Antarctic sea ice. *Savage et al.* [1988] studied the Antarctic/ENSO relationship by using lagged correlation statistics. *Savage et al.* found temperatures at the Amundsen-Scott South Pole Station to be anomalously cold 1 year after a warm phase of ENSO, while the wind data for the same time period showed enhanced downslope flow on the Antarctic ice dome. *Savage et al.* concluded that these anomalous temperature and wind patterns were maintained by a large-scale circulation pattern dynamically linked to the ENSO system.

A dynamic link between Antarctica and the large-scale circulation of the southern hemisphere was suggested by *James* [1988] and *Trenberth* [1980]. Both authors found the topography of Antarctica to be important in forcing the planetary-scale, tropospheric flow patterns of the southern hemisphere. Furthermore, *Trenberth* [1980] discussed a link between the topography of Antarctica and the amplitude and phase of a blocking ridge common to the New Zealand area [*Streten and Zillman*, 1984, Figure 28]. The New Zealand block is important, since *Trenberth* [1980] implied that the block and its associated cutoff low over the Tasman Sea may be related to changes in the strength of the north Australian-Indonesian low of the SO system. Another link between Antarctica and the New Zealand blocking was presented in a case study of a block in June 1982 by *Mo et al.* [1987]. They concluded that the amplitude and longevity of the New Zealand block was strongly influenced by both local land-sea heating contrasts near Australia and by cold air releases from the Antarctic continent. Furthermore, *Parish and Bromwich* [1987] revealed that the airflow on the Antarctic continent is dominated by the topography and likely would concentrate cold air releases at certain focal points along the coast.

The purpose of our research was to analyze the horizontal temperature and pressure patterns in Antarctica to see if they could affect, through formation of the New Zealand block, the Southern Oscillation. Composites of Antarctic pressure and temperature anomalies were created for years when ENSO was and was not in a warm phase to locate any ENSO signal in the climate record. Using the composite results and the work of other authors, we present a hypothesis, based on a simple thickness argument, on how the temperature and pressure anomaly patterns may influence the New Zealand block discussed above, and possibly link Antarctica to ENSO. Three-month composites showing the evolution of the climate anomalies during a warm phase and the individual ENSO warm phases are analyzed to test the thickness hypothesis.

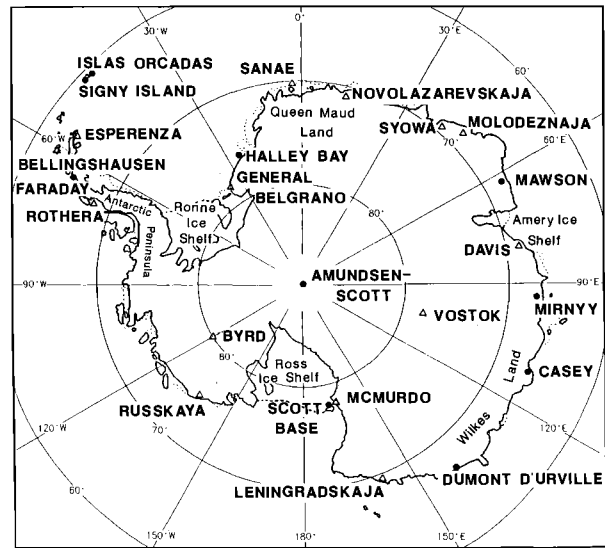


Fig. 1. The locations and names of 24 year-round, manned, weather stations and geographic features in Antarctica. The stations located at the solid circles are the 10 stations with near-perfect records from March 1957 to March 1984.

2. DATA COLLECTION

2.1. Data Selection and Sources

Antarctic climate was represented by monthly mean surface temperature and pressure data from manned year-round stations. The base data set was compiled by *Jones and Limbert* [1987] and contained monthly mean surface pressure (millibars) and temperature (degrees Celsius) data for 29 manned stations from 1957 through 1986. Of these 29 station records, 24 were chosen, based on record length and amount of missing data, for our project. Figure 1 shows the names and locations of the 24 stations and the geographical features referenced later in the text. In an attempt to provide the best data coverage possible over the continent, some shorter records were included. Note that all but three of the stations are along the coastline at elevations of less than 300 m, while the three inland stations vary in elevation from 1515 m at Byrd to 3420 m at Vostok.

Many sources were used to extend the 24 pressure and temperature records past 1986 in an unsuccessful attempt to include the 1987 ENSO event in our composites. The record at Byrd Station was extended using data from an automated weather station (AWS) operating near the old manned station site from 1980 to 1987 [*Stearns and Savage*, 1981]. Data for 1987 through 1989 and some earlier missing months at Amundsen-Scott and McMurdo stations were retrieved from the *Antarctic Journal of the United States*. Monthly mean data from 1987 through 1989 for Mawson, Davis, Casey, Scott Base, S.A.N.A.E., Signy Island, Faraday, Rothera Point, and Halley Bay were obtained from

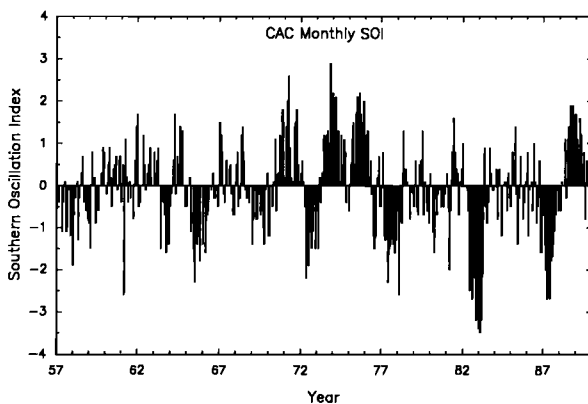


Fig. 2. Histogram of monthly SOI values calculated by the Climate Analysis Center for January 1957 through December 1989.

Australian, New Zealand, South African, and British sources. Some other data voids and obvious errors in the original *Jones and Limbert* [1987] data set were filled using data supplied by the Australian Antarctic Division (see acknowledgments).

To measure the phase of ENSO, we utilized the Southern Oscillation Index (SOI), a twice normalized Tahiti minus Darwin SLP index. Monthly values of the SOI were obtained from the Climate Analysis Center (CAC) of the National Meteorological Center (V. E. Kousky, unpublished data, 1991). The CAC SOI, a nondimensional index which is negative when ENSO is in a warm phase, was calculated using four steps. First, monthly pressure anomalies were derived by subtracting the 1951–1980 monthly means from the SLP data at Tahiti and Darwin. Next the anomalies were normalized using the mean annual standard deviation of the pressure anomalies at each station. The difference of the normalized anomalies, Tahiti minus Darwin, was then taken, and finally the difference time series was standardized by its standard deviation. The resulting monthly SOI values from January 1957 through December 1989 are presented as a histogram in Figure 2.

2.2. Error Analysis

After compiling the data for Antarctic climate and the phase of ENSO, the data were checked for accuracy. The SOI data were checked by recalculating the index using the CAC methods described above. The recomputed data varied by ± 0.1 from the original index we received; however, these small differences were attributed to rounding errors. As a result, the SOI was used as it was received from the CAC.

Unlike the SOI, bad data are common in the Antarctic climate record, and the highly variable climate makes finding errors difficult. The base data set underwent a series of accuracy checks described by *Jones and*

Limbert [1987]; however, the data added from other sources also needed to be screened for errors. Therefore the combined pressure and temperature data for each station underwent a graphical error analysis technique described in detail by *Smith* [1991].

Briefly, our technique involved plotting the monthly pressure and temperature data in two graphical formats and then comparing neighboring stations to find outlying trends in the monthly data. Comparisons were made only for the 21 coastal stations, since differences in elevation and topography caused problems with the inland stations. In general, for the coastal stations, if an outlying trend occurred on the graphs for either of the neighboring stations the outlier was considered good data. If no data were available at neighboring stations to check an outlier, the outlier was considered good by default unless the outlier was radically out of the station's trend, say $\pm 10^{\circ}\text{C}$ or 10 mbar. Our error analysis resulted in the removal or correction of 15 temperature and only four pressure values. A sample of the error corrected data along with instructions for obtaining the complete data set can be found in Appendix 1.

Furthermore, our error analysis revealed the pressure data at McMurdo to be suspect, an error also noted by *Savage et al.* [1988]. Figure 3a, a one to one plot of McMurdo versus Scott Base monthly mean pressure values, reveals large differences between the stations. Since McMurdo and Scott Base are only 1.9 km apart, they should show a better correlation. Further comparisons between these two year-round stations and the AWS at Ferrell and Marble Point [*Stearns and Wendler*, 1988] were made to reveal which manned station was in error. Figures 3b–3f show the one to one pressure plots between these four stations. Note that the correlations between Scott Base and the two AWS (Figures 3d and 3e) are much better than those for McMurdo (Figures 3b and 3c) even though Marble Point is 85 km northwest of the two manned stations and Ferrell is 97 km to the east-southeast. Even the correlation between the two AWS (Figure 3f), some 180 km apart, was better than that between McMurdo and Scott Base. We believe that these graphical correlations reveal an error whereby only part of the McMurdo pressure record was corrected to SLP. This conclusion resulted in our decision to discard McMurdo's pressure data from our research.

The result of our error analysis was a single monthly mean temperature record at 24 stations and a single monthly mean pressure record at 23 stations, most spanning roughly 30 years. Missing data in these records created problems for climatic analyses; thus the handling of missing data is discussed for each analysis in the methodology section below. In some cases, records with missing data were used, while other analyses utilized blocks of data having no missing points over a fixed period of record. Refraining from using averaging techniques to fill in the missing data points was a matter of personal preference. It should be noted, however,

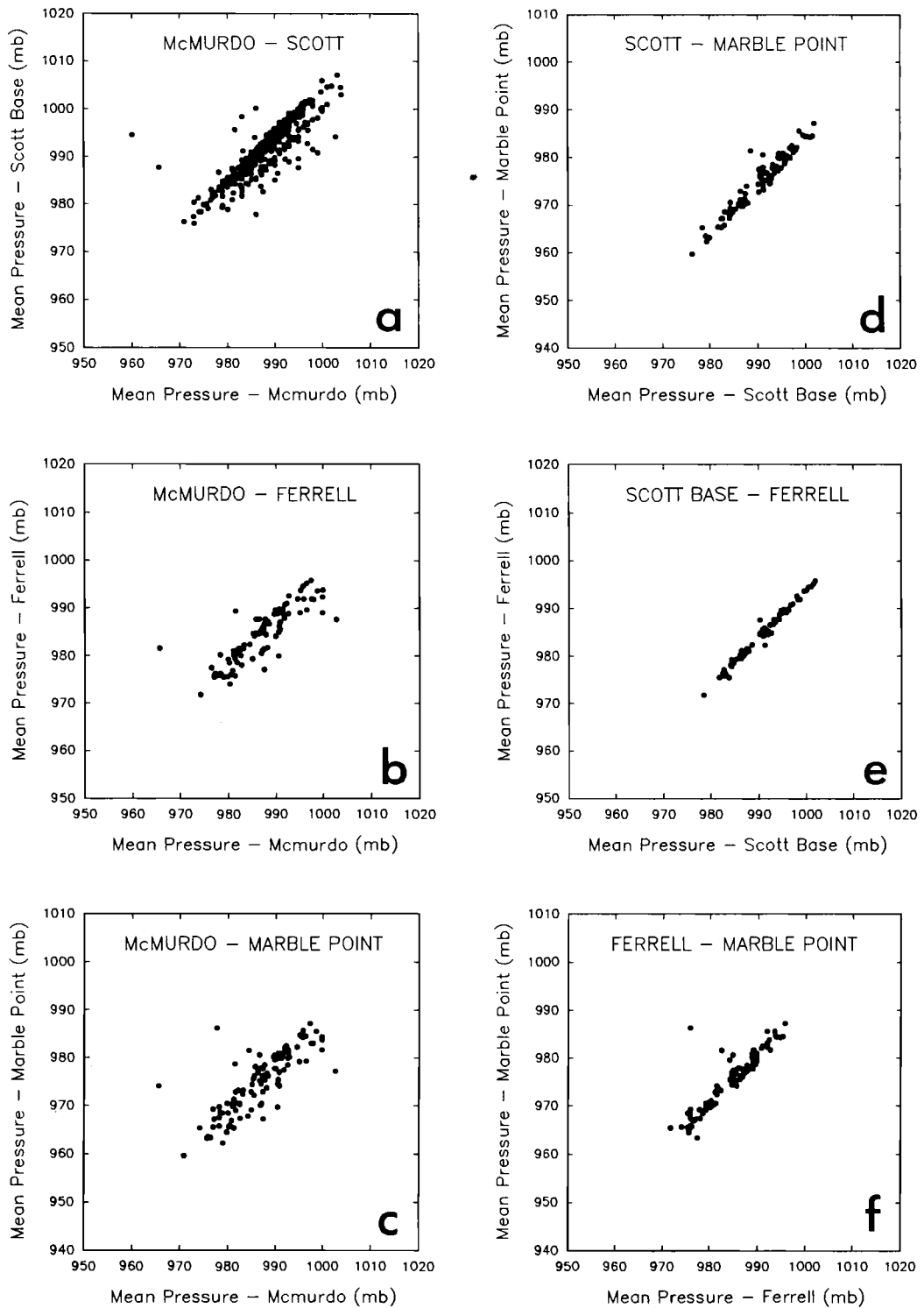


Fig. 3. One to one plots of monthly mean pressure values. (a) McMurdo versus Scott Base. (b) McMurdo versus Ferrell. (c) McMurdo versus Marble Point. (d) Scott Base versus Marble Point. (e) Scott Base versus Ferrell. (f) Ferrell versus Marble Point.

that the number of missing data and the scarcity of long climate records in Antarctica are the major data limitations on our research.

3. METHODOLOGY

3.1. Creation of Anomaly Data

Upon completion of the error analysis, we began our search for an ENSO signal in the Antarctic climate record. Since the annual cycle in the climate data would mask any signal, it was necessary to remove the annual cycle using either simple averaging or Fourier techniques. For this project, a simple arithmetic averaging approach was used, primarily because of the presence of the coreless winter in some of the temperature records. The temperature time series for a typical coreless winter resembles a step function with short pointed summers and the steady winter temperatures as described by *Schwerdtfeger* [1984]. This steplike time series would be difficult to reconstruct by adding a limited combination of sine and cosine waves in a Fourier approach. Though only the three inland stations, Byrd, Amundsen-Scott, and Vostok, exhibited the coreless winter, for consistency we utilized arithmetic averaging to remove the annual cycle at all stations.

The removal method consisted of calculating long-term monthly means first and then subtracting the long-term means from the monthly mean values to create monthly anomalies for each station. Long-term monthly means were calculated using an arithmetic average of monthly data only from calendar years with 12 monthly values. As a result, all long-term monthly means for one station's record were created with the same number of data points. However, when the long-term monthly means were subtracted from the individual monthly mean values to create the monthly anomalies, the subtractions were done on all the monthly means, including those in calendar years with less than 12 monthly values.

The number of data points used to create the long-term monthly means varied from station to station depending on the number of complete calendar years of data. The above method was used, as opposed to fixing the anomalies to a specific period, because of the low quality of some of the data records. Using a different number of data points to create each station's anomalies raised questions about the validity of comparing results from different stations. However, in an effort to use the most data possible for each long-term mean, this conflict was unavoidable. The pressure and temperature monthly anomalies obtained by removing the annual cycle were used to construct all of our composites.

3.2. Compositing Techniques

Annual composites of the monthly temperature and pressure anomalies were created to reveal the ENSO

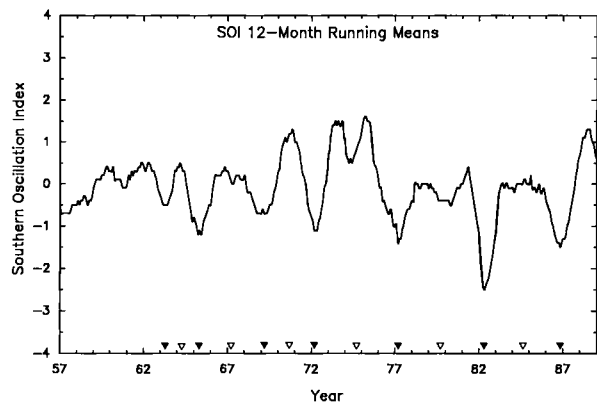


Fig. 4. Time series of the 12-month running means of the SOI created from data for January 1957 through December 1989. The ticks on the year axis represent the January to December annual mean. The solid triangles mark the 12-month running mean values that include the SOI minima, and the open triangles mark the running mean pair values that include the midpoints between each minima pair.

signal in Antarctica. *Meehl* [1987] and *van Loon and Shea* [1985, 1987] found the ENSO events up to the 1980s to have a seasonal component; therefore they defined their ENSO composites using 3-month seasons. However, *Wang* [1992] revealed that the 1982 and 1987 warm events had an evolution that was timed differently from the seasonal cycle used by *Meehl* [1987] and *van Loon and Shea* [1985, 1987]. Thus *Wang* [1992] suggested that, since the timing of each ENSO warm event differs with respect to the seasons, seasonal composites may result in an inadequate representation of all ENSO warm events. We agreed with *Wang* [1992] and decided to center our warm phase composites using the minimum in the SOI time series. Figure 4, a graph of unweighted 12-month running means of the SOI, was used to locate the SOI minima because the smoother series made locating a central minimum for each ENSO warm event easier. Twelve-month running means were used simply to give us the same time scale as the annual composites. Seven minima were found in our period of record, and the solid triangles in Figure 4 mark the 12-month running mean that included the SOI minimum. Therefore the point between the sixth and seventh month of the marked 12-month running mean was the actual date of the SOI minimum. The seven minima were located between these months: October/November 1963, October/November 1965, June/July 1969, October/November 1972, August/September 1977, October/November 1982, and April/May 1987.

Figure 5 shows a schematic of how the annual composites surrounding the SOI minimum for the pressure anomalies were created. Many missing anomalies before and after the 1987 minimum allowed only the first six minima to be used in the composites. The first step was summing the 12 monthly pressure anomalies for the

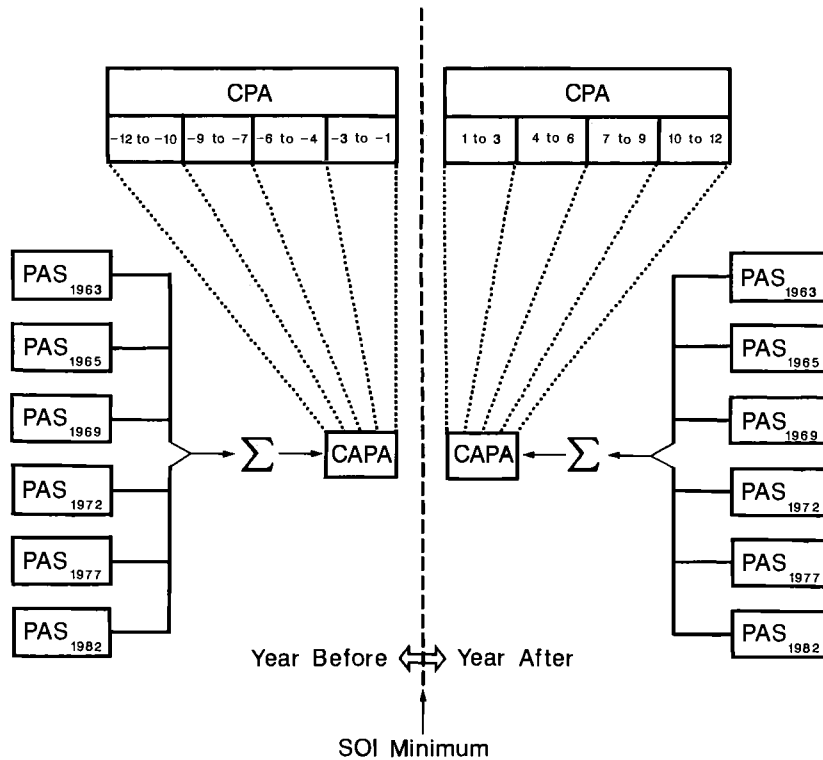


Fig. 5. Schematic of the compositing methods. The pressure anomaly sums (PAS) of 12 monthly anomalies for each of the six SOI minima are summed to create the composite annual pressure anomaly (CAPA) both before and after the SOI minimum. The temperature anomaly sums and the composite annual temperature anomalies are similarly created (see text).

year before and the 12 monthly pressure anomalies for the year after each SOI minimum, creating one annual pressure anomaly sum (PAS) before and after each of the six SOI minima. Next the six PAS before the SOI minimum were added to create a composite annual pressure anomaly (CAPA) for the year before the SOI minimum. Similarly, the six PAS after the SOI minimum were added to create the CAPA after the SOI minimum. The PAS and CAPA were created at all desired stations. Annual temperature anomaly sums (TAS) and the composite annual temperature anomalies (CATA) for the SOI minimum were created using the same method.

In an attempt to create composites without any missing data, the PAS, TAS, CAPA, and CATA were first calculated using 10 stations with near-perfect pressure and temperature anomaly records from March 1957 to March 1984. These 10 stations, marked by solid circles in Figure 1, resulted in a perfect data set for all the composites except for the CAPA surrounding the SOI minimum, where Dumont d'Urville had 1 month of missing data during the 1965 warm event. Note that nine of these 10 stations are along the coastline and that there are two large gaps in the coverage from 20°W to 60°E and from 70°W to the dateline (180°). Therefore when

the composite patterns are presented (section 4), the contours plotted in these data voids are purely subjective. Other CATA and CAPA using the entire anomaly data set were made for confirmation of our results from the 10 station composites.

Using the identical procedure, CATA and CAPA for periods in between the warm phases were created. These non-warm phase composites were centered on the midpoint, the point in time halfway between two SOI minima. The five midpoints between the six SOI minima used in the composites above, marked as above by the open triangles in Figure 4, were located between these months: October/November 1964, August/September 1967, February/March 1971, March/April 1975, and March/April 1980. A sixth midpoint occurred between January and February of 1985; however, many missing anomalies made this midpoint unusable. The midpoint composites were made for the same 10 stations and the same period of record as for the SOI minimum composites.

To analyze the evolution of the anomaly patterns surrounding the minimum in the SOI, 3-month composites were created for the pressure and temperature anomaly data. The first step in creating the 3-month

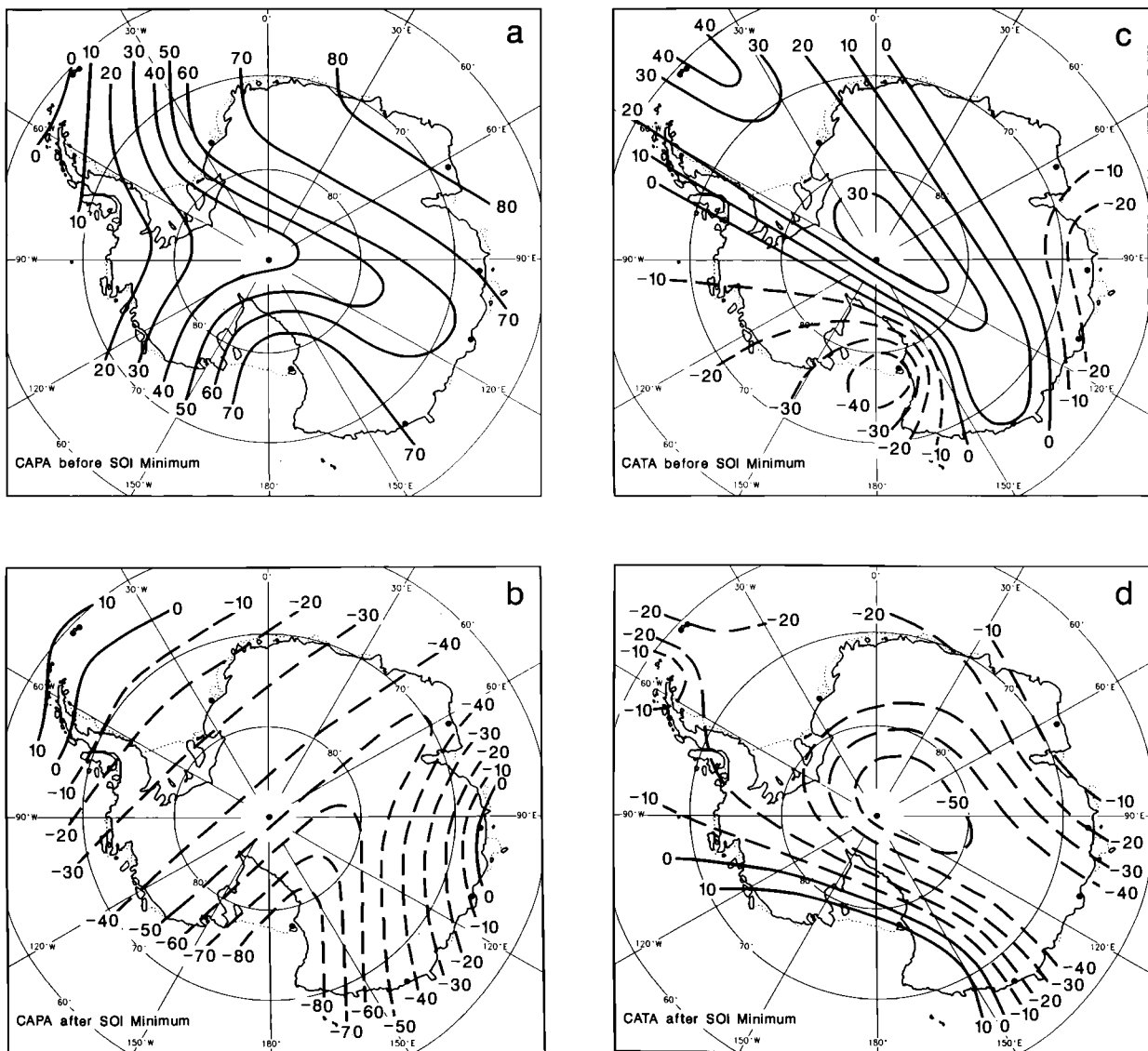


Fig. 6. Composite maps for the SOI minimum. (a) CAPA before minimum. (b) CAPA after minimum. (c) CATA before minimum. (d) CATA after minimum. Pressures are contoured every 10 mbar and temperatures every 10°C. Negative anomalies have dashed contours.

composites was dividing the 24-month period surrounding the SOI minimum into eight 3-month segments as follows: -12 to -10, -9 to -7, -6 to -4, -3 to -1, 1 to 3, 4 to 6, 7 to 9, and 10 to 12 months, with negative and positive months represent months before and after the SOI minimum, respectively (Figure 5). Next, the three monthly anomalies for each 3-month segment were added for all six SOI events. Finally, the six 3-month sums for each time segment were added to create a total of eight 3-month composite temperature anomalies (CTA) and eight 3-month composite pressure anomalies (CPA). The schematic in Figure 5 shows that the CPA are related to the

CAPA basically by dividing the CAPA before and after the SOI minimum into the eight 3-month segments outlined above.

As a test of the reliability of the CAPA and CATA patterns surrounding the SOI minimum, we created new PAS and TAS for each of the six SOI minimum events. These new PAS and TAS were made using all station records that had 24 months of good data surrounding each SOI minimum. The new PAS and TAS (Figures 10–15) for the six SOI minimum events were compared to the CAPA and CATA for the SOI minimum (Figure 6) to see which of the six individual SOI minima resembled the composite patterns.

4. RESULTS

Now that we have outlined the methodology, we present the results of the composites, starting with the CAPA and CATA surrounding the SOI minimum, followed by the midpoint analyses. Section 4.3 introduces the 3-month CTA and CPA, and section 4.4 presents the PAS and TAS for each individual ENSO event. For all the composite maps to follow, the pressure anomalies are plotted in millibars and the temperature anomalies in degrees Celsius. Contours are spaced every 10°C for temperature and 10 mbar for pressure, with the negative anomalies having the dashed contours.

4.1. SOI Minimum Composites

Figure 6 shows the CATA and CAPA before and after the SOI minimum. The CAPA prior to the SOI minimum, shown in Figure 6a, reveals that positive pressure anomalies dominated the continent in the year before the SOI minimum, with the highest anomalies occurring in the vicinity of Scott Base and Mawson stations. A relative minimum in the anomalies cut across the continent from Casey, through Amundsen-Scott, to the Antarctic Peninsula, where anomalies were very small.

A sharp change in the sign of the pressure anomalies occurred over most of the continent for the year after the SOI minimum (Figure 6b). The CAPA were mostly negative, with the largest negative anomalies stretching from a maximum at Scott Base toward Mawson Station. The Antarctic Peninsula, however, retained its low to slightly positive anomalies. Recall that a sign change in the pressure anomalies was also found from yr_{-1} to yr_0 by both Carleton [1988] and van Loon and Shea [1985, 1987].

A sign change also occurred across the SOI minimum in the CATA results, but the sign change was not the same over the entire continent. Figure 6c, the CATA for the year before the SOI minimum, shows a large area of positive temperature anomalies stretching from a maximum over Signy Island, across Amundsen-Scott, toward Dumont d'Urville. Local minima in the anomalies were centered over Scott Base and along the east coast of the continent near Mawson. After the minimum (Figure 6d) the CATA showed strong negative temperature anomalies replacing the positive anomalies over the center of the continent. Meanwhile, weak positive anomalies occurred over Scott Base, a station that was strongly negative before the minimum, and, even though the actual CATA value at Mawson changed little, the region around Mawson was another relative maximum in the CATA pattern after the SOI minimum.

Student's t-tests were done to infer the significance of the CAPA and CATA results both before and after the SOI minimum. Of the CAPA, only three stations, Mawson, Scott Base, and Dumont d'Urville, had CAPA values that were significant above the 90% level. The high significance of the CAPA at these three stations

focused our interest along the Wilkes Land coast from the Amery Ice Shelf to the Ross Ice Shelf. Of the CATA results, only the value at Amundsen-Scott after the SOI minimum was significant above the 90% level (actual 99%). The high significance at Amundsen-Scott further supported the findings of Savage *et al.* [1988] that South Pole is significantly colder in the year after a SOI minimum. The significance levels at Mawson, Scott Base, and Dumont d'Urville, the three focal stations, were all 50% or less. In regard to all the t-tests, however, we must agree with van Loon and Shea [1987], who state that, since only six SOI minima were available to create the composites, the statistical significance levels may be unreliable.

After finding the sign changes in the anomalies surrounding the SOI minimum, we looked for confirmation of the results by reconstructing the CATA and CAPA using all 24 temperature and 23 pressure records. These composites were not at all complete; because of missing data some did not even include all six SOI minima. However, the composites (not shown) were plotted as above and revealed the same sign changes across the SOI minimum as the 10 station composites. Furthermore, though there were some slight differences, the locations of the maxima and minima in the CAPA and CATA patterns found by the 10-station approach were confirmed when all the available data were used.

4.2. Midpoint Composites

For comparison with the SOI minimum composites above (Figure 6), Figure 7 presents the CAPA and CATA for the year before and after the midpoint between two SOI minima. The CAPA prior to the midpoint, shown in Figure 7a, revealed positive pressure anomalies over the entire continent except at Scott Base. During the year after the midpoint, the CAPA were still positive over the continent, including Scott Base (Figure 7b). Though the pattern of the anomalies changed, only Scott Base showed a sign change.

The CATA for the year before and after the midpoint are presented in Figures 7c and 7d, respectively. Before the midpoint the pattern was similar to the SOI minimum case (Figure 6c) except that negative anomalies crossed the center of the continent from Halley Bay to Dumont d'Urville and positive anomalies occurred in the regions on either side of the central cold anomaly. The CATA after the midpoint (Figure 7d) revealed a change in the overall pattern. The negative anomalies shifted toward Queen Maud Land, while positive anomalies dominated the rest of the continent. Hence the CATA for the midpoint had sign changes along with changes in the location of the anomaly centers. Across the SOI minimum the location of the CATA centers did not change significantly.

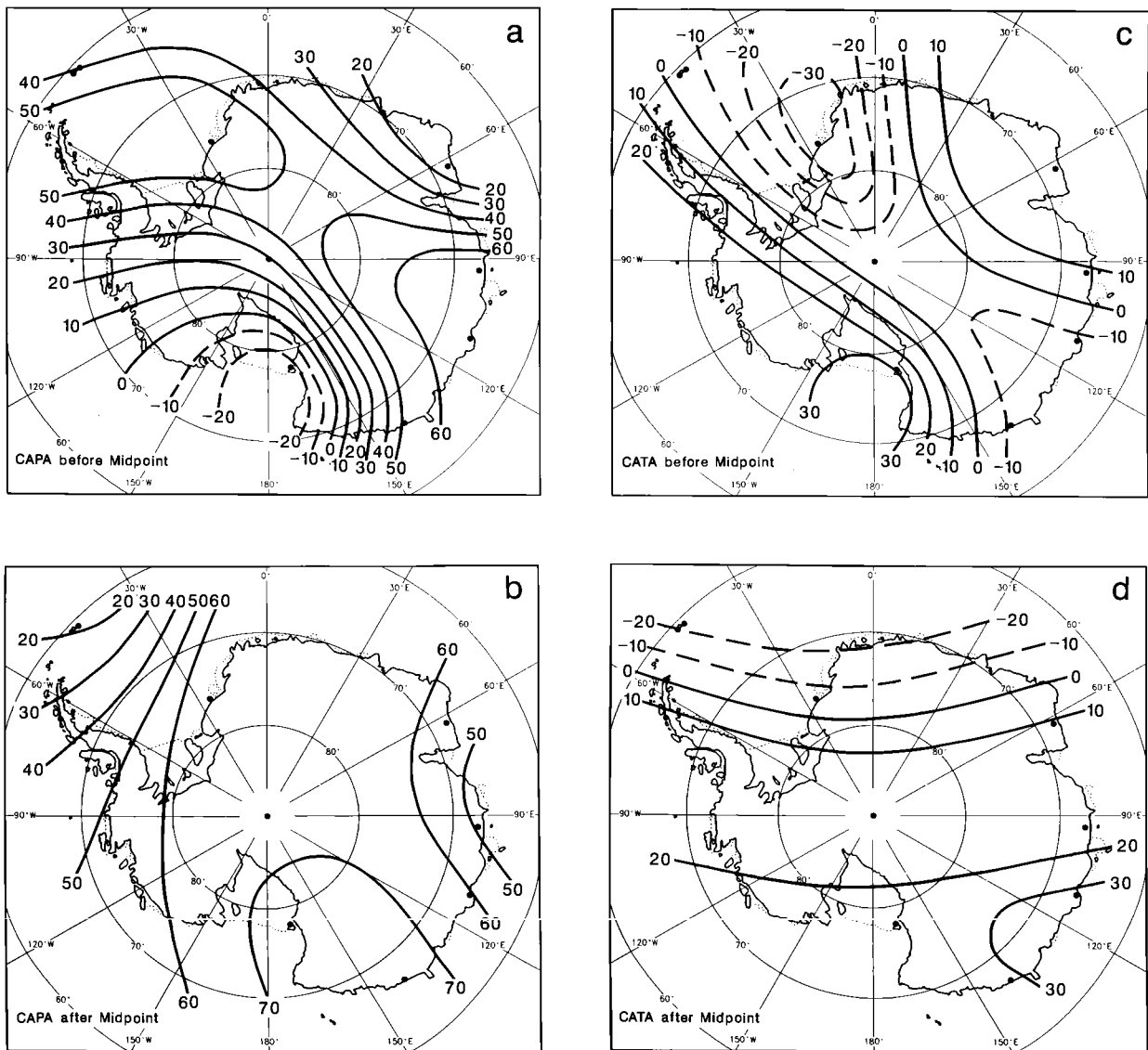


Fig. 7. Same as Figure 6, except composites were created around the midpoint between two SOI minima.

4.3. Three-Month Anomaly Composites

After revealing the sign change in the annual composites, we created the 3-month composite temperature and pressure anomalies to understand how the anomaly patterns evolved over the 24 months surrounding the SOI minimum. The CTA and CPA were calculated for the 3-month periods outlined in the methods section (Figure 5) and are presented in Figures 8a–8g and Figures 9a–9g, respectively. Recall that negative months occurred before the SOI minimum.

The CTA for the year before the SOI minimum are presented in Figures 8a–8d and begin with the –12 to –10 month period, which shows strong negative CTA

over Scott Base with weaker negative CTA covering the center of the continent. During the next three-month period (Figure 8b) the positive CTA strengthened over the Antarctic Peninsula, while the negative CTA weakened over the Ross Ice Shelf. The negative CTA over Amundsen-Scott warmed to become positive anomalies stretching all the way down to the coast at Dumont d'Urville. Meanwhile, the positive CTA found in the previous period near Casey became negative. The positive CTA over the south pole at –9 to –7 months (Figure 8b) split into two regions, one centered over the Antarctic Peninsula and the other over Dumont d'Urville, by the –6 to –4 month period (Figure 8c). The

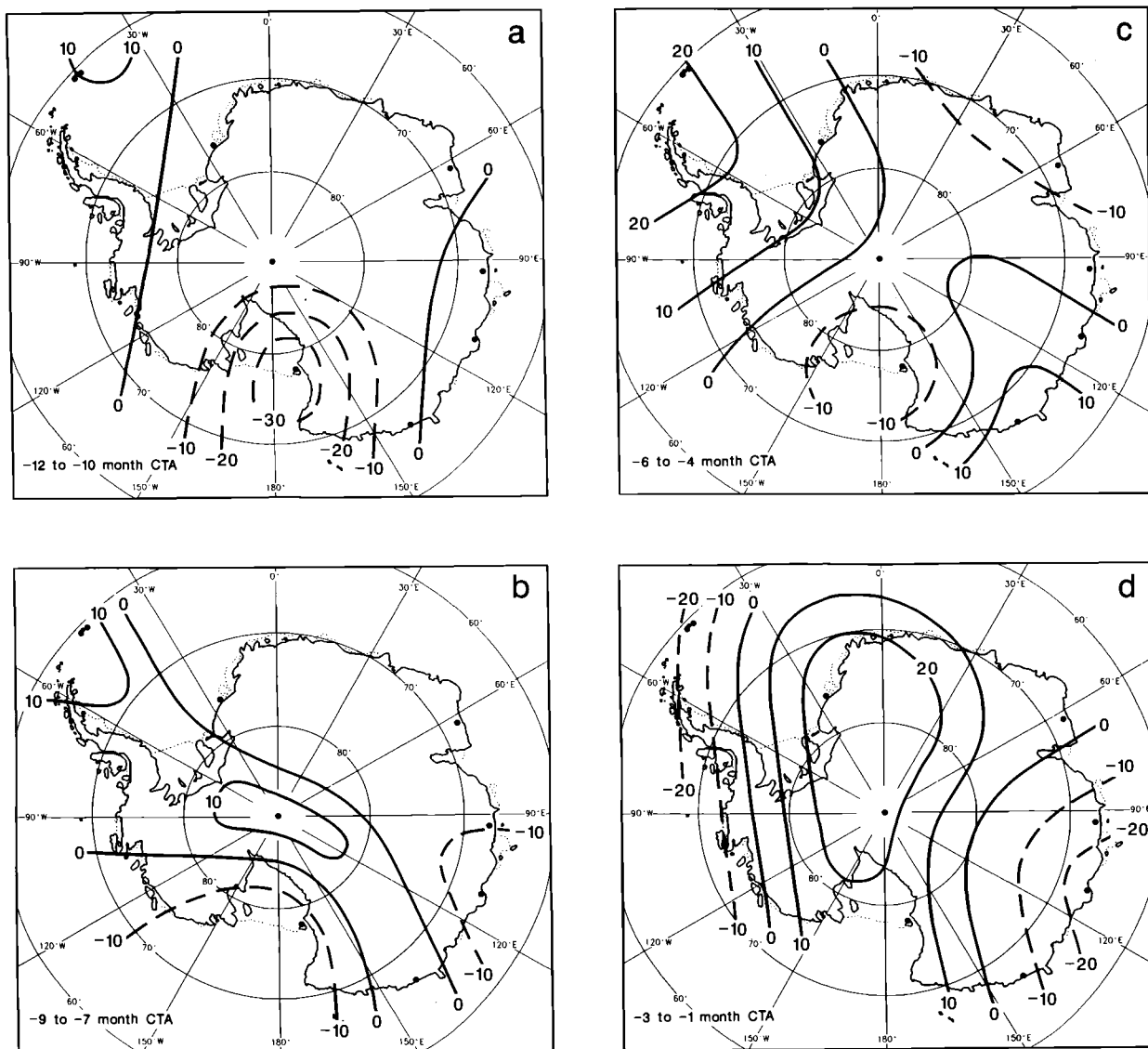


Fig. 8. Three-month CTA for (a) 12–10, (b) 9–7 (c) 6–4, and (d) 3–1 month periods prior to an SOI minimum and for the (e) 1–3, (f) 4–6, (g) 7–9, and (h) 10–12 month periods after an SOI minimum. Contour and unit conventions are the same as in Figure 6.

CTA minimum over Scott Base was still present, while the minimum that was near Casey drifted along the coast to Mawson Station.

Figure 8d reveals the result of a sharp discontinuity in the CTA pattern as the –6 to –4 month period (Figure 8c) evolved into the –3 to –1 month period. Most regions that had positive CTA in the previous 3-month composite now had negative values, and vice versa. For example, Scott Base and Mawson, colder than normal before (Figure 8c), had positive CTA in Figure 8d, while regions around the Antarctic Peninsula and Casey Station, warmer than normal before, now had negative anomalies.

The year after the SOI minimum began with the first 3 months having a weakening of the positive CTA over Amundsen-Scott and the negative CTA over the Antarctic Peninsula, resulting in negative CTA over the entire continent (Figure 8e). The only strong negative anomalies were along the Wilkes Land coast near Casey, and even these dissipated by the 4 to 6 month period (Figure 8f). The 4 to 6 month period was dominated by weak negative CTA over the entire continent, with two weak positive anomalies near Mirnyy and Halley Bay. The CTA amplified by the 7 to 9 month period (Figure 8g), creating a four-cell pattern with negative CTA over the Antarctic Peninsula and Casey

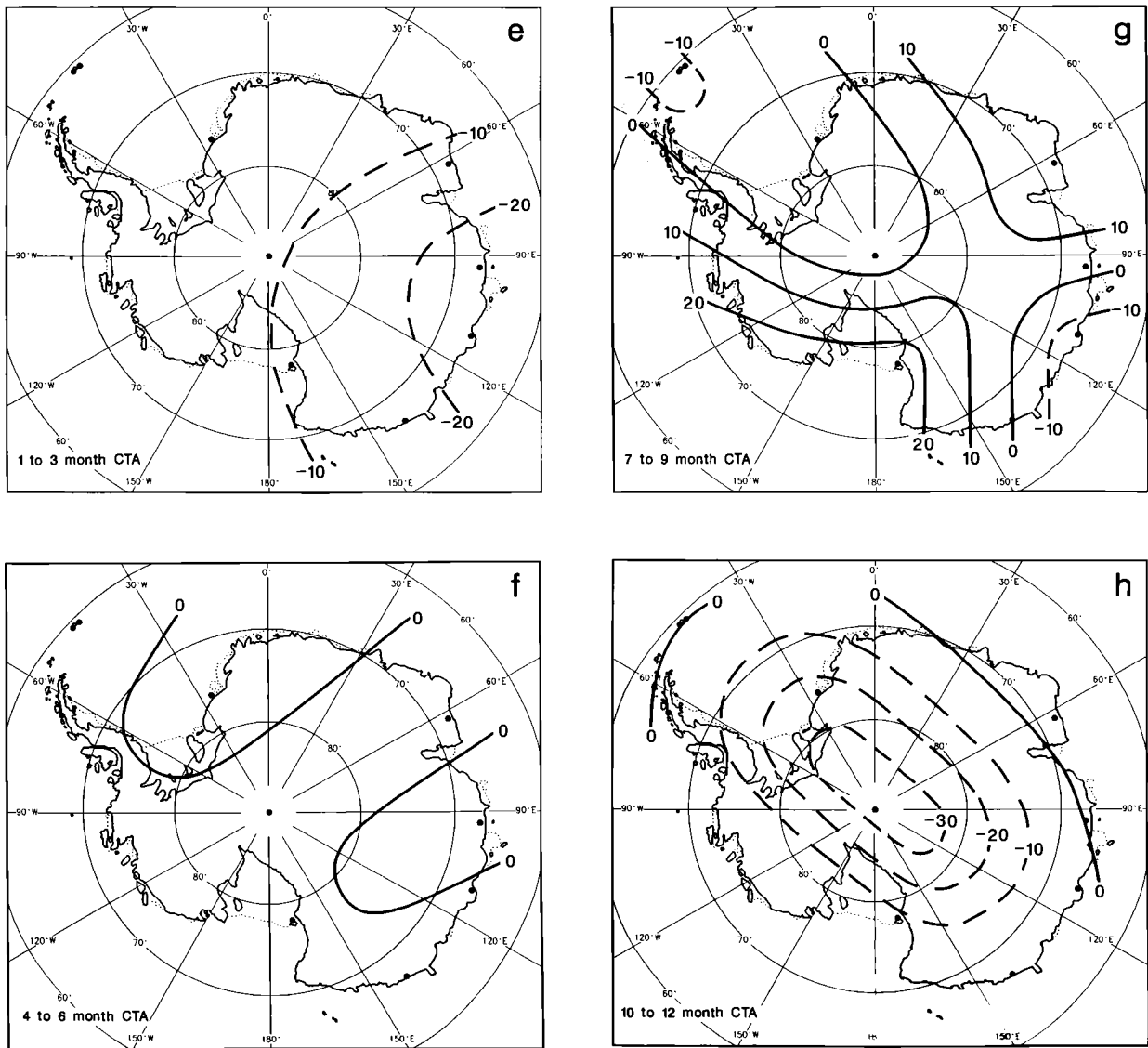


Fig. 8. (continued)

Station and positive CTA centered over Scott Base and Mawson. By the final 3-month period (Figure 8h) the negative CTA over the Antarctic Peninsula and Casey joined to form a single cell with strong negative CTA centered over Amundsen-Scott Station. The pattern of colder than normal temperatures over the south pole 10 to 12 months after the SOI minimum supported the findings of *Savage et al.* [1988].

The 3-month CPA for the year before the SOI minimum (Figures 9a to 9d) began with the continent being dominated by negative CPA (Figure 9a). The largest negative values stretched from Amundsen-Scott to Mawson, and the only positive CPA were near Dumont d'Urville and Casey. A sharp change in the sign of the

CPA occurred by the -9 to -7 month period (Figure 9b). The -9 to -7 month CPA pattern was dominated by positive anomalies with two maxima, one over Scott Base and the other near Halley Bay. The next six months (Figures 9c and 9d) were also dominated by positive CPA over much of the continent, with only one brief occurrence of negative anomalies over the Antarctic Peninsula during the -6 to -4 month period (Figure 9c).

The 3-month CPA in the year after the SOI minimum began with a second sharp change in the sign of the CPA. Figure 9e presents the 3-month CPA for months 1 to 3 and shows the continent dominated by a large area of negative CPA centered over Dumont d'Urville and stretching across the south pole toward Halley Bay.

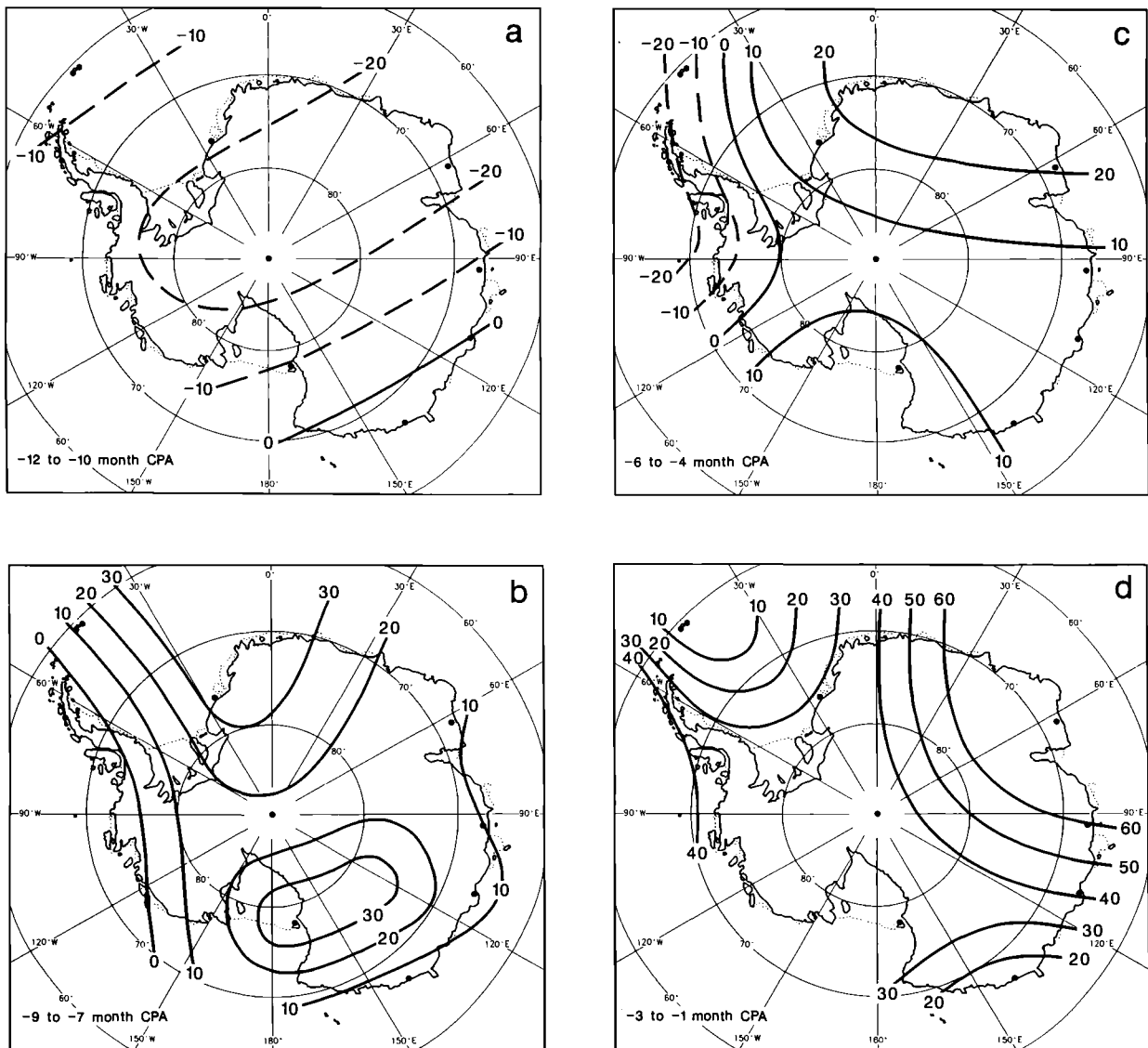


Fig. 9. Same as Figure 8 but for the 3-month CPA.

Negative CPA still covered the entire continent in the 4 to 6 month composite (Figure 9f); however, the negative anomalies weakened and the center moved toward Halley Bay and Signy Island. Figure 9g reveals that months 7 to 9 were dominated by positive CPA, the third sharp sign change in the CPA. Only Scott Base retained the negative CPA that controlled the 4 to 6 month composite. Finally, the 10 to 12 month composite (Figure 9h) presented yet another discontinuity in the pressure progression, with the continent returning to mostly negative CPA.

In summary, the 3-month CTA had smoother transitions from one period to the next than the CPA. Also, a distinct sign change occurred in both composite series

near the SOI minimum. For pressure the sign change coincided with the minimum, while for temperature the change occurred 3 months prior to the SOI minimum. Furthermore, the CATA and CAPA patterns for the SOI minimum can be seen in the 3-month CTA and CPA. During the four 3-month composites before the minimum, CTA over the Ross and Amery ice shelves were mostly negative, while positive CTA covered the center of the continent. The CPA were generally positive over the entire continent. Negative CPA dominated the continent for most of the 3-month periods after the SOI minimum, while a reversal of the CTA signs occurred in most cases over the Ross and Amery ice shelves and the center of the continent.

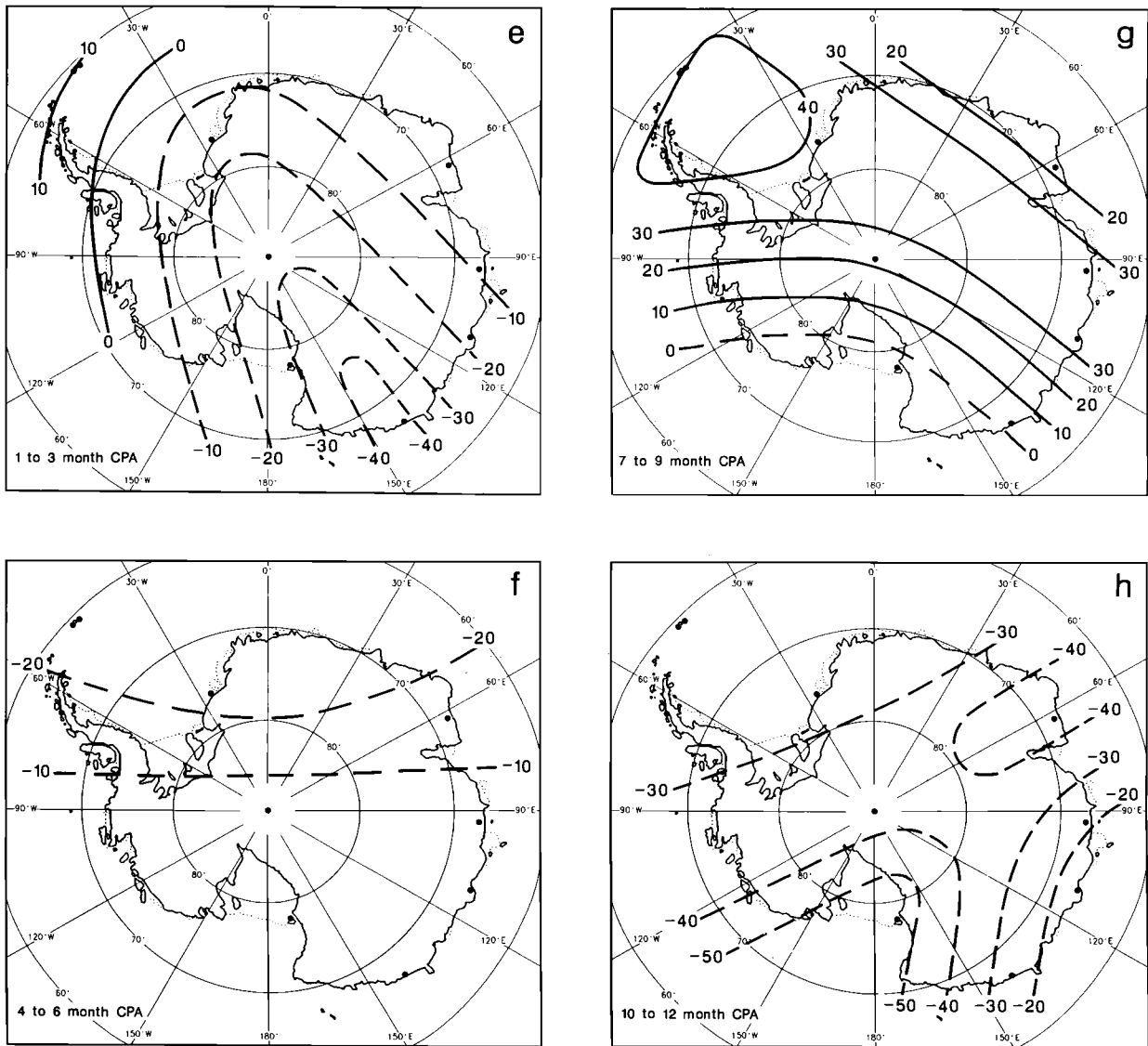


Fig. 9. (continued)

4.4. Event Anomalies

After analyzing the trends of the anomalies we tested the reliability of the composite patterns using the individual SOI minimum events. Figures 10a and 10b present the PAS for the 1963 event and reveal the pattern to be unlike the CAPA pattern for the SOI minimum, since the sign change was both regional and in the opposite direction. The PAS were mostly negative prior to the 1963 minimum (Figure 10a), with weak positive anomalies near Davis, Mirnyy, and Halley Bay. Figure 10b, the PAS after the 1963 minimum, reveals the regional sign changes. Unlike the PAS, the TAS before and after the 1963 event (Figures 10c and 10d, respectively) showed more similarities to the CATA patterns for the SOI minimum. The

main deviation from the CATA before the minimum (Figure 6c) was a less distinct positive anomaly pool over Amundsen-Scott in the TAS prior to the 1963 minimum (Figure 10c). The TAS pattern after the 1963 minimum (Figure 10d) was quite similar to the CATA pattern (Figure 6d), but the largest negative anomaly was located over General Belgrano Station instead of Amundsen-Scott.

Figure 11 presents the annual anomalies for the 1965 event. The 1965 event was controlled by positive PAS before the minimum (Figure 11a), and like the CAPA (Figure 6a and 6b) a sign change to mostly negative PAS occurred after the minimum (Figure 11b). There were some differences in the anomaly centers, but the general trend from positive to negative pressure anom-

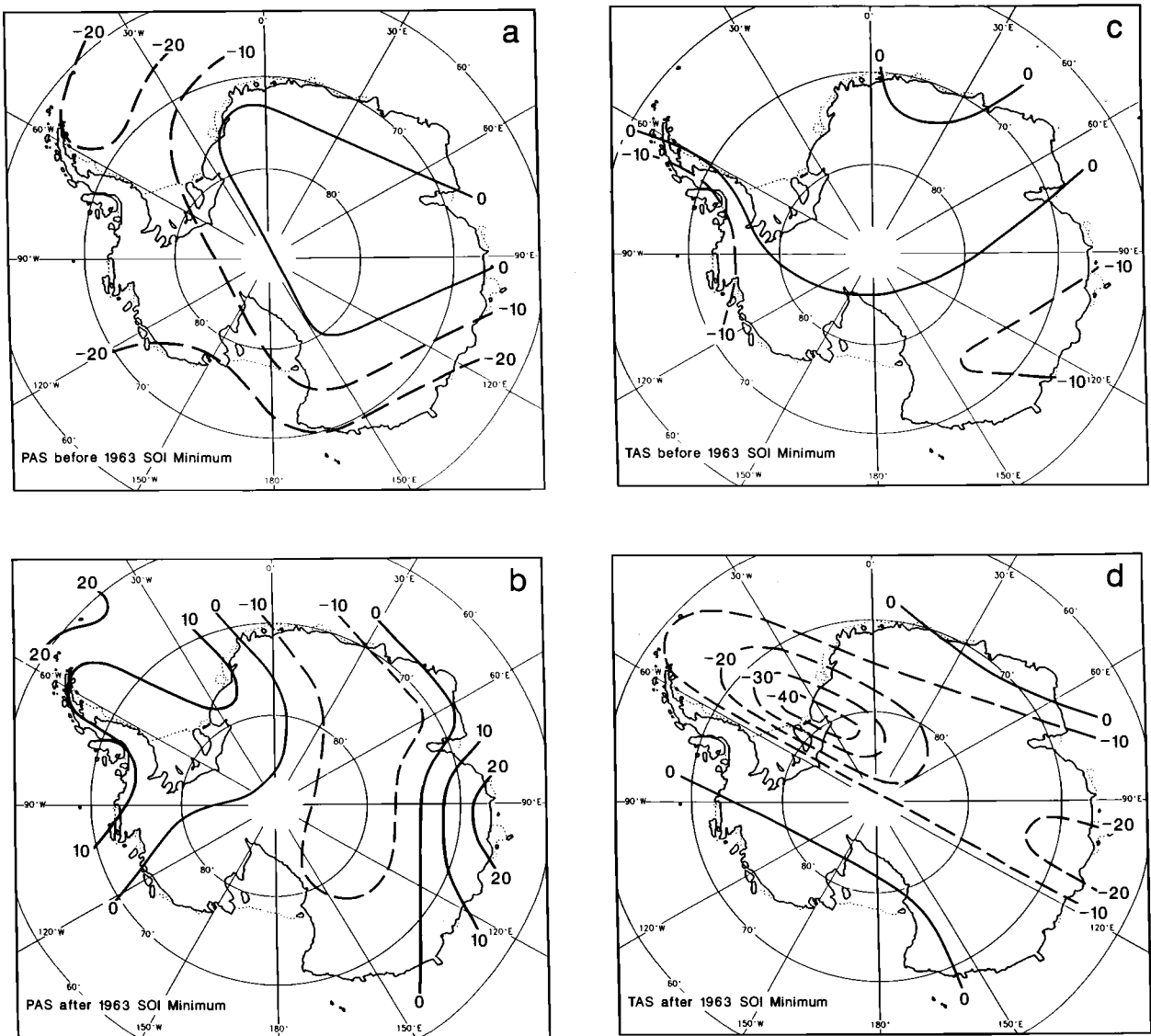


Fig. 10. Annual anomaly sums for the 1963 SOI minimum: (a) pressure before, (b) pressure after, (c) temperature before, and (d) temperature after. Contour and unit conventions are the same as in Figure 6.

alies was present. The TAS before the 1965 event (Figure 11c) had some similarities to the CATA before the SOI minimum and showed a region of positive anomalies over the western half of the continent from the Antarctic Peninsula to Byrd Station. These positive TAS resembled the positive CATA before the SOI minimum in location, but the positive TAS did not extend as far across the continent as the CATA (Figure 6c). After the 1965 minimum (Figure 11d) the resemblance to the CATA was less evident, since very few sign changes occurred in the TAS across the SOI minimum.

The PAS for the 1969 minimum, presented in Figures 12a and 12b, had sign changes and locations of anomaly

centers very similar to the CAPA. Prior to the minimum (Figure 12a) the PAS were dominated by positive anomalies with maxima near the Ross and Amery ice shelves and a relative minimum extending from the Antarctic Peninsula inland towards the south pole. The PAS changed sign to predominantly negative anomalies after the 1969 minimum (Figure 12b) with the largest negative values near Mawson and Scott Base. The 1969 TAS (Figures 12c and 12d) had some regional sign changes; however, only a few of the sign changes were in the same direction as the CATA for the SOI minimum, and the centers of the anomalies were much different from the CATA cases (Figures 6c and 6d).

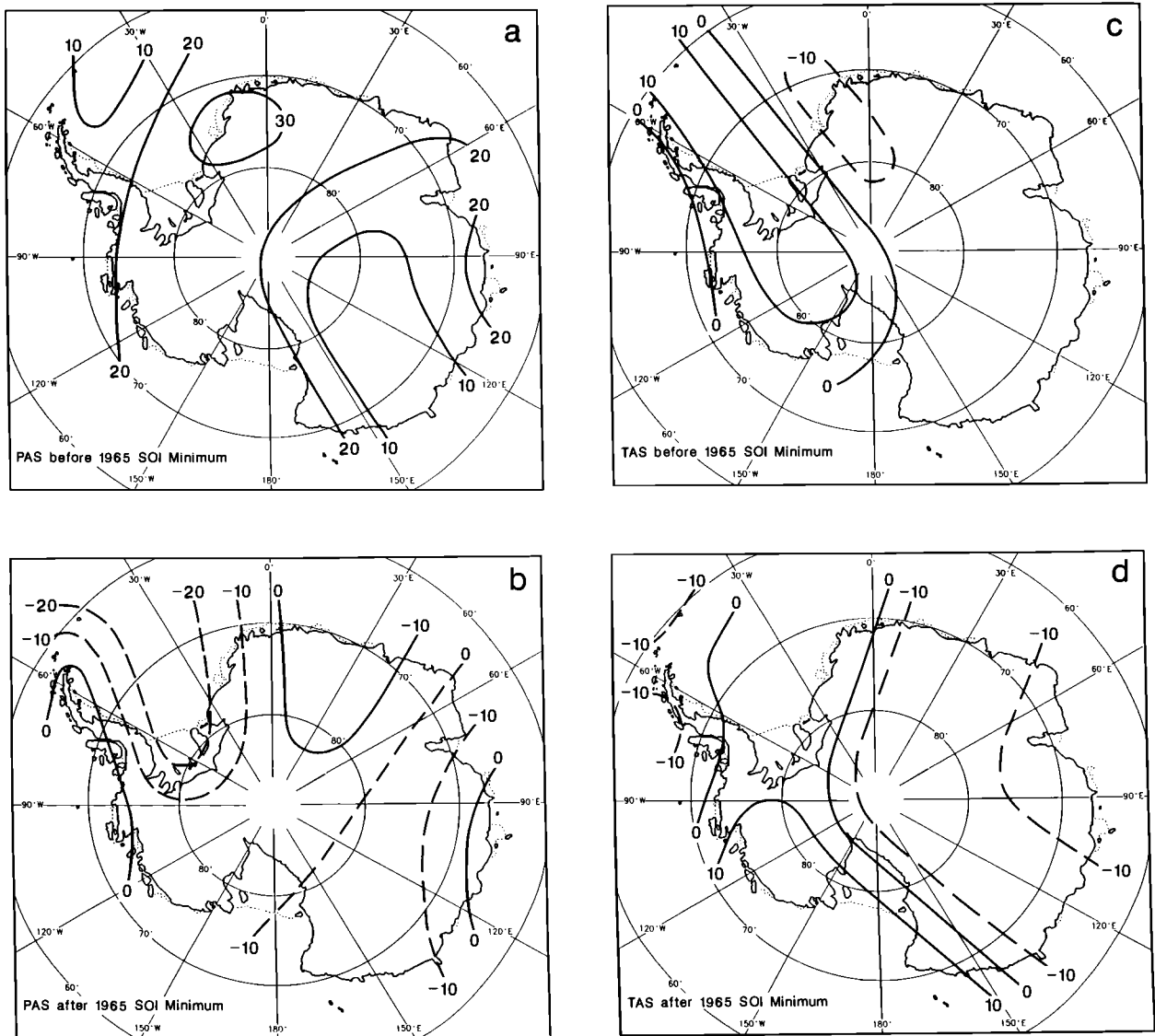


Fig. 11. Same as Figure 10 but for the 1965 SOI minimum.

Figures 13a–13d show the PAS and TAS for the 1972 event. The pressure anomalies switched from positive over the entire continent to mostly negative values over the continent after the 1972 SOI minimum (Figures 13a and 13b). Unlike the CAPA (Figures 6a and 6b), however, the centers of the anomalies were located over Halley Bay before and the Antarctic Peninsula after the 1972 minimum. The TAS for the 1972 SOI minimum (Figures 13c and 13d) were quite different from CATA (Figures 6c and 6d) because the locations of the TAS centers were different and very few sign changes occurred.

The 1977 minimum again showed a sign change from mostly positive PAS before the minimum (Figure 14a)

to mostly negative PAS afterward (Figure 14b), which agrees with the CAPA changes across the SOI minimum. Though the sign change was similar to the CAPA, the patterns of the PAS were much different from the CAPA. The TAS prior to the 1977 minimum, presented in Figure 14c, had a pattern similar to the CATA (Figure 6c). Positive anomalies extended from the Antarctic Peninsula toward Amundsen-Scott, and anomalies were low over the Ross Ice Shelf. However, after the 1977 minimum (Figure 14d), though some sign changes occurred, the pattern did not evolve into one similar to the CATA (Figure 6d).

The 1982 ENSO event had sign changes in the PAS that were opposite what was expected from the CAPA

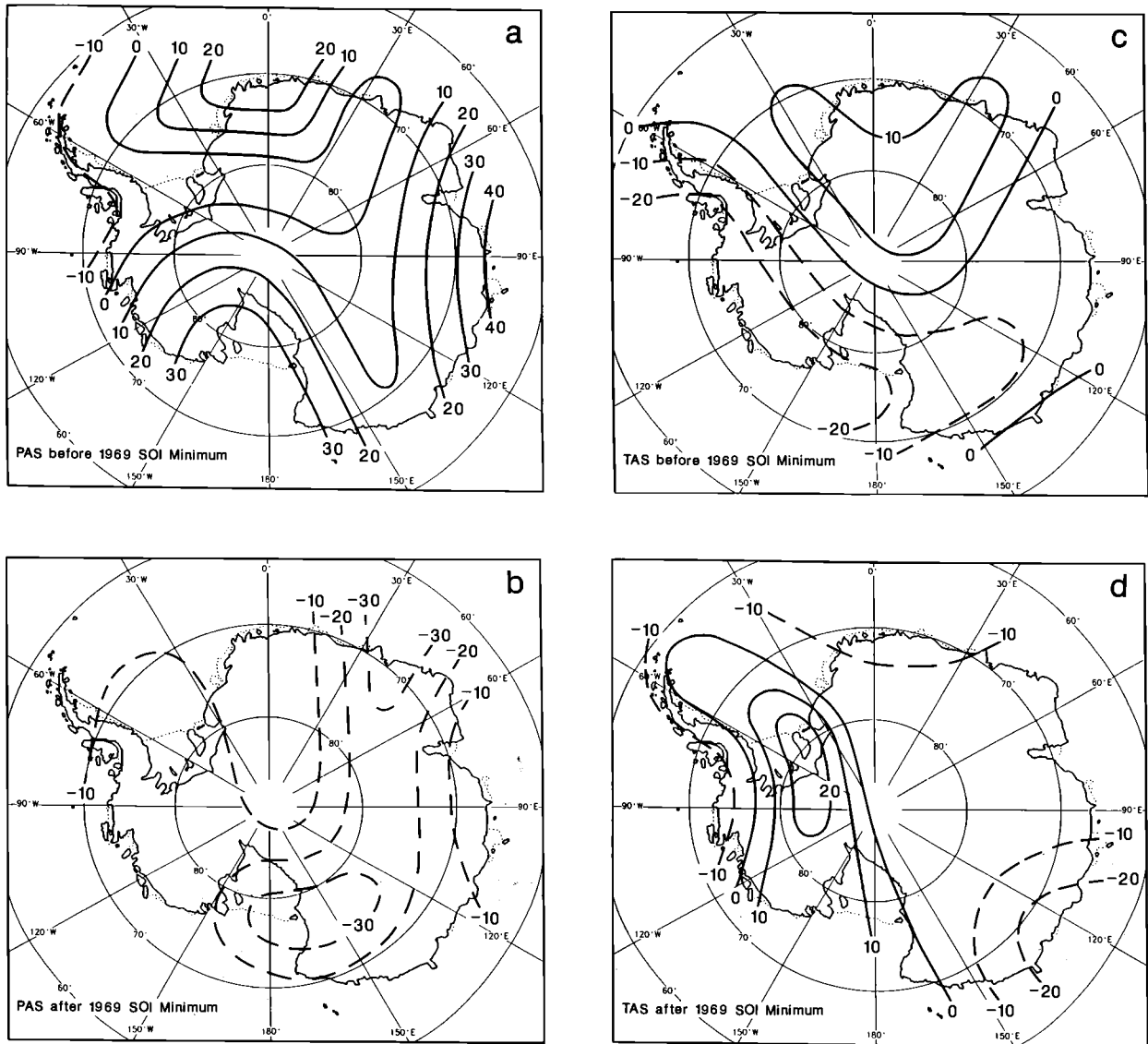


Fig. 12. Same as Figure 10 but for the 1969 SOI minimum.

(Figures 6a and 6b). Before the minimum (Figure 15a) the PAS were negative over the entire continent, and afterward (Figure 15b) the PAS changed to weak positive anomalies over much of the continent. The TAS before the 1982 minimum (Figure 15c) resembled more closely the pattern of the CATA before the minimum (Figure 6c), with positive anomalies over the Antarctic Peninsula and negative anomalies over Mawson and Scott Base. After the 1982 SOI minimum the TAS (Figure 15d) also showed similarities to the CATA after a minimum (Figure 6d), with positive anomalies over Mawson and Scott Base and negative values over Amundsen-Scott. One should note that the 1982 ENSO warm phase developed differently from the other five

minima presented [Rasmusson and Wallace, 1983] and this may be partially responsible for the PAS sign changes that were opposite what was expected from the CAPA.

5. DISCUSSION

We begin our discussion by expanding upon the dynamic link between Antarctica and ENSO, introduced in section 1, using the works of several authors. Next we use the CATA and CAPA results surrounding the SOI minimum to hypothesize how the temperature and pressure patterns found along the Wilkes Land coast may influence the New Zealand ridge and possibly link Antarctica and ENSO. Finally, we discuss the

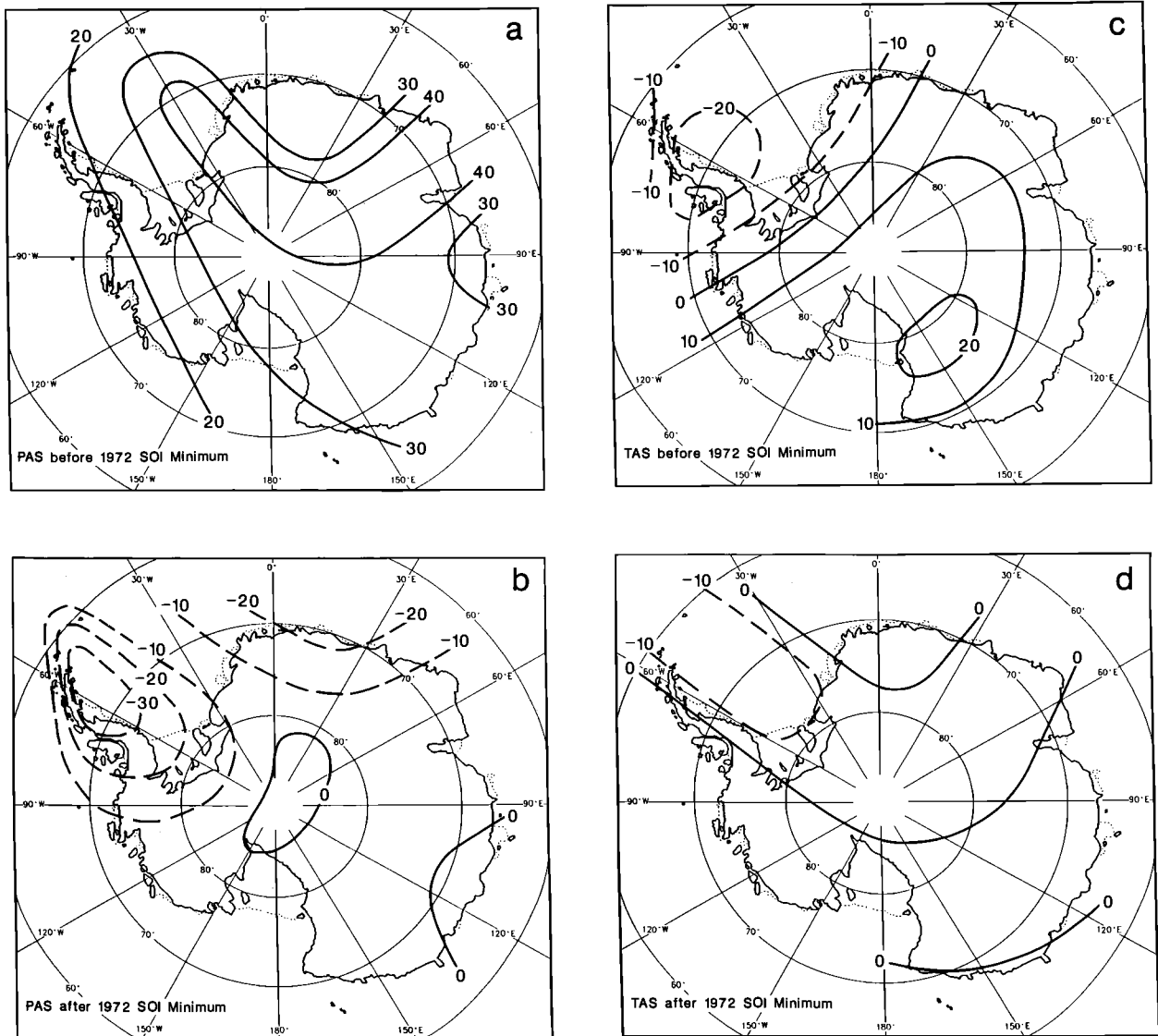


Fig. 13. Same as Figure 10 but for the 1972 SOI minimum.

CATA and CAPA surrounding the midpoint, the 3-month CTA and CPA, and the TAS and PAS along the Wilkes Land coast and show how they support the hypothesis.

5.1. Dynamic Link Between Antarctica and ENSO

James [1988] used a barotropic vorticity equation model to examine how the topography of different continents affected the mean tropospheric, planetary scale, Rossby wave patterns found in the climatology of the southern hemisphere. He concluded that the asymmetry of the Antarctic topography had the largest dynamic impact on the planetary scale Rossby wave patterns over the middle and high southern latitudes. More impor-

tant, James found the orography of Antarctica influential in forcing and maintaining a split flow in the tropospheric jet south of Australia. This split flow was the signature of a 500-mbar blocking pattern found in the climatology of the New Zealand region with a ridge extending south of New Zealand, near 160°E, toward the Antarctic coast and a trough reaching north over the Tasman Sea.

Earlier, Trenberth [1980] also concluded that the amplitude and phase of the mean 500-mbar planetary scale waves in the southern hemisphere were dynamically linked to the asymmetries of the Antarctic continent. Trenberth related the amplitude and phase of the mean planetary scale waves to the strength of the New Zealand blocking ridge and its associated trough, often a

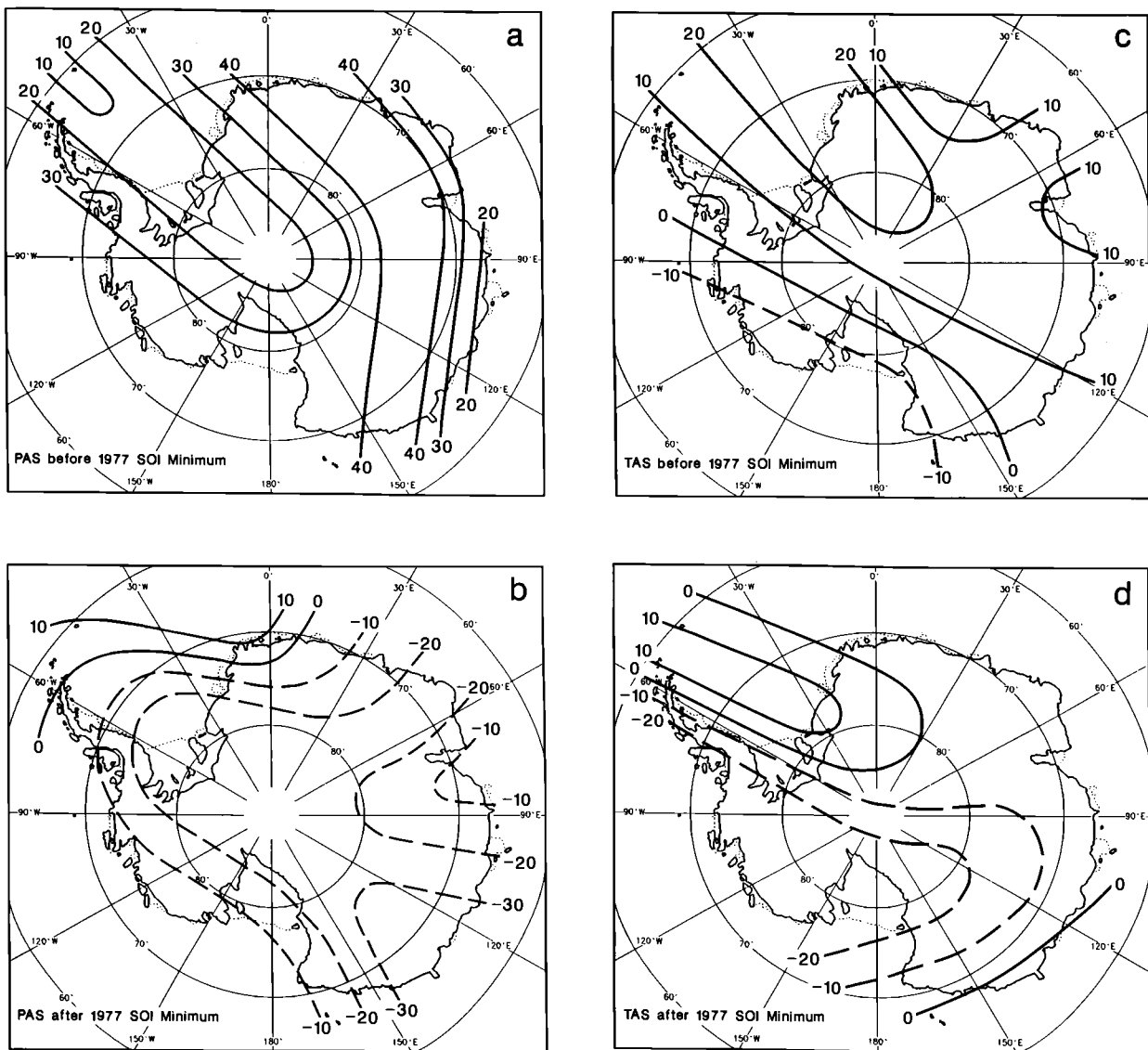


Fig. 14. Same as Figure 10 but for the 1977 SOI minimum.

cutoff low, located north of the ridge over the Tasman Sea. Furthermore, Trenberth noted that when the trough was a cutoff low, large precipitation and temperature anomalies occurred over eastern Australia, and he implied that these anomalies may influence the phase of the SO by changing the strength of the North Australian-Indonesian low.

Mo et al. [1987] further analyzed the cause of persistent New Zealand blocking in a case study for June 1982. The blocking ridge and its associated cutoff low in June of 1982 were located similarly to the climatological position discussed by *James* [1988], with the ridge

extending south of New Zealand to the Antarctic coast over Dumont d'Urville and a deep cutoff low over the Tasman Sea. Two troughs occurred upstream and downstream of the block near the Ross and Amery ice shelves at 160°W and 90°E, respectively. The resulting trough-ridge-trough pattern along the east Antarctic coast resembled the tropospheric pattern that *Trenberth* [1980] hinted may link ENSO to New Zealand blocking. Even though no link was mentioned by *Mo et al.* [1987], the June 1982 block occurred just 5 months prior to the minimum in the SOI associated with the 1982/1983 ENSO warm phase.

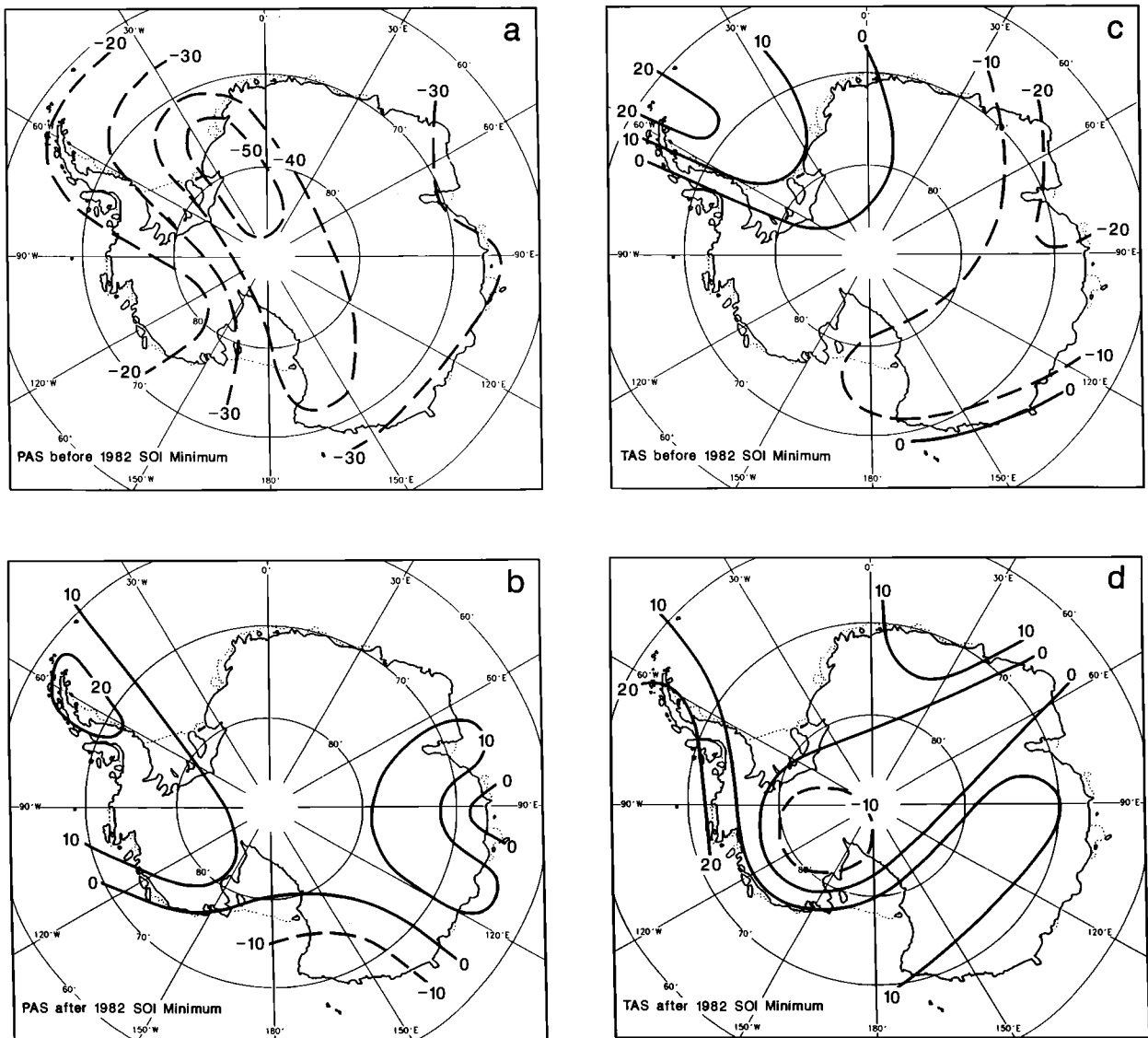


Fig. 15. Same as Figure 10 but for the 1982 SOI minimum.

Mo et al. [1987] were trying to determine what mechanisms in the southern hemisphere affected the strength and persistence of blocking near New Zealand. Using a general circulation model, they created a control forecast, reproducing the mean June 1982 blocking pattern, and then changed the forecast by altering the orography, sea surface temperature anomalies, and other regional heating inputs for the model. *Mo et al.* concluded that regional land-sea heating contrasts near Australia and cold air release from Antarctica were most important in maintaining the persistent blocking over the New Zealand region in June of 1982.

Summarizing, a general pattern of thermal forcing for

blocking near New Zealand, and possibly ENSO, can be outlined. As mentioned in the introduction, *Parish and Bromwich* [1987] showed that the orography of Antarctica concentrates the airflow to the coast in specific regions; thus one would expect the horizontal temperature patterns to be affected by the orography of the continent. The CATA results for the SOI minimum show that in two depressions in the topography, the Ross and Amery ice shelves, the temperature anomalies are similar, while the opposite anomalies occurred along the Wilkes Land coast. These horizontal differences in temperature along the Antarctic coast from 120°W to 60°E, likely related to the topography, may be respon-

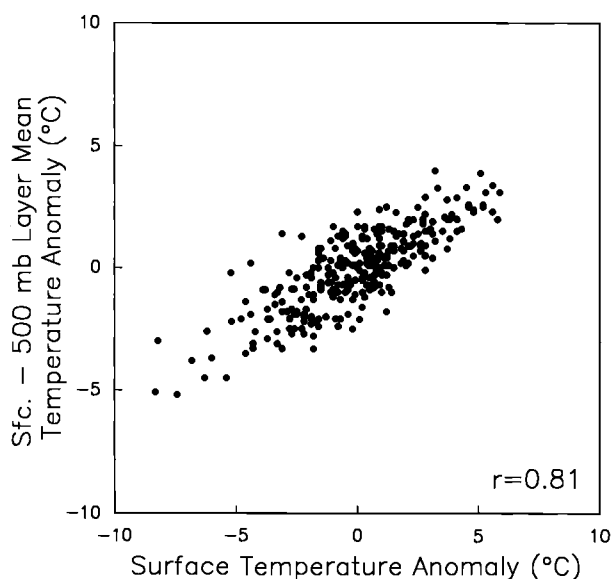


Fig. 16. One-to-one scatter plot: Surface temperature anomalies versus the surface to 500 mbar layer mean temperature anomaly for McMurdo Station. The correlation coefficient of 0.81 is significant at the 99.9% level.

sible for the cold air release from Antarctica which *Mo et al.* [1987] believe supported the development and persistence of the 1982 New Zealand block. Once formed, blocking near New Zealand could affect the strength of the SO through the cutoff low over the Tasman Sea sometimes associated with the block [*Trenberth*, 1980].

5.2. Thickness Hypothesis

Using the concept of the thickness of a layer, we now present a hypothesis on how the temperature differences found in the CATA results for the SOI minimum near the coast of Wilkes Land could result in the amplification of the normal trough-ridge-trough pattern to produce a strong ridge over Dumont d'Urville similar to the 1982 blocking described by *Mo et al.* [1987]. *Wallace and Hobbs* [1977] defined the thickness as

$$Z_2 - Z_1 = \frac{R_d \bar{T}_v}{g_0} \ln \left(\frac{P_1}{P_2} \right) \quad (1)$$

where $Z_2 - Z_1$ is the thickness between two layers with pressures P_2 and P_1 , respectively, R_d is the gas constant for dry air, g_0 is the globally averaged acceleration due to gravity at the Earth's surface, and \bar{T}_v is the mean virtual temperature of the layer. The thickness between two layers, P_1 and P_2 , is directly proportional to \bar{T}_v ; thus when \bar{T}_v is cold, the thickness is small, and when \bar{T}_v is warm, the thickness is large. Given \bar{T}_v and the

surface pressure field, an estimate of the geopotential heights can be made at a lower pressure surface, P_2 , using this proportionality.

Applying equation (1) to the CATA results required us to assume that \bar{T}_v for the entire air column, from the surface to 500 mbar, had the same sign as the temperature anomaly at the surface. This assumption was tested using 27 years of radiosonde data from McMurdo Station. Figure 16 presents a plot of the surface temperature anomaly versus the surface to 500 mbar layer mean temperature anomaly and reveals that the two time series have a high linear correlation, $r = 0.81$, that is significant at the 99.9% level. (Please refer to Appendix 2 for the methodology of the sounding analysis.) We calculated the least squares regression line for Figure 16 and found the relationship between the surface temperature anomaly (STA) and the surface to 500 mbar layer mean temperature anomaly (LMTA) to be

$$\text{LMTA} = -0.0027 + 0.52 \text{ STA} \quad (2)$$

Using equation (2) and the CATA results (Figures 6c and 6d), we estimated the value of the LMTA at Scott Base, Dumont d'Urville, and Mawson. The result was as expected: our LMTA always had the same sign as the STA. By adding the LMTA found using equation (2) to a surface to 500 mbar annual layer mean temperature calculated for the focal stations using the southern hemisphere climate atlas of *Taljaard et al.* [1969] we obtained estimates of \bar{T}_v .

Before we can show how the pressure and temperature anomalies affect the thickness pattern and the 500-mbar heights, we must know the normal pattern. Figure 17a shows a schematic cross section, looking to the south, of the normal conditions along the Antarctic coast from 120°W to 30°E. Note that the solid lines represent arbitrary pressure surfaces. The Ross and Amery ice shelves are characterized by low pressure at the surface and troughing aloft, while the region of Wilkes Land has higher surface pressures and ridging aloft [*Streten*, 1980; *Le Marshall et al.*, 1985]. Also plotted on all the schematics in Figure 17 are the locations of Scott Base (SB), Dumont d'Urville (DD), and Mawson (M) stations.

Now utilizing equations (1) and (2), and by applying the CAPA and CATA result before the SOI minimum (Figures 6a and 6c) to the 12-month mean pressure and temperature at the three focal stations before the SOI minimum, we created in Figure 17b a schematic of how the surface anomalies would affect the normal thickness pattern (Figure 17a) prior to the SOI minimum. Also, though the value of the 500-mbar heights calculated were very dependent upon the slope of the line in Figure 16, we found that the relative magnitudes of the heights from one station to another were unaffected. Therefore schematics are used in Figure 17 since the relative, not the actual, magnitudes were most important to our

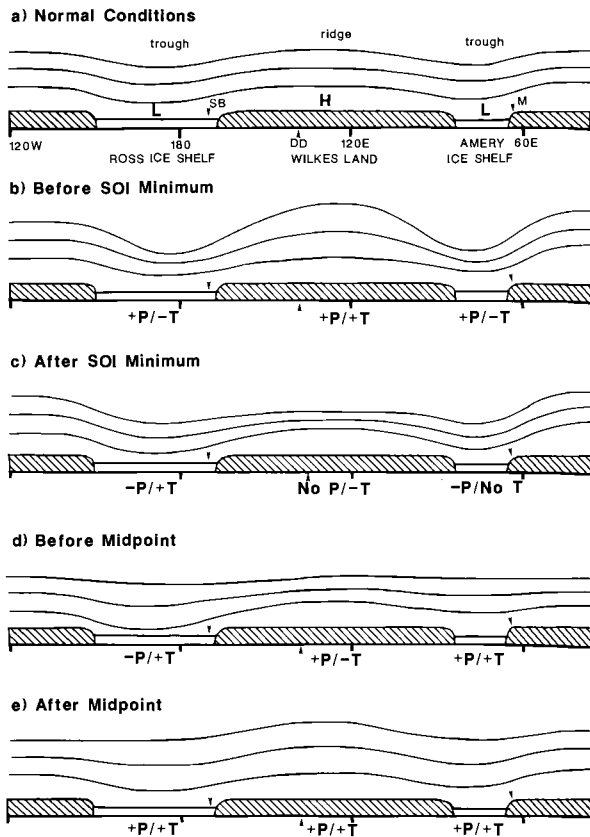


Fig. 17. Schematic representations of the thickness pattern along the coast of Antarctica from 120°W to 30°E. (a) Normal conditions. (b) Before the SOI minimum. (c) After the SOI minimum. (d) Before the midpoint between two SOI minima. (e) After the midpoint. Viewed looking south. The lines represent arbitrary pressure surfaces. Positive and negative CAPA (P) and CATA (T) are marked near the three key stations, Scott Base (SB), Dumont d'Urville (DD), and Mawson (M).

research. Since CAPA was positive (+P) over both ice shelves and Wilkes Land, no change occurred in the lowest pressure level. However, the negative CATA ($-T$) over the ice shelves resulted in cold \bar{T}_v and smaller thicknesses and thus deeper troughs over the ice shelves. Positive CATA (+T) over Wilkes Land similarly resulted in larger thicknesses and a stronger ridge aloft. In general, the anomalies present prior to the SOI minimum amplified the normal 500-mbar pressure pattern and created a strong trough-ridge-trough pattern in a location similar to that of the blocking ridge described by *Mo et al.* [1987]. Whether the pattern forced by our hypothesis forms a block or not is beyond the scope of this paper.

Through similar arguments, equations (1) and (2) can be applied to the CAPA and CATA after the SOI minimum (Figures 6b and 6d), resulting in a deepening

of the 500-mbar troughs over the ice shelves and a weakening of the ridge aloft of Dumont d'Urville. A schematic showing the conditions after the minimum is presented in Figure 17c. The negative CAPA ($-P$) over the ice shelves overwhelmed the weak warming and deepened both the surface lows and the 500-mbar troughs. Strong surface cooling ($-T$) and lower pressures ($-P$) at Dumont d'Urville resulted in cold \bar{T}_v values and smaller thicknesses; thus there was a pronounced decrease in the amplitude of the ridge aloft. In summary, the change in surface anomalies caused height falls at all three locations and resulted in a deepening of the troughs aloft of the ice shelves and a pronounced weakening of the ridge over the Dumont d'Urville region.

5.3. Applying Thickness Hypothesis to Other Observations

Applying equations (1) and (2) to the CAPA and CATA patterns before the midpoint between two SOI minima (Figures 7a and 7c) resulted in the thickness schematic in Figure 17d. The CAPA pattern would create a deeper surface low over the Ross Ice Shelf and weaken the surface low over the Amery Ice Shelf. Positive CAPA will also strengthen the surface high near Dumont d'Urville. However, the positive CATA over the ice shelves and the negative CATA over Dumont d'Urville would weaken both the lows over the ice shelves and the ridge over Wilkes Land with increasing height from the surface. The result would be the deamplification of the normal 500-mbar pattern which may actually be related to the formation of the cold phases of ENSO, three of which occurred in the years between the SOI minima used in this research.

The height calculations from equations (1) and (2) for the year after the midpoint between two SOI minima reveal changes in the thickness pattern that were opposite the SOI minimum case. Instead of having height falls at all three stations, as was found with the SOI minimum, height rises occurred at the three stations after the midpoint. The resulting pattern, shown in Figure 17e, had the ridge over Dumont d'Urville building and the troughs over the ice shelves weakening. The result of this rebuilding of the ridge may actually be the transition back to the stage found prior to the SOI minimum.

Further analysis of the thickness hypothesis was achieved by using the 3-month CTA and CPA (Figures 8 and 9) results to construct the evolution of the 500-mbar patterns. During the first 3-month period (Figures 8a and 9a), troughs would be forced at 500 mbar over the Ross and Amery ice shelves by colder temperatures and lower pressures at the surface. Meanwhile near-normal pressure and temperature anomalies near Dumont d'Urville would support the ridge aloft as expected by the composite annual anomalies. For the next 6 months

(Figures 8b–8c and 9b–9c), below-normal temperatures with positive pressure anomalies over the Ross and Amery ice shelves and above-normal temperatures and pressures present over Dumont d'Urville would still result in a trough-ridge-trough pattern at 500 mbar similar to Figure 17b and to that seen by *Mo et al.* [1987].

A temporary weakening of the 500-mbar troughs over the Ross and Amery ice shelves would occur for the –3 to –1 month period (Figures 8d and 9d), since the ice shelves had positive CTA and CPA. Meanwhile, the weakening of the ridge over Dumont d'Urville, due to negative CTA and positive CPA at the surface, also occurred in the –3 to –1 month period. The deepening of the troughs over the Ross and Amery ice shelves would return for months 1 to 6, as negative CTA and CPA occurred on these ice shelves. The ridge over Dumont d'Urville would likely continue to weaken, as negative CTA and CPA were found here as well. The ice shelf troughs would finally weaken during the final 6 months, when positive CTA and positive and negative CPA were found over the Ross and Amery ice shelves. Negative CTA and CPA dominated Dumont d'Urville for the final 6 months; thus the weak ridge continued. The resulting 500-mbar pattern for the final 6 months resembled Figure 17c. In general, the CTA and CPA patterns amplified the normal trough-ridge-trough pattern along the Wilkes Land coast in the year before the SOI minimum and deamplified the ridge over Dumont d'Urville after the minimum.

The above discussion shows that the evolution of the 3-month composite anomalies agreed fairly well with the thickness hypothesis. As a final test of the thickness hypothesis, 12-month PAS and TAS for each individual ENSO event were analyzed using equations (1) and (2). Applying the thickness hypothesis revealed that two of the six individual events, 1965 and 1969, would amplify the 500-mbar trough-ridge-trough pattern, similar to what is seen in Figure 17b along the Wilkes Land coast from 60°E to 150°W before the SOI minimum. The 1972 event showed amplification of the ridge before the SOI minimum, but the deepening of the ice shelf troughs was delayed. The 1977 event showed a delay in the amplification of the entire trough-ridge-trough pattern, while the 1982 and 1963 SOI minima only partially agreed with the thickness hypothesis.

The 1965 and 1969 ENSO events (Figures 11 and 12, respectively) had the best agreement to the hypothesis. Both had negative TAS and positive PAS over the Ross and Amery ice shelves and weak positive TAS and PAS near Dumont d'Urville before the SOI minimum. The result would be a weak ridge aloft near Dumont d'Urville with a trough both upstream and downstream, similar to the pattern in Figure 17b. A reversal of the anomalies over the Ross and Amery ice shelves and Dumont d'Urville would deepen the troughs over the ice

shelves and weaken the ridge aloft at Dumont d'Urville after both the 1965 and 1969 minima.

The 1972 event (Figure 13) had positive TAS and PAS over the Ross and Amery ice shelves and Wilkes Land before the 1972 minimum. This would result in weaker troughs or over both ice shelves; however, the ridge over Wilkes Land would amplify. After the 1972 minimum, weaker PAS and TAS values would deamplify the ridge and result in a deepening of the ice shelf troughs, as temperatures and pressures there are nearly normal.

The 1977 warm event had a slow evolution that partially resembled the composite pattern before the minimum and looked like Figure 17b after the 1977 minimum. Before the 1977 minimum (Figures 14a and 14c), negative TAS and positive PAS were found over Scott Base, and a positive TAS and PAS occurred over the Amery Ice Shelf and Dumont d'Urville. The result would be a stronger trough at 500 mbar over the Ross Ice Shelf, a stronger ridge over Wilkes Land, and a weaker trough over the Amery Ice Shelf. However, after the 1977 minimum (Figure 14), negative TAS and PAS were present over both the Ross and Amery ice shelves, and positive TAS were still found over Dumont d'Urville. The result would be a trough-ridge-trough 500-mbar pattern similar to Figure 17b. The slow evolution of the 1977 minimum, with the pattern expected before the minimum actually occurring after the minimum, may be partially responsible for the 1977 event having the longest period of negative SOI values (Figure 4).

The 1963 minimum was the first of two that did not fit the thickness hypothesis well. Before the 1963 event the negative TAS and PAS over the Ross Ice Shelf and Wilkes Land would create a deep trough over the Ross Ice Shelf and a very weak ridge or trough aloft at Dumont d'Urville. Positive PAS and zero to negative TAS over the Amery Ice Shelf would probably form a weak trough there as well. Troughing would still dominate aloft of Wilkes Land due to negative TAS and zero PAS near Dumont d'Urville after the 1963 minimum.

The 1982 ENSO warm phase (Figure 15) had negative TAS and PAS over the Ross and Amery ice shelves which produced deep troughs at 500 mbar using the thickness argument, since surface pressures were normally low (Figure 17a). Before the 1982 event the annual anomalies were strong: –28°C and –21 mbar anomalies at Mawson and –17°C and –43 mbar anomalies at Scott Base. These strong 1982 anomalies may be responsible for forcing deep troughs over the ice shelves; however, the TAS at Dumont d'Urville were not very warm, and formation of a strong ridge over Wilkes Land is problematic.

In summary, the 1965, 1969, and 1972 events all support the amplification of the 500 mbar trough-ridge-trough pattern along the coast of east Antarctica before their minima, with only a few subtle differences from the composite patterns. These three events also all show the weakening of the ridge aloft of Dumont d'Urville in the

year after the SOI minimum. The 1977 minimum has a slow evolution but results in a pattern like Figure 17b after the minimum. The 1982 event showed amplification of the ice shelf troughs, but the weak temperature anomalies do not make it clear whether the ridge over Dumont d'Urville will amplify. Finally, the 1963 minimum showed some aspects of the composite patterns, but total agreement did not occur at all three stations. The 1963 and 1982 events reveal that the thickness hypothesis for linking Antarctic climate through the New Zealand block to ENSO may be part of the dynamic link; however, there are many other variables that our research cannot begin to cover.

6. SUMMARY AND CONCLUSIONS

The focus of our research was the search for a link between ENSO and the Antarctic climate record. Using the SOI to represent the phase of ENSO and monthly pressure and temperature anomalies to represent the climate of Antarctica, we were able to arrive at the following results:

1. Compositing the pressure and temperature anomalies for a year before and a year after the SOI minimum revealed that distinct sign changes occurred in the anomalies surrounding the minimum. The pressure anomalies showed a change from positive anomalies before the minimum to negative anomalies after the minimum over most of the continent. The temperature anomalies before the minimum were more regional, with the Ross and Amery ice shelves having negative anomalies, while the center of the continent from the Antarctic Peninsula to Dumont d'Urville had positive anomalies. The signs of the temperature anomalies changed within these regions after the minimum, with the positive anomalies turning negative and the negative anomalies turning positive.

2. Composites of the climate anomalies surrounding the midpoint between two SOI minima did not result in the coherent sign changes observed for the SOI minimum composites.

3. Three-month anomaly composites for the 24 months surrounding the SOI minimum revealed that the evolution of the anomaly patterns had smoother transitions for the temperature than for the pressure anomalies. However, both the pressure and the temperature 3-month anomaly composites showed a distinct sign change within 3 months of the SOI minimum.

A hypothesis was formed using our results and the work of several authors to relate the different temperature and pressure anomalies present along the Wilkes Land coast to the 500-mbar flow and possibly to ENSO. By simple thickness arguments we showed that the CATA and CAPA anomalies present before the SOI minimum would strengthen a trough over the Ross and Amery ice shelves and a ridge aloft near Dumont d'Urville. This amplified trough-ridge-trough pattern

resembled the 500-mbar flow discussed by *Mo et al.* [1987] which contained a block over the New Zealand region. *Mo et al.* concluded that the New Zealand block was partially forced by cold air releases from Antarctica. *Parish and Bromwich* [1987] showed that flow from Antarctica was shaped by the topography of the continent and would be concentrated along the Wilkes Land coast and on the Ross and Amery ice shelves. The presence of the New Zealand block was noted by *James* [1988] and *Trenberth* [1980], both of whom stated that the southern hemispheric 500-mbar flow was forced primarily by Antarctic topography, and *Trenberth* [1980] hinted that the cutoff low associated with the New Zealand block may influence the western branch of the SO. Therefore we conclude that the horizontal differences in temperature, likely created by topographical differences, before the SOI minimum in Antarctica may be responsible for maintaining the New Zealand block and its associated cutoff low; thus the Antarctic climate affects ENSO.

Other results supported the thickness hypothesis relating ENSO to the Antarctic climate. First, the thickness hypothesis can be used to explain why the ridge over Dumont d'Urville weakens after the SOI minimum using the CAPA and CATA results after the SOI minimum. Second, applying the thickness hypothesis to the CAPA and CATA surrounding the midpoint between two SOI minima will weaken the normal 500-mbar pattern and the ridge near New Zealand, which may in fact be linked to an ENSO cold phase. Third, the 3-month CTA and CPA results supported the trough-ridge-trough pattern before the SOI minimum and showed a decay of the pattern afterward. Finally, the thickness hypothesis adequately explains the evolution of four of the six SOI minima and partially explains the evolution of two other warm events in our period of record. The fact that it does not work for all six warm events shows that our hypothesis is far from the whole solution to a complex problem.

This research is just a preliminary study of a complex system, and there are many avenues open for further investigation of the relationships between the ENSO and Antarctic climate. First, the source of the differential temperature patterns along the Antarctic coast need to be identified along with how they relate to the topography of the continent. Second, broader scale studies of the southern hemispheric upper air patterns are needed to determine if a block occurs near New Zealand before all ENSO events. Further analysis of the radiosonde data would result in better estimates of \bar{T}_v for the thickness analysis and reveal if the assumption used for \bar{T}_v in this study is valid. Finally, the relationships between New Zealand blocking, cutoff lows over the Tasman Sea, and the Southern Oscillation need in-depth study. We are presently undertaking an analysis of the southern hemispheric 500-mbar height fields that we hope will answer some of these questions.

APPENDIX 1

This appendix gives a sample of the error corrected monthly mean pressure and temperature values for the 24 stations presented in Figure 1. The temperature units are degrees Celsius and the pressure units are millibars. The value '444.0' represents missing data in both the temperature and pressure data. Even though the McMurdo pressure data were discarded from our research, the data are included in the data set for others to analyze. Also included in the header for each tempera-

ture record are the station's World Meteorological Organization number, latitude in degrees south, longitude in degrees east or west, and elevation in meters. The complete data set is available in its entirety on the disk (ASCII format) enclosed inside the back cover of this book or as paper copy from C. R. Stearns, 1225 West Dayton Street, Madison, Wisconsin 53706 (telephone 608-262-0780; email chucks@ssec.wisc.edu). Alternatively, a paper printout or disk may be requested from C. R. Stearns.

SCOTT BASE	Temperature	WMO#:89665	Lat:77.85	Lon:166.75E	Elev:16
1957	444.0 444.0 -19.8 -27.1 -27.2 -26.2 -30.2 -27.6 -24.5 -22.9 -9.8 -4.6				
1958	-4.0 -7.9 -21.0 -23.9 -29.7 -28.8 -35.6 -32.6 -29.2 -22.4 -11.6 -7.2				
1959	-4.8 -12.2 -19.7 -23.1 -29.2 -26.6 -26.6 -35.0 -26.9 -28.6 -14.8 -3.6				
1960	-8.8 -15.7 -24.6 -26.4 -27.4 -28.2 -31.2 -31.3 -25.4 -19.2 -13.2 -7.4				
1961	-4.3 -9.4 -21.0 -19.4 -24.2 -26.2 -33.7 -32.8 -25.0 -24.6 -10.9 -6.8				
1962	-5.5 -12.5 -26.6 -23.3 -26.2 -25.4 -31.2 -32.3 -33.2 -25.8 -13.0 -6.6				
1963	-5.7 -11.6 -23.1 -27.4 -30.2 -25.0 -29.6 -28.8 -25.8 -21.6 -10.1 -5.6				
1964	-6.8 -12.8 -20.8 -22.2 -29.5 -22.4 -24.2 -35.3 -26.2 -21.3 -10.2 -5.3				
1965	-4.3 -10.2 -24.1 -23.6 -33.5 -31.2 -24.6 -27.2 -27.4 -21.3 -11.0 -3.7				
1966	-6.6 -9.3 -13.0 -24.2 -32.1 -21.9 -26.1 -32.1 -29.5 -21.2 -12.2 -5.1				
1967	-2.9 -6.6 -20.2 -27.2 -25.7 -24.2 -27.7 -25.5 -28.4 -25.1 -12.9 -5.0				
1968	-4.9 -9.4 -16.5 -23.8 -28.1 -27.8 -30.0 -33.9 -37.8 -22.1 -12.7 -6.3				
1969	-4.9 -10.9 -18.8 -25.4 -27.7 -28.4 -35.4 -29.1 -29.2 -23.4 -11.7 -3.8				
1970	-3.2 -9.5 -15.0 -22.3 -27.1 -24.5 -30.3 -33.5 -27.0 -17.7 -13.5 -4.0				
1971	-1.6 -10.4 -20.8 -19.2 -24.6 -26.4 -31.8 -30.4 -23.2 -23.5 -11.6 -5.5				
1972	-5.6 -9.6 -18.1 -26.9 -24.5 -22.5 -26.7 -27.7 -24.7 -19.5 -12.3 -4.7				
1973	-5.0 -13.2 -23.6 -24.5 -25.1 -26.1 -26.9 -26.5 -26.1 -17.2 -9.8 -5.8				
1974	-3.6 -10.4 -21.5 -22.5 -22.6 -24.0 -31.5 -25.0 -32.5 -18.7 -10.2 -3.8				
1975	-4.7 -10.2 -19.4 -24.8 -23.6 -25.1 -27.3 -30.2 -24.2 -21.6 -12.8 -6.6				
1976	-4.7 -10.7 -20.6 -28.2 -31.6 -33.3 -25.7 -32.8 -30.0 -31.9 -13.1 -4.3				
1977	-3.0 -13.3 -23.4 -26.0 -25.9 -27.6 -25.4 -26.8 -34.7 -23.1 -14.5 -7.5				
1978	-8.4 -10.9 -17.1 -23.9 -26.1 -26.3 -31.3 -41.5 -28.1 -23.5 -12.5 -6.4				
1979	-5.4 -9.8 -20.7 -21.4 -29.3 -24.1 -33.3 -34.8 -27.4 -25.9 -10.8 -4.9				
1980	-5.4 -10.0 -19.9 -21.7 -22.2 -28.5 -26.0 -25.8 -27.7 -21.5 -10.9 -3.6				
1981	-4.9 -10.6 -15.3 -27.2 -25.8 -23.0 -25.3 -28.4 -31.7 -23.8 -14.1 -4.8				
1982	-4.4 -9.9 -24.4 -28.4 -28.1 -29.1 -33.0 -26.1 -31.3 -22.4 -10.2 -3.3				
1983	-4.9 -13.7 -20.5 -18.4 -18.1 -28.6 -30.7 -28.9 -28.2 -21.4 -11.7 -5.1				
1984	-4.4 -12.5 -17.7 -20.6 -21.7 -25.4 -27.0 -30.7 -28.1 -19.1 -10.8 -2.8				
1985	-2.5 -13.1 444.0 -24.7 -24.8 -25.5 -35.7 444.0 -28.0 -21.4 -12.8 -4.7				
1986	-4.8 444.0 444.0 -29.1 444.0 -24.8 444.0 444.0 444.0 444.0 444.0 444.0				
1987	-1.9 -12.3 -22.6 -25.3 -25.0 -23.1 -26.1 -30.5 -25.1 -20.9 -12.5 -3.5				
1988	-4.4 -12.5 -22.7 -22.3 -23.2 -23.9 -28.0 -20.9 -22.2 -15.4 -12.1 -5.1				
1989	-4.0 -14.1 -18.9 -21.1 -27.5 -32.2 -27.0 -29.7 -26.5 444.0 444.0 444.0				

SCOTT BASE	Pressure
1957	444.0 444.0 998.5 995.9 997.9 999.3 989.4 992.2 985.6 990.3 991.6 1000.4
1958	993.0 992.8 999.1 1000.0 996.0 1000.0 996.9 991.3 981.5 985.4 987.3 988.1
1959	993.2 991.0 990.7 996.8 997.7 997.2 995.0 998.7 982.4 988.2 981.7 992.8
1960	993.2 992.2 983.8 994.3 989.5 987.6 986.4 994.1 980.4 983.6 988.9 987.8
1961	991.4 1000.1 998.6 990.9 995.5 995.5 990.7 988.5 993.5 983.4 986.8 985.2
1962	987.4 992.1 994.1 985.2 986.9 999.5 988.2 989.8 994.2 984.4 990.8 988.3
1963	986.5 988.6 992.4 991.6 994.1 987.0 989.3 1005.8 990.6 982.8 979.9 991.8
1964	1000.8 994.9 992.0 986.3 979.7 996.2 1004.8 1000.6 978.9 981.0 992.4 994.7
1965	994.9 1004.6 992.2 988.5 1003.1 994.2 992.2 988.2 989.2 987.6 981.7 995.9

1966	991.6	994.2	998.0	992.6	1000.9	985.5	997.8	979.5	982.8	976.1	988.4	994.1
1967	1000.2	996.8	993.7	997.1	993.8	990.8	991.6	981.8	986.6	985.2	994.6	992.6
1968	992.7	993.1	994.8	989.3	1002.2	992.9	983.8	992.6	992.3	989.2	993.2	993.3
1969	1003.0	994.4	991.1	997.5	994.3	1004.6	985.5	981.0	988.5	989.3	985.6	991.2
1970	989.0	989.7	989.1	994.4	985.3	987.8	996.4	977.8	991.8	987.1	987.9	996.7
1971	995.5	989.4	988.3	989.5	998.2	989.4	995.4	994.8	986.6	992.0	988.3	996.9
1972	1001.8	993.7	996.2	1001.6	993.7	998.5	994.8	996.3	988.9	977.5	983.6	995.7
1973	998.9	993.4	986.4	993.4	1000.0	995.2	989.9	983.9	985.9	981.3	988.9	987.2
1974	997.2	985.1	988.7	988.6	992.6	1000.2	993.0	1001.3	984.3	986.4	994.0	996.3
1975	998.4	992.6	993.3	987.8	1001.0	996.1	997.2	987.1	979.8	981.8	989.3	996.9
1976	998.5	992.5	990.0	986.6	993.4	994.7	992.6	987.6	983.4	985.8	992.8	1007.1
1977	999.6	994.5	994.4	995.7	993.1	996.9	990.6	993.9	984.8	978.4	983.1	993.1
1978	991.9	991.1	991.6	995.1	991.8	993.1	1003.6	986.5	986.2	984.5	989.0	991.0
1979	991.5	990.4	986.3	989.3	989.7	984.9	980.9	991.8	984.8	986.2	988.8	997.2
1980	995.6	996.0	994.1	996.6	991.9	987.3	997.6	992.8	996.9	980.0	997.3	992.3
1981	991.3	994.1	996.3	998.0	992.6	984.7	993.5	1001.5	994.7	987.5	982.6	984.3
1982	996.2	992.4	984.0	986.6	992.9	986.8	995.7	981.7	983.0	986.0	990.1	1000.5
1983	998.3	1001.1	992.0	986.2	991.6	994.9	987.8	983.7	990.2	976.3	979.1	991.1
1984	1000.0	995.8	985.3	986.0	994.3	987.1	982.4	991.1	987.9	979.4	984.3	998.1
1985	444.0	444.0	444.0	444.0	444.0	444.0	444.0	444.0	444.0	444.0	444.0	444.0
1986	444.0	444.0	444.0	444.0	444.0	444.0	444.0	444.0	444.0	444.0	444.0	444.0
1987	998.7	994.3	993.1	995.2	990.9	994.7	999.6	982.4	994.7	986.3	984.3	991.2
1988	994.4	991.0	993.0	990.5	997.2	1001.9	984.3	983.1	990.5	996.7	987.4	988.6
1989	991.2	990.8	990.4	995.3	978.4	987.8	986.3	990.2	991.8	444.0	444.0	444.0

APPENDIX 2

Testing the assumption that the surface temperature anomaly was of the same sign as the surface to 500 mbar layer mean temperature anomaly was achieved by using radiosonde data for McMurdo Station. McMurdo was chosen simply because it is close to the Ross Ice Shelf, one of the three regions focused on in the thickness hypothesis, and the data were readily available. The radiosonde data came from the TD-6200 series National Climatic Data Center (NCDC) upper air digital files and are available from NCDC in Asheville, North Carolina. The data we obtained had a period of record from April 1956 to December 1982 with soundings at both 0000 UT and 1200 UT. However, many days were missing one or both of these soundings, and in some cases entire months were missing. The temperature data for all the soundings were extracted from the NCDC files, and these data were checked for transcription and other obvious errors.

In the next step, we created monthly mean temperature profiles using only the 0000 UT soundings, because during the southern winter months only 0000 UT soundings were taken. The mean profiles were created by taking an arithmetic average of the temperatures at each standard level in the soundings. At least 8 days of 0000 UT soundings were necessary to create a monthly mean temperature at a given standard level, otherwise the mean temperature for that month and level was considered missing. The result was monthly mean temperature profiles with data points at the surface and every 50 mbar from 950 to 500 mbar. The annual cycle was

removed from the profiles starting with the creation of long-term monthly mean temperatures at each level from the surface to 500 mbar using an arithmetic average and data only from years with 12 nonmissing monthly mean temperatures at every level in the profile. The long-term monthly means were subtracted from the monthly mean profiles to create monthly temperature anomaly profiles.

The final step in testing our assumption was creating a surface to 500 mbar layer mean anomaly for each month and comparing these layer mean anomalies to the surface temperature anomalies. The layer mean anomaly was taken simply to be an arithmetic average of the temperature anomalies at each level in a profile from the surface to 500 mbar. This layer mean temperature anomaly was created for all months with eight or more mean profiles and is plotted against the surface temperature anomaly in Figure 7. The one-to-one correlation between the two time series was clear and was quantified by a correlation coefficient of 0.81 that was statistically significant at the 99.9% level using a Student's *t*-test.

The results in Figure 7 support our assumption that the surface and the surface to 500 mbar layer mean temperature anomalies have the same sign. Granted this analysis only looked at the radiosonde data at one point on the continent and one must be careful when extrapolating these results to other parts of the continent; however, since our use of the assumption is in a hypothesis that needs further study, we feel our extrapolation of the results is justified. We also hope that more

analysis of the radiosonde data at other stations will follow to further test our assumption.

Acknowledgments. We wish to thank those people who provided us unpublished data to extend our climate records. John C. King of the British Antarctic Survey provided data for Signy Island, Faraday, Halley Bay, and Rothera Point. Hugh Hutchinson of the Australian Bureau of Meteorology provided data for Mawson, Davis, and Casey. Data were also received from the New Zealand Meteorological Service for Scott Base and from the South African Weather Bureau for S.A.N.A.E. Station. Finally, T. H. Jacka from the Australian Antarctic Division provided pressure and temperature data that were used to fill in missing data and correct errors at many stations. Special thanks to Vernon E. Kousky for providing the CAC SOI data and explaining how the SOI was calculated. We also wish to thank the two anonymous reviewers for reading our manuscript and making many helpful comments. The result was a much improved paper. This research was funded by the National Science Foundation's Division of Polar Programs under grant 9015586.

REFERENCES

- Bromwich, D. H., A. M. Carleton, and T. R. Parish, A Review of Precipitation-Related Aspects of West Antarctic Meteorology, *NASA Conf. Publ. 3115, Vol. 2*, 1–22, 1991.
- Carleton, A. M., Sea ice-atmosphere signal of the Southern Oscillation in the Weddell Sea, Antarctica, *J. Climate*, **1**, 379–388, 1988.
- James, I. N., On the forcing of planetary-scale Rossby waves by Antarctica, *Q. J. R. Meteorol. Soc.*, **114**, 619–637, 1988.
- Jones, P. D., and D. W. S. Limbert, A data bank of Antarctic surface temperature and pressure data, *Rep. DOE/ER/60397-H2, Dist. Category UC-11*, 52 pp., U.S. Department of Commerce, Springfield, Va., 1987.
- Le Marshall, J. F., G. A. M. Kelly, and D. J. Karoly, An atmospheric climatology of the southern hemisphere based on ten years of daily numerical analyses (1972–82), I, Overview, *Aust. Meteorol. Mag.*, **33**(2), 65–85, 1985.
- Meehl, G. A., The annual cycle and interannual variability in the tropical Pacific and Indian Ocean regions, *Mon. Weather Rev.*, **115**, 27–50, 1987.
- Mo, K. C., and G. H. White, Teleconnections in the southern hemisphere, *Mon. Weather Rev.*, **113**, 22–37, 1985.
- Mo, K. C., J. Pfaendtner, and E. Kalnay, A GCM study on the maintenance of the June 1982 blocking in the southern hemisphere, *J. Atmos. Sci.*, **44**, 1123–1142, 1987.
- Parish, T. R., and D. H. Bromwich, The surface windfield over the Antarctic ice sheets, *Nature*, **328**, 51–54, 1987.
- Philander, S. G., and E. M. Rasmusson, The Southern Oscillation and El Niño, *Adv. Geophys.*, **28A**, 197–215, 1985.
- Rasmusson, E. M., and T. H. Carpenter, Variations in tropical sea surface temperature and surface wind fields associated with the Southern Oscillation/El Niño, *Mon. Weather Rev.*, **110**, 354–384, 1982.
- Rasmusson, E. M., and J. M. Wallace, Meteorological aspects of the El Niño/Southern Oscillation, *Science*, **222**, 1195–1202, 1983.
- Savage, M. L., C. R. Stearns, and G. A. Weidner, The Southern Oscillation signal in Antarctica, in *Second Conference on Polar Meteorology and Oceanography* (preprints volume), pp. 141–144, American Meteorological Society, Boston, Mass., 1988.
- Schwerdtfeger, W., *Weather and Climate of the Antarctic*, 261 pp., Elsevier, New York, 1984.
- Smith, S. R., Antarctic climate anomalies associated with the minimum of the Southern Oscillation Index, M.S. thesis, University of Wisconsin-Madison, Madison, 1991.
- Stearns, C. R., and M. L. Savage, Automatic weather stations, 1980–1981, *Antarct. J. U.S.*, **16**, 190–192, 1981.
- Stearns, C. R., and G. Wendler, Research results from Antarctic automatic weather stations, *Rev. Geophys.*, **26**, 45–61, 1988.
- Streten, N. A., Some synoptic indices of the southern hemisphere mean sea level circulation 1972–77, *Mon. Weather Rev.*, **108**, 18–36, 1980.
- Streten, N. A., and J. W. Zillman, Climate of the South Pacific Ocean, in *Climates of the Oceans, World Survey of Climatology*, vol. 15, edited by H. van Loon, pp. 263–374, Elsevier, New York, 1984.
- Taljaard, J. J., H. van Loon, H. L. Crutcher, and R. L. Jenne, Temperatures, dewpoints, and heights at selected pressure levels, climate of the upper air: southern hemisphere, *Rep. NAVAIR50-IC-55*, vol. 1, 135 pp., Chief of Naval Operations, Washington, D. C., 1969.
- Trenberth, K. E., Planetary waves at 500 mb in the southern hemisphere, *Mon. Weather Rev.*, **108**, 1378–1389, 1980.
- van Loon, H., and D. J. Shea, The Southern Oscillation, IV, The precursors south of 15°S to the extremes of the oscillation, *Mon. Weather Rev.*, **113**, 2063–2074, 1985.
- van Loon, H., and D. J. Shea, The Southern Oscillation, VI, Anomalies of sea level pressure on the southern hemisphere and of Pacific sea surface temperature during the development of a warm event, *Mon. Weather Rev.*, **115**, 370–379, 1987.
- Wallace, J. M., and P. V. Hobbs, *Atmospheric Science, an Introductory Survey*, 467 pp., Academic, San Diego, Calif., 1977.
- Wang, B., The vertical structure and development of the ENSO anomaly mode during 1979–1989, *J. Atmos. Sci.*, **49**(8), 698–712, 1992.

(Received January 28, 1992;
accepted September 4, 1992.)

VARIATION IN AEROSOL CONCENTRATION ASSOCIATED WITH A POLAR CLIMATIC ITERATION

A. HOGAN,¹ D. RILEY,² B. B. MURPHEY,³ S. C. BARNARD, AND J. A. SAMSON

Atmospheric Sciences Research Center, State University of New York at Albany, Albany, New York 12222

This paper presents analyses which follow warm, aerosol-laden cyclonic systems across the Ross Ice Shelf, using automatic weather station data. Subsequent discussion indicates that marine aerosol deposits in the interior Antarctic ice may reflect a recent climatic iteration of surface temperature and aerosol concentration. The Antarctic continental (cA) air mass is rarely displaced from the south polar plateau, but it is frequently modified by exchange with Antarctic maritime (mA) air advected from the ice shelves or frozen seas or with polar maritime (mP) air advected from the southern oceans. Because the cA air mass resides over an uninhabited and relatively static ice-covered surface, the concentration of aerosol particles in this unique air mass may reflect aerosol variation in the global atmosphere. A continuous series of surface observations began at South Pole Station in 1974 and have continued to the present. Although a large seasonal variation in aerosol concentration is present, little year to year variation in mean seasonal aerosol concentration occurred prior to 1982. A consistent diminution of mean annual aerosol concentration occurred during the 1980s, and a concurrent reduction in sodium concentration in snow and firn was also found. The decrease in aerosol concentration was greatest in late winter and spring, concurrent with decreases in mean air temperature and mean wind speed. This paper describes analytical techniques used to examine these apparent trends. We conclude that the diminution in temperature, aerosol concentration, and sodium deposition are a consequence of a diminution in the frequency of cyclonic-related warming events.

INTRODUCTION

Lettau [1971] proposed the Antarctic atmosphere as a test tube for meteorological theories. The south polar plateau is a well suited proving ground, as it provides the largest, most uniform solid plain on the Earth over which an air mass can reside. The symmetry of ice and water distributions over the surface of the southernmost quarter of the Earth allows the continental Antarctic (cA) air mass to remain over the interior of Antarctica and not be displaced to lower latitudes as similar Arctic air masses are displaced. The snow and firn surface of the plateau receives no incoming solar radiation during one half of the year and is often in radiation deficit during summer [*Weller*, 1986]. There is a surface temperature inversion a few hundred meters deep on most days, which decouples the boundary layer from tropospheric flow, but shallow layers of lapse or convection occur near the surface, according to *Neff* [1981], *Cronn et al.* [1983], *J. S. Obremski et al.* (Observation of recurrent temperature lapse near the surface at the

south pole, unpublished manuscript, 1988), and *D. Fitzgarrald* (personal communication, 1989), allowing exchange to the surface sink.

The cold surface also acts as a trap for vapors, although some may be released again [*Rasmussen et al.*, 1981; *Robinson et al.*, 1983, 1988; *Cronn and Schilling*, 1988]. Particulate matter seems to be permanently deposited in the snow and firn although it may occasionally be possible for drifting snow to sublime while in motion, reentraining a few particles in the boundary layer. While the plateau may not be a penultimate sink, it quite closely approximates a sourceless plane. Air arriving in the interior of Antarctica might be considered near the endpoint of atmospheric particle and vapor removal processes and as free of inhomogeneity of trace component concentrations as air near the surface of the Earth ever becomes [*Shaw*, 1979, 1980, 1982, 1988]. The locations of stations and the direction frequency of 500-mbar winds flowing over South Pole are given in Figure 1.

The cA air mass is not displaced from the plateau, but it is slowly modified by polar maritime (mP) or Antarctic maritime (mA) air masses exchanging with it around its periphery or through vertical exchange [*Schwerdtfeger*, 1970, 1984; *Van Loon*, 1972; *Taljaard*, 1972; *Hogan et al.*, 1990]. The strong surface inversion prevents exchange with the lower troposphere. The elevation of the polar plateau and the resulting katabatic wind regime

¹Also at Cold Regions Research and Engineering Laboratory, Hanover, New Hampshire 03755.

²Now at Vermont Department of Natural Resources, Waterbury, Vermont 05676.

³Now at Department of Earth and Atmospheric Sciences, Georgia Institute of Technology, Atlanta, Georgia 30332-0340.

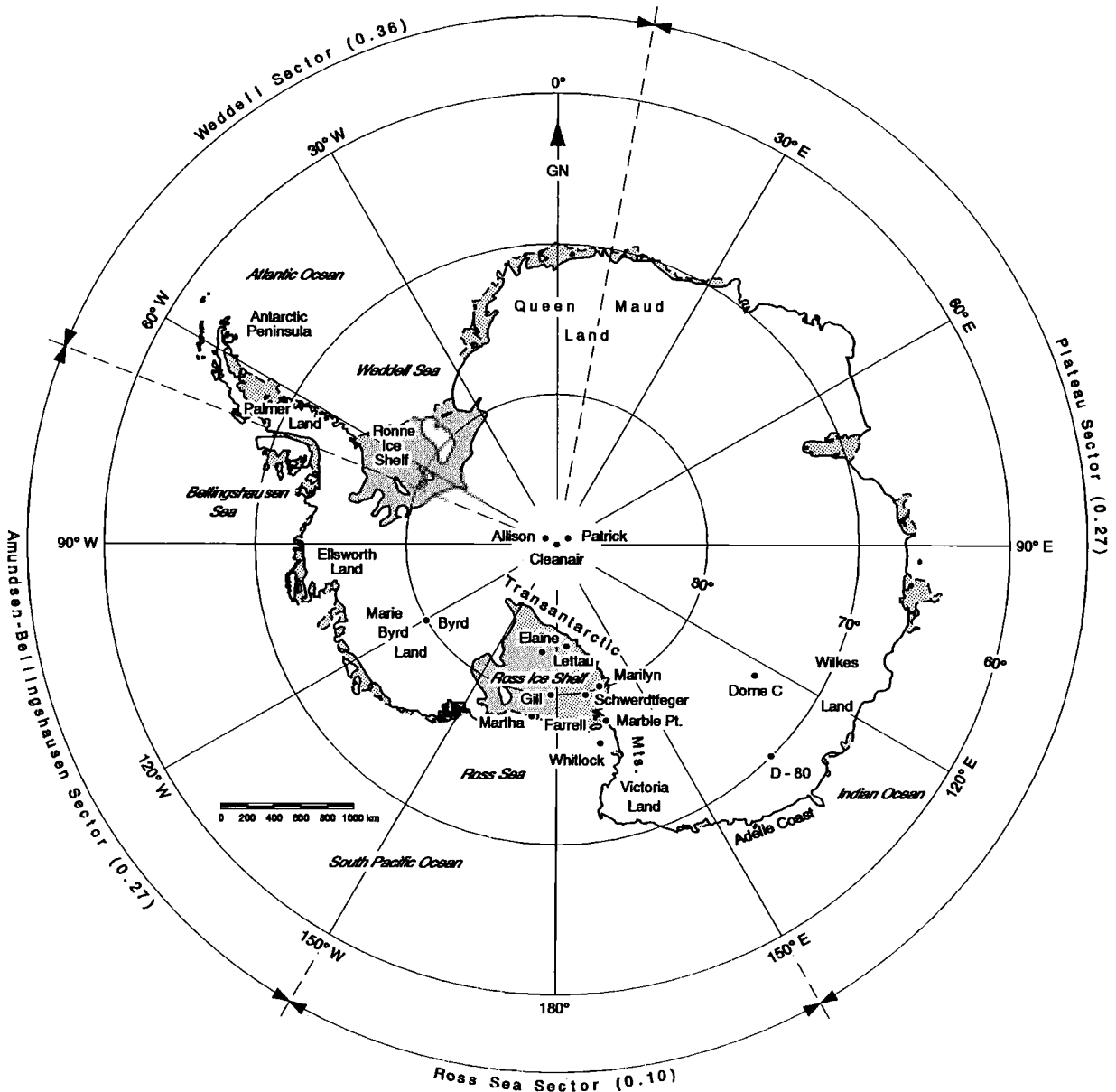


Fig. 1. Annotated map [from *Stearns and Wendler, 1988*] showing locations of Antarctic stations and geographic features. The relative frequency of 500-mbar winds occurring at the south pole from each defined sector is noted within the sector.

[*Mather and Miller, 1966; Kodama and Wendler, 1984; Parish, 1988; Parish and Bromwich, 1987*] limit exchange with surrounding air masses. The cA air mass provides a symmetric, infrequently modified, stable air mass that may be most readily examined for short-term fluctuation [*Stearns and Wendler, 1988; Hogan et al., 1990*]. It is yet to be established if the changes of the cA air mass are indeed recorded in the snow firm and ice, or if these changes reflect other climatic iterations or

fluctuations throughout the troposphere or atmosphere. The time periods of interest here were proposed by Landsberg as quoted by *Griffiths and Driscoll [1982]* as a climatic iteration with a time scale of a decade and a climatic fluctuation with a time scale of a decade to a century. This paper will describe a possible iteration in the temperature, wind, and aerosol climate observed at the south pole [*Samson et al., 1990*] and the record of a portion of it in recent firm [*Legrand and Kirchner, 1988*].

ESTABLISHMENT OF AN AEROSOL CLIMATOLOGY OF THE SOUTH POLE

The initial aerosol research programs conducted at South Pole were to support radioactive particle transport analysis according to *Feeley and Seitz* [1970] and *Feeley et al.* [1977]. *Zoller et al.* [1974], *Duce et al.* [1975], *Maenhut et al.* [1979a, b], *Cunningham and Zoller* [1981], and *Tuncell et al.* [1989] began collecting particulate material for transport analysis in the early 1970s, and J. A. Warburton (personal communication, 1972) measured aerosol concentration at the polar surface. Prior to this, *Voskresenskii* [1968] measured Aitken nuclei [*Vali*, 1985] throughout the year at Mirnyy, and *Kikuchi* [1971] measured cloud condensation nuclei at Syowa.

Meszaros and Vissy [1974] measured marine aerosols over the Antarctic seas, and *Kikuchi and Fujiwara* [1971] attempted to measure the transport of giant sea salt nuclei to the polar plateau during the Syowa-to-South Pole overland traverse of 1968–1969. *Kumai* [1976] determined that clay minerals and sea salts were transported to the south pole through analysis of nuclei remaining after sublimation of precipitated ice crystals. Intrusion of volcanic or mid-latitude aerosol sometimes influences Antarctic radiation through transport in the upper troposphere and stratosphere, as measured by *Flowers and Viebrock* [1968], *Rosen et al.* [1978], *Ito* [1986], and *Ito et al.* [1986].

The National Oceanic and Atmospheric Administration (NOAA) Geophysical Monitoring for Climatic Change (GMCC) program [*Pack*, 1973] began a disciplined climatic record of surface aerosol concentrations [*Hogan*, 1975; *Hogan and Nelson*, 1975; *Bodhaine and Murphy*, 1980; *Bodhaine and Shanahan*, 1990] at the south pole on January 27, 1974. A General Electric (GE) automatic nucleus counter [*Vonnegut*, 1950; *Skala*, 1963], a *Pollak and O'Connor* [1955] version of the Nolan-Pollak nucleus counter as a calibration standard, and a *Rich* [1966] diffuser denuder were the original aerosol instruments. A series of measurements were made daily with the Nolan-Pollak counter, Rich diffuser denuder, and, from 1977 through 1985, a *Sinclair* [1972] diffusion battery coincident with the release of the 00 UT radiosonde at the station. An additional daily measurement was made at some time at least 8 hours removed from the 00 UT release.

The same Nolan-Pollak counter (serial PG15 (prepared by R. Gussman, BGI Inc., Waltham, Massachusetts)) has been in use at South Pole for the duration of these measurements. It is one of a cohort of counters manufactured in the same fixtures that are in use at the Mauna Loa, Samoa, and Barrow observatories of the GMCC program. The calibration [*Metnieks and Pollak*, 1959; *Pollak and Metnieks*, 1960] of the Nolan-Pollak counter has been challenged in literature [*Liu and Pui*,

1974; *Hogan et al.*, 1981; *Miller and Bodhaine*, 1982], but it has more recently been verified [*Liu et al.*, 1975; *Sinclair*, 1984; *Davies and Egilmez*, 1985]. The counter at South Pole has received considerable attention [*Bodhaine and Murphy*, 1980; *Miller and Bodhaine*, 1982] since its installation, and the alignment and linearity of response of its optical system and photocell are periodically examined. It was recently replaced with a newer member of its cohort (B. Bodhaine, personal communication, 1990) while receiving major inspection and service. The simplicity and precision of the Nolan-Pollak counter are compatible with long-time calibration stability; the instrument was initially designed by Pollak to provide the reliability needed to establish long-term climatic records of aerosol concentration.

The aerosol concentration measurements are supported by the National Weather Service (NWS) radiosonde upper meteorological data, the station surface meteorological data, and concurrent observations of meteorological, other aerosol [*Ahlquist and Charlson*, 1969], and trace gas parameters by the Climate Measurement and Dynamics Laboratory (CMDL) (GMCC) observers. A large seasonal variation and major synoptic-scale variation in polar aerosol concentration became apparent in the first year of observations [*Hogan and Nelson*, 1975; *Hogan and Barnard*, 1978]. Additional meteorological observations have been continuously added to support the aerosol observations, culminating in the construction of a 30-m meteorological tower in 1984.

The relocation of the observation station to “New” South Pole camp and the establishment of the Clean Air Facility (CAF) are well documented in literature [*Bodhaine and Shanahan*, 1990; *Samson et al.*, 1990], as is the quality of the observed data. More than 355 observing days per year of aerosol data are available in the South Pole record since the establishment of the CAF in 1977, and only 13 observations were found to be suspected of contamination when *Samson et al.* [1990] defined this data base. The GMCC/Atmospheric Sciences Research Center (ASRC) south pole aerosol data base is probably the longest, best meteorologically supported, most synoptically compatible, and least contaminated [*Komhyr*, 1983] aerosol data base available for analysis.

RESULTS OF OBSERVATIONS: THE METEOROLOGICAL RECORD

Schwerdtfeger [1977] analyzed the temperature record obtained during the first 20 years of observations at the south pole. He used a 5-day running mean averaging technique to smooth the record and performed a harmonic analysis, extracting seasonal and second harmonics. A similar 5-day running mean analysis was performed on 10 years of south pole aerosol, surface temperature, and surface pressure observations

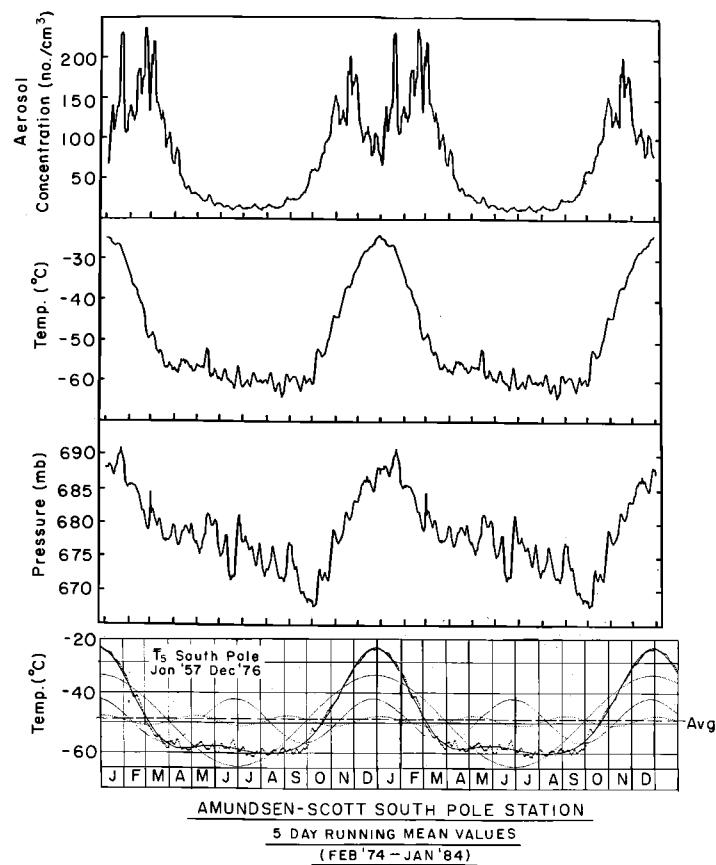


Fig. 2. Composite plot showing aerosol concentration, temperature, and pressure (1974-1984) [from Samson *et al.*, 1990] and seasonal variation of temperature (1957-1976) [from Schwerdtfeger, 1977] at the surface at the south pole.

by Samson *et al.* [1990]. Figure 2 is a composite figure showing these two records, and it indicates the kernlose winter [Wexler, 1959] is reflected in both the surface air temperature and the surface aerosol concentration.

Examination of the Schwerdtfeger and Samson analyses reveals some of the important characteristics of interior Antarctic circulation and local south polar meteorology. The kernlose winter is not uniformly cold, but is broken by advection of relatively warm air to the polar plateau. These warming periods are of major amplitude (20° to 30°C warmer than the mean temperature) but of short duration (often a single day, rarely 3 consecutive days) and appear as peaks impressed upon the nearly constant -58° to -60°C mean temperatures of April through September. These warmings may influence large sectors of Antarctica in both summer and winter according to Sinclair [1981] and Alvarez and Lieskes [1960]. The lowest temperature of the calendar year has often occurred after sunrise during late September; in the mean a temperature increase begins in late September, accelerates on October 1, and continues a near-linear rate of increase to a mean maximum in late

December. A somewhat more ragged but near-linear decrease in temperature begins on January 1 and continues through the beginning of the kernlose winter on about April 1. Noticeable, and apparently repeatable, reversals occur in mid-February and early October, and a slowing of the rate of the temperature increase occurs in early November.

The pressure analysis shows an unusual trend, as the surface pressure continues to decrease, first somewhat in step with the temperature from January 1 through April 1, and then it continues to decrease at nearly the same mean rate through October 1. This appears to be due to the elevation and flatness of the plateau and the extension of Antarctica through the growth of sea ice during winter. Cold air katabatically flows down the slopes and glacier valleys from the polar plateau and across the relatively smooth, snow-covered sea ice [Mather and Miller, 1966; Schwerdtfeger, 1984; Parish, 1982, 1988; Parish and Bromwich, 1987; Stearns and Wendler, 1988; Bromwich *et al.*, 1990] at a more rapid rate than it can be replenished into the region within both the tropospheric and the stratospheric polar vorti-

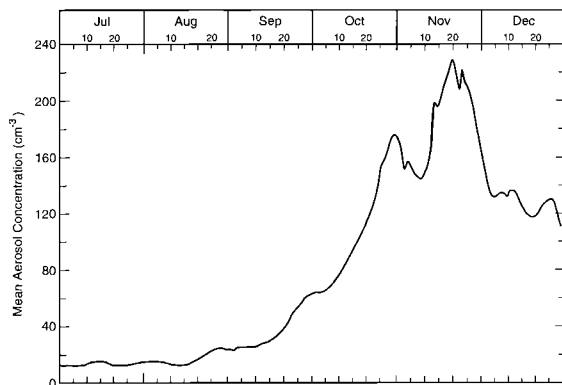


Fig. 3. Nine-day running mean aerosol concentration, calculated from 1974–1984 observations [from *Samson et al.*, 1990]. The additional time smoothing accentuates the mid-November maximum and the late November through December decrease in mean aerosol concentration.

ces. A strengthening of poleward upper winds in spring reverses this deficit, transporting 10^{15} kg of air through 70°S [*Schwerdtfeger*, 1984] and allowing the temperature and barometric pressure to increase simultaneously.

The aerosol analysis presents trends somewhat similar to those of temperature and pressure but with considerably more short-term variability impressed in spring and fall. The data of Figure 2 have been further smoothed by calculating 9-day running means of aerosol concentration, as shown in Figure 3. This smoothing shows that the spring (September, October, November) increase in aerosol concentration parallels the increase in surface temperature, but that midsummer aerosol concentrations decrease on the mean to values less than those of early summer. This cannot be explained by the seasonal variation of circulation and exchange, and it may be indicative of source variation [*Bigg*, 1980; *Bigg et al.*, 1984].

In summary, the elevation of the south polar plateau and its ice and snow cover make it an exporter of cold air and an importer of warm air. Increasing barometric pressure precedes increasing temperatures, stronger surface winds, and cloudiness. The relatively warm, recently imported air that accompanies increased barometric pressure is also enriched in aerosol concentration.

Figures 2 and 3 show that the meteorology of the south polar plateau is not static, as some midsummer visitors might believe, but quite dynamic, with frequent and sudden warmings occurring that cannot be identified as “fronts” using wind shift criteria [*Hogan and Barnard*, 1978]. Several experiments based on aerosol collections of a few hours time resolution have been used to define some of these subtle mixing and exchange parameters.

THE SOUTH POLE AEROSOL AND METEOROLOGICAL DATA SET

The seasonal aerosol trends shown in Figures 2 and 3 are derived from the 00 UT aerosol observations made in conjunction with the radiosonde releases. In some cases the 00 UT observation was missing and the nearest-in-time aerosol observation of that day was used as a surrogate measurement. Application of this criterion provides a data base of more than 355 aerosol observation days per year since the establishment of the Clean Air Facility in 1977. A significant amount of aerosol and supporting data were provided by B. A. Bodhaine from the NOAA/GMCC archive.

The meteorological data base is that of the Amundsen–Scott South Pole Station, collected at “Old Pole,” and in 1975–1976 at “New Pole,” by U.S. Weather Bureau (USWB)/National Weather Service (NWS) observers. The New Zealand Meteorological Service provided observers from 1976 through 1979, and contracted observers have served since that time. The upper air data used are derived from copies of the soundings, archived for us by the station meteorologists since January 1974. Soundings from 1961 through 1974 were obtained through a copy of an archived tape recording from the U.S. NOAA National Climatic Center in Asheville, North Carolina. This data set contains the records of the soundings successfully made during this time. It differs from some other south pole sounding data sets that do not include some soundings that were not synoptically transmitted because of communication difficulties (*E. Danielson*, personal communication, 1985).

The surface data set used is based on copies of the USWB form 733-1, “Local Climatological Data,” and subsequent revisions, containing the original daily entries made at the station. Some of these were supplied by the station meteorologists, some were copied from the originals in the meteorological office at the station, and some were supplied by C. Stearns, who derived them from similar sources. These are the original reporting forms and have not been altered. Hourly observations were necessary to support some of the analysis; these were obtained on microfiche from the National Climatic Data Center. More frequent data were used in some of the field experiments reported. These data were obtained on station from the meteorologist or were extracted from the station record charts.

The automatic weather station (AWS) data used here were provided by *Sievers et al.* [1988] in annual report form or as copies of master disks of the original record. The three AWS observations made nearest to the standard synoptic schedule are directly compared with station observations, although they may not be precisely synoptic.

The nature of variation of polar meteorological data is such that 2 consecutive days of missing data may result

in loss of record of a significant meteorological event. The trends in temperature, pressure, and aerosol concentration shown in Figures 2 and 3 are ill-suited to reporting by calendar months. We have attempted to present a majority of these data on a scale compatible with events, but in some cases it is necessary to use monthly means for comparison with published work.

RESULTS OF OBSERVATIONS: SECULAR TREND IN THE SOUTH POLE AEROSOL

The variation in observed aerosol concentrations at the south pole from *Samson et al.* [1990] is given in the top panel of Figure 4; it shows a diminishing trend in aerosol concentration. This decrease was noted as it was occurring, as there was great interest in determining if the increase in stratospheric aerosol concentration associated with the El Chichon eruption of 1982 [*McCormack and Swisler*, 1983; *Hofmann and Rosen*, 1985; *Hofmann*, 1987, 1988] would be observable in the surface record. A number of approaches were applied to attempt to uniquely define aerosol variation over a sourceless snow field in terms of meteorological parameters, yielding a preliminary correlation between surface wind direction, surface temperature, and aerosol concentration [*Hogan et al.*, 1982].

Bodhaine [1983] analyzed the aerosol recordings made at the south pole with an Ahlquist modified GE counter from 1974 through 1981 and found the annual geometric mean concentrations to be nearly invariant. This analysis is shown in the top panel of Figure 4. *Samson et al.* [1990] analyzed the daily aerosol observations, made from 1974 through 1985, and fitted a diminishing concentration trend to the data. *Bodhaine and Shanahan* [1990] have recently presented an analysis of the south pole condensation nuclei data through 1987, which is shown in the bottom panel of Figure 4. The data bases used in these analyses are not identical. The Ahlquist modified GE counter [*Skala*, 1963] records the aerosol pseudocontinuously (5 times per second); daily mean values are extracted from this recording to provide the NOAA/GMCC *Bodhaine* data set. Three observations obtained over a period of about 10 min, using the previously described protocol, provide the daily Nolan-Pollak counter data set. The months of December 1974, June 1976, and July 1976 are missing from the Nolan-Pollak data base, and several months in mid-1975 and the summer of 1981–1982 are missing from the GE recorded data base. The numerical values are directly comparable, as the recording counter derives its calibration from comparison with the Nolan-Pollak counter.

Bodhaine presents the aerosol chronology in log mean form with a linear trend line, while *Samson et al.* [1990] present arithmetic means through which a time series using a linear sinusoidal and least squares exponential regression is drawn. The combination of these presen-

tations in Figure 4 provides an enhanced insight to interpreting the aerosol trend in time. *Bodhaine's* [1983] analysis shows quite convincingly that the annual mean aerosol concentration was quite invariant during the 1974–1980 era; examination of the same time period in the presentation of *Samson et al.* [1990] indicates that the austral springs and summers of those years were characterized by periods of relatively great aerosol concentration, which produced some large mean values in individual months and a relatively large standard deviation of the aerosol concentration in many months. The record for the years beginning with 1981 shows generally lesser aerosol concentrations in spring and summer months, much smaller standard deviation in summer aerosol concentration, and an absence of the spring and autumn spikes that were almost always present during 1974–1980.

Figure 4 quite convincingly demonstrates that two different analyses of two somewhat different data bases indicate that a diminishing trend in surface aerosol concentration was observed at the south pole during the decade of the 1980s. This is an unexpected observation, as an increase in upper atmospheric aerosol concentrations was widely noted by *Hofmann* and his coworkers [*Hofmann*, 1988] following the eruption of the El Chichon volcano, including several measurements of enhanced stratospheric aerosols over Antarctica.

It is necessary to examine the record of aerosol concentrations observed at the surface of the south polar plateau, relative to meteorological events, the glaciological record, available tracers, and the activities at South Pole Station itself, to determine if this observed decrease in aerosol concentration is representative of the continental Antarctic air mass or is an artifact of the observing system. This will be done by presenting hypotheses describing processes that might influence aerosol transport to South Pole Station and examining variables that may influence these processes.

The surface at the south pole is decoupled from the lower tropospheric circulation by a radiation-induced inversion. To be observed at the surface, aerosol must be exchanged through this inversion by diffusion, wind shear, or gravity waves [*Neff*, 1981] or be introduced beneath the inversion through upslope flow from the periphery of Antarctic. Similar reasoning can be applied to the advection of sensible heat. *Hogan et al.* [1982] showed a wind direction dependent relationship between air temperature and aerosol concentrations in which air arriving from the grid east, beneath a low, strong inversion, was colder and lower in aerosol concentration than air arriving from the grid northwest beneath a higher and weaker inversion. (Definitions of grid directions and wind flow sectors are shown in Figure 1.) Other relationships among temperature, aerosol concentration, and exchange parameters have been found in the southern hemisphere [*Hogan*, 1979, 1986].

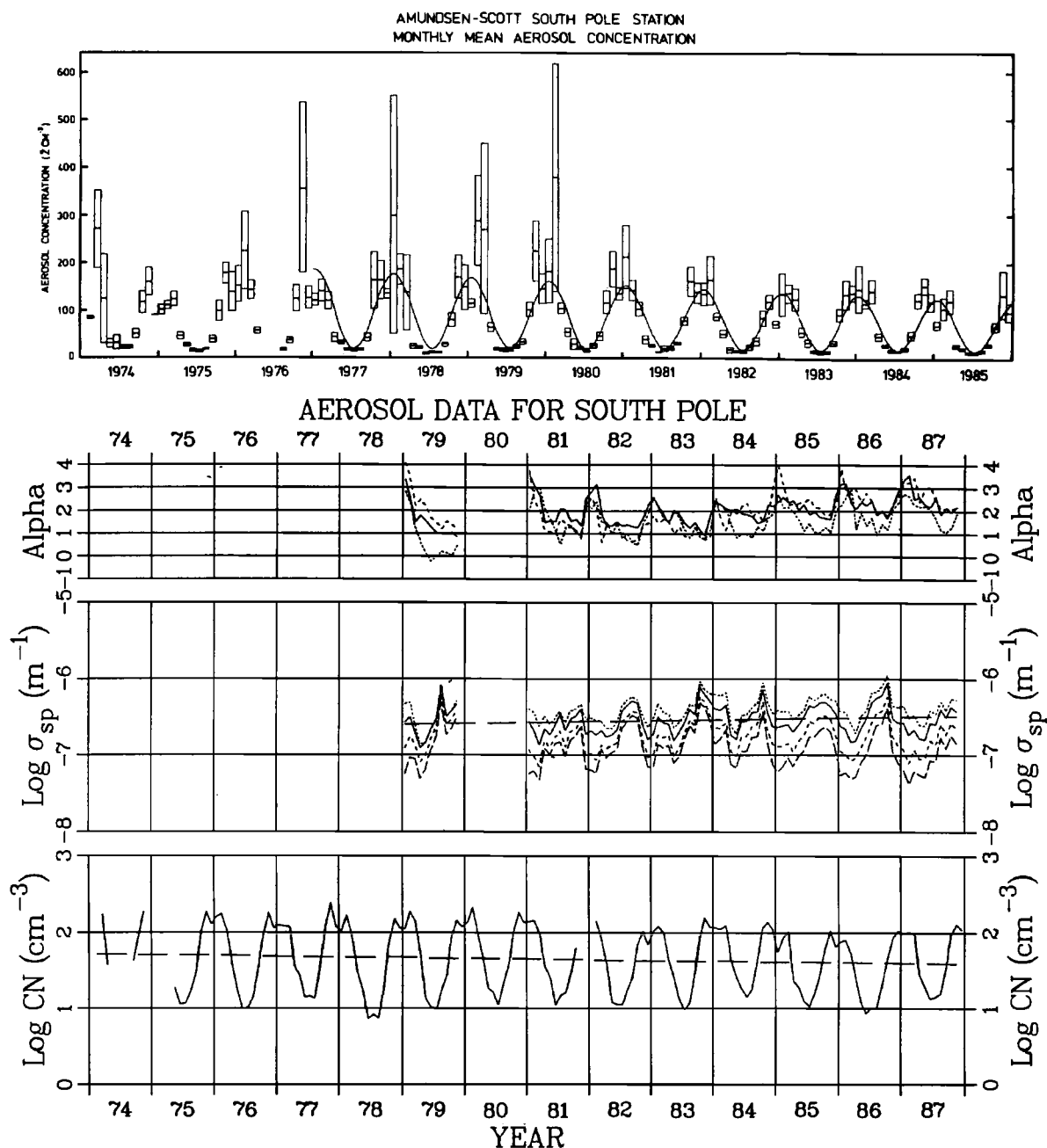


Fig. 4. Aerosol record from the south pole: (top) monthly mean of daily Pollak count, 1974–1985, with harmonic fitted [from *Samson et al.*, 1990]; (bottom) monthly geometric mean of continuous data, 1974–1987 [from *Bodhaine and Shanahan*, 1990]. The diminution in summer aerosol concentration during the 1980s is quite apparent.

COMPARISON OF INSTRUMENTAL AEROSOL RECORD AND SODIUM DEPOSITION

Comparison of the station aerosol record with the glaciochemical record of some aerosol material deposited in snow is not a trivial task. A conservative component of the particulate material must be available and, preferably, this conservative component should be gen-

erally present in the typical aerosol and constitute a sufficient fraction of the aerosol mass to be representative of the general trend of the aerosol. Particulate material from the aerosol will be deposited with falling snow as nuclei [*Kumai*, 1976], may be collected by other falling ice crystals or snow flakes [*Pitter*, 1977; *Kikuchi and Ueda*, 1978; *Miller*, 1990], or can be incorporated as

rime or hoarfrost growth on surfaces [Hogan and Kikuchi, 1975; Linkletter and Warburton, 1976]. Few particles fall to the surface by sedimentation in the Antarctic, but a dry deposition can be inferred from ^{210}Pb measurement in air and surface snow [Polian *et al.*, 1986]. After reaching the surface the particles will drift with the accompanying snow crystal or grain and finally become immobilized in wind crust or firn many days after, and many kilometers from, the place of initial deposition.

Legrand and Kirchner [1988] measured the chemistry of recent (1957–1983) south polar precipitation, including nitrate, chloride, and sodium concentrations in snow and firn. Sodium (Na) is conservative, a major component of the polar aerosol (second to sulfur, according to Maenhut *et al.* [1979a]). It appears in the aerosol record as late-winter sodium storms [Parungo *et al.*, 1979, 1981; Bodhaine and Bortniak, 1981; Bodhaine *et al.*, 1986], bringing relatively large particles to the plateau, and as a major fraction of the aerosol in summer “warm highs” [Hogan *et al.*, 1984a, b]. Legrand and Kirchner [1988] analyzed the sodium concentration in deposited snow representing the period winter 1976 through December 1983, associating maximum Na concentration with winter layers. They observed a decrease in sodium concentration with decreasing depth (time), which they associate with weakening meridional transport in the troposphere.

The Na profiles of Legrand and Kirchner are compared with the station aerosol record in Figure 5. The winter-peaking Na in firn profiles is almost exactly out of phase with the summer-peaking total aerosol record, which has consistent minima in winter. Bodhaine and Bortniak [1981] indicate that the larger light-scattering fraction of the south polar aerosol, which may sometimes constitute a majority of surface aerosol mass, is at a minimum in May and at a maximum in late winter (August) and early spring, coincident with “salt storms.” Cipriano *et al.* [1983] show small salt nuclei to be concurrently produced with the larger particles. A slight modification of the method used to calculate aerosol mass from Nolan-Pollak, Rich, and Sinclair aerosol measurements given by Hogan *et al.* [1984b] has been used to calculate Na mass from the aerosol record. This method was compared in situ with Bodhaine’s nephelometer measurements and was found to quite adequately predict scattering mass during summer of 1983–1984.

Riley [1987] shows that the number of charged particles measured by the Rich [1966] method, which is an input to this mass calculation, varies from a mean of 5 cm^{-3} in June and July, through 25 cm^{-3} in spring, to a maximum of 55 cm^{-3} in November and February. Applying the Na fractions in “warm” and “cold” advection from Hogan *et al.* [1984a, b] gives a range from $10^{-12} \text{ kg m}^{-3}$ of Na aerosol in June and July to $1.5 \times 10^{-12} \text{ kg m}^{-3}$ in November. This is in fair agreement

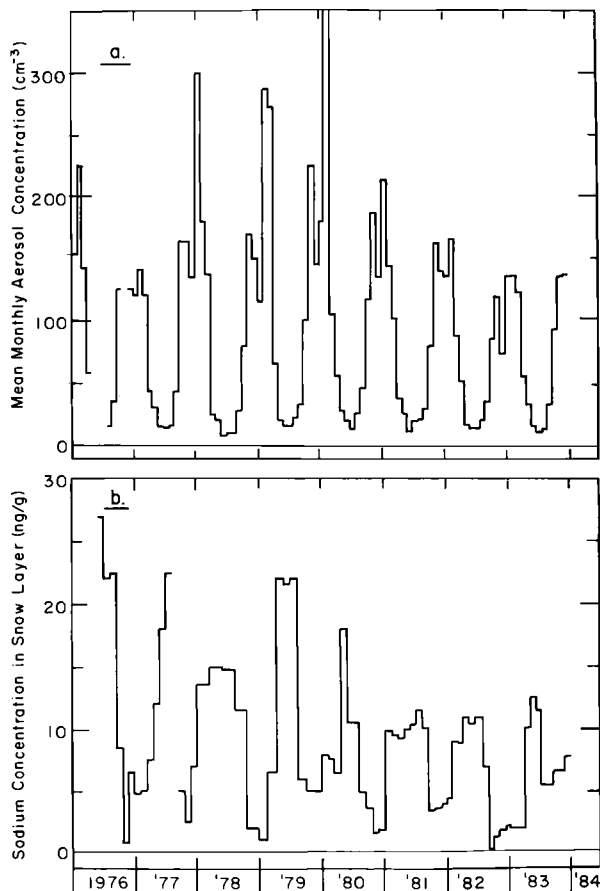


Fig. 5. Chronology of mean monthly aerosol concentrations observed at the south pole [from Samson *et al.*, 1990] and sodium concentrations measured in a shallow snow pit near the south pole by Legrand and Kirchner [1988]. A time axis shift of 6 months, using the hypothesis that sodium precipitated to the polar plateau during the late winter and summer will be accumulated and stored in the following winter layer, similar to the accumulation of snow [Gow, 1965], places the decreasing trends in phase.

with Na aerosol measurements of Maenhut *et al.* [1979a], who measured 2 to $4 \times 10^{-12} \text{ kg m}^{-3}$ Na in December and January. Vertical profiles of aerosol concentration over the Antarctic [Rosen *et al.*, 1978; Hogan, 1986; Saxena *et al.*, 1985], exchange analysis [Hogan *et al.*, 1984a, b], and precipitation analysis [Kumai, 1976] indicate the most Na-rich aerosol lies in and beneath the inversion, and a “dustier,” more sulfurous (Si–Al–S-rich) aerosol resides in the troposphere above the inversion.

Lapse, indicating the top of the inversion, is found on the mean 300 to 700 m above the plateau [Dalrymple, 1966]. The total Na aerosol column available to precipitate to the surface can vary from $5 \times 10^{-10} \text{ kg m}^{-2}$ to $1.5 \times 10^{-8} \text{ kg m}^{-2}$. Legrand and Kirchner [1988] show a range of 1 – $25 \times 10^{-12} \text{ kg Na per gram of water in}$

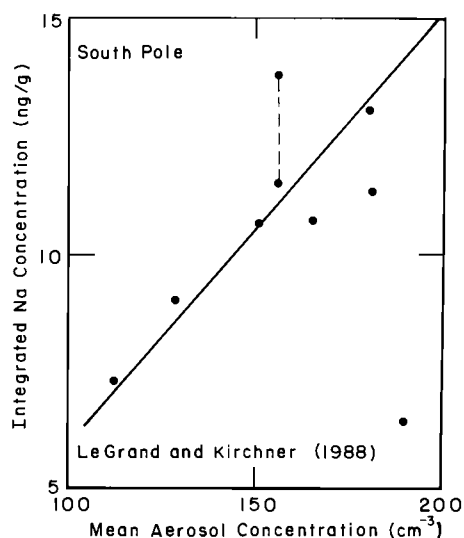


Fig. 6. Comparison of the integrated Na concentration in winter snow layers collected from a shallow snow pit near the south pole by *LeGrand and Kirchner* [1988] and the mean aerosol concentration observed during the previous October–March period at the south pole. The plotted line intersects the origin but is not statistically fitted.

south polar snow during the period 1976 through 1983. A Simpson's rule integration of the data in their Figure 4 gives a mean Na concentration of 9.9×10^{-12} kg Na per kilogram of meltwater. The mean annual accumulation at the south pole is $70 \text{ kg m}^{-2} \text{ yr}^{-1}$ of water [*Giovinetto and Bentley*, 1985; *Bromwich*, 1988]; if we assume the precipitation is equal to the accumulation, the precipitation of Na averages $7 \times 10^{-7} \text{ kg m}^{-2} \text{ yr}^{-1}$. This is about one half of the total Na aerosol transported over the polar plateau, if we base our flux calculations on the mean concentrations, inversion heights, and wind speeds cited.

The Simpson's rule integration was applied to individual "years" in the *LeGrand and Kirchner* [1988] presentation by placing the beginning of the calendar year in the center of each minimum. Annual Na precipitation was compared to observed aerosol concentration using several weightings and phase shifts. The best agreement is found when the sum of aerosol concentration measured from October through March is compared with the following winter's Na accumulation in snow. The result of this comparison is shown in Figure 6, with a straight line intersecting the origin drawn without statistical fitting.

Gow [1965] examined the seasonal accumulation and stratification of snow in proximity to *Giovinetto's* [1961] snow stakes at the south pole. A layer of hoar, formed in early winter, was found beneath a winter accumulation layer; it was used to define the bottom of annual winter layers. Large sastrugi were observed in November; they deflated through sublimation and erosion

through December and January. Summer snow was observed to puddle among the sastrugi, but it did not become consolidated. The winter layer appears to be an accumulation of the erosion products from sublimed sastrugi, unconsolidated late-winter precipitation, and summer precipitation. *Gow's* work provides the hypothesis that sodium precipitated during late winter and summer will be accumulated in the following winter snow layer. It is unfortunate that *LeGrand and Kirchner* [1988] could not collect the snow analyzed adjacent to an accumulation stake of several years record.

Sodium precipitation may involve several physical processes. The snow accumulated at the south pole may have been precipitated a long distance away and more than a year before it was incorporated in the winter layer. The accumulated water may not have fallen as snow but may have been precipitated as hoar or rime [*Kikuchi and Hogan*, 1976]. The results of *LeGrand and Kirchner* [1988] support the diminution of aerosol presented in Figure 4. It is necessary to examine the meteorological record to determine if the "reduced meridional transport" they suggest as a cause of diminished Na precipitation can be identified.

METEOROLOGICAL ANALYSIS OF TRANSPORT AND EXCHANGE PROCESSES ON THE PLATEAU

The initial aerosol measurements at the south pole previously referenced verified the intuitive hypothesis that aerosol concentrations on the polar plateau would be very small in both mass and number. Systematic measurement of these small concentrations can be disrupted by the most minor local contamination, and very extensive analysis of surface meteorology was conducted by *Pack* [1973] and *Watkins* [1976] before the Clean Air Facility was established. It was suggested at the beginning of the program that perhaps there was a constant reservoir of particles in the troposphere above the station and that observed variations were merely due to variation in exchange across the inversion. The vertical profiles and cross-continental transects made during the airborne experiments of 1977 and 1978 shown in Figure 7 define the fair-weather transport of particulate matter [*Hogan*, 1979, 1986], but uncertainties remain relative to "spring," "autumn," and "storm"-related exchange of material to the polar surface.

I. Whillans (personal communication, 1978) had demonstrated in the field that the new, domed South Pole Station altered the drift pattern several kilometers from the station. *Zoller et al.* [1974] were constantly plagued by station contamination, as were *Rasmussen et al.* [1981], who moved their sampling site 5 km grid east of the station and CAF in 1976. *S. Warren* (T. C. Grenfell et al., Absorption of solar radiation at the Antarctic snow surface, unpublished manuscript, 1988) expressed similar concern in sampling soot in the vicinity of the station. *W. Schwerdtfeger* and *H. Lettau* frequently

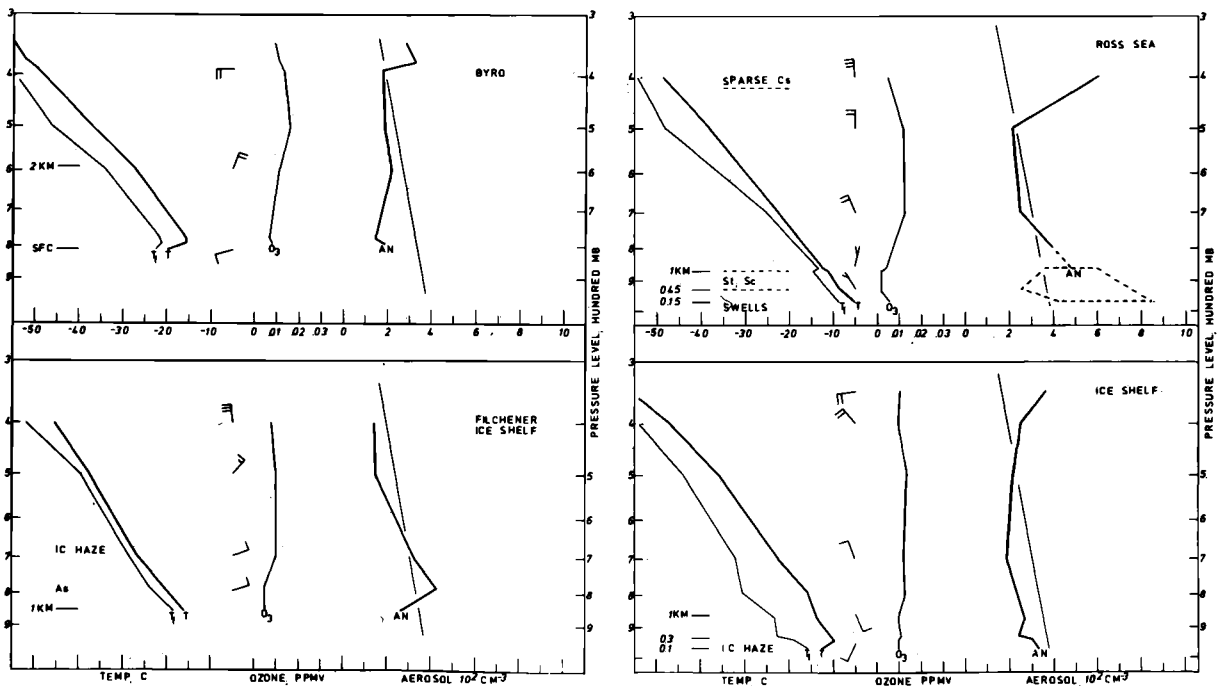
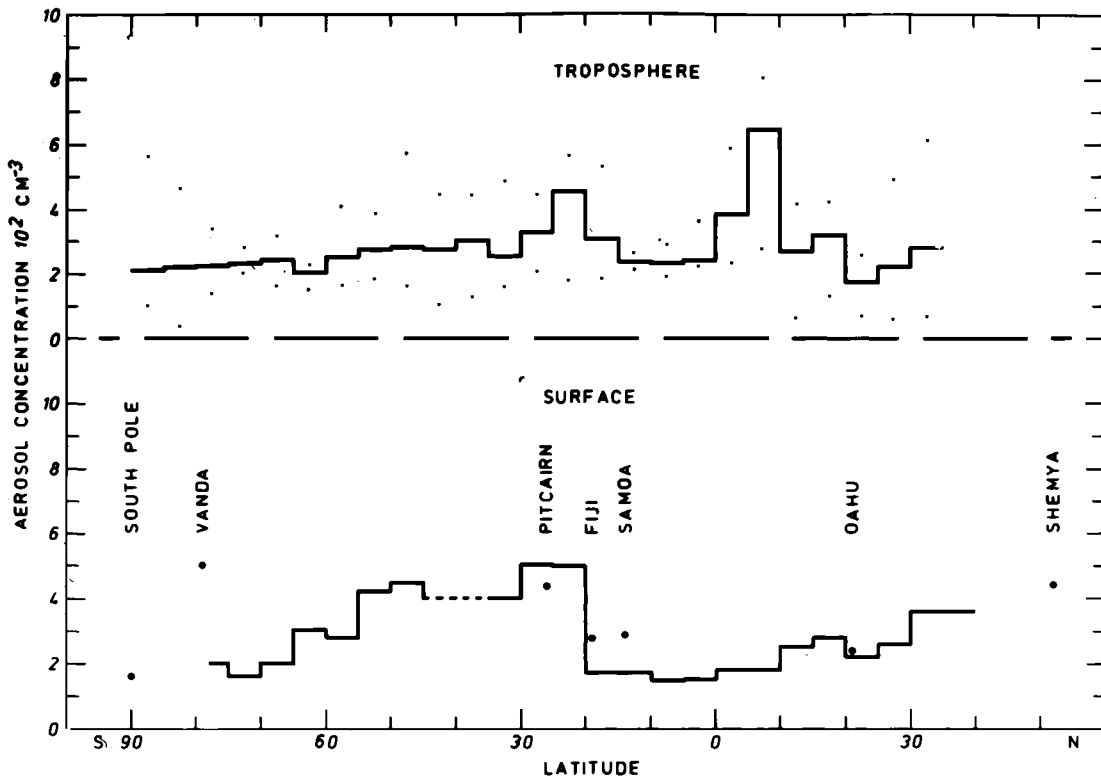


Fig. 7. The latitudinal and vertical variation of tropospheric aerosol concentration, approximately along the 180th meridian. The upper tropospheric measurements were made in October 1977, 1978, and 1980; the surface measurements were collected over many years. The light line plotted in the vertical profiles is the mean aerosol concentration measured at those levels during many soundings over Ross Island and the South Polar Plateau in dry air during 1977 and 1978.

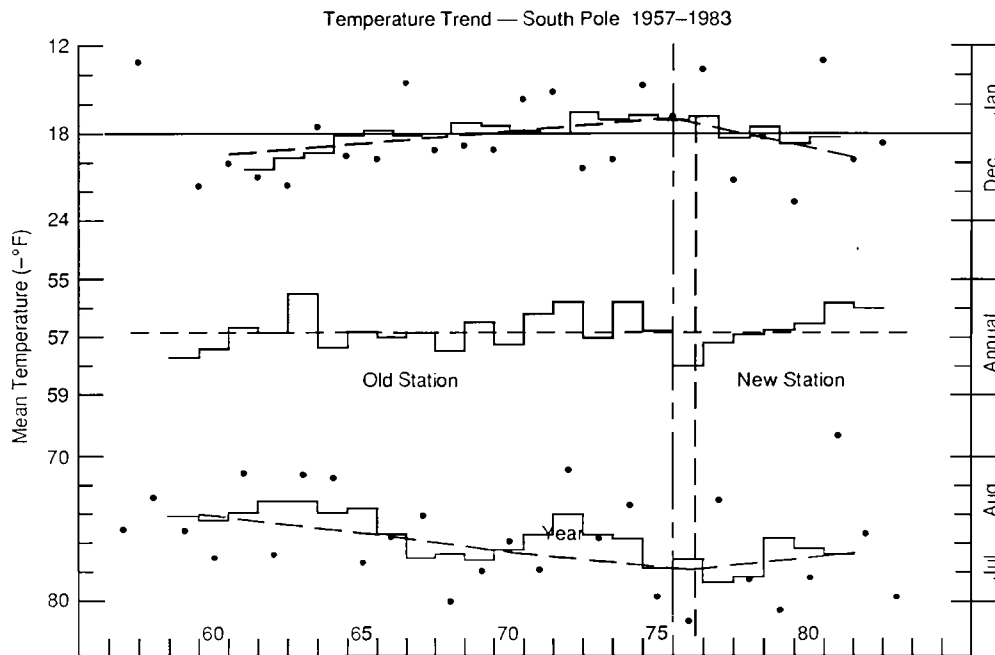


Fig. 8. Surface temperatures measured at the south pole, 1957–1983, in negative degrees Fahrenheit. Summer (December–January) and midwinter (July–August) temperatures are plotted with large dots, with plotted lines indicating the middle-year value of the 5-year running mean temperature. Mean calendar year temperatures are plotted in the center, with a dashed line indicating the 1958–1983 mean temperature. The dashed vertical lines indicate the relocation of the station in December 1974 and the observer change (NWS to New Zealand Meteorological Service) in 1976.

raised questions relative to the maintenance of the proper exposures of the station meteorological instrumentation as the station grew in size. *Samson* [1983] examined the station surface meteorological record in conjunction with her analysis of winds above the station and found the interesting chronology presented in Figure 8. The mean annual (calendar year) temperature was almost invariant during the years 1959–1982 (the initial 2 years of observations, 1957 and 1958, had periods of missing data and are not included). The data base cited previously differs from that of *Jones and Limbert* [1987] in this respect. The peaked summer and midwinter temperatures were quite variable, when compared to the annual mean. Calculation of the 5-year running mean December–January and July–August temperatures indicated that summers were warming while winters were cooling at nearly equal rates during 1960–1975. The pattern appeared to reverse following the relocation to the new station. Several hypotheses, including chance, were considered, but the problem seemed significant to the analysis and interpretation of the south pole aerosol record, and the authors proposed that with NSF support, C. Stearns, M. Savage, and G. Weidner should establish an AWS network in the vicinity of the south pole to investigate the station's influence on local circulation.

APPLICATION OF AUTOMATIC WEATHER STATIONS TO AEROSOL ANALYSIS

Automatic weather stations (AWS) were installed, 20 min of latitude from the south pole, along the 45th (Patrick) and 330th (Allison) meridians of longitude on January 28, 1986 [*Sievers et al.*, 1988]. An additional station, the Clean Air Facility, was installed near the station and research meteorological sensors the following day. The locations are shown in Figure 1. The station along the 45th meridian lies in the sector of most frequent surface flow toward the south pole. The station along the 330th meridian lies along the path of flow of warmer air to the south pole. These two AWSs were equipped with shielded air temperature, barometric pressure, and Aerovane wind sensors and communicated measured variables through the ARGOS satellite system.

The third AWS was similarly instrumented and provides a reference for comparison of nonsynoptic observations between the upwind stations and South Pole. It remains in place to provide long-term empirical evaluation of meteorological instruments in the Antarctic. The upwind stations, Patrick and Allison, were removed during the austral summer of 1987–1988. The stations

yielded 12 and 17 complete months of meteorological data, respectively.

A comparison of the monthly mean and monthly minimum air temperatures recorded at the AWSs with respect to the NWS station observations is shown in Figure 9. The correspondence is good but not conclusive, as the data are recorded in each case as whole numbers, and the differentials are of the order of one or two digits. The similarity between warm-month correspondence and cold-month correspondence indicates that all instruments are properly shielded from stray radiation. A calibration offset of 1°C may be present at station Patrick.

Comparison of recorded mean monthly wind speeds shows near-exact correspondence between the station wind observation and the adjacent AWS at CAF. AWSs Allison and Patrick recorded consistently lesser mean wind speeds than the station anemometer or the CAF AWS. A comparison of station and AWS Patrick wind and temperature records for the period August 16–26, 1986, is shown in Figure 10. Circles denoting south pole observations are not plotted if the two values coincide. Brisk winds of 5 m s^{-1} or greater seem comparable, but the outlying anemometer has been observed to stall when the station record indicates less than 2 m s^{-1} of wind.

These comparisons do not allow us to dismiss all fears that the station influences local circulation and temperature, but they do alleviate major concerns that station heat influences the temperature observed or that station surfaces may be sources or sinks of radiation influencing observed temperature. The comparison of mean monthly and synoptic wind data indicates that the South Pole Station complex does not diminish local wind, but we cannot discount that it may slightly accelerate the nearby wind.

The analysis of AWS data yielded an additional analytical bonus. Examination of warming events indicated that some of them can be traced along the surface from the Ross Ice Shelf through the AWS network.

Murphey *et al.* [1991] collected particles by impaction on Ross Island, Antarctica, for later electron microscopic analysis, during a late-winter storm shown in the chronology in Figure 11. Winds of less than gale force from the northeast (seaward) direction preceded the storm and continued through the initial storm stages. At 00 UT, September 10, 1983, near calm at the surface accompanied weak winds (less than 15 m s^{-1}) from the continental (south) direction, from the 850-mbar level throughout the troposphere, and into the lower stratosphere at the 200-mbar level. Surface ozone concentrations exceeded 100 ppb during this calm period, and collected particle mass was more than 75% Si and Al, with less than 10% Na. These observations are consistent with ozone and particle transport from higher layers during strong subsidence.

Weak seaward winds resumed on September 11 and

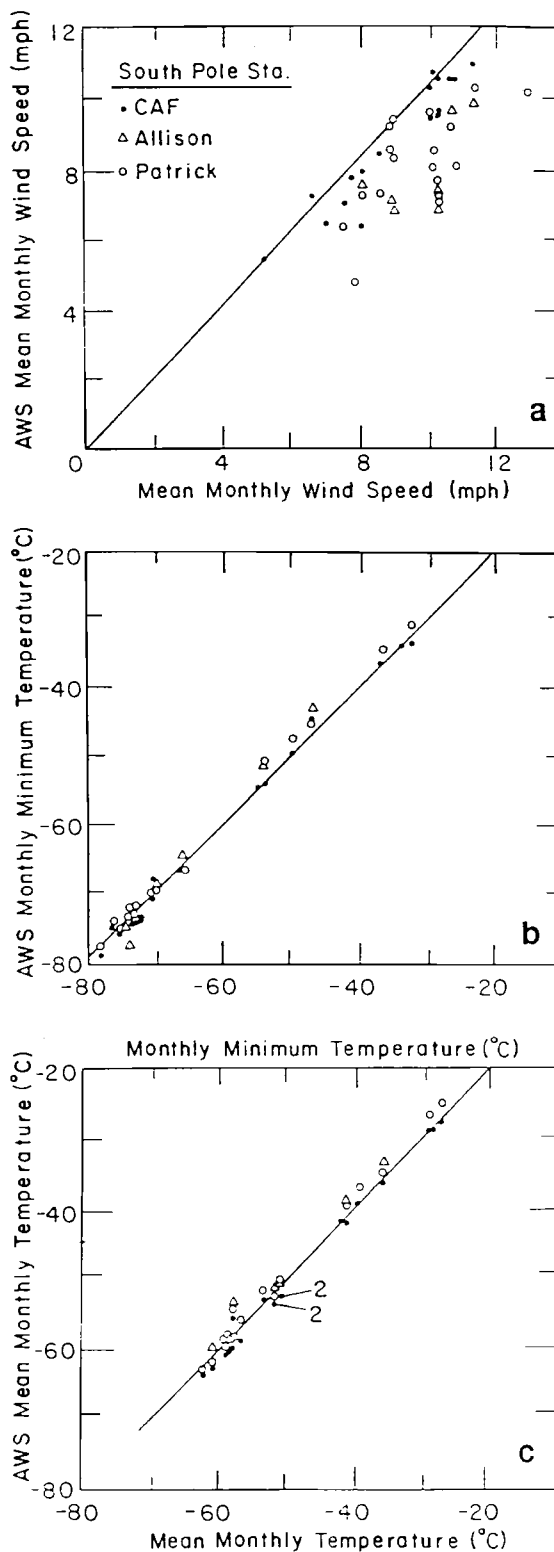


Fig. 9. Temperatures and winds recorded at automatic weather stations (AWSs) relative to station observations at the south pole: (a) mean monthly wind speeds, (b) monthly minimum temperatures, and (c) mean monthly temperatures.

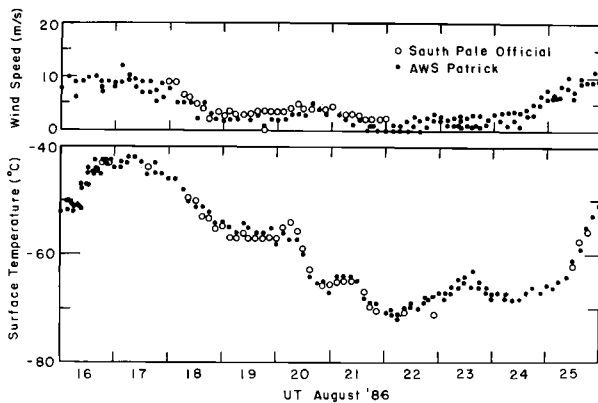


Fig. 10. Comparison of observed winds and temperatures at the south pole and AWS Patrick, 20 NM NE, August 16–25, 1986. Coincident values are plotted singly.

then strengthened and shifted to the south after 12 UT; the wind exceeded gale force from the Ross Ice Shelf (south) at 18 UT and continued to blow at 25 m s^{-1} until after 00 UT on September 12. The surface winds then gradually weakened and shifted through the east across the shelf. The surface ozone concentrations had diminished to less than 20 ppb vol/vol as the winds from the ice shelf accelerated but then increased to more than 100 ppb vol/vol in the strong winds concurrent with a slight warming and peaking of the barometric pressure just after 00 UT on September 12. Energy dispersive X ray analysis (EDXA) of particles collected on September 12 indicates 90% of the mass was sea salt and 10% was Si and Al. A photomicrograph of the particles collected is shown in Figure 12, along with the EDXA analysis. Rectangular crystals of sea salt up to $12 \mu\text{m}$ long are quite clearly distinguishable. Cheng *et al.* [1988] have recently shown that such crystals grow in air, from sea spray in near-water-saturated conditions.

Meteorological analysis, ozone record, and the composition of the collected aerosol indicate that sea spray generated over open water was advected onto the Ross Ice Shelf and survived transport over the shelf to be collected at Ross Island from the continental direction. The coincidence of ozone and sea salt on September 12 indicates that strong exchange [Danielsen and Mohnen, 1977] occurred over the shelf, probably mixing the sea salt through the lower troposphere. Warburton and Linkletter [1978] have previously found evidence for sea salt advection over the shelf through snow and firn analysis.

Examination of the South Pole aerosol record for September 1983 (also in Figure 11) indicates that a major increase in aerosol concentration and size occurred at 12 UT on September 13, but no major increase in ozone concentration was observed, which is in agreement with Oltmanns and Komhyr [1976]. Winds above the inversion at the south pole were quite strong (for Antarctica,

15 to 40 m s^{-1}) along the date line (flow from the Ross Sea direction) from 00 UT on September 11 through 00 UT on September 14. The surface temperature and barometric pressure increased in concert, with temperature changing from -62° to -33°C during this period, which is the warmest air observed during September at the south pole for the period of record. The surface wind was from 240 grid at the time the maximum aerosol concentration was measured; the maximum concentration probably arrived concurrent with the maximum temperature as the surface wind went through the date line (180 grid), but observations cannot be made at CAF with these winds.

There were no AWSs operating on the shelf south of 79°S at the time of these observations. This is unfortunate, as Bodhaine *et al.* [1986] give trajectory analyses that show midtropospheric flow from the Ross–Bellingshausen–Amundsen Sea sector to the polar plateau during late-winter to spring salt storms, although their trajectories generally join the persistent cross-Antarctic tropospheric flow along 300 grid inland of the Transantarctic Mountains. The experiment indicates that organized tropospheric flow may have continued beyond the mountain barrier, disorganized the usual decoupling of the strong inversion over the plateau, and permitted advection of only slightly modified mP air to the surface of the interior of Antarctica. Had AWS data been available during this event, it might be possible to verify the flow route along the surface. AWS data are available for a later event, but this event is not accompanied by coastal aerosol observation.

The period around October 1, 1987, is quite interesting in this respect. There was ample AWS coverage of the Ross Ice Shelf during this time to illustrate the advection of mP air across the shelf prior to an increase in surface temperature and aerosol concentration at the south pole.

The temperatures recorded at the AWSs on the Ross Ice Shelf, at Byrd Station, and at Dome Charlie (Dome C) and the NWS station observations from the south pole are plotted in Figures 13 and 14 for the period September 27 through October 6, 1987, UT. The aerosol concentrations observed at the south pole are plotted between the concurrent South Pole and Dome C temperatures in Figure 14. Warm air was advected onto the polar plateau prior to 12 UT on September 30, 1987, bringing relatively higher aerosol concentrations by 12 UT on October 1 and then apparently drifting about the polar plateau as a warm high, reaching Dome C by 00 UT on October 2.

Referring to Figure 13a, the warm air was first observed at Byrd at 00 UT on September 29, then at the stations Lettau and Elaine at 83°S at the foot of the Transantarctic Mountains at 12 UT on September 30, at Gill at 80°S on the shelf at 00 UT on October 1, and at the other shelf stations to seaward at 12 UT on October 1, simultaneous with its arrival at South Pole. The storm

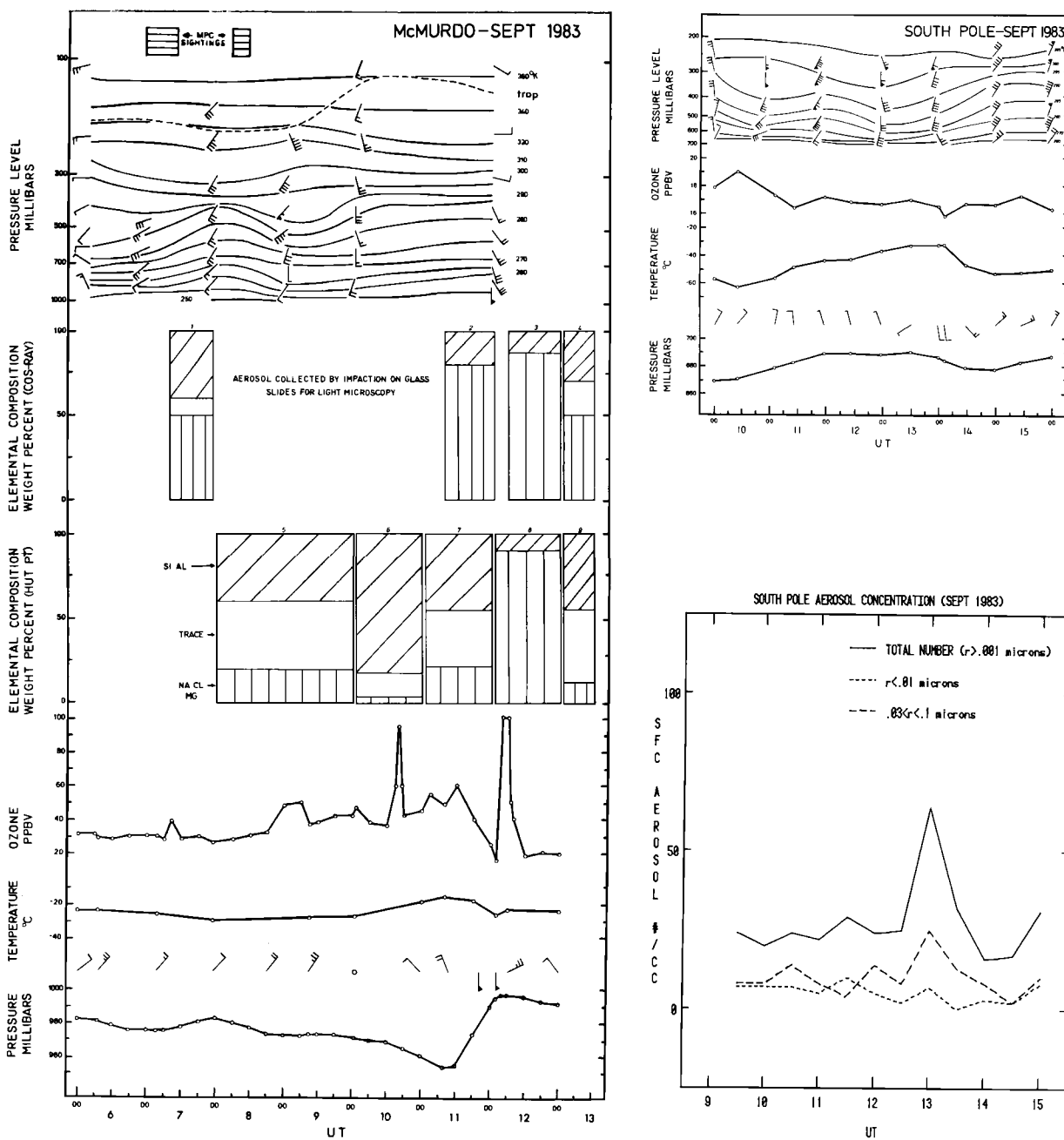


Fig. 11. Chronologies of aerosol and meteorological events at McMurdo and South Pole, during a September storm, September 6-15, 1983. The maximum aerosol concentration probably arrived at the south pole concurrent with the surface wind shift through the date line direction but could not be measured.

trajectory over Byrd to below the Transantarctic Mountains barrier and then northward to the Ross Island area is common [Naval Support Force Antarctica, 1988], but apparently few of these storms influence the surface of the polar plateau because of the mountain barrier and

the strong inversion over the plateau. The absence of AWSs poleward of the Transantarctic range prevents more complete analysis of the dimension and place of penetration of mP air onto the plateau.

The two cases cited provide the mechanism of merid-

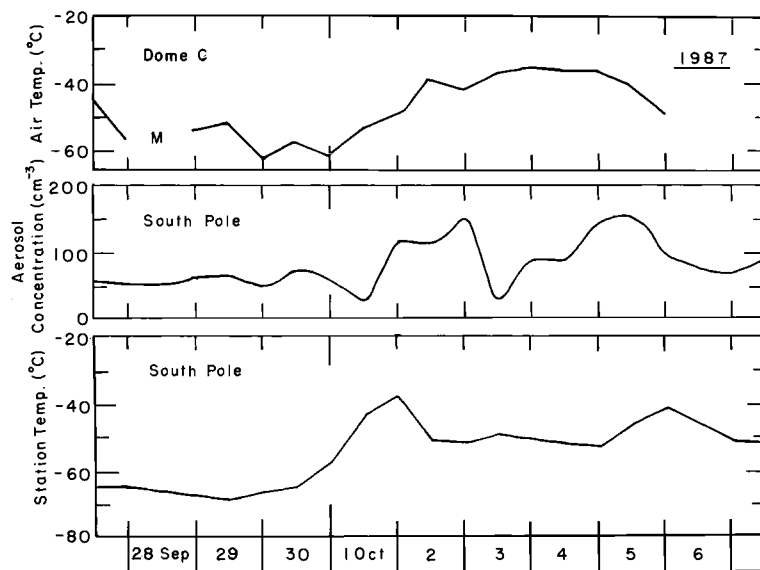


Fig. 14. Air temperatures and aerosol concentration observed on the Antarctic plateau during September 27 through October 6, 1987. Evidence of the same warming was also observed in the AWS D-80 record.

18. This indicates that exchange of enhanced aerosol concentration generally accompanies the exchange of warmer air to the surface of the plateau as barometric pressure increases.

There are 32 years of observational and instrumental records of meteorological variables at the south pole. This period is comparable to the climatic iteration and climatic fluctuation scale proposed by Landsberg. An analysis of the total record may place the duration of aerosol and snow sodium measurement in proper perspective.

The meteorological data set described above has been broken into five periods, representing the calendar years 1960 through 1984, and a shorter record representing 1985–1988. This conveniently breaks the record at the date South Pole Station was relocated. The mean values of surface temperature, barometric pressure, and wind speed are tabulated in Table 1. It is quite apparent that the period of instrumental aerosol measurement at the south pole has been conducted during a time of decreasing wind speeds. The mean monthly wind speeds recorded in 1960–1974 and 1975–1988 are plotted for comparison in Figure 19. The summer months of December and January show only slightly diminished wind speeds, but all other months have mean speed decreases of at least 2 mi h^{-1} ($\sim 1 \text{ m s}^{-1}$). The “salt storm” months of August, September, and October have decreased by more than 3.5 mi h^{-1} ($\sim 1.5 \text{ m s}^{-1}$) on the mean. A similar comparison of temperatures is given in Figure 20. Several months show no change, March is warmer in the recent record, but the August–September–October period is consistently colder than in

the early record. The monthly pentadal breakdown of the temperature record (Figure 20) shows that the relative March warmth has continuously increased during the period of record, while the August–September–October period has become cooler in the latter part of the period.

If the August–September–October cooling is due to a decreased frequency of warm advective events, as occurred on September 10–13, 1983, and September 27 to October 5, 1987, a parallel reduction of advection of sodium could accompany this decrease. A frequency analysis of warm advective events is given in Tables 2, 3, and 4 and Figure 21. Study of several late winter–early spring warm advective events showed that typical south pole surface temperatures of less than -60°C were replaced by air temperatures of $-40^\circ > T > -50^\circ\text{C}$ over a period of 24 to 48 hours. Surface temperatures greater than -50°C indicate strong advection of warm air to the polar plateau in August and September. Schwerdtfeger’s [1977] 1957–1976 temperature analysis shows the mean surface temperature is greater than -50°C after October 20. The number of days with temperatures colder than -50°C remains a fair indicator of exchange vigor in October. November historically is a month of temperatures greater than -50°C , and the opening of the flying season to the south pole is traditionally scheduled for November 1 [Naval Support Force Antarctica, 1988]. The number of days each year (1957–1988) exceeding -50°C , -45°C , -40°C , and -35°C during the calendar months August, September, and October are shown in Tables 2, 3, and 4. The cumulative number of warm days occurring in August,

September, and October is shown in Figure 21. One November day colder than -50°C occurred prior to 1980. Two November days did not reach -50°C in 1981 and 1987, nor did three in 1983.

Lettau [1969] showed that moisture sufficient to account for interior Antarctic precipitation must be advected inland during periods when the air temperature exceeds the monthly mean. Hogan [1986] showed an association between relatively moist or cloudy air and increased aerosol concentration in vertical profiles (Figure 7) obtained in mP, mA, and cA air over Antarctica.

Examination of Figure 21 shows that the relative frequency of warm advection to the surface of the south

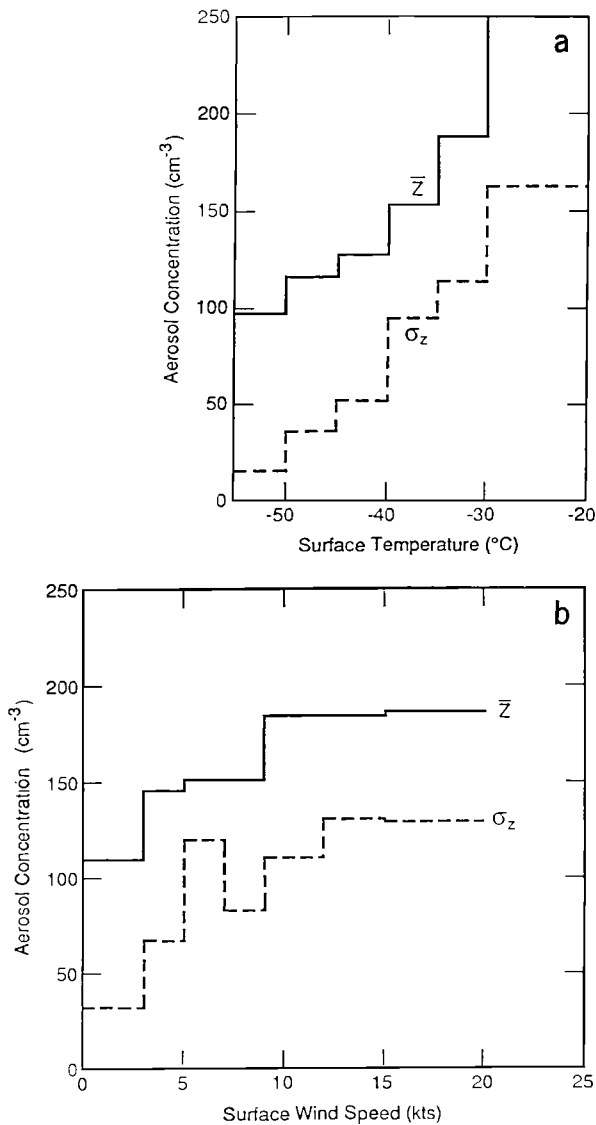


Fig. 15. Mean and standard deviation of aerosol concentration observed at South Pole, as functions of (a) surface temperature and (b) wind speed, for November in 1974–1983 [from Hogan et al., 1990].

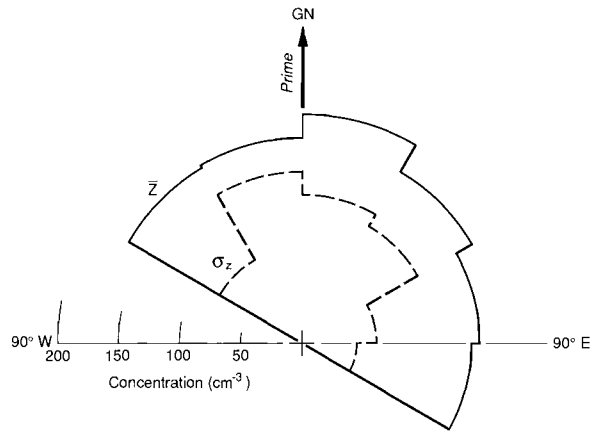


Fig. 16. Mean south pole November aerosol concentration by surface wind sector. The cA air mass appears to be universally modified during this warming period.

polar plateau was greater in the years before 1972 than since. The median number of August + September + October (ASO) days per calendar year with temperatures greater than -50°C is 33 days. Years with less than 32 days of ASO temperatures greater than -50°C are 1957–1959, 1964–1965, 1976–1977, 1979–1981, 1983, 1986, and 1987. The period 1966–1975 had more than the median number of warm advection events each spring, while the period 1976 through 1987 had less than the median number of spring warmings in 8 of 12 years.

DISCUSSION

Samson et al. [1990] and Bodhaine and Shanahan [1990] have shown that the concentration of aerosol observed at the surface on the south polar plateau diminished during the decade of the 1980s with respect to that observed during the decade of the 1970s. Legrand and Kirchner [1988] analyzed Na concentration from snow and firn in a shallow pit near the south pole, representing accumulation years 1976–1983, and found a similar decrease in Na concentration in the meltwater. When the instrumental record of aerosol concentration observed in September through March is compared with the Na stored in the following winter's firn, good correspondence is found.

Legrand and Kirchner attribute the diminution of Na to reduced meridional transport. Examination of the station meteorological record indicates that surface wind speeds and surface air temperatures decreased during this time period when compared to the pre-1975 record. The greatest decrease in wind speeds and temperatures occurs during the months of August, September, and October, which are months of major transport of Na to the plateau, according to Parungo et al. [1979, 1981] and Bodhaine et al. [1986].

A frequency analysis of major spring warming events

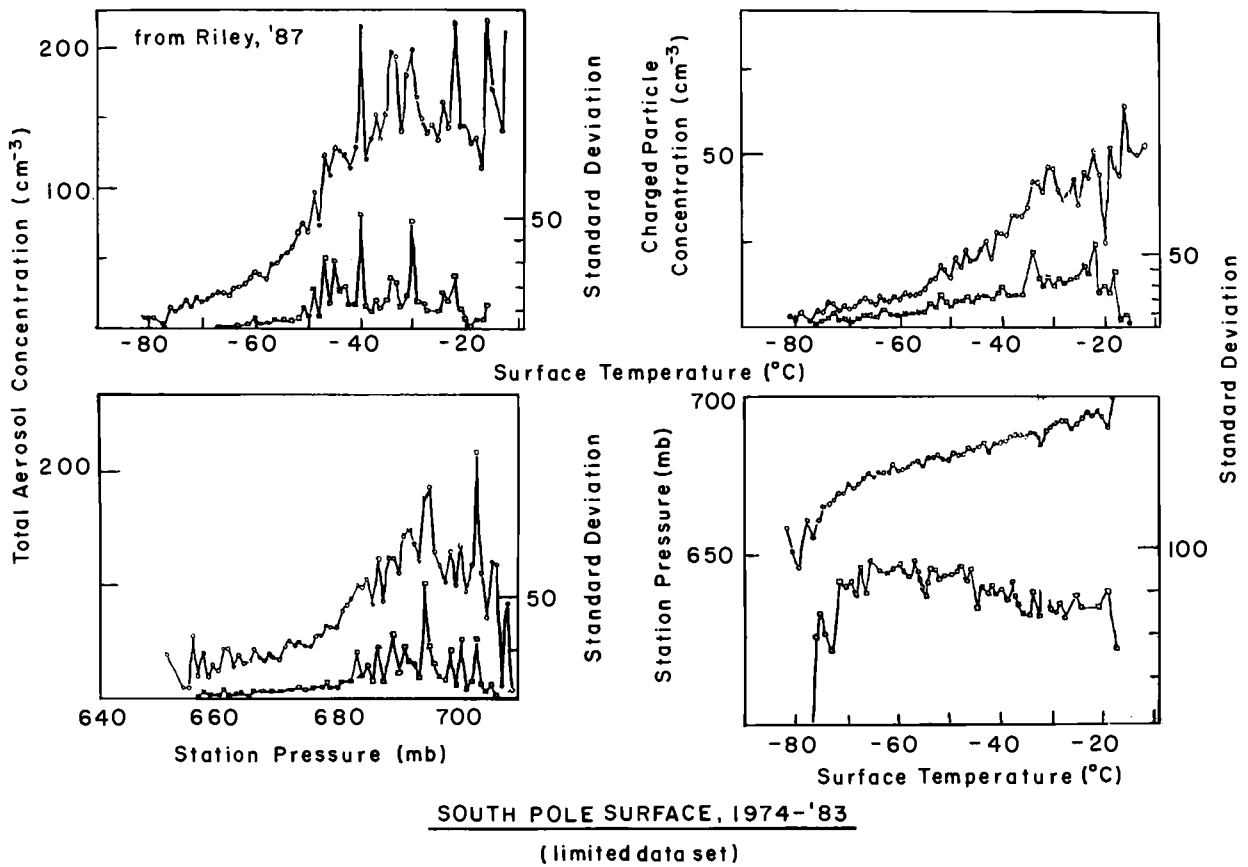


Fig. 17. Relationships among station pressure, surface air temperature, total aerosol concentration, and charged aerosol concentration, observed at South Pole, 1974–1983. The data set is limited to pressure and temperature observations made concurrently with aerosol observations. All data are from Riley [1987].

indicates that these warmings were relatively common during 1966–1975 but less common during the period 1976–1987. This decrease in the number of days of warm advection may account for the “decreased meridional transport” proposed by Legrand and Kirchner [1988]. This decrease in the number of warming events results in a decrease in the mean monthly temperature observed in August, September, and October during the decade of the 1980s and reduces the annual temperature of the calendar year to produce the apparent diminishing trend shown in Table 1. This late-winter and spring cooling is in agreement with a general tropospheric cooling in the south polar region shown by Angell [1988], although it is not possible to align the monthly trends precisely with Angell’s seasonal data. Jones [1988] also shows the interior of Antarctica to be cooling, although prior work [Raper *et al.*, 1984] shows a general warming trend in the Antarctic. An association between a decreased number of warming events, decreased temperatures, diminished aerosol concentration, and reduced Na in snow at the south pole seems to

verify that “decreased meridional transport” was characteristic of the period. The experiment at Ross Island [Murphy *et al.*, 1991] indicates that the Na source and mixing mechanisms are present on the Ross Ice Shelf to enhance the sodium concentration in the meridionally transported air. The AWS analysis verifies that warm, Na-rich air may be advected to the plateau by that route, as shown in some of the trajectory analyses of Bodhaine *et al.* [1986], but without joining the grid-westerly tropospheric fair weather flow, which trajectories sometimes show.

Swanson and Trenberth [1981] showed that the geostrophic wind, geopotential height, and geopotential thickness fields have important interdecadal changes over the southern hemisphere, including Antarctica. Papers describing major changes in lower stratospheric flow into Antarctica during the decade of the 1980s, relative to the Antarctic “ozone hole,” are numerous [Mahlman and Fels, 1986; Komhyr *et al.*, 1986; Solomon, 1988].

It appears that we have observed portions of three, or

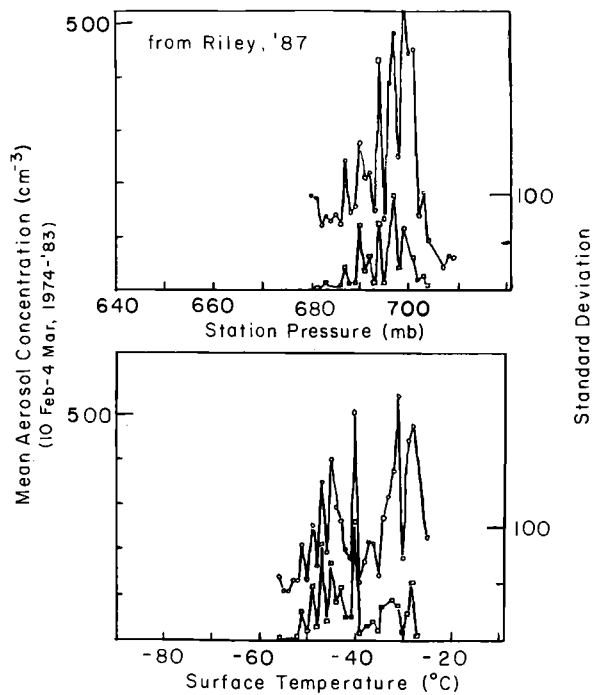


Fig. 18. Variation in aerosol concentration with surface meteorology, during summer-winter transitions, 1974-1983 [from Riley, 1987].

perhaps four (if 1988 is the harbinger of a new trend), climatic iterations during our brief period of instrumental observations at the south pole and that at least one is co-recorded in aerosol measurements and the polar firm. It is important that we use this opportunity to attempt to calibrate the climatic record that seems to be as well chronicled in glaciological storage [Gow, 1965; Jouzel et al., 1983] as in our data files.

The instrumental record of aerosol concentrations observed at the south pole and our supporting meteorological data are somewhat handicapped. The layout of the station and the Clean Air Facility is such that we are able to measure contamination-free aerosol concentrations more than 355 days per year, in the grid NW to ESE surface wind sector. The clean air sector was planned from our knowledge of surface wind frequency and the assumption that marine input would join the predominant northwesterly lower tropospheric flow

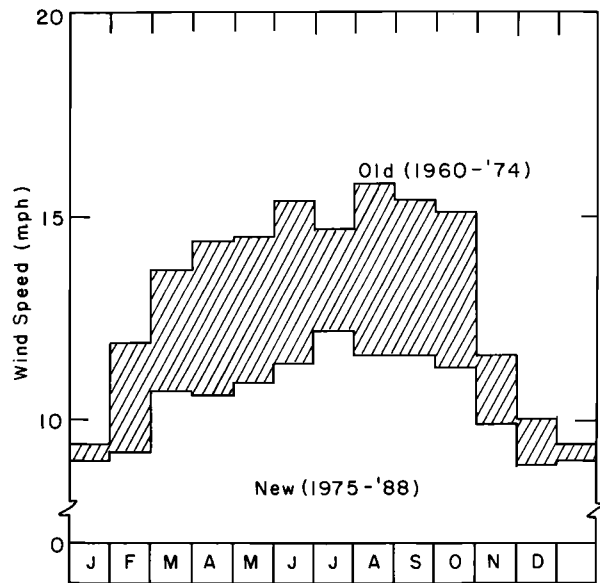


Fig. 19. Mean monthly wind speeds observed at South Pole, 1960-1974 and 1975-1988.

over the plateau. It now appears that those few days of southerly (grid) flow may be major contributors to tracer materials deposited in the snow and firn. Volcanic material from "nearby" Mount Erebus may be transported to the plateau on a few occasions, as suggested by Radke [1982]. It seems necessary to revise some measurement protocols to permit instrumental assessment of aerosol transport during southerly surface flow. South Pole and Vostok are the only upper air sounding stations on the plateau. There is no sounding on the Ross Ice Shelf, although soundings were made for several years at Byrd and Little America. The McMurdo sounding is valuable in determining the presence of strong flow along the date line. It appears that mP air entered Antarctica over Marie Byrd Land, passed over the AWSs at Byrd and Lettau, and then across the shelf to McMurdo on October 1, 1987, in the well-known Minna Bluff storm approach. Some of this relatively warm air ascended the slopes to the south polar plateau, reaching the south pole on October 1 as well, and then drifted about the plateau as a warm high, reaching Dome C and D-80, according to our single-station temperature

TABLE 1. Mean Temperature, Barometric Pressure, and Wind Speed at the South Pole Surface, for 5-Year Periods

Calendar Year Pentad	"Old Station"			"New Station"		
	1960-1964	1965-1969	1970-1974	1975-1979	1980-1984	1985-1988*
Mean surface temperature, °C	-49.3	-49.1	-49.1	-49.4	-49.4	-50.0
Mean station pressure, mbar	680.7	682.4	682.7	681.3	681.0	681.0
Mean wind speed, m s ⁻¹	6.1	5.7	5.8	4.7	4.7	4.4

*Incomplete record.

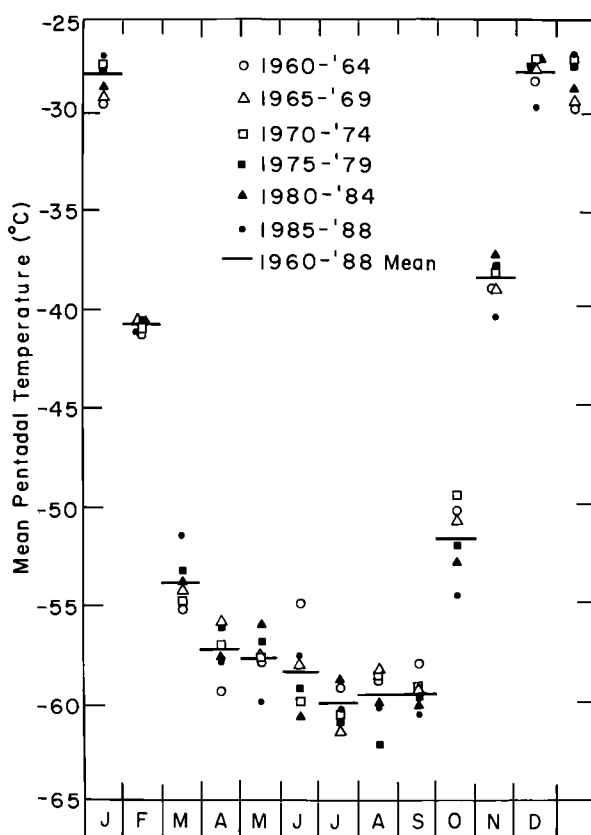


Fig. 20. Mean monthly surface temperatures observed at South Pole, 1960–1988. Five-year mean temperatures are noted by symbols. The month of March has been consistently warmer since 1975; the months of August, September, and October have been consistently colder.

analysis. If this is verifiable, the same marine air may be responsible for the material deposited at Dome C as at the pole, with only the frequency of “strong” deposition varying among the stations.

The existing AWS network made this analysis possible, but it does not have the measurement density and areal coverage necessary to permit plotting isobars and isotherms on the eastern Ross Ice Shelf, on Marie Byrd Land, along the Transantarctic Mountain barrier, or on the south polar plateau. It is necessary to determine the location and magnitude of exchange of mA or mP air into the cA air mass to attempt to assess the modification of cA air quantitatively, to calibrate the magnitude of alteration of meridional transport, and to assess the degree of variation of this transport with climatic iterations, fluctuations, or changes. There is a major need for enhanced instrumental surface meteorological observational capability in Antarctica if we are to investigate the scale and frequency of climatic change objectively.

CONCLUSION

Four independent aerosol-measuring techniques [Parungo *et al.*, 1979, 1981; Hogan *et al.*, 1984a, b; Bodhaine *et al.*, 1986; Tuncell *et al.*, 1989] indicate sodium aerosol is transported to the south polar plateau during well-defined warming events from August through mid-November. Experiments on Ross Island found large salt particles in air accompanying a classic storm approach from the Ross Ice Shelf. Enhanced ozone in the air returning from the shelf indicated that deep mixing had occurred, and examination of the south polar aerosol record indicates that this storm did transport heat and particles to the interior of Antarctica on September 13, 1983.

Meteorological analysis of surface pressure, temperature, and wind data from AWSs and the aerosol record from South Pole show the passage of warm, particle-enriched air across the Ross Ice Shelf to the south pole on October 1, 1987. These independent analyses tend to verify the hypothesis that late-winter and early-spring warmings are the major transporters of sodium to the polar plateau.

TABLE 2. South Pole Daily Maximum Temperature and Number of August Days Warmer Than Stated Temperature

Year	Temperature, °C				$\Sigma > -50$
	-35	-40	-45	-50	
1957			2	7	9
1958			1	1	1
1959			3	3	3
1960			4	4	4
1961	2	1	1	6	10
1962			1	4	5
1963	2	1	7	4	14
1964	1	2		4	7
1965		2	6	4	12
1966			2	4	6
1967		2	1	2	5
1968		1	2	3	6
1969			3	7	10
1970			1	2	3
1971			4	4	8
1972		1	6	8	15
1973				5	5
1974	2	2	1	8	13
1975			4	2	6
1976				2	2
1977		2	1	4	7
1978			3	0	3
1979				3	3
1980				1	1
1981			7	7	14
1982		1	1	5	7
1983				5	5
1984				5	5
1985		3	4	6	13
1986			6	4	10
1987			1		0
1988		3	6	3	12

TABLE 3. South Pole Daily Maximum Temperature and Number of September Days Warmer Than Stated Temperature

Year	Temperature, °C					Σ > -50
	-30	-35	-40	-45	-50	
1957					2	2
1958			5	2	2	9
1959				1	4	5
1960				5	7	12
1961			2	3	5	10
1962				6	4	10
1963			2	6	6	12
1964				2	0	2
1965			1	1	3	5
1966				2	8	10
1967				3	9	12
1968			1	3	4	8
1969		2	2	2	6	12
1970		2	3	1	4	10
1971		1	1	1	2	5
1972					8	8
1973				2	9	11
1974				3	3	6
1975			2	1	5	8
1976			2	2	5	9
1977					2	2
1978			1	3	4	8
1979		1	2	3	8	14
1980			4	1	3	8
1981		1	1		4	4
1982		1	1	0	3	5
1983	2	0	1	3	3	9
1984			3	2	6	11
1985				1	3	4
1986					3	3
1987				1	4	5
1988		1	1	3	6	11

Comparison of late-winter and early-spring instrumental aerosol measurements with *Legrand and Kirchner's* [1988] determination of sodium deposited in the following winter's snow shows good correspondence. There also seem to be sound meteorological and glaciological [Gow, 1965] arguments supporting consolidation of the spring precipitation into the next winter's accumulation. This seems to be an empirically good association, but it is not well supported by established particle removal theory. It is difficult to find a physical argument supporting the repeatability and regularity of the exchange and precipitation processes necessary to provide the agreement between aerosol concentration and deposited sodium shown in Figure 5.

This association includes temperature, wind speed, and aerosol concentration, which diminished simultaneously with the diminution of sodium in snow during the period 1976–1983. Temperature, wind speed, and aerosol concentration have continued to diminish, on the mean, during the period from August through mid-November, through 1988 as well.

All of these arguments tend to support the hypothesis

TABLE 4. South Pole Daily Maximum Temperature and Number of October Days Warmer Than Stated Temperature

Year	Temperature, °C					Σ > -50
	-30	-35	-40	-45	-50	
1957					2	16
1958			4	3	5	8
1959			1	2	5	11
1960				2	2	17
1961	2	2	2	5	7	18
1962				1	9	12
1963				4	8	6
1964					5	6
1965				2	0	5
1966				1	3	19
1967				1	2	11
1968			4	3	10	10
1969			1	9	8	4
1970			5	3	6	6
1971				2	8	12
1972			2	6	7	11
1973					12	11
1974			4	1	3	10
1975				5	11	6
1976				4	7	10
1977					5	7
1978			2	6	7	11
1979				2	2	7
1980				5	4	11
1981					4	5
1982			4	5	2	11
1983					1	10
1984				4	5	9
1985			4	2	6	4
1986				2	3	10
1987			1	4	2	7
1988			4	6	8	7

that we have had the good fortune to observe, and instrumentally measure, the variation in aerosol properties in a unique air mass during an identifiable climatic iteration. This particular set of observations is especially valuable, because most of our theories of aerosol

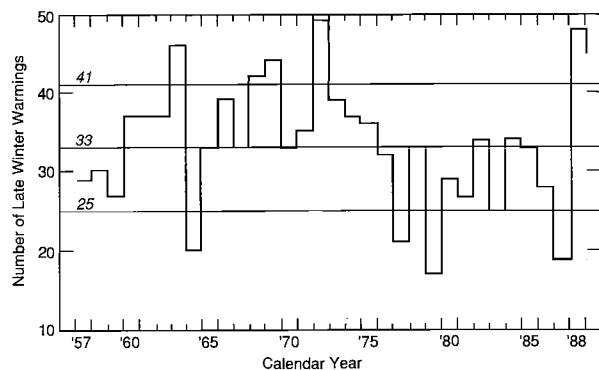


Fig. 21. Frequency analysis of occurrence of spring warmings, which caused the daily maximum temperature to exceed -50°C for the defined period 1957–1988.

transport relate to increasing concentrations, while this circulation change resulted in a period of diminished concentration. It indicates that we may be able to calibrate climatic changes recorded in the glacial record, but only through a broadened understanding of meteorological transport, exchange, and precipitation processes.

The glaciological record near the south pole remains undisturbed and available for additional analysis. It would be productive to date strata in several pits along a circle of 20-km radius about the pole and compare the water and chemical accumulation with the 1957–1990 observation record.

A record of wind speed and direction 300 m above the surface is available in the South Pole radiosonde data. Analysis of this record should identify surface circulation changes attributable to station activity, if any are present. An expanded AWS network is necessary to provide objective analysis of surface transport and exchange.

A major research effort is necessary to identify and assess the magnitude of the processes that cause the precipitation of sodium, or some other conservative aerosol tracer, to the surface of the polar plateau. Identification of climatic or meteorological variation from glaciological records will remain hypothesis until a quantitative precipitation and accumulation theory is established. It is of primary importance to investigate the influence of reduced wind speed on the precipitation and accumulation of particulate matter in south polar snow. It is also necessary to determine if the aerosol–temperature–pressure association observed at the south pole is source independent, or if it reflects a source change in the properties of mP air.

Acknowledgments. This research was supported by NSF-OPP and NSF-DPP, through grants to the Research Foundation of SUNY, over the period 1975–1988. USA CRREL supported the first author during preparation of this manuscript. Thanks are offered to K. Stoner and the Information Management Division of CRREL for preparation and editing of the text and figures. A. J. Gow read the first draft of the manuscript, and discussions with him and B. A. Bodhaine greatly improved several sections of the paper. Additional reviews were provided by E. Andreas and R. Melloh. Special thanks are offered to D. Pack, G. Herbert, M. Johnson, and D. Nelson, who established a long-term climatological aerosol observing program at South Pole; C. Jenkins, who initiated the archiving of meteorological observations to support the program; and the entire sequence of station meteorologists and GMCC observers whose diligence in observation has produced this unique record. This paper is dedicated to W. H. Zoller, the original south polar aerosol scientist.

REFERENCES

- Ahlquist, N. C., and R. C. Charlson, Measurement of the wavelength dependence of atmospheric extinction due to scatter, *Atmos. Environ.*, *3*, 551–564, 1969.
- Alvarez, J. A., and B. J. Lieskes, The Little America blizzard of May, 1957, in *Proceedings of the Symposium on Antarctic Meteorology*, pp. 115–127, Australian Bureau of Meteorology, Melbourne, 1960.
- Angell, J. K., Variations and trends in tropospheric and stratospheric global temperatures, *J. Clim.*, *1*, 1296–1313, 1988.
- Bigg, E. K., Comparison of aerosol at four baseline monitoring stations, *J. Appl. Meteorol.*, *19*, 521–533, 1980.
- Bigg, E. K., J. L. Gras, and C. Evans, Origins of Aitken particles in the remote regions of the southern hemisphere, *J. Atmos. Chem.*, *1*, 203–214, 1984.
- Bodhaine, B. A., Aerosol measurements at four background sites, *J. Geophys. Res.*, *88*, 10,753–10,768, 1983.
- Bodhaine, B. A., and J. C. Bortniak, Four wavelength nephelometer measurements at South Pole, *Geophys. Res. Lett.*, *8*, 539–542, 1981.
- Bodhaine, B. A., and M. E. Murphy, Calibration of an automatic condensation nuclei counter at the south pole, *J. Aerosol Sci.*, *11*, 305–312, 1980.
- Bodhaine, B. A., and M. K. Shanahan, Condensation nucleus and aerosol scattering extinction measurements at the south pole observatory, 1979–1988, *Data Rep. ERL-CMDZ-1*, Natl. Oceanic and Atmos. Admin., Boulder, Colo., April 1990.
- Bodhaine, B. A., J. J. DeLuise, J. M. Harris, P. Houmère, and S. Bauman, Aerosol measurements at the south pole, *Tellus, Ser. B*, *38*, 223–235, 1986.
- Bromwich, D. H., Snowfall in high southern latitudes, *Rev. Geophys.*, *26*, 149–168, 1988.
- Bromwich, D. H., T. R. Parish, and C. A. Zorman, The confluence zone of the intense katabatic winds at Terra Nova Bay, Antarctica, as derived from airborne sastrugi surveys and mesoscale numerical modeling, *J. Geophys. Res.*, *95*, 5495–5510, 1990.
- Cheng, R. J., D. C. Blanchard, and R. J. Cipriano, The formation of hollow sea-salt particles from the evaporation of drops of seawater, *Atmos. Res.*, *22*, 15–26, 1988.
- Cipriano, R. W., D. C. Blanchard, A. W. Hogan, and G. G. Lala, On the production of Aitken nuclei from breaking waves and their role in the atmosphere, *J. Atmos. Sci.*, *40*, 469–479, 1983.
- Cronn, D. R., and K. J. Schilling, Atmospheric trace gas studies in Antarctica, *Rev. Geophys.*, *26*, 497–518, 1988.
- Cronn, D. R., E. Robinson, and M. Loiseaux, Halocarbon and NO₂ profiles in the Antarctic boundary layer, paper presented at Int. Congr. on Polar Meteorol., Int. Union of Geod. and Geophys./Int. Assoc. of Meteorol. and Atmos. Phys., Hamburg, Aug. 16–18, 1983.
- Cunningham, W. C., and W. H. Zoller, The chemical composition of remote area aerosols, *J. Aerosol Sci.*, *12*, 367–384, 1981.
- Dalrymple, P., A physical climatology of the Antarctic plateau, in *Studies in Antarctic Meteorology*, *Antarct. Res. Ser.*, vol. 9, edited by M. J. Rubin, pp. 195–231, AGU, Washington, D. C., 1966.
- Danielsen, E. F., and V. A. Mohnen, Project Dust Storm: In situ measurements and meteorological analysis of tropopause folding, *J. Geophys. Res.*, *82*, 5867–5877, 1977.
- Davies, C. H., and N. Egilmez, The Nolan-Pollak condensation nuclei counter, *J. Aerosol Sci.*, *16*, 245–259, 1985.
- Duce, R. A., G. L. Hoffman, and W. H. Zoller, Atmospheric trace metals at remote northern and southern hemisphere sites: Pollution or natural?, *Science*, *200*, 59–61, 1975.
- Feeley, H. W., and H. Seitz, Use of lead 210 as a tracer of transport processes in the stratosphere, *J. Geophys. Res.*, *75*, 2885, 1970.
- Feeley, H. W., L. E. Toonkel, and M. Shonberg, Radionuclides and lead in surface air, *Rep. HASL 315*, pp. B1–B149,

- U.S. Energy Res. and Dev. Admin., Washington, D. C., 1977.
- Flowers, E. C., and H. J. Viebrock, Comments on the recent decrease in solar radiation at the south pole, *Tellus*, 20, 400–411, 1968.
- Giovinetto, M. B., Mass accumulation in West Antarctica, *Eos Trans. AGU*, 42, 386–389, 1961.
- Giovinetto, M. B., and C. R. Bentley, Surface balance in ice drainage systems of Antarctica, *Antarct. J. U.S.*, 20, 6–13, 1985.
- Gow, A. J., On the accumulation and seasonal stratification of snow at the south pole, *J. Glaciol.*, 40, 461–477, 1965.
- Griffiths, J. F., and D. M. Driscoll, *Survey of Climatology*, Charles E. Morrill Publishing, Columbus, Ohio, 1982.
- Hofmann, D. J., Perturbations of the global atmosphere associated with the El Chichon volcanic eruption of 1982, *Rev. Geophys.*, 25, 743–759, 1987.
- Hofmann, D. J., Balloon borne measurements of middle atmosphere aerosols and trace gases in Antarctica, *Rev. Geophys.*, 26, 113–130, 1988.
- Hofmann, D. J., and J. M. Rosen, Antarctic observations of stratospheric aerosol and high altitude condensation nuclei following the El Chichon eruption, *Geophys. Res. Lett.*, 12, 13–16, 1985.
- Hogan, A. W., Antarctic aerosols, *J. Appl. Meteorol.*, 14, 550–559, 1975.
- Hogan, A. W., Meteorological transport of particulate material to the south polar plateau, *J. Appl. Meteorol.*, 18, 741–749, 1979.
- Hogan, A. W., Aerosol exchange in the remote tropospheres, *Tellus, Ser. B*, 38, 197–213, 1986.
- Hogan, A. W., and S. C. Barnard, Seasonal and frontal variation in Antarctic aerosol concentration, *J. Appl. Meteorol.*, 17, 1458–1465, 1978.
- Hogan, A. W., and D. Nelson, Aerosol observations over the ice caps, *Antarct. J. U.S.*, 10, 310–312, 1975.
- Hogan, A., W. Winters, and S. Barnard, Photoelectric counters for aerosol climatology, *J. Aerosol Sci.*, 12, 477–489, 1981.
- Hogan, A. W., S. C. Barnard, J. A. Samson, and W. Winters, The transport of heat, water vapor, and particulate material to the south polar plateau, *J. Geophys. Res.*, 87, 4287–4292, 1982.
- Hogan, A., J. Samson, K. Kebschull, R. Townsend, S. Barnard, B. Murphey, and T. Hare, On the interaction of aerosol with meteorology, *J. Rech. Atmos.*, 18, 41–67, 1984a.
- Hogan, A., K. Kebschull, R. Townsend, B. Murphey, J. Samson, and S. Barnard, Particle concentrations at the south pole, on meteorological and climatological time scales: Is the difference important?, *Geophys. Res. Lett.*, 11, 850–853, 1984b.
- Hogan, A. W., W. G. Egan, J. A. Samson, S. C. Barnard, D. M. Riley, and B. B. Murphey, Seasonal variation of some constituents of Antarctic tropospheric air, *Geophys. Res. Lett.*, 17, 2365–2368, 1990.
- Ito, T., Study of background aerosols in the Antarctic troposphere, *J. Atmos. Chem.*, 3, 69–91, 1986.
- Ito, T., Y. Morita, and Y. Iwasaka, Balloon observations of aerosols in the Antarctic troposphere and stratosphere, *Tellus, Ser. B*, 38, 214–222, 1986.
- Jones, P. D., Hemispheric surface air temperature variations: Recent trends and an update to 1987, *J. Clim.*, 1, 654–660, 1988.
- Jones, P. D., and D. W. S. Limbert, A data bank of Antarctic surface temperature and pressure data, *Rep. TR038, DOE/ER/60397-H2*, Dep. of Energy, Washington, D. C., June 1987.
- Jouzel, J., L. Merlivat, J. R. Peteit, and C. Lorius, Climatic information over the last century deduced from a detailed isotopic record in the south polar snow, *J. Geophys. Res.*, 88, 2693–2703, 1983.
- Kikuchi, K., Observation of cloud condensation nuclei at Syowa Station, Antarctica, *J. Meteorol. Soc. Jpn.*, 49, 376–383, 1971.
- Kikuchi, K., and K. Fujiwara, Observation of giant sea salt particles from Syowa Station to the south pole, *Sci. Rep. Spec. Issue 2*, pp. 110–112, Jpn. Antarct. Res. Exped., Tokyo, March 1971.
- Kikuchi, K., and A. W. Hogan, Snow crystal observations in summer season at Amundsen–Scott South Pole Station, *J. Fac. Sci. Hokkaido Univ., Ser. VII*, 5, 1–20, 1976.
- Kikuchi, K., and H. Ueda, Cloud droplets and raindrops collected and frozen on the surface of natural snow crystals, in *Snow Crystals in the Arctic Canada*, edited by C. Magono, pp. 83–102, Hokkaido University, Hokkaido, Japan, 1978.
- Kodama, Y., and G. Wendler, Coreless winter in Adélie Land, Antarctica, in 1983, *Antarct. J. U.S.*, 19, 199–201, 1984.
- Komhyr, W. D., An aerosol and gas sampling apparatus for remote observatory use, *J. Geophys. Res.*, 88, 3913–3918, 1983.
- Komhyr, W. D., R. D. Grass, and R. K. Leonard, Total ozone decrease at South Pole, Antarctica, 1964–1985, *Geophys. Res. Lett.*, 13, 1248–1251, 1986.
- Kumai, M., Identification of nuclei and concentrations of chemical species in snow crystals sampled at the south pole, *J. Atmos. Sci.*, 33, 833–841, 1976.
- Legrand, M., and S. Kirchner, Polar atmospheric circulation and chemistry of recent (1957–83) south polar precipitation, *Geophys. Res. Lett.*, 15, 879–882, 1988.
- Lettau, B., The transport of moisture into the Antarctic interior, *Tellus*, 21, 331–340, 1969.
- Lettau, H. H., Antarctic atmosphere as a test tube for meteorological theories, in *Research in the Antarctic*, edited by L. O. Quam, *Publ. 93*, pp. 443–476, Am. Assoc. for the Adv. of Sci., Washington, D. C., 1971.
- Lettau, H. H., A. J. Riordan, and M. Kuhn, Air temperature and two-dimensional wind profiles in the lowest 32 meters as a function of bulk stability, in *Meteorological Studies at Plateau Station, Antarctica*, *Antarct. Res. Ser.*, vol. 25, edited by J. A. Businger, pp. 77–91, AGU, Washington, D. C., 1977.
- Liu, B. Y. H., D. Y. H. Pui, A. W. Hogan, and T. A. Rich, Calibration of the Pollak counter with monodisperse aerosols, *J. Appl. Meteorol.*, 14, 46–51, 1975.
- Maenhut, W., W. H. Zoller, R. A. Duce, and G. L. Hoffman, Concentration and size distribution of particulate trace elements in the south polar atmosphere, *J. Geophys. Res.*, 84, 2421–2431, 1979a.
- Maenhut, W., W. H. Zoller, and D. G. Coles, Radionuclides in the south pole atmosphere, *J. Geophys. Res.*, 84, 3131–3138, 1979b.
- Mahlman, J. D., and S. B. Fels, Antarctic ozone decreases: A dynamical cause, *Geophys. Res. Lett.*, 13, 1316, 1986.
- Mather, K. B., and G. S. Miller, Wind drainage of the high plateau of eastern Antarctica, *Nature*, 209, 281–284, 1966.
- McCormack, M. P., and T. J. Swissler, Stratospheric aerosol mass and latitudinal extension of the El Chichon eruption cloud for October, 1982, *Geophys. Res. Lett.*, 10, 877–880, 1983.
- Meszaros, A., and K. Vissy, Concentration, size distribution and chemical nature of atmospheric aerosol particles in remote oceanic areas, *J. Aerosol Sci.*, 5, 101–109, 1974.
- Metnieks, A. L., and L. W. Pollak, Instructions for using photoelectric condensation nucleus counters, *Geophys. Bull. 16*, School of Cosmic Phys., Dublin Inst. for Adv. Study, Dublin, 1959.
- Miller, N. L., A model for the determination of the scavenging

- rates of submicron aerosols by snow crystals, *Atmos. Res.*, 25, 317–330, 1990.
- Miller, S. W., and B. A. Bodhaine, Calibration of a Pollak condensation nuclei counter using charged monodisperse aerosols, *J. Aerosol Sci.*, 13, 419–428, 1982.
- Murphey, B. B., T. Hare, A. W. Hogan, K. Lieser, J. Toman, and T. Woodgates, Vernal atmospheric mixing in the Antarctic, *J. Appl. Meteorol.*, 30, 494–507, 1991.
- Naval Support Force Antarctica, *McMurdo Forecasters Handbook*, Meteorological Detachment, Port Hueneme, Calif., 1988.
- Neff, W. D., Observational and numerical study of the atmospheric boundary layer overlying the east antarctic ice sheet, *Tech. Memo. NOAA-TM ERL-WPL-67*, 272 pp., Natl. Oceanic and Atmos. Admin., Boulder, Colo., 1981.
- Oltmans, S. J., and W. D. Komhyr, Surface ozone in Antarctica, *J. Geophys. Res.*, 81, 5359–5364, 1976.
- Pack, D. H., Geophysical monitoring for climatic change, *Antarct. J. U.S.*, 7, 253–254, 1973.
- Parish, T., Surface airflow over East Antarctica, *Mon. Weather Rev.*, 110, 84–90, 1982.
- Parish, T. R., Surface winds over the Antarctic continent: A review, *Rev. Geophys.*, 26, 169–180, 1988.
- Parish, T. R., and D. Bromwich, The surface windfield of the Antarctic ice sheet, *Nature*, 327, 51–54, 1987.
- Parungo, F., E. Ackerman, W. Caldwell, and H. K. Weickmann, Individual particle analysis of Antarctic aerosols, *Tellus*, 31, 521–529, 1979.
- Parungo, F., B. A. Bodhaine, and J. C. Bortniak, Seasonal variation of Antarctic aerosol, *J. Aerosol Sci.*, 12, 491–504, 1981.
- Pitter, R. L., A re-examination of riming on thin ice plates, *J. Atmos. Sci.*, 14, 684–685, 1977.
- Polian, G., G. Lambert, B. Ardouin, and A. Jegou, Long-range transport of continental radon in Subantarctic and Antarctic areas, *Tellus, Ser. B*, 38, 178–189, 1986.
- Pollak, L. W., and A. L. Metnieks, Intrinsic calibration of the photoelectric nucleus counter model 1957 with convergent light beam, *Tech. Note 9*, School of Cosmic Phys., Dublin Inst. for Adv. Study, Dublin, 1960.
- Pollak, L. W., and T. C. O'Connor, A photoelectric condensation nucleus counter of high precision, *Geofis. Pura Appl.*, 32, 139–146, 1955.
- Radke, L. F., Sulphur and sulphate from Mt. Erebus, *Nature*, 299, 710–712, 1982.
- Raper, S. C. B., T. M. L. Wigley, P. R. Mayes, P. D. Jones, and M. J. Salinger, Variations in surface air temperatures, 3, The Antarctic, 1957–82, *Mon. Weather Rev.*, 112, 1341–1353, 1984.
- Rasmussen, R. A., M. A. K. Khalil, and R. W. Daluge, Atmospheric trace gases in Antarctica, *Science*, 211, 285–287, 1981.
- Rich, T. A., Apparatus and method for measuring the size of aerosols, *J. Rech. Atmos.*, 2, 79–86, 1966.
- Riley, D. C., A study of the relationship between the variation of aerosol and meteorological parameters at south pole on synoptic, seasonal, and climatological time scales, *ASRC Publ. 1122*, State Univ. of N. Y., Albany, May 1987.
- Robinson, E., D. R. Cronn, F. Menzia, D. Clark, R. Legg, and R. Watkins, Trace gas profiles to 3000 m over Antarctica, *Atmos. Environ.*, 17, 973–981, 1983.
- Robinson, E., D. R. Cronn, F. Menzia, D. Clark, R. Legg, and R. Watkins, Long-term air quality monitoring at the south pole by the NOAA program, Geophysical Monitoring for Climatic Change, *Rev. Geophys.*, 26, 63–80, 1988.
- Rosen, J. M., D. J. Hofmann, and K. H. Kaselau, Vertical profiles of condensation nuclei, *J. Appl. Meteorol.*, 17, 1737–1740, 1978.
- Samson, J. A., Some characteristics of the south polar atmosphere, M.S. thesis, *ASRC Publ. 990*, 207 pp., State Univ. of N. Y., Albany, 1983.
- Samson, J. A., S. C. Barnard, J. S. Obremski, D. C. Riley, J. J. Black, and A. W. Hogan, On the systematic variation of surface aerosol concentration at the south pole, *Atmos. Res.*, 25, 385–396, 1990.
- Saxena, V. K., T. B. Curtin, and F. P. Parungo, Aerosol formation by wave action over Ross Sea, Antarctica, *J. Rech. Atmos.*, 19, 213–224, 1985.
- Schwerdtfeger, W., The climate of Antarctica, in *Climates of the Polar Regions*, edited by S. Orvig, pp. 253–322, Elsevier, New York, 1970.
- Schwerdtfeger, W., Temperature regime of the south pole: Results of 20 years observation at Amundsen–Scott Station, *Antarct. J. U.S.*, 12, 156–159, 1977.
- Schwerdtfeger, W., *Weather and Climate of the Antarctic*, 261 pp., Elsevier, New York, 1984.
- Shaw, G. E., Considerations of the origin and properties of the Antarctic aerosol, *Rev. Geophys.*, 17, 1983–1998, 1979.
- Shaw, G. E., Optical, chemical, and physical properties of aerosols over the Antarctic ice sheet, *Atmos. Environ.*, 14, 911–921, 1980.
- Shaw, G. E., On the residence time of the Antarctic ice sheet sulfate aerosol, *J. Geophys. Res.*, 87, 4309–4313, 1982.
- Shaw, G. E., Antarctic aerosols: A review, *Rev. Geophys.*, 26, 89–112, 1988.
- Sievers, M. F., G. A. Weidner, and C. R. Stearns, Antarctic automatic weather station data for the calendar year 1987, *Rep. 53706*, Dep. of Meteorol., Univ. of Wis., Madison, 1988.
- Sinclair, D., A portable diffusion battery, *Am. Ind. Hyg. Assoc. J.*, 33, 729–735, 1972.
- Sinclair, D., Intrinsic calibration of the Pollak counter—A revision, *Aerosol Sci. Technol.*, 3, 125–134, 1984.
- Sinclair, M. R., Record high temperatures in the Antarctic—A synoptic case study, *Mon. Weather Rev.*, 109, 2234–2242, 1981.
- Skala, G. F., A new instrument for measurement of condensation nuclei, *Anal. Chem.*, 35, 702–705, 1963.
- Solomon, S., The mystery of the Antarctic ozone hole, *Rev. Geophys.*, 26, 131–148, 1988.
- Stearns, C. R., and G. Wendler, Research results from automatic weather stations, *Rev. Geophys.*, 26, 45–61, 1988.
- Swanson, G. S., and K. E. Trenberth, Trends in the southern hemisphere tropospheric circulation, *Mon. Weather Rev.*, 109, 1879–1889, 1981.
- Taljaard, J. J., Synoptic meteorology of the southern hemisphere, in *Meteorology of the Southern Hemisphere, Meteorol. Monogr.*, vol. 13, edited by C. W. Newton, pp. 139–213, American Meteorological Society, Boston, Mass., 1972.
- Tuncell, G., N. K. Aras, and W. H. Zoller, Temporal variations and sources of elements in the south polar atmosphere, 1, Non-enriched and moderately enriched elements, *J. Geophys. Res.*, 94, 13,025–13,038, 1989.
- Vali, G., Nucleation terminology, *Bull. Am. Meteorol. Soc.*, 66, 1426–1427, 1985.
- Van Loon, H., Pressure in the southern hemisphere, in *Meteorology of the Southern Hemisphere, Meteorol. Monogr.*, vol. 13, edited by C. W. Newton, pp. 59–86, American Meteorological Society, Boston, Mass., 1972.
- Vonnegut, B., A continuous recording condensation nuclei meter, in Proceedings of the First National Air Pollution Symposium, Pasadena, Calif., 10–11 November 1949, *Reprint 1711*, General Electric Res. Lab., Schenectady, N. Y., 1950.
- Voskresenskii, A. I., Condensation nuclei in the Mirnii region (in Russian), *Tr. Sov. Antarkt. Eksped.*, 38, 194–198, 1968. (English translation, Antarctic Bibliography.)

- Wang, P. K., A convective diffusion model for the scavenging of submicron aerosol particles by snow crystals of arbitrary shapes—Some comments and corrections, *Atmos. Res.*, *23*, 195–198, 1989.
- Warburton, J. A., and G. O. Linkletter, Atmospheric processes and the chemistry of the snow on the Ross Ice Shelf, Antarctica, *J. Glaciol.*, *20*, 149–162, 1978.
- Watkins, J. A. (Ed.), Geophysical monitoring for climatic change, No. 4, *Summary Rep. 1975*, Natl. Oceanic and Atmos. Admin./Environ. Res. Lab., U.S. Dep. of Commer., Boulder, Colo., 1976.
- Weller, G., Advances in Antarctic geophysical sciences from the IGY to the present, *Antarct. J. U.S.*, *21*, 1–12, 1986.
- Wexler, H., Seasonal and other temperature changes in the Antarctic atmosphere, *Q. J. R. Meteorol. Soc.*, *85*, 196–208, 1959.
- Zoller, W. H., E. S. Gladney, and R. A. Duce, Atmospheric concentrations and sources of trace metals at the south pole, *Science*, *183*, 198–200, 1974.

(Received January 29, 1992;
accepted September 4, 1992.)

CONTINUOUS NANOCLIMATE DATA (1985–1988) FROM THE ROSS DESERT (MCMURDO DRY VALLEYS) CRYPTOENDOLITHIC MICROBIAL ECOSYSTEM

CHRISTOPHER P. MCKAY

Space Science Division, NASA Ames Research Center, Moffett Field, California 94035

JAMES A. NIENOW,¹ MICHAEL A. MEYER,² AND E. IMRE FRIEDMANN

Department of Biological Science, Florida State University, Tallahassee, Florida 32306

We have collected year-round nanoclimate data for the cryptoendolithic microbial habitat in sandstones of the Ross desert, Antarctica, obtained with an Argos satellite data system. Data for two sites in the McMurdo Dry Valleys are available: Linnaeus Terrace, January 1985 to June 1988, and Battleship Promontory, 1986–1987. The focus of this research is ecological, and hence year-round environmental data have been obtained for the ambient environment as well as for conditions within the rock. Using data from the summer, we compare the conditions inside the rock to the outside weather. This demonstrates how the rock provides a shelter for the endolithic microbial community. The most important property of the rock is that it absorbs the summer sunlight, thereby warming up to temperatures above freezing. This warming allows snowmelt to seep into the rock, and the moisture level in the rocks can remain high for weeks against loss to the dry environment.

INTRODUCTION

The Ross desert is a true desert in Antarctica, extending to most of the McMurdo Dry Valleys, the largest ice-free region of the continent. This area is free of ice because it is shielded by the Transantarctic Mountains from the flow of ice from the polar plateau. The entire coastal region near McMurdo Sound, including the polar plateau, receives very little precipitation [Schw-erdtfeger, 1970]. This, together with the low albedo and relatively warm and dry föhn winds descending from the polar plateau, results in extremely arid conditions in the dry valleys [Riordan, 1975, 1982; Bromley, 1985; Clow *et al.*, 1988].

The valleys and the surrounding mountains form an extremely cold desert environment in which there are no visible signs of life. However, microorganisms live hidden in the perennially ice covered lakes [Parker *et al.*, 1982] and below the surface of rocks [Friedmann and Ocampo, 1976; Friedmann, 1982]. The cryptoendolithic ecosystem poses intriguing questions about the survival of organisms in cold dry conditions and has been the subject of investigation for many years. The predominant cryptoendolithic community is the lichen-

dominated community [Friedmann *et al.*, 1988] composed of lichens accompanied by nonlichenized algae, fungi, and bacteria. This community exists in the pore spaces of Beacon sandstone orthoquartzite at a depth of a few millimeters but does not actively bore into the rock. Microbial activity results in the exfoliative weathering of the rock surface [Friedmann, 1982]. Field studies conducted during the austral summers have demonstrated that the nanoclimate conditions in the endolithic zone are very different than those which characterize the macroclimate [Friedmann, 1977; Friedmann *et al.*, 1980; Kappen *et al.*, 1981; McKay and Friedmann, 1985]. These studies have established a need for detailed year-round observations in order to fully understand the differences between the environment within the rock and the outside conditions.

Such a complete set of biological microclimate data is also necessary for a full understanding of the ecosystem and for the construction of numerical models [e.g., Nienow *et al.*, 1988a, b] to predict the system response to perturbations. Unfortunately, ecological research in Antarctica is hampered by the difficulty in obtaining continuous biometeorological data over the entire year. Often, data have only been obtained for time periods when human observers were present in the field, i.e., during periods of relatively clement weather in the summer season. Even if environmental and logistical

¹Now at Waycross College, Waycross, Georgia 31501.

²Now at Desert Research Institute, Reno, Nevada 89506.

difficulties could be surmounted, polar ecosystems are often too fragile to withstand a year-round human presence. Hence automatic data acquisition equipment clearly has a role to play in obtaining the requisite data.

Over the last 10 years there has been an ongoing effort to obtain meteorological data from automatic weather stations in the Antarctic [Renard and Salinas, 1977; Stearns and Savage, 1981; Stearns, 1982; Savage et al., 1985; Stearns and Wendler, 1988]. These stations obtain data using standard meteorological instrumentation once every ~200 s. The data are broadcast by radio, and when one of the National Oceanic and Atmospheric Administration (NOAA) series of polar-orbiting satellites is passing overhead, the data are collected and then relayed to ground stations. The fact that the satellites are in polar orbit makes this system particularly well suited for use in polar regions where data transmission to geostationary satellites is often impossible. The total number of satellite passes over a given location averages about seven per day at the equator and up to 28 per day at the poles. For the data reported in this paper, all readings collected during a single satellite pass are averaged together.

We have successfully adapted this system to monitor biologically important environmental parameters, both within the rock habitat and for ambient conditions, on a year-round basis. The initial summaries of the year-round data results for this system were presented by McKay and Friedmann [1984] and more extensively by Friedmann et al. [1987]. These studies were based at Linnaeus Terrace, a location of extensively colonized sandstone rocks in the Wright Valley. In this paper we report the availability of the complete set of data acquired at Linnaeus Terrace from 1984 to 1988 (the data set for Linnaeus Terrace from 1984 to 1986 are published in full detail by Friedmann et al. [1987]) and from a second site, Battleship Promontory, for the years 1986 and 1987. The data set is extensive, and we do not reproduce it here but focus instead on illustrative subsamples of the data, particularly from the summer months. The full data set for both sites is available from the first author.

A detailed quantitative analysis of the yearly hours of the various temperature-light-water combinations based on the computer analysis of the data set, as well as further biological considerations, is published elsewhere [Friedmann et al., 1993].

METHODS AND INSTRUMENTATION

The system is composed of three components: the sensors, the data-handling and transmitting unit, and the power supply. In this paper we report data obtained from sensors which monitor the air temperature, the temperature of the rock surface in several orientations, the electrical conductivity of the rock (an indication of rock moisture), the wind speed near the ground, the

photosynthetically active radiation flux, and the presence of snow. Air temperature is measured at a distance of about 1 m from the rock sensors and at a height of about 70 cm above the rock surface. The sensor is screened from direct solar radiation by a polished metal cylinder. A complete description of the methods and instrumentation has been given by Friedmann et al. [1987] and is only briefly reviewed here.

The temperature is sensed with a National Semiconductor (Santa Clara, California) LM134 semiconductor sensor which generates a current that is directly proportional to the absolute temperature. A secondary temperature sensor was composed of a Yellow Springs Instrument (Yellow Springs, Ohio) thermistor device. It is composed of a ceramic bead whose electrical resistance is a sensitive function of temperature. Light measurements of the photosynthetically active radiation (PAR) are obtained using a LiCor (Lincoln, Nebraska) quantum sensor. On Linnaeus Terrace the skylight was measured by shielding a light sensor with a tube such that the view of the sky was limited to a ~50° region centered on the zenith. In the dry valleys, where the maximum solar elevation is 36°, this ensures that only skylight reaches the sensor, and hence the ratio of this sensor's output to the output from the total light sensor is an indication of cloud cover. Wind is measured with a standard meteorological cup anemometer.

We have developed a method to determine the presence of liquid water in the rock on the basis of electrical conductivity [Friedmann et al., 1987]. The sensor consists of a pair of electrodes separated by about 1 cm. To attach the electrodes to the rock surface, they are soldered into small holes (about 1 cm deep) drilled into the rocks. The effective conductance between these electrodes is dependent on the mobility of ions that can act as charge carriers. The conductivity depends on all possible current paths on the surface and within the rock to a distance approximately equal to the separation of the two electrodes. When liquid water is present in the rock, salts in solution provide the ions that allow current to flow. If the presence of liquid water is the limiting factor in determining conductivity (i.e., salts are present and the environment is dry), then the conductivity will increase uniformly (but not necessarily linearly) with increasing liquid water. Typical conductivities for the colonized Antarctica rocks saturated with moisture are 1 μ mhos. However, the value of the conductivity that is obtained depends on the total salt content, the porosity of the rock, and the structure of the interstitial channels within the rock. These factors can vary from site to site even within the same rock. For this reason we have not tried to quantify the output of the rock conductivity sensor and use it only as an indicator of the duration of liquid water conditions within the rock. At below freezing temperatures, current can still flow because films of liquid water will still exist. In the rock, water can remain unfrozen in an

undercooled state at least several degrees below the equilibrium freezing temperature [Meyer *et al.*, 1988]. If the rock is below freezing and ice (which does not conduct) forms within the rock, then the conductivity will decrease. However, sufficient amounts of water may remain to form a conductive channel. As the temperature drops, ice will separate out and the solution concentration will increase [see Franks, 1985] in the remaining conductive channels. The volume of the unfrozen liquid is proportional to the initial solute concentration and the freezing point depression of the solution.

To perform, the measurement a 2-M Ω resistor is placed in series with the electrodes and a voltage (5 V) placed across both the fixed resistor and the rock. The voltage drop across the electrodes in the rock (buffered by a unity gain amplifier) indicates the effective conductivity of the rock. The scale of the conductivity reading runs from zero to 255 counts. To prevent polarization of the surface, ac excitation is preferred. However, the low current draw and the low duty cycle allow us to use dc excitation.

We have constructed a device to signal the onset of snowmelt in a qualitative manner [Friedmann and McKay, 1985]. The sensitive element is a NaCl impregnated fiberglass filter paper disk of approximately 5 cm diameter. The disks were soaked in 1M NaCl and then allowed to dry. In the dry state the dc conductance of the disks is virtually zero. When snow is present at temperatures above the eutectic point of NaCl (-22°C), the conductivity of the disk increases dramatically. The input lead to the sensor is a 5-V reference line that pulses only during sampling intervals. The output from the sensor goes directly to the input of the data-handling and transmitting unit. When there is no moisture on the filter paper disk, the input channel records no voltage but becomes a full 5 V when moisture is present. Thus the snow sensor functions as a binary state switch, providing a uniform signal when any snow is present at temperatures above the eutectic point of NaCl. There is very little current draw even in the presence of moisture, since the input impedance of the data-handling system is very high. Despite the use of a dc excitation, polarization of the sensor is not a problem as a result of the low duty cycle times (1 in 200), low current draw, and low moisture levels.

The data are processed by an Argos Data Acquisition Platform (ADAP, manufactured by Polar Research Laboratories, Santa Barbara, California). The ADAP is a self-contained portable data system designed for remote areas. Each unit is capable of sampling 32 channels in the form of analog ground-referenced voltages from zero to 5 V. Preconditioning of the input signals is handled by custom-manufactured electronics (National Research and Technology, Tallahassee, Florida). In operation, the ADAP completes a sampling sequence once every 200 s. In a sampling sequence the unit

samples all 32 channels in 1 s, stores the data, digitizes, and then transmits them to the TIROS/NOAA series of satellites. When a satellite's orbit places it within the view of a platform, the transmissions are received and relayed to a ground station.

The major problem in the design of a monitoring station in Antarctica is to ensure survival throughout the dark cold austral winter. Power is supplied by eight 12-V 40 A h lead-acid gel batteries (Power Sonic, Redwood City, California) recharged during the summer months by an array of solar cells. The average power requirement of the system, including ADAP, ancillary electronics, and sensors, is about 0.6 W. This load can be sustained for over 8 months with the battery supply. All electronic components are rated or tested to -40°C .

STUDY SITES

The first study site is located on Linnaeus Terrace ($77^{\circ}36'\text{S}$, $161^{\circ}05'\text{E}$, 1600–1650 m altitude) in the Asgard Range, on the northern slope of Mount Oliver facing Wright Valley [Friedmann, 1982]. This is also the site of earlier environmental measurements [Kappen *et al.*, 1981; Friedmann *et al.*, 1987]. For a map of the dry valley region see McKay and Friedmann [1985]. Apart from a few dolerite dykes, Linnaeus Terrace consists of Beacon sandstone and is particularly rich in lichen-dominated cryptoendolithic microbial colonization.

The second site is Battleship Promontory ($76^{\circ}55'\text{S}$, $160^{\circ}55'\text{E}$, 1600–1650 m altitude) in the Convoy Range. The name of this large sandstone outcrop facing Alatina Valley aptly expresses its spectacularly ragged morphology. Its geology has been described by Mirsky *et al.* [1965]. The sandstone rocks of Battleship Promontory are colonized by the lichen-dominated cryptoendolithic community. Sandstones adjacent to the dolerite talus slope of Mount Gran are wetted by snowmelt water carried by the dolerite rubble which acts as an aquifer, and here the sandstone is colonized by the *Gloeocapsa-Hormathonema* (cyanobacteria) community which requires more liquid water than lichens [Friedmann *et al.*, 1988].

RESULTS

Daily average temperatures and sunlight on Linnaeus Terrace station are shown in Figure 1. The light is the photon flux (in units of 6.02×10^{20} photons $\text{m}^{-2} \text{s}^{-1}$) in the 400- to 700-nm spectral region. The dichotomy between summer and winter is clearly shown. Also shown in Figure 1 is the temperature on the horizontal surface of a colonized rock. The top surface of this particular rock has been previously monitored [McKay and Friedmann, 1985; Friedmann *et al.*, 1987].

Figure 2 shows the data in more detail for the month of January 1987. Here we also show the results of the sky sensor. When the ratio of the total light to the sky

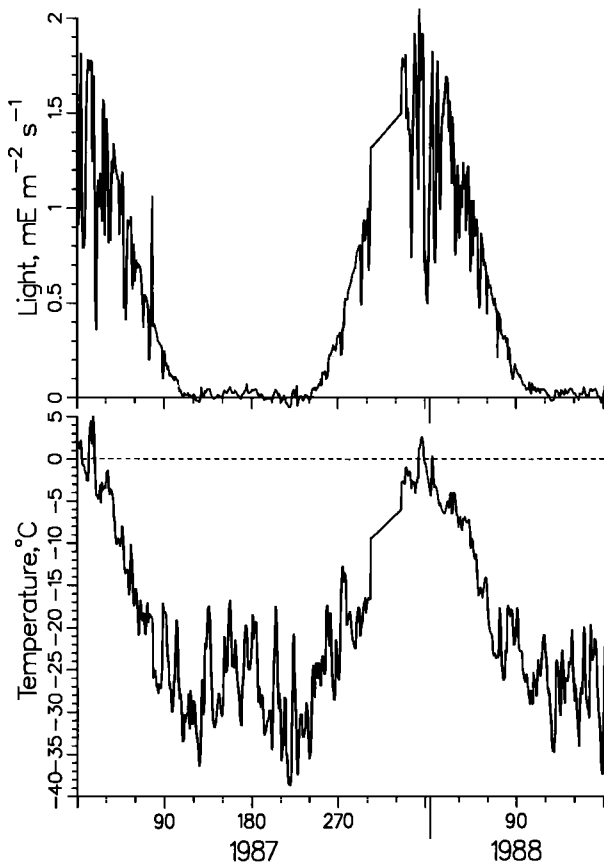


Fig. 1. Daily average light and temperature during 1987 and 1988 on Linnaeus Terrace. Photosynthetically active radiation (400–700 nm) is shown in the top panel ($E = 6.02 \times 10^{23}$ photons). Temperature of a horizontal rock surface is shown in the bottom panel.

light approaches values close to ~ 3 , this is an indication that the sky is completely cloudy. When this occurs, the temperatures drop. The rock and air temperatures are both shown in the bottom panel of Figure 2. As expected [Kappen *et al.*, 1981; McKay and Friedmann, 1985; Friedmann *et al.*, 1987], the rock temperature is warmer than the air temperature. The data shown here are daily averages, and the rock is uniformly about 5°C warmer than the air. The difference varies throughout the day from about $10^\circ\text{--}15^\circ\text{C}$ at midday to nearly zero at midnight [e.g., McKay and Friedmann, 1985].

Figures 3 and 4 show selected climate results for Battleship Promontory. Daily average air temperatures at Battleship Promontory for 1986 and 1987 are shown in the bottom panel of Figure 3. The top panel of that figure shows the temperature difference between an eastern facing rock surface and air. The rock is significantly warmer during the summer months as a result of solar heating. During winter the rock surface is slightly colder

than the air. This is the expected result since the rock surface will cool efficiently by infrared emission.

Figure 4 shows the daily average snow and rock moisture for Battleship Promontory for 1986 and 1987. The presence of snow is detected by NaCl disks, and the rock moisture determined by changes in conductivity. The results are qualitative only and have been normalized. The results suggest that the Battleship Promontory site receives snow with a frequency not unlike that reported for Linnaeus Terrace by Friedmann *et al.* [1987]. Both sites, which are located over 1600 m above the valley floors, receive much more regular snowfalls than the valley floors below [Riordan, 1975; Thompson *et al.*, 1971; Clow *et al.*, 1988].

As seen in Figures 1 and 3, after January the flux of sunlight is reduced, temperatures drop, and the growing season for the endolithic communities is essentially over. Rock temperature on Linnaeus Terrace did not rise above freezing after mid-February. Throughout the winter months the temperatures remain quite low.

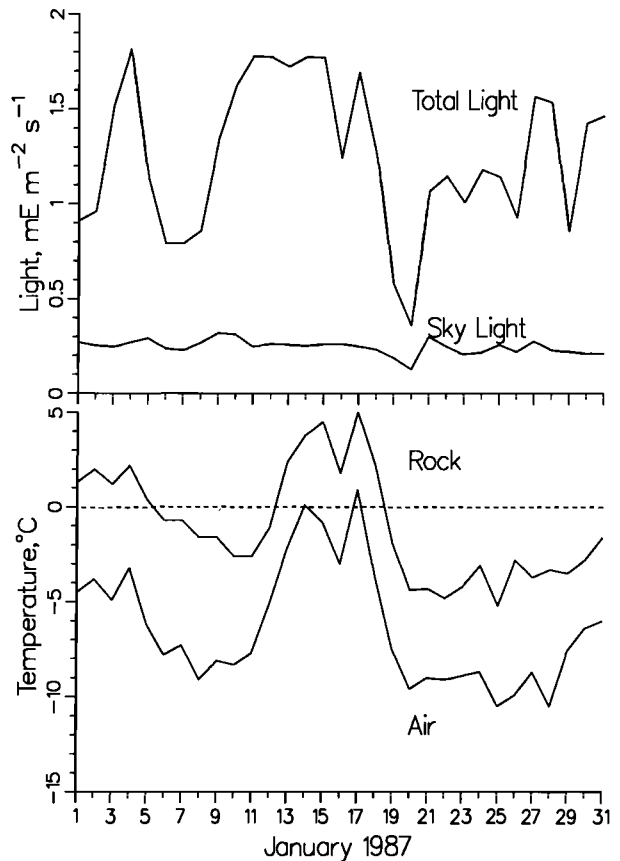


Fig. 2. Daily average light and temperature during January 1987 on Linnaeus Terrace. Light and rock temperature are the same as in Figure 1. Also shown is the sky light (light only from a cone of about 50° centered on the zenith) and the air temperature. Under completely cloudy conditions, total light is about 3 times the sky light.

There is a variation of about 20°C, which can be seen, for example, in the data for winter 1986, 1987, and 1988. The rise in temperature during winter, often by 20°C, is due to föhn winds [Schwerdtfeger, 1970; Riordan, 1975, 1982; Bromley, 1985; Clow *et al.*, 1988]. In September the sunlight becomes measurable again, and the air temperatures begin to rise. Rock surface temperature begins to rise above freezing in November and maximizes in late December and early January. This general pattern repeats from year to year.

DISCUSSION

The year-round data mirror seasonal patterns not only in the Ross desert nanoclimate but also in the mesoclimate of the McMurdo Dry Valleys in general. Summer extends from mid-November to late February and is the period during which virtually all metabolic activity occurs. The phasing of the seasons (the difference

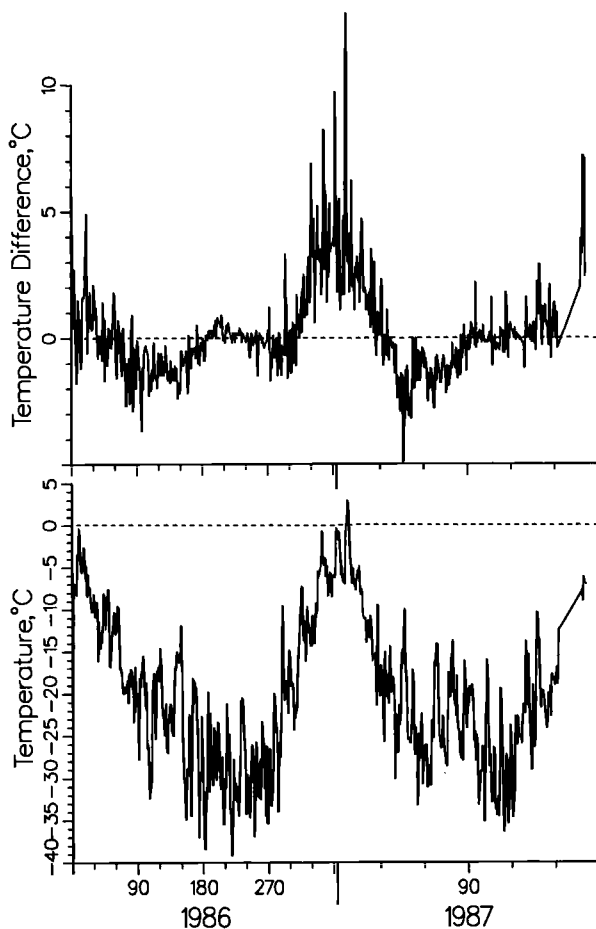


Fig. 3. Daily average air temperatures at Battleship Promontory for 1986 and 1987 are shown in the bottom panel. The top panel shows the temperature difference between rock and air. The rock is significantly warmer during the summer months and slightly cooler in the winter.

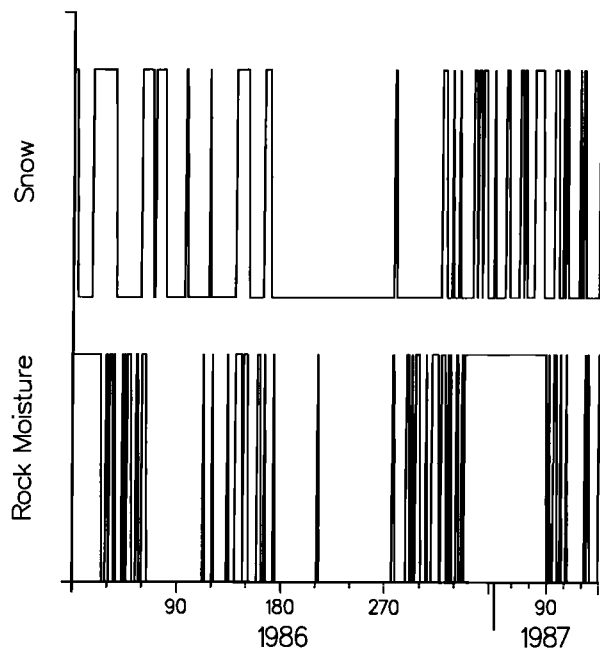


Fig. 4. Daily average snow and rock moisture for Battleship Promontory for 1986 and 1987. The presence of snow is detected by NaCl disks, and the rock moisture determined by changes in conductivity. The results are qualitative only and have been normalized.

between the summer solstice and the warmest day of the year) is dominated by the solar radiation, and hence summer in Antarctica is more symmetrical with respect to the solstice (December 21) than the summer season in the temperate regions of the southern hemisphere. During the austral summer the sun shines continuously, often raising the rock temperatures above the freezing point. The summer is also the period of the most snowfall. This, and the warm rock surfaces, ensure a supply of water within the rocks [Friedmann, 1978]. Once water has seeped into the rock, it is retained long after the ambient conditions return to a dry state. Fall, from late February to mid-April, marks the transition to continuous night and rock temperatures consistently below freezing. Snowfalls continue, but the rock temperatures are too low to result in melting. Winter, from mid-April to August, is the period of continuous darkness, and temperatures are determined by the balance between radiative cooling and heating due to sporadic föhn winds [e.g., Clow *et al.*, 1988]. Spring extends from September to mid-November and represents the transition from continuous night to continuous day. Rock temperatures remain below freezing, and there is no significant melting of snow or metabolic activity.

It is interesting to consider how the pattern of climate varies from year to year because of interannual variability in climate. There are two key processes that control nanoclimate of the endolithic habitat: sunlight warming

TABLE 1. Comparison of the Ambient Conditions and the Advantages of the Cryptoendolithic Environment

Factor	Ambient Condition	Advantages of the Cryptoendolithic Environment
Temperature	Low air temperature.	Direct solar heating warms the rocks and thermal inertia of the rocks dampens variations.
Moisture	Little snow; air humidity averages <<50%.	Rock pore spaces hold moisture for weeks after a snowmelt.
Wind	Abrasion by strong föhn winds.	Protection is given by the rock.
Radiation	Solar ultraviolet flux and intense visible radiation.	The rock significantly attenuates all radiation, particularly UV, but limits depths of colonization.

the rock and snowmelt providing a source of liquid water. The first of these is not likely to vary to a great extent from year to year since the solar radiation is controlled by the solar zenith angle. The second factor, however, does show considerable interannual variation. Some years there are numerous and heavy snowfalls, while other years there are only light and occasional snows. This variation could be tied to larger weather patterns which transport moist air from other regions. Assessing the nature of any interannual variability would require a longer systematic monitoring than we have accomplished.

The climate of the McMurdo Dry Valleys is cold and dry, and on the surface there are virtually no signs of life, especially in the typical desert areas (Ross desert). More humid microsites with mosses, lichens, and cyanobacterial mats occur only when meltwater from glaciers or from snow is available. Yet, within the sandstone of the Ross desert, colonized by cryptoendolithic microorganisms, conditions are suitable for life. On the basis of year-round data we can characterize the ambient environment and assess what advantages the endolithic habitat provides. The environmental factors that make life on the surface of soils or rocks impossible are listed in Table 1. Although we have listed them in a priority order, all of these factors are operating. On the basis of our studies of the cryptoendolithic habitat we can suggest how the rock substrate provides protection to organisms.

Among adverse biological factors the most significant is air temperature, which is generally below freezing, with only brief excursions to temperatures above 0°C. The mean annual air temperature is below -20°C, and even during the warmest month of the year, January, the monthly mean air temperature is several degrees below freezing (see also *Friedmann et al.* [1987]). By contrast, temperatures within the rocks can be relatively warm with tens to hundreds of hours spent above 0°C. In addition, direct solar heating of the rock can raise temperatures to up to 17.8°C and provides a thermally stable environment [*McKay and Friedmann*, 1985].

Water is an essential requirement for life, and the ambient conditions in the valleys are extremely dry compared to the levels necessary to support life. There is little precipitation, and much of it is blown away or sublimates and therefore is unavailable for organisms [*Friedmann*, 1978]. Again, the endolithic habitat provides an advantage. Snow on the surface of the rocks is melted by the absorption of radiation, warming the rock to temperatures above the freezing point. Water then seeps quickly into the porous rock [*Friedmann*, 1978]. Although the ambient environment rapidly dries, water is retained within the rock matrix and only gradually decreases. Typically, new snow recharges the rock water content before the levels have dropped appreciably. The data show (e.g., Figure 4) that after a summer snowmelt the moisture level in the rocks can remain high for weeks while the air relative humidity remains quite low (see also *Kappen et al.* [1981] and *Friedmann et al.* [1987]).

In addition to providing a favorable thermal and moisture regime, the rock habitat functions as a mechanical shield against wind abrasion and extreme ultraviolet or visible light [*Nienow et al.*, 1988b]. Thus the cryptoendolithic habitat, because of the dramatic difference between its nanoclimate and the outside conditions, constitutes a refuge for life in an otherwise abiotic and "hostile" environment.

Acknowledgments. We thank the members of the field parties and the helicopter crews for assistance in deployment of the equipment. This work was supported by NASA grants NSG 7337 and NAGW 1971 and by NSF grants DPP80-17581 and DPP83-14180 to E.I.F.

REFERENCES

- Bromley, A. M., Weather observations, Wright Valley, Antarctica, report, 37 pp., N. Z. Meteorol. Serv., Wellington, 1985.
- Clow, G. D., C. P. McKay, G. M. Simmons, Jr., and R. A. Wharton, Jr., Climatological observations and predicted sublimation rates at Lake Hoare, Antarctica, *J. Clim.*, 1, 715-728, 1988.

- Franks, F., *Biophysics and Biochemistry at Low Temperatures*, Cambridge University Press, New York, 1985.
- Friedmann, E. I., Microorganisms in Antarctic desert rocks from dry valleys and Dufek Massif, *Antarct. J. U. S.*, *12*, 26–30, 1977.
- Friedmann, E. I., Melting snow in the dry valleys is a source of water for endolithic microorganisms, *Antarct. J. U. S.*, *13*, 162–163, 1978.
- Friedmann, E. I., Endolithic microorganisms in the Antarctic cold desert, *Science*, *215*, 1045–1053, 1982.
- Friedmann, E. I., and C. P. McKay, A method for the continuous monitoring of snow: Application to the cryptoendolithic microbial community of the Ross desert, Antarctica, *Antarct. J. U. S.*, *20*, 179–181, 1985.
- Friedmann, E. I., and R. Ocampo, Endolithic bluegreen algae in the dry valleys: Primary producers in the Antarctic desert ecosystem, *Science*, *193*, 1247–1249, 1976.
- Friedmann, E. I., Y. Garty, and L. Kappan, Fertile stages of endolithic lichens in the dry valleys of southern Victoria Land, *Antarct. J. U. S.*, *15*, 166–167, 1980.
- Friedmann, E. I., C. P. McKay, and J. A. Nienow, The cryptoendolithic microbial environment in the Ross desert of Antarctica: Continuous nanoclimate data, 1984 to 1986, *Polar Biol.*, *7*, 273–287, 1987.
- Friedmann, E. I., M. Hua, and R. Ocampo-Friedmann, Cryptoendolithic lichens and cyanobacterial communities of the Ross desert, Antarctica, *Polarforschung*, *58*, 251–259, 1988.
- Friedmann, E. I., L. Kappen, M. A. Meyer, and J. A. Nienow, Long-term productivity in the cryptoendolithic microbial community of the Ross desert, Antarctica, *Microbiol. Ecol.*, *25*, 51–69, 1993.
- Kappen, L., E. I. Friedmann, and Y. Garty, Ecophysiology of lichens in the dry valleys of southern Victoria Land, Antarctica, 1, Microclimate of the cryptoendolithic lichen habitat, *Flora Jena*, *171*, 216–235, 1981.
- McKay, C. P., and E. I. Friedmann, Continuous temperature measurements in the cryptoendolithic microbial habitat by satellite-relay data acquisition system, *Antarct. J. U. S.*, *19*, 170–172, 1984.
- McKay, C. P., and E. I. Friedmann, The cryptoendolithic microbial environment in the Antarctic cold desert: Temperature variations in nature, *Polar Biol.*, *4*, 19–25, 1985.
- Meyer, M. A., G. H. Huang, G. J. Morris, and E. I. Friedmann, The effect of low temperatures on Antarctic endolithic green algae, *Polarforschung*, *58*, 113–119, 1988.
- Mirsky, A., S. B. Treves, and P. E. Calkin, Stratigraphy and petrography, Mount Gran area, southern Victoria Land, Antarctica, in *Geology and Paleontology of the Antarctic*, *Antarct. Res. Ser.*, vol. 6, edited by J. B. Hadley, pp. 145–175, AGU, Washington, D. C., 1965.
- Nienow, J. A., C. P. McKay, and E. I. Friedmann, The cryptoendolithic microbial environment in the Ross desert of Antarctica: Mathematical models of the thermal regime, *Microbiol. Ecol.*, *16*, 253–270, 1988a.
- Nienow, J. A., C. P. McKay, and E. I. Friedmann, The cryptoendolithic microbial environment in the Ross desert of Antarctica: Light in photosynthetically active region, *Microbiol. Ecol.*, *16*, 271–289, 1988b.
- Parker, B. C., G. M. Simmons, Jr., K. G. Seaburg, D. D. Cathey, and F. T. C. Allnut, Comparative ecology of plankton communities in seven Antarctic oasis lakes, *J. Plankton Res.*, *4*, 271–286, 1982.
- Renard, R. J., and M. G. Salinas, The history, operation, and performance of an experimental automatic weather station in Antarctica, *Rep. NPS-63RD7710*, 57 pp., Nav. Postgrad. Sch., Monterey, Calif., 1977.
- Riordan, A. J., The climate of Vanda Station, Antarctica, in *Climate of the Arctic*, edited by G. Weller and S. A. Bowling, pp. 268–275, Geophysical Institute, University of Alaska, Fairbanks, 1975.
- Riordan, A. J., Formulation and testing of a climatonic simulation of the microclimate of the dry valleys and of the Little America V Station in Antarctica, *Boundary Layer Meteorol.*, *24*, 295–329, 1982.
- Savage, M. L., C. R. Stearns, and D. Flemming, Antarctic automatic weather station data for the calendar year 1980, report, 72 pp., Dep. of Meteorol., Univ. of Wis., Madison, 1985.
- Schwerdtfeger, W., The climate of the Antarctic, in *World Survey of Climatology*, vol. 14, *The Climate of the Antarctic*, edited by S. Orvig, pp. 253–355, Elsevier, New York, 1970.
- Stearns, C. R., Antarctic automatic weather stations, 1981–1982, *Antarct. J. U. S.*, *17*, 217–219, 1982.
- Stearns, C. R., and M. L. Savage, Automatic weather stations, 1980–1981, *Antarct. J. U. S.*, *16*, 190–192, 1981.
- Stearns, C. R., and G. Wendler, Research results from Antarctic automatic weather stations, *Rev. Geophys.*, *26*, 45–61, 1988.
- Thompson, D. C., R. M. F. Craig, and A. M. Bromley, Climate and surface heat balance in an Antarctic dry valley, *N. Z. J. Sci.*, *14*, 245–251, 1971.

(Received March 18, 1991;
accepted April 7, 1993.)